

SESS REPORT 2020

The State of Environmental Science
in Svalbard – an annual report

SESS REPORT 2020

The State of Environmental Science
in Svalbard – an annual report

Marta Moreno-Ibáñez, Jon Ove Methlie Hagen,
Christiane Hübner, Heikki Lihavainen,
Agata Zaborska (Editors)

SESS report 2020
The State of Environmental Science in Svalbard
– an annual report

ISSN 2535-809X (printed)
ISSN 2535-6321 (pdf)
ISBN 978-82-691528-9-0 (printed, stapled)
ISBN 978-82-691528-8-3 (pdf)

Publisher: Svalbard Integrated Arctic Earth Observing System (SIOS)
Editors: Marta Moreno-Ibáñez, Jon Ove Methlie Hagen, Christiane Hübner,
Heikki Lihavainen, Agata Zaborska
Editor popular science summaries: Janet Holmén
Layout: Melkeveien designkontor, Oslo
Overview figure: Floor van den Heuvel

CITATION:

Entire report: Moreno-Ibáñez M, Hagen JO, Hübner C, Lihavainen H, Zaborska A (eds) 2021:
SESS report 2020, Svalbard Integrated Arctic Earth Observing System, Longyearbyen
Chapters in report: All authors (2021) Title of chapter. In: Moreno-Ibáñez et al (eds) SESS
report 2020, Svalbard Integrated Arctic Earth Observing System, Longyearbyen, pp xx-xx.
DOI-link of chapter



The report is published as electronic document, available from
the SIOS web site <https://sios-svalbard.org/SESSreport>

Contents

Foreword.....	6
Authors from following institutions contributed to this report:.....	8
Executive Summary	10
Summaries for stakeholders.....	14
1 How representative is Svalbard for future Arctic climate evolution? An Earth system modelling perspective (SvalCLIM)	38
2 Space physics in Svalbard: A study of the energy input in the polar ionosphere using SuperDARN.....	60
3 Scientific Applications of Unmanned Vehicles in Svalbard (UAV Svalbard).....	78
4 Arctic haze in a climate changing world: the 2010-2020 trend (HAZECLIC).....	104
5 Microplastics in the realm of Svalbard: current knowledge and future perspectives (MIREs).....	118
6 Environmental status of Svalbard coastal waters: coastscapes and focal ecosystem components (SvalCoast).....	142
7 From land to fjords: The review of Svalbard hydrology from 1970 to 2019 (SvalHydro).....	176
8 Satellite and modelling based snow season time series for Svalbard: Inter-comparisons and assessment of accuracy (SATMODSNOW).....	202
9 Svalbard snow and sea-ice cover: comparing satellite data, on-site measurements, and modelling results (SvalSCESIA)	220
10 Terrestrial photography applications on snow cover in Svalbard (PASSES).....	236
11 A multi-scale approach to snow cover observations and models (SnowCover).....	252
12 Ground ice content, drilling methods and equipment and permafrost dynamics in Svalbard 2016–2019 (PermaSval)	258
Frequently Asked Questions.....	276

Foreword

Svalbard Integrated Arctic Earth Observing System (SIOS) is an international multidisciplinary research infrastructure in and around Svalbard. SIOS focuses on long-term monitoring of key variables in the Arctic to observe, attribute and describe the effects of global environmental and climate change. SIOS entered into the operational phase in 2018 with a mission to develop an efficient observing system; to share technology, experience, and data; to close knowledge gaps, and to decrease the environmental footprint of science. The annual SESS report is one tool to fulfil this mission.

The SESS report is a way to guide development of the observing system; the recommendations in the SESS reports are used to identify research needs, gaps in observations, and new techniques and methods that can improve and optimise the research infrastructure. This is the third SESS report. Like its forerunners, it is based on multifarious contributions from different disciplines within Earth System Science. The reports' recommendations are already being implemented, either at the initiative of the SIOS Knowledge Centre or by SIOS members as a direct result of collaborating to write a SESS chapter or within SIOS in general. During the coming year, we will synthesise the recommendations from the first three reports and develop a roadmap for their implementation.

The year 2020 has been overshadowed by the global COVID-19 pandemic. The Svalbard community, which is quite dependent on tourism and research, was also hit hard. The nationwide lockdowns in many countries, quarantine regulations, and restrictions on travel to and within Svalbard led to field work being postponed or cancelled. Meetings, workshops, and conferences were all moved online. This is foreseen to continue at least for the first half of 2021.

SIOS reacted swiftly to this new situation with various initiatives. The SIOS Knowledge Centre, with help from the working groups, organised possibilities to patch gaps in field data with satellite or airborne remote sensing, coordinated remote access to research instrumentation, and also intensified the social aspects of SIOS by gathering the community virtually for coffee breaks, webinars and conferences. None of these things would have happened without members' and the SIOS Knowledge Centre's dedication. In some ways, it might be said that the pandemic has made the SIOS community more tightly knit by bringing them together – if only virtually – to share knowledge, solve problems and ensure research continuity.

There is a lot to learn for the future. How will the “new normal” look? How much we will change our behaviour? Will we continue or even expand our use of digital technology to interact with each other? Will we increasingly rely on remote and virtual access to keep measurements running and gather samples? Only time will tell how much of today’s on-site fieldwork will be replaced by remote sensing tools and innovative approaches. SIOS will certainly continue to strive to be at the forefront of developing new methodologies that ensure high quality observations in the Arctic.

I would like to express my appreciation for the editorial board; it was a pleasure to work with such an enthusiastic team. I am deeply grateful to the reviewers for their input on this SESS report; reviewing is hard work, and I thank you. I also acknowledge my colleagues here at SIOS Knowledge Centre. These have been strange times, but we managed to support each other and make the best of a challenging situation.

Longyearbyen, December 2020



Heikki Lihavainen

Director, SIOS

Authors from following institutions contributed to this report:

AARI	Arctic and Antarctic Research Institute, Russia
AMU	Adam Mickiewicz University, Poland
APN	Akvaplan-niva AS, Norway
AWI	Alfred Wegener Institute, Helmholtz Centre for Polar and Marine Research, Germany
BCSS	Birkeland Centre for Space Studies, University of Bergen, Norway
CAS	Institute of Rock Structure and Mechanics of the Czech Academy of Sciences, Czech Republic
CESE-TU	College of Environmental Science and Engineering, Tongji University, China
CPE USB	Centre for Polar Ecology, University of South Bohemia, České Budějovice, Czech Republic
Eurac	Eurac Research, Institute for Earth Observation, Italy
FMI	Finnish Meteorological Institute, Finland
GU	GIS Centre, University of Gdańsk, Poland
HU Berlin	Humboldt-Universität Berlin, Germany
IG PAS	Institute of Geophysics, Polish Academy of Sciences, Poland
IIA-CNR	Institute of Atmospheric Pollution Research, National Research Council of Italy, Italy
IMR	Institute of Marine Research, Norway
INAR	Institute for Atmospheric and Earth System Research, University of Helsinki, Finland
INFN	National Institute for Nuclear Physics, Italy
Insubria Univ.	Insubria University, Italy
IOPAN	Institute of Oceanology Polish Academy of Sciences, Poland
ISP-CNR	Institute of Polar Sciences, National Research Council of Italy, Italy
IVL	IVL Swedish Environmental Research Institute, Sweden

Kolibri Geo Services Kolibri Geo Services, Norway
 Loughborough Univ Loughborough University, United Kingdom
 MET Norway. Norwegian Meteorological Institute, Norway
 MMBI Murmansk Marine Biological Institute, Russia
 MU Masaryk University, Czech Republic
 NCU Nicolaus Copernicus University, Poland
 NGI. Norwegian Geotechnical Institute, Norway
 NILU Norwegian Institute for Air Research, Norway
 NIPR National Institute of Polar Research, Japan
 NIVA Norwegian Institute for Water Research, Norway
 NORCE Norwegian Research Centre AS, Norway
 NPI Norwegian Polar Institute, Norway
 NTNU Norwegian University of Science and Technology, Norway
 NVE The Norwegian Water Resources and Energy Directorate, Norway
 SALT SALT Lofoten AS, Norway
 SU Stockholm University, Sweden
 TU Braunschweig Technische Universität Braunschweig, Germany
 UiB University of Bergen, Norway
 UiO. University of Oslo, Norway
 UiT UiT The Arctic University of Norway, Norway
 UMCS Maria Curie-Skłodowska University, Poland
 UniFi University of Florence, Italy
 UNIS University Centre in Svalbard, Norway
 UofS Institute of Space & Atmospheric Studies, Department of Physics & Engineering
 Physics, University of Saskatchewan, Canada
 UQAR University of Quebec at Rimouski, Canada
 US University of Silesia in Katowice, Centre for Polar Studies, Poland
 UU Uppsala University, Sweden

Executive Summary

Marta Moreno-Ibáñez¹, Jon Ove Methlie Hagen², Christiane Hübner³, Heikki Lihavainen³, Agata Zaborska⁴

1 University of Quebec in Montreal, Canada, 2 University of Oslo, Norway, 3 SIOS Knowledge Centre, Longyearbyen, Norway, 4 Institute of Oceanology of the Polish Academy of Sciences, Sopot, Poland

The State of Environmental Science in Svalbard (SESS) report 2020 aims to document the state of the Arctic environment in and around Svalbard, and highlight research conducted within SIOS. Given its remote but accessible location, Svalbard constitutes a privileged place to observe the Arctic environment in general, including, more specifically, the causes and consequences of climate change in the Arctic.

The Arctic is currently undergoing significant changes due to global warming. The IPCC Special Report on the Ocean and Cryosphere in a Changing Climate (2019)¹ was a wake-up call for climate change action. Over the last two decades, the Arctic has warmed more than twice as fast as the global average. The Arctic sea-ice extent has declined and will continue to decline in the future. For a stabilised global warming of 2°C, there is a 10-35% risk of a sea ice free September occurring at the end of the 21st century.

Svalbard, as the Arctic in general, has undergone substantial changes in near-surface temperature, precipitation and sea-ice extent in response to the warming over the last few decades, and these trends are projected to continue in response to future climate change. The future increases in temperature and precipitation in the Arctic and in Svalbard are expected to be significantly larger than the global mean increase in those variables. Thus, Svalbard is well-suited as an observational supersite for the Arctic ([SvalCLIM](#)).

Knowledge of the spatio-temporal distribution of snow in the Arctic is key to understanding the snow-atmosphere feedbacks involved in Arctic amplification. Long time-series of snow cover from a wide variety of observational platforms provide information at different spatial and time scales. For

instance, satellite monitoring over 1982-2015 has shown an earlier onset of snow-melting in Svalbard, and shortened duration of summer snow cover with the most pronounced decrease in valleys, by 1-2 days per year ([SvalSCESIA](#)). A comparison between satellite-derived snow cover data and the output from several hydrological snow models revealed significant differences in the geographical distribution and the timing of snow cover, which are likely explained by inaccurate inputs to the snow models ([SATMODSNOW](#)). Satellite observations are limited by their relatively low temporal resolution, and they can be affected by cloud cover. In contrast, terrestrial photography is characterised by high temporal resolution and is less affected by the weather; therefore, it can provide a continuous ground-truth for validating remotely sensed observations of snow cover in Svalbard ([PASSES](#)). Integrating these three methodologies allows for a multi-scale approach to snow cover observations and modelling ([SnowCover](#)).

Depending on their composition, aerosols can contribute to warming or cooling of the Arctic atmosphere. The reduction of cooling sulphate aerosol due to air quality legislation in Europe and North America since the 1980s has been proposed to be responsible to a significant part of Arctic warming. Knowledge about the long-term trends of aerosol concentration and composition is therefore essential to understand their role in Arctic warming. A significant increase in aerosol concentration in the Arctic troposphere occurs in winter-spring (Arctic Haze), and has mainly an anthropogenic origin. The Gruebadet and Zeppelin observatories, in Ny Ålesund, provide long-term data on sulphate and ammonium, two central components of Arctic Haze. Long-term trends of those compounds are analysed ([HAZECLIC](#)).

¹ IPCC (2019) Technical Summary. In: Pörtner H-O, Roberts D C, Masson-Delmotte V, Zhai P, Poloczanska E, Mintenbeck K, Tignor M, Alegría A, Nicolai M, Okem A, Petzold J, Rama B, Weyer N M (eds.) IPCC Special Report on the Ocean and Cryosphere in a Changing Climate. In press.

In general, an increase in water runoff has been observed from glacierised catchments due to increased melt of the glaciers. However, over the last decades, there has been a decrease in freshwater fluxes from some small glacierised catchments due to rapid shrinking of glacier area and volume. In contrast, water discharge has increased in rainfall-dominated watersheds due to increased precipitation. The boundaries of the hydrological year have shifted to earlier onset of snowmelt in the spring and later freeze-up in the autumn. The current long-term monitoring of evaporation and condensation, as well as of precipitation change with elevation is sparse and needs to be upgraded ([SvalHydro](#)).

One of the Arctic ecosystems that is directly and indirectly impacted by global warming is the coast. Climate change-induced stressors such as reduction of land and glacier ice, altered wind and wave energy, increased precipitation, thawing permafrost and changes of surface runoff all affect environmental conditions in the coastal waters. Global warming also contributes to more intense human activity in the Arctic (e.g., tourism, natural resources exploration). More comprehensive monitoring of physical, geochemical and biological parameters is necessary to detect, understand and mitigate changes in Svalbard's coasts ([SvalCoast](#)).

Climate change in the Arctic can also lead to an increase in the risks to human populations, such as geohazards. In permafrost landscapes, the thawing of ground ice often leads to ground instability and subsidence. Current knowledge about ground ice in Svalbard is focused on coastal lowlands, valley bottoms and periglacial landforms, while research on ground ice in slope deposits is currently limited. Temperature and pore water pressure sensors in boreholes in slopes could improve our understanding of slope sensitivity to climate change and enable preparedness for geohazards ([PermaSval](#)).

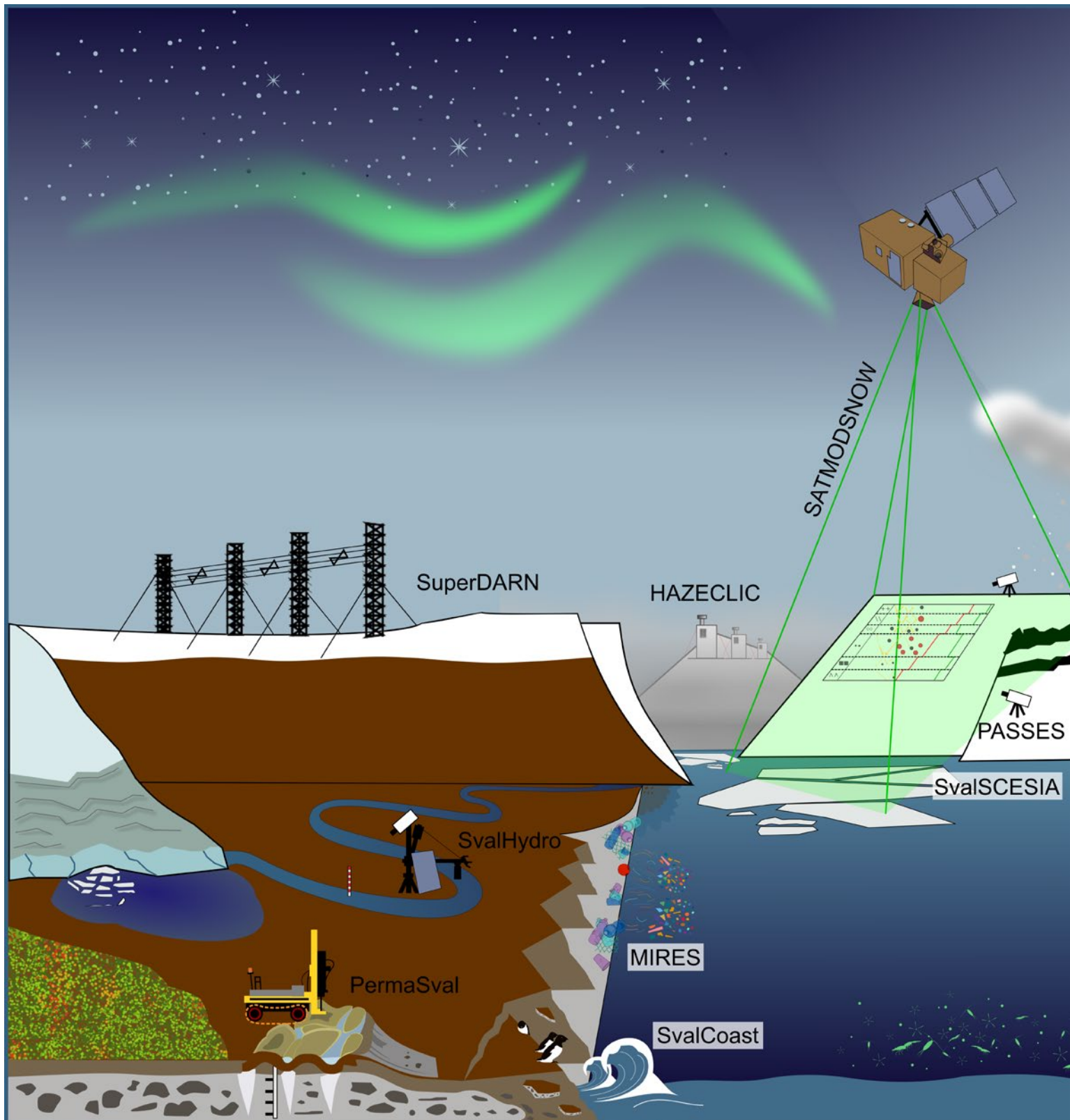
Climate change is not the only problem of anthropogenic origin affecting Svalbard. The

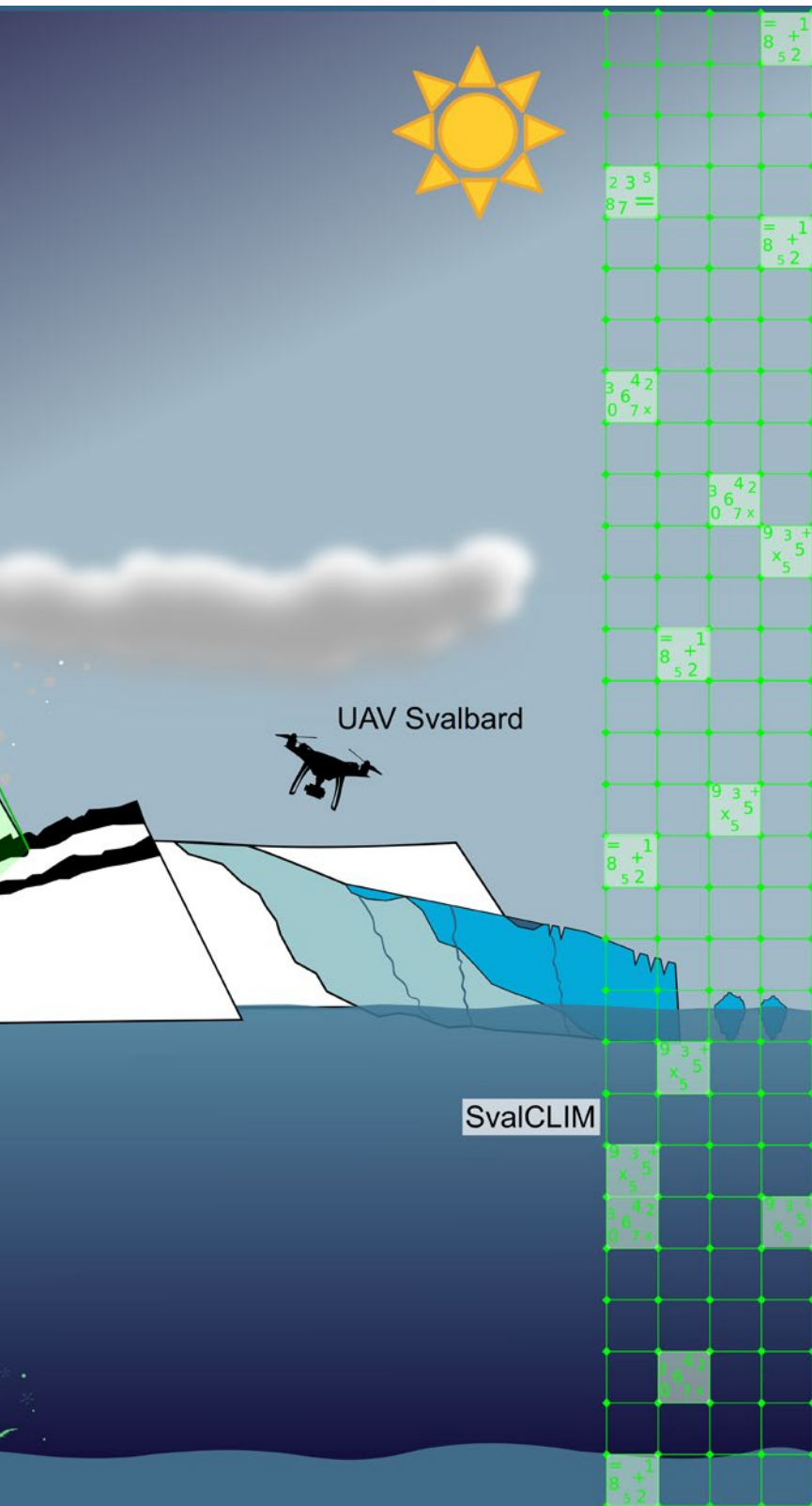
archipelago is also affected by plastic waste, which is an emerging global issue. Microplastics are plastic fragments (1 µm to 5 mm in size) that originate from both primary (e.g. cosmetics) and secondary (fragmentation of plastic products) sources. Microplastics debris has been found in sea ice, snow, water, sediment and biota samples from Svalbard. A holistic view of the microplastics status is crucial for evaluating and communicating the significance of prevention and reduction of plastic pollution in the Arctic ([MIREs](#)).

Developing an integrated Arctic Earth observing system is of utmost importance if we aim to better understand the numerous environmental challenges faced by the Arctic. Among the observational platforms available, unmanned aerial vehicles (UAVs) can provide valuable observations around the Svalbard region. To increase collaboration and to allow establishing long-term monitoring datasets, a system to log past, existing, and planned projects with UAVs in Svalbard should be developed ([UAV Svalbard](#)). Svalbard is also home to space physics infrastructure, including a wide range of optical and radio instruments. The Svalbard SuperDARN radar is part of a global network of high frequency radars that provide information on the structure and dynamics of the Earth's ionosphere. Among other uses, SuperDARN could support space weather monitoring by providing real-time observations. Unfortunately, SuperDARN was damaged by a severe ice storm in 2018, but it will be rebuilt in 2021 ([SuperDARN](#)).

Based on research conducted within the framework of SIOS, the authors of the SESS chapters have highlighted the gaps in our knowledge about the Earth system and suggested concrete actions that should be taken to address these gaps.

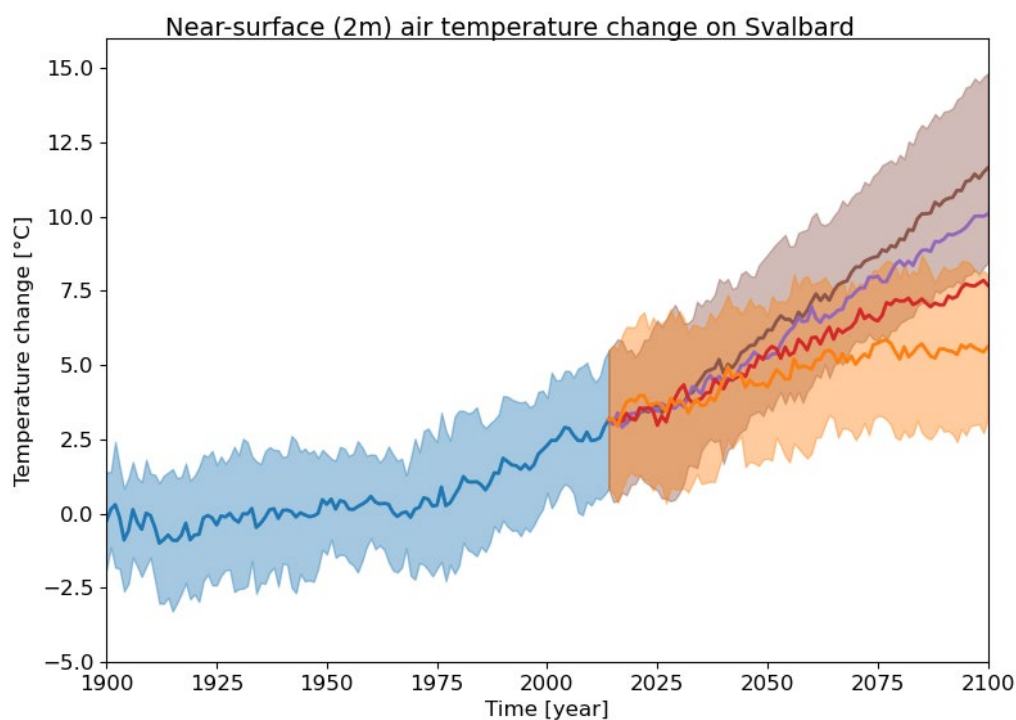
The editors would like to thank the authors for their valuable contributions to the SESS Report 2020. Together, these chapters show how SIOS projects contribute to the advancement in the knowledge of the Svalbard region's role in the Earth system.





Legend

- | | | | |
|---|--|---|---------------------------------|
|  | Aurora |  | Snow covered land |
|  | Glaciers |  | Sea ice and land fast sea ice |
|  | Partly ice-covered lake |  | Melt water |
|  | Permafrost degradation and ground instability Ice wedges |  | Arctic Tundra |
|  | Coastal erosion |  | Zoo- and Phytoplankton |
|  | Plastic litter |  | Microplastics |
|  | Seabirds | | |
|  | Satellites |  | Climate model |
|  | Snow model |  | Hydrological monitoring station |
|  | Aerosol measurements |  | SuperDARN |
|  | Unmanned Aerial Vehicle |  | Time-lapse camera |
|  | Ground temperature measurements |  | Permafrost drilling equipment |



Model results showing near-surface temperature change, averaged over the globe and the year. Lines show the mean, and shading shows the spread of the historical period and four future projections by an ensemble of 23 models. Results for historical runs (1900-2014) are presented in blue. Orange, red, purple, and brown colours present results based on best-case to worst-case scenarios for the future.

How representative is Svalbard for future Arctic climate evolution? An Earth system modelling perspective (SvalCLIM)

[Click here](#) for full chapter

HIGHLIGHTS

- Svalbard displays stronger warming than the Arctic as a whole for the period 1980–2014.
- Over the same period, sea ice melts faster around Svalbard than in the whole Arctic.
- In the worst-case future scenario, winter precipitation and winter temperatures rise less in Svalbard than in the whole Arctic.

AUTHORS

A Gjermundsen (MET Norway)	R Makkonen (FMI, INAR)
LS Graff (MET Norway)	DJL Olivié (MET Norway)
M Bentsen (NORCE)	Ø Seland (MET Norway)
LA Breivik (MET Norway)	P Zieger (SU)
JB Debernard (MET Norway)	M Schulz (MET Norway, UiO)

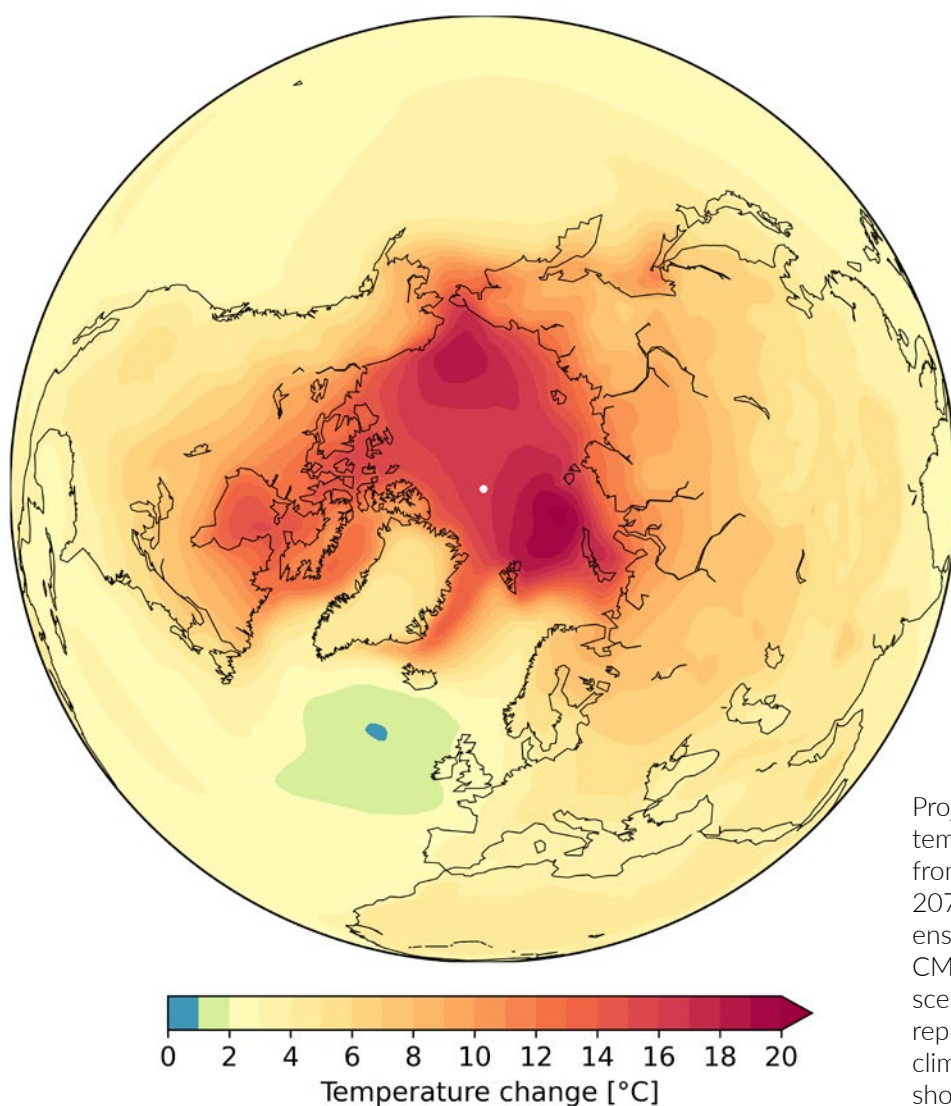
Situated in the Arctic and in a region with relatively pristine conditions, Svalbard is a very important and interdisciplinary observational supersite for the Arctic. In this SESS chapter, we investigate how representative Svalbard is for the Arctic region as a whole using data from numerical simulations with climate models.

In our study comparing model predictions of how temperature, precipitation, and sea-ice extent develop over time, we found that the changes in Svalbard resemble those in the Arctic as a whole, both during the warming period of the past few decades and during projected future climate change. However, some important differences were found (see highlights).

Predicting and characterising climate change in Svalbard will be increasingly important in the 21st century as changes in near-surface air temperature, precipitation and sea-ice extent seem to occur at an extremely high pace in Svalbard, even higher than in the rest of the Arctic. Closer collaboration between experimentalists, observationalists, and the modelling community could help us understand the mechanisms underlying differences between observed and modelled climate changes. SIOS is in a unique position to coordinate and facilitate such collaborative research.

RECOMMENDATIONS

- To cooperate with the Norwegian national Earth System Modelling infrastructure INES to build the modelling tools needed to integrate new SIOS data and explore where comparisons between data from models and observations can provide meaningful answers to questions related to Arctic amplification, abrupt changes, and climate feedbacks.
- To foster e-science tools (and education) so that young researchers working in Arctic climate science can efficiently analyse results from model ensembles, such as CMIP6.
- To initiate and strengthen collaboration with existing pan-Arctic research initiatives and institutions to assemble temporal trends of physical climate variables.
- To identify and document the most efficient international means of cooperation to foster joint understanding of forthcoming Arctic climate changes, possible abrupt climate transitions, and the drivers for such changes.



Projected change in near-surface air temperature in winter (Dec–Jan–Feb) from the baseline (1951–1980) to 2071–2100. The figure shows the ensemble-mean change from 23 CMIP6 models. The future forcing scenario used for these projections represents weak action on mitigating climate change and reducing emissions, shown in purple in figure to the left.



The Svalbard SuperDARN radar, situated at Breinosa. (Photo: Mikko Syrjäsuo / UNIS)

Space Physics in Svalbard: A study of the energy input into the polar ionosphere using SuperDARN

[Click here](#) for full chapter

HIGHLIGHTS

To understand, predict and model the upper atmospheric response to energy input from the Sun, we need continuous, long-term observations from many types of instruments. In Svalbard, these data are provided by a wide range of optical and radio instrumentation, including the Svalbard SuperDARN Radar.

AUTHORS

L Baddeley (UNIS, BCSS)	BCSS)
E Bland (UNIS)	LBN Clausen (UiO)
DA Lorentzen (UNIS, BCSS)	W Miloch (UiO)
K Herlingshaw (UNIS,	K McWilliams (UofS)
	AS Yukimatu (NIPR)

The chapter provides an overview of Norwegian space physics infrastructure in Svalbard (owned either individually or through collaborations) with a particular focus on the Svalbard SuperDARN (Super Dual Auroral Radar Network) radar. This new radar, located on Breinosa near the Kjell Henriksen Auroral Observatory (KHO), is the only Norwegian-owned radar in a global network of more than 30 radars. They are designed for studying flows and turbulence in the upper atmosphere (100-300 km altitude), driven by interactions between the magnetic fields of the Sun and the Earth. The Svalbard SuperDARN radar fills an important gap in the spatial coverage of SuperDARN and complements the other research infrastructure mentioned in the report. The radar operated continuously from October 2016 – October 2018,

before being damaged by a large ice storm. It will be rebuilt in 2021. The report highlights the important scientific achievements of the radar, with an emphasis on localised upper atmospheric processes and studies of a more global nature.

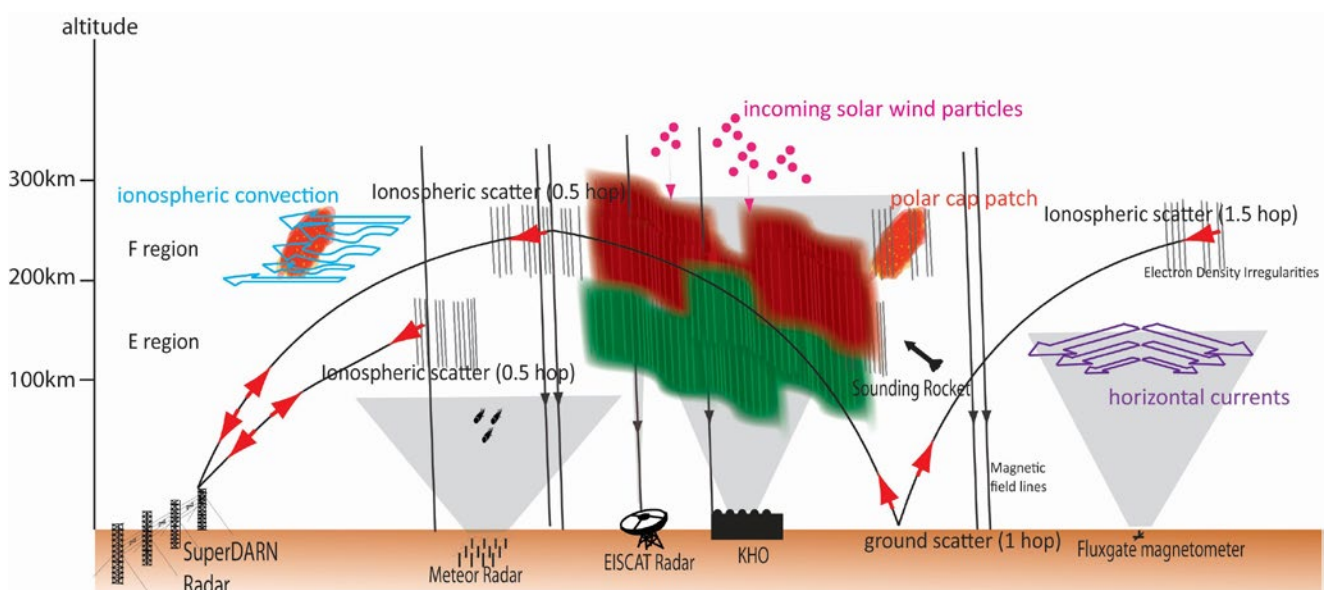


Construction of the Svalbard SuperDARN radar.
(Photo: Mikko Syrjäsoo / UNIS)

RECOMMENDATIONS

1. Rebuild the Svalbard SuperDARN radar, and secure ongoing funding for maintenance and operational costs.
2. Designate the area on Breinosa (which currently includes the SuperDARN and EISCAT radars and KHO) as a research infrastructure zone, and limit land rental costs. Excessive costs unnecessarily deplete research budgets and divert funding away from core research.
3. Construct a second SuperDARN radar on the same site as the current radar, with a field of view covering the region southwest of Svalbard. This would cover the flight path of sounding rockets from Ny-Ålesund and complement the fields of view provided by existing All-Sky Cameras and any newly developed SuperDARN radars in Iceland.
4. Develop a collaboration between Norway and North America to build the real-time space weather monitoring capability of SuperDARN, including tracking of space weather disturbances across the polar cap, and monitoring HF radio absorption.
5. Support an extension to the Longyearbyen meteor radar to allow 2-D measurements of the atmospheric velocities and temperatures in the mesosphere. This would provide a complementary dataset to the higher altitude SuperDARN dataset.

A schematic showing some of the of space physics phenomena and the instrumentation used to study them from Svalbard. (Illustration: Lisa Baddely / UNIS)





Drone operations in front of Nordenskiöldbreen. (Photo: Richard Hann)

Scientific Applications of Unmanned Vehicles in Svalbard (UAV Svalbard)

[Click here](#) for full chapter

HIGHLIGHTS

- We reviewed the scientific usage of unmanned vehicles in Svalbard.
- Off-the-shelf drones are most common, followed by fixed-wings, and marine vehicles.
- We recommend giving SIOS partners access to more platforms and services.
- Long-term data storage and open access to data should be facilitated.

AUTHORS

R Hann (NTNU, UNIS)

B Altstädter (TU Braunschweig)

P Betlem (UNIS, UiO)

K Deja (IOPAN)

K Dragańska-Deja (IOPAN)

M Ewertowski (AMU)

F Hartvich (CAS)

M Jonassen (UNIS)

A Lampert (TU Braunschweig)

M Laska (US)

I Sobota (NCU)

R Storvold (NORCE)

A Tomczyk (AMU)

K Wojtysiak (IG PAS)

P Zagórski (UMCS)

The polar regions are among the most sensitive areas of the Earth and changes in the Arctic have global consequences. Therefore, more and better Arctic research is needed, and unmanned vehicles are an important tool in this research. This report provides a review of research conducted with unmanned vehicles in Svalbard. That includes vehicles that travel in air, on water and underwater. The main focus is on unmanned aerial vehicles (UAVs). UAVs are well-suited for Arctic research for several reasons. The Arctic regions lack high vegetation and big settlements, making them ideal for aerial observations. UAVs can access

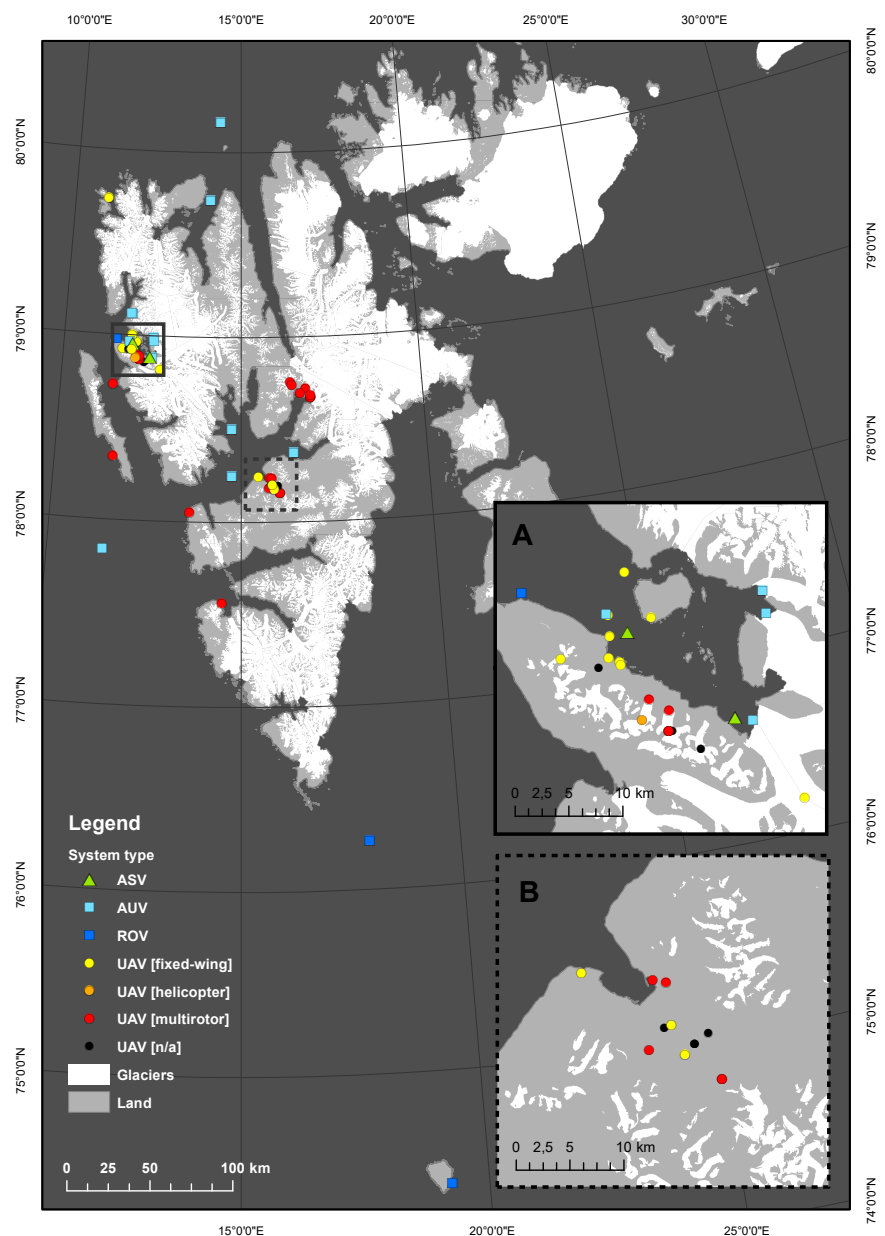
glaciers, mountains, and other difficult areas. They are cheaper and have a lower environmental impact than manned flights. Svalbard has an international research infrastructure and frequent flight connections, making it a hotspot for Arctic research. However, there are several challenges to the use of unmanned vehicles in the Arctic. These include magnetic interference, low temperatures, harsh weather conditions, and wildlife. Most optical sensors cannot be used during the dark season between October and February. This review shows that the researchers using unmanned vehicles in Svalbard can be divided into two groups: basic and advanced users. The majority of researchers today are basic users. They use off-the-shelf UAVs to enhance their fieldwork. The most common application is mapping. A minority of the researchers are advanced users. This group includes users of unmanned marine vehicles and fixed-wing UAVs.

RECOMMENDATIONS

We suggest both increasing the number of basic users, as well as encouraging mature basic users to become advanced users. To achieve this, we have four main recommendations:

1. Establishing an outreach and experience transfer program for SIOS partners to train them in the use of unmanned vehicles.
2. Giving SIOS partners access to more platforms and piloting services, as well as providing consultation on regulations.
3. Developing best-practice standards that include data collection methods, processing methods, specification of sensors and systems, access to raw data, and data formats.
4. Facilitating long-term data storage and open-access sharing of data to make the projects more relevant for long-term monitoring.

Overview of unmanned vehicle activities in Svalbard. Location of study sites: A: Kongsfjorden region; B: Adventdalen region; ASV - Autonomous Surface Vehicle, AUV - Autonomous Underwater Vehicle, ROV - Remotely Operated Vehicle, UAV - Unmanned Aerial Vehicle





Gruvebadet and Mt Zeppelin observatories. (Photo: Mirko Severi)

Arctic haze in a climate changing world: the 2010-2020 trend (HAZECLIC)

[Click here](#) for full chapter

HIGHLIGHTS

Arctic haze is relevant in controlling the Arctic atmosphere. Long-term studies reveal change in the extent and composition of the haze. Sulphate and sulphate:ammonium ratios were analysed at two altitudes in Ny-Ålesund. Sulphate levels have declined in the first decade of the 21st century.

AUTHORS

R Traversi (UniFi)	M Mazzola (ISP-CNR)
S Becagli (UniFi)	A Lupi (ISP-CNR)
M Severi (UniFi)	M Fiebig (NILU)
L Caiazza (UniFi, INFN)	O Hermansen (NILU)
	R Krejci (SU)

The phenomenon of Arctic haze was studied in Ny-Ålesund at two observatories close to each other but at different altitudes (Gruvebadet and Mt Zeppelin, 50 m and 700 m a.s.l.). The sites are influenced by a different mix of sources and transport processes: mainly long-range sources and free troposphere at Mt Zeppelin and short-range inputs at Gruvebadet. These two complementary sites offer a way to better understand advection of polluted air masses to Svalbard at continental and local-to-regional scale. The data series from Mt Zeppelin covers the last 27 years while the Gruvebadet data series begins in 2010. Here we present the first comparison of the available data on chemical tracers for this potentially harmful phenomenon (sulphate and ammonium), to be developed further by taking into account other tracers. Sulphate concentrations in the atmosphere have been decreasing in the Arctic since the 1990s (in line with falling SO₂ emissions). Our data show continued decreases at roughly the same rate also



Walking to Gruvebadet observatory during a day with Arctic haze. (Photo: Rita Traversi)

in the first decade of the 21st century. Moreover, we find that this decrease is particularly intense during Arctic haze months (winter and early spring), whereas in autumn the concentrations are constant or slightly rising. Decreases in sulphate may have opposing fallouts on climate, environment and human health in Svalbard, since the atmosphere is becoming poorer in sulphuric acid, favouring an additional warming of the atmosphere (lower

RECOMMENDATIONS

To confirm the trends described here about sulphate concentration and acidic/alkaline character of the atmosphere, continuous long-term measurements are needed at Gruvebadet and Zeppelin, particularly during winter/early spring (Arctic haze months).

Analysis of the chemical composition (sulphate, ammonium, nitrate, organic and black/elemental carbon) of the particulate matter collected will allow more accurate discrimination between natural and anthropogenic sources.

A thorough comparison between the data series from the two sites is needed to better constrain the impact of the haze and identify a “local” and “long-range” signature in Svalbard.

scattering effect on incoming solar radiation) and modifying the chemistry of the atmosphere (towards a more alkaline character, richer in ammonia).



Trained personnel checking aerosol cut-off devices on the roof of Gruvebadet observatory. (Photo: Rita Traversi)



Photo: Jón Aars

Microplastics in the realm of Svalbard: current knowledge and future perspectives (MIREs)

[Click here](#) for full chapter

HIGHLIGHTS

The findings of microplastics in sea ice, snow, water, sediment, and biota samples in Svalbard show that the archipelago is not isolated from pollution generated in other parts of the world and plastic pollution in the region must be monitored.

AUTHORS

N Singh (NPI)
M Granberg (IVL)
F Collard (NPI)
G Caruso (ISP-CNR)
Z Lu (CESE-TU)

T Kögel (IMR, UiB)
GW Gabrielsen (NPI)

Plastic pollution is an increasing problem worldwide including in Svalbard and the Arctic more widely. This includes microplastics (MPs) i.e. the fraction of plastic smaller than 5 mm. MPs are ingested by a wide range of organisms like zooplankton, crustaceans, fish, seabirds and mammals. Once ingested, MPs can potentially affect the organisms either by obstruction and abrasion, by releasing the associated chemicals and adsorbed contaminants (plasticisers, persistent organics pollutants), or by adverse effects of the particles themselves. Humans are exposed to MPs, amongst other pathways, by consuming contaminated food.

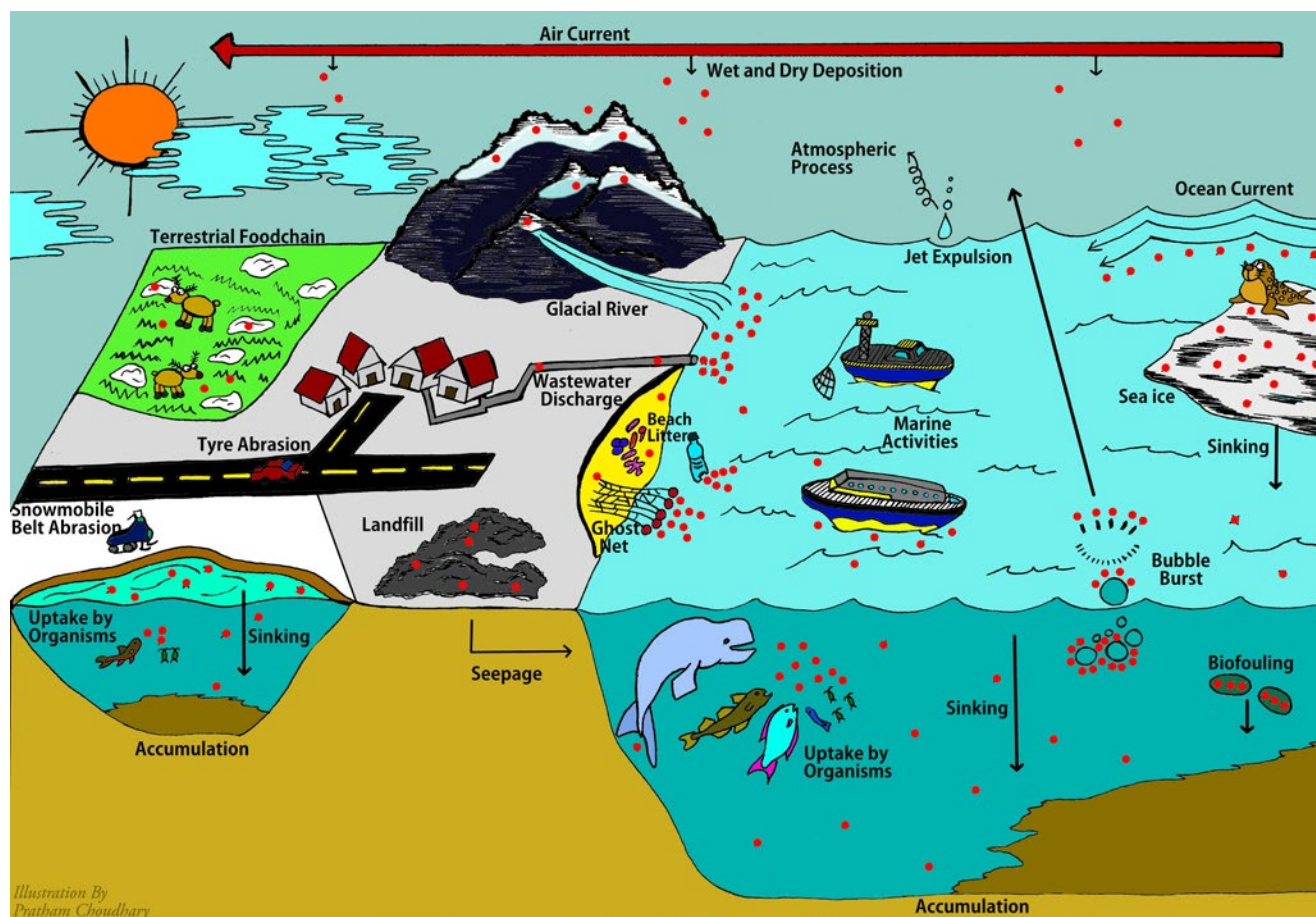
We find MPs in sea ice, snow, water, deep-sea sediment, beaches and organisms (amphipods, fish) at different locations in Svalbard. The best available evidence gathered by monitoring and research suggests that MPs pollution is likely to



Photo: Susanne Kühn

have negative effects in Svalbard, at least at long time scales. A good view of MPs status based on our current understanding and adopting a future perspective is crucial for evaluating and communicating the significance of preventing and reducing plastic pollution in the Arctic.

Potential sources and pathways of microplastics in Svalbard. (Illustration: Pratham Choudhary)



RECOMMENDATIONS

- **Harmonising methodologies:** A workshop is needed to facilitate agreements among international MPs experts on how to start monitoring MPs at Svalbard's four observatories (Hornsund, Barentsburg, Longyearbyen, Ny-Ålesund). The work currently being finalised by AMAP on MPs monitoring will be highly valuable.
- **Long-term monitoring:** A monitoring programme should be designed to consider societal needs such that science can provide advice regarding plastic use in Svalbard, wastewater treatment, effects of cruises and other tourism activities, and fishing.
- **Mapping:** MPs in the unexplored parts of Svalbard, which include terrestrial and marine biota, need to be mapped to establish a proper risk assessment for both the environment and human consumers.
- **Collaboration:** A Svalbard plastics task force should be formed and meet regularly to develop methods and monitoring recommendations, to ensure that there is a concerted effort to fill the identified knowledge gaps.
- **Experiments:** Experimental studies of Arctic key species and the possible trophic transfer of MPs under Arctic conditions should be set up.



Since 2005 a five-fold increase in the macroalgal cover has been observed in western Spitsbergen. In northern and eastern Svalbard, most rocky shores are still barren due to sea ice scouring. (Bohemanneset. Photo: Josef Wiktor, IOPAN)

Environmental status of Svalbard coastal waters: coastscapes and focal ecosystem components (SvalCoast)

[Click here](#) for full chapter

HIGHLIGHTS

- First coastscape mapping of Svalbard
- Recent warming and sea-ice loss has increased intertidal species richness and biomass in western Svalbard
- Ecological losers include cold-adapted species that rely on sea ice
- The next decade's greatest environmental changes are expected in northeastern Svalbard

AUTHORS

JE Søreide (UNIS)

V Pitusi (UNIS)

A Vader (UNIS)

B Damsgård (UNIS)

F Nilsen (UNIS)

R Skogseth (UNIS)

A Poste (NIVA)

AM Bailey (NPI)

KM Kovacs (NPI, UNIS)

C Lydersen (NPI)

S Gerland (NPI)

S Descamps (NPI)

H Strøm (NPI)

PE Renaud (APN/UNIS)

G Christensen (APN)

MP Arvnes (SALT)

P Graczyk (NORCE)

D Moiseev (MMBI)

RK Singh (UQAR)

S Bélanger (UQAR)

J Elster (CPE USB)

J Urbański (GU)

M Moskalik (IG PAS)

J Wiktor (IOPAN)

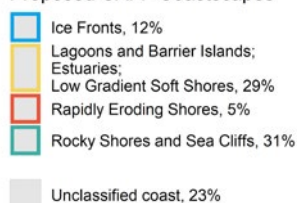
JM Węstawski (IOPAN)



Tidewater glacier fronts are important feeding areas for seabirds and marine mammals. The Ice Front coastscape is particularly vulnerable to climate change. (Photo: Kit M Kovacs and Christian Lydersen, NPI)

Coastal waters are among the most productive regions in the Arctic. These nearshore waters are critical breeding and foraging grounds for many invertebrates, fish, birds, and marine mammals and provide a host of ecosystem services, from private outdoor activities to large-scale tourism and fisheries. Arctic nature coast types (= coastscape) and biodiversity are under growing pressure as climate change and human activities increase in the region. More data on the rates of change in the physical, chemical and biological environments in these highly dynamic and heterogeneous coastscape are urgently needed. Svalbard is warming more rapidly than anywhere else in the Arctic, and the Arctic is warming at 2-3 times the rate of other areas globally. Svalbard experiences steep climate gradients due to being situated at the interface between warm Atlantic and cold Arctic waters. Warming is creating a huge potential for increased colonisation by boreal species, with potential negative impacts on “native” species assemblages and food webs. Changes in physical drivers and biodiversity patterns must be

Proposed CAFF Coastscape

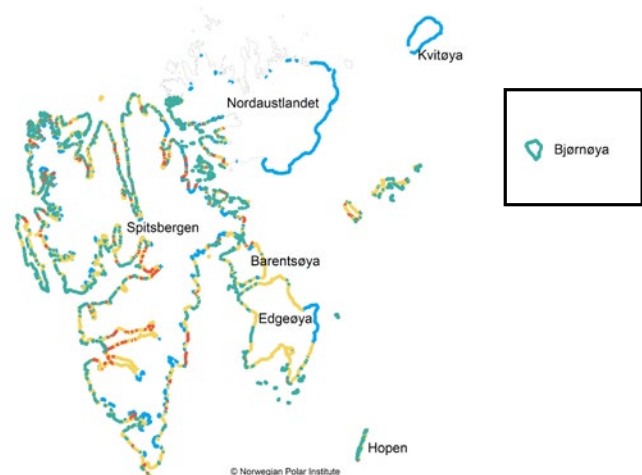


The first mapping of Svalbard’s coastscape as defined by CAFF’s Arctic Coastal Biodiversity Monitoring Plan, based on aerial photos of 8 739 km of coastline taken by the Norwegian Polar Institute (1987-1991). While the dataset requires a final quality check and updates due to subsequent glacial retreat, it is nonetheless the most complete dataset on Svalbard coastal geomorphology today, encompassing 77% of Svalbard’s coastline at 1 km resolution. (Map: Norwegian Polar Institute)

RECOMMENDATIONS

- Monitor environmental and ecosystem trends in both warm and cold regions in Svalbard
- Improve international coordination and cooperation to develop and maintain the infrastructure and activities required to achieve a more holistic coastal observatory in Svalbard
- Generate a list of Svalbard-specific standard coastscape (i.e. nature types)
- Agree on a list of essential focal ecosystem components (e.g. bio-indicators) to be monitored in these coastscape
- Adopt new methods (e.g. molecular methods) and technology (e.g. autonomous observatories, remote sensing) to secure cost-efficient long-term data series

documented to predict upcoming challenges and opportunities as the Arctic changes. This synopsis is the first joint effort across nations, institutes, and disciplines to address current gaps in knowledge and monitoring of Svalbard’s coast – a result of the international workshop Svalbard Sustainable Coasts in Longyearbyen, February 2020. Another important task of this synthesis work was to look into the applicability of the defined coastscape and biodiversity tools in the Arctic Coastal Monitoring plan, initiated by the Arctic Council’s Conservation of Arctic Flora and Fauna (CAFF, www.caff.is), for Svalbard.





An example of a braided river in a glacierised catchment. Adventelva inflow into Adventfjorden. (Photo taken by A Nowak in August 2019)

From land to fjords: The review of Svalbard hydrology from 1970 to 2019 (SvalHydro)

[Click here](#) for full chapter

HIGHLIGHTS

Hydrological response to ongoing environmental revolution in the Arctic is the most important research topic, yet long-term monitoring is sparse. Dramatic warming forces us to rethink water balance. Not all catchments are delivering increasing amounts of water to the polar ocean.

AUTHORS

A Nowak (UNIS)	E Łepkowska (US)
R Hodgkins (Loughborough Univ)	M Majerska (IG PAS)
A Nikulina (AARI)	K Romashova (AARI)
M Osuch (IG PAS)	I Vasilevich (AARI)
T Wawrzyniak (IG PAS)	I Sobota (NCU)
J Kavan (MU)	G Rachlewicz (AMU)

Svalbard was long seen as a canary in the coalmine for climate change. Now this early warning system has suffered irreparable damage. Svalbard has warmed 2-6 times faster than the rest of the world, and we can expect further increase in air temperature (by 4–7°C), precipitation (by 45–65%) and more frequent heavy rainfall and floods.

Contrary to predictions from regional climate models, freshwater fluxes from some glacierised catchments have steadily decreased for over a decade. Yet in rainfall dominated watersheds, water discharge has been increasing. To understand the implications, we must improve hydrological research in Svalbard.

Ground newly uncovered by receding glaciers develops permafrost when exposed to harsh Arctic winters. Simultaneously, permafrost thaw produces new water sources and flowpaths. Current hydrogeological models do not account for such complexity.



UNIS students performing maintenance of a hydrological monitoring station in Adventdalen during flood. (Photo: A Nowak)

The boundaries of the hydrological year have shifted due to earlier onset of snowmelt, and later freeze up.

Other weaknesses in hydrological research come from scarcity of long-term monitoring, outdated methods and data for evaporation and condensation and a lack of data on precipitation change with elevation.

As every new broken record reminds us, it is more urgent than ever to understand Svalbard's hydrology.

Fleinisen, a valley glacier in the process of recession. Dashed line represents the extent of the glacier in the 1920s. (Photo taken by A Nowak in August 2019)



RECOMMENDATIONS

We must close the water budget for the Norwegian High Arctic. We recommend upgrading existing sites (Hornsund, Grøndalen, Adventdalen, DeGeerdalen, Kaffiøyra, Ny-Ålesund) and establishing new supersites for hydrological research. The main action points are:

- **Establish long-term hydrological monitoring** yielding easily accessible data:
- **Autonomous meteorological and hydrological monitoring** on:
 - Svalbard's east coast e.g. Væringsdalen or Eistradalen
 - Northern Svalbard e.g. Svartdalen, Mosselhalvøya
- Permanent hydrological monitoring in Endalen and Gruvedalen (Longyearbyen's drinking water)
- **A network of meteorological stations across a range of elevations** (Longyeardalen, Hornsund, Ny-Ålesund, Svalbard's east and north coasts)
- **Set up time-lapse cameras** in catchments to capture onset of snowmelt
- **Measure water flux in the active layer**
- **Use multi-sensor remote sensing** to obtain water balance data from inaccessible places and improve spatial coverage in monitored areas.



Snow field campaign on Longyearbreen 2018. (Photo: Rolf-Ole Jenssen)

Satellite and modelling based snow season time series for Svalbard: Inter-comparisons and assessment of accuracy (SATMODSNOW)

[Click here](#) for full chapter

HIGHLIGHTS

We compared six time series of snow cover from satellite and models for Svalbard between 1957–2020. The significant differences between datasets could in part be explained by differences in spatial resolution. Future work should lead to better integration of models and improved reanalysis of historical snow data over Svalbard.

AUTHORS

E Malnes (NORCE)	W Van Pelt (UU)
H Vickers (NORCE)	V Pohjola (UU)
SR Karlsen (NORCE)	J Zhang (UU)
T Saloranta (NVE)	L Stendardi (Eurac)
MA Killie (MET Norway)	C Notarnicola (Eurac)

We document differences and similarities between three satellite-based and three model-based snow cover datasets, showing the geographical distribution and amount of snow across Svalbard for several periods from 1957 to 2020. The study shows that the datasets have many differences and that work needs to be done to accurately represent the snow cover in Svalbard. Low resolution datasets tend to predict longer winters than higher resolution datasets.

We studied differences between the datasets and suggest methods to improve each dataset. Satellite data have been available since 1978, but early sensors had low resolution, and can only provide correct information over larger areas. Current sensors, available since 2016, have high resolution. Older low-resolution data may be improved by utilising overlapping time-series of high- and

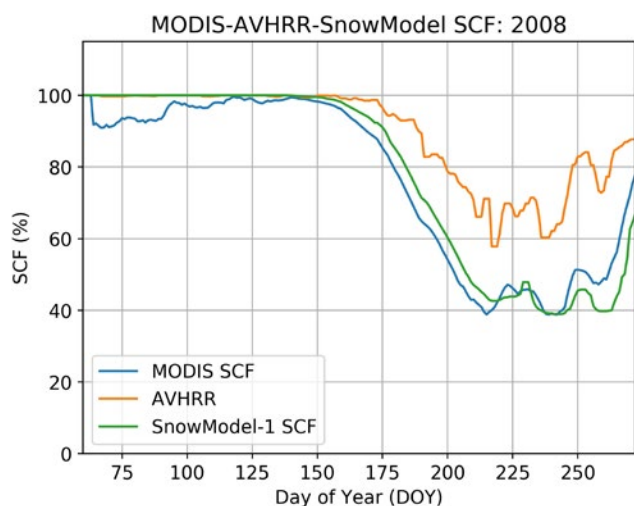
low-resolution data since local snow distribution patterns recur annually with a time-shift depending on average temperature and precipitation during the winter.

The snow models predict in general the amount of snow (Snow Water Equivalent or SWE), but the timing of snow disappearance predicted by the models can be compared with estimates from satellite snow cover observations. Since the snow

models depend on uncertain models of precipitation and temperature to estimate SWE there is potential to integrate satellite data to improve the models for snow in the future.

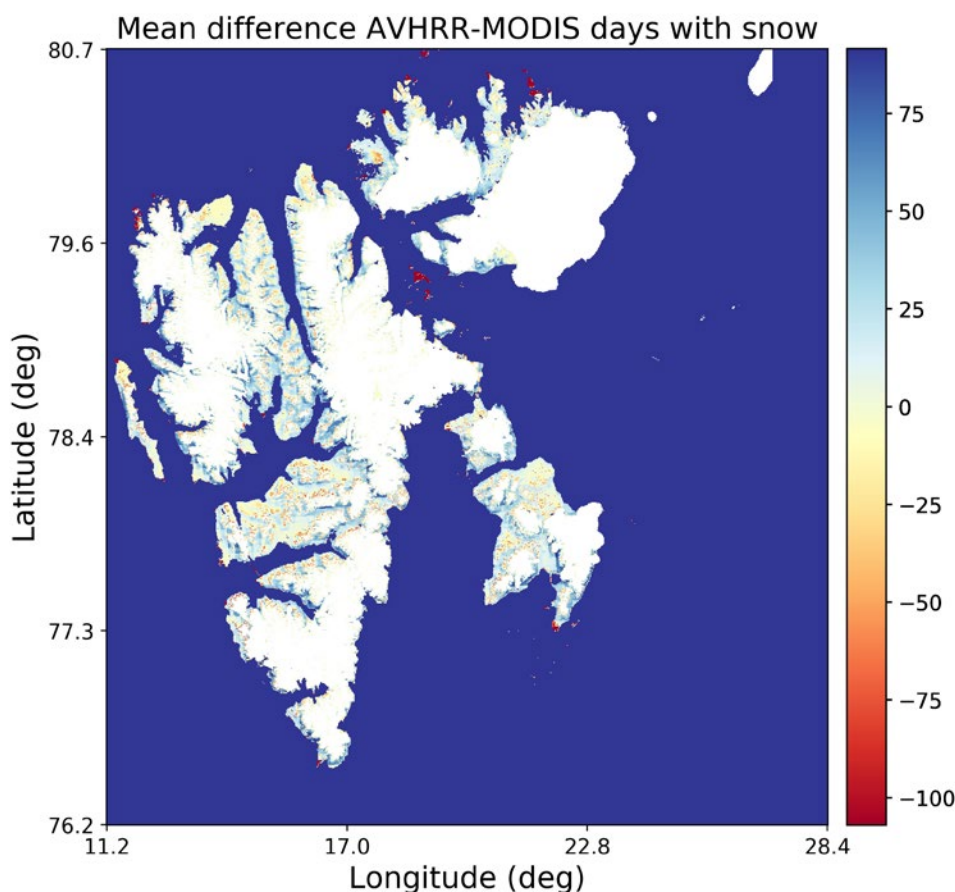
RECOMMENDATIONS

- Combine efforts from snow cover models and Earth Observation (EO) data to compile a long-term time series of snow cover data that covers the period 1978-2020 with as high spatial resolution as possible
- Future efforts should integrate multi-source EO data (in situ, airborne and satellite observations) with new techniques (e.g., AI and data assimilation) to further improve the characterisation of snow cover and SWE in Svalbard
- Hydrologists should utilise EO data from remote sensing to improve hydrological models in order to capture snow cover distribution and simultaneously improve SWE estimates
- Future datasets from EO should be compared with corresponding layers from modelling (e.g. liquid water content)
- Snow measurement infrastructure in Svalbard needs improvements for providing more calibration and validation data for both models and EO datasets



Comparison of the average snow cover fraction (SCF) for entire Svalbard for 2008 based on satellite data from MODIS (moderate resolution) and AVHRR (high resolution) and on predictions by the model from Uppsala University. Note that AVHRR overestimates snow cover during summer, whereas MODIS and SnowModel are in good agreement.

Average difference for the period 2000-2015 in number of snow days between satellite data from MODIS (moderate resolution) and AVHRR (high resolution). AVHRR frequently underestimates snow cover fraction in lowlands and overestimates it in highlands as compared to MODIS.



On-site measurements of the snowpack are performed annually to monitor and analyse its physical properties over time and space, their inter-annual variability and long-term trends. These measurements cover the main ecological and climatic gradients from the outer fjord areas to the inner part of the valley. (Photo: Ketil Isaksen, from March 2019 at Platåberget outside Longyearbyen, view towards Isfjorden)



Svalbard snow and sea-ice cover: comparing satellite data, on-site measurements, and modelling results (SvalSCESIA)

[Click here](#) for full chapter

HIGHLIGHTS

Satellite monitoring over 1982-2015 shows earlier onset of snow melt in Svalbard. The most pronounced shift is in valleys, where the ground is snow-free 1-2 days more every year during summer. Snow cover variability in lowlands correlates with the variability of sea ice in the adjacent seas, especially in June.

AUTHORS

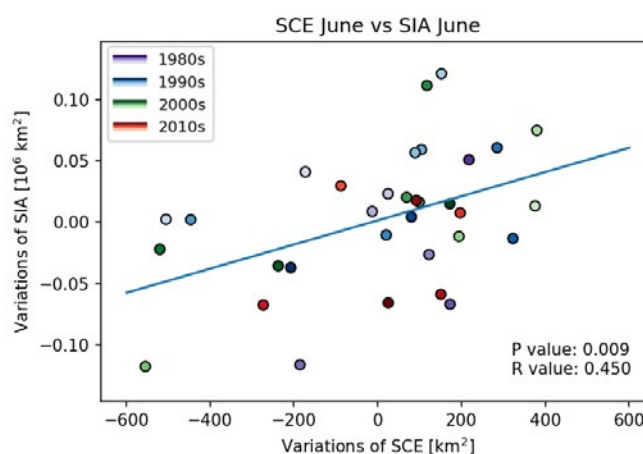
M A Killie (MET Norway)
S Aaboe (MET Norway)
K Isaksen (MET Norway)

W Van Pelt (UU)
Å Ø Pedersen (NPI)
B Luks (IG PAS)

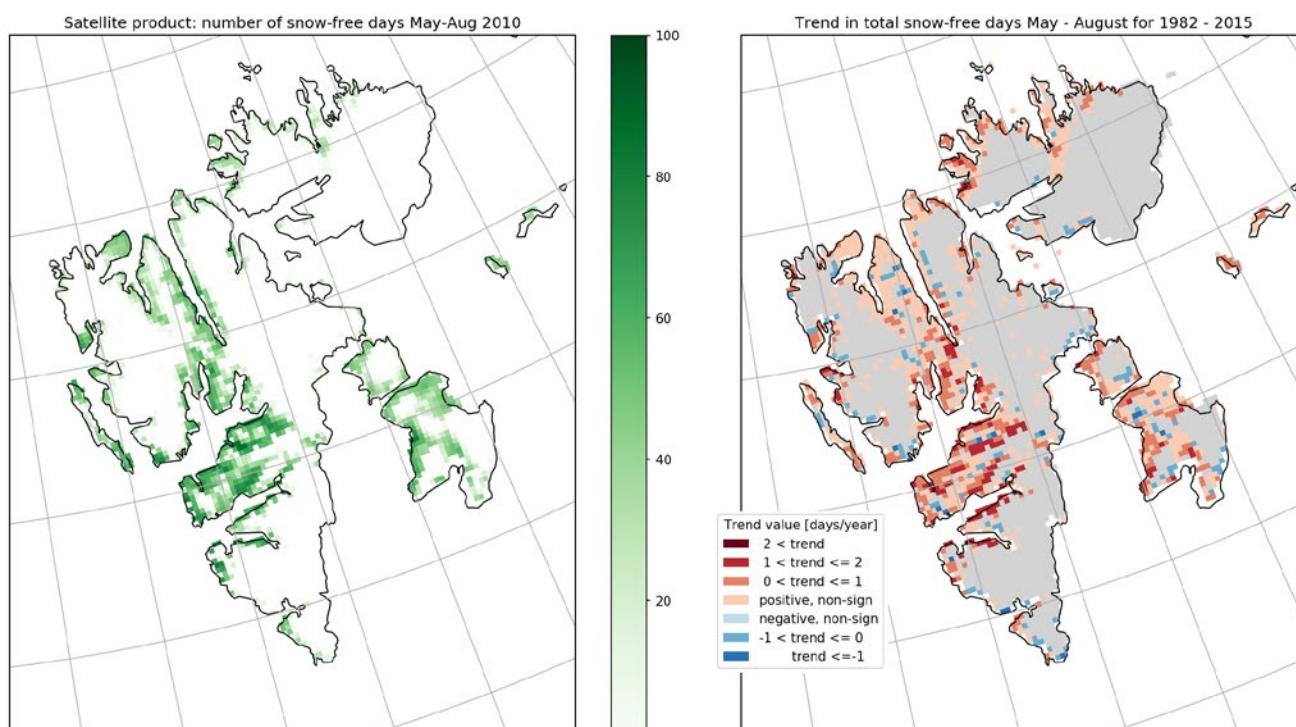
Fundamental knowledge gaps and scaling issues hamper efforts to determine how changes in snow cover and snow distribution affect ecosystems. The presence of snow cover has huge impact on Arctic ecosystems, human activities, atmospheric processes and Earth's surface energy balance. Mapping snow cover over large regions is challenging because of its variability over time and space. Also, the small number of weather stations that measure snow cover contributes to a poor observational base. Svalbard is located on the border between the ice-covered Arctic Ocean and the warmer North Atlantic, which means the sea is a controlling factor for Svalbard's climate. By using remote sensing monitoring it is possible to get a better overview of snow conditions on land. This information can be compared with on-site observations of snow, output from snow models, and evaluated in relation to the sea-ice

extent in the adjacent sea. A 34-year satellite data record for snow cover indicates that snow now starts melting more than a week earlier. The total number of snow-free days in summer is increasing fastest in regions dominated by lowland valleys and coastal plains. Most noticeable are the trends centred near the large valleys of Nordenskiöld Land. Negative trends dominate the extent of the sea ice as well. There is significant and positive correlation between sea-ice area and snow-cover extent at elevations up to 250 m in June, the month when snow melt begins. Snow melt, again, is probably strongly affected by ocean–air interactions and energy exchange when warm (or cold) winds from an open (or ice-covered) ocean come in over land.

The correlation between sea-ice area (SIA) and snow-cover extent (SCE) for June. Each dot represents a year during 1982–2015. The line illustrates the positive correlation between the two.



The left panel shows the number of snow-free days during May–August 2010. The right panel shows the trend in total snow-free days during May–August over the period 1982–2015. Reds indicate trends toward more snow-free days and blues toward fewer snow-free days.



RECOMMENDATIONS

The ecosystem impact of changing snowpack properties in a warming climate is an important arena for interdisciplinary research between ecology and geophysics. Besides co-location of research infrastructure, there is a need to develop a system that merges available observational datasets on snow properties with state-of-the-art, high-resolution (1-to-500-metre scale), physically based snow models. The goal of this data–model fusion system is to create accurate datasets that have good spatial distribution and evolve with time. Such datasets can be used to better understand relationships between ecosystem processes.



Time-lapse camera at the summit of Fugleberget in Hornsund. (Photo: Daniel Kępski)

Terrestrial photography applications on snow cover in Svalbard (PASSES)

[Click here](#) for full chapter

HIGHLIGHTS

Time-lapse cameras are important sources of data, offering an efficient and economically advantageous way to observe changes in the Svalbard environment. For snow cover monitoring using cameras, it is important to identify potential image providers, archived imagery, and processed datasets.

AUTHORS

R Salzano (IIA-CNR)	B Luks (IG PAS)
K Aalstad (UiO)	L Nilsen (UiT)
E Boldrini (IIA-CNR)	R Salvatori (ISP-CNR)
JC Gallet (NPI)	S Westermann (UiO)
D Kępski (IG PAS)	

Ground-based observations are critical requirements for many disciplines that are trying to monitor climate change in a remote environment such as the Svalbard archipelago. This overview of cameras operating in Svalbard has been compiled by searching for specific applications that monitor the snow cover and by collecting information about images that can be accessed on the internet, including those not solely dedicated to cryospheric research. The survey identified 43 cameras operating in the region that are managed by research institutions and private companies. These cameras include facilities operated by different nationalities. The datasets vary, but the feasibility of using them to determine fractional snow cover is generally limited. Identifying the key metadata necessary to survey the available devices revealed problems and knowledge gaps that prevent using the full potential of terrestrial photography networks in Svalbard.



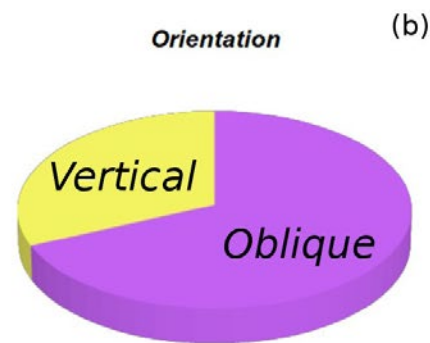
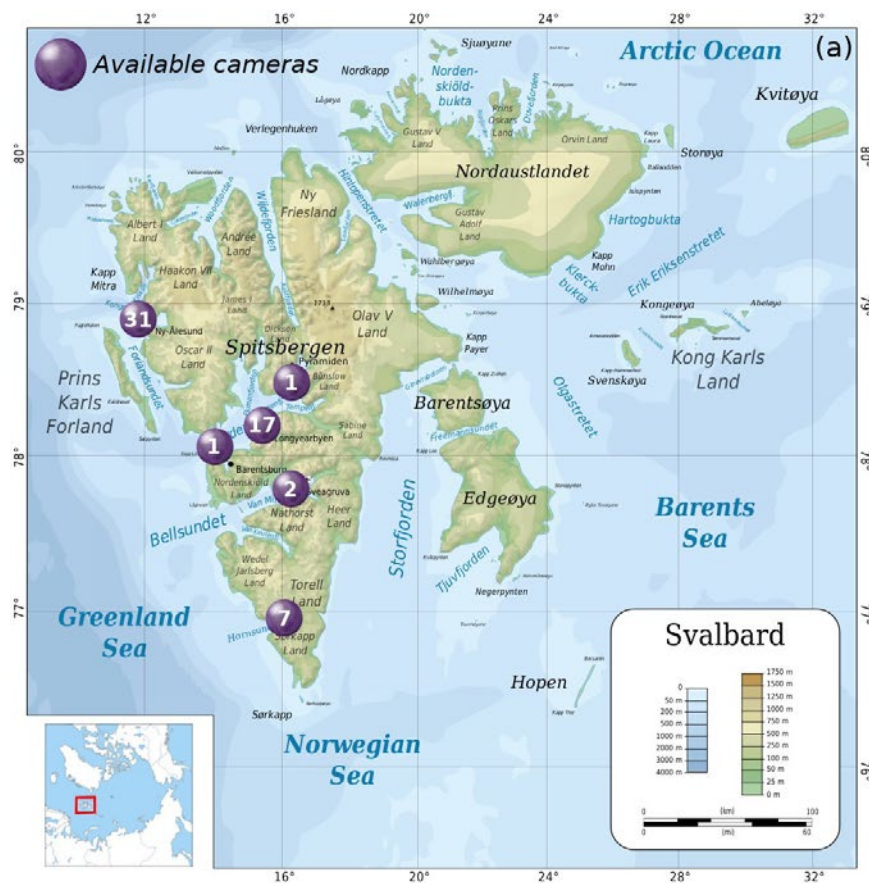
Time-lapse cameras at the Climate Change Tower in Ny-Ålesund. (Photo: Roberto Salzano)

First survey of time-lapse cameras available in Svalbard (a). Fraction of cameras with vertical versus oblique setups (b) and fraction that show snow cover (c). (Figure: Roberto Salzano)

RECOMMENDATIONS

The usefulness of time-lapse camera networks for snow cover monitoring and related studies can be enhanced through:

1. Promoting actions and projects based on using time-lapse cameras, especially in the more remote areas of Svalbard. Most terrestrial photography setups focus on Spitsbergen's shores, close to settlements. There are no cameras that cover terrain at higher elevation. Monitoring such areas is crucial for calibration and validation of satellite snow products.
2. Stimulating the creation of a Svalbard camera system network. Although all cameras provide valuable scientific data, it is currently difficult to use all the data collectively for one scientific purpose. There is a need to establish a common approach for processing images obtained by devices aimed at snow cover applications.
3. Creating a space on the SIOS website that gathers information about actively maintained camera systems in Svalbard.
4. Promoting the estimation of the fractional snow-covered area from images obtained by time-lapse cameras not specifically devoted to snow studies. This will facilitate the involvement of local communities in participatory forms of science.
5. Stimulating the use of time-lapse cameras by different disciplines where high resolution information can be retrieved for various purposes.



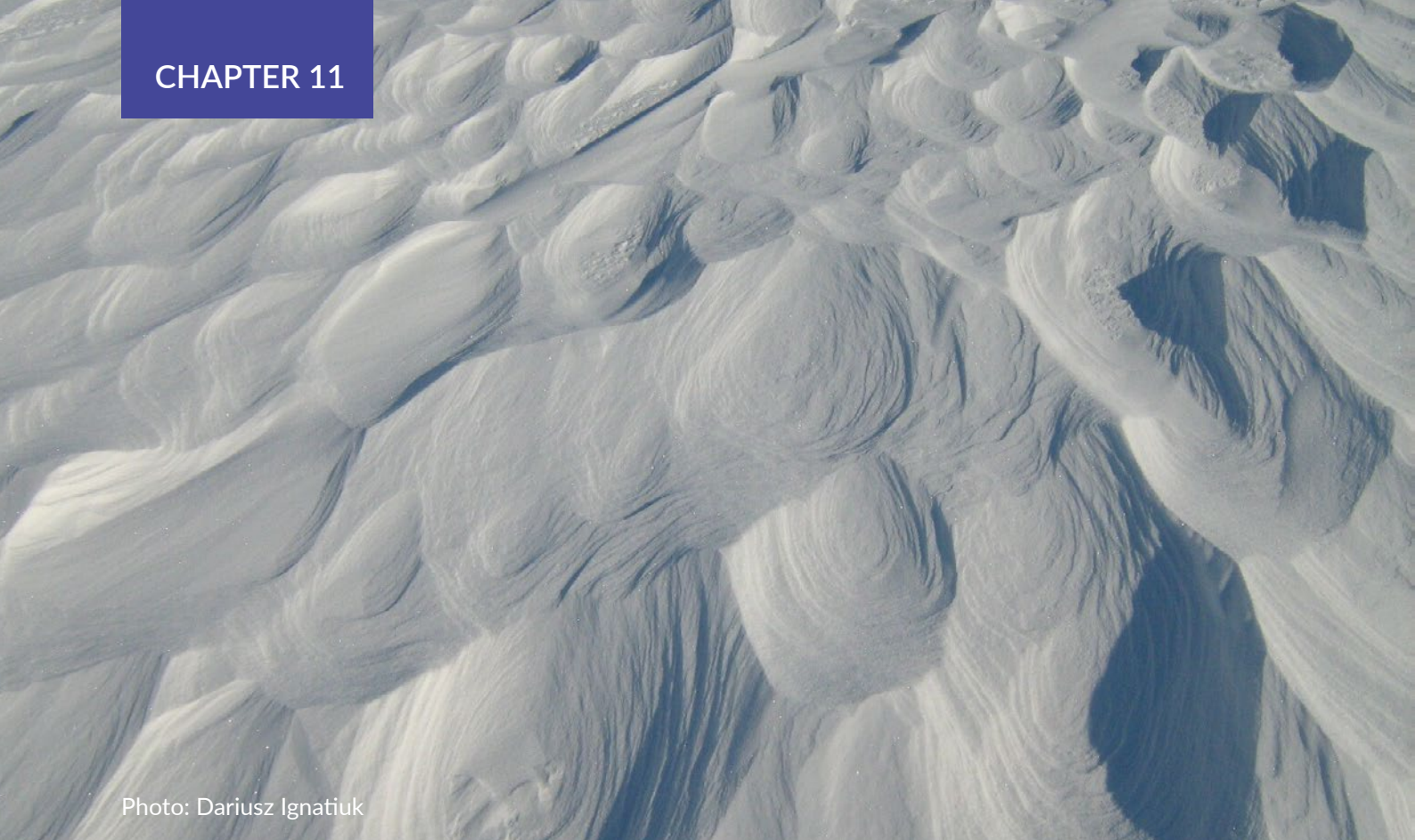


Photo: Dariusz Ignatiuk

A multi-scale approach on snow cover observations and models (SnowCover)

[Click here](#) for full chapter

HIGHLIGHTS

Long time-series on various snow parameters are crucial to many disciplines, including climate research.

Arctic snow cover can be monitored precisely but locally (*in situ* measurements), or broadly but at low resolution (satellite imagery).

Combined, these methods complement and enhance each other.

AUTHORS

R Salzano (IIA-CNR)

B Luks (IG PAS)

MA Killie (MET

E Malnes (NORCE)

Norway)

Data on snow properties such as cover fraction, depth, water equivalents, and melt date are important *per se*, but also as input in various models, and to verify model results. Earth observation (EO) gathers information on these parameters. Different EO methods for snow have different strengths. Manual measurements and locally deployed sensors give precise data, but only at individual sites. Satellite-based methods give huge amounts of data covering vast areas, but at lower resolution, and only when the satellite passes over relevant sites.

Three SIOS projects attempt to bridge the spatial and temporal gaps between remote sensing data and point measurements of snow cover.

PASSES gathers information about time-lapse cameras already deployed around Svalbard for research or other purposes. Most of them show snow-cover extent on an intermediate scale

(10 m² to 10 km²), with good temporal resolution. Some have been in place for 20 years, providing a valuable historic record.

SATMODSNOW finds that discrepancies between satellite data and model results arise from weaknesses in how the models handle precipitation and temperature. Since snow cover disappears in similar patterns every year, with a time shift depending on precipitation and temperature, close examination of satellite observations offers a way to refine hydrological snow models.

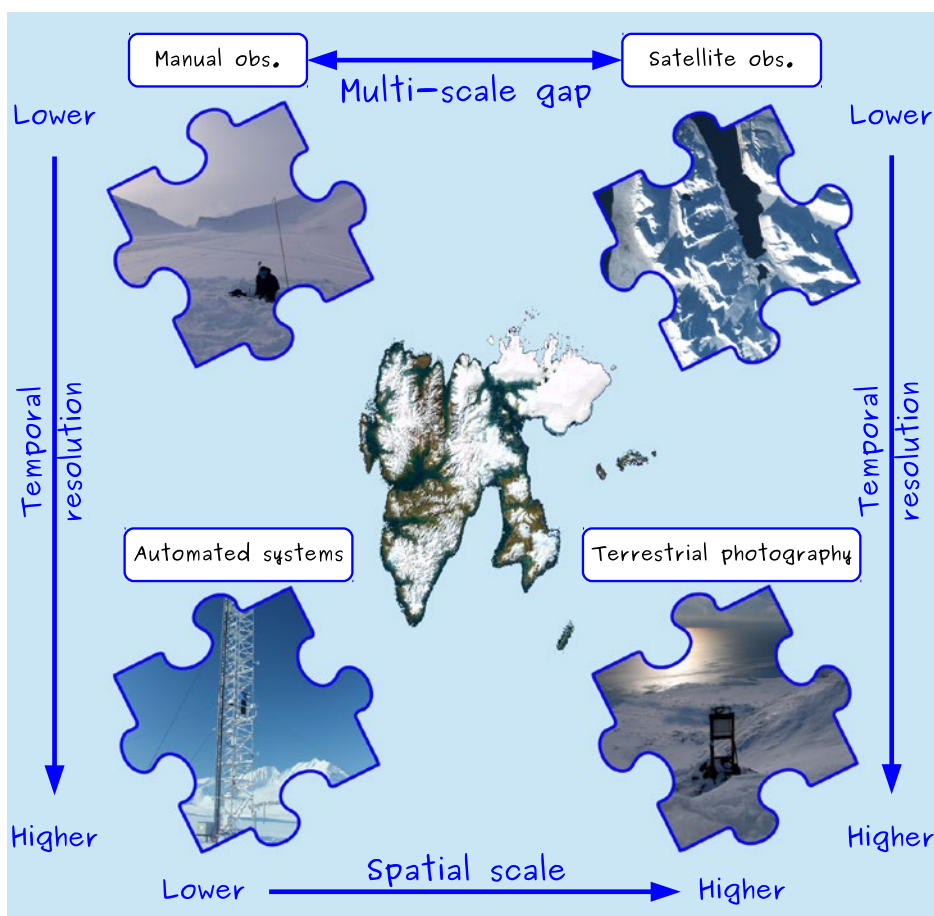
SvalSCESIA compares satellite data on both sea-ice area and snow cover against ground-based monitoring data and snow model output. They find major shifts in the duration of summer snow-free periods, especially in valleys and lowlands. Snow cover also correlates with

RECOMMENDATIONS

- Compare and inter-calibrate snow products covering spatial scales from 4 km to <1 m to better understand melt patterns.
- Establish a SIOS super-site containing snow-related remote sensing data and ground measurements of snow, for calibration/validation activities.
- Create and maintain an inventory of existing EO monitoring systems for snow cover in Svalbard.
- Investigate ways to incorporate EO data into snow-related models.

the ice cover in adjacent seas, indicating a strong effect of energy exchange between land and sea.

Integration and intercomparison of EO data obtained with different methods and on different scales will likely improve snow models.



The representation of a multi-scale strategy aimed at solving the gap existing between in situ measurements and satellite observations: the snow cover observed from different perspectives. The gaps between different spatial and temporal scales need to be bridged using sensors in the intermediate scale range (e.g., airborne sensors) to understand and remove uncertainties in long-term snow time series based on coarse-scaled satellite data and modelling.



Ice-rich permafrost at 150 cm depth from the Endalen borehole site. The darkest parts are ice lenses, while the rest are cobbles and sediment. (Photo: Ullrich Neumann)

Ground ice content, drilling methods and equipment and permafrost dynamics in Svalbard 2016-2019 (PermaSval)

[Click here](#) for full chapter

HIGHLIGHTS

In 2016-2019 the top permafrost cooled and permafrost at 10-20 m continued warming slightly at most Svalbard observation sites. Active layer thicknesses decreased but doubled at a blockfield site. Permafrost ice content is largest in valley bottom sediments up to 160%, but typically below 15% in bedrock.

AUTHORS

HH Christiansen (UNIS)	M Guglielmin (Insubria Univ)
GL Gilbert (UNIS, NGI)	K Isaksen (MET Norway)
U Neumann (Kolibri Geo Services)	M Osuch (IG PAS)
N Demidov (AARI)	J Boike (AWI, HU Berlin)

The observed mean annual permafrost temperature data for the period 2016-2019 at 10-20 m depths show a range from no warming in the Adventdalen, Ny-Ålesund and Barentsburg areas, up to 0.15°C/yr warming in inner Adventdalen at Janssonhaugen. This shows that there is still a response to the general warming that Svalbard has seen over the last decades. During the observation period, the mean annual air temperature declined by 0.6°C, with a particular cooling in the autumns. There was a clear reduction in the amount of precipitation of 100 mm. This caused the top permafrost temperature to decrease at all observation sites ranging from 0.2°C/yr at Kapp Linné to 0.6°C/yr in Barentsburg.

The active layer has mostly decreased slightly in thickness over the 2016-2019 period from 1 cm/yr in Ny-Ålesund to 6.5 cm/yr in Adventdalen, while

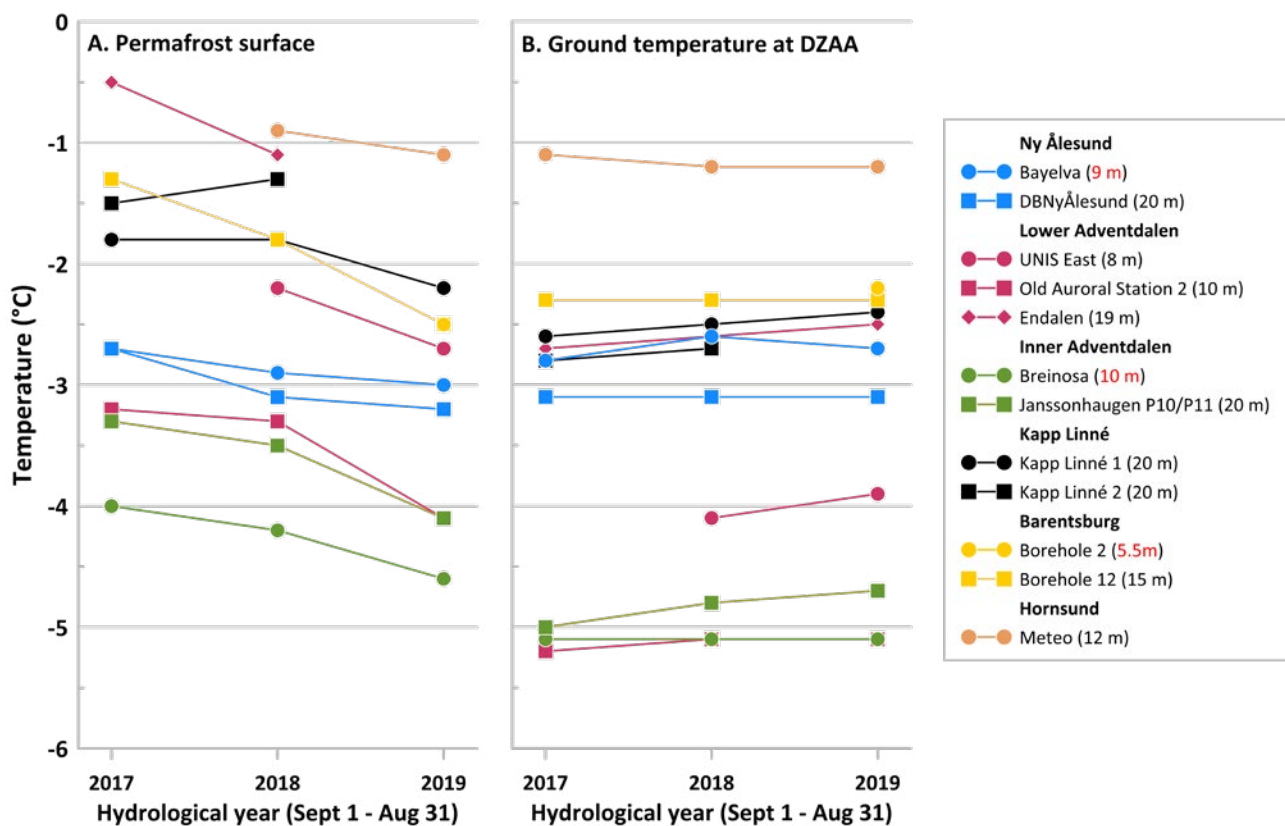
two sites had small increases, 1 cm/yr at Kapp Linne and 3.5 cm/yr at Janssonhaugen. In the blockfield at Breinosa the active layer doubled to 98 cm, while in raised marine sediments in Barentsburg the active layer thinned by 18.5 cm/yr from summer 2017 to summer 2019.

The ground ice content in the Svalbard permafrost observation boreholes is largest in the permafrost in valley bottom sediments, up to 160% (relative to dry weight), with much less ice in the bedrock sites, typically below 15%. In Adventdalen the permafrost has a much higher content of ground ice, reaching 150% in the top 1-3 m, where terrestrial sediments such as loess and solifluction sediment dominate, and clearly lower ice content ~25-30% in the fluvial and marine sediments below.

RECOMMENDATIONS

- Always collect ground ice and stratigraphy data from long-term permafrost observation sites
- Consider expanding the permafrost observation network
- Perform ground ice studies on slopes
- Get more permafrost Essential Climate Variables and SIOS Core Data operational and online

The overview of the drilling equipment demonstrates clearly that Svalbard is now well-equipped for drilling boreholes with a range of equipment, allowing creation of both deep and shallow boreholes. The review of the drilling methods used for the existing observation boreholes shows that most of them, even though made for permafrost observation, did not collect cores, and some do not even have any stratigraphical record.



Mean annual ground temperature development as recorded at (A) the permafrost surface and (B) the depth of zero annual amplitude (DZAA) or deepest sensor, for the hydrological years 2016-2017 to 2018-2019. DZAA (black text) or location of the deepest sensor (red text) is given in brackets beside each borehole in the legend.

How representative is Svalbard for future Arctic climate evolution? An Earth system modelling perspective (SvalCLIM)

Ada Gjermundsen¹, Lise Seland Graff¹, Mats Bentsen², Lars Anders Breivik¹, Jens Bolding Debernard¹, Risto Makkonen^{3,4}, Dirk J.L. Olivié¹, Øyvind Seland¹, Paul Zieger⁵, and Michael Schulz^{1,6}

1 Norwegian Meteorological Institute, Henrik Mohns plass 1, 0313 Oslo, Norway

2 NORCE Norwegian Research Centre and Bjerknes Centre for Climate Research, Nygårdsgaten 112, 5008 Bergen, Norway

3 Climate System Research, Finnish Meteorological Institute, P.O. BOX 503 FI-00101 Helsinki, Finland

4 INAR – Institute for Atmospheric and Earth System Research P.O. Box 64 00014 University of Helsinki, Finland

5 Department of Environmental Science, Stockholm University 106 91 Stockholm, Sweden

6 University of Oslo, Department of Geosciences, P.O. Box 1047 Blindern, 0316 Oslo, Norway

Corresponding author: Ada Gjermundsen, adag@met.no

ORCID number 0000-0002-2053-4689

Keywords: Earth system modelling, Arctic amplification, historical trends, future projections

DOI: <https://doi.org/10.5281/zenodo.4034104>

1. Introduction

It is well known that the world has become warmer in response to emissions of anthropogenic greenhouse gases (GHGs). This warming is however not evenly distributed across the globe, but is amplified in specific regions, such as in the Arctic. This, can for instance, be seen in temperature records from the Svalbard Archipelago, which reveal the greatest increase in temperature in Europe over the last three decades (Nordli et al. 2020).

The amplification of the Arctic temperature signal compared to the global mean is known as Arctic amplification (AA). It is most pronounced during winter and has large ramifications for the cryosphere, the hydrological and biogeochemical cycles and for all life in the Arctic (Meier et al. 2014; Bintanja and Selten 2014; Kim et al. 2019). AA is not merely a result of climate variability (Winton 2011; Notz and Marotzke 2012; Liang et al. 2020), but can be attributed to a number of mechanisms, including changes in surface albedo (associated with melting snow and sea ice), clouds, the vertical distribution of temperature, and hence in the lapse rate, water-vapour content, surface fluxes, and atmospheric and oceanic energy transports (Screen and Simmonds 2010; Doyle et al. 2011; Serreze and Barry 2011; Pithan and Mauritsen 2014; Simpkins 2017; Screen and Blackport 2019). It has also been shown that the surface temperature in the Arctic and in Svalbard can be affected by remote anthropogenic emissions such as of European sulfur (Navarro et al. 2016) and North-Eurasian black carbon (Sand et al. 2013). However, a quantitative understanding of the individual mechanisms contributing to AA is not well known. Specifically in Svalbard, the warming is in part linked to changes in the atmospheric circulation due to extensive sea-ice melt in the fjords and the surrounding ocean (Isaksen et al. 2016; Dahlke et al. 2020).

Being situated in the Arctic and in a region with relatively pristine conditions, Svalbard is a very important and interdisciplinary observational supersite for the Arctic. However, little attention has been paid to how representative observations

from Svalbard are for the entire Arctic region, and studies that compare observations from different sites located in the Arctic suggest that persistent differences beyond year-to-year variability can occur (Freud et al. 2017; Ding et al. 2018; Schmeisser et al. 2018). Here, we investigate how representative Svalbard is for the Arctic region as a whole, using data from numerical simulations with climate models. We assess recent and future changes and trends in the climate in Svalbard, comparing them to corresponding results from the entire Arctic region and to global results.

Climate models are excellent tools for understanding, in a consistent manner, both the global and regional climate. They are mathematical representations of the climate system based on physical, biological, and chemical principles. The models solve the governing equations of the climate system numerically in order to, for instance, simulate future climate scenarios on a 3D-grid (height, latitude, longitude) and consist of several components (e.g. atmosphere, ocean, land, sea ice, vegetation), which interact by transfer of energy, momentum, humidity, and matter. When such a model also includes interactive atmospheric chemistry and biogeochemistry (e.g. the carbon cycle), it is called an *Earth System Model* (ESM).

The spatial and temporal scales of the model components determine which processes are resolved. Processes occurring on even smaller scales than that resolved by the models (so-called sub-grid processes), biological processes, and chemical interactions need to be represented either by mathematical models that capture the essence of the behaviour of the phenomenon or by empirical functions deduced from instance measurements. Examples of such processes are boundary-layer convection, aerosol-cloud interactions, turbulence, oceanic internal- and gravity waves, and molecular processes. Because parameterisations typically only capture first-order effects and are often not valid under all possible conditions, they represent a large source of uncertainties in the models.

ESMs are not constrained by observations in the same way as, for instance, weather prediction models and reanalysis data. ESMs start from an initial state, which can be based on observations or data from a previous ESM run; then they run freely while being forced by solar insolation, GHG concentrations, natural aerosols and chemical species (highly model dependent), emissions from volcanoes, anthropogenic aerosol and GHG emissions, and changes in land use. Such forcing information is given at the temporal and spatial resolution that best represents current knowledge.

In this study, we use data from a large set of state-of-the-art ESMs participating in phase 6 of the Coupled Model Intercomparison Project (CMIP6; see info box for a more detailed description). We

consider data from a vast number of different experiments, including a simulation of the historical period 1850–2014 (Section 2) and projections of future climate change (Section 3). To investigate how realistic the historical simulations are, we compare the model data to several reanalysis products, observationally based global data sets, and to local observations from Svalbard. Reanalysis combine advanced forecast modelling and observations (through data assimilation) to produce a coherent estimate of the recent history of the Earth system and that differs fundamentally from earth system modelling as the former are constrained by the observations, while the latter run freely. See the Data availability section for further details.

INFO BOX: COUPLED MODEL INTERCOMPARISON PROJECT PHASE 6 (CMIP6)

CMIP is a project of the World Climate Research Programme (WCRP)'s Working Group of Coupled Modelling (WGCM), which coordinates climate model experiments, including future scenarios that are considered in the assessment reports by the Intergovernmental Panel of Climate Change (IPCC), involving 33 international modelling teams and more than 70 ESMs; defines common protocols for experiments, forcings, and output to advance scientific understanding of the Earth System; develops experiment sets in phases and is currently in the 6th phase.

The experimental design focuses on three broad scientific questions (Eyring et al. 2016): (1) How does the Earth System respond to forcing? (2) What are the origins and consequences of systematic model biases? (3) How can we assess future climate changes given climate variability, predictability and uncertainties in scenarios?

The CMIP6 experiments consist of a set used to assess the equilibrium state of the ESMs and their sensitivity to idealized changes in CO₂ (the so-called DECK experiments) and historical experiments in which the models are run with observed forcings to recreate the recent historical period (for CMIP6, it is 1850–2014) and 23 different more specialized sets known as model intercomparison projects "MIPs", which are tailored to investigate more specific questions such as, for instance, how the Earth system responds to polar amplification (Polar Amplification MIP; Smith et al. 2019).

Experiments used in this report: Simulations of the pre-industrial (taken as year 1850) climate, the historical experiment described above, and simulations of future scenarios (from ScenarioMIP) for the years 2015–2100.

For more information, see Eyring et al. 2016, the CMIP6 webpages ^{1,2}, and Eyring et al. 2018.

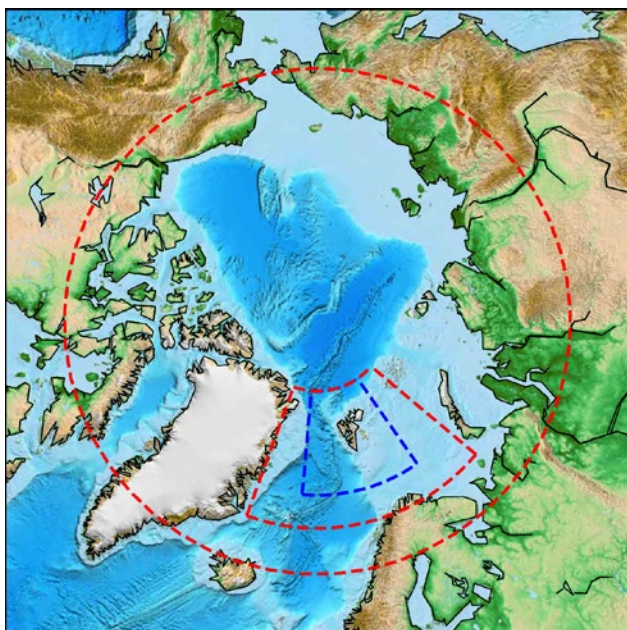
1 <https://www.wcrp-climate.org/wgcm-cmip/wgcm-cmip6>

2 <https://pcmdi.llnl.gov/CMIP6/>

2. Historical trends in temperature, precipitation and sea ice

We consider 3 regions: Svalbard, the entire Arctic, and the globe. *Svalbard* is here defined as the region bounded by 70°N – 83°N, 20°W – 50°E (inner dashed red box in Figure 1). This does include rather large parts of the surrounding ocean, but we find comparable results when using a smaller region that is more confined to the Svalbard Archipelago (indicated by the blue dashed box in Figure 1), albeit with substantially larger variability. Thus, the results presented in this section are from the extended Svalbard region (red box). The *Arctic* is defined as the area within 66°N – 90°N (outer red dashed circle).

We consider recent changes and trends in near-surface (2 m) temperature, precipitation, and sea-ice extent for our three focus regions, using data from the CMIP6 historical experiment from 48 different ESMs (Figure 1) that all performed this experiment. The historical experiment covers 1850–2014, but we focus on the last decades to facilitate more direct comparison with reanalysis products and observations.



2.1. Near-surface temperature

The AA of the near-surface temperature is evident in both observations and models (Figure 2) for all seasons except summer (defined as June, July, and August; JJA), with the warming being most intense during autumn (September, October, and November; SON) and winter (December, January, and February; DJF). The enhanced winter warming compared to summer is largely caused by transport of water vapour by the atmosphere (Doyle et al. 2011; Simpkins 2017; Lee et al. 2017) and by enhanced ocean heat release in response to thinner sea ice and reduced sea-ice extent (Screen and Simmonds 2010; Kim et al. 2019; Cohen et al. 2020).

Figure 2 shows the historical (years 1985–2014) seasonally averaged anomalies against the baseline (years 1951–1980) for near-surface (2 m) temperature, as found in the observationally based temperature data-set GISTEMPv4 (upper) and the CMIP6 ensemble mean (middle). Generally, the

1 ACCESS-CM2	17 CNRM-CM6-1	33 INM-CM5-0
2 ACCESS-ESM1-5	18 CNRM-CM6-1-HR	34 IPSL-CM6A-LR
3 AWI-CM-1-1-MR	19 CNRM-ESM2-1	35 KACE-1-0-G
4 AWI-ESM-1-1-LR	20 E3SM-1-0	36 MIROC6
5 BCC-CSM2-MR	21 E3SM-1-1	37 MIROC-ES2L
6 BCC-ESM1	22 EC-Earth3	38 MPI-ESM1-2-HAM
7 CAMS-CSM1-0	23 EC-Earth3-Veg	39 MPI-ESM1-2-HR
8 CanESM5-CanOE	24 EC-Earth3-Veg-LR	40 MPI-ESM1-2-LR
9 CanESM5	25 FGOALS-f3-L	41 MRI-ESM2-0
10 CAS-ESM2-0	26 GFDL-ESM4	42 NESM3
11 CESM2-FV2	27 GISS-E2-1-G-CC	43 NorCPM1
12 CESM2	28 GISS-E2-1-G	44 NorESM2-LM
13 CESM2-WACCM-FV2	29 GISS-E2-1-H	45 NorESM2-MM
14 CESM2-WACCM	30 HadGEM3-GC31-LL	46 SAM0-UNICON
15 CIESM	31 HadGEM3-GC31-MM	47 TaiESM1
16 CMCC-CM2-SR5	32 INM-CM4-8	48 UKESM1-0-LL

Figure 1: Indicated by the red dashed lines are the regions used for the comparison in this report (left). The Arctic is defined as 66°N–90°N (outer red circle). Svalbard is defined as 70°N–83°N, 20°W–50°E (inner red circle). A narrower region around Svalbard, confined to 73°N–83°N, 5°W–35°E, was included in a sensitivity test (blue dashed line). The names of the 48 ESMs that are part of the CMIP6 ensemble and analysed in this chapter; the number and coloured dots are used in the following scatter plots (right).

Near-surface (2m) temperature difference from (1951-1980)

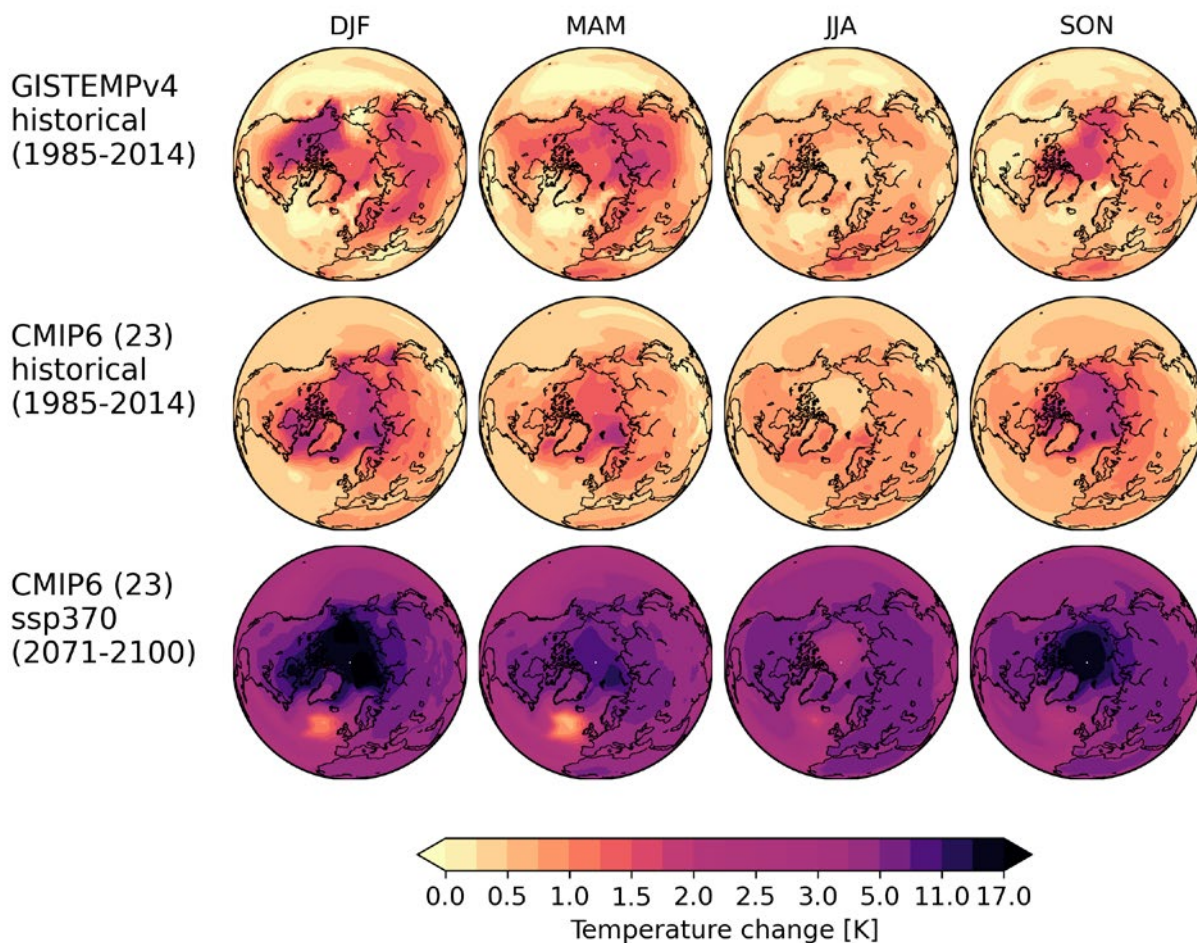


Figure 2: Seasonally averaged anomalies against the baseline (1951–1980) for near-surface (2 m) temperature. The historical (1985–2014) temperature change as found in GISTEMPv4 (upper) and the CMIP6 ensemble mean (middle), and in the projected (2071–2100) temperature change under SSP3-7.0 for CMIP6 (bottom). The numbers in parenthesis after CMIP6 indicate the number of models included in the ensemble mean.

Arctic warming is larger in the CMIP6 ensemble compared to GISTEMPv4. This is especially noticeable in autumn and winter with an AA factor (the ratio of Arctic warming to global warming) of 3.48 (2.24) and 3.75 (2.42) in CMIP6 (GISTEMPv4), respectively. In GISTEMPv4, there is pronounced warming over land, especially in winter and spring (March, April, and May; MAM). In the models, the warming is mostly enhanced over sea ice-covered regions. Interestingly, the region around Svalbard exhibits strong warming compared to the Arctic in winter and spring in both GISTEMPv4 and CMIP6 (see also Table 1).

The AA also shows up clearly in projections of the future climate at the end of the century (here represented by SSP3-7.0; for a description of the SSPs please see Section 3) with an Arctic-averaged winter surface warming of 13°C and as high as 20°C in some regions (Figure 2, bottom panel). In the autumn, the area-averaged surface warming is 10°C for the Arctic and reaches 16°C in some regions. As seen with other warming scenarios (e.g. Graff et al. 2019) AA is less pronounced in an even warmer world than in the present-day climate. The AA factor is slightly reduced in all seasons in SSP3-7.0 at the end of the century compared to the current period in the historical experiment;

Model/Obs	Region	Annual T	Winter T	Annual pr	Winter pr
CMIP6*	Global	0.26	0.27	0.38	0.37
	Arctic	0.70	0.92	2.96	3.12*
	Svalbard	0.78	1.07*	2.66*	2.89*
ERA5	Global	0.16	0.15	0.96	1.08
	Arctic	0.68	0.75	1.49	1.52
	Svalbard	0.75	1.39	2.02	2.69
MERRA-2	Global	0.12	0.10	1.48	2.47
	Arctic	0.41	0.36	-0.14	-1.34
	Svalbard	0.52	1.12	0.09	-1.13
NCEP-DOE 2	Global	0.16	0.09	-	-
	Arctic	0.88	0.92	-	-
	Svalbard	0.81	1.54	-	-
GISTEMPv4	Global	0.16	0.13	-	-
	Arctic	0.66	0.72	-	-
	Svalbard	0.69	0.94	-	-
GPCPv2.3	Global	-	-	0.18	0.60
	Arctic	-	-	3.15	2.30
	Svalbard	-	-	9.78	10.58
Svalbard Lufthavn	Svalbard	1.23	2.49	3.35	4.06
Ny-Ålesund	Svalbard	0.93	2.07	10.08	13.99

Table 1: Linear near-surface temperature (T) trends (°C per decade) and total precipitation (pr) trends (% per decade) for the time period 1980–2014. Trends significant at the 5% level are bold [Mann-Kendall non-parametric test (Mann 1945; Kendall 1975; Hussain and Mahmud 2019)]. For CMIP6, the ensemble-mean value of 48 models (see list in Figure 1) is given in bold if more than 75% of the individual models exhibit a significant trend and an * if the CMIP6 ensemble-mean trend is significant, but less than 75% of the individual models exhibit a significant trend.

for example, it is reduced from 3.75 to 3.42 in winter and from 3.48 to 2.83 in autumn (note that for consistency the numbers are based on the 23 models that simulated both the SSP3-7.0 and the historical experiment – but they are very similar to those reported above based on all 48 models). The Arctic summer warming is 0.70°C in the CMIP6 historical (1985–2014) ensemble average and projected to increase by 7°C by the end of the 21st century in SSP3-7.0. Also for summer, the AA factor of 1.32 is slightly reduced in SSP3-7.0, compared to the historical AA factor of 1.51.

In addition to being able to correctly represent the spatial pattern of the recent changes in near-surface temperature, the CMIP6 models must also capture the temporal evolution of these changes over the historical period. In our representation, with the period of 1981–2010 as baseline, it

appears, that the CMIP6 models exhibit too strong warming after 1980 (Figure 3, left panels and Table 1). It has been shown that this warming partly compensates for a cooling effect prior to and around the year 1970, imposed by possibly too strong aerosol forcing in the models at that time (Flynn and Mauritsen 2020). Another reason why the models are too warm is that they are unable to properly capture the global warming hiatus between 1998 and 2012, when the annual and global mean surface temperature hardly changed for more than a decade in spite of increasing atmospheric GHG concentrations (Kosaka and Xie 2013; Medhaug et al. 2017). The historical timeseries of annual and global mean near-surface temperature anomalies (Figure 3a) reveal a warming trend of 0.26°C per decade over the 35 years from 1980 to 2014 in the CMIP6 ensemble mean, which is significantly higher than in the reanalysis (Table 1).

Annually averaged temperature and precipitation anomalies

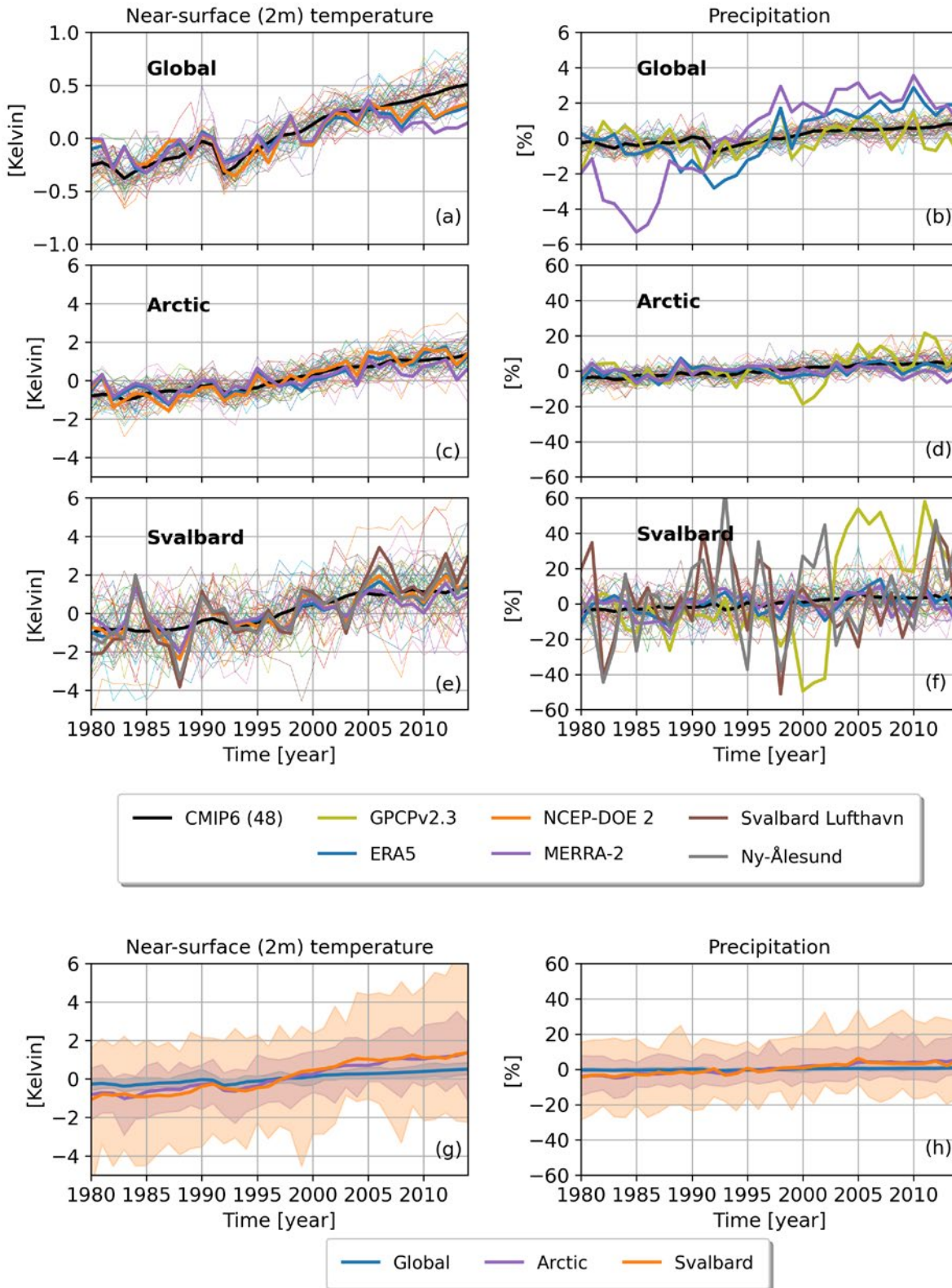


Figure 3: Annually averaged anomalies from the baseline (1981–2010) for near-surface (2 m) temperature (left) and precipitation (right) over the years 1980–2014. The upper 6 panels show the CMIP6 members (thin lines) and the CMIP6 ensemble mean (black line) compared to the reanalysis data: GPCPv2.3 (olive line, only precipitation), ERA5 (blue line), NCEP-DOE 2 (orange line), and MERRA-2 (purple line), in addition to observational records from Svalbard-Lufthavn (brown line), and Ny-Ålesund (grey line). Three regions are considered: global (upper), Arctic (middle) and Svalbard (bottom). The lower 2 panels show the anomalies in temperature (left) and precipitation (right) for the CMIP6 ensemble mean (solid line) and the spread (shading) for the global mean (blue), Arctic mean (purple), and Svalbard (orange).

The CMIP6 ensemble-mean temperature evolution in the Arctic and in Svalbard is within the uncertainty of the reanalysis, and AA is clearly visible (Table 1 and Figure 3c,e)³ with an annual temperature trend (1980–2014) of 0.70°C per decade in the Arctic and 0.78°C per decade in Svalbard. The modelled trends for Svalbard are smaller than the observed temperature trends of 0.93°C per decade in Ny-Ålesund and of 1.23°C per decade in Svalbard Lufthavn (Figure 3e). These trends are higher compared to those reported in Førland et al. (2011): 0.73°C per decade in Ny-Ålesund and 1.04°C per decade in Svalbard Lufthavn for the years 1975–2011. They are clear evidence of the more recent accelerated warming. Updated estimates reveal an even stronger warming trend of 1.66°C per decade over the years 1991 – 2018 in Svalbard Lufthavn (Nordli et al. 2020).

The aforementioned global warming hiatus was in large part dominated by cooling over the Pacific Ocean and over North America towards Eurasia (Kosaka and Xie 2013; Medhaug et al. 2017), and hence is not evident when only the Arctic is considered. The annual mean Arctic warming in CMIP6 is in agreement with ERA5 (Table 1). However, NCEP-DOE 2 exhibits an even stronger warming of 0.88°C per decade. The reanalysis sets agree on a global warming trend of 0.16°C per decade, except for MERRA-2, which exhibits a smaller warming trend of 0.12°C per decade. The smaller annual temperature trend in MERRA-2 is also evident for the Arctic and in Svalbard.

The historical temperature trends for the Arctic and Svalbard are compared for all seasons (Figure 4a). 63% of the CMIP6 models exhibit a stronger temperature trend in winter in Svalbard compared to the Arctic. However, only 13% of the individual models exhibit a statistically significant warming trend at the 5% level (Mann-Kendall non-parametric test; Mann 1945; Kendall 1975; Hussain and Mahmud 2019)⁴. Importantly, the ensemble mean value of 0.92°C per decade for the Arctic and 1.07°C per decade for Svalbard is significant even at the 1% level. The stronger temperature trend

in Svalbard compared to the Arctic in the CMIP6 ensemble mean is present for all seasons, except autumn, with a 0.09°C per decade (annual) and a 0.15°C per decade (winter) enhanced warming trend. Of the reanalysis sets, only MERRA-2 exhibits a significantly stronger warming trend in Svalbard compared to the Arctic with a 0.40°C per decade and 0.70°C per decade warmer trend for the annual and winter mean respectively.

2.2. Precipitation

In conjunction with the temperature increase, the total precipitation increases on a global scale as well as in the Arctic (Figure 3, right panels and Table 1). The historical CMIP6 timeseries of annual mean area-averaged total precipitation exhibits a significant increase of 0.37% per decade in the global mean over the years 1980–2014 compared to 3.12% per decade and 2.89% per decade in the Arctic and in Svalbard, respectively. The CMIP6 ensemble mean and the reanalysis GPCPv2.3 experience a significantly larger trend in the Arctic and Svalbard compared to the global mean. The CMIP6 ensemble mean demonstrates a wetter trend of 2.61% per decade for the Arctic and 2.30% per decade in Svalbard, compared to the global annual mean.

The hydrological cycle has intensified in response to global warming, and consequently the atmospheric moisture transport to the Arctic has increased (Held and Soden 2006; Serreze et al. 2012; Hartmann et al. 2013; Hanssen-Bauer et al. 2019). In addition, amplified temporal fluctuations and the changes in the atmospheric circulation in the mid-latitudes in response to the warming could further enhance the moisture transport into the Arctic (Zhang et al. 2008). The precipitation timeseries (Figure 3, right panels) reveal great disagreement among the CMIP6 models as well as among the reanalyses, reflecting that the hydrological cycle is challenging to model. Precipitation occurs in large part on sub-grid scales and hence is parameterized in climate models. In contrast to temperature, which is a more direct response of radiation, precipitation

³ Please note the different y-axis

⁴ All statistically significant trends in this report are significant at the 5% level, using the Mann-Kendall non-parametric test, if not stated differently

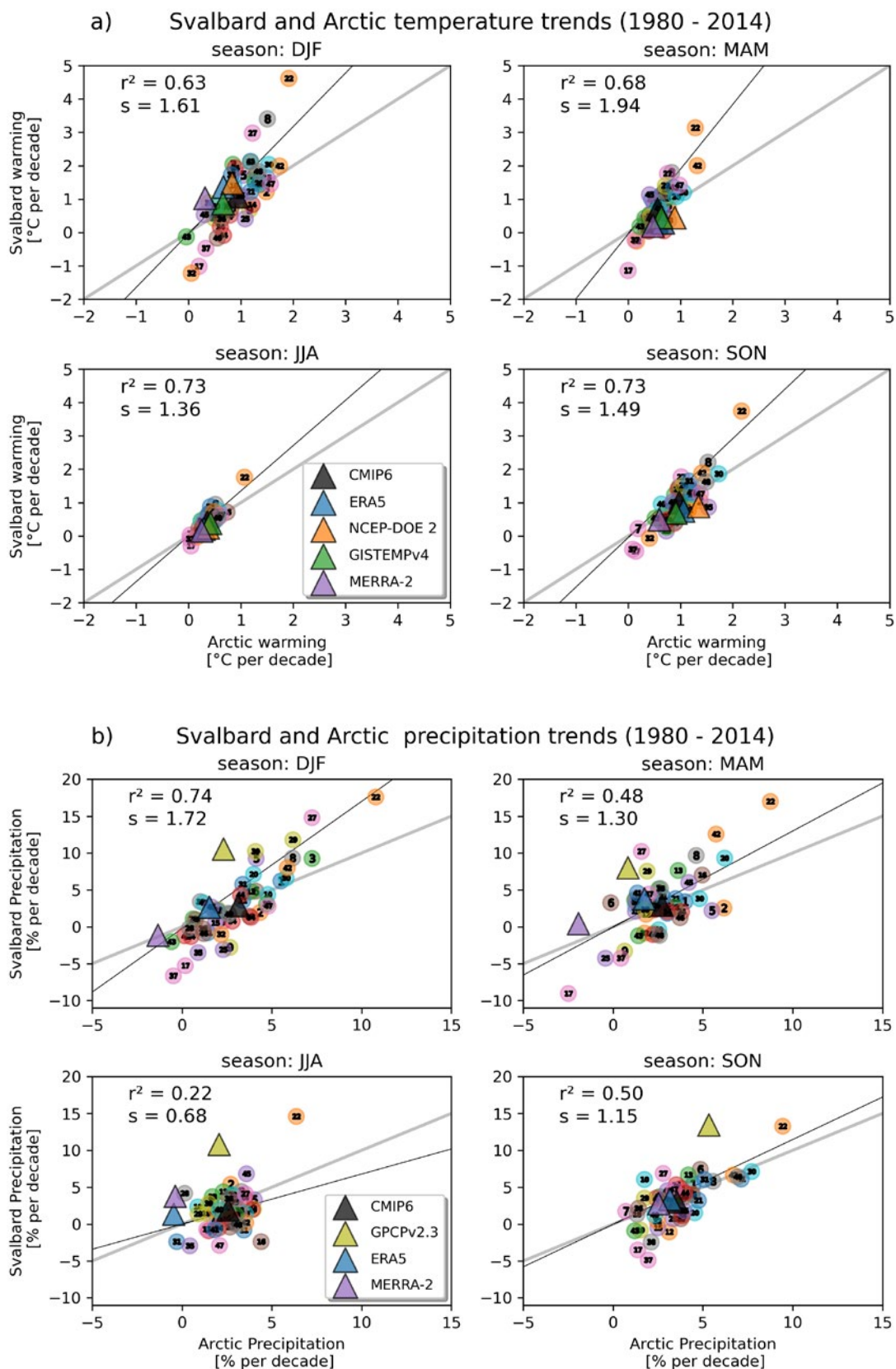


Figure 4: Near-surface (2 m) temperature (upper 4 panels) and precipitation trends (lower 4 panels) for the Arctic and Svalbard for all seasons. All panels show 48 ESM historical simulations (coloured dots) and the CMIP6 ensemble mean (black triangle) and are compared to similar trends in reanalysis and observational datasets: ERA5 (blue triangle), NCEP-DOE 2 (orange triangle), GISTEMPv4 (green triangle), MERRA-2 (purple triangle), and GPCPv2.3 (olive triangle). Also indicated is the 1:1 agreement (grey line) and the linear regression of the CMIP6 model results (black line).

involves various nonlinear interactions of processes such as evaporation, convection, cloud formation, and temperature and pressure fluctuations. In addition, the reanalyses are sensitive to a lack of good observations of precipitation (Zhang et al. 2013). Further, in response to global warming, it is particularly hard to obtain realistic treatment of processes such as degradation of permafrost, Arctic greening and reduction of plant transpiration which can act to intensify the hydrological cycle in addition to the atmospheric circulation changes (Zhang et al. 2013).

The historical precipitation trends for the Arctic and Svalbard are compared for all seasons (Figure 4b, also see Table 1). In the Arctic, 44% of the individual models exhibit a statistically significant increased precipitation trend during winter, and as many as 82% do so during autumn. The CMIP6 ensemble mean exhibits a significant increase in precipitation of 3.12% per decade (winter) and 3.56% per decade (autumn) for the Arctic. In Svalbard, the percentage of individual models exhibiting a significant increasing precipitation trend is reduced to 29% (winter) and 23% (autumn). However, the CMIP6 ensemble mean exhibits a significant increased precipitation trend of 2.89% per decade (winter) and 3.02% per decade (autumn) in Svalbard.

The CMIP6 ensemble mean shows a significantly larger annual precipitation trend in the Arctic than in Svalbard, being 0.23% wetter per decade. This is also evident in the autumn where the Arctic precipitation trend is 0.74% per decade wetter compared to Svalbard. The observed precipitation trends from GPCPv2.3 are wetter in Svalbard compared to the Arctic in summer (7.89% per decade) and autumn (8.35% per decade) and also in the annual mean (5.70% per decade). None of the reanalyses exhibit significant differences in the precipitation trends in the Arctic and Svalbard.

2.3. Sea ice

Sea-ice loss and changes in the associated sea-ice albedo feedback is an important factor contributing to AA (Cohen et al. 2020). The bright sea-ice surface efficiently reflects solar radiation during spring and summer. As the sea ice melts, this bright

reflecting surface is replaced by a dark absorbing ocean. The absorbed heat is returned to the cold atmosphere during autumn and spring (Serreze et al. 2009) causing extensive warming and further sea-ice loss — creating a positive feedback. This feedback loop is one of the main reasons why the Arctic is warming so fast compared to the rest of the world (Pithan and Mauritsen 2014; Kim et al. 2019). Liang et al. (2020) find that in climate models, as much as 21% of the Arctic-averaged near-surface winter temperature are accounted for by the Arctic sea-ice concentration-driven variance over the years 1979–2014.

In fact, the amplified warming in the Arctic causes sea ice melt at a pace greater than that simulated by the climate models (Cohen et al. 2014, 2020). The Arctic experiences sea ice loss across all seasons (Stroeve and Notz 2018) with the greatest loss in the autumn (Figure 5, right columns). 44 models participating in CMIP6 exhibit a declining trend in the September sea-ice extent of $(-0.7 \pm 0.06) \times 10^6$ km² per decade over the years 1979–2014, while the observed trend is even larger $(-0.82 \pm 0.18) \times 10^6$ km² per decade (Shu et al. 2020). In this report, we consider 30 of the 48 models listed in Figure 1, and Arctic sea ice is defined as the Northern Hemisphere total sea-ice extent.

On average, the sea-ice extent in CMIP6 is too large compared to observations and all the reanalyses. This is especially evident in spring (MAM, Figure 5a). 90% of the individual models exhibit a significant decline in sea-ice extent with an ensemble-mean decadal trend over the years 1980–2014 of -0.36×10^6 km² for spring (MAM) and -0.57×10^6 km² for autumn (SON) (Figure 5a,b). The discrepancy between the autumn trend of -0.57×10^6 km² per decade reported in this study and the $(-0.7 \pm 0.06) \times 10^6$ km² per decade listed above, is due to different averaging periods (SON vs. September only) and a different number of models (30 vs. 44). Of the observational dataset (HadISST) and reanalyses (ERA5 and MERRA-2), only ERA5 exhibit a larger decadal decline in Arctic sea-ice extent in the autumn (-0.69×10^6 km²), while the corresponding value for HadISST is -0.55×10^6 km² and in agreement with the CMIP6 ensemble mean value.

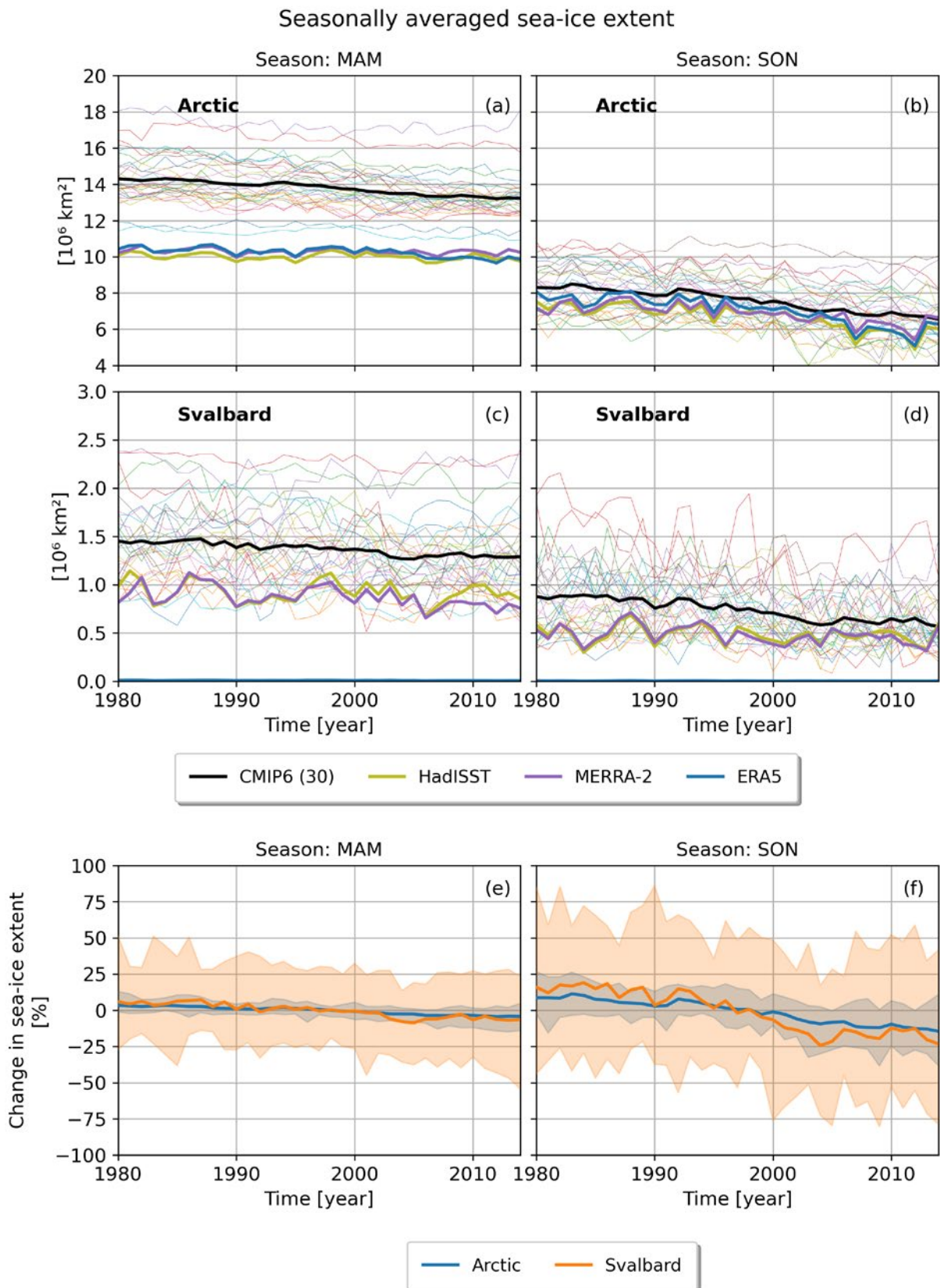


Figure 5: Sea-ice extent in the MAM season and the SON season for the years 1980–2014. The upper 4 panels show the CMIP6 members (thin lines) and the CMIP6 ensemble mean (black line) compared to the reanalysis data: HadISST (olive line), MERRA-2 (purple line), and ERA5 (blue line). Two regions are considered: Arctic (upper) and Svalbard (bottom). The lower 2 panels show the anomalies in sea-ice extent from the baseline (1981–2010) as a percentage change for the MAM season (left) and the SON season (right) for the CMIP6 ensemble mean (solid line) and the spread (shading) for the Northern Hemisphere (blue) and Svalbard (orange).

In Svalbard, 43% and 77% of the individual models exhibit a significant decline in sea-ice extent in spring (MAM) and autumn (SON) (Figure 5c,d). One model (CNRM-CM6-1) exhibits a significant increasing trend in sea-ice extent in spring. The CMIP6 ensemble-mean decadal trend is $-0.06 \times 10^6 \text{ km}^2$ for spring (MAM) and $-0.10 \times 10^6 \text{ km}^2$ for autumn (SON) (Figure 5c,d).

When comparing the decadal decline in sea-ice extent for Arctic and the Svalbard region, we consider the percentage changes (Figure 5, bottom

row). In CMIP6, the sea-ice extent declines faster in the region around Svalbard, compared to the Arctic, and the difference is most prominent in the autumn with a sea-ice loss of -13.7% per decade in Svalbard, compared to -7.5% per decade in the Arctic. 37% of the individual models exhibit a significantly more negative trend in the region around Svalbard compared to the Arctic. The CMIP6 ensemble mean exhibits a significantly faster decline of -6.20% in sea-ice extent around Svalbard compared to the Arctic as a whole.

3. Future projections of Arctic climate

To study how temperature, precipitation, and sea-ice extent may change over the upcoming 80 years, we consider results from four CMIP6 climate projections known as “shared socioeconomic pathways” (SSPs; O’Neill et al. 2016): **SSP1-2.6**, the “best-case” scenario where mitigation and adaptation challenges are low and the radiative forcing due to anthropogenic activities reaches 2.6 W m^{-2} by the end of the 21st century; **SSP2-4.5**, a mid-range scenario with respect to both mitigation and adaptation and with the radiative forcing reaching 4.5 W m^{-2} in 2100; **SSP3-7.0**, a future with high mitigation and adaptation challenges and high radiative forcing of 7.0 W m^{-2} in 2100; **SSP5-8.5**, the “worst-case” scenario with high mitigation challenges, low adaptation challenges, and the radiative forcing exceeding 8.5 W m^{-2} by 2100.

We consider results from the SSPs alongside results from the historical runs using data from the 23 CMIP6 models that provide the necessary data from all simulations.

3.1. Near-surface temperature

The annually and globally averaged near-surface temperature increases by 0.89°C over the historical period (1900–2014; Figure 6). The temperature continues to increase in the future, both in terms of the global mean (Figure 6, upper left) and for the Arctic (middle left) and Svalbard regions (bottom left). The temperature increase is however

substantially larger in the high-latitude regions (note top panel has different y-axis). The scenarios start diverging around 2040, and by 2100, there is considerable spread between the best- and worst-case scenarios, with the global-mean ensemble-mean warming over the last 10 years (2091–2100, compared to the baseline years 1850–1879) ranging from 1.97°C (SSP1-2.6) to 4.85°C (SSP5-8.5), whereas the CMIP6 ensemble-mean warming for the Arctic and Svalbard ranges from 6.80°C to 18.20°C and 7.37°C to 15.35°C , respectively.

The enhanced winter warming in the Arctic and Svalbard is evident in all scenarios (Figure 6). Interestingly, by 2100 Svalbard experiences greater warming compared to Arctic for the historical period and the two mildest future scenarios (SSP1-2.6 and SSP2-4.5). However, for the two warmest scenarios (SSP3-7.0 and SSP5-8.5), the Arctic experiences greater warming. The reason for this shift is probably the lack of sea-ice feedback as all the sea ice in the region around Svalbard has melted by 2100 under the warmest scenarios (Figure 7, right). However, only the winter warming for the SSP5-8.5 scenario is significantly warmer in the Arctic than in Svalbard (Mann-Whitney U Test, $p = 0.007$, Mann and Whitney 1947).

There is vast inter-model spread; for instance, for Svalbard the winter warming over the years 2091–2100 (compared to the baseline years 1850–1879) for SSP5-8.5 ranges from 9.70°C to 25.91°C (see

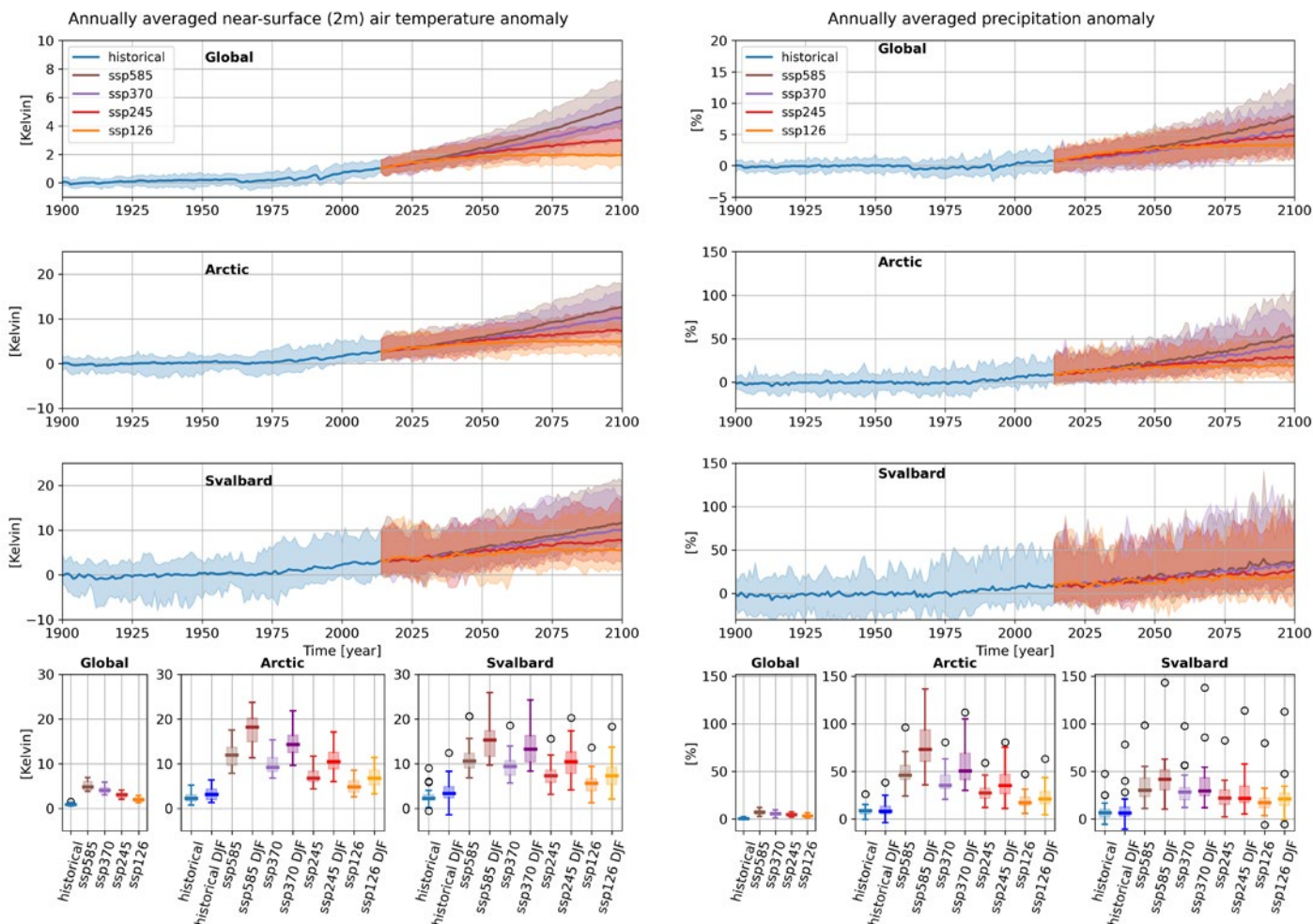


Figure 6: Annual-mean anomalies of near-surface (2 m) temperature (left column) and precipitation (right column) from the historical runs (1900–2014) and future projections (2015–2100) for three regions: the globe (upper row), the Arctic (second row), and Svalbard (third row). The anomalies are taken with the years 1850–1879 as a baseline. The upper four panels show the time evolution of the historical run (blue), SSP5-8.5 (brown), SSP3-7.0 (purple), SSP2-4.5 (red), and SSP1-2.6 (orange) for the CMIP6 ensemble mean (solid lines) and the spread (shading). The bottom row shows the box plots of area-averaged anomalies % of sea-ice extent from the historical runs and future projections for annual-mean global values, global-mean, and DJF values for the Arctic and global-mean and DJF values for Svalbard averaged over 2091–2100 (the last decade shown in the upper four panels). The horizontal line within the box shows the median value, the boxes show the interquartile range, the whiskers extend to the smallest and largest values that are not outliers, and the open circles show the outliers. For the Arctic and Svalbard, plots for DJF are shown alongside.

brown shading in Figure 6). The inter-model spread increases as we zoom in on smaller regions, with Svalbard having the largest spread; the spread is moreover larger when only considering the winter season (Figure 6, bottom panel). Presumably, the inter-model spread of area-averaged quantities is smaller for the larger domain because more data points are included. For smaller domains, the average could be more sensitive to whether values in the tails of the distributions fall within the domain or not. For the Svalbard region, the position of the marginal ice zone, which can vary between the models, exerts a large influence on temperature, potentially causing large inter-model temperature spread. Similarly, the inter-model spread could

be larger for the winter means than the annual means because fewer data (25%) are used when computing the winter means. However, the winter season is also characterised by more variability with, for instance, the North Atlantic storm track being more vigorous and also more tilted toward the pole compared to during summer (Shaw et al. 2016). Further investigation is warranted to understand this properly.

3.2. Precipitation

While the precipitation trend seems to be rather weak (0.5% increase) over the historical period, it clearly increases in the future climates. As with

Sea-ice extent anomaly

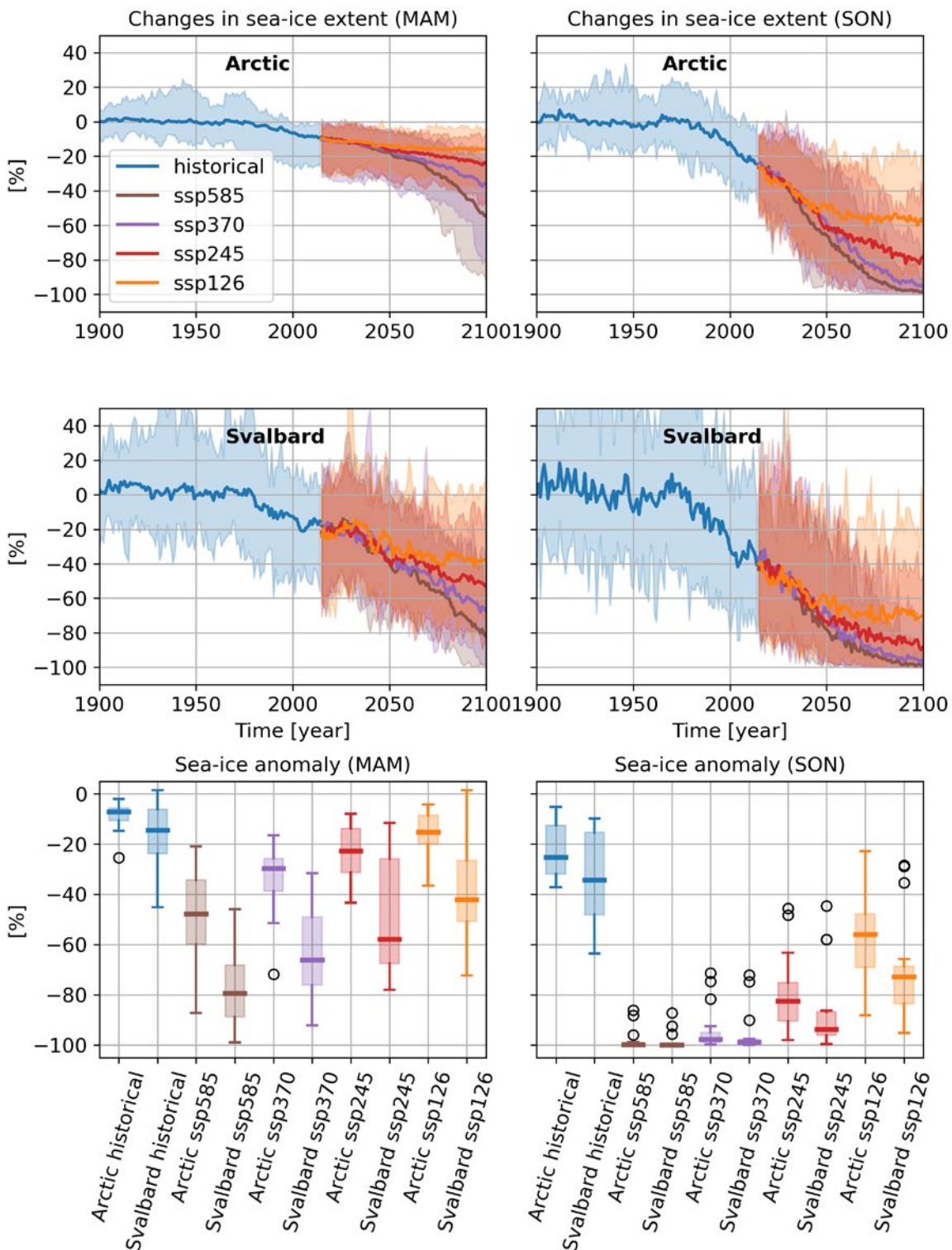


Figure 7: Annual-mean anomalies of the sea-ice extent from the historical runs (1900–2014) and future projections (years 2015–2100) for the Arctic and Svalbard regions for MAM (left column) and SON (right column). The anomalies are taken with the years 1850–1879 as a baseline. The upper four panels show the time evolution of the sea-ice extent anomalies for the historical (blue), SSP5-8.5 (brown), SSP3-7.0 (purple), SSP2-4.5 (red), and SSP1-2.6 (orange) timeseries for the CMIP6 ensemble mean (solid lines) and the spread (shading) for the Arctic (top row) and Svalbard (middle row) regions. The bottom row shows box plots of area-averaged anomalies of sea-ice extent from the historical runs and future projections for the Arctic and Svalbard averaged over 2091–2100 (the last decade shown in the upper four panels). The horizontal line within the box shows the median value, the boxes show the interquartile range, the whiskers extend to the smallest and largest values that are not outliers, and the open circles show the outliers.

temperature, the increase is larger for the Arctic and Svalbard regions than it is globally (note the different y-axis). The global-mean ensemble-mean change in precipitation by year 2100 ranges from 3% for SSP1-2.6 to 7% for SSP5-8.5, whereas the corresponding numbers for the Arctic and Svalbard are 21% to 73% and 21% to 42%, respectively.

As with temperature, the inter-model spread is largest for Svalbard and smallest for the global mean; the spread is also larger when considering just the winter months compared to the whole year. Interestingly, the inter-scenario spread, that is, the spread between the different SSPs, is larger for the Arctic than for Svalbard. This could indicate that for Svalbard, the change in precipitation by 2100 depends less on the chosen scenario than it does for the Arctic as a whole. The ensemble-mean precipitation reaches lower values under SSP5-8.5 for Svalbard than for the Arctic, but higher values for SSP1-2.6, suggesting that Svalbard could experience a larger increase in precipitation than the Arctic under the best-case scenario, while the roles could be reversed under the worst-case scenario. However, only the two warmest and wettest scenarios (SSP3-7.0 and SSP5-8.5) show a significantly larger increase in annual and winter precipitation in the Arctic compared to Svalbard

(Mann-Whitney U Test, $p < 0.001$, Mann and Whitney 1947).

3.3. Sea ice

As expected, the sea-ice extent decreases with time over the historical period and continues to decrease with future warming, both when considering the Arctic (i.e. the Northern Hemisphere sea-ice extent), and when narrowing down to the Svalbard region (Figure 7). The changes are largest in the scenarios with the strongest warming. During spring, the sea-ice extent is projected to decrease by 48% for the worst-case scenario (SSP5-8.5) and 15% for the best-case scenario (SSP1-2.6) for the Arctic and by 79% for the worst-case scenario and 42% for the best-case scenario for Svalbard by 2100.

Ice-free conditions are reached under both the worst-case scenario and SSP3-7.0 during autumn, whereas for the best-case scenario, the sea-ice extent decreases by 56% for the Arctic and 73% for Svalbard. There is large inter-model variability both during the historical period and in the future projections. The variability however decreases as the sea-ice extent decreases, and is very low by the end of the 21st century (Figure 7, bottom right panel).

4. Concluding remarks

Our study shows that compared to the temporal evolution in the global mean of selected climate variables, Svalbard and the Arctic undergo similar and significantly larger changes in response to projected future climate change and to the warming that has occurred over the last few decades. Thus, we find that Svalbard is well-suited as an observational supersite for the Arctic. There are however important differences:

- The Svalbard region displays an even stronger warming trend than the Arctic for the historical period (1980–2014) and for the two mildest future scenarios (SSP1-2.6 and SSP2-4.5).
- In the future, the Arctic experiences a significantly larger increase in annual and winter precipitation compared to Svalbard for the two warmest and wettest (SSP3-7.0 and SSP5-8.5) climate projection scenarios.
- Over the more recent historical period (1980–2014), the sea ice melts faster in the region around Svalbard than in the Arctic.

However, the winter warming for the worst case scenario (SSP5-8.5) is significantly warmer in the Arctic than in Svalbard.

5. Connections and synergies with other SESS report chapters

Good and accurate observations are of critical importance for Earth System Modelling. Observations are needed in order to improve our understanding of the state of the Earth system and distribution of different quantities, processes, and interactions. This knowledge is utilised in the models to make sure that the Earth system is represented as realistically as possible. Observations are also needed to validate the model output and help us identify quantities and processes that are well-represented or that need further improvement. The work presented here therefore has synergies with several other chapters from SESS reports, for instance, in relation to

observations of snow cover and sea ice (“Long-term monitoring of landfast sea-ice extent and thickness in Kongsfjorden, and related applications (FastIce)” by Gerland et al. 2020; “Long-term variability of terrestrial-snow and sea-ice cover extent in Svalbard (SvalSCESIA)” by [Killie et al. 2021](#)), cloud condensation nuclei (“Multidisciplinary research on biogenically driven new particle formation in Svalbard (SVALBAEROSOL)” by Sipilä et al. 2020), atmospheric black carbon (“Atmospheric black carbon in Svalbard (ABC Svalbard)” by Gilardoni et al. 2020) and Arctic haze (“Arctic haze in a climate changing world (HAZECLIC)” by [Traversi et al. 2021](#)).

6. Unanswered questions

Some of the mechanisms contributing to Svalbard/Arctic differences in temperature, precipitation, and sea-ice extent need further investigation and are listed below.

Svalbard lies in the vicinity of the North Atlantic transport pathways, which bring heat, moisture, and matter to the Arctic by both atmospheric and oceanic processes and which connect the Arctic to the larger-scale circulation. Hence, transport changes due to anthropogenic forcing may cause a greater impact in Svalbard compared to the Arctic as a whole, and/or the timescales of impact may differ greatly, but that needs further investigation.

The West Spitsbergen Current (WSC) brings warm and saline Atlantic water into the Arctic and connects the Arctic and the world oceans. The Arctic near-surface temperature and sea-ice extent can be mediated by this inflow, both in the present climate (Chylek et al. 2009; Mahajan et al. 2011) and in projections of future climate change (Nummelin et al. 2017). In our study we found that over the more recent historical period (1980–2014), the sea ice melts faster in the region around Svalbard than in the Arctic. A reduction in sea-ice extent is intimately linked to temperature changes, and our

results show that the Svalbard region displays an even stronger warming trend than the Arctic for the historical period (1980–2014). How these reported changes between Svalbard and the Arctic are linked to the ocean transport needs further investigation.

North Atlantic storms typically travel poleward and eastward from the east coast of the U.S. toward the Barents Sea. The storms bring warm moist air from lower to higher latitudes, and are an important contributor to the atmospheric poleward heat transport. Changes in the pathways of these storms can change this transport and therefore have the potential to affect the Arctic as a whole and perhaps even more so Svalbard, as it is situated in the north-eastern edge of the storm track and is greatly affected by the details of the paths taken by the storms. In addition, the discrepancy between the observed storm tracks and those simulated by the models has implications for atmospheric poleward heat transport, precipitation, and strong winds. It can even be a major cause of why models fail to fully capture observed climate change in Svalbard and the Arctic as a whole.

In order to quantify the most important drivers for climate change in Svalbard and for the Arctic

as a whole, it remains an open question how one can quantify the contributions from the large-scale atmospheric circulation changes, such as shifts in the storm tracks, changes in the oceanic heat transport into the Arctic, and how to disentangle such contributions from the various feedbacks amplifying the warming. Likewise, it is still difficult to differentiate between large-scale drivers and more local changes (Isaksen et al. 2016). How confident

can we be of modelled attribution of climate change when interpreting locally observed timeseries of physical and biogeochemical variables?

In this study, we have considered the Arctic as a whole. Further investigation is needed to understand for which parts of the Arctic the Svalbard region can act as a supersite and can be used as an early warning platform.

7. Recommendations for the future

The climate models are highly complex numerical models, fed with initial conditions (for instance the current state of the Earth system or perturbed states) to simulate, for instance, the historical period or to project future scenarios. Due to the chaotic nature of the system, understanding the data produced by the models is challenging. Although often very impressive in their complexity, the models are imperfect and not always able to accurately reproduce all aspects of the Earth system. To be able to tell where the models fail and where they succeed, we need to understand why they act as they do. In particular, we need to make sure that the correctness of future projections made by these models rest on our understanding of the system. To achieve that, observations and process understanding are of crucial importance. For instance, incorrect atmospheric and oceanic transports of energy into the Arctic have large impacts on the rate of warming. The model community can benefit not only from the great observational data collected on and in the regions around Svalbard, but also from process understanding of experimentalists and observationalists. Likewise, the experimentalists and observationalists can benefit greatly by interacting more with the modelling community and learn from their perspectives – “the purpose of models is not to fit the data, but to sharpen the questions” (Karlin 1983).

Predicting and characterising climate change in Svalbard will be an increasingly important issue in the 21st century as the changes in near-surface air temperature, precipitation and sea-ice extent seem to occur at an extremely high pace in Svalbard,

even higher than in the rest of the Arctic. It is equally important to understand and explain what mechanisms are causing the differences between the observed and modelled climate changes. A closer collaboration between experimentalists, observationalists, and the model community has the potential to improve the understanding of Arctic climate change for the science community, stakeholders, and the public at large. Svalbard Integrated Arctic Earth Observing System (SIOS) is in a unique position to facilitate such a collaboration.

To address the knowledge gaps identified above, we recommend that SIOS supports and initiates consolidated efforts to strengthen the relevant research infrastructure components, both within and outside SIOS. Such efforts will enable other Norwegian and Arctic research institutions to pursue urgently needed research projects in the area of Arctic climate change.

Specifically we recommend:

Supporting efficient data mining and harmonisation efforts, beyond metadata catalogues, which allow the construction and monitoring of energy budgets and energy flux trends in the larger Svalbard region and the Arctic as a whole. Energy flux estimates in the atmosphere, the ocean, and the cryosphere require broad efforts in data assembly and quality assurance, including efforts to seek feedback on usability and usefulness of datasets from model users.

Cooperating with the Norwegian national ESM infrastructure INES to build the modelling tools

needed to integrate the new SIOS data and explore how comparisons between data from models and observations can provide meaningful answers to questions related to Arctic amplification, abrupt changes, and climate feedbacks.

Fostering e-science tools (and education) so that young scientists working in the area of Arctic climate science are able to efficiently analyse results from model ensembles, such as CMIP6.

Initiating and strengthening the collaboration with

existing pan-Arctic research initiatives and institutions to assemble temporal trends of physical climate variables in all spheres, along with those of biogeochemical tracers of system changes (methane, aerosols, carbon isotopes, and water isotopes).

Identifying and documenting the most efficient international means of cooperation to foster joint understanding of forthcoming Arctic climate changes, possible abrupt climate transitions, and the drivers for such changes.

8. Data availability

All original data used in this report are openly accessible via the links in table 2. All code used for

the analysis can be obtained from the corresponding author upon request.

Table 2: Data sets used in this report

Data set	Time period	Region	Data info, providers and access
CMIP6	1850–2100	Global	All CMIP6 data used in this report are made publicly available in a standardised format and are free to download and accessible from any of the portals listed under “model output access” at https://pcmdi.llnl.gov/CMIP6/
ERA5	1979–Present	Global	ERA5 data are provided by the Copernicus Climate Change Service (C3S), from the Copernicus Climate Change Service Climate Data Store (CDS): https://www.ecmwf.int/en/forecasts/datasets/reanalysis-datasets/era5
MERRA-2	1980–Present	Global	MERRA-2 data are provided by NASA, and made available at MDISC, managed by the NASA Goddard Earth Sciences (GES) Data and Information Services Center (DISC): https://gmao.gsfc.nasa.gov/reanalysis/MERRA-2/docs/
GISTEMPv4	1880–Present (baseline 1951–1980)	Global	GISTEMPv4 data are provided by the NOAA/OAR/ESRL PSL, from their website at https://data.giss.nasa.gov/gistemp/
HadiSST v1.1	1871–Present	Global	HadiSST data can be accessed through the Met Office Hadley Centre at http://badc.nerc.ac.uk/view/badc.nerc.ac.uk ATOM dataent_hadisst
GPCPv2.3	1979–Present	Global	GPCP Precipitation data are provided by the NOAA/OAR/ESRL PSL, from their website at https://psl.noaa.gov/
NCEP-DOE 2	1979–Present	Global	NCEP-DOE reanalysis 2 data are provided by National Centers for Environmental Prediction/National Weather Service/NOAA/, from the Research Data Archive at the National Center for Atmospheric Research, Computational and Information Systems Laboratory: https://doi.org/10.5065/KVQZ-YJ93 .

Acknowledgements

The authors thank the Editorial Board, Christiane Hübner, and two anonymous reviewers for their comprehensive and insightful comments, which have led to the improved presentation of this report. This work was supported by the European Framework Programme Horizon 2020 project CRESCENDO (Coordinated Research in Earth Systems and Climate: Experiments, Knowledge, Dissemination and Outreach, grant agreement no. 641816), the Research Council of Norway through

project number 291644, Svalbard Integrated Arctic Earth Observing System – Knowledge Centre, operational phase, INES (270061) and KeyCLIM (295046). High performance computing and storage resources were provided by the Norwegian infrastructure for computational science UNINETT Sigma2 (through projects NN2345K, NN9560K, NN9252K, NS2345K, NS9560K, NS9252K, and NS9034K).

References

- Bintanja R, Selten F (2014) Future increases in Arctic precipitation linked to local evaporation and sea-ice retreat. *Nature* 509(7501):479–482, <http://doi.org/10.1038/nature13259>
- Chylek P, Folland CK, Lesins G, Dubey MK, Wang M (2009) Arctic air temperature change amplification and the Atlantic Multidecadal Oscillation. *Geophys Res Lett* 36(14):L14801, <https://doi.org/10.1029/2009GL038777>
- Cohen J, Screen JA, Furtado JC, Barlow M, Whittleston D, Coumou D, Francis J, Dethloff K, Entekhabi D, Overland J, Jones J (2014) Recent Arctic amplification and extreme mid-latitude weather. *Nat Geoscience* 7(9):627–637, <https://doi.org/10.1038/ngeo2234>
- Cohen J, Zhang X, Francis J, Jung T, Kwok R, Overland J, Ballinger TJ, Bhatt US, Chen HW, Coumou D, Feldstein S, Gu H, Handorf D, Henderson G, Ionita M, Kretschmer M, Laliberte F, Lee S, Linderholm HW, Maslowski W, Peings Y, Pfeiffer K, Rigor I, Semmler T, Stroeve J, Taylor PC, Vavrus S, Vihma T, Wang S, Wendisch M, Wu Y, Yoon J (2020) Divergent consensus on Arctic amplification influence on midlatitude severe winter weather. *Nat Clim Change* 10:20–29, <https://doi.org/10.1038/s41558-019-0662-y>
- Dahlke S, Hughes NE, Wagner PM, Gerland S, Wawrzyniak T, Ivanov B, Maturilli M (2020) The observed recent surface air temperature development across Svalbard and concurring footprints in local sea ice cover. *Int J Climatol* 40(12):5246–5265, <https://doi.org/10.1002/joc.6517>
- Ding M, Wang S, Sun W (2018) Decadal Climate Change in Ny-Ålesund, Svalbard, A Representative Area of the Arctic. *Condensed Matter* 3(2):12, <https://doi.org/10.3390/condmat3020012>
- Doyle JG, Lesins G, Thackray CP, Perro C, Nott GJ, Duck TJ, Damoah R, Drummond JR (2011) Water vapor intrusions into the High Arctic during winter. *Geophys Res Lett* 38(12):L12806, <https://doi.org/10.1029/2011GL047493>
- Eyring V, Bony S, Meehl GA, Senior CA, Stevens B, Stouffer RJ, Taylor KE (2016) Overview of the Coupled Model Intercomparison Project Phase 6 (CMIP6) experimental design and organization. *GMD* 9(5):1937–1958, <https://doi.org/10.5194/gmd-9-1937-2016>
- Eyring V, Flato G, Meehl J, Senior C, Stevens B, Stouffer R, Taylor K (2018) Overview of the Coupled Model Intercomparison Project Phase 6 (CMIP6) Experimental Design and Organization. https://www.wcrp-climate.org/images/modelling/WGCM/CMIP/CMIP6FinalDesign_GMD_180329.pdf, accessed: 2020–11-13
- Flynn CM, Mauritsen T (2020) On the climate sensitivity and historical warming evolution in recent coupled model ensembles. *Atmos Chem Phys* 20(13):7829–7842, <https://doi.org/10.5194/acp-20-7829-2020>
- Førland EJ, Benestad R, Hanssen-Bauer I, Haugen JE, Skaugen TE (2011) Temperature and precipitation development at Svalbard 1900–2100. *Adv Meteorol* 2011, <https://doi.org/10.1155/2011/893790>
- Freud E, Krejci R, Tunved P, Leaitch R, Nguyen QT, Massling A, Skov H, Barrie L (2017) Pan-Arctic aerosol number size distributions: seasonality and transport patterns. *Atmos Chem Phys* 17(13):8101–8128, <https://doi.org/10.5194/acp-17-8101-2017>
- Gerland S, Pavlova O, Divine D, Negrel J, Dahlke S, Johansson AM, Maturilli M, Semmling M (2020) Long-term monitoring of landfast sea-ice extent and thickness in Kongsfjorden, and related applications (FastIce). In: Van den Heuvel et al. (eds): SESS report 2019, Svalbard Integrated Arctic Earth Observing System, Longyearbyen, pp 160–167. https://sios-svalbard.org/SESS_Issue2

- Gilardoni S, Lupi A, Mazzola M, Cappelletti DM, Moroni B, Ferrero L, Markuszewski P, Rozwadowska A, Krecji R, Zieger P, Tunved P, Karlsson L, Vratolis S, Eleftheriadis K, Viola AP (2020) Atmospheric black carbon in Svalbard. In: Van den Heuvel et al. (eds): SESS report 2019, Svalbard Integrated Arctic Earth Observing System, Longyearbyen, pp 196–211. https://sios-svalbard.org/SESS_Issue2
- Graff LS, Iversen T, Bethke I, Debernard JB, Seland Ø, Bentsen M, Kirkevåg A, Li C, Olivie DJL (2019) Arctic amplification under global warming of 1.5 and 2°C in NorESM1-Happi. *ESD* 10(3):569–598, <https://doi.org/10.5194/esd-10-569-2019>
- Hanssen-Bauer I, Førland E, Hisdal H, Mayer S, AB S, Sorteberg A (2019) Climate in Svalbard 2100. A knowledge base for climate adaptation
- Hartmann D, Tank A, Rusticucci M, Alexander L, Brönnimann S, Charabi Y, Dentener F, Dlugokencky E, Easterling D, Kaplan A, et al. (2013) Observations: Atmosphere and surface: Climate Change 2013 the Physical Science Basis: Working Group I Contribution to the Fifth Assessment Report of the Intergovernmental Panel on Climate Change. Cambridge University Press p 159
- Held IM, Soden BJ (2006) Robust Responses of the Hydrological Cycle to Global Warming. *J Clim* 19(21):5686–5699, <https://doi.org/10.1175/JCLI3990.1>
- Hussain M, Mahmud I (2019) pyMannKendall: a python package for non parametric Mann Kendall family of trend tests. *J Open Source Softw* 4(39):1556, <http://dx.doi.org/10.21105/joss.01556>
- Isaksen K, Nordli Ø, Førland EJ, Łupikasza E, Eastwood S, Niedźwiedz T (2016) Recent warming on Spitsbergen— influence of atmospheric circulation and sea ice cover. *J Geophys Res: Atmos* 121(20):11,913–11,931, <https://doi.org/10.1002/2016JD025606>
- Karlin S (1983) quote from the 11th R. A. Fisher Memorial Lecture at the Royal Society of London on 20 April 1983
- Kendall M (1975) Rank correlation methods (4th edn.) Charles Griffin. San Francisco, CA 8
- Killie MA, Aaboe S, Isaksen K, Van Pelt W, Pedersen ÅØ, Luks B (2021) Svalbard snow and sea-ice cover: comparing satellite data, on-site measurements, and modelling results. In: Moreno-Ibáñez et al (eds) SESS report 2020, Svalbard Integrated Arctic Earth Observing System, Longyearbyen, pp 220-235. <https://doi.org/10.5281/zenodo.4293804>
- Kim KY, Kim JY, Kim J, Yeo S, Na H, Hamlington BD, Leben RR (2019) Vertical feedback mechanism of winter Arctic amplification and sea ice loss. *Sci Rep* 9(1):1–10, <https://doi.org/10.1038/s41598-018-38109-x>
- Kosaka Y, Xie SP (2013) Recent global-warming hiatus tied to equatorial Pacific surface cooling. *Nature* 501(7467):403–407, <https://doi.org/10.1038/nature12534>
- Lee S, Gong T, Feldstein SB, Screen JA, Simmonds I (2017) Revisiting the Cause of the 1989–2009 Arctic Surface Warming Using the Surface Energy Budget: Downward Infrared Radiation Dominates the Surface Fluxes. *Geophys Res Lett* 44(20):10,654–10,661, <https://doi.org/10.1002/2017GL075375>
- Liang YC, Kwon YO, Frankignoul C, Danabasoglu G, Yeager S, Cherchi A, Gao Y, Gastineau G, Ghosh R, Matei D, Mecking JV, Peano D, Suo L, Tian T (2020) Quantification of the Arctic Sea Ice-Driven Atmospheric Circulation Variability in Coordinated Large Ensemble Simulations. *Geophys Res Lett* 47(1):e2019GL085397, <https://doi.org/10.1029/2019GL085397>
- Mahajan S, Zhang R, Delworth TL (2011) Impact of the Atlantic meridional overturning circulation (AMOC) on Arctic surface air temperature and sea ice variability. *J Clim* 24(24):6573–6581, <https://doi.org/10.1175/2011JCLI4002.1>
- Mann H (1945) Non-parametric tests against trend. *Econometrica* 13:245 – 259
- Mann HB, Whitney DR (1947) On a test of whether one of two random variables is stochastically larger than the other. *Ann Math Statist* 18(1):50–60, <https://doi.org/10.1214/aoms/1177730491>
- Medhaug I, Stolpe MB, Fischer EM, Knutti R (2017) Reconciling controversies about the 'global warming hiatus'. *Nature* 545(7652):41–47, <https://doi.org/10.1038/nature22315>
- Meier WN, Hovelsrud GK, van Oort BE, Key JR, Kovacs KM, Michel C, Haas C, Granskog MA, Gerland S, Perovich DK, Makshtas A, Reist JD (2014) Arctic sea ice in transformation: A review of recent observed changes and impacts on biology and human activity. *Rev Geophys* 52(3):185–217, <https://doi.org/10.1002/2013RG000431>
- Navarro JA, Varma V, Riipinen I, Seland Ø, Kirkeva g A, Struthers H, Iversen T, Hansson HC, Ekman AM (2016) Amplification of Arctic warming by past air pollution reductions in Europe. *Nat Geoscience* 9(4):277–281, <https://doi.org/10.1038/ngeo2673>
- Nordli Ø, Wyszynski P, Gjeltén HM, Isaksen K, Łupikasza E, Niedźwiedz T, Przybylak R (2020) Revisiting the extended Svalbard Airport monthly temperature series, and the compiled corresponding daily series 1898–2018. *Polar Res* 39, <https://doi.org/10.33265/polar.v39.3614>
- Notz D, Marotzke J (2012) Observations reveal external driver for Arctic sea-ice retreat. *Geophys Res Lett* 39(8):L08502, <https://doi.org/10.1029/2012GL051094>, L08502
- Nummelin A, Li C, Hezel PJ (2017) Connecting ocean heat transport changes from the midlatitudes to the Arctic Ocean. *Geophys Res Lett* 44(4):1899–1908, <https://doi.org/10.1002/2016GL071333>

- O'Neill BC, Tebaldi C, van Vuuren DP, Eyring V, Friedlingstein P, Hurtt G, Knutti R, Kriegler E, Lamarque JF, Lowe J, Meehl GA, Moss R, Riahi K, Sanderson BM (2016) The Scenario Model Intercomparison Project (ScenarioMIP) for CMIP6. *GMD* 9(9):3461–3482, <https://doi.org/10.5194/gmd-9-3461-2016>
- Pithan F, Mauritsen T (2014) Arctic amplification dominated by temperature feedbacks in contemporary climate models. *Nat Geoscience* 7(3):181–184, <https://doi.org/10.1038/NNGEO2071>
- Sand M, Berntsen TK, Seland Ø, Kristjánsson JE (2013) Arctic surface temperature change to emissions of black carbon within Arctic or midlatitudes. *J Geophys Res: Atmos* 118(14):7788–7798, <https://doi.org/10.1002/jgrd.50613>
- Schmeisser L, Backman J, Ogren JA, Andrews E, Asmi E, Starkweather S, Uttal T, Fiebig M, Sharma S, Eleftheriadis K, et al. (2018) Seasonality of aerosol optical properties in the Arctic. *Atmos Chem Phys* 18(16):11599–11622, <https://dx.doi.org/10.5194/acp-18-11599-2018>
- Screen JA, Blackport R (2019) How Robust is the Atmospheric Response to Projected Arctic Sea Ice Loss Across Climate Models? *Geophys Res Lett* 46(20):11406–11415, <http://doi.org/10.1029/2019GL084936>
- Screen JA, Simmonds I (2010) The central role of diminishing sea ice in recent Arctic temperature amplification. *Nature* 464(7293):1334–1337, <https://doi.org/10.1038/nature09051>
- Serreze M, Barrett A, Stroeve J, Kindig D, Holland M (2009) The emergence of surface-based arctic amplification. *The Cryosphere* 3(1):11
- Serreze MC, Barry RG (2011) Processes and impacts of arctic amplification: A research synthesis. *Glob Planet Change* 77(1):85 – 96, <https://doi.org/10.1016/j.gloplacha.2011.03.004>
- Serreze MC, Barrett AP, Stroeve J (2012) Recent changes in tropospheric water vapor over the Arctic as assessed from radiosondes and atmospheric reanalyses. *J Geophys Res: Atmos* 117(D10):D10104, <https://doi.org/10.1029/2011JD017421>
- Shaw TA, Baldwin M, Barnes EA, Caballero R, Garfinkel CI, Hwang YT, Li C, O'Gorman PA, Rivière G, Simpson IR, Voigt A (2016) Storm track processes and the opposing influences of climate change. *Nat Geoscience* 9:656–664, <http://dx.doi.org/10.1038/ngeo2783>
- Shu Q, Wang Q, Song Z, Qiao F, Zhao J, Chu M, Li X (2020) Assessment of Sea-ice extent in CMIP6 With Comparison to Observations and CMIP5. *Geophys Res Lett* 47(9):e2020GL087965, <https://doi.org/10.1029/2020GL087965>
- Simpkins G (2017) Snapshot: Extreme Arctic heat. *Nat Clim Change* 7(2):95–95, <https://doi.org/10.1038/nclimate3213>
- Smith DM, Screen JA, Deser C, Cohen J, Fyfe JC, Garcia-Serrano J, Jung T, Kattsov V, Matei D, Msadek R, Peings Y, Sigmond M, Ukita J, Yoon JH, Zhang X (2019) The Polar Amplification Model Intercomparison Project (PAMIP) contribution to CMIP6: investigating the causes and consequences of polar amplification. *GMD* 12(3):1139–1164, <https://doi.org/10.5194/gmd-12-1139-2019>
- Sipilä M, Hoppe CJM, Viola A, Mazzola M, Krejci R, Zieger P, Beck L, Petäjä T (2020) Multidisciplinary research on biogenically driven new particle formation in Svalbard. In: Van den Heuvel et al. (eds): SESS report 2019, Svalbard Integrated Arctic Earth Observing System, Longyearbyen, pp 168–195. https://sios-svalbard.org/SESS_Issue2
- Stroeve J, Notz D (2018) Changing state of Arctic sea ice across all seasons. *Environ Res Lett* 13(10):103001, <https://doi.org/10.1088/1748-9326/aade56>
- Traversi R, Becagli S, Severi M, Caiazzo L, Mazzola M, Lupi A, Fiebig M, Hermansen O, Krejci R (2021) Arctic haze in a climate changing world: the 2010-2020 trend. In: Moreno-Ibáñez et al (eds) SESS report 2020, Svalbard Integrated Arctic Earth Observing System, Longyearbyen, pp 104-117. <https://doi.org/10.5281/zenodo.4293826>
- Winton M (2011) Do Climate Models Underestimate the Sensitivity of Northern Hemisphere Sea Ice Cover? *J Clim* 24(15):3924–3934, <https://doi.org/10.1175/2011JCLI4146.1>
- Zhang X, Sorteberg A, Zhang J, Gerdes R, Comiso JC (2008) Recent radical shifts of atmospheric circulations and rapid changes in Arctic climate system. *Geophys Res Lett* 35(22):L22701, <https://doi.org/10.1029/2008GL035607>
- Zhang X, He J, Zhang J, Polyakov I, Gerdes R, Inoue J, Wu P (2013) Enhanced poleward moisture transport and amplified northern high-latitude wetting trend. *Nat Clim Change* 3(1):47–51, <https://doi.org/10.1038/nclimate1631>

Space physics in Svalbard: A study of the energy input in the polar ionosphere using SuperDARN

Lisa Baddeley^{1,2}, Emma Bland¹, Dag A. Lorentzen^{1,2}, Katie Herlingshaw^{1,2}, Lasse B. N. Clausen³, Wojciech Miloch³, Kathryn McWilliams⁴, Akira Sessai Yukimatu⁵

1 University Centre in Svalbard, Longyearbyen, Norway

2 Birkeland Centre for Space Studies, University of Bergen, Norway

3 Department of Physics, University of Oslo, Norway

4 Institute of Space & Atmospheric Studies, Department of Physics & Engineering Physics, University of Saskatchewan, Saskatoon, Canada

5 National Institute of Polar Research, Tokyo, Japan

Corresponding author: Lisa Baddeley, Lisa.Baddeley@unis.no

ORCID number 0000-0003-1246-0488

Keywords: Ionosphere, space physics, radar, space weather, aurora

DOI: <https://doi.org/10.5281/zenodo.4293796>

1. Introduction

At approximately 08:00–12:00 local time each day, Svalbard passes through a narrow, funnel-shaped region of the Earth’s magnetic field known as the “cusp”. This region channels charged particles from the Sun into the Earth’s upper atmosphere, producing auroral displays which can be observed from Svalbard during the polar night. The long polar night and the availability of supporting infrastructure make Svalbard the only place on Earth where it is both possible and practical to study the cusp from the ground. It is also an ideal location for observing a wide range of other high-latitude magnetospheric and upper atmospheric processes driven by solar activity. Svalbard has therefore been the focus of major investments in space physics research infrastructure, both from Norway and abroad, over several decades.

The major Norwegian investments in space physics research infrastructure in Svalbard are as follows:

- The Kjell Henriksen Observatory (KHO), the world’s largest optical observatory for auroral and middle atmospheric studies, with 34 instruments, located on Breinosa about 12 km southeast of Longyearbyen;
- Svalrak, a rocket range owned by the Andøya Space Centre, located in Ny-Ålesund;
- The European Incoherent Scatter (EISCAT) Svalbard Radar, located on Breinosa. This radar provides measurements of temperatures, densities and velocities of particles in the upper and middle atmosphere over and around Svalbard.

A recent addition to Svalbard’s space physics research infrastructure is the Svalbard SuperDARN Radar, located on Breinosa near the KHO and EISCAT facilities. SuperDARN (Super Dual Auroral Radar Network) is an international network of more than 30 high frequency (HF) radars designed for studying high-latitude plasma convection driven by interactions between the magnetic fields of the Sun and the Earth (Greenwald et al. 1995; Chisham et al. 2007; Nishitani et al. 2019). The Svalbard

SuperDARN radar fills an important gap in the spatial coverage of SuperDARN and complements the local optical and radio observations from KHO and EISCAT. SuperDARN is operated by researchers from 10 countries and is often cited as a prime example of successful international scientific collaboration (Greenwald 2017). Collectively, the SuperDARN radars provide coordinated observations of global-scale plasma structures and dynamics, whilst individually providing observations of mesoscale (100–500 km) processes and turbulence.

1.1. Energy transfer from space to the upper polar atmosphere

The vast majority of near-Earth space physics phenomena derive their energy from the Sun through a wide range of coupling mechanisms. In addition to light, the Sun emits a stream of ionised energetic particles called the solar wind, which also carries with it the solar or interplanetary magnetic field (IMF). The Earth is protected from the solar wind and the IMF by its own magnetic field; thus, most of the solar wind is deflected around the Earth. At the dayside magnetopause, the IMF and the Earth’s magnetic field can connect (through a process called magnetic reconnection), forming a gateway between the two systems which channels particles and energy directly into the Earth’s upper atmosphere. This process is illustrated in Figure 1. The IMF connects with the Earth’s magnetic field at the magnetopause, forming an ‘open’ field line configuration over the polar regions. One visible consequence of this process is the dayside aurora, which occurs when the solar wind particles collide with atmospheric nitrogen and oxygen in the cusp. The polar cusp in each hemisphere forms at the point where the field lines first become ‘open’ to the IMF, and it is the footprint of this region where the ‘dayside’ aurora can be observed (Figure 1, inset).

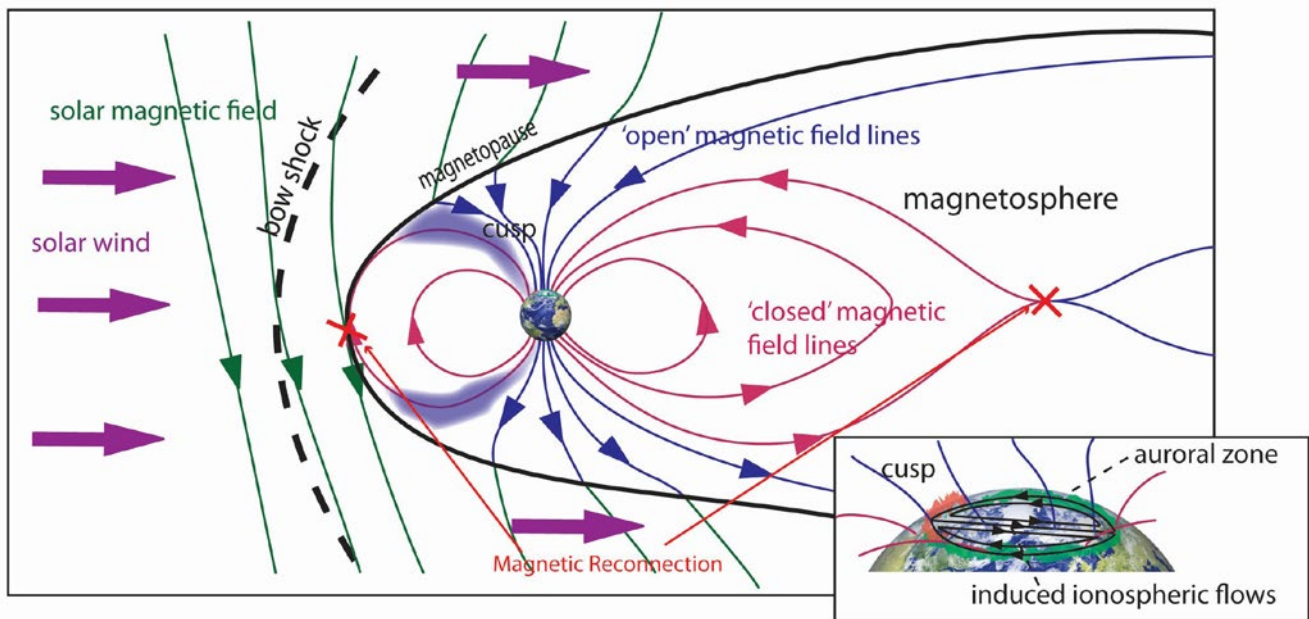


Figure 1: Interaction between the solar magnetic field and the Earth's magnetic field, which drives the ionospheric convection measured by SuperDARN radars.

In addition to providing this gateway for particles, the solar wind flow drags the open magnetic field lines across the polar regions, from the dayside to the nightside. Once on the nightside, these field lines sink into the magnetosphere where they reconnect, forming closed loops between the two hemispheres. The act of closing these field lines transfers energy and momentum from the solar wind into the magnetosphere, which drives auroral activity on the night side of the Earth (Figure 1, inset). Once closed, the field lines convect around the flanks of the magnetosphere to the dayside and the process repeats. This process of opening, convecting and closing of field lines, known as the Dungey cycle (Dungey 1961), sets up large-scale horizontal velocity flows up to 2 km/s over the polar regions, which can be measured by SuperDARN radars at around 250 km altitude (F region ionosphere). The direction, speed and turbulent nature of these ionospheric flows are controlled by the interaction with the IMF. These

processes also induce large horizontal current systems in the 90–120km altitude range (E region ionosphere), dissipating energy into the neutral atmosphere through Joule heating or frictional heating processes (Brekke 2013). Collisional heating and turbulence associated with various auroral processes also serve to dissipate energy into the system (e.g. Frey et al. 2019; Hosokawa et al. 2019). Joule heating and particle precipitation account for 22% of the total global upper atmospheric energy budget, and in cases of extreme solar wind driving, the energy contribution from Joule heating can exceed the energy input from solar UV (Knipp et al. 2005). The coupled solar wind-magnetosphere-ionosphere system thus acts to direct energy into the high latitude atmosphere through a wide variety of processes and over a range of temporal and spatial scales. The term 'space weather' is often used to describe disturbances in this system that may impact technology and infrastructure.

1.2. Space physics research infrastructure on Svalbard

Due to its vast size, it is not possible to monitor the entirety of the Earth's magnetosphere in-situ. However, the outer magnetosphere maps into a relatively small region of the ionosphere at polar and auroral latitudes along the geomagnetic field lines. Magnetospheric processes can therefore be studied by monitoring their footprints in the ionosphere. The signatures of the ionospheric energy deposition assume many different forms; hence, the vast majority of studies must combine data from many types of instrumentation. Moreover, radio instruments such as radars can sometimes be used in place of traditional optical instrumentation during periods of daylight or cloud cover to construct a continuous dataset. Svalbard's extensive research infrastructure and unique location under the cusp make it a world-class location for ground-based remote sensing of the cusp and polar atmosphere using this multi-instrument complementary approach.

In addition to the Kjell Henriksen Observatory and the EISCAT facilities at Breinosa, Norwegian research institutes operate a wide variety of space physics instruments elsewhere in Svalbard. These include cameras, photometers, ground magnetometers and GNSS receiver stations in Ny Ålesund and Hornsund; an ionosonde, meteor radar and mesospheric radar (SOUSY) in Adventdalen and a riometer in Ny Ålesund. A full list of the

current Norway-owned instrumentation and the instrumentation that Norwegian researchers have direct access to through ongoing collaborations is provided in Table 1. A more detailed list of the international instrumentation at the KHO is available on the KHO webpage¹.

Other countries with relevant research infrastructure in Svalbard (either individually or through collaboration) include China, Japan, UK, Sweden, Finland, Denmark, the USA, South Korea, France, Russia, Italy, Ukraine and Poland. Five of these countries (China, Japan, the UK, Italy and the USA) also operate SuperDARN radars. Many of these countries collaborate through data sharing or focused experimental campaigns.

To obtain a detailed understanding of the system and, more importantly, to be able to model and predict the atmospheric responses to external forcing over the long term, consistent, complementary datasets are required. Datasets from Svalbard represent some of the longest time series of measurements of ionospheric processes in the world. These include mesospheric temperature measurements (1980–present), auroral camera observations (1978–present) and EISCAT radar observations (1997–present). The recent addition of the Svalbard SuperDARN radar marks a new era of complementary, long-term and continuous monitoring of the polar atmosphere and cusp by an HF system, joining the global database of SuperDARN observations that stretches over 25 years.

¹ http://kho.unis.no/nordlysstasjon_instr.htm

Table 1: Norwegian owned instrument or instruments to which Norway has direct access (e.g. EISCAT)

Instrument	Parameters	Period	Location	Metadata/Data access	Data provider	Category
Svalbard SuperDARN radar	F-region convection velocity and dynamics, HF absorption, mesoscale processes and turbulence	Nov 2016–Oct 2018, early 2021 -	Breirosa	<p> https://www.bas.ac.uk/project/superdarn/#data. </p>	UNIS	Radars
HF Doppler transmitter/receiver	Horizontal ionospheric velocity	Aug 2020–present	Hornsund/Breirosa	<p> https://www.bas.ac.uk/project/superdarn/#data. </p>	UNIS	Radars
Dynasonde	Electron density profile	May 2020–present	Breirosa	<p> http://kho.unis.no/ionosonde/index.html </p>	UNIS/UIT	Radars
SOUSY radar	Middle atmosphere structure and turbulence	2001–present	Adventdalen	<p> http://kho.unis.no/ionosonde/index.html </p>	UIT	Radars
Riometer	Cosmic noise absorption	2013–present, Dec 2020 - present	Ny Ålesund Adventdalen	<p> http://kho.unis.no/ionosonde/index.html </p>	UIT/ TGO TGO/UNIS	Radars
Meteor radar	Mesospheric velocity	April 2019–present	Adventdalen	<p> http://kho.unis.no/ionosonde/index.html </p>	UIT/ TGO	Radars
EISCAT radar	Ionospheric density, temperatures and velocities (E and F region)	1997–present	Breirosa	<p> http://portal.eiscat.se/madrigal/ </p>	EISCAT	Radars
7 all-sky cameras	Auroral and airglow: morphology, emission intensity, mesospheric studies	Variable depending on instrument (~5 years to 20 years, winter season)	KHO	<p> http://kho.unis.no/keograms/keograms.php </p>	UNIS	Optical
3 all-sky cameras	Emission intensity, auroral morphology	Ny Ålesund: 1997–present, Hornsund: 2019–present, KHO: 1996–present	Ny Ålesund, Hornsund, KHO	<p> http://tid.uio.no/plasma/aurora/ </p>	UiO	Optical

4 spectrometers	Spectral emission intensities, mesospheric temperatures, particle precipitation energies	Variable depending on instrument (~5 years to 40 years, winter season)	KHO	http://kho.unis.no/Keograms/keograms.php	UNIS / U of Alaska / UiT	Optical
2 photometers	Open-closed boundary, particle boundaries, auroral morphology	Variable depending on instrument (~5 years to 20 years, winter season)	KHO	http://kho.unis.no/Keograms/keograms.php	UNIS / U of Alaska	Optical
4 fluxgate magnetometers	Magnetic field motion, waves	KHO: 1993–present, Ny Ålesund: 1980–present, Hopen: 1988–present, Bjornøya: 1997–present	Ny Ålesund, KHO, Hopen, Bjornøya	RiS: 6083 https://flux.phys.uio.no/geomag.html	UiT / TGO	Others
GNSS scintillation receivers	Total electron content, scintillation of GNSS signals	Ny Ålesund: 2009–present, Hornsund: 2018–present	Ny Ålesund, Hornsund	RiS: 10977 http://tid.uio.no/plasma/gps/	UiO	Others
GNSS scintillation receivers	Total electron content, scintillation of GNSS signals	2013–present	Ny Ålesund, KHO, Bjornøya, Hopen	https://site.uio.no/spaceweather/data-and-products/ionospheric-conditions/ionospheric-scintillation/	UiB	Others
SvalIRAK	Rocket, in-situ ionospheric measurements	1997–present	Ny Ålesund	RiS: 10620	Andøya Space Centre	Others

2. Ionospheric and upper atmospheric research using SuperDARN HF radars

SuperDARN radars have provided invaluable knowledge about the large-scale structure and dynamics of the ionospheric convection, energy transfer processes and mesoscale structures over several decades. In the polar cap and auroral zones, including over Svalbard, significant attention has been accorded to determining the location of the boundary between open and closed magnetic field lines using SuperDARN and comparing the results to the optical signature of this boundary (e.g. Chisham et al. 2004; Imber et al. 2013; Chen et al. 2015). The radars have also been used for performing high spatial resolution observations of small-scale velocity features within the large-scale convection pattern (e.g. Herlingshaw et al. 2019; Baddeley et al. 2007), patches of enhanced electron density (polar cap patches) that are transported through the polar caps within the background convection flow (Oksavik et al. 2006; Zhang et al. 2013; Fæhn Follestad et al. 2019) and estimations of Joule heating rates (Billet et al. 2020; Kiene et al. 2018).

In addition to the above applications, focused primarily on the F-region ionosphere, SuperDARN data have also been used in studies focused on E-region structures, such as nightside auroral arcs (e.g. Hosokawa et al. 2010) and large-scale atmospheric tidal motions at 100 km altitude (e.g. van Caspel et al. 2020). Some recent studies have also used SuperDARN data to validate atmospheric and climate modelling results (Hibbins et al. 2019) or develop improved inputs for these models (Bland

et al. 2019, 2020). The SuperDARN radars are therefore highly versatile research tools which can be used to address a wide range of topics in upper and middle atmospheric physics.

2.1. The Svalbard SuperDARN radar (2016–2018)

The Svalbard SuperDARN radar is part of a global network of more than 30 HF radars used for studying the structure and dynamics of the Earth's ionosphere. The SuperDARN network began over 25 years ago. The Svalbard radar was added to the network in 2016 to fill a spatial coverage gap in the cusp and polar cap ionosphere. The field of view of the Svalbard radar is shown in Figure 2 (red shading), along with the fields of view of the other SuperDARN radars in each hemisphere. Each field of view covers an azimuthal sector of at least 52° and extends to over 3500 km in range. Two radars located in Finland and Iceland provide coverage over Svalbard (grey shading), and the data from these radars have been used extensively in studies of cusp and auroral phenomena together with KHO, EISCAT and sounding rocket instrumentation (e.g. Lorentzen et al. 2010; Moen et al. 2012; Oksavik et al. 2012; Chen et al. 2015). These two radars, however, were decommissioned in 2018 and 2019 after more than 20 years of operation. The research groups who are responsible for these radars have obtained funding to refit both radar systems, and it is hoped that they will resume operations in 2022.

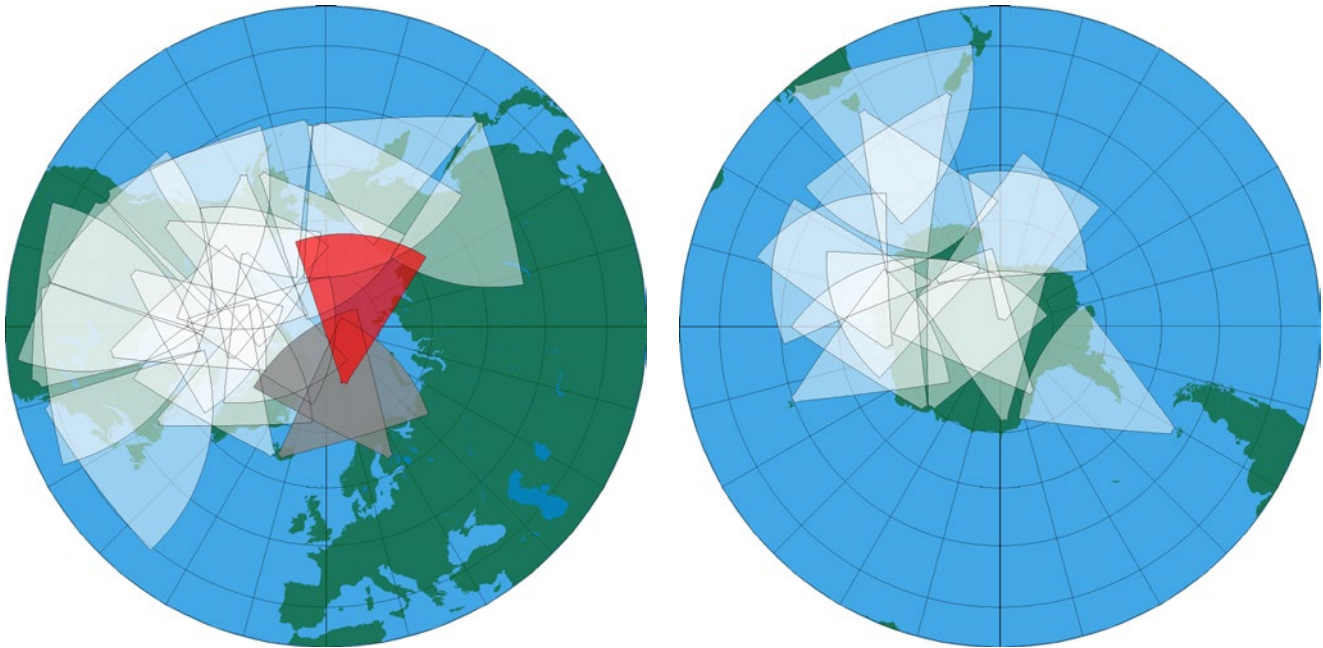


Figure 2: Fields of view of the SuperDARN radars in the northern hemisphere (left) and southern hemisphere (right). The Svalbard SuperDARN radar field of view is shaded red. The two radars in Finland and Iceland that provide coverage over Svalbard are shaded grey.

Funding for the Svalbard SuperDARN radar was obtained by the research group at the University Centre in Svalbard (UNIS) in 2012 through the ConocoPhillips/Lundin High North Research Program.² This radar is located on Breinosa alongside the EISCAT Svalbard Radar and the KHO and is Norway's first SuperDARN radar. Working with an externally employed company, MultiConsult, planning permission was granted on 13 May 2014. Two research groups were brought onboard for the construction phase of the project: the Radio and Space Plasma Physics Group at the University of Leicester (UoL), UK, and the Institute for Space and Atmospheric Studies at the University of Saskatchewan (UoS), Canada. The UoL group designed and built the radar electronics and transmitter elements. They have also built several other SuperDARN radars and operated two of the radars in Iceland and Finland. The UoS group designed and built the radar antenna units and masts. This group has designed several such structures and operates five SuperDARN radars across Northern Canada.

Due to the sensitive nature of the Arctic tundra, all elements of the radar had to be mounted on top of wooden posts driven into the tundra. This ensured minimal environmental impact since no

elements would lie directly on the tundra. To limit environmental impact during the construction phase, the antenna masts were erected by hand by a crew of 10 people from UNIS, UoL and UoS during the summer of 2015. The radar consists of the following 3 elements: a main transmitter array of 18 antenna masts, an interferometer array of six antenna masts placed 100 m behind the main array and a 20 ft shipping container which houses the transmitters and other electronics. After an initial commissioning and testing phase, the radar officially became part of the SuperDARN network in October 2016.

The radar operated continuously until October 2018, when an unusual storm caused heavy icing on both antenna arrays. The storm brought sustained periods of strong winds, snow and supercooled rain. The icing created a total mass loading on the system of 1.6 kg/m, resulting in over 10 tonnes of additional weight on the antenna masts, which caused significant irreparable damage. Following this incident, a climate load report was commissioned from Kjeller Vindteknikk, which outlined the ice and wind loads during the incident and provided recommendations for a new mast design that would be able to withstand a 'once in 50 years' storm with a mass loading up to 6 kg/m.

² http://static.conocophillips.com/files/resources/arctic_approach.pdf

Norconsult was then commissioned to design new masts for the Svalbard SuperDARN radar, given the recommended climate loads. The new masts have been constructed from a durable, corrosion-resistant aluminium alloy and include top plates, custom-made foundation base plates, guy rope brackets and other accessories. The masts have been delivered to Svalbard and the new Svalbard SuperDARN radar will be operational from 2021.

2.2. SuperDARN: A global network

Collectively, SuperDARN performs coordinated observations of the large-scale plasma convection driven by the Dungey cycle. Although there are minor differences in hardware across the network, the radars produce identical data products which can be readily combined into maps of global convection. The radars have no moving parts, allowing them to operate continuously and autonomously with relatively little maintenance. The SuperDARN radars typically have 16 beams (pointing directions), which are scanned

sequentially to sample the entire field of view. The temporal resolution of a complete scan is either 1 or 2 minutes in a standard operating mode, and the standard range (radial) resolution is 45 km. Once transmitted, the radiowaves are modified and refracted by the ionosphere towards the horizontal, where the amount of refraction is determined by the ionospheric electron density along the ray path. The transmitted radiowaves are reflected from decametre electron density irregularity structures in the ionosphere, as illustrated in Figure 3. They then return to the radar where they are analysed. These irregularities are created through a range of instability and turbulent processes in the ionosphere and move at the background convection velocity. If the electron density is sufficiently high, in addition to the ionospheric scatter close to the radar (0.5 hop propagation mode), the radiowaves may be refracted back to the ground (1-hop propagation mode). They can then also be forward-scattered up from the ground and can be scattered from the ionosphere at a much greater distance from the radar (1.5 hop propagation mode).

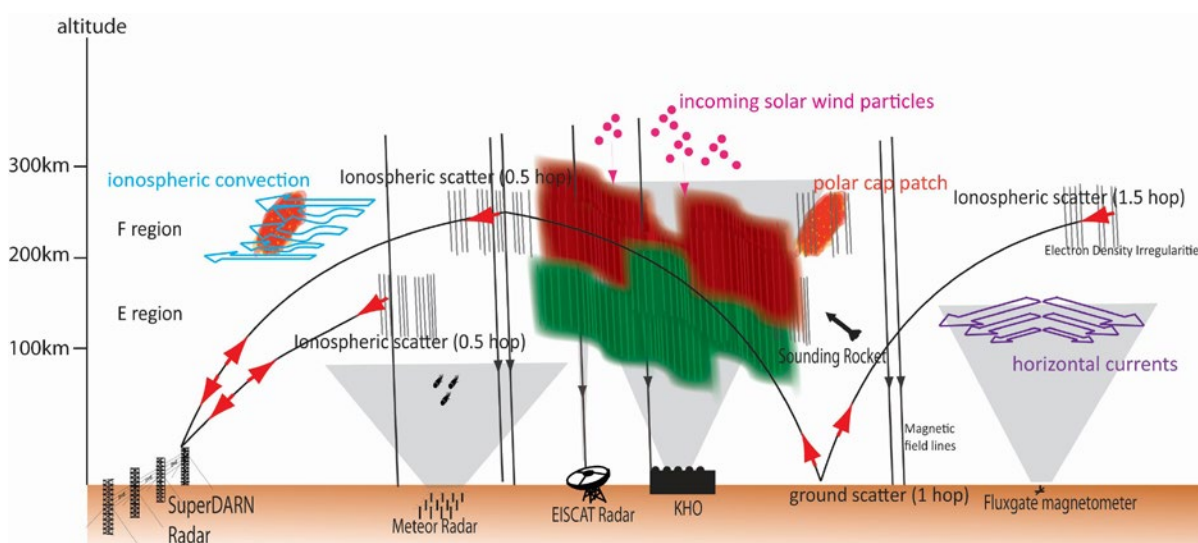


Figure 3: Illustration of space physics phenomena and the instrumentation used to study them from Svalbard.

The primary data products from the radars are the following: backscattered power, line-of-sight Doppler velocity and spectral width. The spectral width parameter is often used as an indicator of turbulence occurring within the scattering volume. Since a single radar can only measure the velocity component parallel to the beam direction, the network is designed with overlapping fields of view

so that the full horizontal velocity vector can be estimated by merging data from radars observing the same geographical area (Hanuise et al.1993; Cerisier and Senior 1994). Data from all radars are combined into a central database, using a grid of nearly equal-area grid cells measuring 1° in geomagnetic latitude, to produce global maps of the ionospheric F-region convection in each

hemisphere (Ruohoniemi and Baker 1995) at a spatial resolution of 1° latitude. Figure 4 shows the typical two-cell convection pattern driven by the Dungey cycle. The radar data are shown as coloured vectors, with the colour and length of the line relating to the magnitude of the flow according to the colour bar. The flow direction is clockwise in the dusk (left) convection cell and anticlockwise in the dawn (right) convection cell. In places where there are no data (i.e. inside the black circled area),

the modelled large-scale convection flow is denoted by black lines. The field of view of the Svalbard SuperDARN radar is also overlaid for reference with the red circle indicating data provided by the radar in an area to the north of Svalbard. In this example, the velocity vectors over Svalbard (LYR) are provided by the (currently non-operational) SuperDARN radar in Hankasalmi, Finland, with the Svalbard SuperDARN radar providing velocity measurements in an area northeast of Svalbard.

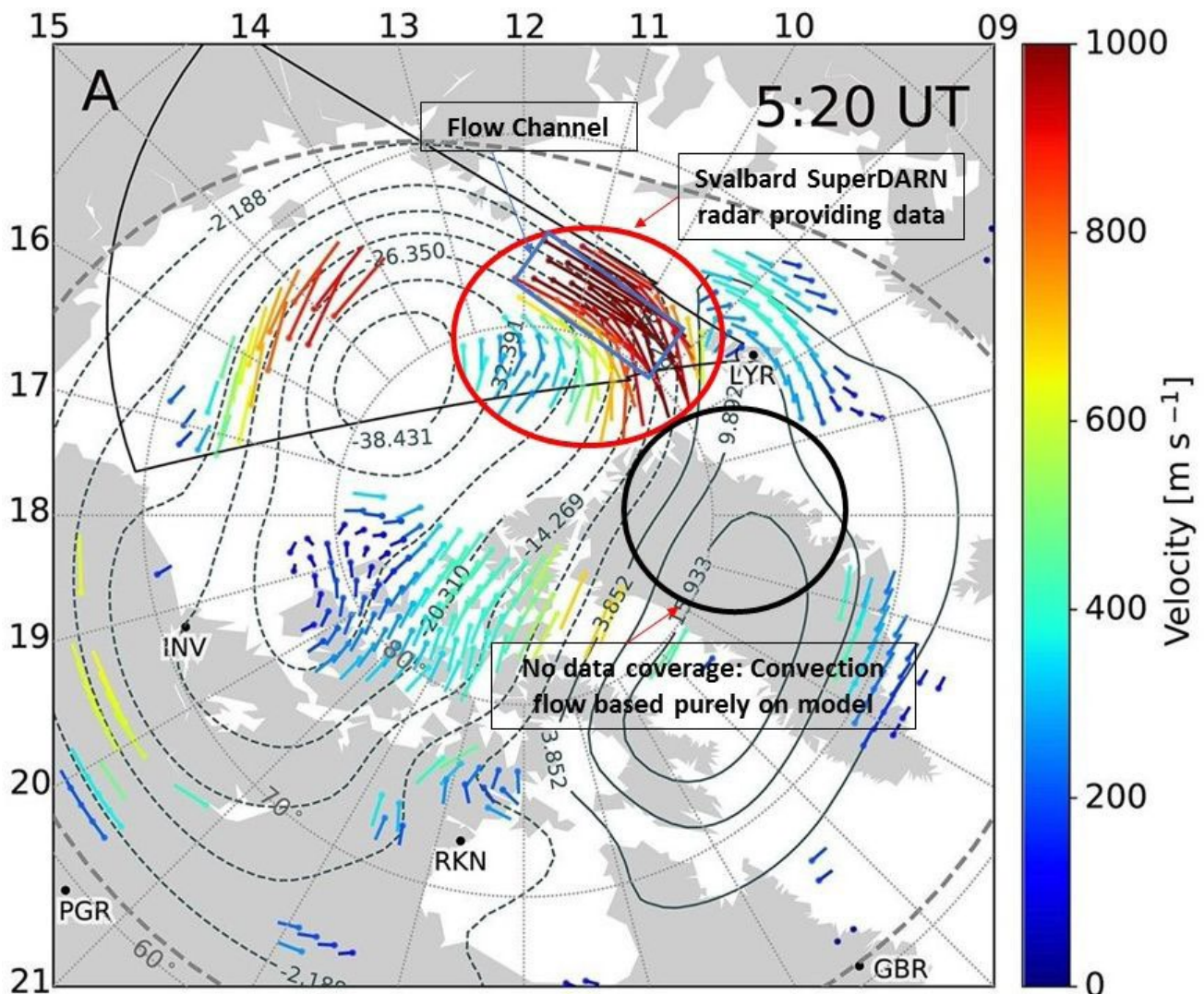


Figure 4: Ionospheric convection map produced from combined observations from the northern hemisphere SuperDARN radars. The Svalbard radar field of view (triangular region, also indicated in red in Figure 2) is shown for reference. The red circle indicates data provided by the Svalbard SuperDARN radar, to the north of Svalbard, and the blue box within that shows a plasma flow channel with velocities up to 1 km/s [Adapted from Herlingshaw et al. (2019)].

These global maps are used extensively across the space and ionospheric physics communities and are unrivalled in their ability to observe large-scale flows. However, there are some caveats. The available propagation modes limit the locations from which ionospheric backscatter can be detected;

thus, most of the data used to determine the convection are line-of-sight velocities from single radars, rather than merged velocity measurements from overlapping fields of view. In areas without any data coverage, the convection pattern is based purely on a model, which introduces a significant

source of error in the large-scale convection. Moreover, the spatial resolution of convection patterns determined using the standard method is unsuitable for studying mesoscale flows and turbulence, which are often under-represented in models of energy dissipation. Bristow et al. (2016) proposed an alternative method that enables the convection to be determined at the native spatial resolution of the radar (typically 45 km), providing

a more detailed representation of the mesoscale ionospheric flow. Expanding the network's spatial coverage by building new radars in strategically-chosen locations would provide a more accurate picture of the large-scale ionospheric convection and also offer new opportunities to study mesoscale structures in combination with other ground-based instrumentation.

3. Scientific highlights

Some examples are given below highlighting some applications of the Svalbard SuperDARN radar, both as a standalone instrument (providing detailed measurements of the cusp and mesoscale ionospheric structures) and as part of the global network of radars (providing observations of the polar cap and cusp for the convection maps in addition to allowing comparative studies with other radars in the network).

3.1. Daily and long-term observations

Figure 5 shows 24 hours of observations from the Svalbard SuperDARN radar, colour-coded according to the power of the returned signals and the Doppler velocity. Positive velocity values indicate plasma flow towards the radar, and negative velocities are directed away from the radar. The slant range (vertical axis) is the distance along the radiowave path to the ionospheric scattering target. Backscatter is detected almost continuously and covers 500–1000 km of range at any given time. The high-power and high-velocity backscatter observed at around 09:00 UT is indicative of the dayside cusp region, where the highly structured

irregularities scatter the radiowaves very efficiently.

A summary of the long-term observations from the radar is shown in Figure 6. These results cover the October 2016–October 2018 period and are divided according to season. In the F region ionosphere (top panel), the greatest amount of ionospheric backscatter was detected in the morning hours (~06:00UT/07:00 local time). This peak is higher in winter compared to summer. This result could be due to the highly structured irregularities in the wintertime cusp acting as efficient scattering targets for the radiowaves. A smaller secondary peak occurs at around 19:00 UT, which might be associated with auroral substorm activity. These findings are similar to those for other polar cap SuperDARN radars (Koustov et al. 2019). In the E region ionosphere (bottom panel), a morning sector peak is also present at around 06:00 UT, with a greater number of detections in the summer months. This may be attributed to the continuous ionisation by solar radiation during summer. Overall, the number of detections during each season is lower in the E region, which reflects its smaller vertical extent.

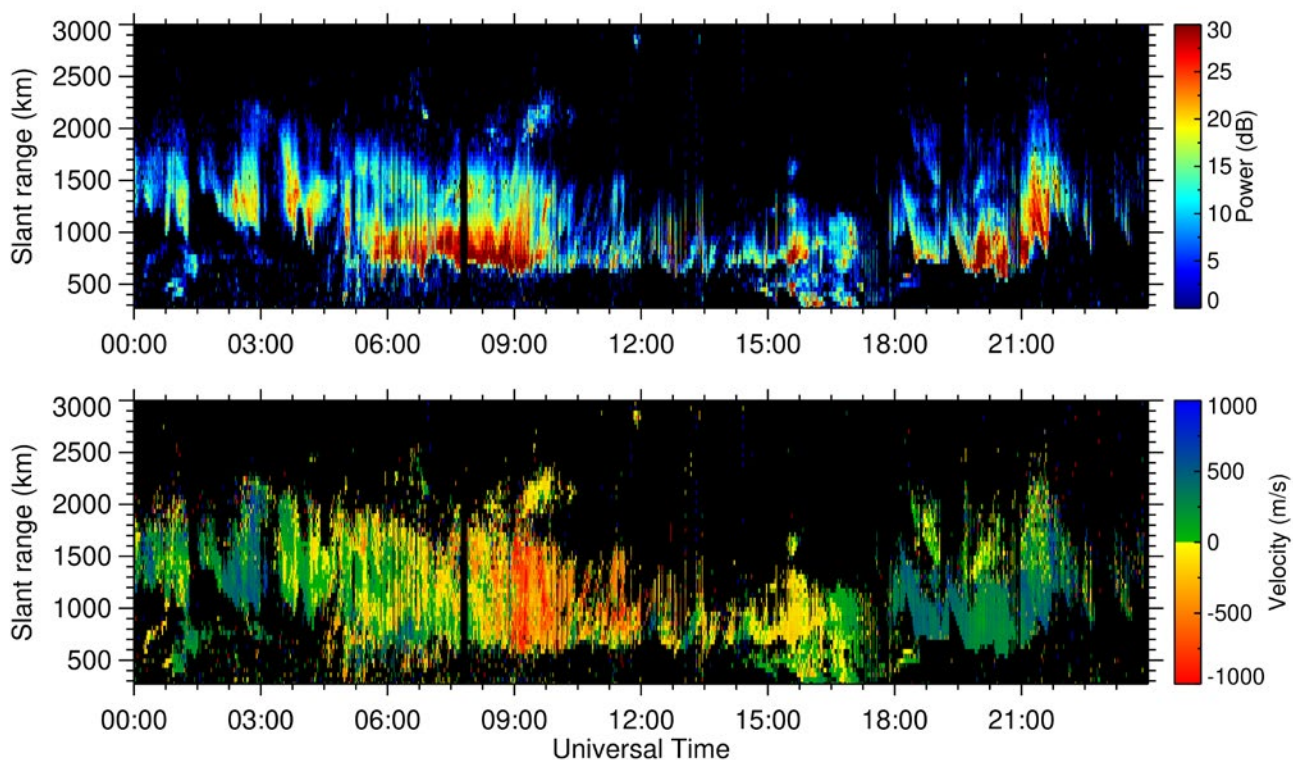


Figure 5: 24-hour summary plot from the Svalbard SuperDARN radar, showing the power of the received backscatter and the line-of-sight velocity measurements.

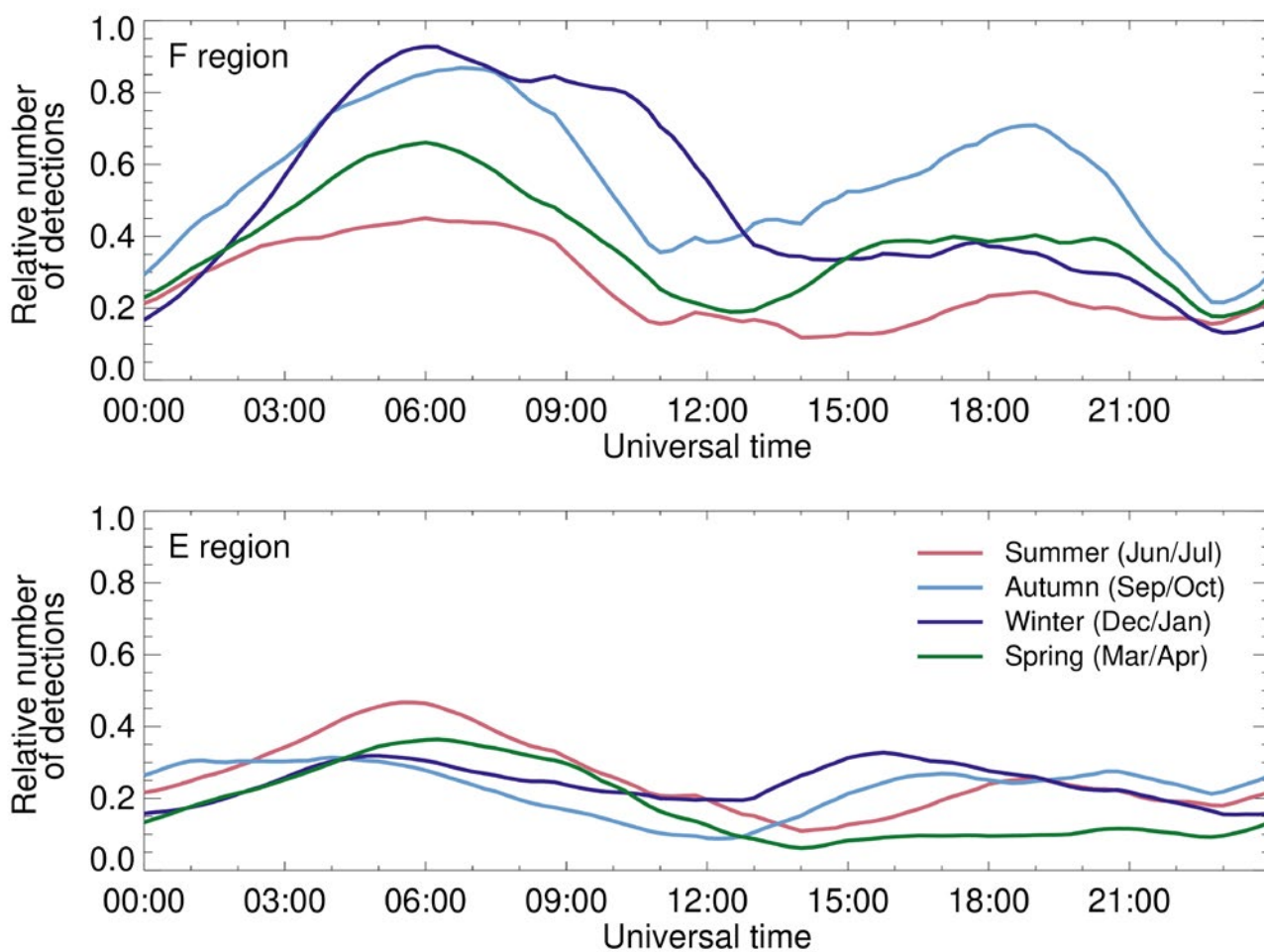


Figure 6: Seasonal and diurnal variations in E region and F region backscatter occurrence for the Svalbard SuperDARN radar, from October 2016 to October 2018.

3.2. Polar cap flow channels

As seen in Figure 5 (bottom panel), the flows in the polar cap ionosphere are highly dynamic both in magnitude and structure. Flow channels are defined as high-speed (>1 km/s) ionospheric flows embedded within the slower moving large-scale background convection and can be identified in SuperDARN radar data as narrow regions of enhanced plasma velocities within the field of view. A new algorithm has been developed to automatically detect these fast flows using the Svalbard SuperDARN radar. An example of a large flow channel identified by the algorithm in the Svalbard radar field of view is marked in a blue box in Figure 4. The flow region extends over 45 degrees in longitude, from Svalbard, across the Arctic Ocean. The proof of concept study (Herlingshaw 2019) indicated that even relatively small (400 km in width) short-lived (13 min) channels can provide a significant fraction (60%) of the total amount of open flux transported across the entire polar cap region by the Dungey cycle. The algorithm was used to perform a quantitative statistical analysis of over 1000 channels and investigate their relationship to the IMF orientation and solar wind conditions (Herlingshaw et al. 2020). This study showed that ~50% of detected flow channels are quite short-lived phenomena, lasting only 3 minutes or less and ranging from about 70 km to 650 km in width (often of a similar magnitude as the resolution of the large-scale convection maps). This work has highlighted the need for increased radar coverage of the polar regions if an accurate representation of the F-region ionosphere is to be obtained.

3.3. Polar cap patch formation and impact on GNSS

Ionospheric plasma irregularities, which SuperDARN radars rely on, impact also the propagation of trans-ionospheric radiowaves, such as Global Navigation Satellite System (GNSS) signals. In the polar cap, irregularities are mostly associated with polar cap patches which get highly structured by plasma instabilities when following the convection pattern and, in particular, when they enter the nightside aurora (Jin et al. 2014). Mitigation of their effects on GNSS signals can

be achieved through a forecast of polar cap patch formation, propagation and modelling of the associated GNSS signal disturbance. Fæhn Follestad et al. (2019) presented a new method to forecast space weather disturbances on GNSS at high latitudes, in which they describe the formation and propagation of polar cap patches and predict their arrival at the nightside aurora. The space weather prediction model incorporates an ionospheric convection model and total electron content (TEC) observations from the Global Positioning System (GPS) network. Fæhn Follestad et al. validated their new forecast by comparing its results to GPS global TEC observations from MIT's Madrigal database, ionospheric convection data from SuperDARN and scintillation data from instruments in Ny Ålesund. They were able to show that the model describes the polar cap patch motion effectively and can be used to predict scintillations of GPS signals at high latitudes. The dynamics of signal scintillations, which are the measure of trans-ionospheric radiowave perturbation, often agree with the plasma velocities deduced from the SuperDARN measurements. Thus, the radar data can be incorporated into both global and local models for the space weather effects on the GNSS signals and hence contribute to precise positioning services in the polar regions.

3.4. Space weather impact on radio communications

Energetic particles and solar X-ray flares cause increased ionisation of the lower ionosphere, leading to strong attenuation of HF radiowaves. This can impact the critical industries that rely on HF radio communications, including aviation, maritime, emergency services and defence (Redmon et al. 2018). Space weather events in September 2017 highlighted the capability of SuperDARN radars for monitoring these impacts in real-time. In the polar regions, energetic proton precipitation resulted in strong radiowave absorption which was detected by multiple SuperDARN radars over a period of 10 days (Bland et al. 2018). At the same time, the mid-latitude SuperDARN radars detected several shortwave fadeout events caused by ionisation by solar X-ray flares (Chakraborty et al. 2018). The absorption response measured by SuperDARN

near the peak of this space weather event is shown in Figure 7. Other recent work has shown that SuperDARN radars are sensitive enough to detect radiowave absorption caused by energetic electron precipitation (EEP) in the auroral zones, providing a new method for determining statistical occurrence rates and spatial coverage of EEP events (Bland et al. 2019, 2020). This information is being used to improve the energetic particle forcing used in climate models.

These results demonstrate that SuperDARN has the potential to support routine space weather monitoring efforts through the provision of real-time observations. In addition to monitoring HF radio absorption, coordinated real-time SuperDARN observations could be used to track space weather disturbances across the polar cap between the Norwegian and Canadian sectors, which would provide advanced notice of approaching disturbances.

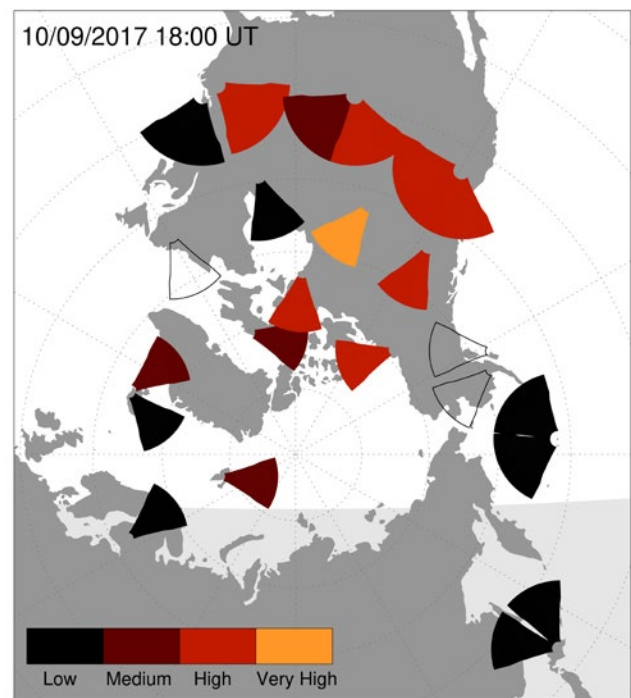


Figure 7: The amount of high frequency radio absorption, rated from 'Low' to 'Very High', observed by the northern hemisphere SuperDARN radars during space weather events in September 2017. Radio blackouts lasting several hours occurred at mid-latitudes, and 10 days of absorption due to energetic proton precipitation was detected in the polar cap.

4. Connections and synergies with other SESS report chapters

Space physics research through the use of rockets has been highlighted in two previous SESS reports. This chapter complements these two previous report chapters by providing a focus on the ground-based instrumentation in Svalbard. Specific points of relevance are as follows:

- Moen et al. (2020) recommended that key parameters from radar instruments should be given status as SIOS core data. As discussed in Section 7 of this report, the Svalbard SuperDARN radar is available online (with full metadata and software tools) in near real-time and has a > 5 years collecting commitment, which makes it suitable to be included as SIOS core data.
- Moen et al. (2019) identifies the critical ground-based observations provided by the instrumentation on Svalbard in regards to rocket campaigns. The Svalbard SuperDARN radar adds to this support network.

5. Unanswered questions

The underlying challenge is to understand, predict and model the response of the atmospheric column as a whole (from the ionosphere, down through the mesosphere and into the stratosphere) to energy input from the Sun and solar wind. Coupling between the neutral and ionised parts of the upper atmosphere is particularly important in the polar regions. Here, the dynamical processes are highly variable in their response to the solar activity levels, with nonlinear processes, instabilities and turbulence in the ionosphere facilitating the energy transfer to the neutral atmosphere. The instrumentation in Svalbard can provide the necessary datasets to assist scientists in several of these aspects.

Specific questions with applications for the Svalbard SuperDARN radar are given below.

- What processes govern the dynamics and structuring of the polar cap patches as they travel across the polar cap ionosphere?
- What are the characteristics of the ionospheric flow channels and how much energy is deposited into the ionosphere through frictional heating both inside and at the edges of flow channels?
- How is the energy originating from ionospheric processes (flow channels, auroral particle

precipitation, waves, etc.) redistributed in latitude and altitude?

- What is the average impact area of energetic electron precipitation into the mesosphere/lower thermosphere region?
- How are the irregularities related to other specific large-scale ionospheric features and what is the physics behind the formation of smaller, deca (< 10 m) and hectometre (< 100 m), irregularities?
- How can the large-scale convection pattern be incorporated into local space weather prediction models related to the positioning accuracy in the European Arctic sector, in particular north and southwest of Svalbard, over the Arctic ocean and towards Greenland?

All these questions address the major open issues in space and upper atmospheric sciences within the context of the energy transfer from space down to the Earth's atmosphere. They are concerned with the upper atmosphere dynamics, its heating, instabilities and turbulence, and addressing them will contribute to the modelling and forecasting of space weather effects. This will increase the resilience of human-based infrastructure to adverse space weather events, thus ensuring safety and continuity of human operations in the polar regions.

6. Recommendations for the future

1. Rebuild the Svalbard SuperDARN radar and secure ongoing funding for maintenance and operational costs.
2. Designate the area on Breinosa (which currently includes EISCAT, the KHO and SuperDARN) as a research infrastructure zone with limited land rental costs. Such costs unnecessarily decimate research budgets diverting funding away from core research.
3. Construct a second SuperDARN radar on the same site as the current radar, with a field of view covering the region southwest of Svalbard.

This would cover the flight path of sounding rockets from Ny Ålesund as well as providing a complementary field of view to existing all-sky cameras and any newly developed SuperDARN radars on Iceland.

4. Develop a collaboration between Norway and North America to build the real-time space weather monitoring capability of SuperDARN, including tracking of space weather disturbances across the polar cap and monitoring HF radio absorption.

5. Support an extension to the Longyearbyen meteor radar to allow 2-D measurements of the atmospheric velocities and temperatures

in the mesosphere. This would provide a complementary dataset to the higher altitude SuperDARN dataset.

7. Data availability

SuperDARN radar data are used throughout the international space physics community. The data are archived in two open-access repositories, where a username and password are required to access the system:

- Globus (<https://www.globus.org/>)
- British Antarctic Survey (<https://www.bas.ac.uk/project/superdarn/#data>)

The SuperDARN community maintains two software packages to support scientific research:

- Radar Software Toolkit (RST), the primary SuperDARN data analysis software
- pyDARN, a python library for SuperDARN data visualisation

These open-source packages are maintained and distributed by an international team of scientists, engineers and software developers. In addition, a web-based interface for visualising the radar data is available from Virginia Tech.³ The Svalbard SuperDARN radar also had (and will have) an online real-time data feed.

Data from the other instrumentation mentioned in this report are available through online databases, some of which are already compatible with the SIOS data access portal (e.g through the already established National Infrastructure for Research Data, NIRD). Table 1 lists the Norway-owned instruments and instrumentation to which Norwegian researchers have direct access through ongoing collaborations.

8. Acknowledgements

Funding for the Svalbard SuperDARN radar is provided through the ConocoPhillips/Lundin High North Research Program. The authors acknowledge the use of SuperDARN data. SuperDARN is a collection of radars funded by national scientific funding agencies of Australia, Canada, China,

France, Italy, Japan, Norway, South Africa, the UK and the USA. The authors were supported by the Research Council of Norway, project number 291644, Svalbard Integrated Arctic Earth Observing System – Knowledge Centre, operational phase in the writing of this report.

³ <http://vt.superdarn.org/tiki-index.php>

References

- Baddeley LJ, Yeoman TK, McWilliams KA, Wright DA (2007) Global Pc5 wave activity observed using SuperDARN radars and ground magnetometers during an extended period of northward IMF. *Planet and Space Sci* 55(6):792–808.
- Billett DD, Hosokawa K, Grocott A, Wild JA, Aruliah AL, Ogawa Y, et al. (2020) Multi-instrument observations of ion-neutral coupling in the dayside cusp. *Geophys. Res. Lett.* 47, e2019GL085590. <https://doi.org/10.1029/2019GL085590>
- Bland EC, Heino E, Kosch MJ, Partamies N (2018) SuperDARN radar-derived HF radio attenuation during the September 2017 solar proton events. *Space Weather* 16(10):1455–69.
- Bland EC, Partamies N, Heino E, Yukimatu AS, Miyaoka H (2019) Energetic electron precipitation occurrence rates determined using the Syowa East SuperDARN radar. *J Geophys Res: Space Physics* 124(7):6253–65.
- Bland E, Tesema F, Partamies N (2020) D-region impact area of energetic particle precipitation during pulsating aurora. *Annales Geophysicae Discussions* 18:1–21.
- Brekke A (2013) *Physics of the upper polar atmosphere*. Springer. ISBN: 978-3-642-27400-8, <https://doi.org/10.1007/978-3-642-27401-5>
- Bristow WA, Hampton DL, Otto A (2016) High-spatial-resolution velocity measurements derived using local divergence-free fitting of SuperDARN observations. *J Geophys Res: Space Physics* 121(2):1349–61.
- Chakraborty S, Baker JB, Ruohoniemi JM, Kunduri B, Nishitani N, Shepherd SG (2019) A study of SuperDARN response to co-occurring space weather phenomena. *Space Weather* 17(9):1351–63.
- Chen XC, Lorentzen DA, Moen JI, Oksavik K, Baddeley LJ (2015) Simultaneous ground-based optical and HF radar observations of the ionospheric footprint of the open/closed field line boundary along the geomagnetic meridian. *J Geophys Res: Space Physics* 120(11):9859–74.
- Chisham G, Freeman MP, Sotirelis T (2004) A statistical comparison of SuperDARN spectral width boundaries and DMSP particle precipitation boundaries in the nightside ionosphere. *Geophys. Res. Lett.* 31(2).
- Chisham G, Lester M, Milan SE, Freeman MP, Bristow WA, Grocott A, McWilliams KA, Ruohoniemi JM, Yeoman TK, Dyson PL, Greenwald RA (2007) A decade of the Super Dual Auroral Radar Network (SuperDARN): Scientific achievements, new techniques and future directions. *Surveys in Geophysics* 28(1):33–109.
- Dungey JW (1961) Interplanetary magnetic field and the auroral zones. *Physical Review Letters* 6(2):47.
- Frey H, U., Han D, Kataoka R, Lessard MR, Milan SE, Nishimura Y, Strangeway RJ, Zou Y (2019) Dayside Aurora. *Space Sci Rev* 215:51. <https://doi.org/10.1007/s11214-019-0617-7>
- Fæhn Follestad A, Clausen LB, Thomas EG, Jin Y, Coster A (2019) Polar cap patch prediction in the expanding contracting polar cap paradigm. *Space Weather* 17(11):1570–83.
- Greenwald RA, Baker KB, Dudeney JR, Pinnock M, Jones TB, Thomas EC, Villain JP, Cerisier JC, Senior C, Hanuise C, Hunsucker RD (1995) DARN/SuperDARN. *Space Sci Rev* 71(1–4):761–96.
- Greenwald RA (2017) The importance of international collaboration in space research. *Radio Sci.* 52:511–515. <https://doi.org/10.1002/2017RS006329>
- Hanuise C, Senior C, Cerisier J-C, Villain J-P, Greenwald RA, Ruohoniemi JM, Baker KB (1993) Instantaneous mapping of high latitude convection with coherent HF radars. *J Geophys Res* 98:17387–17400.
- Herlingshaw K, Baddeley LJ, Oksavik K, Lorentzen DA, Bland EC (2019) A study of automatically detected flow channels in the polar cap ionosphere. *J Geophys Res: Space Physics* 124(11):9430–47.
- Herlingshaw K, Baddeley LJ, Oksavik K, Lorentzen DA (2020) A Statistical Study of Polar Cap Flow Channels and their IMF By dependence. *J. Geophys. Res.: Space Physics*: 125, <https://doi.org/10.1029/2020JA028359>
- Hibbins RE, Espy PJ, Orsolini YJ, Limpasuvan V, Barnes RJ (2019) SuperDARN observations of semidiurnal tidal variability in the MLT and the response to sudden stratospheric warming events. *J Geophys Res: Atmospheres* 124(9):4862–72.
- Hosokawa K, Zou Y, Nishimura Y (2019) Airglow patches in the polar cap region: A review. *Space Sci. Rev.* 215:53. <https://doi.org/10.1007/s11214-019-0616-8>
- Hosokawa K, Motoba T, Yukimatu AS, Milan SE, Lester M, Kadokura A, Sato N, Bjornsson G (2010) Plasma irregularities adjacent to auroral patches in the postmidnight sector. *J Geophys Res: Space Physics.* <https://doi.org/10.1029/2010JA015319>
- Imber SM, Milan SE, Lester M (2013) The Heppner-Maynard boundary measured by SuperDARN as a proxy for the latitude of the auroral oval. *J Geophys Res: Space Physics* 118(2):685–97.
- Jin Y, Moen JI, Miloch WJ (2014) GPS scintillation effects associated with polar cap patches and substorm auroral activity: direct comparison. *J Space Weather Space Clim* 4:A23
- Jin Y, Moen JI, Oksavik K, Spicher A, Clausen LB, Miloch WJ (2017) GPS scintillations associated with cusp dynamics and polar cap patches. *J Space Weather Space Clim* 7:A23.
- Koustov AV, Ullrich S, Ponomarenko PV, Nishitani N, Marcucci MF, Bristow WA (2019) Occurrence of F region echoes for the polar cap SuperDARN radars. *Earth, Planets and Space.* <https://doi.org/10.1186/s40623-019-1092-9>

- Kiene A, Bristow WA, Conde MG, Hampton DL (2018) High-resolution local measurements of *F* region ion temperatures and Joule heating rates using SuperDARN and ground-based optics. *J Geophys Res: Space Physics*. <https://doi.org/10.1029/2018JA025997>
- Lorentzen DA, Moen J, Oksavik K, Sigernes F, Saito Y, Johnsen MG (2010) In situ measurement of a newly created polar cap patch. *J Geophys Res* 115:A12323. <https://doi.org/10.1029/2010JA015710>
- Moen J, Oksavik K, Abe T, Lester M, Saito Y, Bekkeng TA, Jacobsen KS (2012) First in-situ measurements of HF radar echoing targets. *Geophys. Res. Lett.* 39(7).
- Moen J, Spicher A, Rowland DE, Kletzing C, LaBelle J (2019) Grand Challenge Initiative-Cusp: Rockets to explore solar wind-driven dynamics of the top side polar atmosphere. In: Orr et al. (eds): SESS report 2018, Svalbard Integrated Arctic Earth Observing System, Longyearbyen, [pp.184–204](https://sios-svalbard.org/SESS_Issue1). https://sios-svalbard.org/SESS_Issue1
- Moen J, Spicher A, Takahashi T, Rowland DE, Kletzing C, LaBelle J, Larsen M, Conde M, Saito Y, Blix K (2020) Grand Challenge Initiative-Cusp: Observational network for solar wind-driven dynamics of the top atmosphere (GCI-Cusp). In: Van den Heuvel et al. (eds): SESS report 2019, Svalbard Integrated Arctic Earth Observing System, Longyearbyen, pp. [274–284](https://sios-svalbard.org/SESS_Issue2). https://sios-svalbard.org/SESS_Issue2
- Nishitani N, Ruohoniemi JM, Lester M, Baker JB, Koustov AV, Shepherd SG, Chisham G, Hori T, Thomas EG, Makarevich RA, Marchaudon A (2019) Review of the accomplishments of mid-latitude Super Dual Auroral Radar Network (SuperDARN) HF radars. *Pr. Earth and Planet. Sci.* 6(1):1–57.
- Oksavik K, Ruohoniemi JM, Greenwald RA, Baker JB, Moen J, Carlson HC, Yeoman TK, Lester M (2006) Observations of isolated polar cap patches by the European Incoherent Scatter (EISCAT) Svalbard and Super Dual Auroral Radar Network (SuperDARN) Finland radars. *J Geophys Res: Space Physics* 111(A5).
- Oksavik K, Moen J, Lester M, Bekkeng TA, Bekkeng JK (2012) In situ measurements of plasma irregularity growth in the cusp ionosphere. *J Geophys Res: Space Physics* 117(A11).
- Redmon RJ, Seaton DB, Steenburgh R, He J, Rodriguez JV (2018) September 2017's geoeffective space weather and impacts to Caribbean radio communications during hurricane response. *Space Weather* 16(9):1190–201.
- Ruohoniemi JM, Baker KB (1998) Large-scale imaging of high-latitude convection with Super Dual Auroral Radar Network HF radar observations. *J Geophys Res: Space Physics* 103(A9):20797–811.
- Zhang QH, Zhang BC, Lockwood M, Hu HQ, Moen J, Ruohoniemi JM, Thomas EG, Zhang SR, Yang HG, Liu RY, McWilliams KA (2013) Direct observations of the evolution of polar cap ionization patches. *Science* 339(6127):1597–600.

Scientific Applications of Unmanned Vehicles in Svalbard (UAV Svalbard)



Richard Hann^{1,2}, Barbara Altstädter³, Peter Betlem^{1,4}, Kajetan Deja⁵, Katarzyna Dragańska-Deja⁵, Marek Ewertowski⁶, Filip Hartvich⁷, Marius Jonassen¹, Astrid Lampert³, Michał Laska⁸, Ireneusz Sobota⁹, Rune Storvold¹⁰, Aleksandra Tomczyk⁶, Kacper Wojtysiak¹¹, and Piotr Zagórski¹²

1 University Centre in Svalbard, Norway

2 Norwegian University of Science and Technology, Norway

3 Institute of Flight Guidance, Technische Universität Braunschweig, Germany

4 University of Oslo, Norway

5 Institute of Oceanology of the Polish Academy of Sciences, Poland

6 Adam Mickiewicz University in Poznań, Poland

7 Institute of Rock Structure and Mechanics of the Czech Academy of Sciences, Czech Republic

8 University of Silesia in Katowice, Poland

9 Nicolaus Copernicus University in Torun, Poland

10 Norwegian Research Centre, Norway

11 Institute of Geophysics of the Polish Academy of Sciences, Poland

12 Maria Curie-Skłodowska University, Poland

Corresponding Author: Richard Hann, richard.hann@ntnu.no

Keywords: Svalbard, unmanned, drone, UAV, UAS, AUV, ROV, RPAS, review

DOI: <https://doi.org/10.5281/zenodo.4293283>

1. Introduction

The main objective of this State of Environmental Science in Svalbard (SESS) report is to generate an overview of the research conducted in Svalbard with unmanned vehicles. Funding is provided by the Svalbard Integrated Arctic Earth Observing System (SIOS). The report covers unmanned vehicles that travel in air, on the water surface, and underwater. However, due to their prevalence, the main focus will be on aerial systems. This report aims to capture the applications of these unmanned systems in Svalbard and develop recommendations for the future.

This report follows in the footsteps of earlier publications on the use of unmanned vehicles in polar regions. A general overview of unmanned aerial vehicle (UAV) applications in the Arctic, prepared by a working group from the Arctic Monitoring and Assessment Program (AMAP), also gives guidelines for operations in the Arctic (Crowe et al. 2012, Storvold et al. 2013). Bhardwaj et al. (2016) prepared an overview of UAV applications in glaciological applications. An update of this report that was recently published extends the scope to the cryosphere sciences (Gaffey and Bhardwaj 2020). The latter also identified Svalbard as a hotspot for arctic UAV operations. This SESS contribution is unique for its focus on Svalbard and for including not only UAVs but also other types of unmanned vehicles. This allows for a more specific analysis with dedicated recommendations for the Svalbard area.

1.1. Motivation

When compared to the lower latitude regions, global warming occurs significantly quicker in the Arctic (Arctic amplification) because of numerous feedback processes that occur between the atmosphere, the ocean, and the cryosphere (Serreze and Barry 2011). A significantly enhanced sea-ice reduction rate, recession of glaciers, changes in the thickness of the permafrost active layer, and increased activity of morphogenetic processes (e.g. marine, slope) have been observed in the Arctic and Svalbard in recent decades. Due

to its specific character and climate conditions, the Arctic is an important study site for contemporary climate change processes, their feedback, and environmental consequences. The easy access to Svalbard makes it an excellent site for a wide range of polar research disciplines and long-term monitoring programs.

Unmanned vehicles are important tools for conducting research in the Arctic, especially in the field of climate change. This emerging technology allows obtaining complementary datasets to established observation methods such as satellite-based remote sensing and ground observations. Therefore, the use of unmanned vehicles in Svalbard is an important component to develop and enhance the knowledge of current changes in the Arctic and on a global scale.

1.2. Terminology

Different expressions are used to denominate unmanned aircraft. With origin in the military, the terminology “drone” is now used synonymously with all unmanned airborne systems. In scientific applications, the most commonly used expression is unmanned aerial vehicle (UAV), which refers to the airborne vehicle itself. Taking into account the infrastructure belonging to the UAV, such as autopilot and ground control station, the expression most frequently applied is unmanned aerial system (UAS). More recently, the expression remotely piloted aircraft system (RPAS) was introduced by the International Civil Aviation Organization (ICAO) and is used for unmanned vehicles that are controlled and commanded by an operator at a ground control station. Furthermore, the terms unoccupied vehicles or uncrewed vehicles are sometimes used. In this report, the terms “UAV” and “drone” are used synonymously to describe airborne systems.

Several types of marine unmanned vehicles exist. Remotely operated underwater vehicles (ROVs) are controlled by a pilot, whereas autonomous underwater vehicles (AUVs) do not require an

operator or are partially navigated by a pilot (e.g. seaglidern). Unmanned surface vehicles (USVs), sometimes also called autonomous surface vehicles (ASVs), are vehicles that travel on the water surface.

1.3. Types of unmanned vehicles

1.3.1. Multirotors and helicopters

A large range of aerial drones falls under the “multirotor” category. Their common denominator is three or more motors with directly mounted propellers, see Figure 1. They are controlled by adjusting the power directed to each motor when compared to a helicopter that has a collective and controls the aircraft by adjusting the propeller pitch. Multicopters vary in size from a few grams to several hundred kgs. Their main advantage is their mechanical simplicity (the only moving parts are the ball bearings in the motors). Purely battery-operated

multirotors typically have an endurance of 20–40 minutes. Multirotor drones are easy to deploy and some can carry quite a large payload despite not being as large as fixed-wing drones, but extra payload weight reduces endurance. Multirotors are extremely flexible at the cost of reduced range and endurance compared to fixed-wing drones. The biggest manufacturer of commercial (off-the-shelf) multirotor drones is DJI, see Figure 2. They offer several systems that range from small four-rotor (quadcopters) drones weighing a few hundred grams to larger six-rotor (hexacopter) drones with a maximum take-off weight of almost 10kg. These systems are typically very easy to fly and do not require extensive amounts of training. They are mostly operated within the visual line of sight (VLOS) and are typically remotely piloted with low degrees of autonomy.



Figure 1: Example of multirotor (left), fixed-wing (middle), and VTOL hybrid (right) used for scientific data collection and part of the SIOS infrastructure (Photos: NORCE).



Figure 2: Example of off-the-shelf drones from DJI: Phantom 4 Pro (left) and Mavic 2 Pro (Photos: Richard Hann).

1.3.2. Fixed-wing

In fixed-wing drones, the aerodynamic lift is generated by wings, see Figure 1. They are much more energy efficient compared to helicopter and multirotor drones, as the lifting surface is larger and can be optimized to a particular airspeed and wingload. This gives fixed-wing UAVs a much longer range and endurance compared to multirotor drones. The main disadvantage of fixed-wing drones is that they have a minimum airspeed required to stay aloft, i.e. they cannot hover in place. Also, for take-off and landing, fixed-wing UAVs require either a runway or catapult for take-off (small fixed-wings can be thrown manually) and a runway or a net for landing. The operation of fixed-wing drones requires a good amount of training and experience. The endurance is typically one to three hours for purely battery powered systems, whereas combustion systems typically have an endurance of 3–8 hours. Combustion systems can be designed to fly up to 24 hours or longer. The size of fixed-wing drones used for scientific applications will typically vary from 0.5kg to a few hundred kg, with a few exceptions (e.g. NASA operates the Global Hawk at 15t for science missions). Fixed-wing UAVs exhibit typically a high degree of autonomy and can be operated beyond visual line of sight (BVLOS). The main advantage of fixed-wing drones is their ability to cover large distances, to stay aloft for extended periods, and to reach high altitudes (up to several kms). Fixed-wing UAVs have a long history and have, for example, been already used in the 1970s for meteorological research (Konrad et al. 1970).

1.3.3. VTOL Hybrid

Recently, drone designs combining the vertical take-off and landing (VTOL) capabilities of multirotors with a range of fixed-wing have become available, see Figure 1. This design especially benefits operations conducted from ships or field stations, as one does not need runways or catapult and net landing equipment. A VTOL UAV has typically less range and less payload capacity compared to a fixed-wing aircraft of the same size and weight.

1.3.4. Remotely operated underwater vehicles

The origins of this technology dates back to the 1950s, when the first vehicles of this type were used to retrieve lost torpedoes. The following years brought further modernization and expansion of ROVs, mainly in military applications. This technology became indispensable in the oil industry and eventually became an invaluable tool in scientific applications. ROVs are most often built on an open frame with floats attached, with strong light sources and digital cameras transmitting the image directly to the operator's monitor (see Figure 3). Propulsion is usually implemented with electrically driven propellers. ROVs are usually well-balanced and do not require the use of ballast tanks. In addition, they are connected by an umbilical cable with a platform located on the surface or an underwater hangar. Power and data transmission are supplied to the vehicle via the umbilical cable, often with the use of optical fibre technology. ROVs have many classes depending on the weight/size of the vehicle, the depth to which it is able to operate, or the vehicle equipment. Such a movable underwater platform provides a wide range of installation possibilities with various types of measuring equipment: cameras, specialized sensors of physicochemical parameters, manipulators allowing for various types of work or obtaining samples, sonar, acoustic camera and many others. However, the most frequently used devices are high-resolution video cameras that allow for a non-invasive observation of the sea bottom, water column, and the bottom surface of the ice. Most vehicles of this type have an acoustic ultra-short baseline (USBL) navigation system that allows determining the position of the vehicle in relation to the platform from which it was launched (ship, platform, shore, sea ice). If the planned operations are very precise (taking samples from a specific place on the bottom or mooring inspection), the ship should be equipped with a dynamic positioning system. Depending on the complexity of the vehicle, it may have one or more trained operators responsible for individual navigation manipulators.



Figure 3: Example of ROV (top, left), drop camera (top, right), AUV (bottom, left), and USV (bottom, right) used for scientific data collection (Photos: Kajetan Deja).

1.3.5. Autonomous underwater vehicles

As in the case of ROV, the history of this type of construction dates back to the 1950s. In the beginning, these were mainly military-related structures. The advent of modern electronics, efficient power sources, and artificial intelligence has led to an increasing degree of autonomy and the development of autonomous underwater vehicles (AUVs), see Figure 3. The vast majority of AUVs resemble a torpedo, which is dictated by low hydrodynamic resistance (drag) as well as a minimizing of the possibility of catching on underwater obstacles. Typical AUVs contain a battery, electric drive motor, control electronics, and a range of oceanographic instruments (e.g. conductivity, temperature, pressure, pH-value, fluorimeter, sonar, a camera with lights). Some vehicles of this type have a foldable robotic arm. The vehicles are able to carry out missions autonomously after launch. The battery capacity is the main limitation of the operating time, depending on the vehicle class, up to several hours. The exception here is underwater gliders whose

missions can last up to several months – mainly due to the lack of an active propeller. These gliders move by changing their buoyancy, which allows for submersion and ascent, and the change of trim and presence of wings allow for forward movement. Electricity is needed in this case mainly to change the centre of gravity, for e.g. by pumping water or oil. Data are sent to the satellite during ascent – this AUV subtype is “controlled” by the pilot. Vehicles of this type have revolutionized the market, making it possible to perform tasks related to bathymetry or habitat mapping at much lower costs and unprecedented efficiency. They are excellent in all kinds of inspections and are a very important research platform in modern science related to the study of the oceans. Drop cameras are another technology that is often used, but it has been excluded from this report as it is a passive system that does not move on its own, see Figure 3.

1.3.6. Surface vehicles

These are remotely operated vessels (boats) of various sizes. Most often, the units are several

meters long and are equipped with an electric drive with a generator, see Figure 3. They can also use solar and wind energy (saildrone). Remotely controlled units of this type play an increasingly important role in Arctic research. They often allow for a doubling of the studied area and shorten the time needed to collect data when compared to traditional methods that use only a research vessel. They made it possible to enter dangerous waters such as glacier bays or very shallow waters. Due to the high flexibility of the solutions used, they can be adapted to any environmental conditions and are widely used in polar areas.

1.4. Relevance of unmanned vehicles for Arctic research

1.4.1. General

UAVs for scientific data collection have multiple benefits (Pajares 2015). Compared to manned aircrafts, the environmental footprint is orders of magnitude smaller when it comes to noise and fuel consumption, especially in small observation sites. In addition, UAVs are particularly well-suited to bridge the gap between single-point measurements and satellite remote sensing, as both spatial and temporal resolution are highly flexible. Such observations are important for creating consistent time series of surface products like snow albedo, vegetation indices, and biomass/primary production estimates. Satellite-based remote sensing in the Arctic is often limited by the presence of persistent cloud covers and the lack of sunlight during the winter. UAVs also allow access to areas that are dangerous or impossible to access, e.g. crevassed glaciers (Hann et al. 2019). Additionally, UAVs allow a higher flexibility in used sensors and measurements methods, e.g. ultra-wide band radar to measure properties like snow depth and snow water equivalent on land and on sea ice.

One key challenge in using airborne remote sensing generally is the vegetation, buildings, and other obstacles that cover or hide the Earth's surface and the space above it (Gaffey and Bhardwaj 2020). Therefore, the observation of rock structures, animals, or landforms is often obscured or even

impossible. Arctic regions with their lack of higher vegetation, large settlements, and other natural and man-made structures are therefore ideal for aerial remote sensing. Also, the risk of damage, either on the vehicle (UAV) or on the third person's property, not to mention health or life, a common threat in the densely populated areas of Europe, is significantly lower in the vast, obstacle-less plains of the Arctic.

The remoteness and natural character of the Arctic is another reason for the frequent exploitation of UAV technology (Solbø and Storbvold 2013). Mountainous areas, often glacierized, steep cliffs, rock faces, and practically no infrastructure effectively limit the accessibility to many areas except through small boats. However, the operational range of the UAVs (especially fixed-wing), which may exceed several kilometres, allows one to quickly, cheaply, and without any special equipment access to observe many of these remote sites (Stuchlík et al. 2015). Certainly, observations are limited to visual and/or other optical or thermal recordings, but this may be enough for many research tasks.

The undeniable benefit of using underwater vehicles is the ability to observe the environment at depths inaccessible to a diver as well as the analysis of many distant places in a relatively short time. Underwater vehicles also enable minimally invasive observations of the behaviour of animals (observations for many hours). They are well suited for observing the marine environment, where the patches of flora and fauna are natural and point measurements do not give a full picture of the species composition in a given place. Underwater vehicles are a good complement to traditional measurements, giving a wider view and supplementing them with additional observations. They allow for an insight into areas of very poor visibility, typical for glacial bays and glacial estuaries. USVs allow measurements in the close vicinity of a glacier, impossible to perform from a ship for safety reasons. Underwater vehicles are not limited by a specific Arctic light regime and can be used even during the polar night, thanks to the use of artificial lighting or radar.

A general list of technical and operational challenges of using unmanned platforms in polar environments was presented by Kramar (2019). An operational handbook for scientific users of UAVs in the Arctic was produced by the AMAP workgroup (Storvold et al. 2015).

1.4.2. Data resolution

One key benefit of UAVs is their ability to close the “resolution-gap” between ground-based and satellite-based observations. The data resolution of observations typically depends on optical (sensor resolution, lens focal length), environmental (visibility, cloudiness, wind, sun position), and technical (gimbal/sensor stabilisation, flight velocity, flight altitude) conditions. Figure 4 shows the typical resolution of different remote sensing techniques. Satellite-based observations can range from a resolution of approximately 1–100m,

while most products available for the scientific community are on the scale of 20m. In contrast to ground-based observations, this resolution is very coarse and introduces a challenging “gap”. In-situ UAV observations are well suited to contribute to filling this gap. This is mainly related to the lower operational altitude, possible due to those platforms. Such airborne systems can easily provide resolutions in the order of magnitude of 10cm.

The data resolution for ROV, AUV depends mainly on the class of the device and thus the possibility of installing better sensors, both optical – mainly cameras (size and type of sensor, the possibility of changing the focal length) – and measuring environmental parameters (e.g. fluorometer, STD probes) or equipment using sound waves (e.g. sonar, acoustic camera).

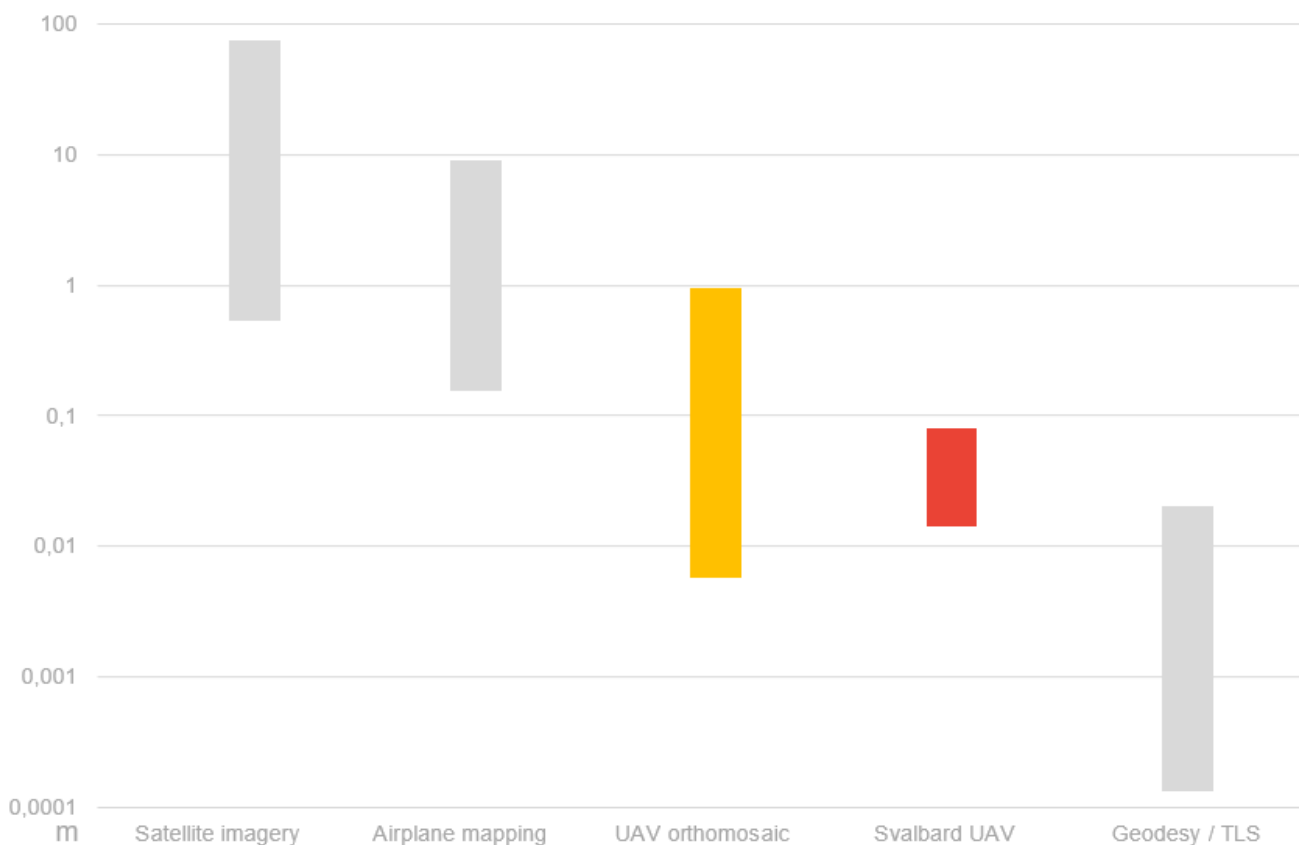


Figure 4: General overview of approximate image/data resolution using various mapping techniques: satellite, airplane, UAV, and terrestrial laser scanning (TLS). Based on this reports database (Svalbard UAV) and literature: Rothermel et al. (2020), Turner et al. (2016), Nex et al. (2014), Westoby et al. (2012), Smith et al. (2009), Prokop et al. (2008), Park et al. (2019) and Goncalves, and Henriques (2015).

1.4.3. Observations of the atmospheric boundary layer

UAVs, especially fixed-wings, are also suitable to fill in a missing gap in atmospheric research: They provide high resolution measurements on small scales, typically up to an altitude of 2km and a horizontal range of a few km, with some long-range applications. This typically requires sophisticated UAV operations. The modern miniaturized data processing units allow measurements with up to 1 kHz resolution.

For studying the exchange processes between the surface and the atmosphere, measurements less than a few 100m above the ground are very important. UAVs are very flexible compared to ground-based measurements like meteorological masts or remote sensing applications (Martin et al. 2011), and they are easier to operate close to the surface than manned systems, which usually have to adhere to a specific minimum flight altitude. Further, the flexibility of UAVs allows making observations at remote locations, which may contribute to enhanced databases for weather forecast (Sun et al. 2020). For investigating specific atmospheric processes, UAVs contribute to local-scale data that can be embedded in larger-scale measurement networks and serve to validate satellite data and numerical simulations with lower spatial resolution. In many large atmospheric projects, UAVs have been deployed to contribute data in small scales.

In addition, UAVS offer the advantage of flexibility concerning the choice of light-weight sensors. Depending on the application, UAVs are equipped with meteorological payload, aerosol sensors, chemical sensors, air sampling capabilities, measurements of radiation, and surface temperature. Last but not the least, for some applications like sampling volcanic eruptions, manned airborne measurements would be too dangerous, but UAV observations are possible, for e.g. (Nicoll et al. 2019).

1.5. Svalbard – a hotspot for unmanned vehicle research across the Arctic

Since 1920, Svalbard has a special status related to the international Spitsbergen Treaty. The regulations of the treaty allowed the signatory states the peaceful use of the area. Therefore, many national and international research facilities fostered cooperation and facilitated the spread of new technologies in various research projects, making Svalbard an important research hotspot.

Another important fact that attracts the researchers using UAVs is the unique natural environment of Svalbard. When compared to the lower latitude regions, heavily glacierized islands with easily perceptible effects of on-going climatic changes on the receding glaciers and related activation of slope and fluvial processes on vast, newly deglaciated areas are very suitable for a temporal observation of these changes (Hartvich et al. 2017, Bernard et al. 2018). Also, the natural processes, to a much smaller degree, are affected by anthropogenic activities. Therefore, monitoring of the state of the glaciers is very important in order to learn about the processes determining its changes, namely the fast degradation of the cryosphere (Bernard et al. 2018). Combining traditional research results with modern UAV methods can be done for modelling the state of cryosphere and the development of scenarios of its changes for much larger areas of the Arctic (Nehyba et al. 2017, Gaffey and Bhardwaj 2020).

It is not only glaciers, snow, and rocks that are studied using UAVs in Svalbard. Glacier runoff also affects the structure of the water layers and supplies huge amounts of suspended sediment to the water column. The use of underwater technologies allows monitoring the presence of Atlantic species that are more often increasingly found in the waters of Svalbard and to study the adaptation and the behaviour of macrofauna or plankton organisms to life in this extremely dynamic and difficult environment. Additionally, the rapid changes in the environment are followed by the dynamic reactions of plants, animals, and other life form populations.

Atmospheric research in Svalbard is focussing on local biogenic emissions and long-range transport processes from lower latitudes, as Svalbard is a relatively pristine environment. Svalbard is located in the Arctic vortex of low temperatures and demonstrates slow mixing of air masses compared to lower latitudes.

Finally, while being geographically relatively remote and isolated, Svalbard is still, compared to similar Arctic regions such as the Canadian archipelago, Severnaya Zemlya, or Franz Josef Land, easily accessible. The archipelago can be reached by commercial flight connections and is regularly visited by cargo ships. In addition, several well-equipped settlements and research facilities are also present there.

2. Results

2.1. Method

The main element of this report is a literature review on the scientific applications of unmanned vehicles in Svalbard. The first step was to identify publications in the peer-reviewed literature that included relevant information. Most of these publications were identified using Google Scholar with a combination of the following keywords: “Svalbard, Spitsbergen, unmanned aerial vehicle, UAV, unmanned aerial system, remotely operated aerial vehicle, RPAS, UAS, autonomous underwater vehicle, AUV, autonomous surface vehicle, ASV, remotely operated underwater vehicle, ROV, unmanned vehicle, drone”. Furthermore, the databases of ResearchGate, Research in Svalbard (RiS), and Svalbox were accessed. The search was conducted in August 2020. Later publications are not considered in this study.

In a second step, the selected publications were investigated in-depth to identify the following key parameters for each study:

- Discipline: the research field of the publication;
- Publication type: the type of publication (article, conference paper, report, thesis);
- Research objective: main purpose of the paper;
- Fieldwork season: the date when the unmanned vehicles fieldwork was conducted;
- Fieldwork location: the location(s) where the unmanned vehicles fieldwork was conducted;
- Unmanned vehicle: the type of unmanned vehicle used;

- Platform name: the name of the unmanned vehicle platform;
- Sensor type: the type of sensors used on the unmanned vehicle platform;
- Post-processing: the software or approach used for post-processing of the sensor data;
- Countries: the origin country of the institutions involved in the research.

2.2. Database

[Appendix 1](#) shows all publications that have been included in the database, along with a few selected variables. The full database is added as an electronic appendix to this report.

2.2.1. Type of unmanned vehicle

An overview of which unmanned vehicles were used mostly in Svalbard is given in Figure 5. The data show that the majority (>80%) of activities in Svalbard were conducted with UAVs. Most of the UAV work was performed with multirotor drones, of which nearly all were conducted with off-the-shelf technologies (i.e. DJI products like Phantom, Mavic, Matrice). This implies that these consumer-grade aircraft, which have a very low barrier, offer a substantial benefit to the scientific community. Fixed-wing UAV operations, which are much more complex due to the requirements in logistics, infrastructure, and trained personnel, were also used intensively. Underwater vehicles and surface vessels are available to a much smaller group of scientists because they are very expensive and require the use of a ship, which additionally increases the costs

and limits the availability of this type of research to oceanographers. Moreover, the use of ROV is quite complicated and time-consuming. Surface vehicles are more increasingly used in projects enabling the safe sampling of the zone at the front of glaciers that is inaccessible with traditional sampling. There are fewer published works on the use of underwater technology than UAV due to the limitations in the availability of this type of equipment.

2.2.2. Products

Generally, the most common products are datasets collected using UAV-mounted optical sensors, such as photomaps, digital elevation models (DEMs), digital surface models (DSMs), digital outcrop models (DOMs), and thermal or other special maps derived from the observed data. Other types of results are represented by point or profile measurements of meteorological, aerosol properties or atmospheric chemistry data. In some cases, observations of life form behaviours are made. Rarely, air, soil, sediment, or biological

material samples are collected from otherwise inaccessible sites. The overview of the product type frequency is given in Figure 6. It has to be noted that there is an uncertainty as not all papers specify the observed data production parameters.

By far, the most common product is an orthophoto (or orthomosaic) map, usually based on digital photographs from visible light cameras. Other types of sensors used for construction of photomaps are IR (infrared), thermal, and multispectral. Often, the orthomosaic map is not the final product but an input into further analyses or processing (therefore, it is sometimes difficult to differentiate it from the derived or special maps category). The orthomosaic maps are used in a variety of research domains, ranging from geology through glaciology and biology to human sciences.

In geomorphology, geology, and glaciology, the DEM/DSM is usually the main goal product, used for further analyses of slope, structures, volume, surface area, and their temporal changes.

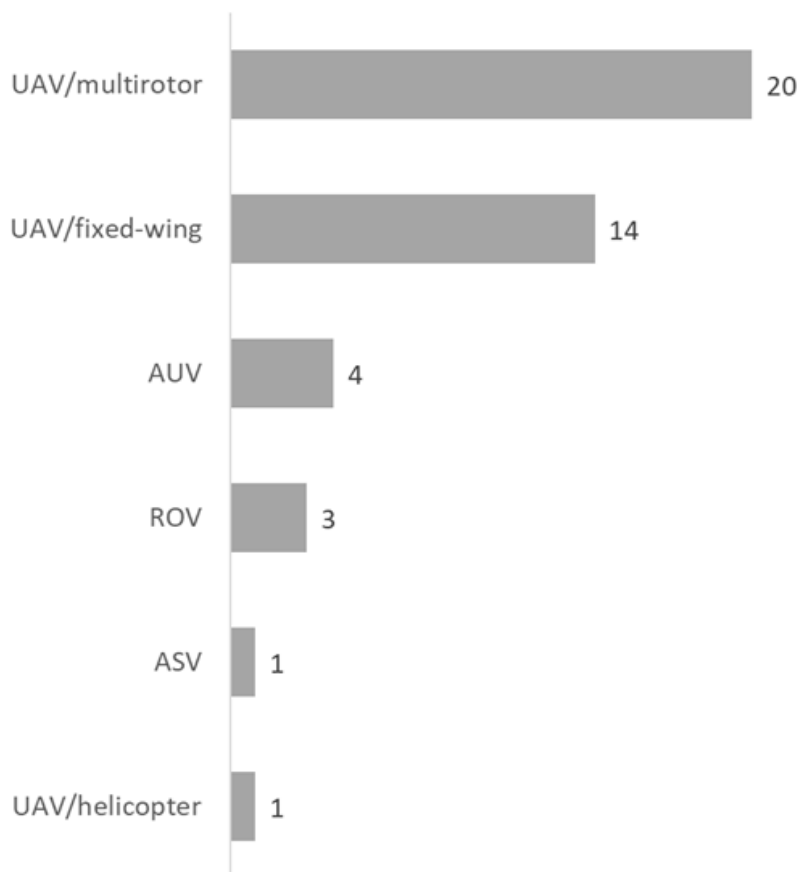


Figure 5: Overview of the different types of unmanned vehicles identified in the database.

The collection of photos, captured by piloted or programmed flight, is usually processed using structure-from-motion technique (SfM, a computerized development of stereoscopic analysis relying on raw computational power of current computers), performed in a specialized software (e.g. Pix4D, Agisoft Metashape, MicMac). As a result, DEM/DSM models are created in various forms (mesh, raster, point cloud, etc.).

Next, a rather wide group of results represents various maps. Often, the maps are derived from orthomosaics, most commonly observing movements of ice, either tracking the individual floating ice blocks (Leira et al. 2017, Albert et al. 2017, Linge, 2019) or extent of glaciers (Hodson et al. 2007, Solbø and Storvold 2013, Howe et al. 2019), mapping of crevasses (Hann et al. 2019), or snow (Stuchlík et al. 2016). Autonomous floating or underwater vehicles are used for bathymetry measurements (Ludvigsen 2018, Howe 2019) or biosphere observations (Hirche 2015, Deja 2019).

Finally, some papers concentrate on the technical side of the UAVs, testing various sensors, settings, or innovative UAVs (Crocker et al. 2012, Fischer 2019, Lampert et al. 2020) or the data processing, visualization, and analyses (Stodle et al. 2014).

A key finding throughout all results is that there seem not to be any standards for how the results and processing methods are documented. Typically, very little information is given on the exact method of data acquisition and processing – mostly just the name of the software. In addition, the results of the publications are typically not made available to the scientific community, which raises issues related to long-term data storage and open-access.

Other uses were recorded in 20% of the papers. Among these, the most frequent use was measuring physical parameters of the atmosphere, such as temperature, humidity, gas and aerosol concentration, etc. (Berman et al. 2012, Bates et al. 2013), either at certain points or in profiles.

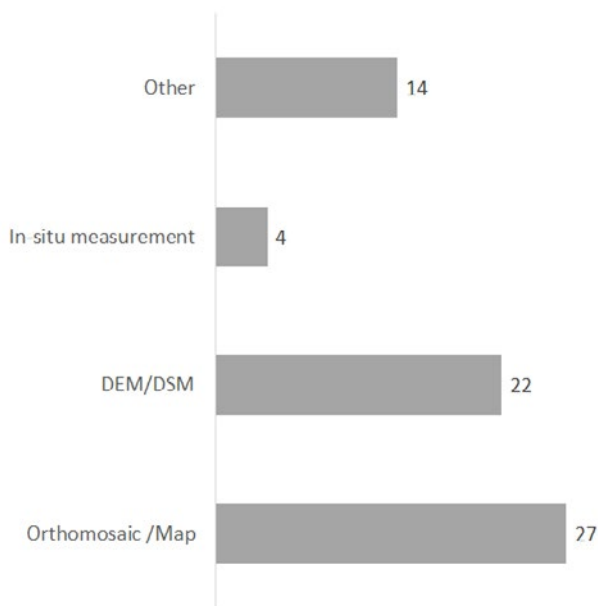


Figure 6: Overview of the different types of products identified in the database.

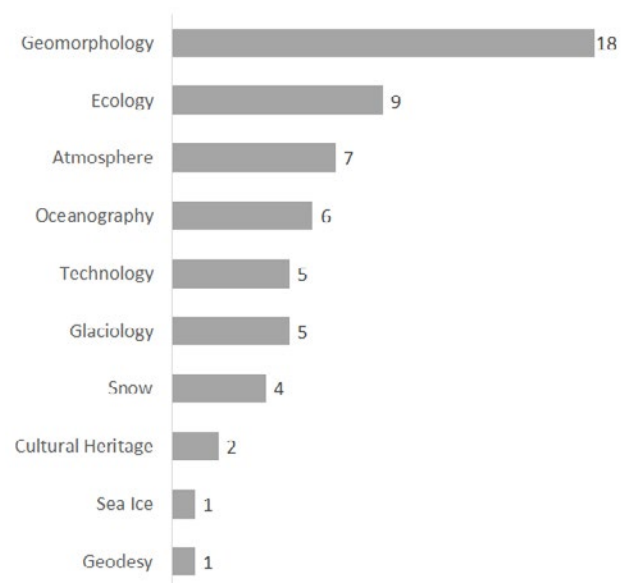


Figure 7: Overview of the different disciplines identified in the database.

2.2.3. Disciplines

Each publication was assigned to one or more disciplines and this distribution is shown in Figure 7. This figure indicates that most of the work with unmanned vehicles has been conducted for geomorphological purposes. The advantage of getting a bird's-eye perspective for describing geomorphological features is clear and explains why this discipline has adapted quadcopter UAVs into their work early on. Similarly, the advantages of using UAVs in the field of atmospheric research are obvious. This field mostly utilized fixed-wing UAVs with specialized sensors for in-situ measurement of atmospheric parameters. The fields of ecology and oceanography are the disciplines that make the most use of ASV, ROV, and AUV technologies.

In general, the datasets indicate that unmanned vehicles offer potential to be used in many different scientific fields. However, the degree of utilization is very different between disciplines. The cryospheric disciplines (snow, sea ice, glaciology) seem to underuse unmanned vehicles, which could indicate a larger potential for growth in these fields in the future.

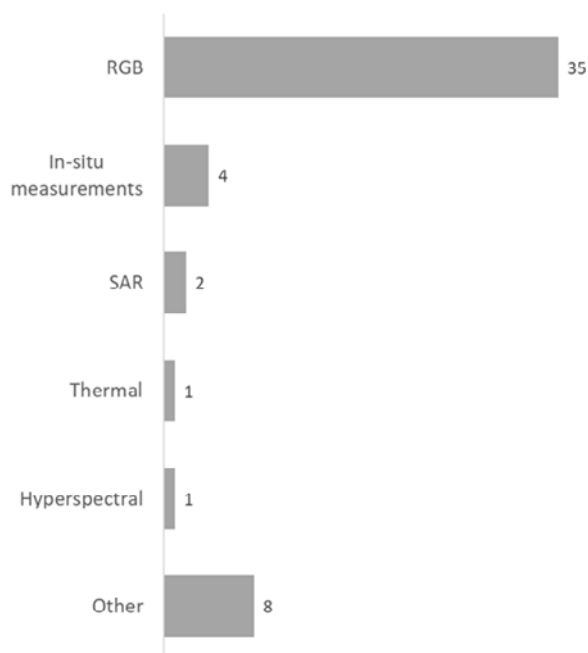


Figure 8: Overview of the different types of sensors identified in the database.

2.2.4. Sensors

The use of different sensor types onboard unmanned vehicles for fieldwork in Svalbard is shown in Figure 8. Since most activities were conducted with off-the-shelf UAVs, it is not surprising that the most frequent sensor type are visual range (RGB) cameras. To a lesser degree, unmanned vehicles were used to obtain in-situ measurements, in particular in atmospheric research (aerosol and meteorological parameters). Very few vehicles used more sophisticated remote sensing instruments like radars, lidars, or hyperspectral cameras. These sensors have clear benefits to many scientific fields and the fact that they are used to a low degree may indicate that the high price and lack of off-the-shelf availability may be a limiting factor. The large number of other sensors indicates that there is also a large degree of customized and specific instrumentation developed and deployed on the unmanned vehicles.

2.2.5. Countries

The graph in Figure 9 shows the country affiliation of all authors' institutions, where each country is only counted once per publication. Countries with less than three publications were summarized

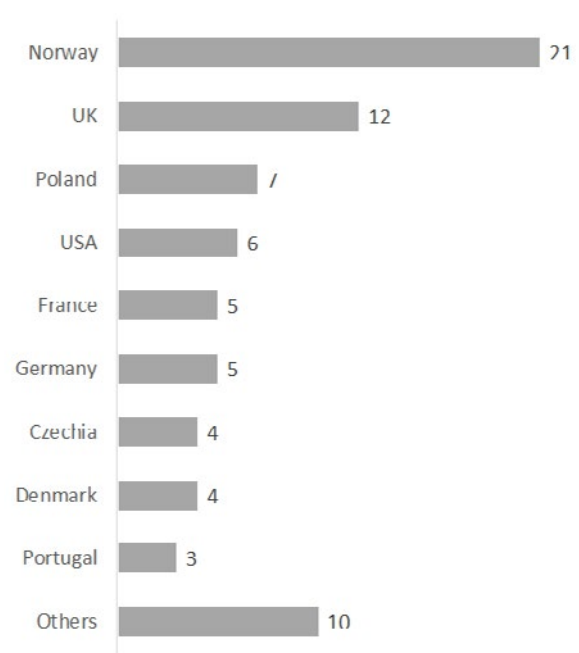


Figure 9: Overview of the different countries identified in the database.

as “others”. The overview data show that a large number of countries are involved in unmanned vehicle research in Svalbard and that the majority of publications included a Norwegian contribution, followed by contributions from the United Kingdom (UK) and Poland.

2.2.6. Fieldwork time

Figure 10 shows the timeline of unmanned vehicle fieldwork activities obtained from published sources. The data indicate that the use of unmanned vehicles in Svalbard started as early as 1998 and that a more frequent use started from 2008. Most activities seem to have been carried out between 2014 and 2016. This coincides with the release of the first commercial off-the-shelf quadcopter drones (DJI Phantom in 2013). Furthermore, it should be noted that the low number of activities in the last few years may be related to the fact that this report only considers published data. The natural “lag” between conducting fieldwork and publishing the results is likely to explain the low frequency of activities.

The data also show that most of the fieldwork has been performed during the summer season, followed by the spring and fall seasons. Only

one field campaign was conducted in winter. This distribution indicates that fieldwork is conducted mostly during the times when access to field sites is the easiest (summer: boat, spring: snowscooter) and daylight is available.

2.2.7. Fieldwork location

Figure 11 shows a map presenting the location of the fieldwork that is described in the published, peer-reviewed papers related to unmanned vehicles in the region of the Svalbard archipelago. We decided to exclude the Fram Strait, where several activities were conducted (eg. Crocker et al. 2012). UAV surveys were focused mostly around three sites: Kongsfjorden, Adventdalen, and Billefjorden. One study concerned eastern Bjørnøya. The geographic extent of the report covers 74°23' N – 80°09' N and 10°59' E – 19°15' E. This shows that there are several hotspots for unmanned vehicle activities in Svalbard. On the one hand, this indicates that these sites could be used in the future for long-term monitoring activities. On the other hand, this means that a large area of Svalbard is not benefiting from these novel technologies yet.

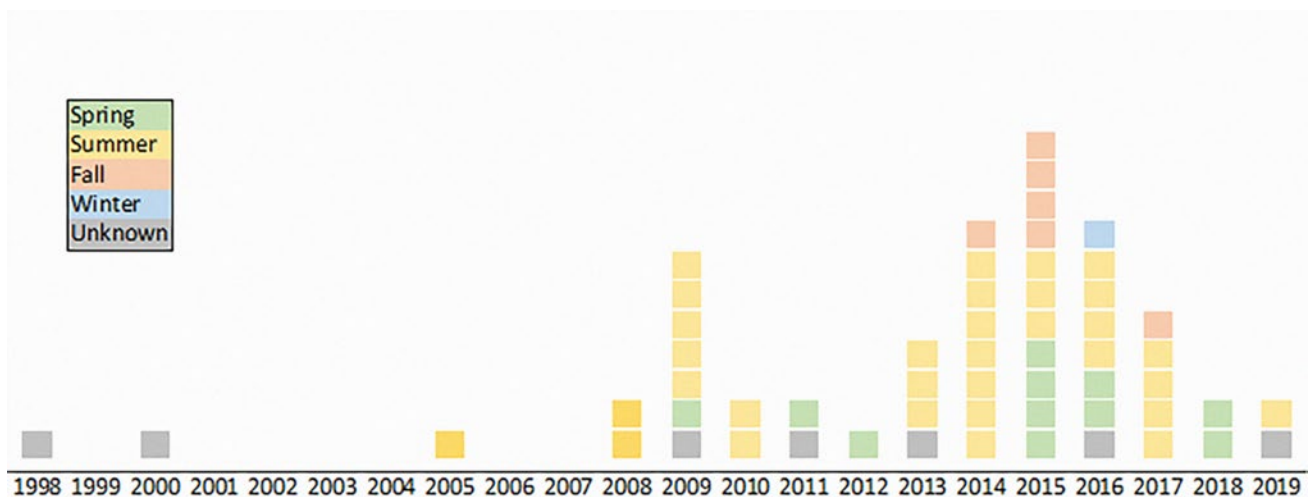


Figure 10: Overview of the timeline and seasons of fieldwork identified in the database.

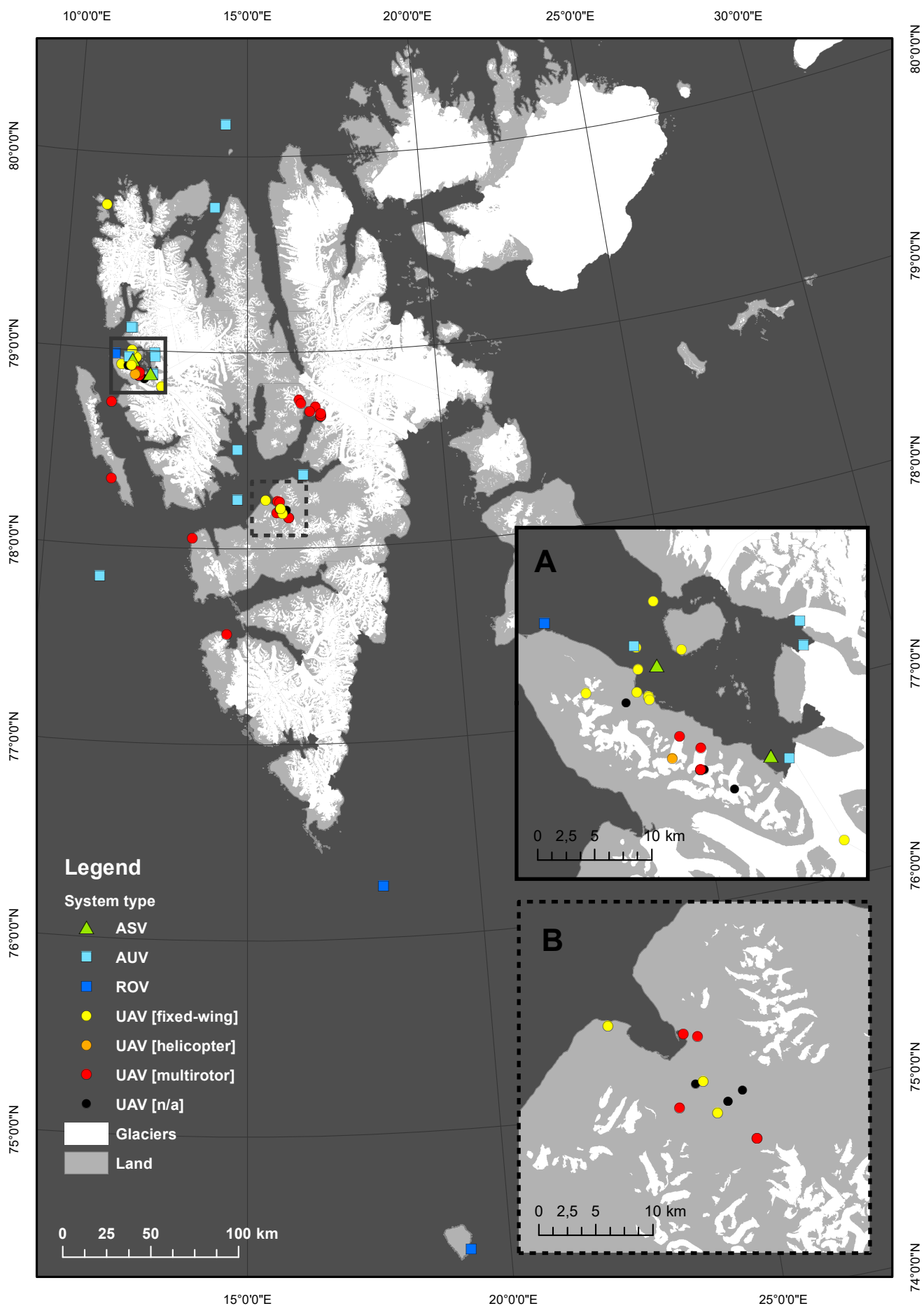


Figure 11: Location of study sites: A: Kongsfjorden region; B: Adventdalen region; ASV - Autonomous Surface Vehicle, AUV - Autonomous Underwater Vehicle, ROV - Remote Operated Vehicle, UAV - Unmanned Aerial Vehicle

2.3. Main conclusions

The results from section 2.2 lead to the following three main conclusions. The first conclusion is that unmanned vehicles offer great benefits for research in the Arctic and are used with an increasing frequency throughout a wide range of scientific disciplines by international operators. Though many disciplines already benefit from using unmanned vehicles, a large untapped potential still remains. Opportunities remain within intensifying the use of existing applications/disciplines, expanding the use to new applications/disciplines, and implementing the use of new types of miniaturized sensors (e.g. radar, lidar, hyperspectral).

The second conclusion is that two user categories of unmanned vehicles in Svalbard can be identified: advanced users and basic users. On the one hand, advanced users are operating complex and sophisticated vehicle systems for specific scientific purposes. Generally, the users of unmanned marine vehicles (ROV, AUVs, ASVs) and fixed-wing UAVs can be considered advanced users. Unmanned marine vehicles are complex in operation and require sophisticated infrastructure and logistics. The technology is applied for very specific research purposes, which, in Svalbard, were mainly on ecological and physical topics. In a similar way, fixed-wing UAVs are typically also complex to operate and require extensive infrastructure and trained pilots. Most fixed-wing UAVs have been used for atmospheric research or for mapping. Fixed-wing mapping activities were conducted mostly before off-the-shelf quadcopter products became widely available (around 2013) or in cases

where large areas needed to be covered. Most fixed-wing operations are conducted beyond visual line of sight with highly autonomous systems.

On the other hand, basic users mostly operate off-the-shelf UAVs for mapping purposes. These small, budget, ready-to-fly multirotors were the most commonly used UAV types in Svalbard. These systems are cheap, easy to transport, and straightforward to operate. With a low level of autonomy, these systems mostly operate within the visual line of sight. Low cost means that researchers can, at least to some extent, test the UAV in different scenarios, even if some of these will result in crashes. The small size of most popular multirotors (e.g. Phantom/Mavic series) allows packing them up in a backpack and hiking for even several tens of kilometers – allowing easy access to remote sites in Svalbard. The operation of these UAVs is very intuitive and requires comparatively little training.

The third and last main conclusion is that most unmanned vehicle operations were part of short-term studies and in limited areas of interest. Typically, the studies focus on small areas, usually limited to 1–2 km². These datasets provide valuable input for many models and simulations but also have the potential to be used for long-term monitoring studies. However, the main limitation of this opportunity is that data are often not shared to the scientific community and stored without long-term potential. Furthermore, most activities were concentrated on very localized areas, mostly around Ny-Ålesund and Longyearbyen.

3. Connections and synergies with other SESS report chapters

The use of unmanned vehicles in Svalbard for remote sensing is a relatively new trend and offers solutions to closing the gap between surface and satellite observations. Therefore, this SESS chapter should serve as a general motivation for all SESS contributions and SIOS partners to evaluate the

potential and benefit of using unmanned vehicles. In particular, future reports should assess how unmanned vehicles are used in their respective field, what potential they offer for the future, and how this potential can be unlocked.

4. Unanswered questions

4.1. Data

The documented use of unmanned vehicles in Svalbard is likely to only represent a fraction of on-going endeavours, as further supported by other reviews on the topic (Ader and Axelsson 2017, Gaffey and Bhardwaj 2020). A significant portion of activity remains beyond the scientifically published domain, i.e. without being peer-reviewed by the wider community and/or as remains hidden through limited access and/or being locally stored. This also applies to reports or theses written in the native language and stored exclusively in academic depositories. Proper care should be given to including such data in future assessments, while further criteria should be implemented for the inclusion of unpublished data. The latter is important given that workflows and reporting procedures remain far from standardised even in published work, and the inclusion of partial datasets may lead to increased ambiguity.

Projects such as Svalbox (Senger 2019, Senger et al. 2020) have enabled access to hundreds of drone-derived DOMs and datasets across Svalbard, yet mostly remain beyond the scientifically published domain. Many UAV-based projects have been conducted but not published yet, e.g. several Polish campaigns near Hornsund, and some have been scientifically published only after the data integration deadline of this study. These projects remain, however, mostly limited in scope to single disciplines, resulting in a highly fragmented data pool when considering Svalbard in full. Data are often stored locally with accessibility granted only through the local data owner. While many allow open access to the data for scientific use, the question of *how to encourage open access data policy as the standard in the field of Arctic UAV use* remains. As with more traditional data and sample sets, data and metadata are often lost along with the termination of the project, and it is therefore important to think about *how to guarantee long-term/permanent storage and availability of both data and metadata*, knowing the size of single datasets. Publicly providing the data after finishing the

project could already be made mandatory during the process of application for UAV operations in Svalbard. This is already the case for several funding agencies such as the German Research Foundation, who require uploading the final processed data alongside the final report. Likewise, the Norwegian Research Council and the National Science Centre in Poland have introduced stricter requirements for open-access sharing of data. Also, US agencies (e.g. NSF, DOE, NASA, NOAA) have well-defined data sharing policies for funded projects.

Prior to determining fitting storage solutions, a draft requirement should be drawn up, covering the kind of data and metadata that should be published. A majority of works reviewed in this contribution did not offer the necessary processing metadata to reproduce the published results, even by offering access to raw data upon request. For scientific reproducibility, products and metadata should be available, including all the processing steps taken and processing parameters applied. Besides the raw data (e.g., images) and processing parameters, the metadata should always include the version and name of the processing software used. *What else should be included*, however, remains an unanswered question and probably requires the support and input of the wider community.

For example, only a handful of the included works provide dedicated processing reports that meet the bare-minimum requirement, even if the generation of processing reports has been available for most major photogrammetry processing software packages (e.g. Agisoft Metashape, Pix4D) for a while. Identifying this gap, the plugins for these processing tools are in active development that standardise the workflow, for e.g. (Betlem et al. 2020). These plugins include the generation of processing reports into a uniform approach. Furthermore, various reviews have outlined *dos and don'ts*, but these either target UAV data acquisition and processing in general (thereby disregarding common issues observed in the Arctic) (Eisenbeiss and Sauerbier 2011, Hugenholtz et al. 2016, Nex and Remondino 2014) or remain mostly discipline-

dependent in favour of the outcome, e.g. DEM, digitised surface features (Bemis et al. 2014, Bhardwaj et al. 2016, Ewertowski et al. 2019).

4.2. UAV Regulations

The operation of UAVs is regulated by aviation authorities in order to ensure safety, security, and privacy. Until 2020, the national aviation authorities issued individual UAV regulations for their countries. In an effort to harmonize the regulations, the EU has introduced common regulations ('EASA' 2020). The new EU regulations were being planned to be implemented in July 2020; however, due to the COVID-19 crisis, the implementation was postponed until January 2021 ('Luftfartstilsynet' 2020). The Civil Aviation Authority of Norway has decided that Norway will follow the new EU regulations and extend them to Svalbard. After the implementation of the new regulation from 1st

January 2021, there will be a gradual transition period where one can still operate after the old regulation and permits until 1st January 2022 (basic operations) and 1st January 2023 (advanced operations).

The introduction of EU-wide regulations is likely going to lower the threshold for more complex UAV operations in Svalbard for non-Norwegian institutions. However, flying drones for scientific purposes in Svalbard will be regarded as commercial operations under the new regulations – this could increase the barrier to conduct even basic operations in the future. In summary, it is unclear to *what extent the new rules differ from the current Norwegian regulations and how this affects future scientific operations in Svalbard*. This generates a large uncertainty for operators and may affect future projects should they not make the necessary adjustments to the new regulations in time.

5. Recommendations for the future

Based on the main conclusions in section 2.3, four recommendations are given below. In general, the recommendations aim to intensify the use of unmanned vehicles for scientific applications in Svalbard and to standardise methods.

The first two recommendations are aimed to promote UAV-based remote sensing in Svalbard. Two separate approaches are suggested for this purpose. The first includes making incentives to increase the number of users of basic drone applications. This may be achieved by lowering the barrier for researchers to get engaged in simple UAV projects, mainly using RGB imagery and off-the-shelf drones. The second is to establish successful use-cases from basic applications and support upscaling them to advanced activities. In practice, this could mean the use of more sophisticated sensors, larger UAV platforms, more complex missions, and larger coverage areas.

The other two recommendations focus on standardisation and open-access. Standardising methods is an equally important task as intensifying

the use of drone-based data acquisition. This is because standards add confidence, transparency, repeatability, and scientific value to the data. Since UAVs are a relatively new technology with many new users, it is natural that a lack of methodical knowledge and standards exists within the scientific community. To overcome this gap, all stakeholders should be involved in the development of best-practice methods for conducting, processing, and sharing data from UAV-based activities.

Recommendation 1: Education, experience transfer, knowledge base, and training

Since unmanned vehicles are still a relatively new technology, education and training are key elements required to promote its use. We recommend an outreach program for SIOS partners to educate and train them in the use of unmanned vehicles but also support knowledge and experience exchange.

- Establish a forum or conference for users of unmanned vehicle technology in Svalbard to share their experience and knowledge.

- Provide education and training on the regulations related to unmanned vehicle operations in Svalbard (e.g. new EU drone law).
- Provide education and training on planning and conducting fieldwork in Svalbard with unmanned vehicles. This includes post-processing of data, data management, standardisation, and best practices.

Recommendation 2: Extend infrastructure and access to advanced systems

Today, there is already a wide range of disciplines, institutions, and researchers that use unmanned vehicles for research in Svalbard. This report shows that the majority of the work is conducted with off-the-shelf drones and RGB cameras. More sophisticated systems are more complicated to operate and substantially more expensive to obtain. We recommend extending the existing SIOS drone infrastructure to help promote the use of unmanned vehicles in Svalbard.

- Provide easy access to a wider range of platforms and piloting services. This can include, for example, access to real-time kinematic (RTK) drones, larger multirotor drones, fixed-wing drones and systems with advanced sensors such as thermal, multispectral, hyperspectral, lidar, and radar.
- Provide consultations on drone regulations and how to apply for specific drone operations that exceed the open category. Collaboration with the Governor of Svalbard (Sysselmannen), Longyearbyen Airport, and RiS to lower the barrier for complex drone operations also included.
- Consider setting up a fixed ground control point network with known coordinates for key sites near Longyearbyen.
- Provide access to electricity for charging batteries in the field.

Recommendation 3: Standardisation of UAV operations, data processing, and data dissemination procedures.

This report shows that there are challenges related to the way how the results from unmanned vehicle operations are reported in the literature. In general, there is a lack of transparency when it comes to the methods of data acquisition and data processing. This undermines the value and confidence of the research results. For this reason, we recommend the development and dissemination of a best practice standard that should include the following information:

- Develop standards for drone operations with manuals, templates, checklists, and risk assessments.
- Develop standards for detailed description of data acquisition methods and parameters (e.g. field site location, fieldwork dates, flight tracks, altitude).
- Develop standards for specification of the sensors, systems and software used for data acquisition (e.g. vehicle type, vehicle modifications, camera specification, post-processing software).
- Promote the publication of raw data and metadata (e.g. photos, raw measurements, coordinates of GCPs), software processing reports, projects files).
- Develop standards for data formats and metadata information.

Recommendation 4: Data storage and data accessibility

Most of the projects that were evaluated in this report were designed as short-term observations. The results from those studies, however, may be very valuable from a future-long term monitoring point of view (e.g. changes in vegetation, glacier recede, coastal erosion). Additionally, not all the collected data are published or are published after a significant time. In order to unlock the long-term

potential, it is essential for data to be stored and shared.

- Develop a system to log past, existing, and planned projects with unmanned vehicles in Svalbard. This should aim to increase collaboration and allow establishing long-term monitoring datasets.
- Generate awareness in the scientific community about data storage and access issues.

- Facilitate for long-term data storage and sharing of data by informing about existing databases that can be used for developing new facilities to SIOS and its partners.
- Support requirements (for publicly funded data acquisition campaigns) to provide open-access to data and to secure their long-term availability.

Acknowledgements

This work was supported by the Research Council of Norway, project number 291644, Svalbard Integrated Arctic Earth Observing System – Knowledge Centre, operational phase.

This study was also carried out as part of the “Changes of north-western Spitsbergen glaciers

as the indicator of contemporary transformations occurring in the cryosphere” (2017/25/B/ST10/00540) project funded by the National Science Centre, Poland.

References

Ader M, David A (2017) Drones in Arctic Environments. KTH Royal Institute of Technology, Stockholm.

Agisoft, LLC., Russia St Petersburg. n.d. Agisoft Metashape User Manual: Professional Edition, Version 1.6, 2020.

Songtao A, Ding X, Tolle F, Wang Z, Zhao X (2019) Latest Geodetic Changes of Austre Lovénbreen and Pedersenbreen, Svalbard. *Remote Sensing* 11(24):2890.

Akbari V, Brekke C, Doulgeris AP, Storvold R, Sivertsen, A (2016). Quad-Polarimetric SAR for Detection and Characterization of Icebergs. *Proceedings of the ESA Living Planet Symposium 2016, Prague, Czech Republic, 9-13 May 2016.*

Albert A, Leira FS, Imsland LS (2017) UAV path planning using MILP with experiments, Modeling, Identification and Control (MIC) 38(1):21-32, 2017

Allaart L, Friis N, Ingólfsson Ó, H\aaakansson L, Noormets R, Farnsworth WR, Mertes J, Schomacker A. 2018. Drumlins in the Nordenskiöldbreen Forefield, Svalbard. *Gff* 140(2):170–188.

Altstädter B, Platis A, Wehner B, Scholtz A, Wildmann N, Hermann M, Käthner R, Baars H, Bange J, Lampert A (2015) ALADINA - an Unmanned Research Aircraft for Observing Vertical and Horizontal Distributions of Ultrafine Particles within the Atmospheric Boundary Layer. *Atmos. Meas. Tech.*, 8, 1627–1639, 2015

Bates TS, Quinn PK, Johnson JE, Corless A, Brechtel FJ, Stalin SE, Meinig C, Burkhart JF (2013) Measurements of Atmospheric Aerosol Vertical Distributions above Svalbard, Norway, Using Unmanned Aerial Systems (UAS). *Atmospheric Measurement Techniques* 6(8):2115–2120.

Bemis, SP, Micklethwaite S, Turner D, James MR, Akciz S, Thiele ST, Bangash HA (2014) Ground-Based and UAV-Based Photogrammetry: A Multi-Scale, High-Resolution Mapping Tool for Structural Geology and Paleoseismology. *Journal of Structural Geology* 69:163–78.

Berman, Elena SF, Matthew Fladeland, Jimmy Liem, Richard Kolyer, and Manish Gupta (2012) Greenhouse Gas Analyzer for Measurements of Carbon Dioxide, Methane, and Water Vapor Aboard an Unmanned Aerial Vehicle. *Sensors and Actuators B: Chemical* 169:128–135.

Bernard, É, Jean-Michel Friedt, Florian Tolle, Ch Marlin, and Madeleine Griselin. 2017. ‘Using a Small COTS UAV to Quantify Moraine Dynamics Induced by Climate Shift in Arctic Environments’. *International Journal of Remote Sensing* 38(8–10):2480–2494.

Bernard, Eric, Jean Michel Friedt, Sophie Schiavone, Florian Tolle, and Madeleine Griselin. 2018. ‘Assessment of Periglacial Response to Increased Runoff: An Arctic Hydrosystem Bears Witness’. *Land Degradation & Development* 29(10): 3709–3720.

- Betlem P, Birchall T, Mosočiová T, Sartell AMR, Senger K (2020) From seismic-scale outcrop to hand sample: streamlining SfM photogrammetry processing in the geosciences. ARCEX annual conference 2020, 19–22 October, 2020.
- Bernard É, Friedt J-M, Tolle F, Griselin M, Marlin Ch, Prokop A (2017) Investigating Snowpack Volumes and Icing Dynamics in the Moraine of an Arctic Catchment Using UAV Photogrammetry'. *The Photogrammetric Record* 32(160):497–512.
- Bhardwaj A, Sam L, Martín-Torres FJ, Kumar R, et al (2016) UAVs as Remote Sensing Platform in Glaciology: Present Applications and Future Prospects'. *Remote Sensing of Environment* 175:196–204.
- Bruzzone G, Odetti A, Caccia M, Ferretti R (2020) Monitoring of Sea-Ice-Atmosphere Interface in the Proximity of Arctic Tidewater Glaciers: The Contribution of Marine Robotics'. *Remote Sensing* 12(11):1707.
- Cimoli E (2015) Determining Snow Depth Distribution from Unmanned Aerial Vehicles and Digital Photogrammetry'. MSc Thesis, M. Sc. thesis, Civil Engineering, Technical University of Denmark, 2015.
- Cimoli E, Marcer M, Vandecrux B, Bøggild CE, Williams G, Simonsen SB (2017) Application of Low-Cost UASs and Digital Photogrammetry for High-Resolution Snow Depth Mapping in the Arctic. *Remote Sensing* 9(11):1144.
- Crowe W, Davis KD, Cour-Harbo, A la, Vihma T, Lesenkov S, Eppi R, Weatherhead EC, Liu P, Raustein M, Abrahamsson M (2012) Enabling Science Use of Unmanned Aircraft Systems for Arctic Environmental Monitoring. AMAP Technical Report No. 6. Arctic Monitoring and Assessment Programme (AMAP), Oslo, Norway. 30 pp.
- Deja K, Ormańczyk M, Dragańska-Deja K (2019) Plankton or Benthos: Where Krill Belongs in Spitsbergen Fjords? (Svalbard Archipelago, Arctic). *Polar Biology* 42(8):1415–30.
- 'EASA' (2020) EU Unmanned Aircraft Systems Regulations. www.easa.europa.eu/regulations#regulations-uas---unmanned-aircraft-systems
- Eisenbeiss H, Sauerbier M (2011) Investigation of UAV Systems and Flight Modes for Photogrammetric Applications. *The Photogrammetric Record* 26(136):400–421.
- Ewertowski, MW, Evans DJA, Roberts DH, Tomczyk AM (2016) Glacial Geomorphology of the Terrestrial Margins of the Tidewater Glacier, Nordenskiöldbreen, Svalbard'. *Journal of Maps* 12(sup1):476–487.
- Ewertowski MW, Tomczyk AM (2020) Reactivation of Temporarily Stabilized Ice-Cored Moraines in Front of Polythermal Glaciers: Gravitational Mass Movements as the Most Important Geomorphological Agents for the Redistribution of Sediments (a Case Study from Ebbabreen and Ragnarbreen, Svalbard). *Geomorphology* 350:106952.
- Ewertowski, MW, Tomczyk AM, Evans DJA, Roberts DH, Ewertowski W (2019) Operational Framework for Rapid, Very-High Resolution Mapping of Glacial Geomorphology Using Low-Cost Unmanned Aerial Vehicles and Structure-from-Motion Approach'. *Remote Sensing* 11(1):65.
- Fraser NJ, Skogseth R, Nilsen F, Inall ME (2018) Circulation and Exchange in a Broad Arctic Fjord Using Glider-Based Observations'. *Polar Research* 37(1):1485417.
- Gaffey C, Bhardwaj A (2020) Applications of Unmanned Aerial Vehicles in Cryosphere: Latest Advances and Prospects. *Remote Sensing* 12(6):948.
- Geoffroy M, Cottier FR, Berge J, Inall ME (2017) 'AUV-Based Acoustic Observations of the Distribution and Patchiness of Pelagic Scattering Layers during Midnight Sun'. *ICES Journal of Marine Science* 74(9):2342–2353.
- Gonçalves JA., Henriques R (2015). UAV Photogrammetry for Topographic Monitoring of Coastal Areas. *ISPRS Journal of Photogrammetry and Remote Sensing* 104:101–11.
- Hann R, Hodson AJ, Jonassen MO (2019) Glacier Mapping and Wind Estimation with UAVs on Svalbard. In: Conference proceedings: Svalbard Science Conference 2020, Oslo.
- Hann, Richard, and Tor A. Johansen. 2020. 'Unsettled Topics in UAV Icing. SAE Technical Paper.
- Hartvich F, Blahut J, Stemberk J (2017) Rock Avalanche and Rock Glacier: A Compound Landform Study from Hornsund, Svalbard. *Geomorphology* 276:244–56.
- Hill ML, Konrad TG, Meyer JH, Rowland JR (1970) A Small, Radio-Controlled Aircraft as a Platform for Meteorological Sensors'. *Johns Hopkins APL Technical Digest*.
- Hirche, H-J, Jürgen Laudien, and Friedrich Buchholz. 2016. 'Near-Bottom Zooplankton Aggregations in Kongsfjorden: Implications for Pelago–Benthic Coupling'. *Polar Biology* 39(10):1897–1912.
- Hodson AJ, Nowak A, Redeker KR, Holmlund ES, Christiansen HH, Turchyn AV (2019) Seasonal Dynamics of Methane and Carbon Dioxide Evasion from an Open System Pingo: Lagoon Pingo, Svalbard. *Frontiers in Earth Science* 7:30.
- Hodson A, Anesio AM, Ng F, Watson R, Quirk J, Irvine-Fynn T, Dye A et al (2007) A Glacier Respires: Quantifying the Distribution and Respiration CO₂ Flux of Cryoconite across an Entire Arctic Supraglacial Ecosystem'. *Journal of Geophysical Research: Biogeosciences* 112 (G4).
- Hong W-L, Latour P, Sauer S, Sen A, Gilhooly WP, Lepland A, Fouskas F (2020) Iron Cycling in Arctic Methane Seeps". *Geo-Marine Letters*, 1–11.
- Howe JA, Husum K, Forwick M, Abernethy C, Macdonald F, Kohler J (2016) Past and Present Glacial Sedimentary Environments in Krossfjorden, Western Svalbard: Glacier Front Evolution. *AGUFM* 2016: EP13C–1041.

- Howe JA, Husum K, Inall ME, Coogan J, Luckman A, Arosio R, Abernethy C, Verchili D (2019) Autonomous Underwater Vehicle (AUV) Observations of Recent Tidewater Glacier Retreat, Western Svalbard. *Marine Geology* 417:106009.
- Hugenholtz C, Brown O, Walker J, Barchyn T, Nesbit P, Kucharczyk M, Myshak S (2016) 'Spatial Accuracy of UAV-Derived Orthoimagery and Topography: Comparing Photogrammetric Models Processed with Direct Geo-Referencing and Ground Control Points'. *Geomatica* 70(1): 21–30.
- Kramar, V (2019) UAS (Drone) Arctic Challenges: Next Steps. Proceedings of the FRUCT'25, Helsinki, Finland, 5-8 November 2019.
- Lampert A, Altstädter B, Bärfuss K, Bretschneider L, Sandgaard J, Michaelis J, Lobitz L et al (2020) Unmanned Aerial Systems for Investigating the Polar Atmospheric Boundary Layer—Technical Challenges and Examples of Applications'. *Atmosphere* 11(4):416.
- Laudien J, Orchard J-B (2012) The Significance of Depth and Substratum Incline for the Structure of a Hard Bottom Sublittoral Community in Glacial Kongsfjorden (Svalbard, Arctic)—an Underwater Imagery Approach. *Polar Biology* 35(7):1057–1072.
- Leira FS, Johansen TA, Fossen TI (2017) 'A UAV Ice Tracking Framework for Autonomous Sea Ice Management. In 2017 International Conference on Unmanned Aircraft Systems (ICUAS), 581–590. IEEE.
- Linge, S, et al (2019) Detection and Characterization of Icebergs in Kongsfjorden (Svalbard) Based on Ground-Based Radar Images and Additional Remote Sensing Data. Master thesis, Aalto University, Helsinki
- Long DG, Zaugg E, Edwards M, Maslanik J (2010) The MicroASAR Experiment on CASIE-09'. In 2010 IEEE International Geoscience and Remote Sensing Symposium, 3466–3469. IEEE.
- Lousada M, Pina P, Vieira G, Bandeira L, Mora C (2018) Evaluation of the Use of Very High Resolution Aerial Imagery for Accurate Ice-Wedge Polygon Mapping (Adventdalen, Svalbard). *Science of the Total Environment* 615:1574–1583.
- Ludvigsen M, Berge J, Geoffroy M, Cohen JH, Pedro R, Normes SM, Singh H, Sørensen AJ, Daase M, Johnsen G (2018) Use of an Autonomous Surface Vehicle Reveals Small-Scale Diel Vertical Migrations of Zooplankton and Susceptibility to Light Pollution under Low Solar Irradiance'. *Science Advances* 4(1):eaap9887.
- Luftfartstilsynet. 2020. Nytt EU-Regelverk. 2020. www.luftfartstilsynet.no/droner/nytt-eu-regelverk/
- Magiera J (2020) The effects of tractor driving on Arctic vegetation at Kapp Linné, Svalbard. PhD Thesis, Gothenburg University
- Martin S, Bange J, Beyrich F (2011) Meteorological Profiling of the Lower Troposphere Using the Research UAV "M2AV Carolo". *Atmospheric Measurement Techniques* 4(4):705.
- Mayer, S, Jonassen MO, Sandvik A, Reuder J (2012) Profiling the Arctic Stable Boundary Layer in Advent Valley, Svalbard: Measurements and Simulations. *Boundary-Layer Meteorology* 143(3):507–526.
- Midgley, NG, Tonkin TN, Graham DJ, Cook SJ (2018) Evolution of High-Arctic Glacial Landforms during Deglaciation. *Geomorphology* 311:63–75.
- Mora C, Vieira G, Pina P, Lousada M, Christiansen HH (2015) Land Cover Classification Using High-Resolution Aerial Photography in Adventdalen, Svalbard. *Geografiska Annaler: Series A, Physical Geography* 97(3):473–488.
- Nehyba S, Hanáček M, Engel Z, Stachoň Z (2017) Rise and Fall of a Small Ice-Dammed Lake-Role of Deglaciation Processes and Morphology". *Geomorphology* 295: 662–679.
- Nex, F, Remondino F (2014) UAV for 3D Mapping Applications: A Review. *Applied Geomatics* 6(1):1–15.
- Nicoll K, Airey M, Cimarelli C, Bennett A, Harrison G, Gaudin D, Aplin K, Koh KL, Knuever M, Marlton G (2019) First in Situ Observations of Gaseous Volcanic Plume Electrification. *Geophysical Research Letters* 46(6):3532–39.
- Pajares G (2015) Overview and Current Status of Remote Sensing Applications Based on Unmanned Aerial Vehicles (UAVs). *Photogrammetric Engineering & Remote Sensing* 81(4):281–330.
- Palomino Gonzalez A (2019) Drones and Marine Mammals in Svalbard. Master's Thesis, UiT The Arctic University of Norway, Tromsø
- Park S, Lee, H, Chon J (2019) Sustainable Monitoring Coverage of Unmanned Aerial Vehicle Photogrammetry According to Wing Type and Image Resolution. *Environmental Pollution* 247:340–48.
- Pasculli L, Piermattei V, Madonia A, Bruzzone G, Caccia M, Ferretti R, Odetti A, Marcelli M (2020) New Cost-Effective Technologies Applied to the Study of the Glacier Melting Influence on Physical and Biological Processes in Kongsfjorden Area (Svalbard). *Journal of Marine Science and Engineering* 8(8):593.
- Pina P (2014) Polygonal Pattern Analysis on Mars Based on Svalbard Analogues'. In Proceedings of the V Iberian Conference of the International Permafrost Association, University of Barcelona.
- Pix4D, SA (2017) Pix4Dmapper 4.1 User Manual. Pix4D SA: Lausanne, Switzerland.
- Prokop A, Schirmer M, Rub M, Lehning M, Stocker M (2008) A Comparison of Measurement Methods: Terrestrial Laser Scanning, Tachymetry and Snow Probing for the Determination of the Spatial Snow-Depth Distribution on Slopes. *Annals of Glaciology* 49:210–16.
- Reuder J, Båserud L, Jonassen MO, Kral ST, Müller M (2016) Exploring the Potential of the RPA System SUMO for Multipurpose Boundary-Layer Missions during the BLLAST Campaign. *Atmospheric Measurement Techniques* 9(6):2675–88.
- Rothermel M, Gong K, Fritsch D, Schindler K, Haala N (2020) Photometric Multi-View Mesh Refinement for High-Resolution Satellite Images. *ISPRS Journal of Photogrammetry and Remote Sensing* 166:52–62.

- Senger, K (2019) Svalbox: A Geoscientific Database for High Arctic Teaching and Research. In Proceedings of the AAPG Annual Convention and Exhibition, San Antonio, TX, USA, 19–22.
- Senger K, Betlem P, Birchall T, Buckley SJ, Coakley B, Eide CH, Flaig PP, Forien M, Galland, O, Gonzaga Jr L, et al (2020) Using digital outcrops to make the high Arctic more accessible through the Svalbox database. *Journal of Geoscience Education* (published online)
- Serreze MC, Barry RG (2011) Processes and impacts of Arctic amplification: A research synthesis. *Global and Planetary Change* 77(1–2):85–96.
- Smith MJ, Chandler J, Rose J (2009) High Spatial Resolution Data Acquisition for the Geosciences: Kite Aerial Photography. *Earth Surface Processes and Landforms* 34(1):155–61.
- Solbø S, Storvold R (2013) Mapping Svalbard Glaciers with the Cryowing UAS. *International Archives of the Photogrammetry, Remote Sensing and Spatial Information Sciences* 1: W2.
- Storrar RD, Ewertowski M, Tomczyk AM, Barr LD, Livingstone SJ, Ruffell A, Stoker BJ, Evans DJA (2020) Equifinality and Preservation Potential of Complex Eskers. *Boreas* 49(1):211–231.
- Storvold R, Sweatte C, Ruel P, Wuennenberg M, Tarr K, Raustein M, Hillesøy T, Lundgren T, Sumich M (2015) Arctic Science RPAS Operator's Handbook. Arctic Monitoring and Assessment Programme (AMAP), Oslo. 25 pp.
- Storvold R, Mulac B, Lesenkov S, Marshall D, Burkhardt J (2013) Use of Unmanned Aircraft for Scientific Data Collection in the Arctic. *The Arctic Herald* 1(5):64–71.
- Stuchlík R, Rusznák J, Plojhar T, Stachoň Z (2016) Measurement of Snow Cover Depth Using 100×100 Meters Sampling Plot and Structure from Motion Method in Adventdalen, Svalbard. *Czech Polar Reports* 6(2):155–168.
- Stuchlík R, Stachoň Z, Láska K, Kubiček P (2015) Unmanned Aerial Vehicle—Efficient Mapping Tool Available for Recent Research in Polar Regions. *Czech Polar Reports* 5(2):210–221.
- Sun Q, Vihma T, Jonassen MO, Zhang Z (2020) Impact of Assimilation of Radiosonde and UAV Observations from the Southern Ocean in the Polar WRF Model. *Advances in Atmospheric Sciences*, 1–14.
- Telg H, Murphy DM, Bates TS, Johnson JE, Quinn PK, Giardi F, Gao R-S (2017) A Practical Set of Miniaturized Instruments for Vertical Profiling of Aerosol Physical Properties. *Aerosol Science and Technology* 51(6):715–723.
- Thuestad AE, Tømmervik H, Solbø SA (2015) Assessing the Impact of Human Activity on Cultural Heritage in Svalbard: A Remote Sensing Study of London. *The Polar Journal* 5(2):428–445.
- Thuestad AE, Tømmervik H, Solbø S, Barlindhaug S, Flyen AC, Myrvoll ER, Johansen B (2015) Monitoring cultural heritage environments in Svalbard: Smeerenburg, a whaling station on Amsterdam Island. *EARSeL eProceedings*, 14(1): 37–50
- Tomczyk AM, Ewertowski MW, Stawska M, Rachlewicz G (2019) Detailed Alluvial Fan Geomorphology in a High-Arctic Periglacial Environment, Svalbard: Application of Unmanned Aerial Vehicle (UAV) Surveys. *Journal of Maps* 15(2):460–473.
- Tømmervik H, Karlsen S-R, Nilsen L, Johansen B, Storvold R, Zmarz A, Beck PS et al (2014) Use of Unmanned Aircraft Systems (UAS) in a Multi-Scale Vegetation Index Study of Arctic Plant Communities in Adventdalen on Svalbard. *EARSeL eProceedings* 13(S1): 47–52
- Tonkin TN, Midgley NG, Cook SJ, Graham DJ (2016) 'Ice-Cored Moraine Degradation Mapped and Quantified Using an Unmanned Aerial Vehicle: A Case Study from a Polythermal Glacier in Svalbard. *Geomorphology* 258:1–10.
- Turner IL, Harley MD, Drummond CD (2016) UAVs for Coastal Surveying. *Coastal Engineering* 114:19–24.
- Westermann S, Langer M, Boike J (2011) Spatial and Temporal Variations of Summer Surface Temperatures of High-Arctic Tundra on Svalbard—Implications for MODIS LST Based Permafrost Monitoring. *Remote Sensing of Environment* 115(3):908–922.
- Westoby MJ, Brasington J, Glasser NF, Hambrey MJ, Reynolds JM (2012) 'Structure-from-Motion' Photogrammetry: A Low-Cost, Effective Tool for Geoscience Applications. *Geomorphology* 179: 300–314.
- Zagórski P, Jarosz K, Superson J (2020) Integrated Assessment of Shoreline Change along the Calypsostranda (Svalbard) from Remote Sensing, Field Survey and GIS. *Marine Geodesy*, 1–39.

Appendix 1

Overview of all publications related to scientific unmanned vehicle operations in Svalbard.

Title	Discipline	Fieldwork location(s)	Unmanned system	Publication type	Reference
A glacier respire: Quantifying the distribution and respiration CO ₂ flux of cryoconite across an entire Arctic supraglacial ecosystem	Glaciology, Ecology	Midtre Lovénbreen, Svalbard	UAV/helicopter	Article	A. Hodson et al. 2007
The MicroASAR experiment on CASIE-09	Sea ice	Ny-Ålesund	UAV/fixed-wing	Conference paper	Long et al. 2010
Spatial and temporal variations of summer surface temperatures of high-arctic tundra on Svalbard – Implications for MODIS LST based permafrost monitoring	Atmosphere	Brøgger	UAV	Article	Westermann, Langer, and Boike 2011
The significance of depth and substratum incline for the structure of a hard bottom sublittoral community in glacial Kongsfjorden (Svalbard, Arctic)—an underwater imagery approach	Ecology	Kongsfjordheset	ROV	Article	Laudien and Orchard 2012
Profiling the Arctic Stable Boundary Layer in Advent Valley, Svalbard: Measurements and Simulations	Atmosphere	Adventdalen	UAV/fixed-wing	Article	Mayer et al. 2012
Greenhouse gas analyzer for measurements of carbon dioxide, methane, and water vapor aboard an unmanned aerial vehicle	Atmosphere	Ny-Ålesund	UAV/fixed-wing	Article	Berman et al. 2012
Mapping Svalbard Glaciers With The Cryowing UAS	Glaciology, Technology	Kongsvegen	UAV/fixed-wing	Conference paper	Solbø and Storvold 2013
Measurements of atmospheric aerosol vertical distributions above Svalbard, Norway, using unmanned aerial systems (UAS)	Atmosphere	Kongsfjorden	UAV/fixed-wing	Article	Bates et al. 2013
Use Of Unmanned Aircraft Systems (UAS) In A Multi-Scale Vegetation Index Study Of Arctic Plant Communities In Adventdalen On Svalbard	Ecology	Adventdalen	UAV/fixed-wing	Conference paper	Tømmervik et al. 2014
Polygonal pattern analysis on Mars based on Svalbard analogues	Geomorphology	Adventdalen (3 small sites)	UAV	article	Pina 2014
Unmanned Aerial Vehicle - Efficient mapping tool available for recent research in polar regions	Geomorphology, Technology	Nordenskiöldbreen	UAV/multirotor	Report	Stuchlik et al. 2015
Monitoring Cultural Heritage Environments In Svalbard: Smeerenburg, A Whaling Station On Amsterdam Island	Cultural Preservation	Smeerenburg	UAV/fixed-wing	Article	Thuestad et al. 2015
Assessing the impact of human activity on cultural heritage in Svalbard: a remote sensing study of London	Cultural Preservation	London	UAV/fixed-wing	Article	Thuestad, Tømmervik, and Solbø 2015

Determining Snow Depth Distribution from Unmanned Aerial Vehicles and Digital Photogrammetry	Snow	Breinosa	UAV/multirotor	Thesis	Cimoli 2015
Surface morphology of fans in the high-Arctic periglacial environment of Svalbard: Controls and processes	Geomorphology	Adventdalen	UAV	Article	De Haas et al. 2015
Land Cover Classification Using High-Resolution Aerial Photography In Adventdalen, Svalbard	Geomorphology, Ecology	Adventdalen	UAV	Article	Mora et al. 2015
Ice-cored moraine degradation mapped and quantified using an unmanned aerial vehicle: A case study from a polythermal glacier in Svalbard	Geomorphology	Austre Lovénbreen	UAV/multirotor	Article	Tonkin et al. 2016
Glacial geomorphology of the terrestrial margins of the tidewater glacier, Nordenskiöldbreen, Svalbard	Geomorphology	Nordenskiöldbreen	UAV/multirotor	Article	Ewertowski et al. 2016
Measurement of snow cover depth using 100x100 meters sampling plot and Structure from Motion method in Adventdalen, Svalbard	Snow	Adventdalen	UAV/multirotor	Article	Stuchlik et al. 2016
Near-bottom zooplankton aggregations in Kongsfjorden: implications for pelago-benthic coupling	Ecology	Kongsfjorden	ROV	Article	Hirche, Laudien, and Buchholz 2016
Quad-Polarimetric SAR For Detection And Characterization Of Icebergs	Technology	Kongsfjorden	UAV/fixed-wing	Conference paper	Akbari et al. 2016
Past and Present Glacial Sedimentary Environments in Krossfjorden, Western Svalbard: Glacier Front Evolution	Glaciology, Oceanography	Fjortendejullbuka	AUV	Abstact	J. Howe et al. 2016
Investigating snowpack volumes and icing dynamics in the moraine of an Arctic catchment using UAV photogrammetry	Geomorphology, Snow	Austre Lovénbreen	UAV/multirotor	Article	Éric Bernard et al. 2017
Using a small COTS UAV to quantify moraine dynamics induced by climate shift in Arctic environments	Geomorphology	Austre Lovénbreen	UAV/multirotor	Article	É Bernard et al. 2017
A UAV ice tracking framework for autonomous sea ice management	Technology	Ny-Ålesund	UAV/fixed-wing	Conference paper	Leira, Johansen, and Fossen 2017
UAV Path Planning using MILP with Experiments	Technology	Ny-Ålesund	UAV/fixed-wing	Article	Albert, Leira, and Imsland 2017
Application of Low-Cost UAVs and Digital Photogrammetry for High-Resolution Snow Depth Mapping in the Arctic	Snow	Breinosa	UAV/multirotor	Article	Cimoli et al. 2017
A practical set of miniaturized instruments for vertical profiling of aerosol physical properties	Atmosphere	Ny-Ålesund airport and Kongsfjorden	UAV/fixed-wing	Article	Telg et al. 2017
Rise and fall of a small ice-dammed lake – Role of deglaciation processes and morphology	Geomorphology	Nordenskiöldbreen / Adolffbukta	UAV/multirotor	Article	Nehyba et al. 2017

Title	Discipline	Fieldwork location(s)	Unmanned system	Publication type	Reference
AUV-based acoustic observations of the distribution and patchiness of pelagic scattering layers during midnight sun	Oceanography, Ecology	Norskebanken, Woodfjorden, Kongsfjordbanken and Isfjordbanken	AUV	Article	Geoffroy et al. 2017
Evaluation of the use of very high resolution aerial imagery for accurate ice-wedge polygon mapping (Adventdalen, Svalbard)	Geomorphology	Adventdalen	UAV	Article	Lousada et al. 2018
Drumlins in the Nordenskiöldbreen forefield, Svalbard	Geomorphology	Nordenskiöldbreen	UAV/multirotor	Article	Allaart et al. 2018
Evolution of high-Arctic glacial landforms during deglaciation	Geomorphology	Midtre Lovénbreen	UAV/multirotor	Article	Midgley et al. 2018
Circulation and exchange in a broad Arctic fjord using glider-based observations	Oceanography	Isfjorden, Nordfjorden, Sassenfjorden	AUV	Article	Fraser et al. 2018
Use of an Autonomous Surface Vehicle reveals small-scale diel vertical migrations of zooplankton and susceptibility to light pollution under low solar irradiance	Ecology	Kongsfjorden	ASV	Article	Ludvigsen et al. 2018
Detailed alluvial fan geomorphology in a high-arctic periglacial environment, Svalbard: application of unmanned aerial vehicle (UAV) surveys	Geomorphology	Dynamisk Creek alluvial fan	UAV/multirotor	Article	Tomczyk et al. 2019
Detection and characterization of icebergs in Kongsfjorden (Svalbard) based on ground-based radar images and additional remote sensing data	Oceanography	Kongsfjorden	UAV/fixed-wing	Thesis	Linge and others 2019
Latest Geodetic Changes of Austre Lovénbreen and Pedersenbreen, Svalbard	Glaciology	Austre Lovénbreen; Pedersenbreen.	UAV	Article	Ai et al. 2019
Drones and marine mammals in Svalbard	Ecology	Forlandsøyane Prins Karl Forland	UAV/multirotor	Thesis	Palomino Gonzalez 2019
Assessment of periglacial response to increased runoff: An Arctic hydrosystem bears witness	Geomorphology	Austre Lovénbreen	UAV/multirotor	Article	E. Bernard et al. 2018
Operational Framework for Rapid, Very-high Resolution Mapping of Glacial Geomorphology Using Low-cost Unmanned Aerial Vehicles and Structure-from-Motion Approach	Geomorphology	Hørbyevee	UAV/multirotor	Article	Ewertowski et al. 2019
Seasonal Dynamics of Methane and Carbon Dioxide Evasion From an Open System Pingo: Lagoon Pingo, Svalbard	Atmosphere	Lagoon Pingo, Adventdalen	UAV/multirotor	Article	A. J. Hodson et al. 2019
Autonomous underwater vehicle (AUV) observations of recent tidewater glacier retreat, western Svalbard	Glaciology, Oceanography	Fjortende Julibreen (Krossfjorden), Conwaybreen, Kongsbreen and Kronebreen (Kongsfjorden)	AUV	Article	J. A. Howe et al. 2019

Reactivation of temporarily stabilized ice-cored moraines in front of polythermal glaciers: Gravitational mass movements as the most important geomorphological agents for the redistribution of sediments (a case study from Ebbabreen and Ragnarbreen, Svalbard)	Geomorphology	Ebbabreen	UAV/multirotor	Article	Ewertowski and Tomczyk 2020
The effects of tractor driving on arctic vegetation at Kapp Linné, Svalbard	Ecology	Kapp Linné	UAV/multirotor	Thesis	Magiera 2020
Integrated Assessment of Shoreline Change along the Calypsostranda (Svalbard) from Remote Sensing, Field Survey and GIS	Geomorphology, Geodesy	Calypsostranda	UAV/multirotor	Article	Zagórski, Jarosz, and Superson 2020
Iron cycling in Arctic methane seeps	Oceanography	Storfjordrenna, Bjørnøyrenna, Ullsfjorden, Høla trough	ROV	Article	Hong et al. 2020
Equifinality and preservation potential of complex eskers	Geomorphology	Hørbyebeen	UAV/multirotor	Article	Storarr et al. 2020
Unmanned Aerial Systems for Investigating the Polar Atmospheric Boundary Layer—Technical Challenges and Examples of Applications	Atmosphere	Ny-Ålesund	UAV/ fixed-wing	Article	Lampert et al. 2020

Arctic haze in a climate changing world: the 2010-2020 trend (HAZECLIC)



Rita Traversi¹, Silvia Becagli¹, Mirko Severi¹, Laura Caiazzo^{1,2}, Mauro Mazzola³, Angelo Lupi³, Markus Fiebig⁴, Ove Hermansen⁴, and Radovan Krejci⁵

1 University of Florence, Department of Chemistry “Ugo Schiff”, Sesto F.no, I-50019, Florence, Italy

2 University of Florence & INFN-Firenze, Department of Physics, Sesto F.no, I-50019, Florence, Italy

3 The National Research Council of Italy, Institute of Polar Sciences, I-40129, Bologna, Italy

4 Norwegian Institute for Air Research (NILU), PO Box 100, N-2027, Kjeller, Norway

5 Stockholm University, Department of Environmental Science, Atmospheric Science Unit, S 106 91, Stockholm, Sweden

Corresponding author: Rita Traversi, rita.traversi@unifi.it

ORCID number 0000-0002-9790-2195

Keywords: Arctic Haze, sulphate, aerosol, Ny-Ålesund, chemical composition, PM10

DOI: <https://doi.org/10.5281/zenodo.4293826>

1. Introduction

Rapid changes in the Arctic environment including increasing temperatures, extending warm seasons, depleting sea ice, reducing surface albedo and changing long-range transport patterns of air pollutants (IPCC 2013) have become and will continue to be the focus of intense research efforts to better understand the processes that control Arctic climate (Arctic Monitoring and Assessment Programme [AMAP] 2011).

Since high-latitude climate variability has been shown to be an early indicator of global climate changes, unravelling the processes leading to Arctic amplification of radiative forcing becomes particularly relevant (Serreze and Barry 2011).

During winter–spring, the combination of intense isentropic transport from mid-latitudes to the Arctic and strong surface-based temperature inversions leads to significant increase of tropospheric aerosol concentration known as Arctic Haze (Quinn et al. 2007). The most relevant contributions to Arctic pollution in mid-winter is of SO₂, which is oxidized to sulphate by both particle (aqueous phase) processes in winter (Wang et al. 2020) and photochemical processes in spring (Ye et al. 2018) through a number of inorganic and organic drivers and intermediates. The synergetic effect of the increased residence time in wintertime and springtime sunlight makes the polar atmosphere act like a large chemical reactor, increasing the number of particles that can scatter solar radiation (Russell and Shaw 2015).

In contrast to the Arctic Haze period, pollutant concentrations during summer are much lower owing to their limited long-range transport into the Arctic from the lower latitudes, as the polar front retreats to the High Arctic (Stone et al. 2014).

Arctic Haze is mainly anthropogenic in origin due to emissions from mid-latitude areas (Europe, former Soviet Union and North America) that are transported to and trapped in the Arctic air mass during winter and early spring (between January and April). These long-range emissions add up to

the inputs from remote Arctic locations, which are minor during the Haze period. Concerning the source areas, sources from Europe and North America become significant at an altitude > 2km, while at higher elevations (> 3km) emissions from deserts, biomass burning regions and Asia play a role (Sharma et al. 2013; Shindell et al. 2008).

The Haze is mostly made of particles belonging to the accumulation mode, which are very efficient at scattering visible solar radiation; however, they also become weakly absorbing particles due to the presence of black carbon (BC; AMAP 2011; Zhao and Garrett 2015).

The net result of the strong scattering and weak absorption is a marked reduction in visibility up to a few km or less. This “weak” absorption exerts large climatic influences when the “dark” Haze expands over the highly reflective Arctic snow cover, since the highly reflective surface amplifies aerosol-radiative interactions due to multiple scattering between the surface and the Haze (Aoki 2013).

In particles mostly belonging to the accumulation mode (Tunved et al. 2013), the Arctic Haze mainly comprises a varying mixture of sulphate and organic particulate matter and, to a lesser extent, ammonium, nitrate, dust, BC and heavy metals (Li and Barrie 1993; Quinn et al. 2007).

Based on the measurements of sulphate and optical properties (light scattering and extinction) of the aerosol, the amount of the Haze reaching the Arctic was found to be either relatively constant or decreasing between the 1980s and early 1990s (Quinn et al. 2007). Moreover, based on data from many sites in the High Arctic, it appears that sulphate has continued to decrease during the first decade of the 21st century from North America and Greenland (Alert, Barrow, Station Nord) to Svalbard Islands (Zeppelin), Northern Norway (Karasjok, Svanvik), Finland (Oulanka) and western Russia (Janiskoski) such as Barrow and Alert (Quinn et al. 2007). This decreasing trend has been confirmed by recent works, such as Sharma et al.

(2019), that show a consistent drop (about 52%) in sulphate concentration at Alert over a 34-year-long period (1980–2013). In particular, at Zeppelin site, non-sea salt sulphate was found to decrease by 21.5% on average between 1990 and 2008, with the most remarkable decline occurring during the early 1990s (AMAP 2015).

Regarding Svalbard Islands, a drop of 21.5% during the period 1998–2008 was found at Zeppelin by Hirdman et al. (2010) by applying a trend analysis based on annual mean geometric concentrations. Similarly, Zeppelin shows the steepest decrease during the early 1990s.

By combining measurement data with calculations using a Lagrangian particle dispersion model (flexible particle dispersion model [FLEXPART]), Hirdman et al. (2010) identified high-latitude Eurasia (mainly Eastern Europe and the metal smelting complexes at Norilsk) as the dominant source region for sulphate at Zeppelin.

Such a trend can be particularly relevant in terms of climate owing to multiple reasons. Among these, recent studies based on present simulations with an Earth system model including comprehensive aerosol physics and chemistry (Acosta Navarro et

al. 2016) suggest that sulphate aerosol reductions in Europe since the 1980s can explain a significant part of Arctic warming over that period.

Moreover, although Arctic warming increases mainly in cold seasons (fall and winter), it is actually triggered in spring/summer by the increase in incoming solar radiation together with a more efficient poleward oceanic and atmospheric heat transport. The summertime energy surplus can reduce sea ice-cover, possibly leading to a heat transfer from the Arctic Ocean to the atmosphere (Acosta Navarro et al. 2016). Thus, it would be important to establish if air quality regulations in the Northern Hemisphere, the ocean and atmospheric circulation, and Arctic climate are related and to what extent.

Thus, a thorough investigation on the chemical markers of the Haze in different areas of the High Arctic can help monitor the temporal evolution of this process in the medium and long run as well as its potential impact on the radiative balance and atmospheric reactivity, with a special attention to possible de-acidification of the atmosphere due to a decreasing content of sulphuric acid and a relatively constant content of ammonia.

2. Overview of existing data and analysis of new data

This report presents an analysis of both existing and new data of sulphate and ammonium concentration in PM₁₀ aerosol from Gruebadet Observatory (GVB; 78.918°N, 11.895°E) and Mt. Zeppelin Observatory (ZEP; 78.908°N, 11.881°E). Both sites are located in Ny-Ålesund (78°55' N, 11°56' E); they are close (about 1.5 km as the crow flies) but have different elevations (about 50 m and 474 m a.s.l., respectively) and distance from Ny-Ålesund research village (about 700 m for GVB). The ZEP is owned and managed by the Norwegian Polar Institute and is part of the Global Atmospheric Watch network.

The monitoring of aerosol (PM₁₀) chemical composition at GVB began in 2010 and is still

ongoing; aerosol samples were collected during the spring–summer period at different resolutions (1–2 days) by several sampling devices, including PM₁₀ samplers and multi-stage impactors. Since winter 2018/2019, all-year-round samplings have started.

The dataset presented here refers to one-to-two-day PM₁₀ aerosol samples collected on 47 mm diameter PTFE filters (Pall Corporation and Cobetter Filtration Group) using a low-volume sampler (TECORA Skypost). The sample filters were prepared under a laminar flow hood in Florence and shipped to Ny-Ålesund; after sampling, the filters were stored in a freezer at “Dirigibile Italia” Station and then shipped back to Florence together with field blanks. The filters were cut into two parts; one

half was analyzed for metals (Giardi et al. 2018) or archived. The PM₁₀ mass was determined by weighing the filter before and after the sampling by means of a five-digit microbalance (Sartorius ME235P). The filters were conditioned for 48 h (25°C and 50% RH) before weighing.

The portion of the filter devoted for chemical analysis was diluted with 10 mL of ultrapure water (18 MΩ. cm, Millipore MilliQ grade) and extracted in ultrasonic bath for 20 minutes. Sulphate and ammonium were measured by two Ion Chromatographic systems performing the analysis of inorganic anions and inorganic cations, respectively. The detailed procedure is described in Becagli et al. (2011).

For both the parameters, reproducibility on real samples was better than 5%, and filter blanks were found to be lower than the detection limit. As reported by Giardi et al. (2016), detection limits for sulphate and ammonium are 0.08 and 0.09 ng m⁻³, respectively, considering the most conservative conditions of sampled volume (i.e. 55 m³ for daily resolution).

Regarding measurements at Zeppelin site, sampling and analytical determination were accomplished by using the methods described in the EMEP Manual v1996, as reported in the EBAS NILU website.

Here, we report the record of sulphate and ammonium concentrations and sulphate/ammonium ratio measured at GVB during the 2010–2019 time period. These data series are compared with the corresponding longer time series from Mt. Zeppelin and all the publicly available data covering the 1993–2019 time period at daily resolution (www.ebas.nilu.no). These are reported to highlight trend similarities and differences.

Figure 1 shows the temporal profile of sulphate concentrations at ZEP and GVB sites; the temporal profile from ZEP is split into two plots (1993–2009 and 2010–2019) to better appreciate the temporal pattern at both seasonal and interannual scale.

Considering the entire investigated period, concentration levels are quite similar at the two sites. Regarding the 2010–2019 time period, mean values are quite close (0.338 mg m⁻³ at ZEP and 0.350 mg m⁻³ at GVB), and median values are practically coincident (0.210 mg m⁻³) at the two sites. Such a similarity can also be observed clearly in the box plots given in Figure 1, which shows that the 50% of the values range between 0.1 and 0.8 mg m⁻³ at both the sites in the 2010–2019 decade. By analyzing a longer trend at Zeppelin, i.e. covering the previous 17 years, higher background and mean values can be observed yielding an average of 0.434 mg m⁻³ and a median value of 0.270 mg m⁻³. Moreover, distribution plots show a higher occurrence of larger values, causing a clear widening of the box containing the 50% of the data.

As stated in the Introduction section, such a result is consistent with the reduction of sulphur emissions from the former Soviet Union and Europe during the 1990s (Quinn et al. 2007; Sirois and Barrie 1999). Sulphate has been shown to continue its declining trend into the 21st century, as well, but at a slower rate (Quinn et al. 2007). In Ny-Ålesund, non-sea salt sulphate was found to decrease at ZEP by 21.5% on average between 1990 and 2008, with the most remarkable decline occurring during the early 1990s (AMAP 2015). In particular, during the Haze season, concentrations decreased at a rate of about 2 % yearly (Udisti et al. 2020).

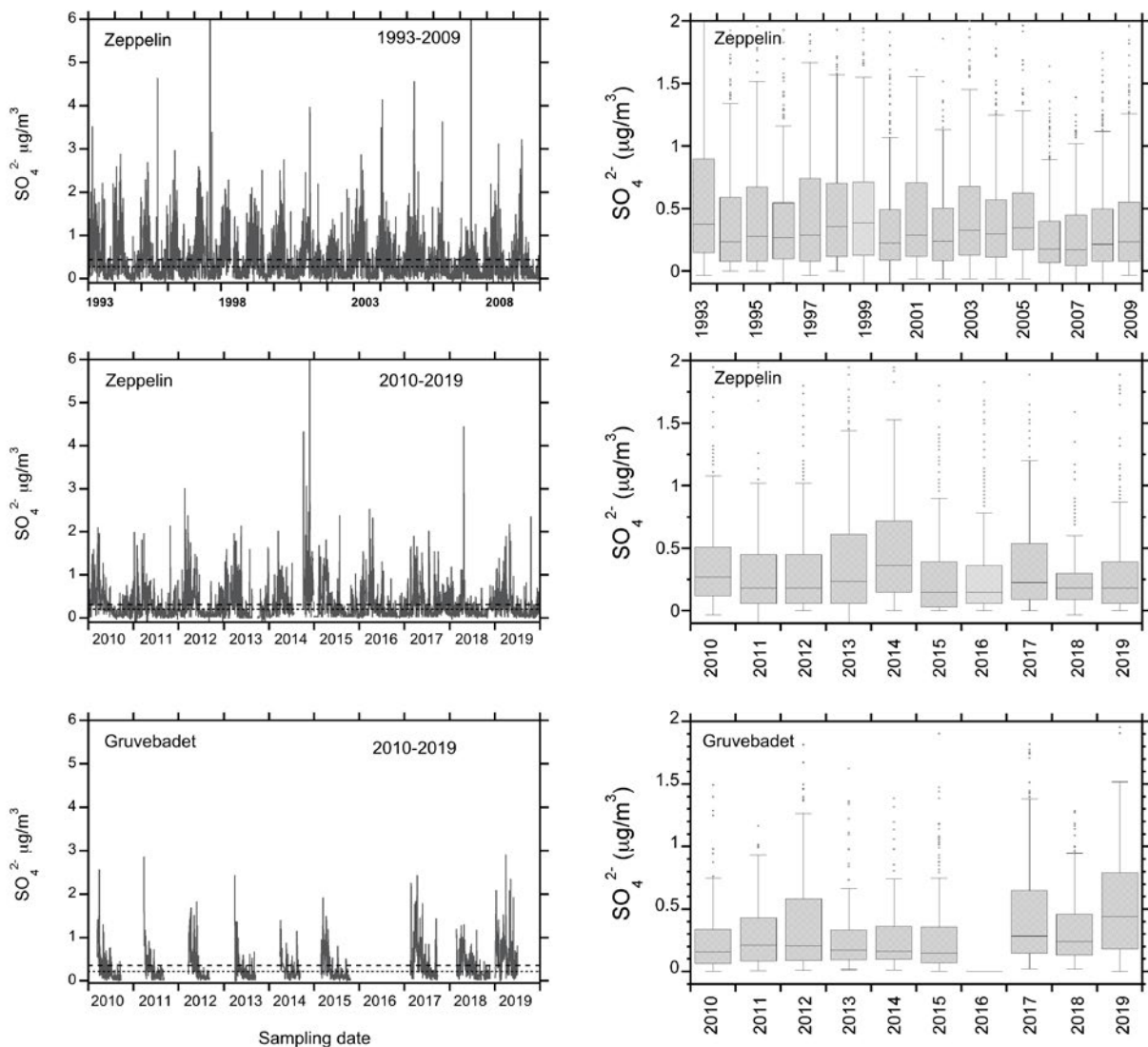


Figure 1: Sulphate concentration trends at Zeppelin (top and mid plot) and Gruvebadet (bottom plot) for the entire investigated period. The plots on the left display raw data at full resolution, while plots on the right show the data distribution as annual box plots separately for different years. Dashed and dotted lines represent mean and median values, respectively, over the investigated period.

The dataset reported here allows extending the trend to the 2010–2020 decade and assessing the extent of the drop. Considering ZEP site, by providing the longer dataset, a continuous sulphate decrease can be observed throughout the 27-year-long period. By dividing the time interval in three periods and applying a linear regression, we can observe a different decreasing rate for the last decade: The drop rate is around 20% during the 1993–1999 and 2000–2009 timeframes, while a steeper decrease is assessed for the 2010–2019 period (around 30%).

Conversely, possibly due to the shorter time period, no significant evidence of a decrease in sulphate at

GVB can be observed through a preliminary data analysis.

Similar decreases were also observed for equivalent black carbon (eBC) in various Arctic sites for 2000–2008 (Hirdman et al. 2010) and 1980–2013 (Sharma et al. 2019). Moreover, a strong correlation was also observed between Zeppelin and two other Arctic sites (Pallas and Alert) by Eckhardt et al. (2015) and captured by models belonging to different classes. This confirms earlier evidence of a common source region for sulphate and eBC and common mixing and removal processes for these aerosol components (Quinn et al. 2007).

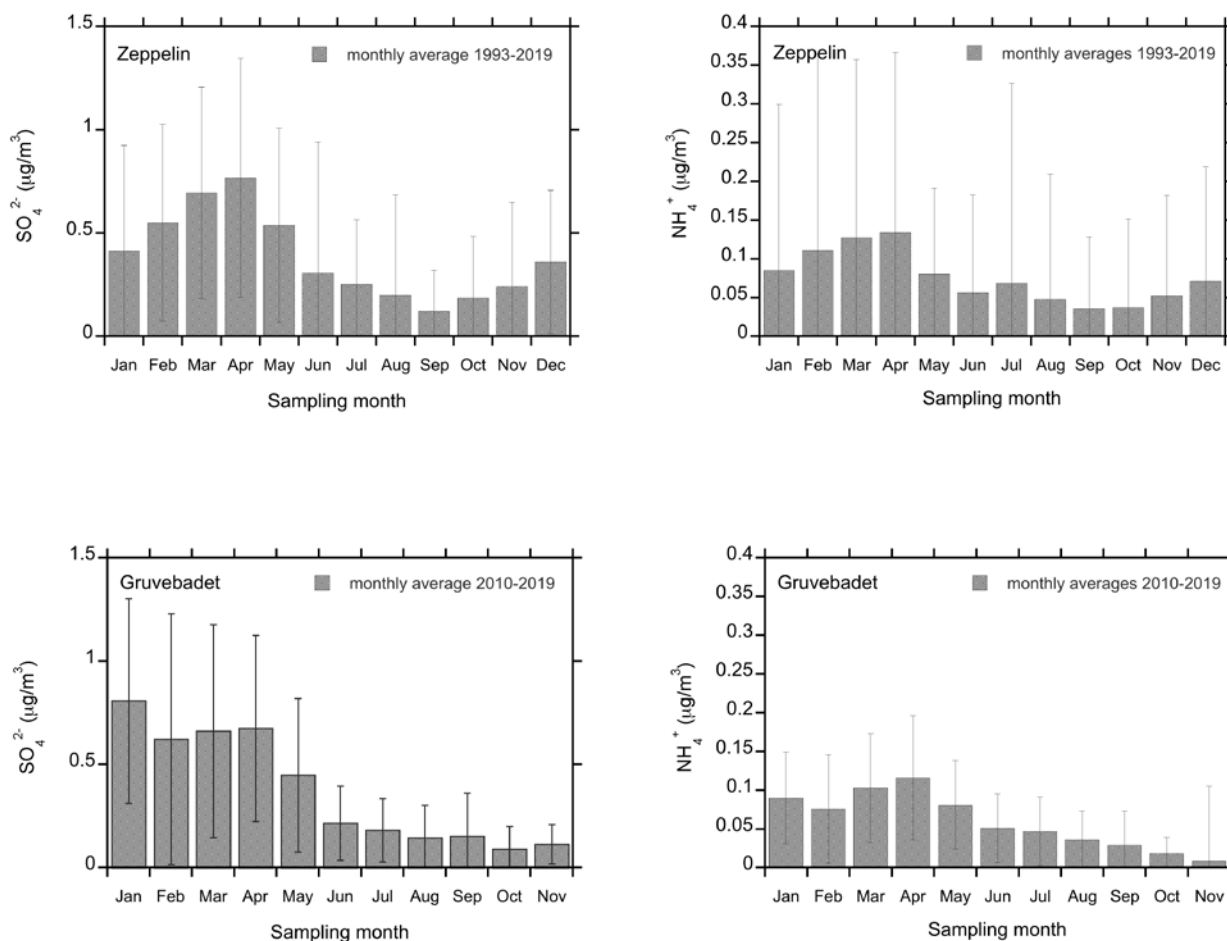


Figure 2: Monthly average of sulphate (left) and ammonium (right) concentrations at Zeppelin and Gruvebadet Observatories (top and bottom plot, respectively) over the time period covered by the available data. Vertical bars refer to the standard deviation of the measurements.

The seasonal pattern of sulphate that can only be barely spotted in Figure 1 can be clearly observed in Figure 2, which shows monthly averages for the entire periods covered by available data at the two sites. Temporal pattern of sulphate as well as ammonium is mainly controlled by the Arctic Haze, with concentrations maximizing during late winter–early spring due to build-up of Haze and then declining and minimizing during summer. The shape of sulphate’s winter maximum at GVB is different from the one at ZEP. At the latter site, one can observe the highest values in April, whereas at GVB a larger maximum is shown during the late winter–early spring period (i.e. February and March). Given that the sampling coverage is different for GVB and Zeppelin (i.e. November and January were sampled only during 2018/2019 field season), this has to be taken only as a preliminary hint; therefore, the difference between the two sites needs to be confirmed through further measurements.

By combining the evidence given by Figures 1 and 2, it is reasonable to assume that a change in sulphate emissions is connected to a change in the chemical composition (or at least sulphate content) in the Haze. Indeed, by analyzing the pattern of sulphate’s monthly averages of different years, it comes out that the months affected by the Haze are driving the sulphate drop along the years.

Indeed, few studies have estimated the contribution of various sulphate sources in Ny-Ålesund, and anthropogenic sources were confirmed to be dominant during winter/spring in terms of crustal, sea-salt and biogenic sources (Udisti et al. 2016; Yang et al. 2018). For instance, according to a source apportionment performed by Udisti et al. (2016) on the basis of aerosol chemical composition at GVB in 2014, biogenic sulphate fraction reached up to 70% in summer, becoming dominant as the anthropogenic component decreases in this season.

Figure 3 shows the temporal profile of sulphate concentration in March and September for the entire range of available datasets at the two sites; the two months were chosen as representative of “Haze” and “no-Haze” periods. In March, sulphate average shows a progressive decrease with time, while September average remains either constant or increases both at ZEP and GVB. These trends show statistically significant linear correlation coefficients (> 95%); the slope of the corresponding regression line is shown for ZEP in Figure 4. From the figure, it appears that there is a seasonal pattern in sign and extent of sulphate trends along the year; substantial decreasing trends can be observed for late winter–early spring (January–April), slightly declining trend is seen during late spring–summer (May–August) and then again in December, and slightly positive trends are observed in Autumn (September – November). This pattern is in line with the dominance of the Haze in the first part of the year and its changing through last decades, but the constant or slightly increasing levels during summer and autumn at both ZEP and GVB sites does not have a straightforward interpretation. Given that marine biogenic source dominates sulphate emissions during late spring–summer, the data shown in Figure 4 may hint towards a progressive increase of intensity or transport processes related to this source along the last decades at Ny-Ålesund even though it is unclear why this could affect autumn months.

The decrease of sulphate concentration in aerosol mainly reflects a decrease in sulphuric acid, it being the main component of the Arctic Haze and particularly of the aerosol accumulation mode (Udisti et al. 2016, 2020) dominating the Haze size distribution. Such a change may have a relevant influence on the chemistry of the Arctic atmosphere in terms of neutralization capacity. According to Sharma et al. (2019), there has been a shift from a generally acidic particulate (sulphuric acid) to a more neutral one (mainly due to ammonium sulphate) due to the larger decline in SO_2 emissions with respect to ammonia emissions in the source regions. The analysis of ammonium concentration and $\text{SO}_4^{2-}/\text{NH}_4^+$ ratio in the aerosol can provide useful information about this likely evolution of the chemistry of the atmosphere along the last decades.

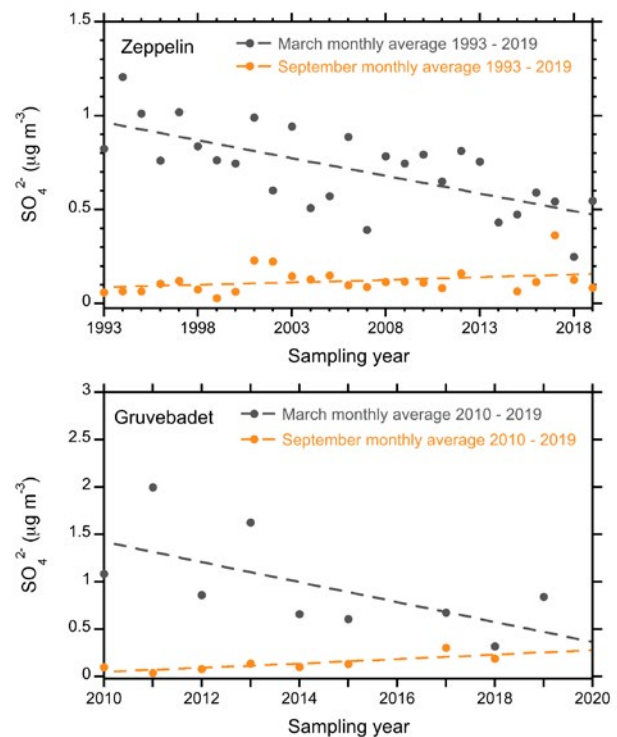


Figure 3: Temporal trend of monthly averages of sulphate concentrations for two selected months (March and September) from the entire sampling period at Zeppelin and Gruvebadet sites.

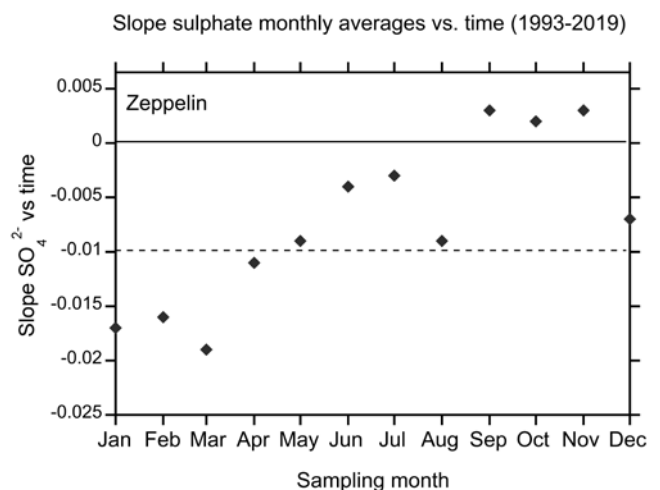


Figure 4: Decreasing/increasing rate of sulphate in the long run (1993–2019) at Zeppelin for each month of the year. Dotted and continuous lines separate the season, showing different trends.

Figure 5 shows $\text{SO}_4^{2-}/\text{NH}_4^+$ ratio (w/w) at monthly (plots on the left) and yearly (plots on the right) resolution at ZEP and GVB over the entire period covered by available data. Previous works already showed that sulphate is present in the aerosol found in Ny-Ålesund mainly as ammonium salt, often both as $(\text{NH}_4)_2\text{SO}_4$ and $(\text{NH}_4)\text{HSO}_4$ during spring–summer (Giardi et al. 2016; Udisti et al. 2016, 2020). Both monthly and yearly averages exhibit a general excess of sulphuric acid with respect to $(\text{NH}_4)_2\text{SO}_4$ and $(\text{NH}_4)\text{HSO}_4$ ratios, with usually higher values at ZEP than GVB indicating an overall dominance of sulphuric acid over neutralized salts. By looking into details at a seasonal scale (see Figure 6), it appears that sulphate/ammonium ratios are particularly high, ranging between 11.6 and 12.2 at ZEP and between 6.7 and

9.7 at GVB as monthly mean during the Haze period (January–April; see Figure 5). These values are much higher than 5.33 – the ratio marking the formation of NH_4HSO_4 salt during the Haze period; however, in summer, the values are found to be around 5.33. These results indicate the presence of an excess of sulphate with respect to the stoichiometric amount needed to neutralize ammonia, confirming that during the Arctic haze months, a significant fraction of sulphuric acid is present together with the most acidic form of sulphate salts (i.e. NH_4HSO_4). The minima of the ratios get slightly shifted during August and September at ZEP and during July and August at GVB, but the general seasonal trend remains quite similar.

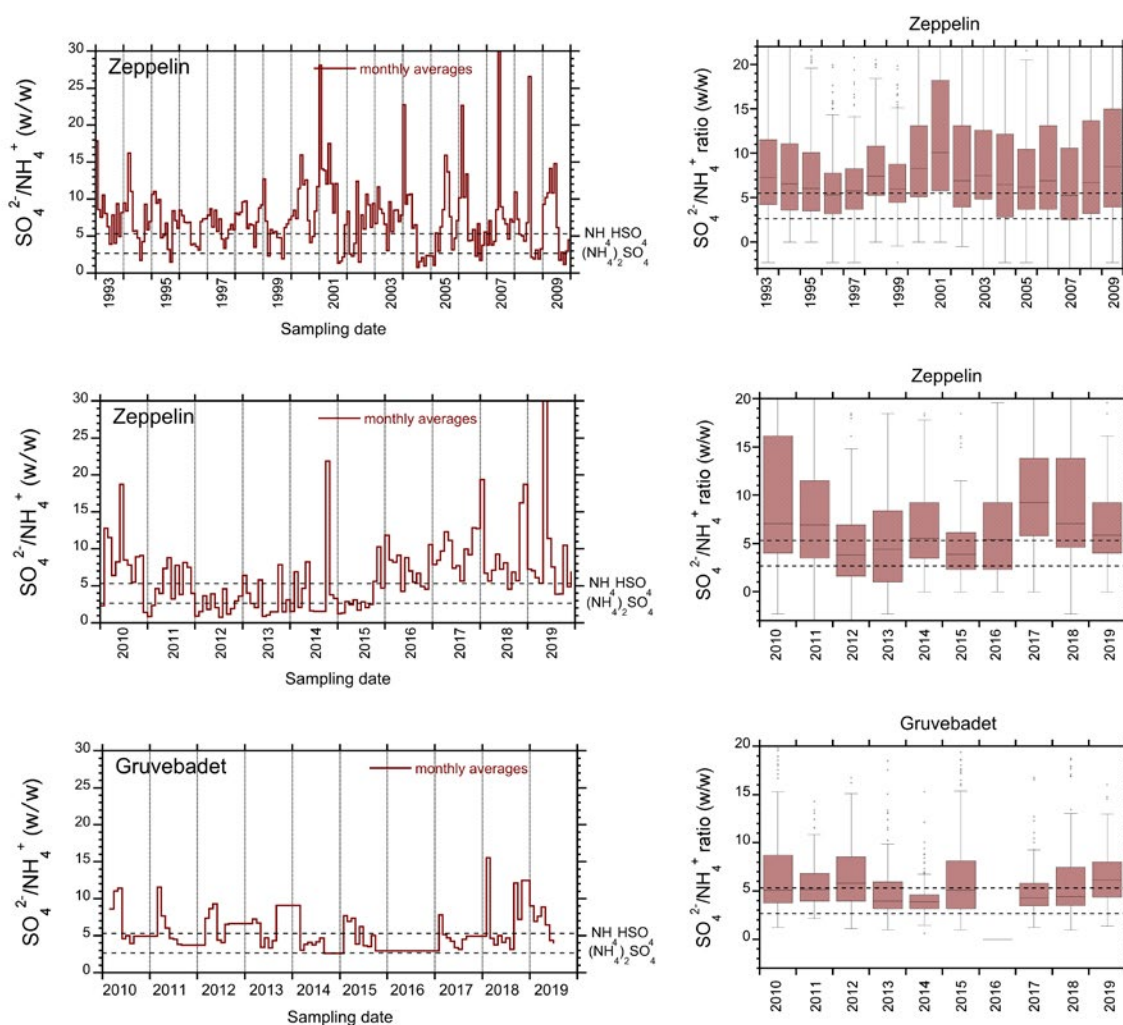


Figure 5: Sulphate/ammonium ratio at monthly resolution and distribution box plot at Zeppelin and Gruebadet Observatories (top plots and bottom plot, respectively) over the entire time period covered by the available data. Dotted lines mark the value of the sulphate/ammonium ratio (w/w) in NH_4HSO_4 (5.33) and $(\text{NH}_4)_2\text{SO}_4$ (2.66)

It is interesting to notice that previous works at GVB (Giardi et al. 2016; Udisti et al. 2016) that focused on single years (2013 and 2014, respectively) found different results from that of the summer sulphate/ammonium ratio, with smaller values, around 2.66, corresponding to the complete neutralization of H_2SO_4 with ammonia to yield $(\text{NH}_4)_2\text{SO}_4$. Nevertheless, comparing the ratios at the two sites for the time period of 2010–2019, both monthly averages and distribution plots at yearly resolution show generally higher values for ZEP. Since sulphate levels are basically similar at the two sites and measured ammonium concentrations are lower at ZEP, the latter drives the ratio. It is likely that differences in the analytical determination and

detection limits of the methods used for ZEP and GVB can explain different values of the ratios at the two sites.

Regarding the long-term trend of the ratio, it appears to be highly variable. Moreover, in this case also, it is possible that a relatively large uncertainty on low ammonium concentrations prevents from observing trends over the years. Sticking to the available data, it appears that there is no clear trend towards a more neutralized atmosphere, but to ascribe it to increasing ammonia emission and compensating decreasing sulphate, further measurements and harmonized protocols are needed.

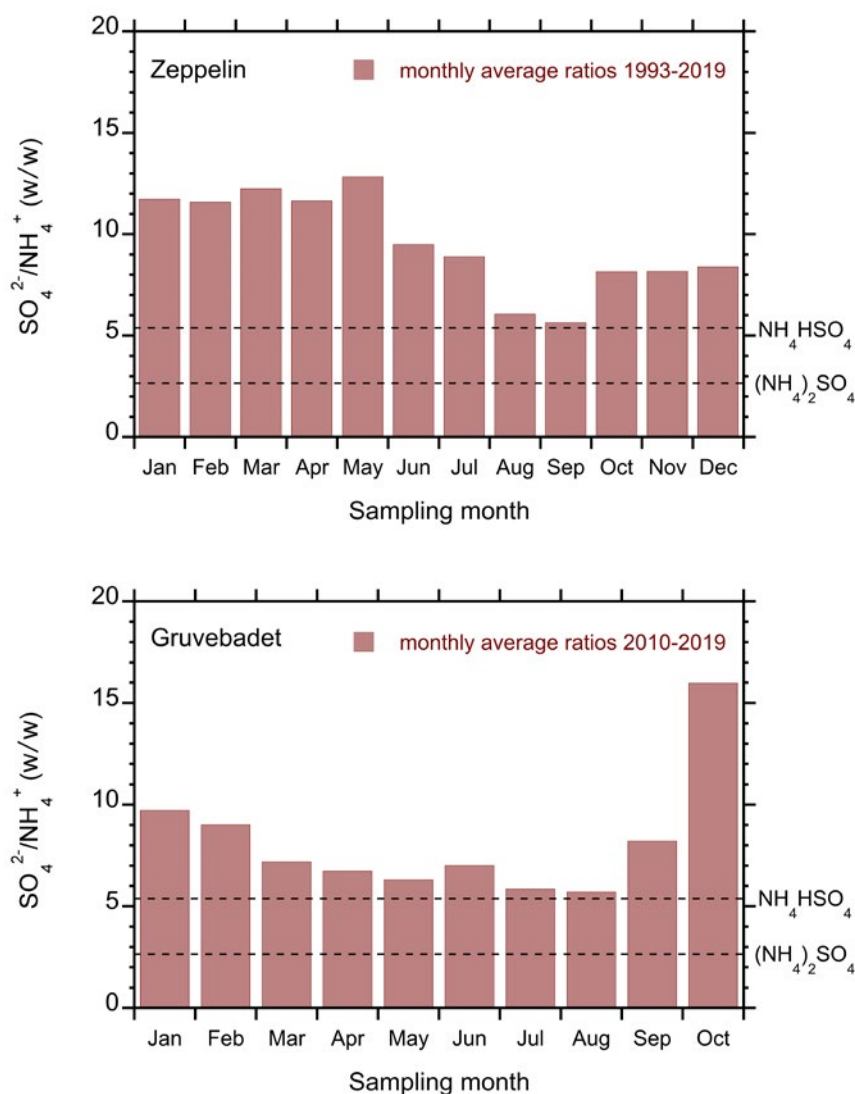


Figure 6: Monthly averages of sulphate/ammonium ratios at Zeppelin and Gruebadet Observatories (top and bottom plot, respectively) over the entire time period covered by the available data.

3. Connections and synergies with other SESS report chapters

This report is in synergy with the SESS Report 2019 chapter “Atmospheric black carbon in Svalbard (ABC Svalbard)” (Gilardoni et al. 2020), which presents an overview of existing data on BC from the same sites as investigated here (ZEP and GVB). BC being another relevant marker of the Arctic Haze, the merger of the datasets presented here and of “ABC Svalbard” would yield a more comprehensive view of the changes in the Haze in Ny-Ålesund.

The datasets and results presented here also fit some of the recommendations in the SESS Report 2019 chapter “Multidisciplinary research on biogenically driven new particle formation in Svalbard (SVALBAEROSOL)” (Sipilä et al. 2020). In the chapter, the authors strongly suggest the continuation of current dimethylsulfide (DMS) and aerosol measurements at Gruvebadet and Zeppelin stations, possibly simultaneously, to better understand the present and predict the

future CCN concentration and optical properties. For this purpose, a more detailed knowledge of the secondary aerosol formation pathways must be achieved. Both sulphuric acid and ammonia have been proven to work as triggers of new particle formation processes in different continental environments (Kirkby et al. 2011; Kulmala et al. 2013); however, the exact mix of reagents which is responsible for such processes in the Arctic is not known yet (Sipilä et al. 2020).

Possible connections can be found with SESS Report 2020 chapter “How representative is Svalbard for future Arctic climate evolution? An Earth system modelling perspective (SvalCLIM)” (Gjermundsen et al. 2021) by using the long-term data reported here to feed predictive models, which pays special attention to the changing features of the Arctic Haze and its impact on overall Arctic climate.

4. Unanswered Questions

Although not completely satisfactory, our current knowledge of the chemical and physical features of the Arctic Haze can be considered as promising.

Long-term and permanent observatories measure aerosol species, including particularly sulphate and other chemical proxies of the Haze (e.g. ammonium, nitrate, BC, organic carbon), as well as size distribution and optical properties of the aerosol that can be related to such process.

A large dataset on the surface concentrations of this kind of aerosol and their seasonal/annual variability is now available, and long-term trends have shown that sulphate has decreased and aerosol has become less acidic.

Nevertheless, the available datasets cover different temporal ranges (from the last few years to the last four decades) at the different sites and with different temporal resolutions so that the merging

of all the datasets to draw significant conclusions on the trends in the Arctic is not straightforward and needs to be accomplished accurately not to be misleading.

In addition, the same datasets have been obtained by applying different protocols of sampling (low- and high-volume samples, sampling medium), sample storage and treatment and, especially, chemical analysis (different analytical performances, blank levels, numbers and kinds of measured analytes), possibly compromising the reliability of a comparison.

A relevant open point of consideration that is connected to aerosol chemical composition and related sources is the vertical structure of boundary layer (BL) in Ny-Ålesund. A number of studies present consistent meteorological datasets on the long-term (e.g. 1993–2011, Maturilli et al. 2013) performed comparisons of eddy covariance measurements

with model results (Jocher et al. 2015) and derived vertical variations of momentum, heat fluxes and kinetic energy (Mazzola et al. 2016). However, although these datasets provide a good picture of the atmospheric variables in the area, they are still not sufficient to describe the vertical structure of the BL. A more detailed knowledge of this aspect would help in better interpreting the observed features in

chemical composition at GVB and ZEP.

In terms of environmental interpretation of the observed changes in the Arctic Haze, a challenging open point concerns the cause of the observed trends: Are they entirely due to changed emissions or does a changing atmospheric reactivity have a role to play?

5. Recommendations for the future

To discriminate between the contribution of sources (changing in terms of chemical composition and/or intensity and possibly different transport routes due to changes in atmospheric circulation patterns) and different chemistry of the atmosphere, continuous long-term measurements are required from strategic sites, such as GVB and ZEP; moreover, existing observations need to be continued and enlarged to further parameters.

In fact, since the two sites are located at different altitudes but at close distance, the differences in concentration levels and seasonal/interannual trends observed at the two sites can help to better understand the impact of local sources and long-range sources of sulphate and the other Haze proxies.

The measurement of other climatically relevant parameters (such as Cloud Condensation Nuclei [CCN and Ice-Nucleating Particle [INP]) and examination of specific studies (dealing with parameters such as single particle composition, mixing state of BC aerosol) has been performed during spot campaigns at both the observatories, but it is strongly suggested to continue it for the long term, in parallel with other ongoing observations.

In particular, regarding single particle size and composition analysis and INP properties of such particles, there is increasing evidence that such information is pivotal to understand the cloud-aerosol feedback in the Arctic, while the mixing state of BC with organic and inorganic aerosol species (including brown carbon) could provide relevant information to understand BC radiative forcing.

For this purpose, an accurate source apportionment by refined statistical tools (particularly Positive Matrix Factorization [PMF]) is mandatory. Hence, a broad spectrum of chemical and physical parameters measured at high and regular resolution is needed. Although data series for some of the mentioned parameters are available, there exists a lack of observation for some species, especially primary and secondary organic aerosols, needed for apportionment of particles to natural and anthropogenic sources.

Therefore, the measurement of methanesulphonic acid (MSA) would provide a valuable support in assessing the biogenic contribution to sulphate budget; this is because MSA is an univocal marker of marine biological activity (also related to sea-ice dynamics; Becagli et al. 2016, 2019) and sulphate/MSA ratio has already been used to reconstruct biogenic source in Ny-Ålesund (Udisti et al. 2016). Hence, there is a clear need to complement ongoing surface-based experimental observations.

GVB can be considered as a representative of ground-level concentrations of the investigated markers, and it is well within the BL. Conversely, Zeppelin observatory has a more dynamic relationship with BL (being often above the BL during winter season and sometimes within it during summer months); however, this phenomenon remains unanswered, and further meteorological and physical observations are needed. Hence, a thorough comparison between the datasets obtained at the two sites is needed to better constrain the impact of the Haze both at surface level and above the BL; this would help to have a

sort of both “local” and “long-range” signature in Svalbard Islands.

To improve the reliability and effectiveness of such a comparison, it is recommended to harmonize the protocols for aerosol sampling and measurements between the two sites. For instance, it would be helpful to set common cut off and/or to use multiple size classes, temporal resolutions, sampling material, extraction and analysis procedures. Later, data analysis tools could also be shared and used on the combined datasets. Moreover, periodic intercalibration exercises (e.g. round robin tests) on same samples are recommended to detect possible significant discrepancies and figure out the best

strategy to match the data series.

Future collaboration among the institutes and stations working on the topics discussed in this report should be solicited, with special attention to the research groups already working in Ny-Ålesund (Alfred Wegener Institut [AWI], Institut Polaire Français Paul-Émile Victor [IPEV], University of Helsinki and Finnish Meteorological Institute [FMI], Stockholm University, Korea Polar Research Institute [KOPRI]). These Institutes have already established collaboration over the past years. Other Institutes concerned with the research topics discussed here should also be encouraged to join efforts with existing collaborations.

6. Data availability

The data that will be collected and discussed in this report include

1. Long-term measurements of sulphate and ammonium concentration in atmospheric aerosol collected at GVB during the 2010–2020 period.

2. Long-term measurements of sulphate and ammonium concentration in atmospheric aerosol collected at ZEP during the 1993–2019 period.

Dataset	Parameters	Period	Location/Area	Metadata/Data access (URL/DOI)	Data provider
PM10 chemistry at GVB	Sulphate and ammonium concentration in PM10 aerosol	2010–2019	Gruvebadet Observatory (GVB) - Ny-Ålesund	http://ebas.nilu.no/ SIOS data access portal: https://bit.ly/2HF8IDE (click 'Search')	Rita Traversi rita.traversi@unifi.it
PM10 chemistry at Zeppelin	Sulphate and ammonium concentration in PM10 aerosol	1993–2019	Zeppelin Observatory (ZEP) - Ny-Ålesund	http://ebas.nilu.no/ SIOS data access portal: https://bit.ly/2HF8IDE (click 'Search')	EBAS NILU

Acknowledgements

This work was supported by the Research Council of Norway, project number 291644, Svalbard

Integrated Arctic Earth Observing System – Knowledge Centre, operational phase.

References

- Acosta Navarro JC, Varma V, Riipinen I, Seland Ø, Kirkevåg A, Struthers H, Iversen T, Hansson HC, Ekman AML (2016) Amplification of Arctic warming by past air pollution reductions in Europe. *Nat Geosci* 9:277–281. <https://doi.org/10.1038/ngeo2673>
- AMAP (2011) The Impact of Black Carbon on Arctic Climate. By: Quinn PK, Stohl A, Arneth A, Berntsen T, Burkhardt JF, Christensen J, Flanner M, Kupiainen K, Lihavainen H, Shepherd M, Shevchenko V, Skov H, Vestreng V. AMAP Technical Report No. 4. Arctic Monitoring and Assessment Programme (AMAP), Oslo, Norway, pp 72.
- AMAP (2015) Black carbon and ozone as Arctic climate forcers. AMAP Assessment 2015. Arctic Monitoring and Assessment Programme (AMAP), Oslo, Norway, vii + 116 pp. Arctic Monitoring and Assessment Programme, 2015. ISBN: 978-82-7971-092-9.
- Aoki T (2013) Reflection properties of snow surfaces. In: Light Scattering Reviews, 7th edn. Springer Praxis Books, Springer, Berlin, Heidelberg. https://doi.org/10.1007/978-3-642-21907-8_5
- Becagli S, Amore A, Caiazzo L, Di Iorio T, di Sarra A, Lazzara L, Marchese C, Meloni D, Mori G, Muscari G, Nuccio C, Pace G, Severi M & Traversi R (2019) Biogenic aerosol in the Arctic from eight years of MSA data from Ny Ålesund (Svalbard Islands) and Thule (Greenland). *Atmosphere* 10: 349.
- Becagli S, Ghedini C, Peeters S, Rottiers A, Traversi R, Udisti R, Chiari M, Jalba A, Despiou S, Dayan U, Temara A (2011) MBAS (methylene blue active substances) and LAS (linear Alkylbenzene sulphonates) in Mediterranean coastal aerosols: Sources and transport processes. *Atmos Environ* 45: 6788–6801. <https://doi.org/10.1016/j.atmosenv.2011.04.041>
- Becagli S, Lazzara L, Marchese C, Dayan U, Ascanius SE, Cacciani M, Caiazzo L, di Biagio C, Di Iorio T, di Sarra A, Eriksen P., Fani F, Giardi F, Meloni D, Muscari G, Pace G, Severi M, Traversi R, Udisti R (2016) Relationships linking primary production, sea ice melting, and biogenic aerosol in the Arctic. *Atmos Environ* 136:1–15. <http://dx.doi.org/10.1016/j.atmosenv.2016.04.002>
- Eckhardt S, Quennehen B, Olivie B, Cherian R, Christensen JH, Collins W, Crepinsek S, Daskalakis N, Flanner M, Herber A, Heyes C, Hodnebrog Ø, Huang L, Kanakidou M, Klimont Z, Langner J, Law KS, Lund MT, Mahmood R, Massling A, Myriokefalitakis S, Nielsen IE, Nøjgaard JK, Quaas J, Quinn PK, Raut JC, Rumbold ST, Schulz M, Sharma S, Skeie RB, Skov H, Uttal T, von Salzen K, Stohl A (2015) Current model capabilities for simulating black carbon and sulfate concentrations in the Arctic atmosphere: A multi-model evaluation using a comprehensive measurements data set. *Atmos Chem Phys* 15:9413–9433. DOI: 10.5194/acp-15-9413-2015
- Giardi F, Becagli S, Traversi R, Frosini D, Severi M, Caiazzo L, Ancillotti C, Cappelletti D, Moroni B, Grotti M, Bazzano A, Lupi A, Mazzola M, Vitale V, Abollino O, Ferrero L, Bolzacchini E, Viola A, Udisti R (2016) Size distribution and ion composition of aerosol collected at Ny-Ålesund in the spring-summer field campaign 2013. *Rend Fis Acc Lincei* 27:S47–S58. <https://doi.org/10.1007/s12210-016-0529-3>
- Giardi F, Traversi R, Becagli S, Severi M, Caiazzo L, Ancillotti C, Udisti R (2018) Determination of Rare Earth Elements in multi-year high-resolution Arctic aerosol record by double focusing Inductively Coupled Plasma Mass Spectrometry with desolvation nebulizer inlet system. *Sci Total Environ* 613–614: 1284–1294. <https://doi.org/10.1016/j.scitotenv.2017.09.247>
- Gilardoni S, Lupi A, Mazzola M, Cappelletti D, Moroni B, Ferrero L, Markuszewski P, Rozwadowska A, Krejci R, Zieger P, Tunved P, Karlsson L, Vratolis S, Eleftheriadis K, Viola AP (2020) Atmospheric black carbon in Svalbard. In: Van den Heuvel et al (eds): SESS report 2019, Svalbard Integrated Arctic Earth Observing System, Longyearbyen, pp. 197–211. https://sios-svalbard.org/SESS_Issue2
- Gjermundsen A, Graff LS, Bentsen M, Breivik LA, Debernard JB, Makkonen R, Olivie DJL, Seland Ø, Zieger P, Schulz M (2021) How representative is Svalbard for future Arctic climate evolution? An Earth system modelling perspective. In: Moreno-Ibáñez et al (eds) SESS report 2020, Svalbard Integrated Arctic Earth Observing System, Longyearbyen, pp. 38–59 <https://doi.org/10.5281/zenodo.4034104>
- Hirdman D, Sodemann H, Eckhardt S, Burkhardt JF, Jefferson A, Mefford T, Quinn PK, Sharma S, Ström J, Stohl A (2010) Source identification of short-lived air pollutants in the Arctic using statistical analysis of measurement data and particle dispersion model output. *Atmos. Chem. Phys.* 10:669–693, <https://doi.org/10.5194/acp-10-669-2010>
- IPCC, 2013: Summary for Policymakers. In: Climate Change 2013: The Physical Science Basis. Contribution of Working Group I to the Fifth Assessment Report of the Intergovernmental Panel on Climate Change. In: Stocker, T.F., D. Qin, G.-K. Plattner, M. Tignor, S. K. Allen, J. Boschung, A. Nauels, Y. Xia, V. Bex and P.M. Midgley (eds.), Cambridge University Press, Cambridge, United Kingdom and New York, NY, USA
- Jocher G, Schulz A, Ritter C, Neuber R, Dethloff K, Foken T (2015) The sensible heat flux in the course of the year at Ny-Ålesund, Svalbard: Characteristics of eddy covariance data and corresponding model results. *Adv Meteorol* 2015: 852108, <https://doi.org/10.1155/2015/852108>
- Kirkby J et 77 al. (2016) Ion-induced nucleation of pure biogenic particles. *Nature* 533(7604):521. <https://doi.org/10.1038/nature17953>

- Kulmala M, Kontkanen J, Junninen H, Lehtipalo K, Manninen HE, Nieminen T, Petäjä T, Sipilä M, Schobesberger S, Rantala P, Franchin A, Jokinen T, Järvinen E, Äijälä M, Kangasluoma J, Hakala J, Aalto PP, Paasonen P, Mikkilä J, Vanhanen J, Aalto J, Hakola H, Makkonen U, Ruuskanen T, Mauldin RL 3rd, Duplissy J, Vehkamäki H, Bäck J, Kortelainen A, Riipinen I, Kurtén T, Johnston MV, Smith JN, Ehn M, Mentel TF, Lehtinen KE, Laaksonen A, Kerminen VM, Worsnop DR (2013) Direct observations of atmospheric aerosol nucleation. *Science*. 339(6122):943–946. <https://doi.org/10.1126/science.1227385>
- Li SM, Barrie LA (1993) Biogenic sulfur aerosol in the Arctic troposphere: 1. Contributions to total sulphate. *J Geophys Res* 1993, 98(D11):20613–20622. <https://doi.org/10.1029/93JD02234>
- Maturilli M, Herber A, König-Langlo G (2013) Climatology and time series of surface meteorology in Ny-Ålesund, Svalbard. *Earth Syst Sci Data* 5:155–163. <https://doi.org/10.5194/essd-5-155-2013>
- Mazzola M, Tampieri F, Viola A, Lanconelli C, Choi T (2016) Stable boundary layer vertical scales in the Arctic: observations and analyses at Ny-Ålesund, Svalbard. *QJR Meteorol Soc* 142:1250–1258. <https://doi.org/10.1002/qj.2727>
- Quinn PK, Shaw G, Andrews E, Dutton EG, Ruoho-Airola T, Gong SL (2007) Arctic haze: current trends and knowledge gaps. *Tellus* 59B:99–114. <https://doi.org/10.1111/j.1600-0889.2006.00236.x>
- Russell LM, Shaw GE (2015) Arctic Haze. In: *Encyclopedia of Atmospheric Sciences* 2nd edn. 1:116–121. <https://doi.org/10.1016/B978-0-12-382225-3.00073-6>
- Serreze MC, Barry, RG (2011) Processes and impacts of Arctic amplification: A research synthesis. *Glob Planet Change* 77(1):85–96. <https://doi.org/10.1016/j.gloplacha.2011.03.004>
- Sharma S, Barrie LA, Magnusson E, Brattstrom G, Leaitch WR, Steffen A, Landsberger S (2019) A factor and trends analysis of multidecadal lower tropospheric observations of arctic aerosol composition, black carbon, ozone, and mercury at Alert, Canada. *J Geophys Res Atmos* 124(14):133 –14161. <https://doi.org/10.1029/2019JD030844>
- Sharma S, Ishizawa M, Chan D, Lavoue D, Andrews E, Eleftheriadis K, Maksyutov S (2013) 16-year simulation of Arctic black carbon: Transport, source contribution, and sensitivity analysis on deposition. *J. Geophys. Res. Atmos* 118(2):943–964. <https://doi.org/10.1029/2012JD017774>
- Shindell DT, Chin M, Dentener F, Doherty RM, Faluvegi G, Fiore AM, Hess P, Koch DM, MacKenzie IA, Sanderson MG, Schultz MG, Schulz M, Stevenson DS, Teich H, Textor C, Wild O, Bergmann DJ, Bey I, Bian H, Cuvelier C, Duncan BN, Folberth G, Horowitz LW, Jonson J, Kaminski JW, Marmer E, Park R, Pringle KJ, Schroeder S, Szopa S, Takemura T, Zeng G, Keating TJ, Zuber A (2008) A multi-model assessment of pollution transport to the Arctic. *Atmos Chem Phys*, 8(17):5353–5372. ISSN 1680-7316. <https://doi.org/10.5194/acp-8-5353-2008>
- Sipilä M, Hoppe CJM, Viola A, Mazzola M, Krejci R, Zieger P, Beck L, Petäjä T (2020) Multidisciplinary research on biogenically driven new particle formation in Svalbard. In: Van den Heuvel et al (eds): *SESS report 2019, Svalbard Integrated Arctic Earth Observing System, Longyearbyen*, pp. 169–194. https://sios-svalbard.org/SESS_Issue2
- Sirois A, Barrie LA (1999) Arctic lower tropospheric aerosol trends and composition at Alert, Canada: 1980–1995. *J Geophys Res* 104(D9):11599–11618. <https://doi.org/10.1029/1999JD900077>
- Stone S, Sharma S, Herber A, Eleftheriadis K, Nelson DW (2014) A characterization of Arctic aerosols on the basis of aerosol optical depth and black carbon measurements. *Elementa: Science of the Anthropocene* 2:000027. <https://doi.org/10.12952/journal.elementa.000027>
- Tunved P, Ström J, Krejci R (2013) Arctic aerosol life cycle: linking aerosol size distributions observed between 2000 and 2010 with air mass transport and precipitation at Zeppelin station, Ny-Ålesund, Svalbard. *Atmos Chem Phys* 13:3643–3660. <https://doi.org/10.5194/acp-13-3643-2013>
- Udisti R, Bazzano A, Becagli S, Bolzacchini E, Caiazzo L, Cappelletti D, Ferrero L, Frosini D, Giardi F, Grotti M, Lupi A, Malandrino M, Mazzola M, Moroni B, Severi M, Traversi R, Viola AP, Vitale V (2016) Sulfate source apportionment in the Ny-Ålesund (Svalbard Islands) Arctic aerosol. *Rend Fis Acc Lincei* 27:S85–S94. <https://doi.org/10.1007/s12210-016-0517-7>
- Udisti R, Traversi R, Becagli S, Tomasi C, Mazzola M, Lupi A, Quinn PK (2020) Chapter 4. Arctic aerosol. In: Kokhanovsky A, Tomasi C (ed) *Physics and chemistry of the Arctic atmosphere*. Springer Nature Switzerland AG, Cham, Switzerland. ISBN 978-3-030-33566-3.
- Wang J, Li J, Ye J, Zhao J, Wu Y, Hu J, Liu D, Nie D, Shen F, Huang X, Huang DD, Ji D, Sun X, Xu W, Guo J, Song S, Qin Y, Liu P, Turner JR, Lee HC, Hwang S, Liao H, Martin ST, Zhang Q, Chen M, Sun Y, Ge X, Jacob DJ (2020) Fast sulfate formation from oxidation of SO₂ by NO₂ and HONO observed in Beijing haze. *Nat Commun* 11: 2844. <https://doi.org/10.1038/s41467-020-16683-x>
- Yang, Y, Wang H, Smith S, Easter R, Rasch P (2018) Sulfate Aerosol in the Arctic: Source Attribution and Radiative Forcing. *J Geophys Res Atmos* 123(3): 1889–1918. <https://doi.org/10.1002/2017jd027298>
- Ye J, Abbatt JP, Chan AW (2018) Novel pathway of SO₂ oxidation in the atmosphere: reactions with monoterpene ozonolysis intermediates and secondary organic aerosol. *Atmos Chem Phys* 18: 5549–5565. <https://doi.org/10.5194/acp-18-5549-2018>
- Zhao CF, Garrett TJ (2015) Effects of Arctic haze on surface cloud radiative forcing. *Geophys Res Lett* 42: 557–564. <https://doi.org/10.1002/2014GL062015>

Microplastics in the realm of Svalbard: current knowledge and future perspectives (MIREs)

Neelu Singh¹, Maria Granberg², France Collard¹, Gabriella Caruso³, Zhibo Lu⁴, Tanja Kögel^{5,6}, and Geir Wing Gabrielsen¹

1 Norwegian Polar Institute, Fram Centre, Tromsø, Norway

2 IVL Swedish Environmental Research Institute, Sweden

3 Institute of Polar Sciences, National Research Council of Italy, Messina, Italy

4 College of Environmental Science and Engineering, Tongji University, China

5 Institute of Marine Research, Bergen, Norway

6 University of Bergen, Faculty of Mathematics and Natural Sciences, Bergen, Norway

Corresponding authors: Neelu Singh, neelu.singh0387@gmail.com, and Geir Wing Gabrielsen, geir.wing.gabrielsen@npolar.no

Keywords: Microplastics, Svalbard, climate change, atmospheric currents, ocean currents

DOI: <https://doi.org/10.5281/zenodo.4293836>

1. Introduction

Plastic and our society have become inseparable. Almost all aspects of daily life involve plastics. Plastics are found, for example, in electronics, home appliances, vehicles, food/goods packaging material, cosmetics, and a range of textiles. Plastic industries have assessed that in 2018 about \approx 359 million tons of plastics were manufactured, globally out of which 62 million tons were produced in Europe (Plastics Europe 2019). Resultantly, plastic pollution has become a critical point of concern, on account of the rapid production and disposal rate of plastic combined with poor waste handling and the slow degradation rate of the material. Merely a few decades into the rapid rise of plastic mass production, we have generated a huge volume of plastic debris in the environment, potentially leaving classifiable fossil records for future generations (Zalasiewicz et al. 2015). Furthermore, plastics are mostly produced from carbon-based raw materials, mainly natural gas and crude oil (Plastics Europe 2019). Different reactions of polymerization contribute to regulating the properties of plastics such as its hardness or softness, opacity or transparency, flexibility or stiffness. Chemical additives such as plasticisers, flame-retardants, and dyes are added to plastics to modulate their flexibility, durability, or other characteristics. First used in environmental sciences two decades ago (Thompson et al. 2004), the term “microplastics” (MPs) encompasses plastic fragments 1 μ m to 5 mm in size. Sources of MPs overlap with those of meso- (2.5 cm – 0.5 cm) and macro-plastic (1 m – 2.5 cm) in many instances. Based on their origin, MPs can be distinguished into the following two types: primary and secondary. Primary MPs are small-sized and commonly used as exfoliants/scrubbers in cosmetics and industrial abrasives (Cole et al. 2011; Leslie 2014), plastic beads that serve as drug vectors in medicines (Patel et al. 2009), or precursors in the production of other plastic products. Conversely, secondary MPs originate from the fragmentation of meso or macro or even larger plastics under the influence of light, mechanical abrasion, and/or temperature

fluctuations. Further fragmentation from MPs to smaller sized (below 1 μ m) particles are known as nano plastics (MSFD Technical Group on Marine Litter 2013). The focus of this review is only on the microplastic (MPs) category.

Not only is plastic production and littering on the rise globally but the high buoyancy of many plastics leads to long-distance transport in the ocean. Plastic is widely distributed in almost all zones from the polar region to tropics and habitats from the sea surface and pelagic zone to the benthos and deep sea. In the Arctic, remote from large populations, plastic debris dominates observations of marine litter (Grøsvik et al. 2018) and has been suggested to have negative effects on the Arctic biota and threatening the ecosystem (Halsband and Herzke 2019; Tanaka et al. 2020). The most common fatal interaction of Arctic organisms with plastic litter is entanglement and ingestion (Derraik 2002). Reported observations of entanglement and ingestion of mega/macropastics by terrestrial and marine organisms are numerous. Entanglement in abandoned fishing gear and other marine litter on the beaches of Svalbard, Norway, by reindeer and seabirds is common (Figure 1) (Hallanger and Gabrielsen 2018; Nashoug 2017; Øritsland 1986). Moreover, ingestion of plastics has been found in organisms at lower and higher levels of the Arctic food web including benthic organisms like starfish, shrimp, and crabs (Fang et al. 2018), fish (Kühn et al. 2018; Morgana et al. 2018), whales (Finley 2001), and seabirds (Poon et al. 2017; Provencher et al. 2017; van Franeker et al. 2011; Trevail et al. 2015). Seabirds, in particular, are vulnerable to marine plastics, mainly on account of their high trophic position and their extensive foraging range. For these reasons, and because their colonies are relatively easily accessed by researchers once a year, seabirds are considered ideal monitoring sentinels for marine plastic pollution in the environment (Herzke et al. 2016; Avery-Gomm et al. 2012; van Franeker et al. 2011).



Figure 1: Interaction of local organisms with plastic litter. Photos: Jon Aars (Reindeer), Susanne Kühn (Fulmar), Governor of Svalbard (Arctic tern, polar bear)

1.1. Adverse effects of MPs

While the adverse effects of larger plastic litter are obvious as the observations mentioned above demonstrate, our knowledge of the adverse effects of MPs is very limited. Biological effects of micro- and nano-plastics have only been observed in laboratory studies. From the available data, the adverse effects of MPs can be divided into mechanical effects, chemical toxicity, and pathogenic microbial toxicity.

Mechanical effects: Unlike macroplastics, the mechanical effects of MPs are hard to assess. Hard and sharp-edged MPs can potentially injure or scratch the soft tissues of the lungs, liver, and gastrointestinal tract (GI) (Hwang 2019; Fry 1987), which may lead to infection and sometimes even death (Duis and Coors 2016). MPs are widely reported to be excreted after ingestion (De Sales-Ribeiro et al. 2020) but they have also been reported to cause obstruction or create a false satiated feeling by residing in the GI tract, leading to death

due to starvation in organisms. MPs have been reported to affect the GI microbiome in organisms (Cox et al. 2019; Wright et al. 2017; Fackelmann et al. 2019) and rare observations report that MPs with a diameter of $\leq 250 \mu\text{m}$ may translocate into tissues in fish (Gomiero et al. 2020) and also in mammals exposure studies (Volkheimer 1975).

Chemical toxicity: The chemical toxicity of MPs can be mediated by plastic additives or contaminants adsorbed to the plastic particles as they travel through the environment. Additives are chemicals added at the time of production, which can be fillers, plasticizers, flame retardants, colorants, stabilizers, lubricants, foaming agents, and antistatic agents (Groh et al. 2019). Chemicals that sorb onto the plastic particles include persistent organic pollutants (POPs), heavy metals, and pharmaceuticals (Magara et al. 2019; Zhang et al. 2019; Sikdokur et al. 2020; Tang et al. 2020). These chemicals can potentially alter physiological functions after being ingested with the plastic particles (Cole et al. 2011; Watts et al. 2014; Wang et al. 2018). On the other hand,

some studies show no correlation between the body burden of organic pollutants and the gut content of MPs in seabirds (Herzke et al. 2016). Whether chemicals associated with or sorbed to plastics play a greater role than other sources of toxic chemicals is yet to be investigated. MPs may not be a net to the most important vector for environmental pollutants other than for those primarily associated with plastics as additives.

Pathogenic microbial toxicity: Plastics, including MPs, are a suitable substrate and vector for pathogenic

microbes in the environment (Oberbeckmann et al. 2015; Koelmans et al. 2016; Hartmann et al. 2017). By colonizing and growing on the surface of MPs, microbes form dense biofilms, the so-called “plastisphere” (Kirstein et al. 2019; Zettler et al. 2013). Organisms can get infected by ingesting MPs colonized by pathogenic microbes (Bhattacharya and Khare 2020). Pathogenic antibiotic-resistant bacteria have been found on MPs collected in the intertidal zone in western Norway (Radisic et al. 2020).

2. Overview of existing knowledge

Different studies of MPs pollution in Svalbard have used different methods and units of measurement ([Appendix 1](#)), making it difficult to discern trends and draw comparisons. Furthermore, many studies do not satisfactorily assess measurement uncertainties. Harmonised analytical protocols and data reporting, as well as method inter-calibration with proficiency tests, are essential to enable us to compare datasets and observe trends. Advice on plastic monitoring in the Arctic regarding sampling and measurement methods is currently being developed through the Arctic Monitoring and Assessment Programme (AMAP). To our knowledge, two ring test regimes are ongoing on a European basis, organised by Quasimeme and the European Commission Joint Research Centre (JRC)/German Federal Institute for Materials Research and Testing (BAM), respectively.

Reports of MP in sea ice, snow, seawater, beach sand, deep-sea and shallow sediments, invertebrates, fish, and seabirds allow to coinciding that MPs have become ubiquitous in the Svalbard ecosystem ([Appendix 1](#)). Knowledge of the ecological and social impacts of this is vital for making informed decisions and policies regarding MPs pollution. Therefore, by exploring the following points, we aim to synthesise the existing knowledge of MPs pollution in and around Svalbard and to identify new insights from current research and gaps and challenges to be addressed by future research.

2.1. Known and potential sources of MPs in Svalbard

MPs have numerous points of entry into the environment, complicating it to pinpoint their particular source. However, based on current knowledge, the sources of MPs in Svalbard can be divided into local and long-range distances (Figure 2). Local sources include industrial activities (e.g. fishing and shipping), tourism, domestic activities such as the washing of synthetic textile clothing, personal care products such as cosmetics containing MPs (e.g. toothpaste, exfoliators, etc.), dumpsites and landfills, sewage, vehicle tyres, and snowmobile belt. Long-distance sources are mostly in similar categories as local sources but on a larger scale. From long-distance sources, MPs travel to Svalbard via atmospheric and ocean currents (Obbard et al. 2018). Before the discovery of atmospheric transportation of MPs, ocean currents were considered as the main pathway for MPs to remote locations such as the polar regions (Cózar et al. 2017). Lately, the detection of MPs in snow, ice and air samples (Bergmann et al. 2019) has highlighted the role of air currents as an important pathway for MPs as well as challenged our current understanding of their global transport. A recent modelling study found the high transport efficiencies of MPs particles produced by road traffic (tyre wear particles [TWP] and brake wear particles [BWP]) to remote regions via the air (Evangelidou et al. 2020).

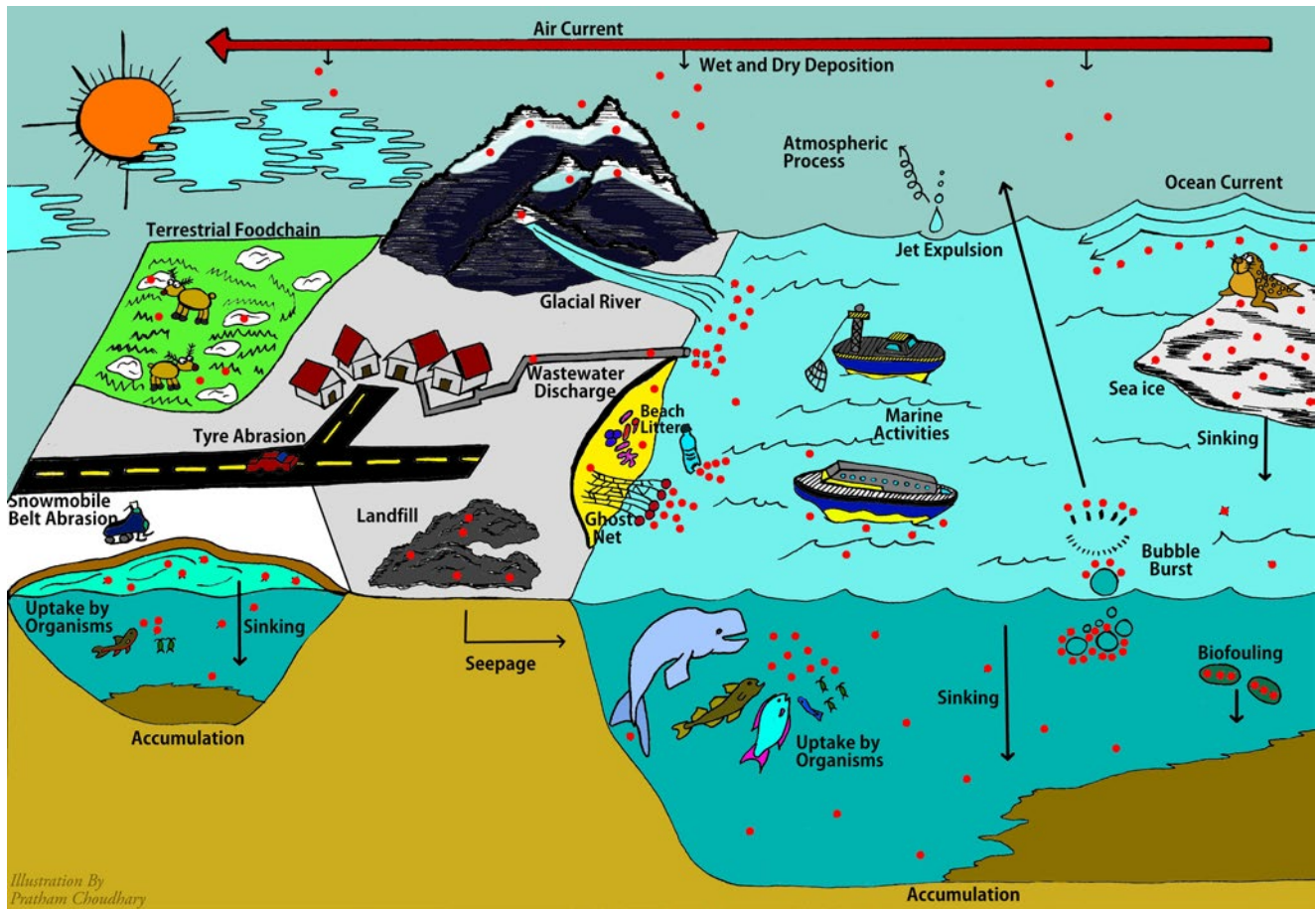


Figure 2: Potential sources and pathways of MPs in Svalbard

2.2. Pathways and movement of MPs between environmental compartments

Glaciers: Glaciers are likely deposition areas for debris and pollutants transported by air, as glacier ice forms through the transformation of accumulated snowfalls, which are particularly efficient at scavenging dust, soot, contaminants, and MPs from the atmosphere (Bergmann et al. 2019). Cryoconite – the dust on a glacier – absorbs solar radiation and forms vertical cylindrical holes. These holes are likely to retain and accumulate atmospherically transported contaminants such as heavy metals (Nagatsuka et al. 2010; Łokas et al. 2016; Baccolo et al. 2017; Singh et al. 2017; Huang et al. 2019), organic compounds (Ferrario et al. 2017; Weiland-Bräuer et al. 2017) and MPs (Ambrosini et al. 2019) from local and distant sources. Seasonal and climate change-induced temperature rise may result in the release of cryoconite/glacial debris-bound MPs to watersheds and the ocean.

Wetlands: Wetlands consist of shallow and perennial lakes and ponds. These environments play an important role in ecosystem structure by sustaining most of the Arctic microbial biodiversity and providing natural refuges and feeding places for wildlife (Walseng et al. 2018). Wetlands are potentially susceptible to the deposition of atmospherically transported MPs from local and distant sources and seabirds (Luoto et al. 2019) to some extent.

Marine environment: The Svalbard ecosystem is mainly influenced by the West Spitsbergen Current, which carries water from the Atlantic northwards and along the western coast of Svalbard (Svendsen et al. 2002), and brings MPs from North Atlantic fisheries to Svalbard (Bergmann et al. 2017). The eastern coasts of Svalbard receive Arctic water from the northeast (Misund et al. 2016), which could be expected to be more influenced by MPs from sea maritime industries and activities (shipping, fishing, cruise ships, and scientific expeditions) from lower latitudes. In addition, MPs may also originate

from local sources such as sewage/wastewater discharge, fishing and tourist activities, and dumpsites and landfills among other local sources. After reaching Svalbard, MPs with a higher density than seawater would sink and accumulate in the sediments (Woodall et al. 2014; Alomar et al. 2016), whereas MPs with a lower density would float on surface water (Suaria and Aliani 2014). The density of floating MPs can be altered through 'biofouling', a process in which biofilm that forms on the surface of floating MPs increases the density of MPs, thereby increasing sinking (Caruso 2020). Floating MPs may be distributed by wind and waves to the fjords and/or washed onto the shores. MPs input into fjords can also be expected from glaciers as a result of iceberg calving, surface melting, runoff, or melting under floating ice shelves. Corroborating this hypothesis, the highest concentrations of MPs measured in Arctic sediments were found close to glaciers (Huntington et al. 2020) and sea-ice fronts (Bergmann et al. 2017; von Friesen et al. 2020).

Sea ice plays a triple role for MPs: a temporary sink, a secondary source, and a transport medium (Obbard et al. 2014; Peeken et al. 2018; Kanhai et al. 2020). Forming sea-ice traps MPs from the surrounding water and sediments. Additionally, atmospheric MPs deposits on sea-ice floes. When sea ice drifts, it transports MPs and release trapped MPs by melting caused by seasonal or climate-induced warming. Regardless of transport, sea ice will release previously trapped MPs into the ocean again, due to seasonal and/or climate change-induced melting.

Generally, the ocean acts as a sink and conveyance for MPs from one to the other location; recently, however, an additional role of the ocean as an indirect source of MPs has been highlighted (Allen et al. 2020). According to Allen et al. MPs may enter the atmosphere from the ocean in a similar way as sea salt aerosol and organic matter do under the influence of wave action, adding a new aspect to the environmental plastic cycle.

Terrestrial environments: MPs in the terrestrial environment may enter via atmospheric currents from long-distance/local sources and be deposited on land, vegetation, water bodies, etc. Earlier it was

believed that mainly marine organisms are at risk of MPs contamination. However, with the discovery of the pervasiveness of MPs via atmospheric currents, it has become clear that MPs may also enter the terrestrial food chain (Bergmann et al. 2019). This has raised questions about not only the security of terrestrial wildlife but also for people living in Svalbard because terrestrial wildlife (e.g. reindeer) is a culturally and nutritionally important traditional food.

Seabirds can also be a source of MPs to the terrestrial environment since MPs can be contained in their regurgitates and faeces. Plastic ingested by seabirds is thought to be retained in the gizzard and mechanically broken down over time until the small pieces are able to pass through the intestines and be excreted (Reynolds and Ryan, 2018).

2.3. Status of MPs in different environmental compartments

Atmosphere: Atmospheric long-distance transport of MPs to the Arctic was not reported until last year when snow samples from Fram Strait and Svalbard were shown to contain MPs (Bergmann et al. 2019). Although the significance of atmospheric transport has been highlighted in a few studies from Svalbard and other remote locations, no data are available on the route and transportation pattern of MPs, except the recently published atmospheric model-based study (Evangelidou et al. 2020), which suggests that the Arctic may be a receptor region for atmospherically transported MPs.

Ice and snow: There are only very few published reports of MPs in snow and sea ice from Svalbard MPs ([Appendix 1](#)). MPs in ice cores from the Fram Strait and north of Svalbard have been observed as a result of local sources (Peeken et al. 2018) and via air currents, transported over long distances to the Arctic (Bergmann et al. 2019). So far, no publication quantifies the deposition of MPs on glaciers in Svalbard. However, there is evidence of MPs in glacial debris from the Forni Glacier (Italian Alps) (Ambrosini et al. 2019), which could be considered instrumental to conduct similar research by the unexplored glaciers of Svalbard. In light of this, we can hypothesise that similar processes may occur for MPs transportation and deposition on glacial

debris/cryoconite in Svalbard. MPs records in glacial ice cores could provide indications for temporal variations, in a similar way to lake sediments that act as a lacustrine archive of MPs (Turner et al. 2019).

Open ocean: MPs in Arctic seawater are relatively well studied in comparison to the other compartments ([Appendix 1](#)). MPs have been reported in surface waters and sub-surface waters near Svalbard, potentially as a result of the breakdown of larger items (transported over a long distance or originating from local vessels) or derived from sewage and wastewater from coastal areas (Lusher et al. 2015). MPs were detected through the entire water column of the Arctic Ocean (Tekmann et al. 2020), suggesting that the Arctic is an accumulation area for MPs coming from (i) the North Atlantic via the thermohaline circulation, (ii) north of the Fram Strait entrained in sea ice and released during melting, (iii) the Barents Sea, (iv) ships in the vicinity, (v) different directions through the atmosphere and precipitations, and/or (vi) rivers discharge.

Coastal and fjord waters: MPs have been detected in seawater, sea-ice samples from different fjords in Svalbard as a result of summer sea-ice melting (von Friesen et al. 2020), and wastewater outlets near settlements (Sundet et al. 2016; von Friesen et al. 2020); they have also been seen to come from local activities as well as distant ones (Purver 2019) via Atlantic ocean currents (Scott 2019).

Freshwater bodies: Despite their importance for the Svalbard ecosystem, freshwater bodies are not well studied for MPs contamination. To date, two studies of MPs in freshwater from Svalbard are available. A study of MPs in sediment from Lake Revvatnet suggested that the increased little auk (*Alle alle*) population acts as a source for MPs (Luoto et al. 2019). However, in another study, MPs in sediment from Lake Knudsenheia (near the western shore of Kongsfjorden) was discussed as a result of atmospheric deposition from local or distant sources (Gonzalez-Pleiter et al. 2020).

Marine sediment and beaches: Detection of MPs in the deep-sea sediment of the Arctic Basin and from the HAUSGARTEN deep-sea observatory in eastern Fram Strait suggested the Arctic as an accumulation zone for MPs particles transported from long distance and/or local sources (Woodall et al. 2014; Bergmann et al. 2017; Tekman et al. 2020). MPs in sediment from the Barents Sea reported at a depth between 650 and 508 meters were discussed as a result of the accumulation of debris (Møskeland et al. 2018). MPs have been detected in shallow sediment from Svalbard coastal areas, in the Kongsfjord-Krossfjord system, Rijpfjorden, Grønnfjorden, Adventfjorden, and Breibogen and are discussed as a result of local and/or long-distance MPs pollution (Sundet et al. 2016; Granberg et al. 2019; von Friesen 2018; Granberg et al. In press).

Terrestrial environment: Even though plastic pollution mainly originates from terrestrial sources, terrestrial systems have not received much scientific attention. To date, there is no publication describing the MPs distribution in terrestrial surface (soil, vegetation) in Svalbard.

2.4. Variability of MPs characteristics and their spatial distribution

MPs in the environment, including the Svalbard region, show huge variability in shapes, sizes, colours, and polymers (Lusher et al. 2015; Duis and Coors 2016; Peeken et al. 2018; von Friesen et al. 2020) for many reasons. First, plastic materials consist of diverse polymers and additives. Once in the environment, these additives continue to modify the fate of plastics. MPs with UV stabilisers will resist for a longer time to degradation compared to a plastic material without such additives. The fragmentation rate will then be different, which will result in a difference in size. The colour also influences the MPs fate since some animals are attracted by specific colours and specifically ingest some and overlook others (Ory et al. 2018; Roch et al. 2020). MPs have a range of intrinsic densities which commonly range from 0.9 to 2.3 g/cm³ (Hidalgo-Ruz et al. 2012). The shape and the density of MPs will also play a role in their sinking rate (Kowalski et al. 2016; Kane et al. 2019). Their

density determines their fate and increases their vertical ubiquity in the aquatic environments, while the shape influences buoyancy. The more rounded, the faster MPs will sink under the same environmental conditions (Kowalski et al. 2016). MPs can also originate from a tremendous number of sources and all inhabited regions of the world, contributing to spatial variability in the environment. In addition to the numerous sources, oceanic and atmospheric currents transport MPs all around the globe, increasing their occurrence in remote areas such as Svalbard. Those currents affect the fate of MPs at both a large and a small scale (Van Sebille et al. 2020). All these parameters simultaneously determine the spatial and vertical distributions and the fate of MPs, leading to the high variability of MPs occurrence in the Svalbard aquatic environments.

2.5. Effects of climate change on MPs distribution

The most important factors affecting the weathering and breakdown of plastic debris to MPs and nano plastics are UV-light and temperature (Andrady 2011). How Arctic conditions, in particular, affect plastic litter weathering is largely unexplored (PAME 2019). Cold winter temperatures and intense 24-hour summer sunlight are both unexplored in their influence on plastic. The harsh weather conditions on the very exposed coasts are further likely to cause fragmentation of already brittle pieces of macroplastic (Brandon et al. 2016). Due to the complexity of the weathering process, it cannot be concluded by deduction if plastic fragmentation is occurring more rapidly in the Arctic than, e.g. in the tropics until now. However, the Arctic is a

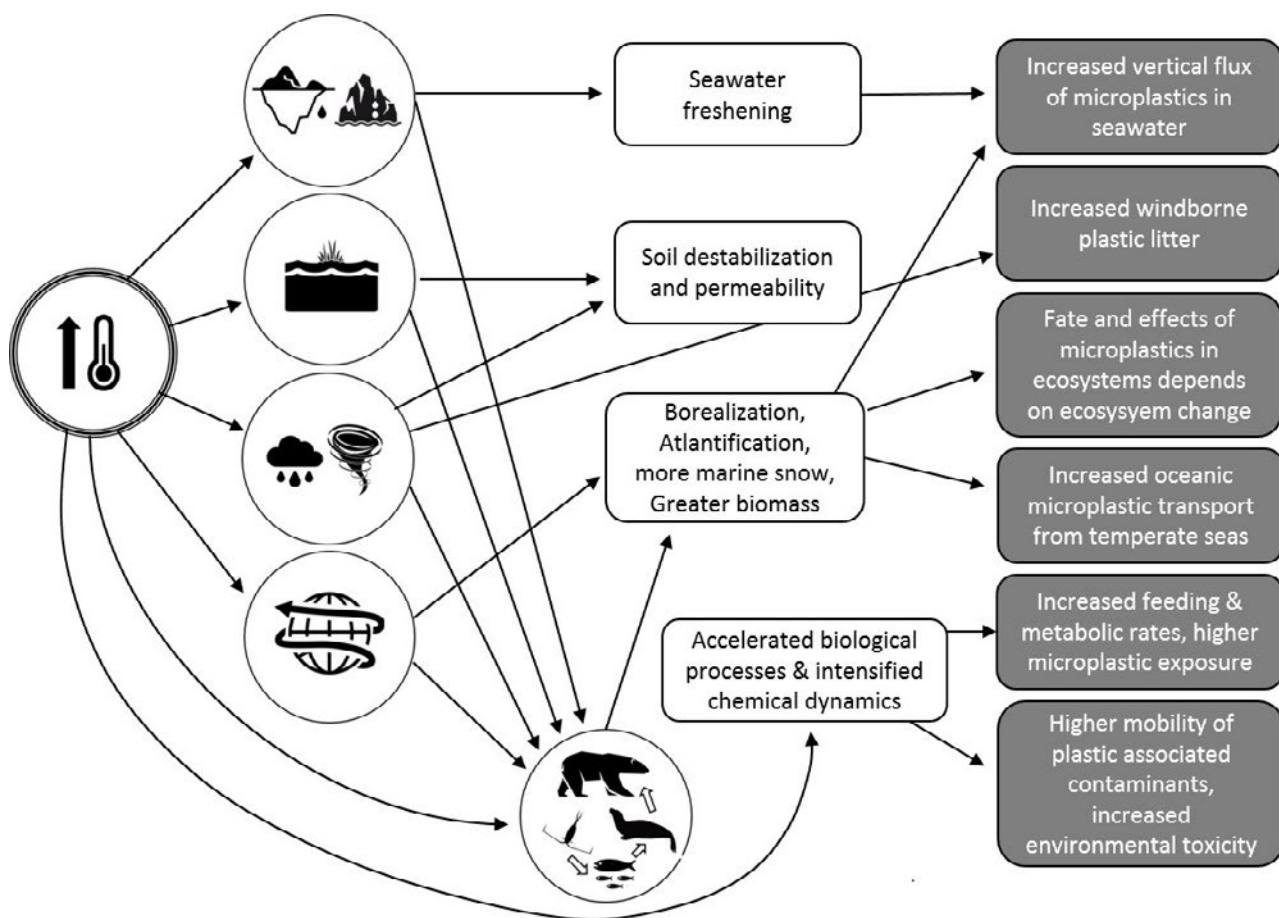


Figure 3: Conceptual illustration showing the potential effects of climate change on plastic pollution in the Svalbard environment

global 'hot-spot' for climate change and is warming more rapidly than other places on the planet due to polar amplification. The term 'polar amplification' refers to a greater temperature change near the poles compared to the rest of the globe for a given global climate force such as a change in greenhouse gasses (Screen and Simmonds 2010; Adakudlu et al. 2019). The major impact of climate change in the Arctic is the loss of sea ice, permafrost thawing, ice melting, glacier reduction, soil destabilization, weather pattern changes, and ocean current alterations (Figure 3). Such climate-induced changes in environmental variables will likely have sizeable impacts on the distribution of MPs in Svalbard and should be investigated.

Changing climate and melting of sea ice and glaciers: The Arctic cryosphere, consisting of ice and snow, is highly sensitive to climate change. Based on satellite images from 1979 to the present, a 40 % decline in Arctic sea ice has been observed (Parkinson and DiGirolamo 2016). Climate models predict that with the current rate of atmospheric CO₂ increase, the Arctic will be ice-free in summer by as early as the 2030s (AMAP 2017). The IPCC further estimates that the earth will pass the threshold of a 1.5°C increase in temperature by 2030 (IPCC 2018), which is considered a 'guardrail' beyond which the effects of climate change will become increasingly severe and difficult to adapt to (Schoolmeester 2019). Increasing warm temperatures accelerate the melting of sea ice and snow and influence MPs distribution. Seasonal expansion and contraction of ice are considered to contribute to the flux of MPs, as particles become trapped as water freezes and released when it melts. It is also projected that the melting of ice may result in the release of the entrained plastics (Obbard et al. 2014). Furthermore, the melting of ice and snow will lead to the freshening of seawater along coasts and sea-ice edges (Woosley and Millero 2020). As freshwater has a lower density than seawater, many floating polymers supported by high saline seawater will now sink and the vertical flux of MPs to deeper waters and sediments will likely increase (Welden and Lusher 2017, Kanhai et al. 2018). As sea ice and glaciers retreat, new shipping routes open up, and resource exploitation will be possible

in previously inaccessible areas, making the neo-industrialized Arctic an increasingly important region in the global economy (Avango et al. 2013; AMAP 2017). Plastic, as well as other pollutants, are likely to increase in the Arctic with increased human industrial activity (Granberg et al. 2017). The sources for MPs will thus likely change the distribution and increase as a whole.

Changing climate and melting permafrost: As permafrost melts, the soil becomes destabilized. Old dumping sites in Svalbard and the wider Arctic are placed directly on the permafrost and become undermined as permafrost melts (Granberg et al. 2017). Dumping sites contain a mix of debris and associated pollutants. The increased permeability of land soil leads to increased water-borne transport through the ground, likely carrying all types of pollutants including MPs and its associated chemicals to lakes and coastal waters (Walvoord 2016) (Figure 2).

Changing climate and weather patterns: In the last decades, the frequency of heavy rainfalls and storms has increased in the Arctic and is projected to further increase (IPCC 2018). The Arctic has generally become a wetter and warmer place as indicated by river discharge spikes being heavier and occurring earlier in the spring (Lammers et al. 2001). Future wind patterns will potentially determine the MPs loads deposited from the atmosphere in the Arctic. Heavy rain will also flush MPs from land to the sea at higher rates. Along with this, 'rain-on-snow' events have always occurred in Svalbard as a product of the strong oceanic influence on weather systems in the archipelago (Svendsen et al. 2002) but winter warming is making such events more frequent (Førland et al. 2012). Winter rains may encapsulate pieces of discarded plastics in ice, making the plastics very brittle and liable to break into MPs, which may end up in lakes or the ocean. More and bigger storms will likely lead to greater losses of larger plastic pieces – such as fishing nets and broken snowmobile parts – from ships and dumping sites and land-based activities (Welden and Lusher 2017). Such plastic debris, whether intentionally or unintentionally discarded, are likely to end up in seas, lakes, and other water bodies.

Changed ocean circulation: Ocean circulation and coastal oceanography are undergoing dramatic changes in the wake of climate change. Around Svalbard, Atlantic water thrusts farther north, bringing along the water from more industrialised parts of the world. Lusher et al. (2015) detected higher concentrations of MPs in Atlantic water than in seawater collected closer to glacial outflows, suggesting Atlantic water to function as a vector for MPs pollution to Svalbard and the Arctic. Fibres constituted the majority (95%) of detected MPs. As the Atlantic water input is predicted to increase as climate change progresses (Polyakov et al. 2020), waterborne MPs pollution from southern latitudes is likely to increase in the Svalbard region.

Ecosystem change and biochemical interactions: It is difficult to predict how ecosystems will change in response to global warming and even more difficult to estimate how the distribution and effects of MPs will be altered in relation to ecosystem change. However, as biological borealisation progresses, i.e. the climate change-induced transformation from the Arctic towards more boreal or temperate ecosystems, information gained from scientific investigations in more southern latitudes may become more relevant for the Arctic. In a modelling study, Kvale et al. (2020) predicted an increase in the transport of MPs from surface waters to deeper waters and sediments in the Arctic Ocean as the sea ice melts and exposes more water to sunlight, stimulating increased primary production and microalgal growth. Marine snows (sinking particulate organic matter) and ingestion (and subsequent egestion) by zooplankton (e.g. Cole et al. 2013 and 2016) become vehicles for MPs transport to the ocean depths. This coincides with the predicted increase in marine biomass stimulated by borealisation (Polyakov et al. 2020). However, Lannuzel et al. (2020) predict a decrease in vertical carbon flux close to the sea ice. As first-year ice will replace multiyear ice the developed microalgal ecosystem can no longer be sustained but may instead be replaced by opportunistic microalgal species of low food quality, e.g. *Phaeocystis* sp. (Assmy et al. 2017). This change will cascade through the pelagic food web and smaller grazing zooplankton producing small faecal pellets will replace large sympagic amphipods and *Calanus*

species. Small faecal pellets do not sink and vertical flux of organic matter and associated particles will thus slow down and particulates kept in surface waters. Processes near coasts will likely differ from those close to the sea-ice edge (Lannuzel et al. 2020).

Luoto et al. (2019) further showed that the species composition and trophic interactions in Lake Revvatnet, Svalbard, changed with the increased input of turbid glacier meltwater. Colonies of little auks (*Alle alle*) have also grown as the lake remains unfrozen for a longer period. A higher MPs content in lake sediments coincides with these changes, and the authors suggest seabird guano as a vector for MPs pollution, as previously suggested for northern fulmars by Provencher et al. (2018). The birds mistake MPs for food when foraging at sea, which has been observed in little auks in Greenland (Amélineau et al. 2016)

Increased temperatures will accelerate all biological processes and intensify chemical dynamics. For example, ingestion and respiration increase in many invertebrates as temperature rises (Acheampong et al. 2014; Grote et al. 2015; Zhang et al. 2016). Elevated seawater temperatures may thereby lead to increased ingestion of MPs by marine organisms. As the dynamics and mobility of plastic-associated contaminants increase with rising temperatures, the bioavailability of these chemicals may elevate environmental toxicity.

2.6. The ultimate fate of MPs in Svalbard

In aquatic environments, it is expected that the majority of MPs will eventually be transported to the oceans via rivers and coastal areas. The distribution of MPs in the ocean is affected by hydrodynamic forces (waves, tides, and currents) (Rocha-Santos and Duarte 2014). As a result of ocean currents and the wind, ocean garbage patches can be regarded as temporal sinks. The Barents Sea is assumed to become another major convergence zone and, thus, a large sink for plastic debris (Cózar et al. 2017). Svalbard, which borders the Barents Sea on the archipelago's east, would consequently be increasingly exposed to both macro and MPs.

In addition to long-distance transport from other regions of the world, Svalbard will be more exposed to local plastic pollution due to an increase in shipping, tourism, and fishing activities as explained in the previous section (v). The fate of this plastic debris in Svalbard is largely unknown. We expect an accumulation of plastic in different compartments: sediment, beaches, glaciers, and sea ice. Once in the Svalbard region, MPs will be exposed to cold temperatures, entrapment in sea ice (van Sebille et al. 2020), and continuous and absent UV exposure for several months. These parameters will influence the fate of MPs in Svalbard in different ways. Cold temperatures will lower the degradation rate by microorganisms (Bergmann and Klages 2012; Urbanek et al. 2017), resulting in a higher accumulation rate compared to temperate and tropical regions. The cold temperatures and absence of sunlight in winter will inhibit biofilm formation (Chen et al. 2019), and floating MPs will stay longer at the water surface in winter. In the summer, the continuous sunlight might support the formation of a biofilm and the fragmentation of MPs compared to the winter season. However, the average temperature of surface waters around Svalbard remains low even in the summer (for example from 4°C to 7°C in Kongsfjorden) (Tverberg et al. in Hop and Wiencke 2019), limiting the density increase due to biofilm formation. The consequences of MPs entrapment in sea ice are currently unknown. On one hand, the physical abrasion of MPs due to ice formation and movements can be expected; on the other, MPs might be protected from direct exposure to sunlight (Chen et al. 2019).

Despite the influence of these parameters, it can be assumed that MPs will eventually sink to the seafloor, end up on beaches, or be trapped in sea ice temporarily, or might cycle in abiotic and biotic ecosystem compartments. The finding of a great deal of MPs in the deep sea near the HAUSGARTEN observatory (Tekman et al. 2017) suggests that future research should investigate whether under-sea canyons are accumulation locations for plastics. To a certain extent, the Svalbard marine fauna can be considered as a temporary sink and transport medium, but literature is lacking regarding MPs trophic transfer, retention times, whether MPs simply pass through the GI of larger organisms or

get accumulated. More data are urgently needed to understand the fate of MPs in cold regions and worldwide in general. Especially, experiments investigating the degradation and sinking rates under Arctic conditions are needed to understand the fate of MPs in Svalbard.

On the seafloor, MPs will be available to many organisms such as snow crabs (*Chionoecetes opilio*) (Sundet 2014) deep-sea starfish (*Hymenaster pellucidus*) (Courtene-Jones et al. 2017) and from sea ice to polar cod (*Boreogadus saida*) due to melting (Kühn et al. 2018). From a food security perspective, the presence of MPs in harvested marine species raises concerns for people.

2.7. Sociological impacts of MPs (e.g. food safety)

As research on MPs has expanded beyond observations highlighting their ubiquity in the oceans, the focus has shifted towards ecological and health risks (GESAMP 2015; Cox et al. 2019). MPs are considered widespread contaminants, ingested directly, or indirectly by trophic transfer through the marine food web (Vandermeersch et al. 2015; Lusher et al. 2015; Desforges et al. 2015; Wright et al. 2013; Nelms et al. 2018). With the identification of MPs in a variety of Arctic organisms (Diepens and Koelmans 2018; Fang et al. 2019; Kühn et al. 2018; Provencher et al. 2018), it has become clear that marine organisms can ingest and even transfer MPs along with the Arctic food webs into top predators including fish and marine mammals. However, little is known today about trophic transfer dynamics, retention times, and whether, and under which conditions, MPs simply pass through the GI of biota or get accumulated in other tissues.

Most of the MPs' research on living organisms has concentrated on marine organisms. Terrestrial organisms have not been regarded as threatened as they are not part of the ocean system, which was considered the main pool of MPs. Recently this perception has changed, and it is now recognised that terrestrial organisms (e.g. reindeer) may be exposed to MPs (Bergmann et al. 2019) and that from them MPs may distribute

to their predators. Reindeer (*Rangifer tarandus*) is an important traditional food in Svalbard and is, therefore, a potentially significant contaminant pathway to humans. There is no information available on the MPs ingestion or accumulation in terrestrial harvested wildlife. Therefore, to provide knowledge-based advice for environmental agencies, food security stakeholders (e.g. UN organisations), consumers, and food producers and to enable educated management, there is an immediate need to develop a baseline database of MPs in harvested terrestrial wildlife.

There is ample evidence of MPs ingestion by fish destined for human consumption, including Arctic species (Kühn et al. 2018; Bråte et al. 2016; Morgana et al. 2018; Fischer and Scholz-Bottcher 2017; Leclerc et al. 2012; Nielsen et al. 2014; Welden and Cowie; 2016; Sundet 2014). In bivalves in the Arctic, MPs are reported in blue mussels (Bråte et al. 2018; Halldórsson and Guls 2018; Granberg et al. 2020) and Greenland smoothcockle (von Friesen et al. 2018). Generally, low counts of MPs in seafood species obscured any differences between collection sites, but MPs in fish are commonly analysed in the (GI) only. Often, only larger MPs, such as above 300 μm , are investigated, and sometimes only by visual inspection without chemical identification. Moreover, estimates of larger MPs in the GI can provide rough estimates of MPs ingestion. However, MPs of such size are unlikely to cross the intestinal barrier or to accumulate in any tissue (Pedà et al. 2016; Grigorakis et al. 2017). Additionally, there is evidence from exposure studies that smaller MPs are of higher concern in terms of negative health effects on aquatic organisms and mammals (Kögel et al. 2020). Hence, to investigate if such accumulation is of concern for seafood security at current pollution levels, quantifications of smaller MPs in the consumed tissues are required. The thresholds for translocation or accumulation are not clarified yet, as very little data from the environment is available, and exposure studies do not cover many polymer types and often use round beads instead of the angular fragments and fibres, which are common in the environment. However,

a recent report – although not from fish from Arctic regions – describes the occurrence of MPs in fish muscle and liver, but none above 250 μm (Gomiero et al. 2020). Reports including findings of MPs smaller than 50 μm in other seafood species were recently summarized in Kögel et al. 2020a. However, data is scarce, and additionally neither harmonized nor fully quantitative due to methodological challenges (Kögel et al. 2020b). However, the only field studies analysing MPs in seafood species from Arctic regions including MPs below 300 μm , point towards that also Arctic seafood species are no exception to containing MPs. Thus, rather low MPs were reported in 11 species of benthic invertebrates sampled from the Bering and Chukchi Seas (>100 μm , Fang et al. (2019), in the gastrointestinal tract of Polar cod (*Boreogadus saida*) (> 35 μm ; Kühn et al. 2018) and of Greenland Cod (*Gadus ogac*) (>20 μm , (Granberg et al. 2020). From exposure studies, there is plenty of evidence that uptake of smaller MPs into other tissues does occur. Nano plastic administered in high doses experimentally reached the brain of fish and nano plastic and MPs lead to altered behavior that may affect the fishes' capability of sustenance (Mattsson et al. 2015; Mattson et al. 2017; Chae et al. 2018; Barboza et al. 2018).

In conclusion, sufficient knowledge of the concentrations per size distribution and uptake and effects of MPs to establish a proper risk assessment for both the environment and human consumers is still lacking (Skåre 2019; Backaus et al. 2018), even though MSFD 2008/56/EC and decision 2017/848/EU require that the situation be documented: "The amount of [...] micro-litter ingested by marine animals is at a level that does not adversely affect the health of the species concerned. [...] Micro-litter shall be monitored [...]". Resultantly, there is an immediate need for an analysis of the occurrence and levels of MPs in seafood organisms as a foundation for knowledge-based advice for food safety authorities, environmental agencies, food security stakeholders, such as UN organisations, and Arctic Inuit authorities and those of other Arctic people, consumers and food producers.

3. Connections and synergies with other SESS report chapters

Many SESS report chapters explore issues that have been identified as gaps related to our understanding of plastics in Svalbard. Figure 4 shows that merging

or forming trans-chapter workgroups or task forces must be a way forward for SIOS to utilise the full breadth of competence within the consortium.



Figure 4: Potential connections with other chapters: SvalCLIM (Gjermundsen et al. 2021), SvalHydro (Nowak et al. 2021), PASSES (Salzano et al. 2021), SvalGLac (Schuler et al. 2020), FastIce (Gerland et al. 2020), and ABC Svalbard (Gillardoni et al. 2020).

4. Unanswered questions

On the basis of the knowledge presented in sections 2.1 - 2.7, we have noted the following knowledge gaps, which are important to be filled for a good understanding of the status of MPs in the realm of Svalbard:

- a. *Trends*: The lack of conformity in sampling, analytical protocols, and data units and the paucity of data make it difficult to determine MPs trends in different environmental compartments.
- b. *Sources*: There is a lack of information regarding the relative importance of distant and local MPs pollution sources in Svalbard and the Arctic in general.
- c. *Toxicological effect*: MPs have been detected in fish and other marine organisms, but there is limited information on the effects MPs cause themselves in environmentally relevant sizes, doses, and combinations and through leakage or uptake of plastic additives (plasticisers and stabilisers) or from the pollutants present in the environment (POPs). As such knowledge emerges, it will be necessary to evaluate to what degree Svalbard deviates from other environments concerning toxicological effects.
- d. *Fate*: The long-term transformation and deposition reservoirs of MPs need further investigation in the Svalbard environment. The interactions between physical and biological compartments regarding MPs are poorly understood and effects on ecosystems therefore highly unpredictable.
- e. *Effect of climate change*: Global climate change is likely to affect the concentrations, transformation processes, and mobility of MPs in the ecosystem. Such effects are currently mainly speculative and need to be quantified.
- f. *Food Security*: MPs concentrations in harvested terrestrial wildlife, marine mammals, fish, and shellfish are poorly documented. It is further unknown whether ingested MPs may have any adverse effect on humans.
- g. *Exchange*: Information on MPs levels in the air and their influence on terrestrial environments is lacking.

5. Recommendations for the future

Harmonising methodologies: A workshop is needed to facilitate agreements among international MPs experts on how to start monitoring MPs at the four observatories in Svalbard (Hornsund, Barentsburg, Longyearbyen, Ny-Ålesund). Here, the work currently being finalised by AMAP on MPs monitoring will be highly valuable.

Long-term monitoring: A monitoring programme should be designed to consider societal needs such that the science can provide advice regarding plastic use in Svalbard, wastewater treatment, effects of cruises and other tourism activities, and fishing.

Mapping: MPs in the unexplored parts of Svalbard, which include terrestrial and marine biota needs to be mapped in order to establish a proper risk assessment for both the environment and human consumers.

Collaboration: It is recommended that a Svalbard plastics task force be formed and meet regularly to develop methods and monitoring recommendations to ensure that there is a concerted effort to fill the identified knowledge gaps.

Experiments: Experimental studies of Arctic key species and the possible trophic transfer of MPs under Arctic conditions should be set up.

6. Data availability

This review chapter is an overview of published articles, thesis, and reports. Information about the

literature used in this chapter can be found in the reference section.

Acknowledgments

This work was supported by the Norwegian Polar Institute (Tromsø), the Research Council of Norway, project number 291644, Svalbard Integrated Arctic Earth Observing System – Knowledge Centre (SIOS-KC), operational phase, and the Institute of

Marine Research. We thank Pratham Choudhary for the illustration work, Helle Goldman for checking the language consistency, and the anonymous reviewers for their careful reading of the manuscript and constructive remarks.

References

- Acheampong E, Hense I, St John, MA (2014) A model for the description of feeding regulation by mesozooplankton under different conditions of temperature and prey nutritional status. *Ecol. Modell* 272:84–97. <https://doi.org/10.1016/j.ecolmodel.2013.09.009>
- Adakudlu M, Andresen J, Bakke J, Beldring S, Benestad R, Bilt W, et al. (2019) Climate in Svalbard 2100 – a knowledge base for climate adaptation. Norway: Norwegian Environmental Agency. ISSN Nr. 2387–3027
- Allen S, Allen D, Moss K, Le Roux G, Phoenix VR, et al. (2020) Examination of the ocean as a source for atmospheric microplastics. *PLoS ONE* 15(5). <https://doi.org/10.1371/journal.pone.0232746>
- Alomar C, Estarellas F, Deudero S (2016) Microplastics in the Mediterranean Sea: deposition in coastal shallow sediments, spatial variation and preferential grain size. *Mar Environ Res* 115:1–10. <https://doi.org/10.1016/j.marenvres.2016.01.005>
- AMAP (2017) Snow, water, ice and permafrost in the Arctic (SWIPA) 2017. Arctic Monitoring and Assessment Programme (AMAP), Oslo, Norway. Xiv: 269
- Ambrosini R, Azzoni RS, Pittino F, Diolaiuti G, Franzetti A, Parolini M (2019) First evidence of microplastic contamination in the supraglacial debris of an alpine glacier. *Environ Pollut* 253:297–301. <https://doi.org/10.1016/j.envpol.2019.07.005>
- Amélineau F, Grémillet D, Bonnet D, Le Bot T, Fort J (2016) Where to forage in the absence of sea ice? bathymetry as a key factor for an Arctic seabird. *PLoS one* 11:e0157764. <https://doi.org/10.1371/journal.pone.0157764>
- Andrady AL (2011) Microplastics in the marine environment. *Mar Pollut Bull* 62(8):1596–1605. <https://doi.org/10.1016/j.marpolbul.2011.05.030>
- Assmy P, Fernandez-Mendez M, Duarte P, Meyer A, Randelhoff A, Mundy CJ, et al. (2017) Leads in Arctic pack ice enable early phytoplankton blooms below snow-covered sea ice. *Sci Rep* 7: 40850. <https://doi.org/10.1038/srep40850>
- Avango, D, Nilsson, AE, Roberts P (2013) Assessing Arctic futures: voices, resources and governance. *The Polar Journal* 3:431–446. <https://dx.doi.org/10.1080/2154896X.2013.790197>
- Avery-Gomm S, O'Hara PD, Kleine L, Bowes V, Wilson LK, Barry KL (2012) Northern fulmars as biological monitors of trends of plastic pollution in the eastern North Pacific. *Mar Pollut Bull* 64:1776–1781. <http://dx.doi.org/10.1016/j.marpolbul.2012.04.017>
- Baccolo G, Di Mauro B, Massabò D, Clemenza M, Nastasi M, Delmonte B, et al. (2019) Cryoconite as a temporary sink for anthropogenic species stored in glaciers *Sci Rep* 7:9623. <https://doi.org/10.1038/s41598-017-10220-5>
- Backhaus T, Wagner M (2018). Microplastics in the environment: much ado about nothing? A debate. *Peer J Preprints*, 6: e26507v26506. <https://doi.org/10.7287/peerj.preprints.26507v6>
- Barboza LGA, Vieira LR, Guilhermino L (2018) Single and combined effects of microplastics and mercury on juveniles of the European seabass (*Dicentrarchus labrax*): changes in behavioural responses and reduction of swimming velocity and resistance time. *Environ Pollut* 236:1014–1019. <https://doi.org/10.1016/j.envpol.2017.12.082>
- Bergmann M, Klage, M (2012) Increase of litter at the Arctic deep-sea observatory HAUSGARTEN. *Mar Pollut Bull* 64:2734–2741. <http://dx.doi.org/10.1016/j.marpolbul.2012.09.018>

- Bergmann M, Mützel S, Primpke S, Tekman MB, Trachsel J, Gerdt G (2019) White and wonderful? Microplastics prevail in snow from the Alps to the Arctic. *Sci Adv* 5(8):eaax1157. <https://doi.org/10.1126/sciadv.aax1157>
- Bergmann M, Tekman MB, Gutow L (2017) Sea change for plastic pollution. *Nature* 544:297. <https://doi.org/10.1038/544297a>
- Bhattacharya A, Khare SK (2020) Ecological and toxicological manifestations of microplastics: current scenario, research gaps, and possible alleviation measures. *J Environ Sci Health C Environ Carcinog Ecotoxicol Rev Part C* 38(1):1–20. <https://doi.org/10.1080/10590501.2019.1699379>
- Brandon J, Goldstein M, Ohman MD (2016) Long-term aging and degradation of microplastic particles: comparing in situ oceanic and experimental weathering patterns. *Mar Pollut Bull* 110:299–308. <http://dx.doi.org/10.1016/j.marpolbul.2016.06.048>
- Bråte IL, Blazquez M, Brooks SJ, Thomas KV (2018) Weathering impacts the uptake of polyethylene microplastics from toothpaste in Mediterranean mussels (*M. galloprovincialis*). *Sci Total Environ* 626:1310–1318. <https://doi.org/10.1016/j.scitotenv.2018.01.141>
- Caruso G (2020) Microbial Colonization in Marine Environments: Overview of Current Knowledge and Emerging Research Topics. *J Mar Sci Eng* 8:78. <https://doi.org/10.3390/jmse8020078>
- Chae Y, Kim D, Kim SW, An YJ (2018) Trophic transfer and individual impact of nano-sized polystyrene in a four-species freshwater food chain. *Sci Rep* 8:284. <https://doi.org/10.1038/s41598-017-18849-y>
- Chen X, Xiong X, Jiang X, Shi H, Wu C (2019) Sinking of floating plastic debris caused by biofilm development in a freshwater lake. *Chemosphere* 222:856–864. <https://doi.org/10.1016/j.chemosphere.2019.02.015>
- Choy CA, Robison BH, Gagne TO, Erwin B, Firl E, Halden RU, et al. (2019) The vertical distribution and biological transport of marine microplastics across the epipelagic and mesopelagic water column. *Sci Rep* 9: 7843. <https://doi.org/10.1016/j.chemosphere.2019.02.015>
- Cole M, Lindeque P, Fileman E, Halsband C, Goodhead R, Moger J, et al. (2013) Microplastic ingestion by zooplankton. *Environ Sci Technol* 47:6646–6655. <https://doi.org/10.1021/es400663f>
- Cole M, Lindeque PK, Fileman E, Clark J, Lewis C, Halsband C, et al. (2016) Microplastics alter the properties and sinking rates of zooplankton faecal pellets. *Environ Sci Technol* 50:3239–3246. <https://doi.org/10.1021/acs.est.5b05905>
- Cole M, Lindeque P, Halsband C, Galloway TS (2011) Microplastics as contaminants in the marine environment: a review. *Mar Pollut Bull* 62:2588–2597. <https://doi.org/10.1016/j.marpolbul.2011.09.025>
- Courtene-Jones W, Quinn B, Gary SF, Mogg AOM, Narayanaswamy B (2017) Microplastic pollution identified in deep-sea water and ingested by benthic invertebrates in the Rockall Trough, North Atlantic Ocean. *Environ Pollut* 231:271–280. <https://doi.org/10.1016/j.envpol.2017.08.026>
- Cox KD, Covernton GA, Davies HL, Dower JF, Juanes F, Dudas SE (2019) Human consumption of microplastics. *Environ Sci Technol* 53:7068–7074. <https://doi.org/10.1021/acs.est.9b01517>
- Cózar A, Martí E, Duarte CM, García-de-Lomas J, van Sebille E, Ballatore TJ, et al. (2017) The Arctic Ocean as a dead end for floating plastics in the North Atlantic branch of the Thermohaline Circulation. *Sci Adv* 3:e1600582. <https://doi.org/10.1126/sciadv.1600582>
- De Sales-Ribeiro C, Brito-Casillas Y, Fernandez A, Caballero MJ, et al. (2020) An end to the controversy over the microscopic detection and effects of pristine microplastics in fish organs. *Sci Rep* 10:12434. <https://doi.org/10.1038/s41598-020-69062-3>
- Derraik, JGB (2002) The pollution of the marine environment by plastic debris: a review. *Mar Pollut Bull* 44:842–852. [https://doi.org/10.1016/S0025-326X\(02\)00220-5](https://doi.org/10.1016/S0025-326X(02)00220-5)
- Desforges JW, Galbraith M, Ross PS (2015) Ingestion of Microplastics by Zooplankton in the Northeast Pacific Ocean. *Arch Environ Contam Toxicol* 69:320–330. <https://doi.org/10.1007/s00244-015-0172-5>
- Diepens NJ, Koelmans AA (2018) Accumulation of plastic debris and associated contaminants in aquatic food webs. *Environ Sci Technol* 52:8510–8520. <https://doi.org/10.1021/acs.est.8b02515>
- Duis K, Coors A (2016) Microplastics in the aquatic and terrestrial environment: sources (with a specific focus on personal care products), fate and effects. *Environ Sci Eur* 28:1–25. <https://doi.org/10.1186/s12302-015-0069-y>
- Evangelio N, Grythe H, Klimont Z, Heyes C, Eckhardt S, Lopez-Aparicio S, Stohl A (2020) Atmospheric transport is a major pathway of microplastics to remote regions. *Nat Commun* 11:3381. <https://doi.org/10.1038/s41467-020-17201-9>
- Fackelmann G, Sommer S (2019) Microplastics and the gut microbiome: how chronically exposed species may suffer from gut dysbiosis. *Mar Pollut Bull* 143:193–203. <https://doi.org/10.1016/j.marpolbul.2019.04.030>
- Fang C, Zheng R, Chen H, Hong F, Lin L, Lin H, et al. (2019) Comparison of microplastic contamination in fish and bivalves from two major cities in Fujian province, China and the implications for human health. *Aquaculture*, 512:734322. <https://doi.org/10.1016/j.aquaculture.2019.734322>
- Fang C, Zheng R, Zhang Y, Hong F, Mu J, Chen M, et al. (2018) Microplastic contamination in benthic organisms from the Arctic and sub-Arctic regions. *Chemosphere* 209:298–306. <https://doi.org/10.1016/j.chemosphere.2018.06.101>

- Ferrario C, Pittino F, Tagliaferri I, Gandolfi I, Bestetti G, Azzoni RS, et al. (2017) Bacteria contribute to pesticide degradation in cryoconite holes in an Alpine glacier. *Environ Pollut* 230:919–926. <https://doi.org/10.1016/j.envpol.2017.07.039>
- Finley KJ (2001) Natural history and conservation of the Greenland whale or Bowhead, in the northwest Atlantic. *Arctic* 54:55–76. <https://doi.org/10.14430/arctic764>
- Fischer M, Scholz-Böttcher BM (2017) Simultaneous trace identification and quantification of common types of microplastics in environmental samples by pyrolysis-gas chromatography–mass spectrometry. *Environ Sci Technol* 51:5052–5060. <https://doi.org/10.1021/acs.est.6b06362>
- Foekema EM, De Gruijter C, Mergia MT, van Franeker JA, Murk AJ, Koelmans AA (2013) Plastic in North Sea fish. *Environ Sci Technol* 47:8818–8824. <https://doi.org/10.1021/es400931b>
- Førland EJ, Benestad R, Hanssen-Bauer I, Haugen JE, Skaugen TE (2012) Temperature and precipitation development at Svalbard 1900–2100. *Adv Meteorol* 1–14. <https://doi.org/10.1155/2011/893790>
- Fry MD, Fefer SI, Sileol L (1987) Ingestion of plastic debris by Laysan albatrosses and wedge-tailed shearwaters in the Hawaiian Islands. *Mar Pollut Bull* 18:339–343. [https://doi.org/10.1016/S0025-326X\(87\)80022-X](https://doi.org/10.1016/S0025-326X(87)80022-X)
- GESAMP (2015) Sources, Fate and effects of Microplastics in the Marine Environment: A Global Assessment 96 IMO/FAO/UNESCO-IOC/UNIDO/WMO/IAEA/UN/UNEP/UNDP Joint Group of Experts on the Scientific Aspects of Marine Environmental Protection ISSN 1020–4873 (GESAMP Reports & Studies Series) <http://agris.fao.org/agris-search/search.do?recordID=XF2017002714>
- Gerland S, Pavlova O, Divine D, Negrel J, Dahlke S, Johansson AM, et al.(2020) In: van den Heuvel et al (eds) SESS report 2019. Svalbard Integrated Arctic Earth Observing System, Longyearbyen, pp 160-167 . https://sios-svalbard.org/SESS_Issue2
- Gilardoni S, Lupi A, Mazzola M, Cappelletti DM, Moroni B, Ferrero L, et al. (2020) In: van den Heuvel et al (eds) SESS report 2019. Svalbard Integrated Arctic Earth Observing System, Longyearbyen, pp 196-211 . https://sios-svalbard.org/SESS_Issue2
- Gjermundsen A, Graff LS, Bentsen M, Breivik LA, Debernard JB, Makkonen R, et.al (2021) How representative is Svalbard for future Arctic climate evolution? An Earth system modelling perspective. In: Moreno-Ibáñez et al (eds) SESS report 2020, Svalbard Integrated Arctic Earth Observing System, Longyearbyen, pp 38-59 . <https://doi.org/10.5281/zenodo.4034104>
- Gomiero A, Haave M, Bjørøy Ø, Herzke D, Kögel T, Nikiforov V, et al. (2020) NORCE report 8-2020. ISBN 978-82-8408-085-7
- González-Pleiter M, Velázquez D, Edo C, Carretero O, Gago J, Barón-Sola Á et al. (2020) Fibers spreading worldwide: Microplastics and other anthropogenic litter in an Arctic freshwater lake. *Sci Total Environ* 722:137904. <https://doi.org/10.1016/j.scitotenv.2020.137904>
- Granberg, ME, von Friesen LW, Ask A, Collard F, Magnusson K, Eriksson Wiklund A-K, et al. (2020) Microlitter in arctic marine benthic food chains and potential effects on sediment dwelling fauna. *Tema Nord Report No. 528: 1– 77*. <https://doi.org/10.6027/temanord2020-528>
- Granberg ME, Ask A, Gabrielsen GW (2017) Local contamination in Svalbard, Overview and suggestions for remediation actions. Brief report 044. Norwegian Polar Institute, Tromsø, Norway ISBN 978-82-7666-409-6
- Granberg ME, von Friesen LW, Bach L, Collard F, Gabrielsen GW (2019) Anthropogenic microlitter in wastewater and marine samples from Ny-Ålesund, Barentsburg and Signehamna IVL Swedish Environmental Research Institute, Svalbard.C373, ISBN: 978-91-7883-020-6. <http://www.vliz.be/imisdocs/publications/338993.pdf>
- Grigorakis S, Mason SA, Drouillard KG (2017) Determination of the gut retention of plastic microbeads and microfibers in goldfish (*Carassius auratus*). *Chemosphere* 169:233–238. <https://doi.org/10.1016/j.chemosphere.2016.11.055>
- Groh KJ, Backhaus T, Carney-Almroth B, Geueke B, Inostroza PA, Lennquist A, et al. (2019) Overview of known plastic packaging-associated chemicals and their hazards. *Sci Total Environ* 651(2):3253–3268. <https://doi.org/10.1016/j.scitotenv.2018.10.015>
- Grøsvik BE, Prokhorova T, Eriksen E, Krivosheya P, Horneland PA, Prozorkevich D (2018) Assessment of Marine Litter in the Barents Sea, a Part of the Joint Norwegian–Russian Ecosystem Survey. *Front Mar Sci* 5:72. <https://doi.org/10.3389/fmars.2018.00072>
- Grote U, Pasternak A, Arashkevich E, Halvorsen E, Nikishina A (2015) Thermal response of ingestion and egestion rates in the Arctic copepod *Calanus glacialis* and possible metabolic consequences in a warming ocean. *Polar Biol* 38:1025–1033. <https://doi.org/10.1007/s00300-015-1664-5>
- Hallanger IG, Gabrielsen GW (2018) Plastic in the European Arctic. Brief report 045. Norwegian Polar Institute, Tromsø, Norway ISBN 978-82-7666-414-0
- Halldórsson HP, Guls HD (2018) Könnun á örplastmengun í kræklingi við Ísland. https://ust.is/library/Skrar/Orplast_kraeklingur_2018_skyrsla_UST_HI_Sudurnes.pdf
- Halsband C, Herzke D (2019) Plastic litter in the European Arctic: what do we know? *Emerg Contam* 5:308–318. <https://doi.org/10.1016/j.emcon.2019.11.001>
- Hartmann NB, Rist S, Bodin J, Jensen LH, Schmidt SN, Mayer P, et al. (2017) Microplastics as vectors for environmental contaminants: Exploring sorption, desorption, and transfer to biota. *Integr Environ Assess Manag* 13:488–493. <https://doi.org/10.1002/ieam.1904>

- Herzke D, Anker-Nilssen T, Nøst TH, Götsch A, Christensen-Dalsgaard S, Langset M, et al. (2016) Negligible Impact of Ingested Microplastics on Tissue Concentrations of Persistent Organic Pollutants in Northern Fulmars off Coastal Norway. *Environ Sci Technol* 50:1924–1933. <https://doi.org/10.1021/acs.est.5b04663>
- Hidalgo-Ruz V, Gutow L, Thompson RC, Thiel M (2012) Microplastics in the marine environment: a review of the methods used for identification and quantification. *Environ Sci Technol* 46:3060–3075. <https://doi.org/10.1021/es2031505>
- Huang J, Kang S, Ma M, Guo J, Cong Z, Dong Z, et al. (2019) Accumulation of Atmospheric Mercury in Glacier Cryoconite over Western China. *Environ Sci Technol* 53:6632–6639. <https://doi.org/10.1021/acs.est.8b06575>
- Huntington A, Corcoran PL, Jantunen L, Thaysen C, Bernstein S, Stern GA, et al. (2020) A first assessment of microplastics and other anthropogenic particles in Hudson Bay and the surrounding eastern Canadian Arctic waters of Nunavut. *FACETS* 5:432–454. <https://doi.org/10.1139/facets-2019-0042>
- Hwang J, Choi D, Han S, Choi J, Hong J (2019) An assessment of the toxicity of polypropylene microplastics in human derived cells. *Sci Total Environ* 684:657–669. <https://doi.org/10.1016/j.scitotenv.2019.05.071>
- IPCC (2018) Global Warming of 1.5 °C: An IPCC special report on the impacts of global warming of 1.5 °C above pre-industrial levels and related global greenhouse gas emission pathways, in the context of strengthening the global response to the threat of climate change, sustainable development, and efforts to eradicate poverty. Summary for Policymakers (IPCC SR1.5). Released October 6, 2018.
- Kane IA, Clare MA (2019) Dispersion, Accumulation, and the Ultimate Fate of Microplastics in Deep-Marine Environments: A Review and Future Directions. *Front Earth Sci* 7:80. <https://doi.org/10.3389/feart.2019.00080>
- Kanhai DK, Gårdfeldt K, Lyashevskaya O, Hassellöv M, Thompson RC, O'Connor I (2018) Microplastics in sub-surface waters of the Arctic Central Basin. *Mar Pollut Bull* 130:8–18. <https://doi.org/10.1016/j.marpolbul.2018.03.011>
- Kirstein IV, Wichels A, Gullans E, Krohne G, Gerdt G (2019) The Plastisphere – Uncovering tightly attached plastic “specific” microorganisms. *PLoS ONE* 14(4):e0215859. <https://doi.org/10.1371/journal.pone.0215859>
- Koelmans AA, Bakir A, Burton GA, Janssen CR (2016). Microplastic as a vector for chemicals in the aquatic environment: critical review and model-supported reinterpretation of empirical studies. *Environ Sci Technol* 50:3315–3326. <https://doi.org/10.1021/acs.est.5b06069>
- Kögel T, Bjørøy Ø, Toto B, Bienfait AM, Sanden M (2020) Micro- and nanoplastic toxicity on aquatic life: Determining factors. *Sci Total Environ* 709:136050. <https://doi.org/10.1016/j.scitotenv.2019.136050>
- Kögel T, Refosco A, Maage A (2020) Surveillance of Seafood for Microplastics. In: Rocha-Santos T, Costa M, Mouneyrac C (eds) *Handbook of Microplastics in the Environment*. Springer, Cham. https://doi.org/10.1007/978-3-030-10618-8_28-1
- Kowalski N, Reichardt AM, Waniek JJ (2016) Sinking rates of microplastics and potential implications of their alteration by physical, biological, and chemical factors. *Mar Pollut Bull* 109:310–319. <https://doi.org/10.1016/j.marpolbul.2016.05.064>
- Kühn S, Schaafsma FL, van Werven B, Flores H, Bergmann M, Egelkraut-Holtus M, et al. (2018) Plastic ingestion by juvenile polar cod (*Boreogadus saida*) in the Arctic Ocean. *Polar Biol* 41:1269–1278. <https://doi.org/10.1007/s00300-018-2283-8>
- Kvale KF, Friederike Prowe AE, Oschlies A (2020) A Critical Examination of the Role of Marine Snow and Zooplankton Fecal Pellets in Removing Ocean Surface Microplastic. *Front Mar Sci* 6:808. <https://doi.org/10.3389/fmars.2019.00808>
- Lammers RB, Shiklomanov AI, Vörösmarty CJ, Fekete BM, Peterson BJ (2001) Assessment of contemporary Arctic river runoff based on observational discharge records. *J Geophys Res* 106:3321–3334. <https://doi.org/10.1029/2000JD900444>
- Lannuzel D, Tedesco L, van Leeuwe M, Campbell K, Flores H, Delille B, et al. (2020) The future of Arctic sea-ice biogeochemistry and ice-associated ecosystems. *Nat. Clim. Change* 10: 983–992. <https://doi.org/10.1038/s41558-020-00940-4>
- Leclerc LME, Lydersen C, Haug T, Bachmann L, Fisk AT, Kovacs KM (2012) A missing piece in the Arctic food web puzzle? Stomach contents of Greenland sharks sampled in Svalbard, Norway. *Polar Biol* 35:1197–1208. <https://doi.org/10.1007/s00300-012-1166-7>
- Leslie HA, PhD (2014) Review of microplastics in cosmetics. Scientific background on a potential source of plastic particulate marine litter to support decision-making. V.U. Institute for Environmental Studies, Amsterdam, 33. http://www.ivm.vu.nl/en/Images/Plastic_ingredients_in_Cosmetics_07-2014_FINAL_tcm234-409859.pdf
- Łokas E, Zaborska A, Kolicka M, Różycki M, Zawierucha K (2016) Accumulation of atmospheric radionuclides and heavy metals in cryoconite holes on an Arctic glacier. *Chemosphere* 160:162–172. <https://doi.org/10.1016/j.chemosphere.2016.06.051>
- Luoto TP, Rantala MV, Kivilä EH, Nevalainen L, Ojala AEK (2019) Biogeochemical cycling and ecological thresholds in a High Arctic lake (Svalbard). *Aquat. Sci.* 81:34. <https://doi.org/10.1007/s00027-019-0630-7>
- Lusher A (2015) Microplastics in the marine environment: distribution, interactions and effects. In: Bergmann, M, Gutow, L, Klages, M. (eds.), *Marine Anthropogenic Litter*. Springer International Publishing 245–307. https://doi.org/10.1007/978-3-319-16510-3_10

- Magara G, Khan FR, Pinti M, Syberg K, Inzirillo A, Elia AC (2019) Effects of combined exposures of fluoranthene and polyethylene or polyhydroxybutyrate microplastics on oxidative stress biomarkers in the blue mussel (*Mytilus edulis*) J Toxicol Environ Health—Part A Curr Issues 82:616–625. <https://doi.org/10.1080/15287394.2019.1633451>
- Mattsson K, Ekvall MT, Hansson LA, Linse S, Malmendal A, Cedervall T (2015) Altered behavior, physiology, and metabolism in fish exposed to polystyrene nanoparticles. Environ Sci Technol 49:553–561. <https://doi.org/10.1021/es5053655>
- Mattsson, K, Johnson EV, Malmendal A, Linse S, Hansson LA, Cedervall (2017) Brain damage and behavioural disorders in fish induced by plastic nanoparticles delivered through the food chain. Sci Rep 7:11452. <https://doi.org/10.1038/s41598-017-10813-0>
- Misund OA, Heggland K, Skogseth R, Falck E, Gjørseter H, Sundet J, et al. (2016) Norwegian fisheries in the Svalbard zone since 1980. Regulations, profitability and warming waters affect landings. Polar Sci 10:312–322. <http://dx.doi.org/http://dx.doi.org/10.1016/j.polar.2016.02.001>
- Morgana S, Ghigliotti L, Estévez-Calvar N, Stifanese R, Wieckzorek A, Doyle T, et al. (2018) Microplastics in the Arctic: a case study with sub-surface water and fish samples off Northeast Greenland. Environ Pollut 242:1078–1086 <https://doi.org/10.1016/j.envpol.2018.08.001>
- Mørskeland, T (2018) Microplastics in sediments on the Norwegian continental shelf. Report for the Norwegian Environment Agency (Miljødirektoratet). Report number M-976. Available at <https://www.miljodirektoratet.no/globalassets/publikasjoner/M976/M976.pdf>
- MSFD 2008/56/EC. <https://eur-lex.europa.eu/legal-content/EN/TXT/?uri=CELEX%3A52020SC0060>
- MSFD Technical Group on Marine Litter 2013 <https://mcc.jrc.ec.europa.eu/>
- Nagatsuka N, Takeuchi N, Nakano T, Kokado Y, Li Z (2010) Sr, Nd and Pb stable isotopes of surface dust on Ürümqi glacier No. 1 in western China. Ann Glaciol 51:95–105. <https://doi.org/10.3189/172756411795931895>
- Nashoug BF (2017) Sources of Marine Litter –Workshop Report, Svalbard 4th–6th September 2016. SALT report. 1017, Lofoten, Norway, 1–23
- Nelms, S, Duncan E, Broderick A, Galloway T, Godfrey M, Hamann M, Lindeque P, Godley B (2016) Plastic and marine turtles: a review and call for research. ICES J Mar Sci 73(2):165–181. <https://doi.org/10.1093/icesjms/fsv165>
- Nielsen J, Hedeholm RB, Simon M, Steffensen JF (2014) Distribution and feeding ecology of the Greenland shark (*Somniosus microcephalus*) in Greenland waters. Polar Biol 37:37–46. <https://doi.org/10.1007/s00300-013-1408-3>
- Nowak A, Hodgkins R, Nikulina A, Osuch M, Wawrzyniak T, Kavan J, et al. (2021) From land to fjords: The review of Svalbard hydrology from 1970 to 2019. In: Moreno-Ibáñez et al (eds) SESS report 2020, Svalbard Integrated Arctic Earth Observing System, Longyearbyen, pp 176–201. <https://doi.org/10.5281/zenodo.4294063>
- Obbard RW, Sadri S, Wong YQ, Khitun AA, Baker I, Thompson RC (2014) Global warming releases microplastic legacy frozen in Arctic sea ice. Earth's Future 2:315–320. <https://doi.org/10.1002/2014EF000240>
- Obbard, RW (2018) Microplastics in Polar Regions: The role of long range transport. Curr Opin Environ Sci Health 1:24–29. <https://doi.org/10.1016/j.coesh.2017.10.004>
- Oberbeckmann S, Löder MGJ, Labrenz M (2015) Marine microplastic-associated biofilms – a review. Environ Chem 12(5):551–562. <http://dx.doi.org/10.1071/EN15069>
- Øritsland NA (1986) Svalbardreinen og dens livsgrunnlag. Otta, Norway: Universitetsforlaget AS. ISBN13 9788200077282.fang
- Ory NC, Gallardo C, Lenz M, Thiel M (2018) Capture, swallowing, and egestion of microplastics by a planktivorous juvenile fish. Environ Pollut 240:566–573. <https://doi.org/10.1016/j.envpol.2018.04.093>
- PAME (2019) Desktop Study on Marine Litter Including Microplastics in the Arctic. Protection of the Arctic Marine Environment, Arctic Council (May 2019). <https://pame.is/projects/arctic-marine-pollution/desktop-study-on-marine-litter>
- Parkinson CL, DiGirolamo NE (2016) New visualizations highlight new information on the contrasting Arctic and Antarctic sea-ice trends since the late 1970s Remote Sens Environ 183:198–204. <http://dx.doi.org/10.1016%2Fj.rse.2016.05.020>
- Patel MM, Goyal BR, Bhadada SV, Bhatt JS, Amin AF (2009) Getting into the brain: approaches to enhance brain drug delivery. CNS Drugs 23:35–58. <https://doi.org/10.2165/0023210-200923010-00003>
- Pedà C, Caccamo L, Fossi MC, Gai F, Andaloro F, Genovese L, et al. (2016) Intestinal alterations in European sea bass *Dicentrarchus labrax* (Linnaeus, 1758) exposed to microplastics:Preliminary results. Environ Pollut 212:251–256. <https://doi.org/10.1016/j.envpol.2016.01.083>
- Peeken I, Primpke S, Beyer B, Gütermann J, Katlein C, Krumpfen T, et al. (2018) Arctic sea ice is an important temporal sink and means of transport for microplastic. Nat Commun 9:1505. <https://doi.org/10.1038/s41467-018-03825-5>
- Plastics Europe (2019) Plastics—The Facts 2019. https://www.plasticseurope.org/application/files/9715/7129/9584/FINAL_web_version_Plastics_the_facts2019_14102019.pdf
- Polyakov IV, Alkire MB, Bluhm BA, Brown KA, Carmack EC, Chierici M, et al. (2020) Borealization of the Arctic Ocean in Response to Anomalous Advection From Sub-Arctic Seas. Front Mar Sci 7:491. <https://doi.org/10.3389/fmars.2020.00491>
- Poon FE, Provencher JF, Mallory ML, Braune BM, Smith PA (2017) Levels of ingested debris vary across species in Canadian Arctic seabirds. Mar Pollut Bull 116:517–520. <https://doi.org/10.1016/j.marpolbul.2016.11.051>

- Provencher JF, Bond AL, Avery-Gomm S, Borrelle SB, Rebolledo ELB, Hammer S, et al. (2017) Quantifying ingested debris in marine megafauna: a review and recommendations for standardization. *Anal Methods* 9(9):1454–1469. <https://doi.org/10.1039/C6AY02419J>
- Provencher JF, Vermaire JC, Avery-Gomm S, Braune BM, Mallory ML (2018) Garbage in guano? Microplastic debris found in faecal precursors of seabirds known to ingest plastics. *Sci Total Environ* 644:1477–1484. <https://doi.org/10.1016/j.scitotenv.2018.07.101>
- Purver M (2019) Understanding the occurrence and fate of microplastics in the Arctic fjords of Svalbard, University of Akureyri, Faculty of Business and Science, Borgir, 600 Akureyri, Iceland
- Radisic V, Nimje PS, Bienfait AM, Marathe NP (2020) Marine Plastics from Norwegian West Coast Carry Potentially Virulent Fish Pathogens and Opportunistic Human Pathogens Harboring New Variants of Antibiotic Resistance Genes. *Microorganisms* 8:1200. <https://doi.org/10.3390/microorganisms8081200>
- Reynolds C, Ryan PG (2018) Micro-plastic ingestion by waterbirds from contaminated wetlands in South Africa. *Mar Pollut Bull* 126:330–333. <https://doi.org/10.1016/j.marpolbul.2017.11.021>
- Roch S, Walter T, Ittner LD, Friedrich C, Brinker A (2019) A systematic study of the microplastic burden in freshwater fishes of South-Western Germany—are we searching at the right scale? *Sci Total Environ* 689:1001–1011. <https://doi.org/10.1016/j.scitotenv.2019.06.404>
- Rocha-Santos T, Duarte AC (2014) A critical overview of the analytical approaches to the occurrence, the fate and the behavior of microplastics in the environment. *TrAC Trends Anal Chem* 65:47–53. <https://doi.org/10.1016/j.trac.2014.10.011>
- Schoolmeester T, Gjerdi HL, Crump J, Alfthan B, Fabres J, Johnsen KI, et al. (2019) Global Linkages: A graphic look at the changing Arctic. Nairobi and Arendal. www.grida.no.
- Salzano R, Aalstad K, Boldrini E, Gallet JC, Kępski D, Luks B, et al. (2021) Terrestrial photography applications on snow cover in Svalbard. In: Moreno-Ibáñez et al (eds) SESS report 2020, Svalbard Integrated Arctic Earth Observing System, Longyearbyen, pp 236–251. <https://doi.org/10.5281/zenodo.4294084>
- Schuler TV, Glazovsky A, Hagen JO, Hodson A, Jania J, Kääh A, et al (2020) In: van den Heuvel et al (eds) SESS report 2019. Svalbard Integrated Arctic Earth Observing System, Longyearbyen, pp 108–135. https://sios-svalbard.org/SESS_Issue2
- Scott N, (2019) Investigating the environmental partitioning of microplastics in two contrasting marine ecosystems. Thesis, University of Exeter.
- Screen JA, Simmonds I (2010) The central role of diminishing sea ice in recent Arctic temperature amplification. *Nature* 464:1334–1337. <https://doi.org/10.1038/nature09051>
- Sikdokur E, Belivermiş M, Sezer N, Pekmez M, Bulan ÖK, Kılıç Ö (2020) Effects of microplastics and mercury on manila clam *Ruditapes philippinarum*: feeding rate, immunomodulation, histopathology and oxidative stress. *Environ Pollut* 262:114247. <https://doi.org/10.1016/j.envpol.2020.114247>
- Singh SM, Avinash K, Sharma P, Mulik RU, Upadhyay AK, Ravindra S (2017) Elemental variations in glacier cryoconites of Indian Himalaya and Spitsbergen. *Arctic Geosci Front* 8:1339–1347. <https://doi.org/10.1016/j.gsf.2017.01.002>
- Skåre JU, Alexander J, Haave M, Jakubowicz I, Knutsen HK, Lusher A, et al. (2019) Microplastics; occurrence, levels and implications for environment and human health related to food. Opinion of the Steering Committee of the Norwegian Scientific Committee for Food and Environment. VKM report 2019:16. ISBN: 978-82-8259-332-8. <https://munin.uit.no/handle/10037/16566?locale-attribute=en>
- Suaria G, Aliani S (2014) Floating debris in the Mediterranean Sea. *Mar. Pollut Bull* 86:494–504. <https://doi.org/10.1016/j.marpolbul.2014.06.025>
- Sundet JH, Bakanev S (2014) Snow crab (*Chionoecetes opilio*) –a new invasive crab speices becoming an importnat player in the Barent Sea ecosystem. ICES CM 2014/F: 04. <http://www.ices.dk/sites/pub/CM%20Documents/CM-2014/Theme%20Session%20F%20contributions/F0414.pdf>
- Sundet JH, Herzke D, Jenssen M (2016) Forekomst og kilder av mikroplastikk i sediment, og konsekvenser for bunnlevende fisk og evertebrater pa Svalbard. RIS prosjekt nr 10495. Svalbards Miljøvernfond.
- Svendsen H, Beszczynska-Møller A, Hagen JO, Lefauconnier B, Tverberg V, Gerland S et al. (2002), The physical environment of Kongsfjorden–Krossfjorden, an Arctic fjord system in Svalbard. *Polar Res* 2:133–166. <https://doi.org/10.3402/polar.v21i1.6479>
- Tanaka K, Watanuki Y, Takada H, Ishizuka M, Yamashita R, Kazama M et al. (2020) In vivo Accumulation of Plastic-Derived Chemicals into Seabird Tissues. *Curr Biol* 30:e723–728. <https://doi.org/10.1016/j.cub.2019.12.037>
- Tang Y, Rong J, Guan X, Zha S, Shi W, Han Y, et al. (2020) Immunotoxicity of microplastics and two persistent organic pollutants alone or in combination to a bivalve species. *Environ Pollut* 258:113845. <https://doi.org/10.1016/j.envpol.2019.113845>
- Tekman MB, Krumpfen T, Bergmann M (2017) Marine litter on deep Arctic seafloor continues to increase and spreads to the North at the HAUSGARTEN observatory. *Deep-Sea Res I Oceanogr Res Pap* 120:88–99. <https://doi.org/10.1016/j.dsr.2016.12.011>
- Tekman MB, Wekerle C, Lorenz C, Primpke S, Hasemann C, Gerds G, Bergman M (2020) Tying up loose ends of microplastic pollution in the Arctic: distribution from the sea surface, through the water column to deep-sea sediments at the HAUSGARTEN observatory. *Environ Sci Technol* 54:4079–4090. <https://doi.org/10.1021/acs.est.9b06981>

- Thompson RC, Olsen Y, Mitchell RP, Davis A, Rowland SJ, John AWG, et al. (2004) Lost at sea: where is all the plastic? *Science* 304:838. <https://doi.org/10.1126/science.1094559>
- Trevail AM, Gabrielsen GW, Kühn S, van Franeker JA (2015) Elevated levels of ingested plastic in a high Arctic seabird, the northern fulmar (*Fulmarus glacialis*). *Polar Biol* 38:975–981. <https://doi.org/10.1007/s00300-015-1657-4>
- Turner S, Horton AA, Rose NL, et al. (2019) A temporal sediment record of microplastics in an urban lake, London, UKJ. *Paleolimnol* 61, 449–462. <https://doi.org/10.1007/s10933-019-00071-7>
- Tverberg V, Skogseth R, Cottier F, Sundfjord A, Walczowski W, Inall ME, et al. (2019) The Kongsfjorden transect: seasonal and inter-annual variability in hydrography. In: Hop H and Wiencke C (eds) *The Ecosystem of Kongsfjorden, Svalbard*, Springer, Cambridge, pp 49–104. https://doi.org/10.1007/978-3-319-46425-1_3
- Urbanek AK, Rymowicz W, Strzelecki MC, Kociuba W, Franczak L, Mironczuk AM (2017) Isolation and characterization of Arctic microorganisms decomposing bioplastics. *AMB Express* 7:148. <https://dx.doi.org/10.1186%2Fs13568-017-0448-4>
- van Franeker JA, Blaize C, Danielsen J, Fairclough K, Gollan J, Guse N, et al. (2011) Monitoring plastic ingestion by the northern fulmar *Fulmarus glacialis* in the North Sea. *Environ Pollut* 159:2609–2615. <https://doi.org/10.1016/j.envpol.2011.06.008>
- van Sebille E, Aliani S, Law KL, Maximenko N, Alsina JM, Bagaev A, et al (2020) The physical oceanography of the transport of floating marine debris. *Environ Res Lett* 15(2):1–32. <https://doi.org/10.1088/1748-9326/ab6d7d>
- Van Sebille E, England MH, Froyland G (2012) Origin, dynamics and evolution of ocean garbage patches from observed surface drifters. *Environ Res Lett* 7:044040. <http://dx.doi.org/10.1088/1748-9326/7/4/044040>
- Vandermeersch G, Van Cauwenberghe L, Janssen CR, Marques A, Granby K, Fait G, et al. (2015) A critical view on microplastic quantification in aquatic organisms. *Environ Res* 143:46–55. <https://doi.org/10.1016/j.envres.2015.07.016>
- Volkheimer G (1975) Hematogenous dissemination of ingested polyvinyl chloride particles. *Ann N Y Acad Sci* 246:164–171. <https://doi.org/10.1111/j.1749-6632.1975.tb51092.x>
- von Friesen LW, Granberg ME, Pavlova O, Magnusson K, Hassellöv M, Gabrielsen GW (2020) Summer sea ice melt and wastewater are important local sources of microlitter to Svalbard waters. *Environ Int* 139:105511. <https://doi.org/10.1016/j.envint.2020.105511>
- Walseng B, Jensen T, Dimante-Deimantovica I et al. (2018) Freshwater diversity in Svalbard: providing baseline data for ecosystems in change. *Polar Biol* 41:1995–2005. <http://dx.doi.org/10.1007/s00300-018-2340-3>
- Walvoord MA, Kurylyk BL (2016) Hydrologic impacts of thawing permafrost—a review. *Vadose Zone J* 15:6. <https://doi.org/10.2136/vzj2016.01.0010>
- Wang F, Wong C, Chen D, Lu X, Wang Fei Zeng, E (2018) Interaction of toxic chemicals with microplastics: a critical review. *Water Res* 139:208–219. <https://doi.org/10.1016/j.watres.2018.04.003>
- Watts AJ, Lewis C, Goodhead RM, Beckett SJ, Moger J, Tyler CR, Galloway TS (2014) Uptake and retention of microplastics by the shore crab *Carcinus maenas*. *Environ Sci Technol* 48:8823–8830. <https://doi.org/10.1021/es501090e>
- Weiland-Bräuer N, Fischer MA, Schramm KW, Schmitz RA (2017) Polychlorinated Biphenyl (PCB)-Degrading Potential of Microbes Present in a Cryoconite of Jamtalfjerner. *Glacier Front Microbiol.* 8:1105. <https://doi.org/10.3389/fmicb.2017.01105>
- Welden NA, Lusher A (2017) Impacts of changing ocean circulation on the distribution of marine microplastic litter. *Integr Environ Assess Manage* 3:483–487. <https://doi.org/10.1002/ieam.1911>
- Welden NAC, Cowie PR (2016) Long-term microplastic retention causes reduced body condition in the langoustine, *Nephrops norvegicus*. *Environ Pollut* 218:895–900. <https://doi.org/10.1016/j.envpol.2016.08.020>
- Woodall LC, Sanchez-Vidal A, Canals M, Paterson GLJ, Coppock R, Sleight V, et al. (2014) The deep sea is a major sink for microplastic debris. *R Soc Open Sci* 1:1–8. <https://doi.org/10.1098/rsos.140317>
- Woosley RJ, and FJ Millero (2020) Freshening of the western Arctic negates anthropogenic carbon uptake potential. *Limnol Oceanogr* <https://doi.org/10.1002/lno.11421>
- Wright SL, Thompson RC, Galloway TS (2013) The physical impacts of microplastics on marine organisms: a review. *Environ Pollut* 178:483–492. <https://doi.org/10.1016/j.envpol.2013.02.031>
- Wright SL, Kelly FJ (2017). Plastic and human health: a micro issue? *Environ Sci Technol* 51:6634–6647. <https://doi.org/10.1021/acs.est.7b00423>
- Zalasiewicz J, Waters CN, Ivar do Sul JA, Corcoran PL, Barnosky AD, Cearreta A, et al. (2016) The geological cycle of plastics and their use as a stratigraphic indicator of the Anthropocene. *Anthropocene* 13:4–17. <https://doi.org/10.1016/j.ancene.2016.01.002>
- Zettler ER, Mincer TJ, Amaral-Zettler LA (2013) Life in the 'Plastisphere': Microbial communities on plastic marine debris. *Environ Sci Technol* 47:7137–7146. <https://doi.org/10.1021/es401288x>
- Zhang HY, Shin PKS, Cheung SG (2016) Physiological responses and scope for growth in a marine scavenging gastropod, *Nassarius festivus* (Powys, 1835), are affected by salinity and temperature but not by ocean acidification. *ICES J Mar Sci* 73:814–824. <http://dx.doi.org/10.1093/icesjms/fsv208>
- Zhang P, Yan Z, Lu G, Ji Y (2019) Single and combined effects of microplastics and roxithromycin on *Daphnia magna*. *Environ Sci Pollut Res* 26:17010–17020. <https://doi.org/10.1007/s11356-019-05031-2>

Appendix 1

MPs in different abiotic compartments of Svalbard

Location	Year	Medium	Range	Unit	Sampling method	Analytical method	Reference
Ice and Snow							
Svalbard and Fram Strait	2016 – 18	Snow	0 – 14,400	Particles L ⁻¹	Surface sample with a spoon	Vacuum filtration (1 mL aliquot) and Fourier-transform infrared microspectroscopy (μFTIR)	Bergmann et al. 2019
Fram Strait, north of Svalbard	2014 – 15	Sea ice	(1.1 0.8) x 10 ⁶ – (1.2 1.4) x 10 ⁷	Particles m ⁻³	Ice coring	Vacuum filtration and μFTIR (FPA detector)	Peeken et al. 2018
Svalbard	2017	Sea ice	0.158	MPs m ⁻³	Boat hook	Visual analysis under stereomicroscope and Fourier transform infrared spectroscopy (FTIR)	Von-Friesen et al. 2020
Water							
Norwegian Sea (Transect from Tromsø up to SW Svalbard (78.07°))	2014	Water (surface)	0 – 11.5	Particles m ⁻³	Manta net (330 μm)	Gravity separation, light microscopy and FTIR	Lusher et al. 2015
		Water (subsurface)	0 – 1.31	Particles m ⁻³	Seawater intake	Vacuum filtration, light microscopy and FTIR	
Svalbard	2017	Water (0–1000m)	0.0007 – 0.048	MPs m ³	Niskin bottles	Visual analysis under stereomicroscope and FTIR	Von-Friesen et al. 2020
Adventfjorden	2018	Water	0 – 3.32	MPs/m ³	manta net and a high-capacity pump system	Visual identification by microscope and FTIR	Purver 2019
Grønifjorden			0.1 – 1.09				
Dicksonfjorden			0.12 – 1.67				
Oxaasdalen			4.0				
Ekmanfjorden			0.36 – 0.83				
Nordfjorden	3.85						
Kongsfjorden	2018	Surface water	23.7 ± SD 11.9 – 74.1 ± SD 43.9	Particles m ⁻³	Surface trawl by using Plankton net	vacuum filtration and FTIR	Scott 2019
Kongsfjorden	2018	Subsurface (160m depth)	53.8 ± SD 3.2 – 92.3 ± SD 12.8	Particles m ⁻³		vacuum filtration and FTIR	Scott 2019
Svalbard	2015	Water (near wastewater outflow)	97 (Mean)	Particles L ⁻¹	n/a	n/a	Sundet et al. 2016

Svalbard	2016	Subsurface water	n.d	Particles L ⁻¹	Seawater intake	Vacuum filtration and visual sorting	Sundet 2017
Fram Strait (HAUSGARTEN observatory)	2016	Water	0 – 1287	Particles m ⁻³	High volume pump	Vacuum filtration, visual sorting and FTIR	Tekman et al. 2020
Svalbard	2017	Incoming and outgoing wastewater	Inflow: 14,207 Outflow:83	Particles L ⁻¹	Water pump	Enzymatic digestion, vacuum filtration, light microscopy and FTIR	Granberg 2019
		Subsurface water	18.6 – 61.2	Particles L ⁻¹	Water pump	Sequential filtration, light microscopy and FTIR	
Sediment							
Knudsenheia lake (western shore of Kongsfjorden)	2018	sediments adhered to rocks	400 (average)	microparticles/m ²		Raman Microscopy, μ FTIR and Synchrotron Radiation μ FTIR (SR-FTIR)	Gonzalez-Pleiter et al. 2020
Lake Revvatnet	2013	Sediment	7.4	particles/cm ⁻¹	Kajak corer	n/a	Luoto et al. 2019
Dicksonfjorden	2018	Sediment	0 – 0.63	MP/kg	Sediment sampler	Visual identification by microscope and FTIR	Purver 2019
Fram Strait (HAUSGARTEN observatory)	2015	Sediment	42 – 6595	Particles kg ⁻¹	Multicorer	Microplastic sediment separator, Fenton's reagent, visual sorting, FTIR	Bergmann et al. 2017
Barents Sea	2017	Sediment	830 – 3900	Particles kg ⁻¹	Grab sample	Density separation, digestion, filtration and visual sorting	Møskeland et al. (2018)
Svalbard	2015	Sediment	0 – 9.2	Particles kg ⁻¹ DW	Van Veen grab	Density, filtration and visual sorting	Sundet et al. 2016
		Beach sediment	0 – 6.4	Particles kg ⁻¹ DW	Beach Sand collection		
Svalbard	2016	Sediment	2 – 10	Particles L ⁻¹	Van Veen grab	Density separation (NaCl), vacuum filtration and visual sorting	Sundet et al. 2017
Svalbard	2017	Sediment	0 – 134	Particles kg ⁻¹ DW	Van Veen grab	Density separation (NaCl), vacuum filtration, light microscopy and FTIR	Granberg et al. 2019
		Beach sediment	11 – n/a	Particles kg ⁻¹ DW	Metal shovel		
Fram Strait (HAUSGARTEN observatory)	2016	Sediment	239 – 13,331	Particles kg ⁻¹	Multicorer	Density separation, vacuum filtration, visual sorting and FTIR	Tekmann et al. 2020
Fram Strait	2001 – 2011	Deep-sea sediment	10 – 15	Particles 50 mL	Subsample of a box/megacore	Density separation (NaCl), visual sorting, FTIR	Woodall et al. 2014

Environmental status of Svalbard coastal waters: coastscapes and focal ecosystem components (SvalCoast)



Janne E. Søreide¹, Vanessa Pitusi¹, Anna Vader¹, Børge Damsgård¹, Frank Nilsen¹, Ragnheid Skogseth¹, Amanda Poste², Allison Bailey³, Kit M. Kovacs^{1,3}, Christian Lydersen³, Sebastian Gerland³, Sébastien Descamps³, Hallvard Strøm³, Paul E. Renaud^{1,4}, Guttorm Christensen⁴, Maria P. Arvnes⁵, Piotr Graczyk⁶, Denis Moiseev⁷, Rakesh Kumar Singh⁸, Simon Bélanger⁸, Josef Elster⁹, Jacek Urbański¹⁰, Mateusz Moskalik¹¹, Józef Wiktor¹², and Jan Marcin Węśławski¹²

1 University Centre in Svalbard, Longyearbyen, Norway

2 Norwegian Institute for Water Research, Tromsø, Norway

3 Norwegian Polar Institute, Fram Centre, Tromsø, Norway

4 Akvaplan-niva AS, Tromsø, Norway

5 SALT Lofoten AS, Svølvær, Norway

6 NORCE Norwegian Research Centre AS, Bergen, Norway

7 Murmansk Marine Biological Institute, Murmansk, Russia

8 University of Quebec at Rimouski, Canada

9 Centre for Polar Ecology, University of South Bohemia, České Budějovice, Czech Republic

10 GIS Centre, University of Gdańsk, Poland

11 Institute of Geophysics, Polish Academy of Sciences, Warsaw, Poland

12 Institute of Oceanology, Polish Academy of Sciences, Sopot, Poland

Corresponding author: Janne E. Søreide, Janne.Soreide@unis.no

ORCID number 0000-0002-6386-2471

Keywords: Climate change, Arctic, physical drivers, sea ice, biodiversity, productivity, ecosystem change

DOI: <https://doi.org/10.5281/zenodo.4293849>

1. Introduction

Coastal waters are among the most productive regions in the Arctic (Leu et al. 2015; Smola et al. 2017; Ardyna et al. 2020). In these areas, a strong coupling exists between the sea and the land, and the shallow depths create a tight pelagic-benthic coupling (McGovern et al. 2020). These regions are also critical breeding and foraging grounds for many invertebrates, fish, bird, and marine mammal species (Dunton et al. 2012). When combined, these various groups of animals provide a valuable host of ecosystem services. Many of the Arctic marine species included in these groupings are vulnerable to anthropogenic and climate-induced stressors (Kovacs et al. 2011; Descamps et al. 2017). In Svalbard, nearshore ecosystems are being impacted directly by global warming—causing the reduction of landfast sea ice, the retreat of marine terminating (also called tidewater) glaciers, and altered wind and wave, circulation and stratification patterns)—as well as somewhat more indirectly by climate change on land (e.g. permafrost thaw, melting of glaciers, changes in precipitation and runoff) (e.g. Adakudlu et al. 2019). This has and will have a broad range of implications for physical and biogeochemical conditions in Svalbard's coastal waters, including changes in nutrient concentrations and the underwater light regime, as well as direct physical changes to coastal habitat structure (Dunton et al. 2012; McGovern et al. 2020). In turn, these changes are likely to impact the primary productivity and biodiversity of Svalbard's coastal waters (Leu et al. 2015; Descamps et al. 2017).

The loss of Arctic sea ice creates the possibility for expansion of commercial activity in Svalbard and the Arctic in general (e.g. fishing, shipping, tourism, and potentially marine mining of minerals, oil and gas exploration, etc.) (Misund et al. 2016; Stocker et al. 2020). The growth of global trade, urbanization, and travel activity create opportunities for organisms to move across previously isolated regions, thus advancing biotic homogenization and extinctions. At present, the extent of protected coastal marine ecosystems in

the Arctic remains minute in comparison to the terrestrial environment (CAFF¹). Arctic biodiversity is under growing pressure as climate change and human activities such as shipping and exploitation of natural resources increase. Government managers, industries, conservation organisations, and communities thus need access to timely and complete biodiversity status and trend data. For example, all Arctic endemic marine mammals are ice-associated, and hence, under extreme threat due to the ongoing trends in sea-ice losses (Kovacs et al. 2011). Recently a Coastal Expert Monitoring Group (CEMG) was established as part of the Circumpolar Biodiversity Monitoring Program (CBMP²) under the Arctic Council's Conservation of Arctic Flora and Fauna (CAFF) working group. The primary goal of the CEMG is to develop a long-term, integrated, multi-disciplinary circumpolar Arctic coastal biodiversity monitoring plan³ 'State of Arctic Coastal Biodiversity Report' in 2023. This synopsis, which comprises an overview of Svalbard coastscapes (Rocky shore, Ice fronts etc.) and the essential focal ecosystem components (FECs) inhabiting them, will be an important contribution to this pan-Arctic synthesis from the Norwegian High Arctic.

The following three main objectives were addressed in this Svalbard synopsis:

1. Provide an overview of the extent of the different coastscapes in the Svalbard Archipelago (using the terminology of the Coastal Expert Monitoring Group in CAFF, 2019).
2. Identify the key environmental drivers (physical, chemical, biological, and anthropogenic) that influence biodiversity and ecosystem functioning in the defined coastscapes.
3. Map the status of essential Focal Ecosystem Components (FEC), defined by CAFF (2019), in these coastscapes in Svalbard, and identify gaps in current knowledge and monitoring.

1 www.caff.is

2 www.cbmp.is

3 www.caff.is/coastal

2. Overview of existing knowledge

2.1. Geographical location and climate

The Svalbard Archipelago extends from 74° to 81° N and from 10° to 35° E and is situated in the middle of the main gateway to the Arctic Ocean, halfway between mainland Norway and the North Pole. The largest island is Spitsbergen in the west, followed by Nordaustlandet in the northeast, and then Edgeøya and Barentsøya on the east side of the archipelago⁴. The distance from southern Spitsbergen to mainland Norway is approximately 680 km, with Bjørnøya, the southernmost island of Svalbard, located halfway to the mainland. Furthest to the east, in the western Barents Sea, the island Hopen is located. Long open sea expanses act as effective barriers against dispersal of organisms. Particle tracking models estimate that ocean currents can transport passive organisms over a distance of 1000 km (i.e. Lofoten, Norway to Isfjorden, Svalbard) in roughly one month (Berge et al. 2005). Strong climatic gradients over short distances characterises the Svalbard Archipelago. Warm Atlantic water impacts the southwest and northwest parts of Svalbard, whereas cold Arctic water and extensive seasonal ice cover dominate the northeast and east coasts of Svalbard. Three main climatic regions can therefore be identified for Svalbard: 1) West Svalbard with a sub-Arctic climate and very little sea-ice presence, 2) North Svalbard with a mixed Atlantic and Arctic climate exposed to the Arctic Ocean and consolidated pack ice, and 3) East Svalbard with a cold Arctic climate and extensive seasonal sea-ice formation.

2.2. Physical environment

Hydrographical observatories (moorings) in fjords in West Svalbard (Kongsfjorden and Isfjorden), operated since 2002, show an increase of 2°C over the 20-year record of observations with the strongest sea temperature increase in winter (Cottier et al. 2019). For fjords in Northeast

Svalbard (Rijpfjorden), no distinct increase in sea temperatures since 2006 has been identified (Cottier et al. 2019), while in East Svalbard, continuous time series from moored observatories are lacking. The sea-ice extent and sea-ice thickness mirror the sea temperatures. In western Svalbard, sea-ice extent and thickness have been monitored in Kongsfjorden since 2003 (Gerland and Renner 2007), in Grønfjorden since 1974 (Zhuravskiy et al. 2012), and Van Mijenfjorden since 2006 (Høyland 2009; Karulina et al. 2019), and both sea-ice extent and thickness have significantly declined after 2006 (Muckenhuber et al. 2016, Pavlova et al. 2019; Gerland et al. 2020; Johansson et al. 2020). In northern Svalbard, SAR satellite products, which have been available since season 2002/03, show indications of shorter sea-ice seasons in Rijpfjorden since winter 2012/13 (Johansson et al. 2020). In eastern Svalbard (Inglefieldebukta), sea-ice monitoring has been undertaken since 2006. Data and analysis for eastern Svalbard are however too incomplete for statements about trends⁵. In southeastern Svalbard, the thickness of coastal sea ice has been monitored at Hopen since 1966 and there is a decreasing trend over the period 1966–2007 (Gerland et al. 2008). Based on SAR satellite data for the period 2005–2018 and a machine learning model, it has been possible to reconstruct landfast ice distribution from standard meteorological temperature data in the period 1973–2000⁶. From this model, fast ice with a duration of two months or longer were estimated to cover an area of 12,000 km² in Svalbard in the years 1973–2000, while in the years 2005–2018 this number was reduced to 8000 km², which was further reduced in 2014–2019 to only 6000 km² (Figure 1). Shallower side arms and sill fjords in Isfjorden still freeze in winter, but the sea-ice season has been reduced up to five months due to later sea-ice formation and earlier break-up (Figure 1).

⁴ <https://toposvalbard.npolar.no/>

⁵ For further information, contact S Gerland, NPI, Norway.

⁶ For further method details, contact JA Urbanski, Gdansk University, Poland.

1973 - 2000 model - 2014 - 2018 observation

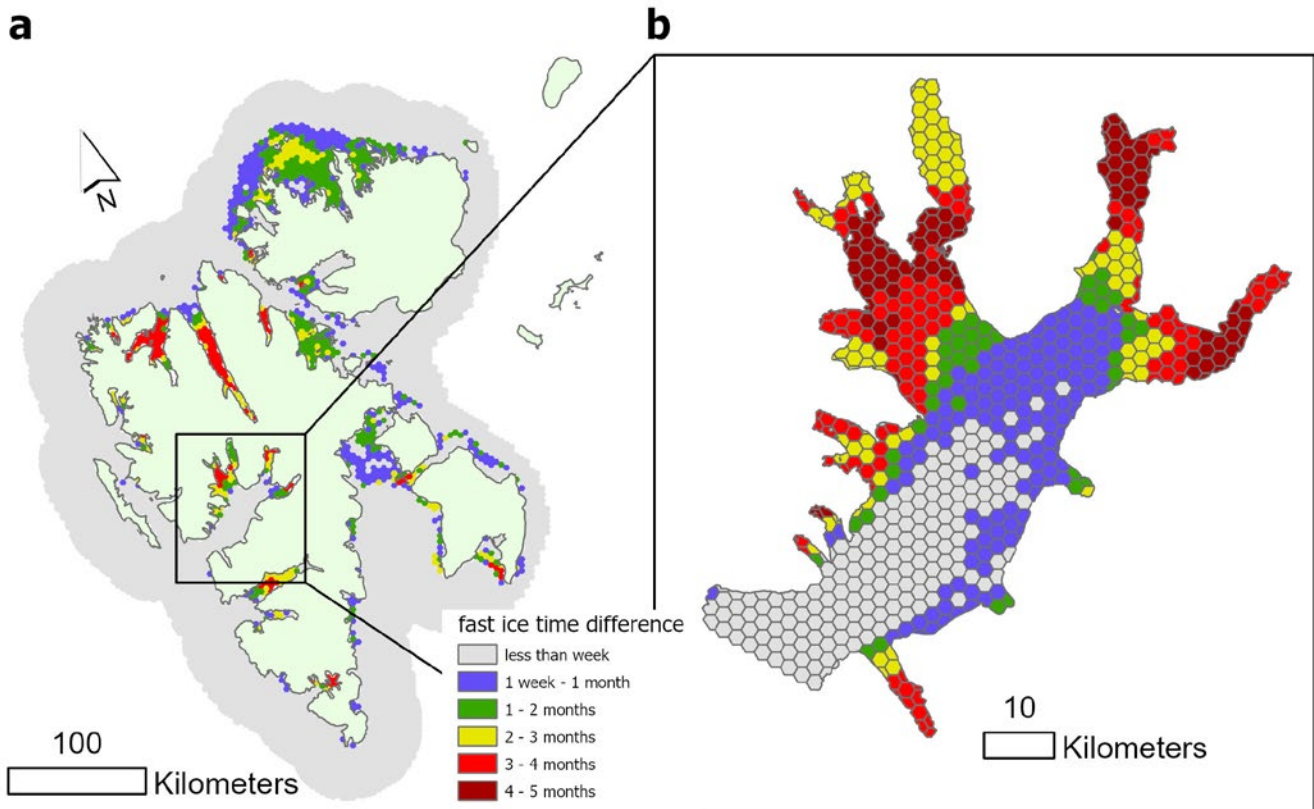


Figure 1. Reduction in land fast sea ice for the period 1973–2000 (based on model data) versus fast ice during 2014–2018 (based on observational data) in Svalbard (a) and specifically for Isfjorden (b). Model results show that fast ice coverage with a duration of two months or more has been reduced by the half over the last 30 years (from 12,000 km² to 6000 km² while the average fast ice duration has decreased between one (green) to five (dark red) months, with the most severe reduction in western Svalbard. For more details about the model results and observations, contact JA Urbanski, Gdansk University, Poland.

With reduced landfast ice and increased storm activity, coastal erosion has increased (Wojtysiak et al. 2018). As an example, between 1960 and 2011, a gravel-dominated coast in Isbjørnhamna, Hornsund experienced a significant shift from being protected by prolonged sea-ice conditions (fast ice) towards a storm-affected and rapidly changing coast. Mean shoreline erosion rates of 0.08 to 0.26 m yr⁻¹ from 1960 to 1990 almost doubled to 0.13-0.45 m yr⁻¹ for the years 1990 to 2011 in Isbjørnhamna (Zagórski et al. 2015). Coastal erosion, increased river runoff (Nowak et al. 2021) and increasing glacial melt is resulting in increased particle loads in coastal waters (i.e. “browning of the Arctic”) which impacts the underwater light availability and thus, primary productivity (Pavlov et al. 2019). In contrast to several studies from the open sea which show that reduced sea ice leads to increased Photosynthetically Active Radiation (PAR)

and increased primary production (Pabi et al. 2008; Arrigo and van Dijken 2011; Kauko et al. 2017) the counteracting effect may occur in coastal waters due to increased light attenuation by terrigenous particles (Smyth et al. 2005; McGovern et al. 2020;). Another factor affecting the penetration of PAR is the increasing cloudiness, which results in reduced PAR entering the water column (Bélanger et al. 2013). Comparison of the chlorophyll-a (Chl-a) concentration (calculated using Shanmugam et al., 2018) and SPM (calculated using Nechad et al. 2010) in a cold and relatively sea ice rich year (2008) versus a warm year with very limited seasonal sea ice (2016) in Svalbard, using MODIS-Aqua data, is shown in Figure 2. Distinct differences in productivity and turbidity between the years is seen with an overall higher primary productivity (Chl-a biomass) and particle load (turbidity) in the warmer year. However, sea-ice algae and under-ice

blooms are not detectable by satellites, as a result, a significant component of the primary productivity in seasonal ice-covered regions is not accounted for in Figure 2. Field studies or other autonomous platforms are therefore needed to monitor changes in the overall primary productivity in Svalbard. Macroalgae (seaweed) and brackish water diatom colonies and other groups of eukaryotic algae and cyanobacteria (microphytobenthos) growing on

intertidal mudflats (Kviderova et al. 2019, Wiktor et al. 2016) are other important primary producers in coastal regions of which we yet have much to learn since our knowledge of their productivity and ecosystem roles are fragmented and poor for the High Arctic (e.g. von Biela et al. 2016).

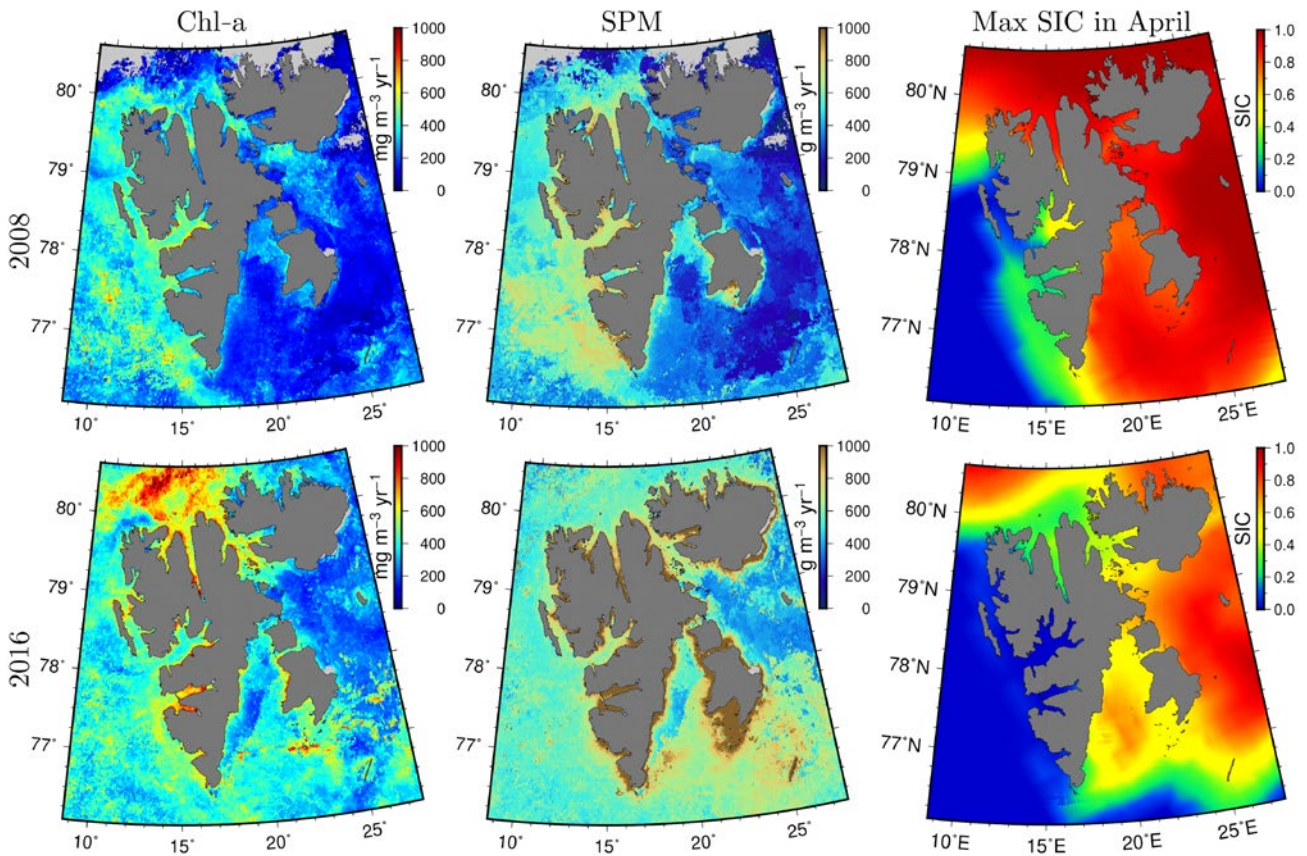


Figure 2. Spatial distribution of chlorophyll-a (Chl-a) concentration and Suspended Particulate Material (SPM) concentration integrated over the months from March to October for the year 2008 (colder year, upper panels) and 2016 (warmer year, lower panels), as well as the maximum sea-ice concentrations (April) in the two years. Sea-ice concentration (SIC) acquired from the National Snow and Ice Data Center. For more details, contact R.K. Singh and S. Belanger, UQAR, Canada.

3. Coastscapes

A pan-Arctic synthesis of coastal biodiversity is scheduled for completion in 2023 (CAFF, 2019). Seven different pan-Arctic coastscapes have been identified (see below and [Appendix 3](#)) and these coastal 'landscapes' will create the basis for comparison of characteristic coastal biota, i.e. Focal Ecosystem Components (FECs), across the Arctic. The selected FECs ([Appendix 4](#)) were chosen because they are considered to be good bio-indicators of the overall health and environmental state of the system, or simply because they are important for food security.

Since Svalbard is located in the High Arctic with marked influences from the warm West Spitsbergen Current, it is a bellwether for climate change impacts on a broader scale. Its unique mix of climatic conditions over small geographic scales makes it an ideal site to monitor the impact of

climate change on Arctic marine systems. Thus, we recommend that monitoring approaches should focus on establishing the status and rate of change for the different coastscapes in all three regions in Svalbard, or at a minimum in one cold and one warm region.

Of the seven coastscapes, the most studied in Svalbard is the fjord coastscape (Figure 3; Weslawski et al. 1993; Wlodarska-Kowalczyk et al. 2012; Berge et al. 2015; Hop et al. 2019). The other six coastscapes represent the shoreline; and in Svalbard these nearshore ecosystems are understudied. However, an extensive coastal mapping project, based on aerial photos (Figure 4), was undertaken by the Norwegian Polar Institute (NPI) between 1987-1991 in order to determine the vulnerability of Svalbard coasts to a potential oil spill.

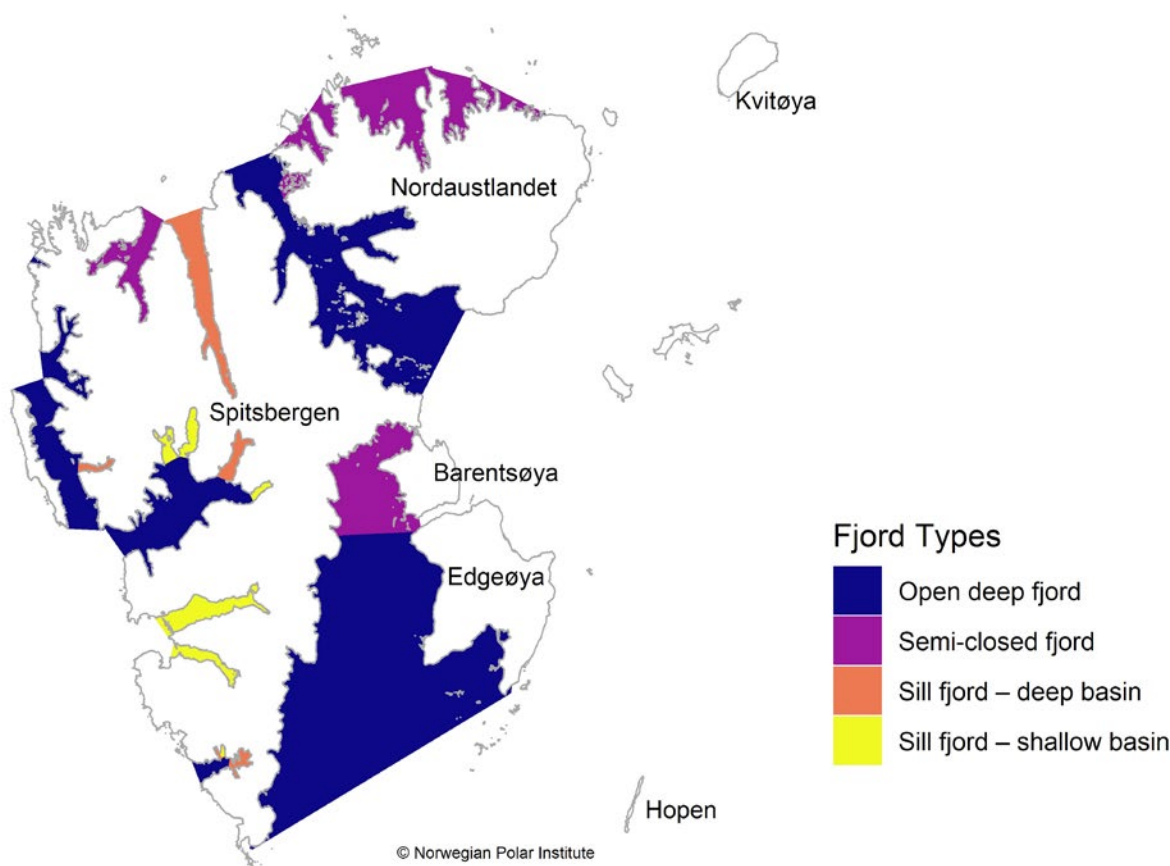


Figure 3. Svalbard fjords classified according to bathymetry and the presence or absence of a shallow sill, or threshold, which restricts the inflow of nearby oceanic water masses into the fjord. Sill fjords are further differentiated by the depth of their inner basin, with “deep” indicating a basin inside the sill deeper >120m. Semi-closed fjords were defined as fjords with an extensive, shallow shelf in front of the fjord mouth that restricts the connectivity with deep oceanic water masses.

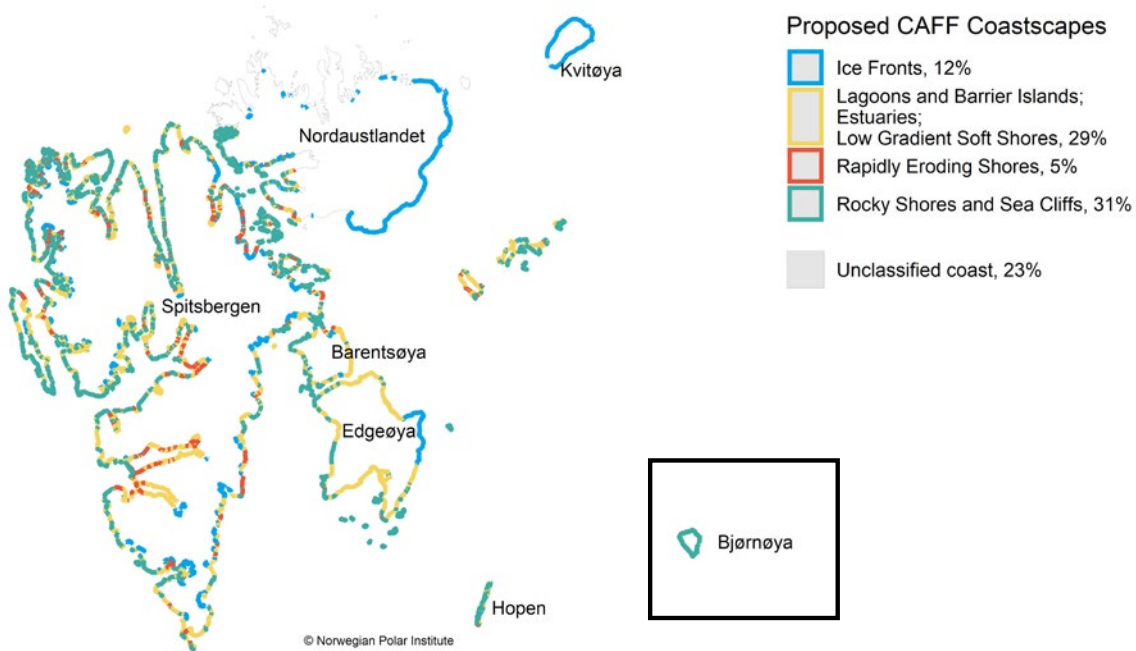


Figure 4. Geomorphological data from aerial photos (1987–1991) (unpublished data, Norwegian Polar Institute) were used to estimate the extent of coastscapes defined by CAFF (2019) in Svalbard. See [Appendix 2](#) for the classification of geomorphology categories into coastscapes. The coastscapes low gradient soft shores, lagoons and barrier islands, and estuaries were not distinguishable based on the geomorphological data available, but see Figure 6 for more details.

NPI mapped the geomorphological characteristics of much of the Svalbard coastline, including the grain size of beach sediments (Figure 5) and special features, such as lagoons, tidal flats, and river deltas (Figure 6). While the dataset requires a final quality check and updates due to subsequent glacial retreat, it is nonetheless the most complete

dataset on Svalbard coastal geomorphology today, encompassing 77% of the coastline of Svalbard at 1 km resolution (8,739 km). The yet-unmapped coastline is primarily in Nordaustlandet, but also includes some newly exposed coastline that is the result of glacial retreat since the aerial pictures were taken in the late 1980s.

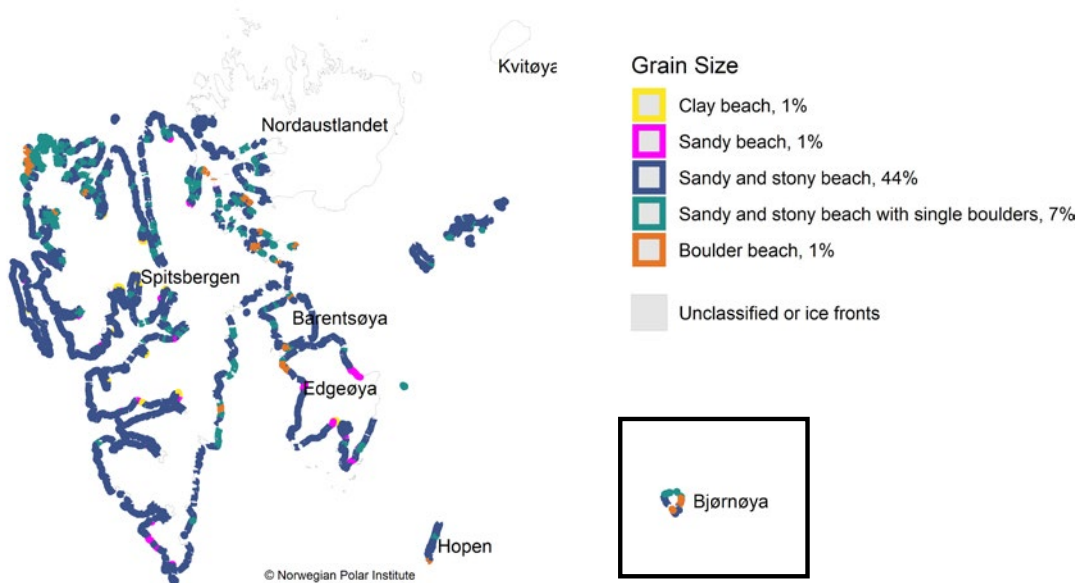


Figure 5. Coastline of Svalbard defined by sediment grain size, as classified from aerial photos (1987–1991) (unpublished data, Norwegian Polar Institute). Grey coastline indicates either unclassified coast or ice fronts. For ice fronts see also Figure 4.

Studies of biota in the intertidal zone were conducted at the same time in a collaborative project with the Institute of Oceanology Polish Academy of Sciences. They inspected, in total, 1400 km coastline by inflatable boats, targeting beaches/coastal habitats characteristic in intervals of 10 km coastline (e.g. gravel beach, sandy beach, boulder beach etc) from Isfjorden in the west to Storfjorden in the east (Weslawski et al. 1990,1997, 1999); some selected sites were revisited in 2015 and 2016 (Weslawski et al. 2018).

The geomorphological and special feature data obtained from the NPI coastal mapping project were assigned to the CAFF coastscapes as indicated in Figures 5 and 6. Certain coastscapes were more easily mapped from the geomorphological data (i.e. ice fronts, rocky shores,

and sea cliffs), while other ones were less easily identifiable from geomorphology alone and will require field investigations in the future to ensure correct classification. The CAFF coastscapes 'low gradient soft shores', 'estuaries' and 'lagoons and barrier islands' are therefore currently pooled for Svalbard (Figure 4). In CAFF, there is only one fjord coastscape, but we recommend dividing it further based on bathymetry (Figure 3). From Figure 5, we see that the two most dominant shoreline coastscapes in Svalbard are rocky shore and sea cliffs (32%) and low gradient soft shores (29%), followed by not mapped (23%), ice fronts (12%) and rapidly eroding shores (4%). The environmental status for the fjord and shoreline coastscapes in Svalbard is presented briefly below, with some future perspectives and recommendations for research and monitoring.

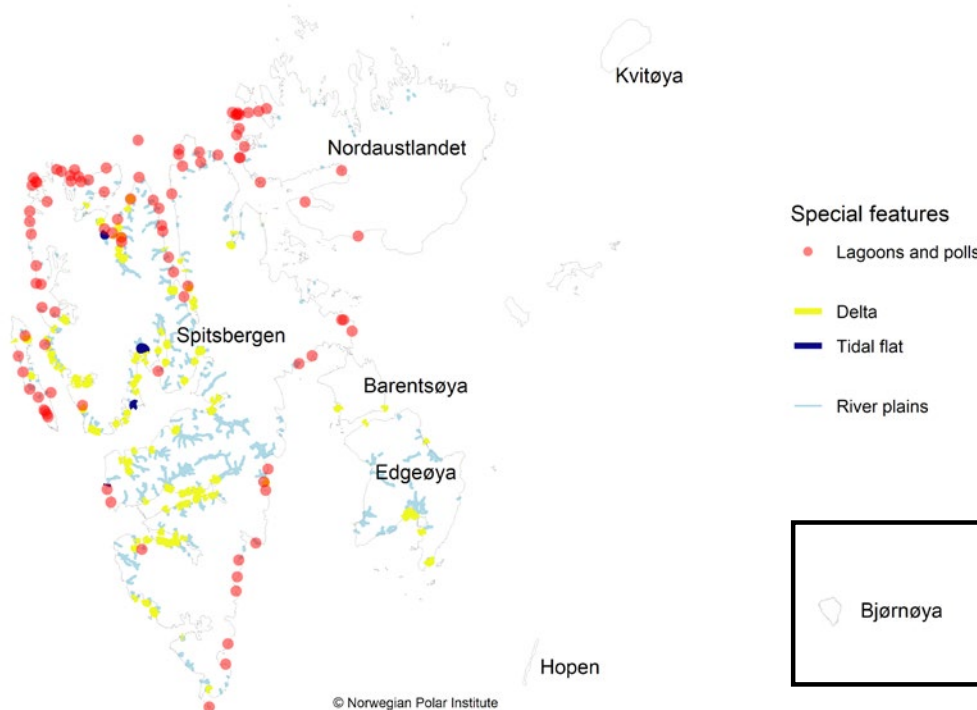


Figure 6. Lagoons and polls (= small water ponds) in Svalbard, according to the Norwegian Polar Institute report (Haug et al. 2016) with delta and tidal flats from aerial photos (1987–1991; unpublished data, Norwegian Polar Institute) and river plains (Norwegian Polar Institute mapping data, 2014).

3.1. Fjords

In Svalbard, fjords are commonly formed from drowned glacial valleys reaching depths down to 450 m, but typically they are shallower with one or more sills present. Ocean-shelf-fjord and land connectivity depend largely on the fjord's geographical location (e.g. west or east Svalbard), its bathymetry and size, and whether there are marine terminating glaciers or river deltas present. Since these factors strongly impact the fjord's biodiversity and productivity, we recommend dividing the fjord coastscape into four main types: 1) deep, open fjords, 2) semi-closed fjords, 3) shallow sill fjords (inner basin <120 m), and 4) deep sill fjords (inner basin >120 m). Deep open fjords are mainly located along west Spitsbergen (e.g. the well-studied Kongsfjorden). These are strongly influenced by warm Atlantic water and thus, harbour a more boreal community than elsewhere in Svalbard (Berge et al. 2015; Gluchowska et al. 2016; Hop et al. 2019a). These fjords are characterised by high biodiversity and productivity since they have a mixture of boreal and Arctic species and a long open water season (Hegseth et al. 2019; Hop et al. 2019a). In contrast, fjords where the advection of Atlantic water is restricted due to a shallow threshold (sill fjords) or a wide, shallow shelf (semi-closed fjords) are colder and often have seasonal ice cover. The semi-closed Rijpfjorden in Nordaustlandet and the deep sill fjord Billefjorden in inner Isfjorden, often have extensive seasonal ice cover, but can nonetheless be as similarly productive as the deep open fjords (Søreide et al. 2013). These cold relatively deep fjords tend to be dominated by a few Arctic species that are specialists, such as the copepod *Calanus glacialis* (Arnkvaern et al. 2005; Søreide et al. 2008; Christensen et al. 2018; Hop et al. 2019b) and the polar cod *Boreogadus saida* (Nahrgang et al. 2014). Shallow sill fjords (e.g. Van Mijenfjorden) are generally less productive than other fjords. These are often strongly freshwater-influenced and highly turbid due to the combination of massive river runoff and restricted circulation, providing poor light conditions for primary producers. For the pelagic biota, warmer sea temperatures and

less sea ice in the last few decades have resulted in a more boreal species composition in Svalbard fjords and especially in the deep open fjords in west and northwest Svalbard (e.g. Berge et al. 2014, Gluchowska et al. 2016; Hop et al. 2019a; Vithakari et al. 2018) due to massive intrusions of warm Atlantic water since 2005 (Muckenhuber et al. 2016; Cottier et al. 2019; Tverberg et al. 2019; Skogseth et al. 2020). For the benthos, a similar 'atlantification' of the community composition has been seen in western Svalbard, but in threshold fjords with glacial basins the Arctic benthic communities have largely survived, demonstrating the importance of these cold isolated habitats in the otherwise warm Atlantic influenced fjords for securing the overall biodiversity (Renaud et al. 2007, Gilg et al. 2016; Drewnik et al. 2017).

Tidewater glaciers (glaciers terminating in sea) are common in Svalbard's fjords and they are often associated with small lateral streams with deltas and estuaries. Glaciers and rivers bring melt water and sediments from land into the fjords, which typically feature species-poor soft bottom communities close to tidewater glaciers or river deltas where sedimentation rates are high (Figure 7). There tends to be a gradual increase in species richness towards the opening of such fjords (Wlodarska-Kowalczyk et al. 2012; Hop et al. 2012; Molis et al. 2019). Overall, the biodiversity of zoobenthos in Svalbard fjords is lower than in surrounding shelf seas, which is partly due to the effect of space availability and the often more stressful environment in fjords (e.g. high sedimentation, lower light availability, less mixing and sediment disturbance) (Molis et al. 2019). Among the marine zoobenthos distributed in the Barents-Greenland seas, less than 30% is found in the fjords (Wlodarska-Kowalczyk et al. 2012). High abundance of the benthic crustacean *Lepidepecreum umbo* and the mollusc *Portlandia arctica* are associated with cold Arctic conditions (Drewnik et al. 2017). A compilation of existing benthos monitoring in Svalbard is given in [Appendix 5](#), for sampling locations and more details see Renaud and Bekkeby (2013).

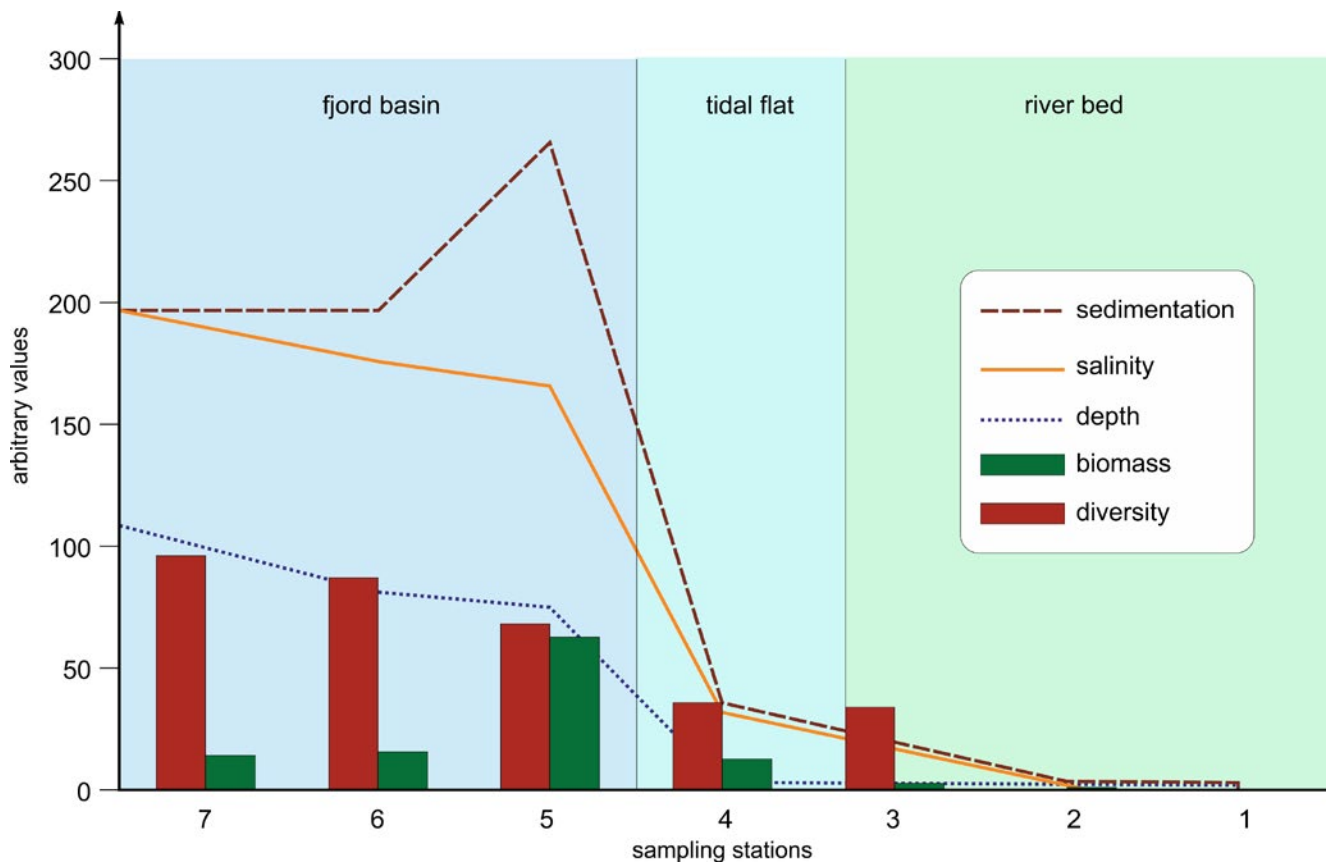


Figure 7. Biomass and diversity of zoobenthos in relation to environmental gradients across a river bed, tidal flat to fjord basin (arbitrary scale) from Weslawski et al. (1999) based on data from Adventfjorden, Spitsbergen.

Phytoplankton is regularly monitored in Svalbard, especially in fjords in western Svalbard (Hegseth et al. 2019); monthly studies are conducted in Adventfjorden year-round (Kubiszyn et al. 2017; [Appendix 5](#)). Some seasonal and time series studies also exist from Rijpfjorden (Leu et al. 2010, 2015; Hop et al. 2019b). With declining sea ice and warmer waters, the onset and magnitude of the ice algal and phytoplankton blooms are changing (Leu et al. 2015, Hegseth et al. 2019). Such distinct changes in bloom phenology are worrying since the grazers may partly miss the bloom (i.e. mismatch) with cascading impacts on higher trophic levels (Leu et al. 2011). Zooplankton abundance and community composition provide important information on the productivity and overall state of the marine fjord ecosystem (Gluchowska et al. 2016; Hop et al. 2019a). Zooplankton are important prey for many fish, seabirds, and marine mammals (Vihtakari et al. 2018) and zooplankton via seabirds fertilize the coastal tundra (Skrzypek et al. 2015). Zooplankton are not regarded as an essential FECs by CAFF in the fjord coastscapes (CAFF, 2019). However, zooplankton are an important ecosystem component

in Svalbard fjords and we strongly recommend zooplankton to be monitored as an essential FEC here. In Svalbard, there is a mixture of Arctic and boreal zooplankton species. Most species are found everywhere in Svalbard, but in very different numbers depending on whether they are primarily Arctic or boreal. The relative proportion of Arctic versus boreal (Atlantic) species and vice versa provides information on the overall “fjord climate” (e.g. Leu et al. 2011; Gluchowska et al. 2016; Hop et al. 2019a;). The Arctic copepod *Calanus glacialis* and the North Atlantic *C. finmarchicus*, are regarded valid climate indicator species for respective cold and warm sea climate in Svalbard (e.g. Hop et al. 2019a). Long zooplankton time series exists from several fjords in west Svalbard Kongsfjorden since 1998 (Hop et al. 2019a); Hornsund since 1987 (Węstawski et al. 1991), and Isfjorden since 2001 (Arnkvaern et al. 2005; Gluchowska et al. 2016, Christensen et al. 2018) and from northeast Svalbard (Rijpfjorden since 2003; Søreide et al. 2010; Weydmann et al. 2013, Hop et al. 2019b), while in eastern Svalbard only a few sporadic studies exist (e.g. Weslawski et al. 1997; Hirche and Kosobokova 2011).

Svalbard fjords are vital habitats for all of the Arctic endemic marine mammal species in the region, including ringed seals, bearded seals, walrus, polar bears, and white whales (Storrie et al. 2018; Bengtsson et al. 2020); the rarer whale species, bowheads, and narwhals also visit fjord environments intermittently, though they spend most of their time in recent decades in the marginal ice zone. Svalbard fjords are becoming important habitats for migratory whales since more Atlantic water comes into the fjords, which again leads to increase in the biomass of boreal fish species and krill (Berge et al. 2015; Misund et al. 2016; Vihtakari et al. 2018). Additionally, harbour seals that have previously been restricted to Prins Karls Forland furthest West, are now occupying many fjords along the west coast of Spitsbergen. Soft-bottom communities within fjords provide food for benthic foraging marine mammals, such as walrus, bearded seals, and white whales. Additionally, young seals of all species target shallow coastal waters to feed on amphipods and other available prey. Fish are important food for many marine mammals and recently a marked change in fish communities in western Svalbard has been documented (Berge et al. 2015), and a significant change in movement patterns has been detected for white whales that suggests that a change in diet has taken place, with the whales spending more time in fjords where Atlantic fish species dominate (Hamilton et al. 2019c). Sea bird diets have also changed according to the available prey species as a result of warming within the fjords (Vihtakari et al. 2018). Some species do not readily shift diet, and these species are likely to suffer negative consequences as the community changes (e.g. Hamilton et al. 2019c). Strong year classes of Atlantic cod combined with massive intrusions of warm Atlantic waters into the west-facing deep fjords have been beneficial for those feeding on them, while for most others this large cod fish is a new predator in the system; which is likely to put pressure on polar cod, a key Arctic fish species that has been a very important trophic linkage in the past (Nahrgang et al. 2014).

3.2. Low Gradient Soft Shores, Lagoons and Barrier Islands, and Estuaries

3.2.1. Low gradient shores

Low gradient shores with varying thicknesses of surficial materials over bedrock, characterised by mudflats, wetlands, and beaches are widely found in Svalbard (Figure 4). A closer look at beaches in Svalbard and their grain size (Figure 5) shows that sandy and stony beaches dominate (44%), followed by sandy and stony beaches with boulders (7%). There are only a few; clay (1%), sandy (1%) and boulder (1%) beaches identified within the archipelago. Estuaries, lagoons, and barrier islands are also naturally included in the beaches above, but these are very special ecosystem features and thus, defined as their own coastscapes by CAFF (2019). A compilation of where these unique coastscapes are located can be found in Figure 6, but for tidal flats and river deltas only old, not quality controlled data exist and thus the classification of this coastscape needs to be revisited.

3.2.2. Lagoons and Barrier Islands

Lagoons are a common feature in Svalbard (Figure 6). These highly productive ecosystems are important feeding grounds and resting sites for migratory birds and resident marine mammals. Lagoons are transitional zones between land and sea, with variable physical and chemical conditions depending on their morphology, inflow of freshwater, and degree of exchange with the open marine system (Dunton et al. 2012). These systems are extensively studied along the Alaskan Arctic coastline, which supports large populations of migratory fish and waterfowl that are essential to the culture of Iñupiat communities (Harries et al. 2018). In Svalbard, however, lagoons are poorly studied. Based on aerial photography, NPI has identified as many as 127 lagoons (Figure 6). Most of these lagoons are very shallow, and approximately two thirds of them have a visible opening to the sea. Many of these lagoons are also strongly influenced by glaciers, either terminating in the lagoon, or delivering glacial melt water to

the lagoon via rivers (Haug et al. 2016). Svalbard's lagoons are important habitat for several species of birds, anadromous Arctic charr, and also for some marine mammals. In particular shallow, extensive tidal flats may be important feeding grounds for birds (Haug et al. 2016). A preliminary study in Richardlaguna (Forlandet) indicated high abundances of soft-bottom benthos, littoral amphipods, and small fish (e.g. sculpins, (McKnight 2019). In general, there are very few data available on physical and biogeochemical conditions, or the biological communities in these lagoons, and there is an urgent need for more knowledge on salinity and depth, benthic community composition and sediment properties, habitat use by higher trophic animals and mapping of coastal geology and lagoons in Svalbard (Haug et al. 2016).

3.2.3. Estuaries

River estuaries are highly dynamic environments in both space and time, where strong physical and chemical gradients play a key role in structuring biological communities. In Svalbard, a large number of rivers drain to the coast (Figure 5), many of which are glacier-fed. Some of the larger rivers have given rise to extensive braided deltas and tidal flats, which provide important habitats for seabirds, waders and other shorebirds (Haug et al. 2016). River discharge in Svalbard is highly seasonal with nearly all runoff occurring between May/June and September (Nowak et al. 2021) and most rivers freeze during the winter. These estuaries are particularly vulnerable to climate change, given that runoff in Svalbard is expected to increase dramatically, due to increases in glacial melt, melting of permafrost, and precipitation (Adakudlu et al. 2019; Hansen-Bauer et al. 2019; Nowak et al. 2021).

Biological communities in estuarine habitats need to cope with a high degree of variability in salinity, temperature, sedimentation, light, nutrient availability, and strong water currents linked to estuarine circulation patterns. Svalbard's estuaries receive large fluxes of particulate matter, leading to high light attenuation in turbid river plumes, as well as high sedimentation rates (e.g. Weslawski et al. 1999). Furthermore, given the high rate of removal of particulate matter and associated

nutrients, organic matter, and terrestrially-derived contaminants (such as mercury), there is a substantial delivery of terrigenous material to estuarine sediments, with important implications for benthic communities. Soft-bottom benthic communities in these areas are thus, often low in species richness and biomass and show abrupt changes in species numbers and biomass across the tidal flats into the fjord basin (Figure 7). Taxa that are able to cope with high sedimentation rates dominate, such as the deposit feeding bivalves *Macoma* sp. and *Chaetozone* sp., as well as the motile filter-feeding bivalve *Thyasira* sp. (Włodarska-Kowalczyk et al. 2012; Pedersen-Ugledstad 2019). Waders feed extensively in tidal flat areas and their numbers in Svalbard appear to be increasing. Tidal flats have the potential to harbour brackish water diatom colonies and other groups of eukaryotic algae and cyanobacteria. Such microphytobenthos communities have been found in Adventfjorden (Kvídárová et al. 2019; Wiktor et al. 2016). The phenomenon and significance of the occurrence of such autotrophic communities should be the target of future research.

Salmonids are considered an essential FECs in soft shores, lagoons, and river estuaries (CAFF, 2019). In Svalbard, there are three different species of anadromous salmonids: Arctic charr (*Salvelinus alpinus*), Atlantic salmon (*Salmo salar*) and pink salmon (*Oncorhynchus gorbuscha*). Arctic charr have a circumpolar distribution and are the world's northernmost freshwater fish and the only freshwater fish that lives and reproduces in watercourses in Svalbard. There are two main forms; a stationary form that stays in fresh water throughout its life and anadromous char which migrate into the marine environment in the summer for four to eight weeks, feeding in nearshore waters. There are probably 100–150 lakes with stationary charr, while populations of anadromous Arctic charr are found in approximately 20 lake systems in Svalbard. There is currently little knowledge about the anadromous Arctic charr migrations and habitat use in the marine environment in Svalbard. Atlantic salmon and pink salmon are relatively new species in Svalbard and most likely do not reproduce successfully within the archipelago (yet). Pink salmon is an alien species that has been monitored

in Svalbard since 2015⁷. New data indicates that there is dietary overlap in nearshore areas and hence, competition between anadromous Arctic charr and pink salmon.

3.3. Rocky Shores and Sea Cliffs

The rocky shores and sea cliffs coastscape are the dominant coastscape in Svalbard (Figure 4). Waves or strong currents remove all loose material from exposed rocky shores, and the shores can be steep and reach considerable depths within a short distance from land. The rocky coast is a biologically

rich environment and can include many different habitat types, such as steep rocky cliffs, platforms, rock pools, and boulder fields. Sea bird cliffs are a prominent feature within this coastscape (Figure 8). Warmer sea temperatures and less sea ice have already significantly changed the rocky shore intertidal (Weslawski et al. 2018) and sublittoral zone in Svalbard (Kortsch et al. 2012; Al-Hababeh et al. 2020). The majority of macrophyte species and biomass is found along sheltered fjordic coastlines (Kruss et al. 2006; Bischof et al. 2019; Fredriksen et al. 2019) and a five-fold increase in seaweed coverage in west Spitsbergen has been recorded

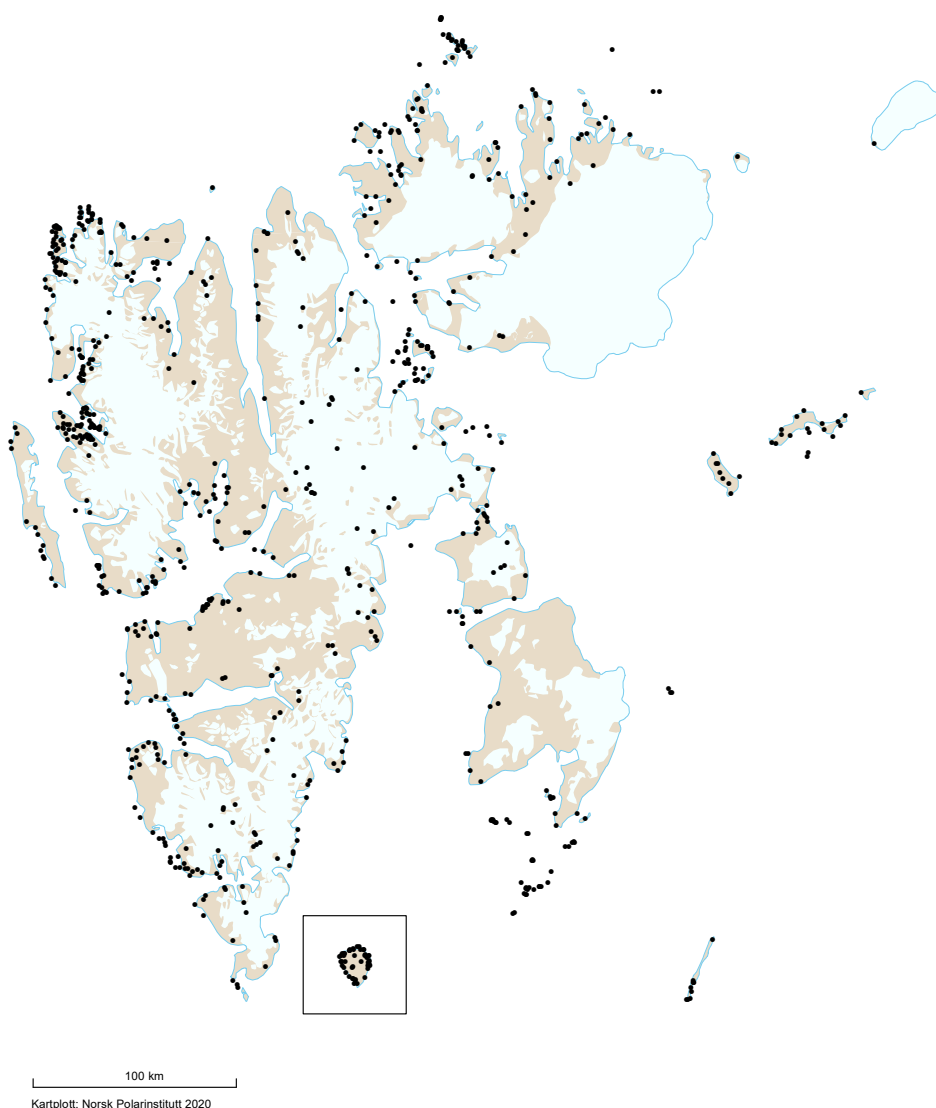


Figure 8. Seabird colonies in Svalbard (Strøm et al. 2008). The majority of the 20 species of seabirds in Svalbard hatch and raise their young close to the coast.

7 For more information contact G. Christensen, Akvaplan-via, Tromsø

since 1984 (Kortsch et al. 2012; Weslawski et al. 2018; Bischof et al. 2019). In east Svalbard, ice scouring is still restricting macroalgal establishment in the intertidal zone; it occurs primarily beyond 3 m depth in eastern Svalbard. Underwater “forests” of macroalgae are an important nursery ground for many invertebrates and fish species and facilitate a rich species diversity and assemblage. Seafloor mapping to identify suitable substrates for macroalgae may therefore be an important task to identify areas of special biological value (e.g. Bekkeby et al. 2017). Common fishes associated with kelp include several species of sculpins which is an understudied focal ecosystem component in Svalbard coastal regions. Reappearance of the blue mussel in Isfjorden in 2005, after 1000 years of absence, is one of many results of ongoing climate warming (Berge et al. 2005) and currently blue mussels are commonly spotted in the intertidal zone in Isfjorden (Leopold et al. 2018).

The kelp-barnacle (*Fucus-Balanus*) assemblages covering the rocky shoreline of western Spitsbergen, where warm Atlantic water prevents sea ice from forming, is the intertidal assemblage with the highest biomass in Svalbard (Weslawski et al. 1992). In eastern Svalbard, *Balanus* spp. were not detected in the intertidal zone in the 1990s (Weslawski et al. 1992). However, with less sea-ice scouring the previously identified cut-off border for *Balanus* at Sørkapp has moved further East and North with tiny *Balanus* spp. now settling in the intertidal zone in Storfjorden⁸.

3.4. Rapidly Eroding Shores

The combination of permafrost-rich, soft coastal sediments often with in-ground ice are typical for rapidly eroding shores. This is the dominant coastscape along the Beaufort Sea in Canada and Alaska, and along the coasts of the Laptev and eastern Siberian Seas in Russia (Lantuit et al. 2012). In Svalbard, this coastscape is spatially very limited (<5%). Biota is particularly scarce and the biodiversity poor in this extreme environment. All types of FEC birds (e.g. waterfowl, omnivorous, diving planktivores, surface and diving piscivores) are considered essential here, in addition to

phytoplankton, zooplankton, and pelagic fishes (CAFF, 2019). In Svalbard, this coastscape is poorly studied and it will probably remain little studied in the years to come since other more ecologically important coastscapes will be prioritized to study. When it comes to physical changes, these rapidly eroding shores may experience large losses of mass, as well as large collapses due to melting ground ice.

3.5. Ice Fronts

Glaciers that terminate at the sea, so-called tidewater glaciers, form a type of unique coastscape. In Svalbard, over 150 such tidewater glaciers are spread across the archipelago, with frontal areas that stretch across approximately 1000 km of Svalbard’s coastline (Figure 4; Dowdeswell 1989; Blaszczyk et al. 2009). Some tidewater glaciers sit on the seafloor, while others have floating termini; the floating glaciers are particularly active, calving glacier ice into the fjords, producing large floating ice islands or icebergs of variable sizes that melt and freshening the surface waters. However, all tidewater glaciers contribute significant amounts of freshwater to the fjords, particularly during the summer melt period, when glacial rivers have their greatest outflows and calving is not restricted by the presence of landfast ice that usually forms in at least the inner parts of fjords in winter in Svalbard. The outflows from tidewater glaciers significantly impact the circulation patterns in fjords (Sundfjord et al. 2017); wind driven forcing combined with glacier river outputs cause upwelling and mixing at glacier fronts that induce seasonal productivity hotspots (Meire et al. 2016); zooplankton advected from the outer parts of the fjord towards the glacier fronts when fjord water replaces surface waters pushed offshore add to the diversity and biomass of zooplankton available in these areas (Lydersen et al. 2014). Nutrient rich sediments at tidewater glacier fronts create areas where krill and other invertebrates aggregate (Deja et al. 2019). High fish densities, particularly high concentrations of polar cod, occur in the cold water refugia created by glacier outputs, feeding on the invertebrates that occupy these waters (particularly when the fronts are deep; Szczucka et al. 2017).

8 Observation by JE Søreide, UNIS, September 2020

The presence of both large zooplankton and fish attract top predators including sea birds, seals and Arctic whales to tidewater glacier fronts (Lydersen et al. 2014; Urbanski et al. 2017). Surface-feeding seabirds including kittiwakes, fulmars, arctic terns, and glaucous gulls are the most common avian species at tidewater glacier fronts in Svalbard (Draganska-Deja et al. 2020). They occur in extremely high concentrations, intermittently, when upwelling is very pronounced, leading to prey being available at the surface. Diving predators, including seals and whales can take advantage of prey at depth and hence, are found more consistently at tidewater glacier fronts, though they also seem to specifically target plumes of subglacial discharge that appear to concentrate prey (Everett et al. 2018). Ringed and bearded seals also take advantage of the availability of glacier ice pieces, which they use as resting platforms when annually formed ice is not available (Hamilton et al. 2019b). Bearded seals have also started to give birth and nurse their young on floating glacier ice pieces,

following the collapse of fast-ice formation in west coast fjords 1.5 decades ago (Kovacs et al. 2020a). In Svalbard, adult ringed seals live in close association with tidewater glacier fronts on a year-round basis, occupying small territories that encompass only one or a few glacier fronts (Figure 9; Hamilton et al. 2016a, b, 2019b). Calved glacier ice freezes into annually formed landfast ice, when fjords freeze in the fall creating areas where snow accumulates on the sea ice, which in turn creates ringed seals breeding habitat. Such areas are important spring hunting habitat for polar bears when females first emerge from dens with young cubs that cannot swim long distances (Freitas et al. 2012; Hamilton et al. 2017). White whales in Svalbard also spend most of their time at tidewater glacier fronts in Svalbard (Lydersen et al. 2001; Vacquie-Garcia et al. 2019). In a recent survey of white whales in Svalbard waters, 82% of whales seen were associated with tidewater glacier fronts (Vacquié-Garcia et al. 2020).

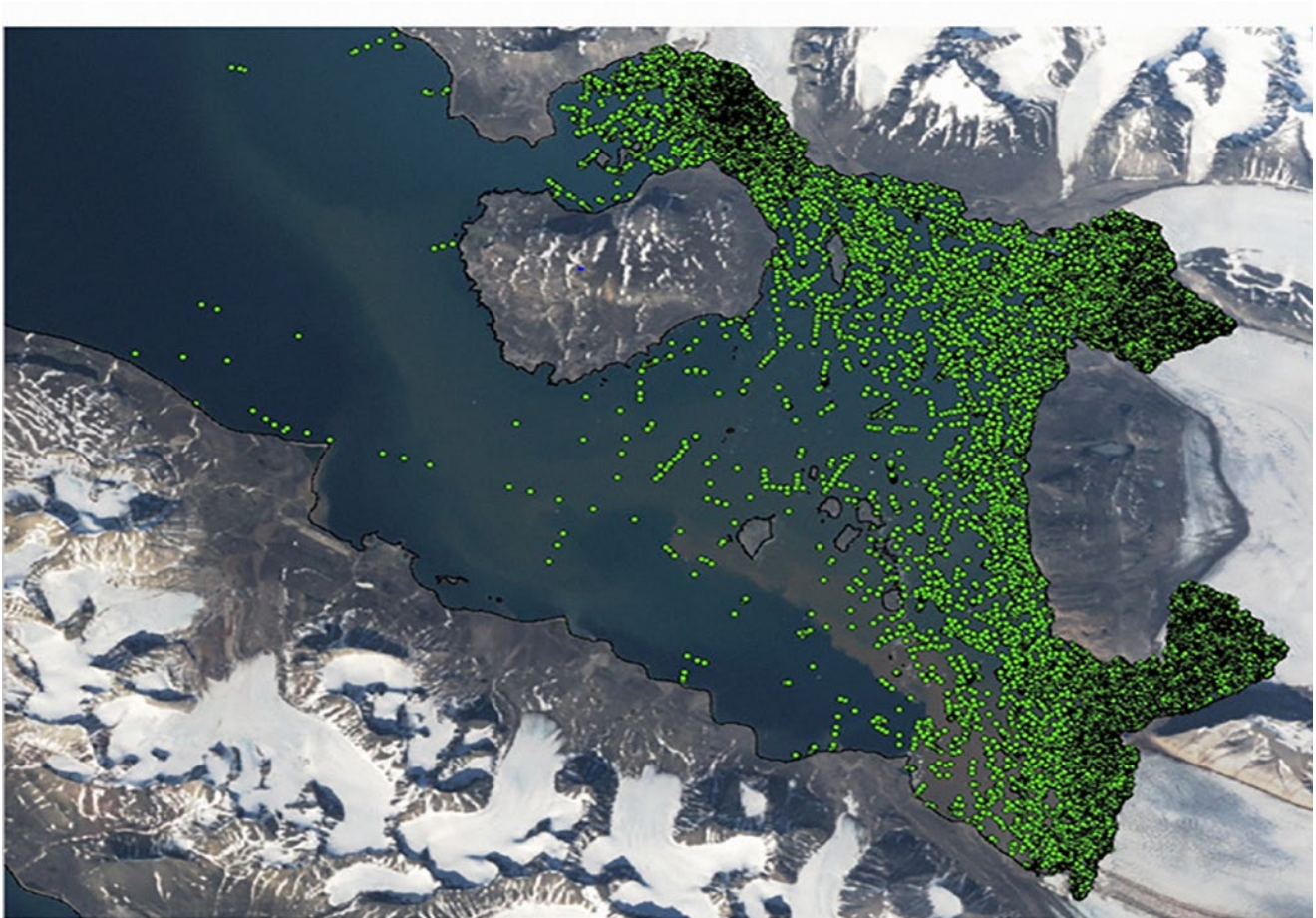


Figure 9. GPS locations (n=62,000) from six tagged ringed seals in Kongsfjorden Svalbard during 2011–2013, displaying this species' tight association with tidewater glacier fronts (ringed seal data presented in a track format in Hamilton et al. 2019b).

This important habitat for Arctic animals in Svalbard is currently threatened by global warming, with tidewater glaciers melting and withdrawing onto shore rapidly (e.g. Blaszczyk et al. 2009). These areas have received limited research attention in the past because they are highly dynamic and logistically challenging to work in. However, new robotic (underwater drone) technology will allow for rapid advances in knowledge of these important/threatened habitats (Hop et al. 2019c; Howe et al. 2019).

3.6. Seasonal Ice Edge Habitat

Most studies in the above coastscapes are conducted in summer, but all the listed coastscapes (especially those in northern and eastern Svalbard) feature sea ice in winter and spring. These seasonal sea-ice environments provide habitats that are critical for the survival of many ice dependent birds and mammals (see Ice Front coastscape; Hamilton et al. 2017; Vacquié-Garcia et al. 2017; Lone et al. 2018; Kovacs et al. 2020b; Gilg et al. 2016), and for an under-studied assemblage of biota inside the sea ice itself (Leu et al. 2010; Bluhm et al. 2018; Marquardt et al. 2018). Plants and animals living inside of sea ice are termed 'sympagic' (= living with ice). Microscopic algae specialized to grow under

low light conditions in sea ice (ice algae) may start to bloom up to two months earlier than the pelagic phytoplankton spring bloom (Leu et al. 2010, 2015; Søreide et al. 2010). An unknown number of tiny larvae take advantage of this early nutritious food source after a long unproductive winter by migrating from the water column or seafloor into the mosaic of brine channels inside sea ice. Here, they can feed safely since most predators are too large and inflexible to access this brine-channel habitat. Sympagic meiofauna has barely been studied in Svalbard or elsewhere in the Arctic (Wiktor and Szymelfenig 2002) since sampling can be challenging and larval species identification is tricky. Available studies show that these small metazoans can be very numerous (>100.000 ind. m⁻²) in the bottom 3 cm of landfast sea ice in Svalbard (Pitusi 2019) and that nematodes dominate, followed by polychaete juveniles and eggs of various species (including those of polar cod). In addition, high numbers of ciliates have been observed. Ongoing barcoding and ecological studies (Marquardt et al. 2018; Pitusi 2019; Andreasen 2019) will eventually increase our knowledge of these unique sea-ice communities and thus their broader importance in Arctic coastal ecosystems which is urgent due to the rapid decline in coastal sea ice (see above Figure 1).

4. Connections and synergies with other SESS report chapters

Coastal ecosystems in Svalbard are impacted by large scale atmospheric (Viola et al. 2019; Sipilä et al. 2020) and oceanic circulation patterns (Bensi et al. 2020), pushing heat, nutrients and organisms northwards into the fjords and nearshore (Cottier et al. 2019; Edwards et al. 2020). This again impacts coastal sea-ice formation (Gerland et al. 2020) and land-to-sea interactions with earlier onset of snow melt (Killie et al. 2021), glacier melt (Schuler et al. 2020), permafrost thawing (Christiansen et

al. 2021) and prolonged river runoff (Nowak et al. 2021). Further, pollution is a major threat and negative impacts of microplastics may be of special concern for Arctic coastal ecosystems (Singh et al. 2021). Autonomous observatories (Cottier et al. 2019, Hann et al. 2021) and remote sensing (Karlsen et al. 2020) will be important tools in the years to come to understand the highly dynamic and complex coastal environments.

5. Unanswered questions

The coastal areas in Svalbard are subject to substantial socio-economic impact, providing a range of ecosystem services, ranging from local recreation to large scale tourism operations, shipping and fisheries (Misund et al. 2016; Stocker et al. 2020). Increased marine activities, combined with climate change, will create new challenges for future coastal management in Svalbard. Seasonal baseline studies of key drivers, biodiversity and bio-indicators will be necessary to detect, understand, and mitigate changes in Svalbard coastscapes. Models of ecological changes are likely to be important tools for predicting future coastal change. However, the lack of baseline data and the complexity of coastal environments urge for continued and expanded monitoring to track changes and provide inputs to model development and scenario-building. Some fundamental, overarching questions are:

- Can we differentiate climate change impacts from seasonal and natural variability, when baseline data are largely lacking from the physical and biological environment?
- Do lack of species identification, or misidentification, combined with limited knowledge on species and ecosystem resilience lead to erroneous predictions regarding future climate change impacts?
- Which focal ecosystem components are the most important to monitor in the different coastscapes in Svalbard?
- What is the ecological role of the understudied unique nature types in coastal Svalbard: lagoons, river deltas/tidal flats and seasonal sea ice?
- Are the rates of environmental and ecosystem changes in the colder, poorly studied northern and eastern regions of Svalbard similar to those recorded in the warmer region of western Svalbard?

6. Recommendations for the future

There is an urgent need for more comprehensive monitoring of physical, biogeochemical, and biological parameters in coastal environments in Svalbard. Such monitoring data are vital to meet the needs of communities, industry, academia, and our national government's management of coastal ecosystems in the Arctic, as well as meeting Norway's commitments and responsibilities to international objectives, such as those outlined in the Arctic Biodiversity Assessment (CAFF, 2013) and by the Convention on Biological Diversity⁹. This requires the application of multi-disciplinary studies gathering circum-Svalbard data through various observational methods ranging from satellite data to local community-based observations and measurements. These new data should be connected to and possibly adjusted according to existing monitoring programs to enable long-term databases. For this, there is a need for integrated

knowledge exchange across disciplines and communication between diverse research teams in order to coordinate ongoing monitoring efforts, opportunities, and future plans. Below, some key recommendations¹⁰:

- Improve international coordination and cooperation to develop and maintain the infrastructure and activities required to achieve a more holistic and cost-efficient coastal observatory in Svalbard.
- Generate a list of Svalbard-specific standard coastscapes (i.e. nature types).
- Agree on a list of essential focal ecosystem components (e.g., bio-indicators) to be monitored in these coastscapes.
- Monitor environmental and ecosystem trends in both the warm and the cold regions in Svalbard.
- Adopt new methods (e.g. molecular methods)

⁹ <https://www.cbd.int/cop/>

¹⁰ See also recommendations for future research and monitoring in [Appendix 6](#).

and technology (e.g. autonomous observatories, remote sensing) to secure cost-efficient long-

term data series.

7. Data availability

Coastal environmental data from Svalbard are many and diverse, and are not found through one portal. In [Appendix 5](#), we have compiled monitoring and long-time series data from Svalbard coastal waters relevant for this chapter. This is a work in progress. Datasets listed below will be available through the SIOS data access portal with links and contact information to where the data are stored. Some of the data sets are currently under work and not yet published, but within year 2021 they should

be available and therefore they are included here. Further, we recommend a closer look at the recent established Svalbard coastal data base, where all archival taxa data observation from Svalbard from 1983 till present from Institute of Oceanology, Polish Academy of Science (IOPAN) are stored, including photos: https://adamant.iopan.pl/adamant/taxa_observations/. This is a dynamic database which will be continuously supplied with new data from also others in the future.

Acknowledgements

This work was supported by the Research Council of Norway, project number 291644, Svalbard Integrated Arctic Earth Observing System – Knowledge Centre, operational phase. This review is a result of the workshop Svalbard Sustainable Coasts arranged in Longyearbyen February 2019, funded by Svalbard Science Forum strategic funding (RCN, project number 296647) and in-kind contributions from several institutions. Further this coastal initiative was motivated and funded by the ongoing project: ‘De-icing of the Arctic coast: critical or new opportunities for marine biodiversity and ecosystem services (ACCES)’, funded through the 2017–2018 Belmont Forum and BiodivERsA joint call for research proposals, under the BioDivScen ERA-Net COFUND programme, and with the funding organisations RCN (project number 296836), NCN and FRQ.

We sincerely thank the many partners who have undertaken this work for their willingness to share data and knowledge that has made this review possible. Some of these contributions include:

- Norwegian Polar Institute mapping department for sharing the shape files from the coastal mapping project.
- Polish Polar Station Hornsund and Institute of Geophysics Polish Academy of Science for the realisation of oceanographical monitoring in Hornsund.
- NASA Ocean Biology Processing Group for developing and maintaining the SeaDAS software.
- NASA Ocean Biology Distributed Active Archive Center for providing MODIS-Aqua Level-1A data.
- National Snow and Ice Data Center for distributing the sea-ice concentration data.

References

- Adakudlu M, Andersen J, Bakke J, Beldring S, Benestad R, Bilt WV, Bogen J, Borstad C, Breili K, Breivik Ø, Børshem KY (2019) Climate in Svalbard 2100—a knowledge base for climate adaptation. <https://www.miljodirektoratet.no/globalassets/publikasjoner/M1242/M1242.pdf>
- Al-Hababeh AK, Kortsch S, Bluhm BA, Beuchel F, Gulliksen B, Ballantine C, Cristini D, Primicerio R (2020) Arctic coastal benthos long-term responses to perturbations under climate warming. *Philos T R Soc A* 378(2181):20190355. <https://doi.org/10.1098/rsta.2019.0355>
- Andreassen MH (2019) Community composition, population structure and phylogeny of coastal sympagic meiofauna in eastern Svalbard. MSc thesis, The University of Bergen. <http://hdl.handle.net/1956/20217>
- Ardyna M, Mundy CJ, Mayot N, Matthes LC, Oziel L, Horvat C, Leu E, Assmy P, Hill V, Gale M, Arrigo KR (2020). Under-Ice Phytoplankton Blooms: Shedding Light on the “Invisible” Part of Arctic Primary Production.” *Frontiers in Marine Science* 7(985). <https://doi.org/10.3389/fmars.2020.608032>
- Arnkvaern G, Daase M, Eiane K (2005) Dynamics of coexisting *Calanus finmarchicus*, *Calanus glacialis* and *Calanus hyperboreus* populations in a high-Arctic fjord. *Polar Biol* 28(7):528–38. <https://doi.org/10.1007/s00300-005-0715-8>
- Arrigo KR, van Dijken GL (2011) Secular trends in Arctic Ocean net primary production. *J Geophys Res* 116:C09011. <https://doi.org/10.1029/2011JC007151>
- Bischof K, Buschbaum C, Fredriksen S, Gordillo FJL, Heinrich S, Jimenez C, Lutz C, Molis M, Roleda MY, Schwanitz M, Wiencke C (2019) Kelps and environmental changes in Kongsfjorden: Stress perception and responses. In H Hop and C Wiencke (eds) *The Ecosystem of Kongsfjorden, Svalbard. Avances in Polar Ecology 2. The Ecosystem of Kongsfjorden, Svalbard.* Springer, pp 423–483. <https://doi.org/10.1007/978-3-319-46425-10>
- Bekkeby T, Albretsen J, Kuipers B, Renaud P, Gundersen H, Włodarska-Kowalczyk M (2017) Kartfesting og klassifisering av marin natur på Svalbard – et prosjekt for Svalbards miljøvernfond. NIVA-rapport ISSN 1894-7948, pp 25.
- Bélanger S, Babin M, Tremblay J-É (2013) Increasing cloudiness in the Arctic damps the increase in phytoplankton primary production due to sea ice receding. *Biogeosciences* 10:4087–4101. <https://doi.org/10.5194/bg-10-4087-2013>
- Bengtsson O, Hamilton CD, Lydersen C, Andersen M, Kovacs KM (2020) Distribution and habitat characteristics of pinnipeds and polar bears (*Ursus maritimus*) around the Svalbard Archipelago, based on observations from 2005–2018. *Polar Res* in press.
- Bensi M, Kovacevic V, Langone L, Miserocchi S, Demarte M, Ivaldi R (2020) Spitsbergen Oceanic and Atmospheric interactions. In: Van den Heuvel et al. (eds): *SESS report 2019, Svalbard Integrated Arctic Earth Observing System, Longyearbyen, pp 250–261*. https://sios-svalbard.org/SESS_Issue2
- Berge J, Johnsen G, Nilsen F, Gulliksen B, Slagstad D (2005) Ocean temperature oscillations enable reappearance of blue mussels *Mytilus edulis* in Svalbard after a 1000-year absence. *Mar Ecol Prog Ser* 303:167–175. <https://doi.org/10.3354/meps303167>
- Berge J, Heggland K, Lønne OJ, Cottier F, Hop H, Gabrielsen GW, Nøttestad L, Misund OA, (2015) First records of Atlantic mackerel (*Scomber scombrus*) from the Svalbard archipelago, Norway, with possible explanations for the extensions of its distribution. *Arctic* 68(1):54–61. <http://www.jstor.org/stable/24363888>
- Blaszczyk M, Jania JA, Hagen JO (2009) Tidewater glaciers of Svalbard: recent changes and estimates of calving fluxes. *Pol Polar Res* 30:85–142.
- Bluhm BA, Hop H, Vihtakari M, Gradinge, R, Iken K, Melnikov IA, Soreide JE (2018) Sea ice meiofauna distribution on local to pan-Arctic scales. *Ecol Evol* 8:2350–64. <https://doi.org/10.1002/ece3.3797>
- CAFF (2013). Arctic biodiversity assessment. Status and trends in Arctic biodiversity. Conservation of Arctic Flora and Fauna International Secretariat: Iceland, Akureyri 557. ISBN: 978-9935-431-22-6 <https://www.caff.is/assessment-series/233-arctic-biodiversity-assessment-2013>
- Christensen GN, Renaud P, Søreide J, Eikrem W, Kulinski P, Fagerli CW, Velvin R, Mannvik HP, Engesmo A, Gitmark JK, Bryntesen T (2018) Økokyst – delprogram Svalbard. Årsrapport 2018, Rapport M-1387, Miljødirektoratet. <https://www.miljodirektoratet.no/publikasjoner/2019-oktober-2019-okokyst--delprogram-svalbard-arsrapport-2018/>
- Cottier F, Skogseth R, David D, Berge J (2019) Temperature time-series in Svalbard fjords. A contribution from the integrated marine observatory partnership (iMOP). In: Orr et al. (eds): *SESS report 2018, Svalbard Integrated Arctic Earth Observing System, Longyearbyen, pp 108–118*. https://sios-svalbard.org/SESS_Issue1
- Deja K, Ormańczyk M, Dragańska-Deja K (2019) Plankton or benthos: where krill belongs in Spitsbergen fjords? (Svalbard Archipelago, Arctic). *Polar Biol* 42(8):1415–30. <https://doi.org/10.1007/s00300-019-02524-1>
- Dowdeswell JA (1989) On the nature of Svalbard icebergs. *J Glaciol* 35:224–34. <https://doi.org/10.3189/S002214300000455X>
- Draganska-Deja K, Blaszczyk M, Deja K, Weslawski JM, Rodak J (2020) Tidewater glaciers as feeding spots for the black-legged kittiwake (*Rissa tridactyla*): a citizen science approach. *Pol Polar Res* 41:69–93. <https://doi.org/10.24425/ppr.2020.132570>
- Drewnik A, Węstawski JM, Włodarska-Kowalczyk M (2017) Benthic Crustacea and Mollusca distribution in Arctic fjord—case study of patterns in Hornsund, Svalbard. *Oceanologia* 59(4):565–75. <https://doi.org/10.1016/j.oceano.2017.01.005>

- Dunton KH, Schonberg SV, Cooper LW (2012) Food web structure of the Alaskan nearshore shelf and estuarine lagoons of the Beaufort Sea. *Estuar Coast* 35(2):416–35. <https://doi.org/10.1007/s12237-012-9475-1>
- Edwards M, Helaouet P, Ostle C, Johns D, Wootton M, Strand E, Bagoien E (2020) The continuous plankton recorder survey-monitoring plankton in the Nordic Sea (CPR Survey). In: Van den Heuvel et al. (eds): SESS report 2019, Svalbard Integrated Arctic Earth Observing System, Longyearbyen, pp 262–273. https://sios-svalbard.org/SESS_Issue2
- Everett A, Kohler J, Sundfjord A, Kovacs KM, Torsvik T, Pramanik A, oehme OL, Lydersen C (2018) Subglacial discharge plume behaviour revealed by CTD-instrumented ringed seals. *Sci Rep* 8:13467. <https://doi.org/10.1038/s41598-018-31875-8>
- Fredriksen S, Karsten U, Bartsch I, Woelfel J, Koblowsky M, Schumann R, Moy SR, Steneck RS, Wiktor JM, Hop H, Wiencke C (2019) Biodiversity of benthic macro- and microalgae from Svalbard with special focus on Kongsfjorden. In H Hop and C Wiencke (eds) *The Ecosystem of Kongsfjorden, Svalbard. Avances in Polar Ecology 2. The Ecosystem of Kongsfjorden, Svalbard.* Springer, pp 331–373. <https://doi.org/10.1007/978-3-319-46425-9>
- Freitas C, Kovacs KM, Andersen M, Aars J, Sandven S, Skern-Mauritzen M, Pavlova O, Lydersen C (2012) Importance of fast ice and glacier fronts for female polar bears and their cubs during spring in Svalbard, Norway. *Mar Ecol Prog Ser* 447:289–304. <https://doi.org/10.3354/meps09516>
- Gerland S, Renner AHH (2007) Sea ice mass balance in an Arctic fjord. *Ann Glacio* 46:435–442. <https://doi.org/10.3189/172756407782871215>
- Gerland S, Renner AHH, Godtlielsen F, Divine D, Løyning TB (2008) Decrease of sea ice thickness at Hopen, Barents Sea, during 1966–2007. *Geophysical Research Letters*. Vol. 35, L06501. <https://doi.org/10.1029/2007GL032716>
- Gerland S, Pavlova O, Divine D, Negrel J, Dahlke S, Johansson AM, Maturilli M, Semmling M (2020) Long-term monitoring of landfast sea ice extent and thickness in Kongsfjorden, and related applications (FastIce). In: Van den Heuvel et al. (eds): SESS report 2019, Svalbard Integrated Arctic Earth Observing System, Longyearbyen, pp 160–167. https://sios-svalbard.org/SESS_Issue2
- Gilg O, Istomina L, Heygster G, Strøm H, Gavrilov MV, Mallory ML, Gilchrist G, Aebischer A, Sabard B, Huntemann M, Mosbech A, Yannic G (2016) Living on the edge of a shrinking habitat: the ivory gull, *Pagophila eburnea*, an endangered sea-ice specialist. *Biol. Lett.* 12:20160277. <https://doi.org/10.1098/rsbl.2016.0277>
- Gluchowska M, Kwasniewski S, Prominska A, Olszewska A, Goszczko I, Falk-Petersen S, Hop H, Weslawski JM (2016) Zooplankton in Svalbard fjords on the Atlantic–Arctic boundary. *Polar Biol* 39(10):1785–1802. <https://doi.org/10.1007/s00300-016-1991-1>
- Hamilton CD, Kovacs KM, Ims RA, Aars J, Lydersen C (2016a) An Arctic predator-prey system in flux: climate change impacts on coastal space use by polar bears and ringed seals. *J Anim Ecol* 86:1054–64. <https://doi.org/10.1111/1365-2656.12685>
- Hamilton CD, Lydersen C, Ims RA, Kovacs KM (2016b) Coastal habitat use by ringed seals *Pusa hispida* following regional sea-ice collapse: importance of glacial refugia in a changing Arctic. *Mar Ecol Prog Ser* 545:261–77. <https://doi.org/10.3354/meps11598>
- Hamilton CD, Kovacs KM, Ims RA, Aars J, Strøm H, Lyderen C (2017) Spatial overlap among an Arctic predator, prey and scavenger in the marginal ice zone. *Mar Ecol Prog Ser* 573:45–59. <https://doi.org/10.3354/meps12184>
- Hamilton CD, Kovacs KM, Lydersen C (2019b) Sympatric seals use different habitats in an Arctic glacial fjord. *Mar Ecol Prog Ser* 615:205–20. <https://doi.org/10.3354/meps12917>
- Hamilton CD, Vacqu e-Garcia, Kovacs KM, Ims RA, Kohler J, Lydersen C (2019c) Contrasting changes in space use induced by climate change in two Arctic marine mammal species. *Biol Lett* 15:20180834. <https://doi.org/10.1098/rsbl.2018.0834>
- Hann R, Altst dter B, Betlem P, Deja K, Dragańska-Deja K, Ewertowski M, Hartvich F, Jonassen M, Lampert A, Laska M, Sobota I, Storbvold R, Tomczyk A, Wojtysiak K, Zagórski P (2021) Scientific Applications of Unmanned Vehicles in Svalbard. In: Moreno-Ib  ez et al. (eds) SESS report 2020, Svalbard Integrated Arctic Earth Observing System, Longyearbyen, pp 78-103 <https://doi.org/10.5281/zenodo.4293283>
- Harris CM, McTigue ND, McClelland JW, Dunton KH (2018) Do high Arctic coastal food webs rely on a terrestrial carbon subsidy? *Food Webs* 15:e00081. <https://doi.org/10.1016/j.fooweb.2018.e00081>
- Haug FD, Myhre PI, and Mari N, Mathisen S (2016) Naturtyper p  Svalbard: laguner og pollers betydning, med katalog over lokaliteter. NPI Kortrapport 40. <http://hdl.handle.net/11250/2424238>
- Hegseth EN, Assmy P, Wiktor JM, Wiktor J, Kristiansen S, Leu E, Tverberg V, Gabrielsen TM, Skogseth R, Cottier F (2019) Phytoplankton seasonal dynamics in Kongsfjorden, Svalbard and the adjacent shelf. In *The Ecosystem of Kongsfjorden, Svalbard.* Springer, Cham, pp 173–227.
- Hirche HJ, KN Kosobokova (2011) Winter studies on zooplankton in Arctic seas: the Storfjord (Svalbard) and adjacent ice-covered Barents Sea. *Mar Biol* 158(10): 2359–76. <https://doi.org/10.1007/s00227-011-1740-5>
- Hop H, Pearson T, Hegseth EN, Kovacs KM, Wiencke C, Kwasniewski S, Eiane K, Mehlum F, Gulliksen B, Wlodarska-Kowalczyk M, Lydersen C (2002) The marine ecosystem of Kongsfjorden, Svalbard. *Polar Res* 21(1):167–208. <https://doi.org/10.3402/polar.v21i1.6480>

- Hop H, Wiencke C, Vögele B, Kovaltchouk NA (2012) Species composition, zonation, and biomass of marine benthic macroalgae in Kongsfjorden, Svalbard. *Bot Mar* 55(4):399–414. <https://doi.org/10.1515/bot-2012-0097>
- Hop H, Assmy P, Wold A, Sundfjord A, Daase M, Duarte P, Kwasniewski S, Gluchowska M, Wiktor JM, Tatarek A, Wiktor Jr J (2019b) Pelagic ecosystem characteristics across the Atlantic water boundary current from Rijpfjorden, Svalbard, to the Arctic Ocean during summer (2010–2014). *Front Mar Sci* 6:181. <https://doi.org/10.3389/fmars.2019.00181>
- Hop H, Wold A, Vhtakari M, Daase M, Kwasniewski S, Guchowska M, Lischka S, Buchholz F, Falk-Petersen S (2019a) Zooplankton in Kongsfjorden (1996–2016) in relation to climate change (2019) In H Hop and C Wiencke (eds) *The Ecosystem of Kongsfjorden, Svalbard. Advances in Polar Ecology 2. The Ecosystem of Kongsfjorden, Svalbard.* Springer, pp 229–302. https://doi.org/10.1007/978-3-319-46425-1_7
- Hop H, Cottier F, Berge J (2019c) Autonomous marine observatories in Kongsfjorden, Svalbard. In H Hop and C Wiencke (eds) *The Ecosystem of Kongsfjorden, Svalbard. Advances in Polar Ecology 2. The Ecosystem of Kongsfjorden, Svalbard.* Springer, pp 515–533. https://doi.org/10.1007/978-3-319-46425-1_13
- Howe JA, Husum K, Inall ME, Coogan J, Luckman A, Arosio R, Abernethy C, Verchili D (2019) Autonomous underwater vehicle (AUV) observations of recent tidewater glacier retreat, western Svalbard. *Mar Geol* 417:106009. <https://doi.org/10.1016/j.margeo.2019.106009>
- Høyland KV (2009) Ice thickness, growth and salinity in Van Mijenfjorden, Svalbard, Norway. *Polar Res* 28(3):339–352. <https://doi.org/10.3402/polar.v28i3.6141>
- Johansson AM, Malnes E, Gerland S, Cristea A, Doulgeris AP, Divine DV, Pavlova O, Lauknes TR (2020) Consistent ice and open water classification combining historical synthetic aperture radar satellite images from ERS-1/2, Envisat ASAR, RADARSAT-2 and Sentinel-1A/B. *Ann Glaciol* 1–11. <https://doi.org/10.1017/aog.2019.52>
- Jones T, Behe C, Arvnes M, Wesseberg S, Serienko L, Harris C, Harcharek Q (2019) Arctic Coastal Biodiversity Monitoring Plan. Conservation of Arctic Flora and Fauna International Secretariat: Akureyri, Iceland. ISBN 978-9935-431-76-9
- Karlsen SR, Stendardi L, Nilsen L, Malnes E, Eklundh L, Julitta T, Burkart A, Tømmervik H (2020) Sentinel satellite-based mapping of plant productivity in relation to snow duration and time of green-up. In: Van den Heuvel et al. (eds): *SESS report 2019, Svalbard Integrated Arctic Earth Observing System, Longyearbyen*, pp 42–57 https://sios-svalbard.org/SESS_Issue2
- Karulina M, Marchenko A, Karulin E, Sodhi D, Sakharov A, Chistyakov P (2019) Full-scale flexural strength of sea ice and freshwater ice in Spitsbergen Fjords and North-West Barents Sea. *Appl Ocean Res* 90:101853. <https://doi.org/10.1016/j.apor.2019.101853>
- Kauko HM, Taskjelle T, Assmy P, Pavlov AK, Mundy CJ, Duarte P, Fernández-Méndez M, Olsen LM, Hudson SR, Johnsen G, Elliott A (2017) Windows in Arctic sea ice: Light transmission and ice algae in a refrozen lead. *J Geophys Res Biogeosci* 122(6):1486–505. <https://doi.org/10.1002/2016JG003626>
- Killie MA, Aaboe S, Isaksen K, Van Pelt W, Pedersen ÅØ, Luks B (2021) Svalbard snow and sea-ice cover: comparing satellite data, on-site measurements, and modelling results. In: Moreno-Ibáñez et al. (eds) *SESS report 2020, Svalbard Integrated Arctic Earth Observing System, Longyearbyen*, pp 220–235. <https://doi.org/10.5281/zenodo.4293804>
- Kortsch S, Primicerio R, Beuche, F, Renaud PE, Rodrigues J, Lonne OJ, Gulliksen B (2012) Climate-driven regime shifts in Arctic marine benthos. *Proc Natl Acad Sci (US)* 109: 14052–57. <https://doi.org/10.1073/pnas.1207509109>
- Kovacs KM, Lydersen C, Overland JE, Moore SE (2011) Impacts of changing sea-ice conditions on Arctic marine mammals. *Mar Biodiv* 41:181–94. <https://doi.org/10.1007/s12526-010-0061-0>
- Kovacs KM, Krafft B, Lydersen C (2020a) Bearded seal (*Erignathus barbatus*) pup growth-body size, behavioral plasticity and survival in a changing climate. *Mar Mamm Sci* 36:276–84. <https://doi.org/10.1111/mms.12647>
- Kovacs KM, Lydersen C, Vacquière-García J, Shpak O, Glazov D, Heide-Jørgensen MP (2020b) The endangered Spitsbergen bowhead whales' secrets revealed after hundreds of years in hiding. *Biol Lett* 20200148. <https://doi.org/10.1098/rsbl.2020.0148>
- Kruss A, Tęgowski J, Wiktor J, Tatarek A (2006) Acoustic estimation of macrophytes in the Hornsund fjord (the Svalbard Archipelago). *Hydroacoustics* 9:89–96. <https://doi.org/10.1371/journal.pone.0112881.t001>
- Kubiszyn AM, Wiktor JM, Wiktor Jr JM, Griffiths C, Kristiansen S, Gabrielsen TM (2017) The annual planktonic protist community structure in an ice-free high Arctic fjord (Adventfjorden, West Spitsbergen). *J Mar Syst* 169:61–72. <https://doi.org/10.1016/j.jmarsys.2017.01.013>
- Kvıderová J, Souquieres CE, Elster J (2019) Ecophysiology of photosynthesis of *Vaucheria* sp. mats in a Svalbard tidal flat. *Polar Sci* 21:172–85. <https://doi.org/10.1016/j.polar.2018.11.006>
- Lantuit H, Overduin PP, Couture N, Wetterich S, Aré F, Atkinson D, Brown J, Cherkashov G, Drozdov D, Forbes DL, Graves-Gaylord A (2012) The Arctic coastal dynamics database: a new classification scheme and statistics on Arctic permafrost coastlines. *Estuar Coast* 35(2):383–400. <https://doi.org/10.1007/s12237-010-9362-6>
- Leopold P, Renaud PE, Ambrose WG, Berge J (2019) High Arctic *Mytilus* spp.: occurrence, distribution and history of dispersal. *Polar Biol* 42(1):237–44. <https://doi.org/10.1098/rsbl.2008.0484>

- Leu E, Wiktor J, Søreide JE, Berge J, Falk-Petersen S (2010) Increased irradiance reduces food quality of sea ice algae. *Mar Ecol Prog Ser* 411:49–60. <https://doi.org/10.3354/meps08647>
- Leu E, Søreide JE, Hessen DO, Falk-Petersen S, Berge J (2011) Consequences of changing sea-ice cover for primary and secondary producers in the European Arctic shelf seas: timing, quantity, and quality. *Prog Oceanogr* 90(1-4):18–32. <https://doi.org/10.1016/j.pocean.2011.02.004>
- Leu E, Mundy CJ, Assmy P, Campbell K, Gabrielsen TM, Gosselin M, Juul-Pedersen T, Gradinger R (2015) Arctic spring awakening—Steering principles behind the phenology of vernal ice algal blooms. *Prog Oceanogr* 139:151–70. <https://doi.org/10.1016/j.pocean.2015.07.012>
- Lone K, Merkel B, Lydersen C, Kovacs KM, Aars J (2018) Sea ice resource selection models for polar bears in the Barents Sea subpopulation. *Ecography* 1(4): 567–78. <https://doi.org/10.1111/ecog.03020>
- Lydersen C, Martin AR, Kovacs KM, Gjertz I (2001) Summer and autumn movement of white whales *Delphinapterus leucas* in Svalbard, Norway. *Mar Ecol Prog Ser* 219:265–74. <https://doi.org/10.3402/polar.v32i0.11206>
- Lydersen C, Assmy P, Falk-Petersen S, Kohler J, Kovacs KM, Reigstad M, Steen H, Strøm H, Sundfjord A, Varpe Ø, Walczowski W, Weslawski JM, Zajaczkowski M (2014) The importance of tidewater glaciers for marine mammals and seabirds in Svalbard, Norway. *J Mar Syst* 129:452–71. <https://doi.org/10.1016/j.jmarsys.2013.09.006>
- Marquardt M, Majaneva S, Pitusi V, Søreide JE (2018) Pan-Arctic distribution of the hydrozoan *Sympagohydra tuuli*? First record in sea ice from Svalbard (European Arctic). *Polar Biol* 41(3):583–88. <https://doi.org/10.1029/2007GL031972>
- McGovern M, Pavlov AK, Deininger A, Granskog MA, Leu E, Søreide JE and Poste AE (2020) Terrestrial inputs drive seasonality in organic matter and nutrient biogeochemistry in a High Arctic fjord system (Isfjorden, Svalbard). *Front Mar Sci* 7:542563. <https://doi.org/10.3389/fmars.2020.542563>
- McKnight C (2019). Establishing the food web structure and mercury concentrations in an Arctic coastal lagoon. MSc thesis. NTNU, Norway. <https://ntnuopen.ntnu.no/ntnu-xmlui/handle/11250/2617023>
- Meire L, Mortensen J, Rysgaard S, Bendtsen J, Boone W, Meire P, Meysman FJR (2016) Spring bloom dynamics in a subarctic fjord influenced by tidewater outlet glaciers (Godthåbsfjord, SW Greenland). *J Geophys Res* 121:1581–92. <https://doi.org/10.1002/2015JG003240>
- Miller AW, Ruiz GM (2014) Arctic shipping and marine invaders. *Nat Clim Change* 4(6): 413–16. <https://doi.org/10.1038/nclimate2244>
- Misund OA, Heggland K, Skogseth R, Falck E, Gjørseter H, Sundet J, Watne J, Lønne OJ (2016) Norwegian fisheries in the Svalbard zone since 1980. Regulations, profitability and warming waters affect landings. *Polar Sci* 10(3):312–22. <https://doi.org/10.1016/j.polar.2016.02.001>
- Molis M, Beuchel F, Laudien J, Włodarska-Kowalczyk, Buschbaum C (2019) Ecological drivers of responses by Arctic benthic communities with an emphasis on Kongsfjorden, Svalbard. In H Hop and C Wiencke (eds) *The Ecosystem of Kongsfjorden, Svalbard*. Advances in Polar Ecology 2. The Ecosystem of Kongsfjorden, Svalbard. Springer, pp 229–302. https://doi.org/10.1007/978-3-319-46425-1_11
- Muckenhuber S, Nilsen F, Korosov A, Sandven S (2016) Sea ice cover in Isfjorden and Hornsund, Svalbard (2000–2014) from remote sensing data. High resolution sea ice monitoring using space borne Synthetic Aperture Radar. <https://doi.org/10.5194/tc-10-149-2016>
- Nahrgang J, Varpe Ø, Korshunova E, Murzina S, Hallanger IG, Vieweg I, Berge J (2014) Gender specific reproductive strategies of an Arctic key species (*Boreogadus saida*) and implications of climate change. *PLoS One* 9(5):e98452. <https://doi.org/10.1371/journal.pone.0098452>
- Nechad B, Ruddick KG, Park Y (2010) Calibration and validation of a generic multisensor algorithm for mapping of total suspended matter in turbid waters. *Remote Sens Environ* 114:854–66. <https://doi.org/10.1016/j.rse.2009.11.022>
- Nowak A, Hodgkins R, Nikulina A, Osuch M, Wawrzyniak T, Kavan J, Łepkowska E, Majerska M, Romashova K, Vasilevich I, Sobota I, Rachlewicz, G (2021) From land to fjords: The review of Svalbard hydrology from 1970 to 2019. In: Moreno-Ibáñez et al. (eds) *SESS report 2020, Svalbard Integrated Arctic Earth Observing System, Longyearbyen*, pp 176–201. <https://doi.org/10.5281/zenodo.4294063>
- Norwegian Polar Institute (2014) Kartdata Svalbard 1:250 000 (S250 Kartdata) [Data set]. Norwegian Polar Institute. <https://doi.org/10.21334/npolar.2014.a23acc28>
- Pabi S, van Dijken GL, Arrigo KR (2008) Primary production in the Arctic Ocean, 1998–2006. *J Geophys Res* 113:C08005. <https://doi.org/10.1029/2007JC004578>
- Pavlova O, Gerland S, Hop H (2019) Changes in sea-ice extent and thickness in Kongsfjorden, Svalbard, and related ecological implications. *Advances in Polar Ecology*. In: Hop H, Wiencke C (eds.) *The Ecosystem of Kongsfjorden, Svalbard*. Springer, Cham, *Advances in Polar Ecology* 2:105–136 https://doi.org/10.1007/978-3-319-46425-1_4
- Pedersen-Ugelstad C (2019) Riverine and glacial influence on infaunal benthic communities in Isfjorden, Svalbard. MSc thesis. UiT–The Arctic University of Norway. <https://hdl.handle.net/10037/15950>
- Pitusi V (2019) Seasonal abundance and activity of sympagic meiofauna in Van Mijenfjorden, Svalbard. MSc thesis, UiT–The Arctic University of Norway. <https://hdl.handle.net/10037/15941>
- Renaud Włodarska-Kowalczyk M, Trannum H, Holte B, Węśławski JM, Cochrane S, Dahle S, Gulliksen B (2007) Multidecadal stability of benthic community structure in a high-Arctic glacial fjord (van Mijenfjord, Spitsbergen). *Polar Biology* 30(3): 295–305. <https://doi.org/10.1007/s00300-006-0183-9>

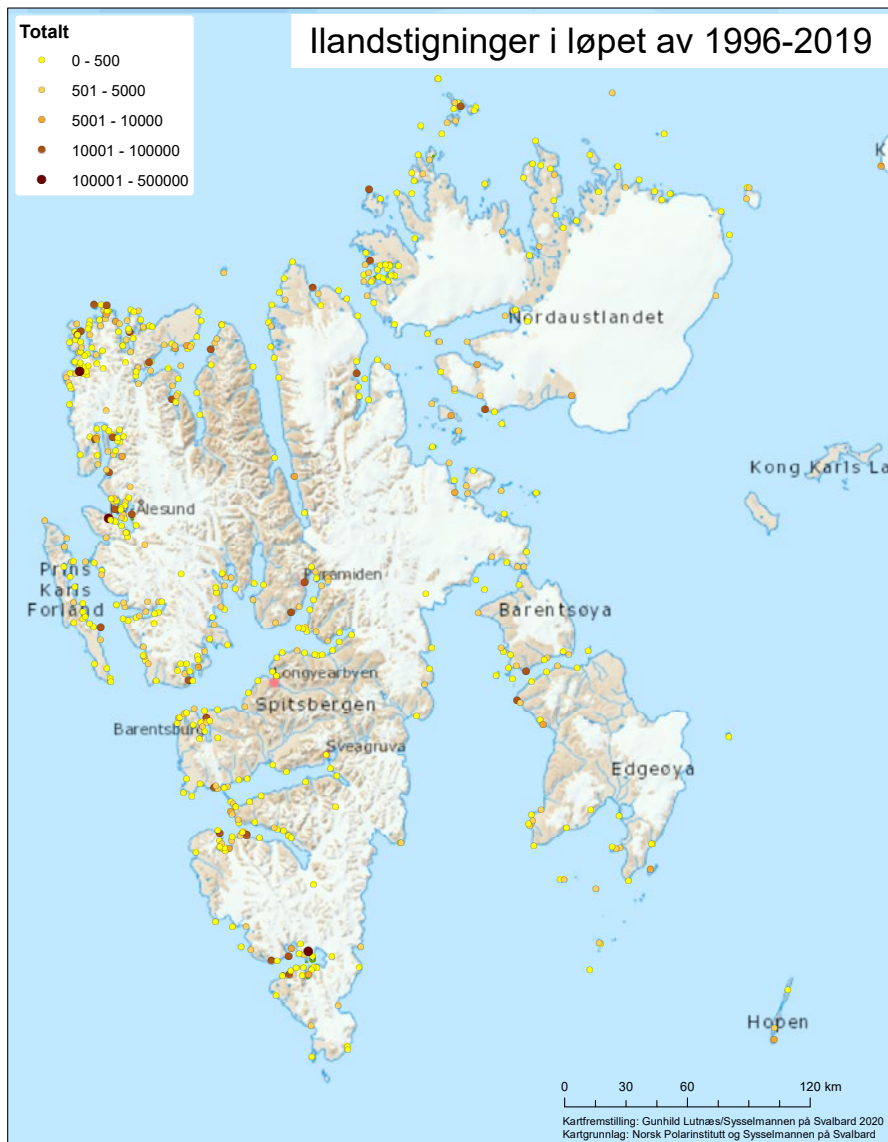
- Renaud P, Bekkeby T (2013) Existing time-series of marine biodiversity and the need for nature type mapping in Svalbard waters: Status, financing, and value for developing management strategies in a changing Arctic. Report 6229 – 2. pp 44
- Renaud PE, Sejr MK, Bluhm BA, Sirenko B, Ellingsen IH (2015) The future of Arctic benthos: expansion, invasion, and biodiversity. *Prog Oceanogr* 139:244–57. <https://doi.org/10.1016/j.pocean.2015.07.007>
- Schuler TV, Glazovsky A, Hagen JO, Hodson A, Jania J, Kääh A, Kohler J, Luks B, Malecki J, Moholdt G, Pohjola V, van Pelt W (2020) New data, new techniques and new challenges for updating the state of Svalbard glaciers. In: Van den Heuvel et al. (eds): SESS report 2019, Svalbard Integrated Arctic Earth Observing System, Longyearbyen, pp 108-134. https://sios-svalbard.org/SESS_Issue2
- Shanmugam P, He X, Singh RK, Varunan T (2018) A modern robust approach to remotely estimate chlorophyll in coastal and inland zones. *Adv Sp Res* 61:2491–2509. <https://doi.org/10.1016/j.asr.2018.02.024>
- Singh N, Granberg M, Collard F, Caruso G, Lu Z, Kögel T, Gabrielsen GW (2021) Microplastics in the REalm of Svalbard: current knowledge and future perspective. In: Moreno-Ibáñez et al. (eds) SESS report 2020, Svalbard Integrated Arctic Earth Observing System, Longyearbyen, pp 118–141. <https://doi.org/10.5281/zenodo.4293849>
- Sipilä M, Hoppe CJM, Viola A, Mazzola M, Krejci R, Zieger P, Beck L, Petäjä T (2020) Multidisciplinary research on biogenically driven new particle formation in Svalbard. In: Van den Heuvel et al. (eds): SESS report 2019, Svalbard Integrated Arctic Earth Observing System, Longyearbyen, pp 169-194. https://sios-svalbard.org/SESS_Issue2
- Skogseth R, Olivier LL, Nilsen F, Falck E, Fraser N, Tverberg V, Ledang AB, Vader A, Jonassen MO, Søreide J, Cottier F (2020) Variability and decadal trends in the Isfjorden (Svalbard) ocean climate and circulation—An indicator for climate change in the European Arctic. *Prog Oceanogr* 187:102394. <https://doi.org/10.1016/j.pocean.2020.102394>
- Skrzypek G, Wojtuń B, Richter D, Jakubas D, Wojczulanis-Jakubas K, Samecka-Cymerman A (2015) Diversification of nitrogen sources in various tundra vegetation types in the High Arctic. *PLoS One* 10(9):e0136536. <https://doi.org/10.1371/journal.pone.0136536>
- Smoła ZT, Tatarek A, Wiktor JM, Wiktor JM, Kubiszyn A, Węstawski JM (2017) Primary producers and production in Hornsund and Kongsfjorden—Comparison of two fjord systems. *Pol Polar Res* 38(3). <https://doi.org/10.1515/popore-2017-0013>
- Smyth TJ, Tilstone GH, Groom SB (2005) Integration of radiative transfer into satellite models of ocean primary production. *J Geophys Res* 110:C10014. <https://doi.org/10.1029/2004JC002784>
- Stocker AN, Renner AHH, Knol-Kauffman M (2020). Sea ice variability and maritime activity around Svalbard in the period 2012–2019. *Scientific Reports* 10 (1): 17043. <https://doi.org/10.1038/s41598-020-74064-2>
- Søreide JE, Falk-Petersen S, Hegseth EN, Hop H, Carroll ML, Hobson KA, Blachowiak-Samolyk K (2008) Seasonal feeding strategies of *Calanus* in the high-Arctic Svalbard region. *Deep Sea Res Part II Top Stud Oceanogr* 55(20-21):2225–44. <https://doi.org/10.1016/j.dsr2.2008.05.024>
- Søreide JE, Leu EV, Berge J, Graeve M, Falk-Petersen ST (2010) Timing of blooms, algal food quality and *Calanus glacialis* reproduction and growth in a changing Arctic. *Glob Chang Biol* 16(11):3154–63. <https://doi.org/10.1111/j.1365-2486.2010.02175.x>
- Søreide JE, Carroll ML, Hop H, Ambrose Jr WG, Hegseth EN, Falk-Petersen S (2013) Sympagic-pelagic-benthic coupling in Arctic and Atlantic waters around Svalbard revealed by stable isotopic and fatty acid tracers. *Mar Biol Res* 9(9):831–50. <https://doi.org/10.1080/17451000.2013.775457>
- Storrie L, Lydersen C, Andersen M, Wynn RB, Kovacs KM (2018) Determining the species assemblage and habitat use of cetaceans in the Svalbard Archipelago, based on recorded observations from 2002–2014. *Polar Res* 37:1463065. <https://doi.org/10.1080/17518369.2018.1463065>
- Strøm H, Descamps S, Bakken V, Lorentzen E (2008) Seabird Colonies by the Barents Sea, White Sea and Kara Sea [Data set]. Norwegian Polar Institute. <https://doi.org/10.21334/npolar.2008.fd4fd3aa>
- Sundfjord A, Albertsen J, Kasajima Y, Skogseth R, Kohler J, Nuth C, Skarohamar J, Cottier F, Nilsen F, Asplin L et al. (2017) Effects of glacier runoff and wind on surface layer dynamics and Atlantic Water exchange in Kongsfjorden, Svalbard; a model study. *Estuar Coast Shelf Sci* 187:260–72. <https://doi.org/10.1016/j.ecss.2017.01.015>
- Szczucka J, Hoppe L, Schmidt B, Fey DP (2017) Acoustical estimate of fish distribution and abundance in two Spitsbergen fjords. *Oceanologia* 59:585–91. <https://doi.org/10.1016/j.oceano.2017.04.007>
- Tverberg V, Skogseth R, Cottier F, Sundfjord A, Walczowski W, Inall ME, Falck E, Pavlova O, Nilsen F (2019) The Kongsfjorden Transect: seasonal and inter-annual variability in hydrography. In: H Hop and C Wiencke (eds) *The Ecosystem of Kongsfjorden, Svalbard. Advances in Polar Ecology 2. The Ecosystem of Kongsfjorden, Svalbard.* Springer, pp 49–104. https://doi.org/10.1007/978-3-319-46425-1_3
- Urbanski JA, Stempniewicz L, Weslawski JM, Draganska-Deja K, Wochna A, Goc M, Iliszko L (2017) Subglacial discharges create fluctuating foraging hotspots for seabirds in tidewater glacier bays. *Sci Rep* 7:43999. <https://doi.org/10.1038/srep43999>
- Vacquié-Garcia J, Lydersen C, Marques TA, Aars J, Ahonen H, Skern-Mauritzen M, Øien Ø, Kovacs KM (2017) Late summer distribution and abundance of ice-associated whales in the Norwegian High Arctic. *Endang Spec Res* 32:59–70. <https://doi.org/10.3354/esr00791>
- Vacquié-Garcia J, Lydersen C, Kovacs KM (2019) Diving behaviour of adult male white whales (*Delphinapterus leucas*) in Svalbard, Norway. *Polar Res* 38:3605. <https://doi.org/10.33265/polar.v38.3605>

- Vacquié-Garcia J, Lydersen C, Marques TA, Andersen M, Kovacs KM (2020) First abundance estimate for white whales *Delphinapterus leucas* in Svalbard, Norway. *Endang Spec Res* 41:253–63. <https://doi.org/10.3354/esr01016>
- Vihtakari M, Welcker J, Moe B, Chastel O, Tartu S, Hop H, Bech C, Descamps S, Gabrielsen GW (2018) Black-legged kittiwakes as messengers of Atlantification in the Arctic. *Sci Rep* 8(1):1–1. <https://doi.org/10.21334/npolar.2017.26dbd004>
- Viola AP, Hudson SR, Krejci R, Ritter C, Pedersen CA (2019) The Lower Atmosphere above Svalbard (LAS): Observed long term trends, small scale processes and the surface exchange. In: Orr et al. (eds): SESS report 2018, Svalbard Integrated Arctic Earth Observing System, Longyearbyen, pp 148–169. https://sios-svalbard.org/SESS_Issue1
- von Biela VR, Newsome SD, Bodkin JL, Kruse GH, Zimmerman CE (2016) Widespread kelp-derived carbon in pelagic and benthic nearshore fishes suggested by stable isotope analysis. *Estuar Coast Shelf Sci* 181:364–74. <https://doi.org/10.1016/j.ecss.2016.08.039>
- Weslawski JM, Kwasniewski S, Swerpel S, Wiktor J, Zajaczkowski M, Ostrowski M, Siwecki R (1990) Summer environmental survey of Gipsvika, Svalbard. Environmental atlas Gipsdalen, Svalbard. *Norsk Polarinstitutt Rapport* 61 111–31. <https://www.iopan.pl/projects/Adamant/Gipsvika/Rapport061.pdf>
- Węsławski JM, Jankowski A, Kwaśniewski S, Swerpel S, Ryg M (1991) Summer hydrology and zooplankton in two Svalbard fiords. *Pol Polar Res* 445–60.
- Węsławski JM, Wiktor J, Duris Z, Zajaczkowski M (1992) Summer marine biological survey at Bolscheoya, Eastern Svalbard 1992. *Arctic Ecology Group Report* 1:22.
- Weslawski JM, Wiktor J, Zajaczkowski M, Swerpel S (1993) Intertidal zone of Svalbard. *Polar Biol* 13(2):73–79. <https://doi.org/10.1007/BF00241052>
- Weslawski JM, Wiktor J, Zajaczkowski M, Futsaeter G, Moe KA (1997) Vulnerability assessment of Svalbard intertidal zone for oil spills. *Estuar Coast Shelf Sci* 44:33–41. [https://doi.org/10.1016/S0272-7714\(97\)80005-4](https://doi.org/10.1016/S0272-7714(97)80005-4)
- Weslawski JM, Szymelfenig M, Zajaczkowski M, Keck A (1999) Influence of salinity and suspended matter on benthos of an Arctic tidal flat. *ICES J Mar Sci* 56:194–202. <https://doi.org/10.1006/jmsc.1999.0620>
- Węsławski JM, Kotwicki L (2018) Macro-plastic litter, a new vector for boreal species dispersal on Svalbard. *Pol Polar Res* 165–74. <https://doi.org/10.24425/118743>
- Weydmann A, Søreide JE, Kwaśniewski S, Leu E, Falk-Petersen S, Berge J (2013) Ice-related seasonality in zooplankton community composition in a high Arctic fjord. *J Plankton Res* 35(4):831–42. <https://doi.org/10.1093/plankt/fbt031>
- Wiktor J, Szymelfenig M (2002) Patchiness of sympagic algae and meiofauna from the fast ice of North Open Water (NOW) Polynya. *Pol Polar Res* 175–84
- Wiktor J, Tatarek A, Węsławski JM, Kotwicki L, Poulin M (2016) Colonies of *Gyrosigma eximium*: a new phenomenon in Arctic tidal flats. *Oceanologia* 58(4):336–40. <http://dx.doi.org/10.1016/j.oceano.2016.04.007>
- Włodarska-Kowalczyk M, Renaud PE, Węsławski JM, Cochrane SK, Denisenko SG (2012) Species diversity, functional complexity and rarity in Arctic fjordic versus open shelf benthic systems. *Mar Ecol Prog Ser* 463:73–87. <https://doi.org/10.3354/meps09858>
- Wojtysiak K, Herman A, Moskalik M (2018) Wind wave climate of west Spitsbergen: seasonal variability and extreme events. *Oceanologia* 60(3):331–43. <https://doi.org/10.1016/j.oceano.2018.01.002>
- Zagórski P, Rodzik J, Moskalik M, Strzelecki M, Lim M, Błaszczak M, Promińska A, Kruszewski G, Styszyńska A, Malczewski A (2015) Multidecadal (1960–2011) shoreline changes in Isbjørnhamna (Hornsund, Svalbard). *Pol Polar Res* 36(4):369–90. <https://doi.org/10.1515/popore-2015-0019>
- Zhuravskiy D, Ivanov B, Pavlov A (2012) Ice conditions at Gronfjorden Bay, Svalbard, from 1974 to 2008. *Polar Geogr* 35(2). <https://doi.org/10.1080/1088937X.2012.662535>

Appendix 1

Cruise tourism in Svalbard has increased the last decade especially among smaller expedition cruises that offer landings (= 'ilandstigninger' in Norwegian, see map, source: The Governor in Svalbard). The number of these expedition vessels (24 to 59 vessels) and passengers (10.040 to 21.000 passengers) has doubled from 2008 to 2018 (Stocker et al. 2020). Large overseas cruise ships offer primarily landings in Longyearbyen, the main settlement in Svalbard (not included in map below). The number of these overseas ships has

actually decreased from 2008 to 2018 (28 to 15 ships) but the ships have become larger so the number of overseas cruise passengers has almost doubled (28.697 to 45.900 passengers; Stocker et al. 2020). West Spitsbergen is the most visited region in Svalbard. However, reduction in sea ice has opened up for more landings in northern and eastern Svalbard and allowed for an extension by starting earlier and ending later the operational season. For more detailed information see Stocker et al. 2020¹¹:



11 Stocker AN, Renner AHH, Knol-Kauffman M (2020). Sea-ice variability and maritime activity around Svalbard in the period 2012–2019. Scientific Reports 10(1): 17043. <https://doi.org/10.1038/s41598-020-74064-2> (open access)

Appendix 2

Geomorphological data from aerial photos (1987–1991) (unpublished data, Norwegian Polar Institute) were used to estimate the extent of coastscapes

defined by CAFF¹² in Svalbard. This table show how geomorphology and special feature classifications from NPI were assigned to the CAFF coastscapes.

CAFF Coastscapes	NPI coastal mapping for Svalbard	
	Geomorphology classifications	Special features
Rapidly Eroding Shores	Talus cones High cliff of unconsolidated material Low cliff of unconsolidated material	
Lagoons and Barrier Islands Estuaries Low Gradient Soft Shores	Barrier (beach ridge) Miscellaneous	Delta Lagoon and delta Lagoon Tidal flat
Rocky Shores and Sea Cliffs	Rocky shore Low cliff of bedrock High cliff of bedrock	
Ice Fronts	Glacier front terminating in the sea	

¹² Coastal Biodiversity Monitoring Plan. Conservation of Arctic Flora and Fauna International Secretariat: Akureyri, Iceland. ISBN 978-9935-431-76-9

Appendix 3

Coastscape description and distribution as defined by CAFF 2019¹³.

COASTSCAPES	GENERAL DESCRIPTION AND DISTRIBUTION
Fjords	Long narrow inlets with steep sides and cliffs usually formed by Quaternary sub-sea level glacial erosion. They are commonly headed by tide water glaciers with associated melt water streams, and feature frequent small lateral side streams with small deltas and estuaries. Fjords are the predominant coastscape in Norway, Iceland, Greenland and the eastern Canadian Arctic.
Rapidly Eroding Shores	Coastal areas with soft shores, often containing significant ground ice, that are eroding at moderate to rapid rates to create offshore bars, spits and mudflats. Occur mostly along the southern coast of the Beaufort, East Siberian, and Laptev Sea.
Lagoons and Barrier Islands	Coasts that feature low-lying, shallow, brackish lake and wetland systems protected from the ocean by barrier bars and spits, usually connected by a relatively small stream that flows in both directions with the tide. Frequently flooded by storms that can significantly alter salinity and turbidity characteristics. Often occur with Rapidly Eroding Shore and Low Gradient Soft Shores Coastscape that supply sediment for land building. Common in Russia, Alaska, and Canada along the Bering, Chukchi, and Beaufort Sea, and along the Iceland coasts.
Rocky shores and Sea cliffs	Low gradient to steep coasts (including sea cliffs) with exposed bedrock to the waterline that frequently include rock pools, beaches and small wetlands. Scattered throughout the Arctic and often associated with the Fjord Coastscape.
Estuaries	Estuaries develop at the mouths of most rivers where sediments are deposited. Often featuring extensive low gradient networks of wetlands, streams and brackish ponds with broad mudflats. Occur along the Arctic coast wherever rivers enter the sea; ranging from very small to very large estuaries such as the Lena, Ob, Yukon and Mackenzie.
Low Gradient Soft Shores	Low gradient coasts with varying thickness of surficial materials over bedrock, and characterised by mudflats, wetlands, and beaches. Scattered throughout the Arctic, but cover large coastal areas of the Canadian Arctic Archipelago, along the Alaskan Chukchi and Beaufort Sea, and along the Russian and Icelandic coasts.
Ice Fronts	Ice Fronts develop where glaciers reach the sea and usually produce floating ice by calving from the glacier front. They occur predominately on the east coast of Greenland, but also in the Baffin Bay area, in southern Alaska and on Svalbard, Norway. Meltwater emanating seasonally from the bottom of the glacier rises as a plume to the surface providing nutrients for lower trophic levels, and supports productive populations of surface feeding seabirds, diving seabirds and marine mammals.

¹³ Coastal Biodiversity Monitoring Plan. Conservation of Arctic Flora and Fauna International Secretariat: Akureyri, Iceland. ISBN 978-9935-431-76-9

Appendix 4

List of essential Focal Ecosystem Components (FECs). The selection of FECs for each coastscape followed a stochastic dominance process based on selection criteria established by the Coastal Expert

Monitoring Group (CEMG). They were assessed based on input from CEMG FEC workshops and selected scientists. For more detailed information see CAFF 2019¹⁴

ESSENTIAL FECS	COASTSCAPES						
	Rocky Shores	Eroding Shores	Lagoons	River Estuaries	Soft Shores	Fjords	Ice Fronts
Waterfowl		X	X	X	X	X	
Seabirds: omnivores	X	X			X		
Seabirds: diving planktivore	X	X			X		
Seabirds: surface piscivores	X	X	X	X	X		X
Seabirds: diving piscivores	X	X	X		X		
Seabirds: benthivores	X	X	X	X	X		
Subtidal flora, intertidal macroalgae	X		X	X		X	
Pinnipeds	X				X	X	X
Whales				X	X	X	X
Pelagic fishes	X	X	X			X	X
Demersal fishes	X		X	X		X	X
Salmonids			X	X	X		
Phytoplankton	X	X		X		X	X
Meso- and macro-zooplankton		X					X
Benthos	X		X	X	X	X	X
Large herbivores						X	
Coastal wetlands			X	X		X	

¹⁴ Coastal Biodiversity Monitoring Plan. Conservation of Arctic Flora and Fauna International Secretariat: Akureyri, Iceland. ISBN 978-9935-431-76-9

Appendix 5

Data sets referred to through various publications in this chapter. The datasets are primarily ongoing monitoring and long-time series on the physical, chemical and biological environment in Svalbard coastal waters. These datasets are (or will be within 2021) available through the SIOS Data Access Portal¹⁵. In this metadata portal general information on the metadata and links to the data themselves are provided. The compilation of environmental coastal data from Svalbard is work in progress. The overall aim is to make relevant coastal data from Svalbard more easily available to the scientific and public community.

Dataset	Parameter	Period	Location	Metadata access (URL)	Dataset provider
Physical –chemical environment					
Hydrography	Water column temperature and salinity	1996-present	Hornsund and Kongsfjorden	Data will be available from 2021 through the IOPAN data portal. http://www.iopan.gda.pl/index.html	IOPAN office@iopan.gda.pl
	Water column temperature and salinity Waves and tides	2013-present	Hornsund	Data will be available from 2021 through IG PAS Data Portal – http://dataportal.igf.edu.pl	Mateusz Moskalik (IG PAS) mmosk@igf.edu.pl
	Water column temperature and salinity	1990-present	Isfjorden	sios.metsis.met.no Svalbard Integrated Arctic Earth Observing System (sios-svalbard.org)	Ragnheid Skogseth (UNIS) Ragnheid5@UNIS.no
Fast ice cover	Percentage of fjord area	Monthly (Feb-Jun) since 2003	Inner Kongsfjorden	https://data.npolar.no/dataset/74c7b236-b94d-48c5-a665-ffcd54e8e1b7	Sebastian Gerland (NPI) sebastian.gerland@npolar.no Olga Pavlova (NPI) olga.pavlova@npolar.no
Sea ice	Time lapse photography	2015-present	Hornsund	Data will be available from 2021 through IG PAS Data Portal – http://dataportal.igf.edu.pl	Mateusz Moskalik (IG PAS) mmosk@igf.edu.pl
Sedimentology	SSC Sediment flux LOI	2015-present	Hornsund	Data will be available from 2021 through IG PAS Data Portal – http://dataportal.igf.edu.pl	Mateusz Moskalik (IG PAS) mmosk@igf.edu.pl

¹⁵ https://sios-svalbard.org/metadata_search

Biogeochemistry	Chlorophyll a (mg/m ³) Nutrients (mmol/m ³) POC/PON (µg/L)	2000-present	Kongsfjorden and adjacent shelf	https://data.npolar.no/dataset/6a4eaafa-10da-40d5-9a52-0268afbed4aa	Haakon Hop (NPI) haakon.hop@npolar.no Anette Wold (NPI) anette.wold@npolar.no
Seasonal Time Series					
Isfjord-Adventfjorden time series (ISA)	Hydrography Nutrients Phytoplankton taxonomy Chlorophyll a DNA (water) Zooplankton community	Bi-weekly to monthly data since 2011; all year	Adventfjorden (approx. 90-m depth)	In preparation for SIOS portal Data in NIRD	Anna Vader (UNIS) anna.vader@unis.no
Isfjorden Marine Observatory Svalbard (IMOS)	Hydrography Nutrients Phytoplankton taxonomy Chlorophyll a Zooplankton community	Seasonal time series since 2015 4 to 8 times per year	Isfjorden transect	In preparation for SIOS portal Data in NIRD	Janne E. Søreide (UNIS) janne.soreide@unis.no
Ecosystem monitoring in coastal waters of Svalbard "Økokyst Svalbard"	Physical parameters (temperature, salinity, oxygen) Water chemistry Phytoplankton Zooplankton Soft bottom benthic fauna Settlement plates	Monthly data; May-September 2018	Three stations in Isfjorden and Hornsund (2019-2020)	https://vanmiljo.miljodirektoratet.no/	Guttorm Christensen (Akvaplan-niva) guttorm.christensen@akvaplan.niva.no
Plankton					
Phytoplankton diversity	Abundance (cells/L)	2000-present	Kongsfjorden and adjacent shelf	https://data.npolar.no/dataset/6a4eaafa-10da-40d5-9a52-0268afbed4aa (work in progress)	Haakon Hop (NPI) haakon.hop@npolar.no Anette Wold (NPI) anette.wold@npolar.no Philipp Assmy (NPI) philipp.assmy@npolar.no
Zooplankton	Abundance (Ind/m ³)	1996-present (every July)	Kongsfjorden and adjacent shelf	https://data.npolar.no/dataset/6a4eaafa-10da-40d5-9a52-0268afbed4aa (work in progress)	Haakon Hop (NPI) haakon.hop@npolar.no Anette Wold (NPI) anette.wold@npolar.no
	Abundance (Ind/m ³)	2005; 2014-2019	Van Mijenfjorden	In preparation for SIOS portal Data in NIRD	Janne Søreide (UNIS) janne.soreide@unis.no

Dataset	Parameter	Period	Location	Metadata access (URL)	Dataset provider
Sea-ice flora and fauna					
Sympagic meiofauna	Abundance (Ind/m ²)	2014-present	Svalbard landfast ice	In preparation for SIOS portal Data in NIRD	Janne Søreide (UNIS) janne.soreide@unis.no
Benthic invertebrates					
Intertidal organisms	Flora and fauna Taxonomy Biomass Density	1981-88; 1999-2008; 2014-present	Around Svalbard	https://adamant.iopan.pl/adamant/taxa_observations/	sios.metis.met.no Svalbard Integrated Arctic Earth Observing System (sios-svalbard.org)
Soft bottom benthos	Sublittoral macrofauna Taxonomy Biomass Density Photography	1996-present	Hornsund and Kongsfjorden	Data will be available from 2021 through IOPAN data portal http://www.iopan.gda.pl/index.html	IOPAN office@iopan.gda.pl
Hard bottom benthos	Shallow sublittoral hard bottom fauna photography	2000-present	Isfjorden	http://www.polarlimelapse.net/	IOPAN office@iopan.gda.pl
Fish					
Pelagic fish		Annually – autumn since 2010; winter since 2011; spring since 2015	Kongsfjorden, Isfjorden, Rijpfjorden and Hinlopen Strait (when sea-ice conditions allow for trawling)	In preparation for SIOS portal Data in NIRD	From UNIS, UIT and Akvaplan-niva Paul Renaud (Akvaplan-niva) paul.renaud@akvaplan.niva.no
Demersal fish		Annually – autumn since 2010; winter since 2011; spring since 2015	Kongsfjorden, Isfjorden, Rijpfjorden and Hinlopen Strait (when sea-ice conditions allow for trawling)	In preparation for SIOS portal Data in NIRD	From UNIS, UIT and Akvaplan-niva Paul Renaud (Akvaplan-niva) paul.renaud@akvaplan.niva.no

Seabirds						
Seabirds	Colony locations and total counts	1960-present	Throughout Svalbard	Historical data: https://data.npolar.no/dataset/fd4fd3aa-7249-53c9-9846-6e28c5a42587 New data upon request	Hallvard Strøm (NPI) hallvard.strom@npolar.no Sébastien Descamps (NPI) sebastien.descamps@npolar.no	
	Population trends	Annual since 1987	Bjørnøya and Spitsbergen	http://www.mosj.no/en/fauna/marine/	Hallvard Strøm (NPI) hallvard.strom@npolar.no Sébastien Descamps (NPI) sebastien.descamps@npolar.no	
Marine mammals						
Marine mammal distribution	Sighting records for all marine mammal species	Annual since 2002	Throughout Svalbard	Upon request	Kit Kovacs (NPI) kit.kovacs@npolar.no	
Polar bear ecology	Dens and sea-ice cover Cubs per litter Cubs per female Body condition	Annually since 1979	Throughout Svalbard	http://www.mosj.no/en/fauna/marine/polar-bear.html	Jon Aars (jon.aars@polar.no)	
Walrus	Population size	1980-present (every 5 th year)	Throughout Svalbard	http://www.mosj.no/en/fauna/marine/walrus-population.html	Kit Kovacs (NPI) kit.kovacs@npolar.no	

Appendix 6

Overview of recommendations for future monitoring/ time series rated with priority 1 to 3 (1= critical/urgent parameters; 2 = important parameters and 3 = support parameters). Climate

region W = West Svalbard, E = East Svalbard, NE = Northeast Svalbard, and All = Whole Svalbard), Coastscape (see list, [Appendix 3](#)) and Focal Ecosystem Component (see list [Appendix 4](#))

Climate region	Coastscape	FEC	Parameter	Priority (1-3)	Comment
All	Lagoons	Needs to be identified	Biodiversity, productivity, ecological role	1	No previous data
All	Estuaries, tidal flats	Phytoplankton (microphytobenthos), invertebrates and waterfowl	Biodiversity, productivity, ecological role	1	No previous data, except from Adventfjorden river delta
E/ NE	Rocky shore	Subtidal flora and intertidal macroalgae	Biodiversity, Coverage and growth (size)	1	No previous data
All	Fjords	Pelagic and demersal fish	Biodiversity, population data, biomass	1	No monitoring programme established for Svalbard fjords
All	Ice fronts, Seasonal sea, Fjords	All resident Arctic endemic marine mammals in Svalbard (only polar bears currently have marginally adequate monitoring coverage)	All relevant CAFF marine mammal FECs	1	Current monitoring is very limited and needs a major expansion for all marine mammal FECs that have been selected by CAFF
All	All vulnerable coastscapes via <i>in situ</i> measurements	Phytoplankton	Chl-a concentration, Turbidity/SPM concentration, coloured dissolved organic matter, dissolved organic carbon, PAR and primary productivity	2	Cal/Val work in progress, but still in an early phase, more research is therefore needed.
All	All vulnerable coastscapes via space borne/airborne measurements		Operation process chain to derive the parameters recorded <i>in situ</i> (listed above) and periodic calibration and validation of the algorithms.	2	
E	Fjords	Physical background data, Phytoplankton	Hydrography, turbidity, PAR, chlorophyll a	2	Autonomous observatory
All	Seasonal sea ice	Physical background data	Snow and sea-ice thickness	3	<i>In situ</i> sampling, SIMBA ice tethered buoys

From land to fjords: The review of Svalbard hydrology from 1970 to 2019 (SvalHydro)

Aga Nowak¹, Richard Hodgkins², Anna Nikulina³, Marzena Osuch⁴, Tomasz Wawrzyniak⁴, Jan Kavan⁵, Elżbieta Łepkowska⁶, Marta Majerska⁴, Ksenia Romashova³, Igor Vasilevich³, Ireneusz Sobota⁷, and Grzegorz Rachlewicz⁸

1 Department of Arctic Geology, The University Centre in Svalbard, PO BOX 156 Longyearbyen, Svalbard, Norway

2 Department of Geography, Loughborough University, United Kingdom

3 Arctic and Antarctic Research Institute, St. Petersburg, Russia

4 Institute of Geophysics, Polish Academy of Sciences, Warszawa, Poland

5 Department of Geography, Polar-Geo-Lab, Masaryk University, Czech Republic

6 University of Silesia, Centre for Polar Studies, Katowice, Poland

7 Department of Hydrology and Water Management, Polar Research Center, Faculty of Earth Sciences and Spatial Management, Nicolaus Copernicus University in Torun, Poland

8 Institute of Geoecology and Geoinformation, Adam Mickiewicz University, Poznan, Poland

Corresponding author Aga Nowak, Aga.Nowak@unis.no

ORCID number 0000-0002-7130-1383

Keywords: Arctic hydrology, hydrological monitoring in Svalbard, water balance, climate change in the Arctic, freshwater fluxes into polar ocean, water resources, hydrological processes, water budget in Svalbard

DOI: <https://doi.org/10.5281/zenodo.4294063>

1. Introduction: A Story of Change

Since the turn of the century, Svalbard has been considered a canary in the coalmine for climate change. Two decades later, the Earth's warning system located in the Norwegian High Arctic experienced irreparable damage, and the title has been passed onto Greenland. Unfortunately, latest research suggests that the new canary has also just reached the point of no return, and its fate might no longer be dependent upon our efforts to limit carbon dioxide emissions (see King et al. 2020). Despite Greenland's record melt-year, the forefront of environmental change affecting Earth's ecosystems continues to be in Svalbard. Here, the warming is two to six times faster than the rest of the world (see Wawrzyniak and Osuch 2020), and the consequences of a shrinking cryosphere have already impacted terrestrial and marine environments.

The magnitude of the climatic changes in the Arctic was evident during the summer melt-season of 2020, when not only Svalbard but also Siberia suffered record-breaking high air temperatures (>21 °C in Svalbard and >38 °C in Siberia). Yet, it is the long-term increase in surface air temperature that is responsible for often irreversible changes associated with the reduction in snow cover, accelerated glacier surface melt and their further recession (AMAP 2017, IPCC 2019). Latest research based on glacier mass balance indicates that in the last 60 years, the above changes, in conjunction with a decrease in glacier refreezing rates, have caused glacier runoff to double, while surface runoff from non-glacierised areas surprisingly remained almost unchanged (van Pelt et al. 2019). In this report, we show that this is not the case for Svalbard catchments when analysing in-situ collected hydrological datasets.

The consequence of hydrological changes in Svalbard is not restricted to local coasts and seas. It is estimated that in the last two decades, melting Arctic glaciers contributed to the global sea level rise at the same rate as the Greenland Ice Sheet. Although climate change predictions vary, depending on the greenhouse gas emissions scenario, there is no doubt that in the High Arctic we can expect further increase in air temperature (by 4–7 °C) and precipitation (by 45–65%) with increased occurrence of heavy rainfall and flood events (NCCS 2019). As a result, total surface discharge is also expected to increase further, although downscaled models and runoff simulations suffer from insufficient data.

Unfortunately, confirmation of the above predictions will be difficult to achieve because:

1. Current long-term hydrological monitoring in Svalbard is sparse, with a clear westward bias (see Figure 1).
2. Monitoring is divided between various institutions and countries, making collaboration limited and data exchange inefficient or often non-existent.
3. Short-term projects performed by various international research teams, that do measure freshwater discharge in easily accessible parts of Svalbard, present mostly partial data from one melting season (generally from July, which is recognized as the month with the highest discharge), or at most, two seasons only (due to funding restrictions). In consequence, they produce an incomplete representation of surface hydrology, while the data are often difficult to access.

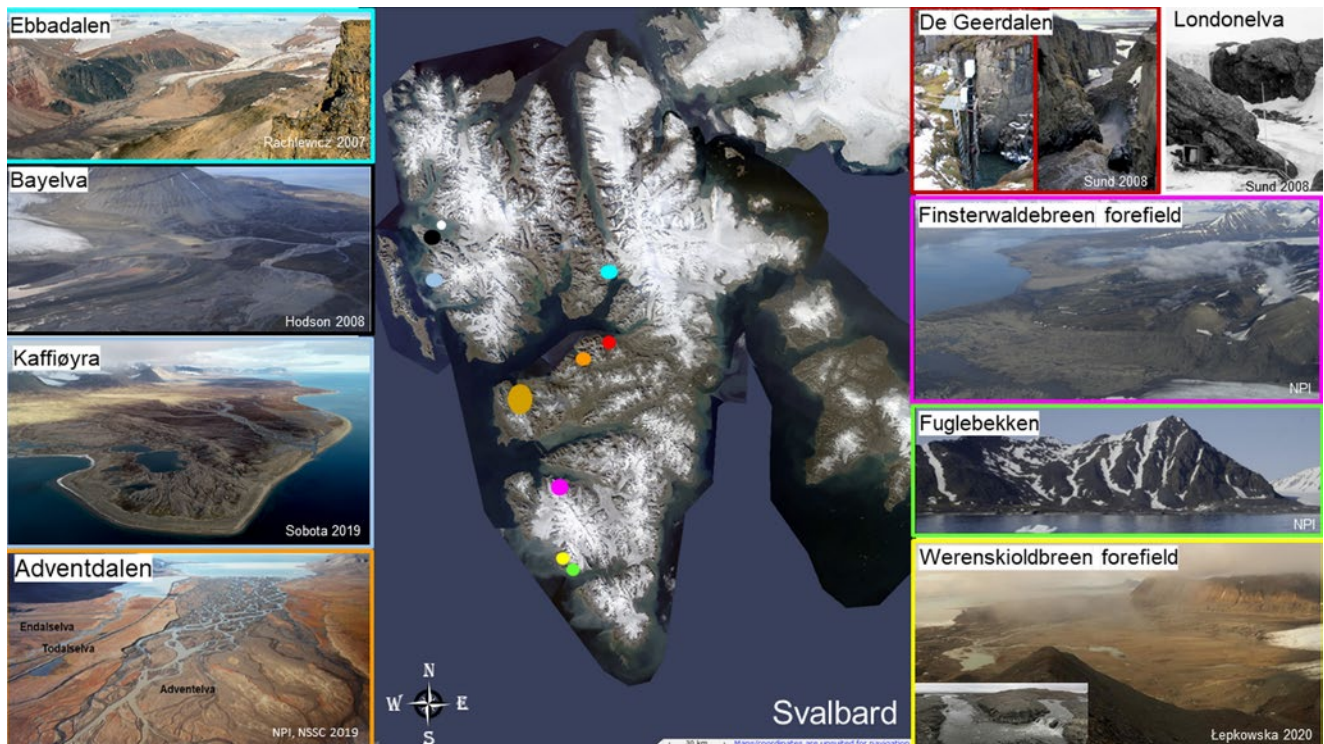


Figure 1: Map of catchments with long-term hydrological monitoring also showing a westward bias for Svalbard research. From south to north: (green) Hornsund – Fuglebekken, (yellow) Nottinghambukta – Werenskioldbreen, (pink) Van Keulenfjorden – Finsterwalderbreen, (brown) Grønfjorden - Grøndalen, Grønfjordbreen, Algedondabreen, Kongressdalen; (orange) Adventfjorden – Adventdalen; (red) Sassenfjorden – DeGeerdalen, (turquoise) Petuniabukta – Bartilelva, Ferdinandelva, Ebbaelva, Elsaelva; (blue) Kafføyra - Waldemarbreen, Kongsfjorden – (black) Bayelva and (white) Londoneelva. Not all monitoring sites are represented in the pictures. See [Appendix 1](#) for details on all sites

As a result, the most widely available and used dataset for producing estimates and predictions of surface runoff from glacierised areas across the entire Svalbard usually come from state-run monitoring programs of the Norwegian Water Resources and Energy Directorate (NVE) and/or the Norwegian Polar Institute (NPI).

The above means that the observations and projections of hydrological changes for the Norwegian High Arctic are based on just two catchments: Bayelva transferring water into Kongsfjorden, and De Geerelva flowing into Sassenfjorden (e.g. NCCS 2019). These monitoring stations are located in the central part of the island, with the former being more northward (see Figure 1, [Appendix 1](#)).

However, research shows that meteorological conditions vary greatly across Svalbard (e.g. Førland et al. 2011, Nordli et al. 2014, Osuch and Wawrzyniak 2017a), as does the surface runoff.

This is because local conditions influence air temperature, precipitation, evaporation, occurrence of winter rainfall, capacity for groundwater storage and the length of melting season. Yet, the influence of the above on surface runoff and consequently water balance is rarely mentioned in the literature (Nowak and Hodson 2013).

We already know that polar regions of the future will be very different to what we can see today, but given the heterogeneity of the Arctic environment, the level of that change will depend on general and local variables intrinsically linked to the air temperature, precipitation and changes in the cryosphere's capacity for storage or release of water.

Given the above, it is unsurprising that hydrological response to undergoing environmental revolution has been named one of the most important research needs in the High Arctic (NCCS 2019; Retelle et al. 2019).

Therefore, through this report we:

4. Present the first ever comprehensive hydrological dataset from all institutions performing long-term hydrological monitoring in Svalbard, in order to **depict the magnitude and direction of hydrological changes**, as well as to highlight the heterogeneity of the environment.
5. Seed the **SvalHydro** initiative to create a long-term hydrological observatory across Svalbard. The aim is to establish and strengthen collaboration between all institutions performing long-term monitoring on the island.
6. **Indicate gaps in knowledge that require our immediate attention**, and in some cases, necessity for new investments. This is to produce more accurate hydrological predictions and recommend actions that need to be taken for environmental protection.

2. Overview of Existing Knowledge

2.1. Water balance, the High Arctic problem

A water balance (or water cycle) is the movement of water from the atmosphere (through condensation and precipitation) to the ground (in the form of snow, ice and runoff) and its return to the atmosphere (through evaporation, see Figure 2).

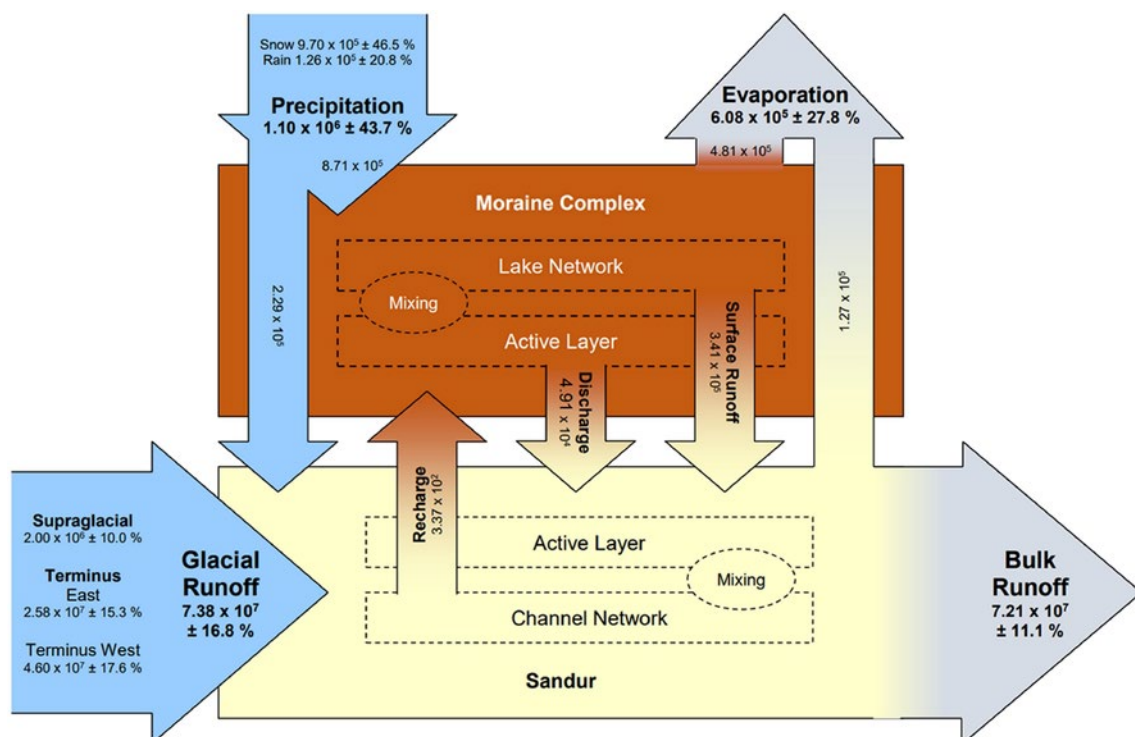


Figure 2: An example of a water cycle in a glacierised catchment in the High Arctic (Finsterwalderbreen watershed). Blue arrows: water inputs; grey arrows: water outputs; other arrows: internal transfers; dashed lines: minor multi-directional, stores/exchanges that cannot be quantified from the data available. All the water fluxes are in m^3 , with estimates of probable error, except for channel recharge, active-layer discharge and surface runoff, these fluxes must be viewed as first-order estimates. The determination of errors in all other water fluxes are described in detail in Hodgkins et al. 2009. Modified from Cooper et al. 2011.

To describe those movements during a hydrological year (i.e. water inputs and outputs from 1st October to 30th September), a water balance equation was created (see Eq 1).

$$P+C-Q-Q_g-E_a \pm \Delta S = \epsilon \quad (\text{Eq 1})$$

Where P is precipitation [mm/y], C is condensation [mm/y], Q is surface runoff [mm/y], Q_g is groundwater runoff [mm/y], E_a is evaporation [mm/y], ΔS is change in storage [mm/y] and ϵ [mm/y] is a residual error term representing water that is not properly accounted for (as the inputs and outputs in the equation should be in balance).

While many forms of this equation exist with different levels of complexity, a study by Nowak and Hodson (2013) modified the most-used versions of it [described in Hagen and Lefauconnier (1995) and Killingtveit et al. (2003)] for providing accurate results in glacierised catchments of the changing High Arctic (see Eq 2).

$$P_{\text{winter(ngs)}} + (P_{\text{JJAS}} + P_Q) + B_s + C - E_a \pm \Delta S = \epsilon \quad (\text{Eq 2})$$

Where $P_{\text{winter(ngs)}}$ is areal winter snowfall from non-glacierised areas [mm/y], P_{JJAS} is areal precipitation during June–September [mm/y], P_Q is daily winter precipitation causing discharge [mm], B_s is summer mass balance of glaciers occupying a catchment [mm/y], C is condensation [mm/y] and E_a is evaporation [mm/y].

Although Eq 2 renders the smallest errors in the water balance due to its appreciation of High Arctic conditions, the equation is far from perfect.

For example, some of its components such as condensation (C) and evaporation (E_a) are still based on artificial assumptions and constants created from sparse measurements performed over 30 years ago ($C = 9.38$ mm/y, $E_a = 46.88$ mm/y Killingtveit et al. 1994). Although using those constants had merits, we now know that meteorological conditions vary greatly across Svalbard, and even small differences between locations of measuring sites may cause substantial changes in the obtained results (Wawrzyniak and Osuch 2020). Therefore, a constant created for a catchment in the north where the climate is colder and more continental

will not reflect conditions in the south where the climate is much warmer and maritime. In addition, the rapidly warming Arctic that observes **dramatic increase in precipitation and air temperature leaves three-decade-old measurements outdated.**

Likewise, measurements of precipitation in the High Arctic are sparse, and gauging stations are located at the sea level. However, majority of the catchments in Svalbard contain mountainous areas, so calculation of the total precipitation needs to include a correction for the elevation gradient. In Eq 2, the assumption was made – based on the results of old measurements and hydrological modelling – that a 19% per 100 m increase of snowfall and rainfall alike will yield the best results. Yet, since **no active measurements of precipitation at various elevations are currently made in Svalbard**, it is another approximation of the conditions that could be close to reality but may not reflect the true values.

Another source of uncertainty in the water balance calculations, and in some cases a source of large errors, come from the change in water storage term (ΔS). It is still commonly accepted that the Arctic conditions allow for the assumption that ΔS is negligible. This is because catchments are underlined by continuous permafrost, while glaciers covering the surface undergo little changes. In addition, the duration of hydrological monitoring used in calculations is usually long, so small annual changes should not, in theory, influence the results in a significant way. However, Nowak and Hodson (2013) also indicated that the **water storage term can no longer be considered negligible** due to changes that follow warming of the High Arctic climate (i.e. thawing of the permafrost, thickening of the active layer, rapid retreat of glaciers coupled with their thermal regime change, or most importantly, increased occurrence of extreme winter rainfall events, causing ground icings).

The final problem that the Arctic hydrology is facing is a change in the boundaries of the hydrological year. The artificial dates of 1st October until 30th September were established based upon data indicating that all precipitation that falls in the form of rain or snowfall from October will stay on the ground until the melt season begins in May. However, there is increasing amount of evidence that extreme rainfall events following climatically driven changes now cause river discharge to happen well into October, November or in some cases December (see for e.g. Majchrowska et al. 2015). **Shifting the theoretical boundaries of the hydrological year is therefore necessary in view of the changing climate.**

Therefore, in this report, we present the evidence that the hydrological research in the High Arctic is in dire need of a 'facelift' that will take into consideration dramatic changes following climate warming. We also demonstrate the importance of long-term hydrological datasets by showing that while freshwater discharge from non-glacierised catchments and catchments with large glacier cover continues to increase, water fluxes from catchments with smaller glaciers, where ice has already retreated markedly, have been in fact decreasing for one or more decades.

Rethinking the water balance equation is a crucial step towards achieving understanding of the current hydrological conditions in the Arctic, as well as being able to accurately predict its contribution to the global water cycle. Especially, when every record-breaking measurement is a painful reminder that the changes we are facing here are beyond the point of no return.

2.2. Air temperature, a winter problem

In the mountainous catchments of Svalbard, snow and ice significantly affect water circulation by temporarily storing and releasing water on various time scales. Many studies have revealed that increase in melt and hydrological activity are directly proportional to increase in air temperature (see Hock 2003). Furthermore, air temperature is also responsible for distinct variability in annual and diurnal discharge.

Data collected from monitoring stations across Svalbard (Hornsund, Longyearbyen and Ny-Ålesund) show that in the last 40 years, the number of positive degree days (days with air temperature above 0°C) almost doubled. We also observe a latitudinal difference in the speed of that warming as the most southward located Hornsund experienced much more positive degree days than central Longyearbyen and the most northward Ny-Ålesund. This is also the case when we look at the length of the period where temperatures continuously stay above 0°C (Figure 3). In addition, melt season across Svalbard continues to start earlier while the freeze-up, marking the beginning of winter, continues to start later (Figure 3b, c). **The summer season is getting longer,** but research also indicates that **it is the winter that sees the most severe consequences of the warming** (see Nowak and Hodson 2013). Increasing number of warm weather episodes that result in intense rainfall almost immediately create extensive icings and ground ice. The former two prevent reindeer from grazing, lead to vegetation browning and impact soil temperatures (Vikhamar-Schuler et al. 2016), while the latter can alter water balance in affected catchments for more than one hydrological year (Nowak and Hodson 2013).

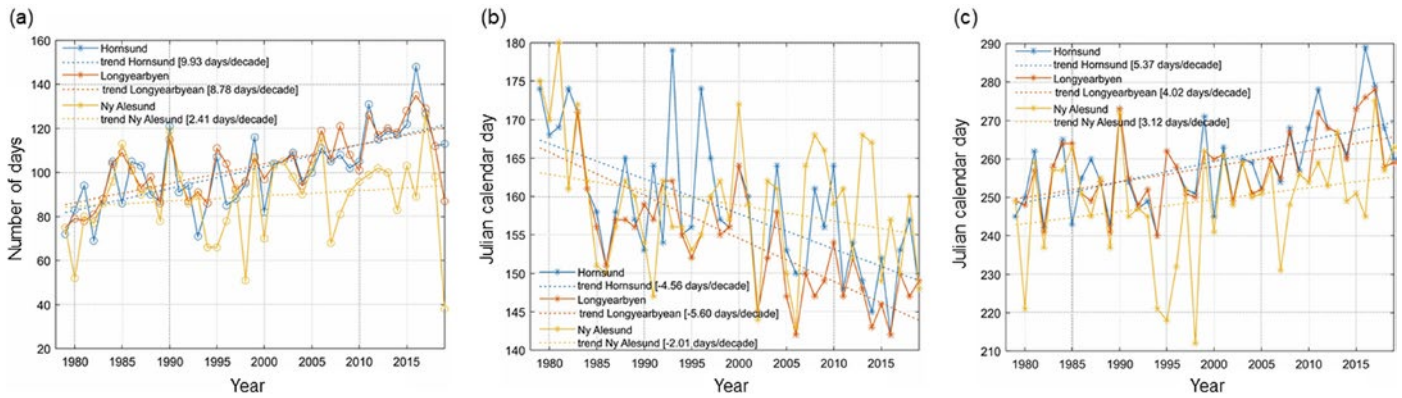


Figure 3: Variability of (a) the length of the longest period with positive air temperature, (b) start date and (c) end date of the continuous period with positive air temperature at Hornsund, Longyearbyen and Ny-Ålesund in the period 1979–2019. Trends were estimated by the modified Mann-Kendall test. The slope of the trend was estimated using Sen’s method (Sen 1968).

2.3. Precipitation, the end of season dilemma

An immediate consequence of continuous increase in air temperature is the increase in precipitation. The trends we see do not follow increase in air temperature exactly, as local climate alters the magnitude of observed rainfall. For example, the maritime location of Hornsund is responsible for

the largest decadal increase in rainfall and decrease in snowfall (see Figure 4). However, Longyearbyen – which is located in the central part of the island where climate is more continental – observed the smallest decadal changes, although the trends are in the same direction. Finally, in the most northward located Ny-Ålesund, both summertime rainfall and wintertime snowfall continue to increase.

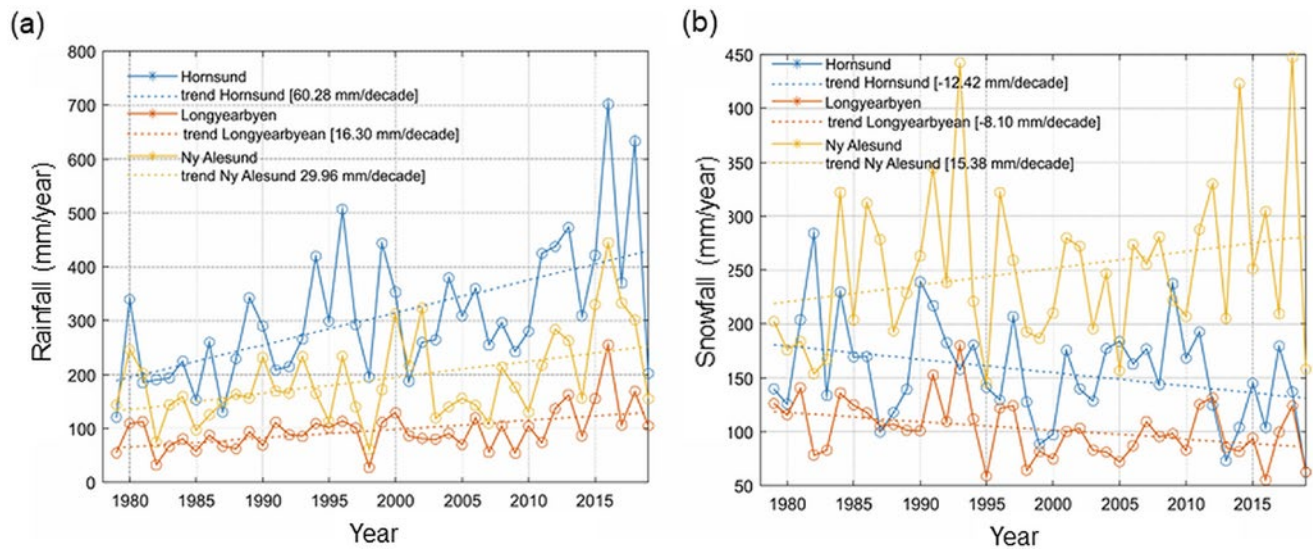


Figure 4: Variability of annual (a) sum of rainfall, (b) sum of snowfall at Hornsund, Longyearbyen, and Ny-Ålesund in the period 1979–2019. It was assumed that rainfall occurred during positive degree days ($>0^{\circ}\text{C}$)

Nonetheless, the consequences of the above changes have an influence upon water balance in all catchments across the archipelago. Increased rainfall is followed by increased occurrence of slushflows (Jaedicke et al. 2008), landslides and rockfalls (Lewkowicz and Way 2019). The changes are most noticeable in the shoulder seasons. While March and April are most affected by the increase in air temperatures shifting the beginning of snowmelt season earlier, September and October have also been getting wetter. The change is **prolonging the melting season and freshwater flux from terrestrial environments well outside the assumed boundaries of a hydrological year.**

The measurements of snowfall and rainfall are however sparse and not without errors. Available studies indicate that Arctic catchments often exhibit a pattern in which runoff appears to significantly exceed precipitation (Killingtveit et al. 2003). This can be attributed to a combination of measurement errors, non-representative locations of precipitation stations, net glacial ablation as well as knowledge gaps caused by insufficient monitoring.

Measurements are often underestimated in upland areas as rain gauges are only located at the sea level (Førland et al. 1997). Measurements of the end-of-winter, snowpack water-equivalent flux also remain challenging for hydrological studies. Sources of potential error in estimates relate to snow-depth measurements and the fact that the snow depth is often interpolated or extrapolated using a regression on elevation. The spatial variation of accumulation seems to contribute by far the most to overall error, being greater, for instance, than the inter-annual variability (Hodgkins et al. 2005). The

probable error range for the snowpack water flux can be as high as $\pm 44\%$ (Hodgkins et al. 2009).

Killingtveit et al. (2003) made the same point in suggesting that residual error in water balance calculations (ϵ in Eq 1 and Eq 2) is probably related to problems of precipitation correction. However, a study by Nowak and Hodson (2013) discovered that if the residue (ϵ) is considerably large, this theoretical surplus of water in a catchment cannot be construed as an error and is in fact a result of extreme winter rainfall events. This is because such unaccounted **rainfall can be stored in the active layer for the duration of one or two hydrological years.**

2.4. Glacier mass balance, a change in storage

Glaciers of Svalbard have been losing mass for the last half of the century, although the tendency to a more negative balance has been observed for the last twenty years (-8 ± 6 Gt/y, Schuler et al. 2020, also see Figure 5). This year (2020) is no different. Although glacier mass balance measurements for 2020 are underway at the time of writing of this report, preliminary results already suggest that 2020 will be another year of very negative mass balance, particularly due to the record low snow water equivalent measured in spring (JC Gallet and J Kohler, personal communication. Also observed by A Nowak, I Sobota and A Hodson on Bogerbreen, Waldemarbreen and Foxfonna, personal communication).

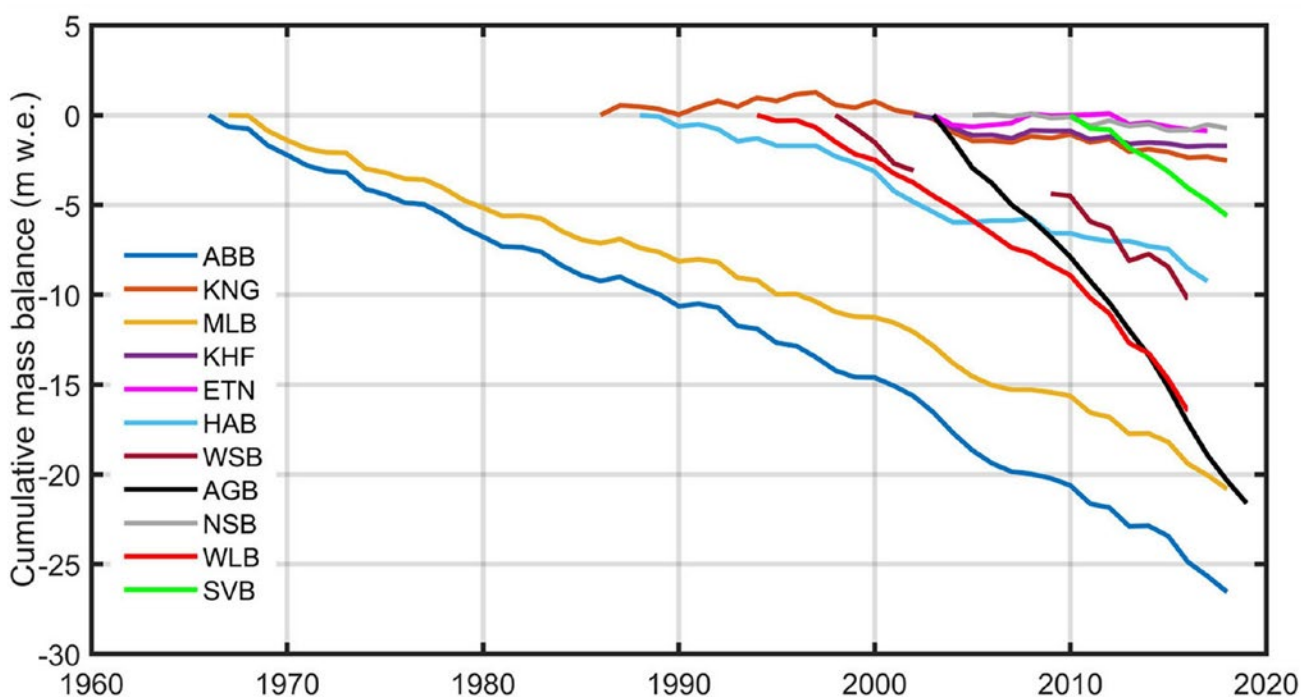


Figure 5: Cumulative surface mass balance of selected Svalbard glaciers. ABB – Austre Broggerbreen, KNG – Kongsvegen, MLB – Midtre Lovenbreen, KHF – Kronebreen/Holtedahlfonna, ETN – Etonbreen, HAB – Hansbreen, WSB – Werenskioldbreen, AGB – Austre Grønfiordbreen, NSB – Nordenskioldbreen, SVB - Svenbreen (Source: Schuler et al 2020)

In Svalbard, smaller and thinner glaciers with modest snow accumulation area respond to the warming (i.e. retreat) much faster than larger ones where the accumulation zones are sizeable (Schuler et al. 2020). The former can be found in the central and southern part of the island, where the climate is milder, while the latter are mostly in the northern part of the island where the climate is much colder and drier. The type of Svalbard glaciers varies from cirque to valley glaciers, ice caps and ice fields, and so does their thermal regime. Smaller glaciers with thickness below 100m are typically cold-based, with the entire ice temperature below the pressure melting point (except for summer surface ice). They are frozen to their beds and their internal water storage freezes during winter. In contrast, larger and thicker glaciers are polythermal, which means that they consist of both cold and temperate ice (see Figure 6). The latter is at the pressure melting point (i.e. warmer) and permits the presence of liquid water. As a result, polythermal glaciers can transport, store and release water from subglacial and/or englacial channels even during winter. According to a study from 1993 by Hagen et al., the majority of glaciers in Svalbard are of the latter type.

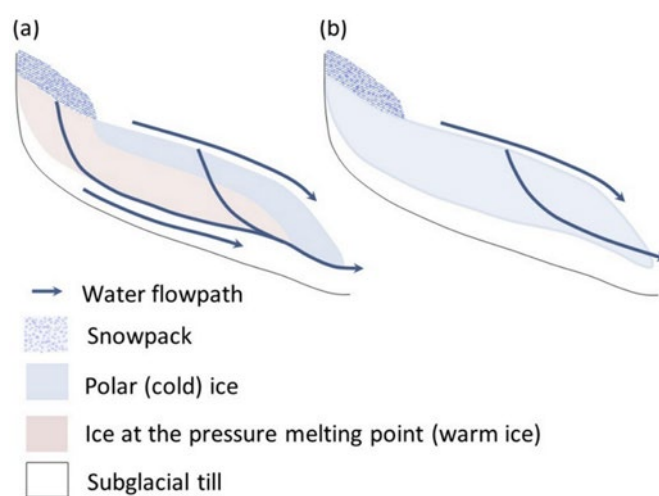


Figure 6: Simplified diagram of (a) polythermal glacier; (b) cold-based (polar) glacier thermal regime and drainage system (Source: Nowak-Zwierz 2013)

However, if we consider that the marked warming of the High Arctic in recent decades has resulted in continuous glacier thinning as well as their rapid recession, we also need to be aware that since 1993, many polythermal glaciers have transformed, or are in the process of transformation, into cold-based (e.g. Austre Brøggerbreen, Bogerbreen, Tellbreen, and Scott Turnerbreen). Such thermal regime change has a significant effect upon fluxes

of water, suspended sediments as well as transport of major ions and nutrients into downstream environments (see Nowak and Hodson 2014).

Suddenly, subglacial drainage ceases, and glacial storage – a contribution of winter discharge into a catchment's water budget – is replaced by an increased summer meltwater delivery from rapidly receding glaciers. Fluxes of ions into coastal waters are enriched due to intensified chemical weathering of freshly released suspended sediments.

Transformation of glaciers' thermal regime and their subsequent recession presents a challenge for calculations of the water balance, as it influences the change in storage term (ΔS)

of the water balance equation in more than one way. Receding glaciers also uncover ground that is now subjected to cold Arctic conditions. As a result, those areas undergo a slow transformation from unfrozen ground (that used to be protected from harsh temperatures by the glacier ice) into permafrost (Szafranec and Dobinski 2020). Although changes in the ground thermal regime of deglaciating catchments are marked, they still need to be included in the hydrogeological models. These so far only consider changes in a catchment's hydrology due to permafrost degradation (e.g. Bense et al 2009; Bense et al 2012).

2.5. Surface discharge, dire need for long term monitoring

Cryospheric changes that occur in Arctic catchments have, and will continue to have, a marked effect on hydrology in glacierised watersheds. A study by Huss and Hock (2018) indicated that globally, even in large-scale basins where the ice cover fraction is minimal, downstream hydrological effects of glacier recession can be substantial. If we consider that freshwater discharge in some catchments in

Svalbard consists of 50–70% of glacial meltwater (Majchrowska et al. 2015; Sobota et al. 2016), marked glacial recession observed in recent years in various watersheds will carry major consequences for the entire downstream ecosystems, terrestrial or coastal, that are dependent upon freshwater supply. Water fluxes, sediment, nutrient and major ion transports, drinking water supply or in some cases hydropower are and will continue to be affected.

In order to prepare for the above we need to be aware of the current hydrological conditions in catchments across the Arctic. Yet, research in high-latitude hydrology continues to be challenging despite technological advancements. The infrastructure remains very limited, and the extreme seasonality reduces the utility of many standard techniques, e.g. even where weir structures have been built, they typically fail to capture early-season runoff adequately because of snow- and ice-blocking of channels at the beginning of the melting season (e.g. Sund 2008). Significant challenges persist in measuring precipitation reliably and representatively; this not only hinders process analysis and water resources management, but also makes climate change detection difficult (e.g. Førland and Hanssen-Bauer 2003).

Measuring and monitoring the discharge of even moderately sized, glacially fed rivers is a demanding task because of the temporal and spatial instability of their flow regimes (see examples in Figure 7), particularly if continuous, complete time series are required. Furthermore, the majority of rivers are extremely braided, (see Figure 1 for an example), and there is no certainty which braid will be active for the entire summer. Therefore, long-term monitoring remains restricted to easily accessible places where local geology allows for collection of all discharge in one channel.

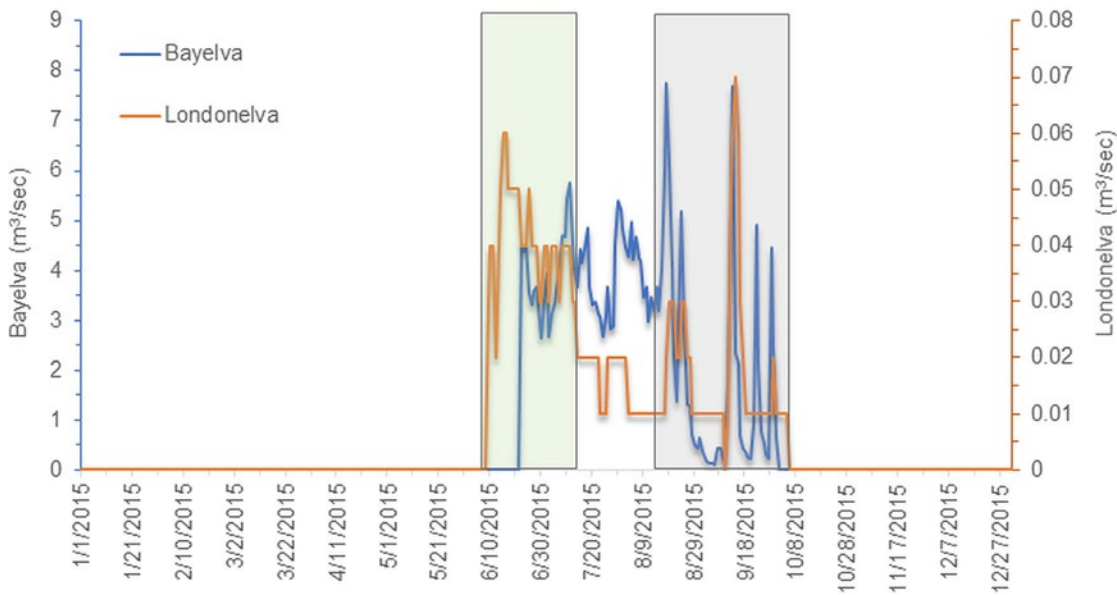


Figure 7: An example of a seasonal hydrograph from a glacierised catchment (Bayelva) and a non-glacierised catchment (Londoneiva). Grey rectangle on the hydrograph covers rainfall-dominated discharge. Green rectangle indicates snowmelt-dominated discharge. White area in between corresponds to discharge dominated by glacier ice-melt.

2.5.1. Have we passed ‘peak water’?

Despite the above, measurements undertaken at sparse hydrological monitoring stations on the west coast of Svalbard indicate that freshwater fluxes from glacierised and non-glacierised watersheds are changing.

In case of the former, rapid glacier recession opens water stores previously locked in the long-term storage (glacier ice). Thus, in catchments dominated

by glaciers, we should observe an increase in annual glacier runoff until ‘peak water’ (or a maximum) is reached. After that, a decline in water discharge is expected due to reduced glacier area that cannot support a steady increase in discharge anymore (Huss and Hock 2018, see Figure 8). However, since glacier coverage, and therefore meltwater contribution to total surface discharge, will vary between different catchments, so will their water fluxes and the timing of peak water.

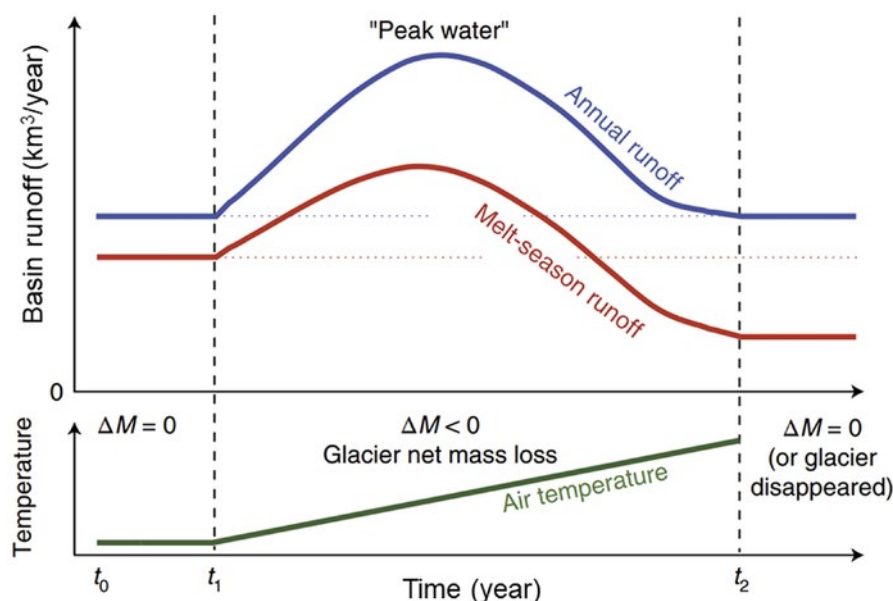


Figure 8: Changes in runoff from a glacierised catchment as a result of continuous climate warming (after Huss and Hock 2018)

Table 1: Average decadal freshwater fluxes (Qavg) into marine environment from three types of catchments (non-glacierised, lacustrine, and glacierised) and watersheds with various level of glaciation. See catchments' description in [Appendix 1](#).

Catchment type	Site name	Qavg 1970- 1980	Qavg 1980- 1990	Qavg 1991- 2000	Qavg 2001- 2010	Qavg 2011-2019
		x103 m ³ /year				
Non-glacierised	Fuglebekken ¹	162	362	453	421	534
	Londonelva	-	-	271	-	647
	Dynamiskbekken	-	-	-	241	-
	Elsaelva (almost non-gl)	-	-	-	-	1,106
Non-glacierised lacustrine	Kongresselva 2017–2019	-	-	-	-	10,695
Glacierised	Werenskioldbreen ²	57,000	52,000	65,000	74,000	83,000
	Adventelva ³	-	-	286,836	313,737	376,143
	Bayelva – started in 1989	-	25,696	27,533	33,683	30,889
	De Geerelva	-	-	42,290	41,953	38,156
	Aldegondabreen 2017–2019	-	-	-	-	23,699
	Finstervaldabreen 1999–2000	-	-	73,800	-	-
	Ferdinandelva	-	-	-	-	3,190
	Ragnarelva 2001–2003	-	-	-	19,777	-
	Horbyeelva 2001–2003	-	-	-	44,243	-
	Ebbaelva	-	-	-	47,508	-
	Bertielva	-	-	-	-	7,260
	Waldemarelva	-	-	6,904	5,587	5,231
	Grøndalselva 2017–2019	-	-	-	-	45,618

¹Simulated discharge using the Nordic-HBV model calibrated on discharge observations from the period 2014–2019 and validated on archival flow observations; discharge;

²unpublished data based on 21 hydrologically active seasons between 1970 and 2019;

³data based on the Nordic-HBV model calibrated on the De Geerelva discharge observations from 1991 to 2019

Table 1 indicates that in Svalbard, catchments with **smaller glaciers that have receded markedly have already achieved 'peak water'** and are on the falling limb of the runoff curve (see Bayelva, De Geerelva, Waldemarelva). In contrast, those **watersheds with larger glaciers** and perhaps higher percentage of non-glacierised area (e.g. Adventelva, Werenskioldbreen) **are still on the rising limb**. Similarly, **non-glacierised catchments** (e.g. Fuglebekken, or Bratteggbekken, an 8 km² watershed south of Werenskioldbreen; personal communication with E Łepkowska) **see an increase in discharge, most likely due to increase in**

precipitation (and ground ice melt within the freshly thawed active layer).

Lack of long-term monitoring data precludes us from accurate estimation of the current and future freshwater fluxes from partially glacierised terrestrial environments into the coastal waters of the Arctic.

Hydrological data also show that **we can no longer rely on Arctic freshwater forecasting based solely on changes in glacier mass balance** as glacier cover in watersheds vary greatly (from 10% to 70%). In

addition, glacier recession does have an influence on subsurface water stores which now more than ever needs to be acknowledged in surface water hydrology.

2.6. Groundwater contribution, the holy grail of Arctic hydrology

Studies of sub-surface hydrology in Svalbard tend to focus on sub-permafrost groundwater with relatively little attention paid to water flow within the active layer. We know that the groundwater flowpath in areas of continuous permafrost depends on location (geology), type of recharge (glaciers, rainfall, lakes, rivers) hydraulic gradients and water quality (temperature and chemical composition). Water transfers are restricted by ground ice, and the most visible outflows are pingos and springs, with the latter being the most obvious during winter when all other surface discharge is frozen (Orvin 1944; Vtyurin 1994). The two best known groundwater systems in Svalbard are located in Grøndalen (see Demidov et al. 2019) and Adventdalen (see e.g. Hodson et al. 2019, Hodson et al. 2020). Yet, still little is known about the sub-permafrost water fluxes, even though the direction of the movement has been studied (e.g. Booij et al. 1998 or Haldorsen and Heim 1999).

For example, if a catchment has a direct connection to a fjord, seawater intrusions into land can reach even a few kilometres into the land. These intrusions then form saline sub-permafrost aquifers that can result in surface discharge (Demidov et al. unpublished; Hodson et al. 2020). Such cryopegs (or taliks, lenses of salt or brine over cooled water) were encountered under both the Grøndalselva and Adventelva estuaries. Sub-permafrost aquifers are also fed by glacier meltwaters (see Figure 9). These aquifers, however, have a very different chemical signature, as firstly they were created by diluted ice melt and then altered by subsurface migration through valley deposits and saturated by chemical weathering or cryogenic metamorphism (Woo 2012; Demidov et al. 2019; Hodson et al. 2019). Although the chemical signature of groundwater within and under permafrost is relatively easy to study via their surface outflows (see a review of the Arctic region groundwaters by Lecher 2017), using it to estimate water flux produces large errors and uncertainties. Therefore, research usually focuses upon identifying groundwater discharge and their chemical characteristics, while the only continuous discharge measurements of such water in Svalbard were performed by Hodson et al. (2020).

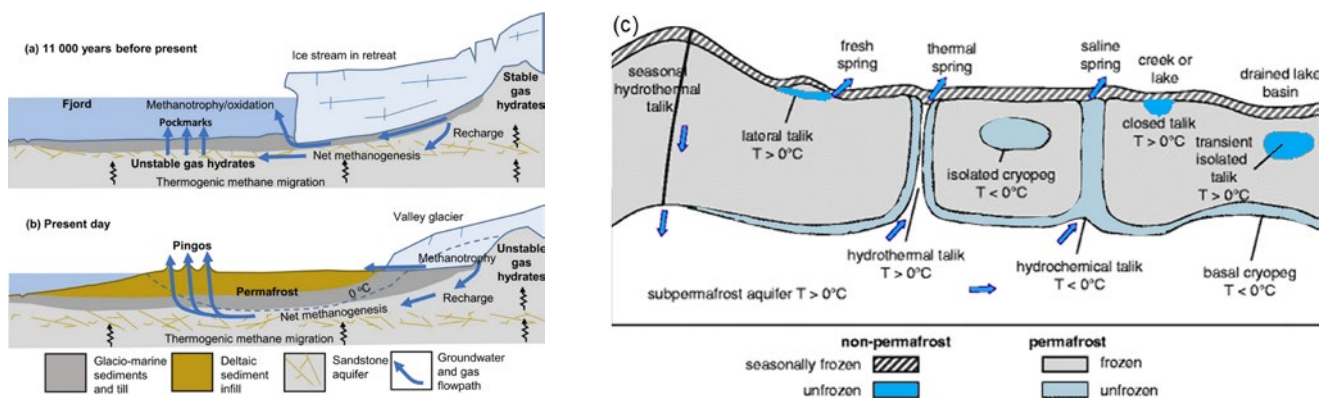


Figure 9: A schematic of sub-permafrost water flowpath in (a, b) glacierised catchments (Hodson et al. 2020) (c) non-glacierised catchments (Woo 2012)

The hydrology of aquifers residing on top of permafrost (in the seasonally frozen active layer) to date has received even less attention (see Cooper et al. 2011), though we know that water from the active layer can discharge in the form of spring or small water seeps anywhere in a valley, estuarine area and beneath the slopes. Surface discharge is usually easier to spot at the end of summer, when all the snow has thawed, glaciers have reduced their melt and the ground has not started freezing yet. As with sub-permafrost groundwaters, active layer hydrology is identified mostly with hydrochemical studies. Its chemical composition is variable, reflecting properties of the sediments it drains.

Even though **we do not directly measure groundwater fluxes in Svalbard**, hydrochemical research shows that **groundwater plays a role in surface runoff** (Figure 10) and the annual formation of the active layer is hydrologically significant (Stäblein 1971). Downward-thawing

rates are initially high, although variations in microtopography and the persistence of patchy snow cover may result in the development of an irregular permafrost table with thawed troughs and frozen ridges, though this irregularity tends to subside as the melt season progresses. The potential for sub-surface water storage and flow in the active layer increases in line with the gradual increase in the depth of the permafrost table, which constitutes the lower boundary layer for water movement (Pecher 1994; Osuch et al. 2019). Sub-surface flow in the active layer may increasingly contribute to proglacial throughputs of runoff, as larger fluxes of water are observed at the surface due to increased glacier melt and increased precipitation. Increased precipitation in the autumn that is following the changing climate also coincides with the deepest active layer, influencing recharge and throughput of the shallow groundwater fluxes. **Yet we know next to nothing about the hydrology of this rapidly changing groundwater system.**

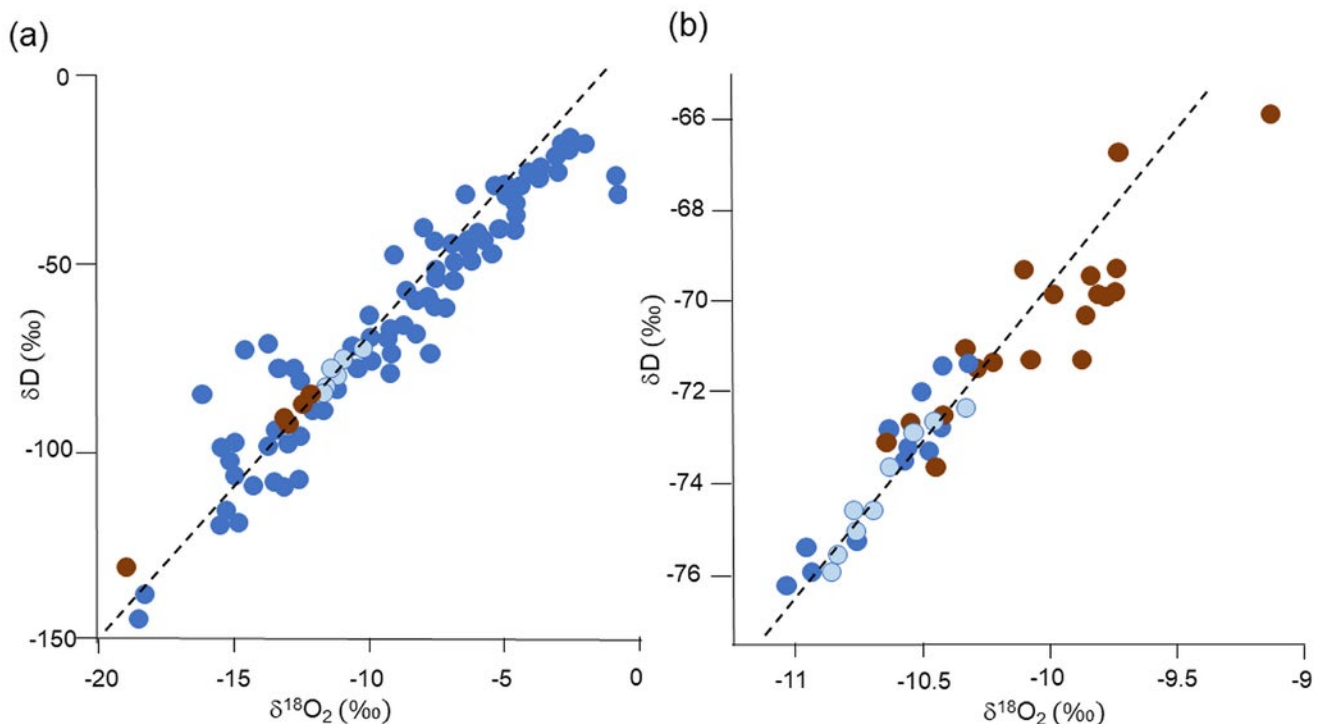


Figure 10 Groundwater contribution to surface runoff. An example of isotopic signature of rainfall (dark blue), river water (light blue) and groundwater (brown) in (a) Grøndalen and (b) Kongressdalen. Dashed lines represent global meteoric water in (a) Barentsburg and meteoric water in (b) (Demidov et al. 2019, Skakun et al. 2020)

3. Connections and synergies with other SESS report chapters

Water is the link that connects all environments; therefore, any changes within those environments (whether atmospheric, terrestrial or marine) will immediately be reflected in changes in the water cycle (i.e. water budget). Hydrological research in the Arctic is challenging, lacks investments and long-term monitoring, yet it is a fantastic bridge that allows us to connect interdisciplinary studies.

For example, this report also includes chapters dedicated to improving our knowledge on snow cover distribution and enhancing snow cover data

collection, thus contributing to minimising errors in the water budget calculations. PASSES ([Salzano et al. 2021](#)) provides a picture of terrestrial photography applications, while SvalSCESIE ([Killie et al. 2021](#)) compares an existing satellite-based, long-term climate data record with the model output for snow water equivalent and in-situ measurements. Lastly, SATMODSNOW ([Malnes et al. 2021](#)) studies the relationships between satellite observations and hydrological snow models and quantifies the difference.

4. Unanswered questions

4.1. Precipitation

As indicated above, one of the most urgent questions concerning Arctic hydrology in the changing climate is related to precipitation. Current observations, as well as most recent predictions, indicate that the amount of rainfall in Svalbard will continue to increase. However, despite the general consensus on the direction of the change, we still do not know the following:

1. How much of that precipitation can be accounted for as snowfall and how much as rainfall?
2. What is the precipitation gradient change with elevation?
3. How we can reliably quantify and monitor winter rainfall (i.e. rain on snow) to provide information on slush flows, as well as water infiltration into ground for rockslides and landslides?
4. How will glacierised catchments across Svalbard respond to increasing precipitation, especially when considering variability in local climate?
5. How flash floods caused by extreme rainfall events will change sediment transport from Arctic catchments? What will be the sediment transport from glacierised and deglaciating

catchments after such events? Focus should be given to changes in bank erosion and increased occurrence of debris slides and debris flows

4.2. Evaporation & Condensation

The rate of evaporation begins to assume significance following the recession of the snowpack, reflecting the increase in air temperatures and the abundance of surface water available for evaporation. However, as the melt season proceeds, the rate of evaporation gradually declines, reflecting the progressive drying out of the ground surface. Observed changes in air temperature and precipitation as well as length of the melting season mean that there is also a dire need for up-to-date measurements of evaporation and condensation. These should be performed across the Arctic following the example from Hornsund, with appreciation of heterogeneity of the meteorological conditions and vegetation across the island.

4.3. Water Storage

Rapid changes in ground temperature, thickening of the active layer and thawing of the permafrost yield several unanswered questions that need to be addressed before we can confidently describe

the Arctic's contribution to the freshening of the Arctic ocean.

What is the glacial contribution to the groundwater system? The linkages between two frozen bodies that are rapidly changing need to be explored. A coupled glacier–groundwater model needs to be developed to investigate the effects of different climate scenarios on freshwater transport into marine environments

What is the capacity of the thickening active layer for water storage and water transfer? Measurements need to be undertaken to help answer questions on groundwater contribution to surface discharge, nutrient flux into terrestrial and coastal areas, and to help answer questions related to risk management of geohazards, such as landslides, erosion or debris flow. In addition, changes to the waterlogged active layer will have an indirect influence upon fluxes of gasses such as carbon dioxide (CO₂) and methane (CH₄)

Finally, we should start addressing the lack of appreciation for modelling of permafrost changes in glacierised catchments, which also needs to include permafrost aggradation due to glacier recession.

4.4. Rethinking water balance in the High Arctic

Given the above, it is unsurprising that the **Arctic hydrology is in a desperate need of a 'facelift'**. Rapid warming shifting the timing of onset of snowmelt and prolonging the meltwater season means that the hydrological year should be redefined. Dramatic changes in precipitation patterns also need to be addressed, and precipitation measurements across a range of elevations should be performed to provide data that correspond to the current climatic conditions. Change in freshwater storage can no longer be assumed negligible, even in glacierised catchments with continuous permafrost. This is because glaciers in Svalbard change their thermal regime from polythermal to cold-based, and so their internal water storage and interaction with groundwaters also change. Furthermore, active layer depth is rapidly increasing as permafrost is thawing. This creates possibilities for new water flowpaths as well as water storage to the next hydrological year. All this has a profound effect upon surface hydrology and all downstream environments, whether terrestrial or marine.

This report shows a **steady decrease in freshwater fluxes from some glacierised catchments of the High Arctic for one or more decades**. However, water fluxes from rainfall-dominated watersheds have been increasing. In order to know the aerial extent of that transition, we must improve hydrological research in Svalbard.

5. Recommendations for the future

We recommend a series of actions deemed necessary to close the water budget for the Norwegian High Arctic. To do so, we suggest the **development of existing sites and the establishment of new supersites for hydrological research**. The main action points are:

Return of long-term hydrological monitoring projects delivering data that are easy to access, as these are vital for providing information on consequences and the speed of changes occurring

as a result of climate warming. The data are also crucial for hydrological modelling in glacierised and deglaciating catchments across the Arctic.

Set up of autonomous meteorological and hydrological monitoring on:

The East coast of Svalbard. Possible locations include catchments advecting water into Agardhbukta (e.g. Væringsdalen or Eistradalen). Locations were chosen based on the relative ease

of access and short distance from Longyearbyen.

In addition, autonomous monitoring should be established in the North of Svalbard (e.g. Svartdalen (Wijdefjorden) or Mosselhalvøya).

A permanent hydrological monitoring station should be re-established in (partially glacierised) Endalen and (non-glacierised) Gruvedalen, as these are the only catchments supplying drinking water to neighbouring Longyearbyen.

Establish a **network of meteorological stations across a range of elevations** at key locations in Svalbard (e.g. Longyeardalen, Hornsund, Ny-Ålesund, as well as the East coast)

Set up time-lapse cameras in the catchments under hydrological monitoring (see above) to allow for discharge monitoring during the beginning of

snowmelt season, when hydro stations are still frozen over and do not provide reliable water discharge data.

Perform measurements of water fluxes **in the active layer** (e.g. via boreholes) in conjunction with already established research on active layer thermal regime changes. These should ideally be undertaken in catchments where long-term hydrological monitoring is already (or will be) established

Conduct **multi-sensor remote sensing studies** in locations that are difficult to access. The versatility of remote sensing means that remote research can now provide information on surface moisture content, ground dynamics, snow water equivalent, ice freeze/thaw cycles and vegetation mapping, thereby delivering new data. It can also improve spatial coverage in catchments that are already under in-situ monitoring.

6. Data availability

Due to a large number of partners and available

data, information is provided in the Appendix 2.

Acknowledgements

This work was supported by the Research Council of Norway, project number 291644, Svalbard Integrated Arctic Earth Observing System – Knowledge Centre, operational phase. The authors kindly thank the Norwegian Water Resources and Energy Directorate (NVE) for supplying the discharge data from Bayelva, Londonelva and De

Geerdalen. They also thank the Norwegian Polar Institute for comments on the 2020 glacier mass balance as well as Dr Lena Rubensdotter (NGU) for providing information on the geomorphology in Adventdalen.

References

AMAP (2017) Snow, Water, Ice and Permafrost in the Arctic (SWIPA) 2017. Arctic Monitoring and Assessment Programme (AMAP), Oslo, Norway. ISBN 978-82-7971-101-8

Bense V, Ferguson G, Kooi H (2009) Evolution of shallow groundwater flow systems in areas of degrading permafrost. *Geophys Res Lett* 36 (22), 1-6. <https://doi.org/10.1029/2009GL039225>

Bense V, Kooi H, Ferguson G, Read T (2012) Permafrost degradation as a control on hydrogeological regime shifts in a warming climate. *J Geophys Res Earth Surf* 117 (Issue F3), 1-18. <https://doi.org/10.1029/2011JF002143>

Booij M, Leijnse A, Haldorsen S, Heim M, Rueslåtten H. (1998) Subpermafrost groundwater modelling in Ny-Ålesund. *Nord Hydrol* 29:385–396.

- Brázdil R., Chmal H., Kida J., Klementowski J., Konečný, M., Pereyma J., Piasecki J., Prošek P., Sobik M., Szczepankiewicz-Szmyrka A. (eds.), 1988. Results of investigations of the Geographical Research Expedition, Spitsbergen 1985. Univerzita Purkyně, Brno: 337 pp.
- Cooper R, Hodgkins R, Wadham J, Tranter M (2002) The hydrology of the proglacial zone of a High Arctic glacier (Finsterwalderbreen, Svalbard): Sub-surface water fluxes and complete water budget. *J Hydrol* 406:88–96.
- Demidov N, Wetterich S, Verkulich S, Ekaykin A, Meyer H, Anisimov M, Shirrmeister L, Demidov V, Hodson AJ (2019) Geochemical signatures of pingo ice and its origin in Grøndalen, west Spitsbergen. *The Cryosphere* 13(11): 3155–3169. <https://doi.org/10.5194/tc-13-3155-2019>
- Elvevold S, Dallmann W, Blomeier D (2007) *Geology of Svalbard*. Norwegian Polar Institute: Grafisk Nord AS, 37.
- Førland EJ, Hanssen-Bauer I, Nordli PØ (1997) Climate statistics and long-term series of temperature and precipitation at Svalbard and Jan Mayen. *Klima* 21/97. Oslo, Norwegian Meteorological Institute.
- Førland EJ, Hanssen-Bauer I (2003) Past and future climate variations in the Norwegian Arctic: Overview and novel analyses. *Polar Res* 22(2):113–124.
- Førland E J, Benestad R, Hanssen-Bauer I, Haugen J E, Skaugen T E (2011) Temperature and precipitation development at Svalbard 1900–2100. *Adv Meteorol* 893790. <https://doi.org/10.1155/2011/893790>
- Geological map Svalbard 1:100 000 (1991) Spitsbergen Norsk Polarinstitutt Temakart nr. 16.
- Hagen JO, Lefauconnier B (1995) Reconstructed runoff from the High Arctic basin Bayelva in Svalbard based on mass balance measurements. *Nord Hydrol* 26:285–296.
- Hagen JO, Liestøl O, Roland E, Jørgensen T (1993) *Glacier atlas of Svalbard and Jan Mayen*. Nor Polarinst Medd 129. Oslo, Norwegian Polar Institute
- Haldorsen S, Heim M (1999) An arctic groundwater system and its dependence upon climatic change: an example from Svalbard. *Permafrost Process* 10:137–149.
- Hanssen-Bauer I, Kristensen Solås M, Steffensen EL (1990) *The climate of Spitsbergen*. Oslo, Norsk Meteorologiske Institutt Rapport, 39/90
- Harland WB (1997) *The geology of Svalbard*. The Geological Society, London, ISBN 1-897799-93-4
- Hjelle A (1993) *The geology of Svalbard*. Polarhåndbook 7. Oslo, Norwegian Polar Institute ISBN 13: 9788276660579
- Hock R (2003) Temperature index melt modelling in mountain areas. *J Hydrol* 282:104–115, doi:[10.1016/S0022-1694\(03\)00257-9](https://doi.org/10.1016/S0022-1694(03)00257-9).
- Hodgkins R, Cooper R, Wadham J, Tranter M (2005) Inter-annual variability in the spatial distribution of winter accumulation at a high-Arctic glacier (Finsterwalderbreen, Svalbard), and its relationship with topography. *Ann Glaciol* 42:243–248.
- Hodgkins R, Cooper R, Wadham J, Tranter M (2009) The hydrology of the proglacial zone of a High Arctic glacier (Finsterwalderbreen, Svalbard): atmospheric and surface water fluxes. *J Hydrol* 378:150–160.
- Hodson A, Nowak A, Redeker K, Holmlund ES, Christiansen HH, Turchyn AV (2019) Seasonal dynamics of methane and carbon dioxide evasion from an open system pingo: Lagoon pingo, Svalbard. *Front Earth Sci* 7:30 <https://doi.org/10.3389/feart.2019.00030>
- Hodson A, Nowak A, Senger K, Redeker K, Christiansen HH, Jessen S, Hornum T, Betlem P, Thornton SF, Turchyn AV, Olausen S, Marca A (2020) Open system pingos as hotspots for sub-permafrost methane emission in Svalbard. *Cryosphere Discuss.* 14, 3829–3842 <https://doi.org/10.5194/tc-2020-11>
- Hodson A, Tranter M, Gurnell A, Clark M, Hagen JO (2002) The hydrochemistry of Bayelva, a High Arctic proglacial stream in Svalbard. *J Hydrol* 257:91114
- Humlum O, Instanes A, Sollid JL (2003) Permafrost in Svalbard: a review of research history, climatic background and engineering challenges. *Pol Res* 22(2):191–215.
- Huss M, Hock R (2018) Global-scale hydrological response to future glacier mass loss. *Nat Clim Change Lett* 8:135–140. doi: [10.1038/s41558-017-0049-x](https://doi.org/10.1038/s41558-017-0049-x)
- Ignatiuk D, Migala K (2013) Werenskiöld glacier. In: Zwolinski Z, Kostrzewski A, Pulina M (eds) *Ancient and modern geosystems of Spitsbergen*. Poznan, Poland: Association of Polish Geomorphologists, 96–99.
- IPCC, 2019: *IPCC Special Report on the Ocean and Cryosphere in a Changing Climate* [H.-O. Pörtner, D.C. Roberts, V. Masson-Delmotte, P. Zhai, M. Tignor, E. Poloczanska, K. Mintenbeck, A. Alegría, M. Nicolai, A. Okem, J. Petzold, B. Rama, N.M. Weyer (eds) In press
- Jaedicke C, Kern MA, Gauer P, Baillifard MA, Platzer K (2008) Chute experiments on slushflow dynamics. *Cold Reg Sci Technol* 51(2–3):156–167. <https://doi.org/10.1016/j.coldregions.2007.03.011>
- Killie MA, Aaboe S, Isaksen K, Van Pelt W, Pedersen ÅØ, Luks B (2021) Svalbard snow and sea-ice cover: comparing satellite data, on-site measurements, and modelling results In: Moreno-Ibáñez et al (eds) *SESS report 2020*, Svalbard. Integrated Arctic Earth Observing System, Longyearbyen, [pp 220-235. https://doi.org/10.5281/zenodo.4293804](https://doi.org/10.5281/zenodo.4293804)
- Killingtveit Å, Pettersson LE, Sand K (1994) Water balance studies at Spitsbergen, Svalbard. In: Sand K, Killingtveit Å (eds) *Proceedings of the 10th International Northern Research Basins Symposium and Workshop*, Norway. SINTEF Rep. 22 A96415. Trondheim, Norwegian Institute of Technology, 77–94
- Killingtveit Å, Pettersson LE, Sand K (2003) Water balance investigations in Svalbard. *Polar Res* 22:161174

- King MD, Howat IM, Candela SG, Noh MJ, Jeong S, Noel MR, van den Broeke MR, Wouters B, Negrete A (2020) Dynamic ice loss from the Greenland Ice Sheet driven by sustained glacier retreat. *Commun Earth Environ* 1:1. <https://doi.org/10.1038/s43247-020-0001-2>
- Lecher A (2017) Groundwater discharge in the Arctic: A review of studies and implications for biogeochemistry. *Hydrology* 4:41. <https://doi.org/10.3390/hydrology4030041>
- Lewkowicz AG, Way RG (2019) Extremes of summer climate trigger thousands of thermokarst landslides in a High Arctic environment. *Nature Comm* 10:1329. <https://doi.org/10.1038/s41467-019-09314-7>
- Majchrowska E, Ignatiuk D, Jania J, Marszałek H, Wasik M (2015) Seasonal and interannual variability in runoff from the Werenskioldbreen catchment, Spitsbergen. *Pol Polar Res* 36:197–224.
- Malnes E, Vickers H, Karlsen SR, Saloranta T, Killie MA, Van Pelt W, Pohjola V, Zhang J, Stendardi L, Notarnicola C (2021) Satellite and modelling based snow season time series for Svalbard: Inter-comparisons and assessment of accuracy. In: Moreno-Ibáñez et al (eds) SESS report 2020, Svalbard Integrated Arctic Earth Observing System, Longyearbyen, pp 202–219. <https://doi.org/10.5281/zenodo.4294072>
- NCCS 2019 Hanssen-Bauer I E, Førland J, Hisdal H, Mayer S, Sandø AB, Sorteberg A. (eds), 2019. Climate in Svalbard 2100 - A knowledge base for climate adaptation. Rapport 1/2019, Norwegian Environment Agency (Miljødirektoratet). ISSN 2387-3027
- Nordli Ø, Przybylak R, Ogilvie, AE, Isaksen K 2014. Long-term temperature trends and variability on Spitsbergen: The extended Svalbard airport temperature series, 1898–2012. *Polar Res* 33:21349, <https://doi.org/10.3402/polar.v33.21349>
- Nowak-Żwierz A (2013) Hydrological and biogeochemical response of a High Arctic glacierised catchment to climate change. A long-term study from Bayelva watershed, Svalbard. PhD thesis, University of Sheffield. UK
- Nowak A, Hodson A (2013) Hydrological response of a High Arctic catchment to changing climate over the past 35 years: a case study of Bayelva watershed, Svalbard. *Polar Res* 2013(32):19691. <https://doi.org/10.3402/polar.v32i0.19691>
- Nowak A, Hodson A (2014) Changes in meltwater chemistry over a 20-year period following a thermal regime switch from polythermal to cold-based glaciation at Austre Brøggerbreen, Svalbard. *Polar Res* 33:1. <https://doi.org/10.3402/polar.v33.22779>
- Orvin AK (1934) Geology of the Kings Bay region, Spitsbergen. *Skrifter om Svalbard og Ishavet* 57. Oslo, Norway's Svalbard and Arctic Ocean Survey (Norwegian Polar Institute).
- Orvin AK (1944) Litt om kilder på Svalbard. *Norsk Geografisk Tidsskrift* 1:16–38.
- Osuch M, Wawrzyniak T (2017a) Inter- and intra-annual changes of air temperature and precipitation in western Spitsbergen. *Int J Climatol* 37:3082–3097. <https://doi.org/10.1002/joc.4901>
- Osuch M, Wawrzyniak T (2017b) Variations and changes in snow depth at meteorological stations Barentsburg and Hornsund (Spitsbergen). *Ann Glaciol* 58 (75), 11–20.
- Osuch M, Wawrzyniak T, Nawrot A. 2019. Diagnosis of the hydrology of a small Arctic permafrost catchment using HBV conceptual rainfall-runoff model. *Hydrol Res* 50.2, 459–478.
- Pecher K (1994) Hydrochemical analysis of spatial and temporal variations of solute composition in surface and subsurface waters of a high arctic catchment. *Catena* 21:305–327
- Romashova KV, Chernov RA, Vasilevich II (2019) Study of the glacial flow of rivers in the Grønfjord bay basin (Western Svalbard). *Arct Antarct Res* 65(1):34–45. (in Russian) <https://doi.org/10.30758/0555-2648-2019-65-1-34-45>
- Salzano R, Aalstad K, Boldrini E, Gallet JC, Kępski D, Luks B, Nilsen L, Salvatori R, Westermann S (2021 a) Terrestrial photography applications on snow cover in Svalbard. In: Moreno-Ibáñez et al (eds) SESS report 2020, Svalbard Integrated Arctic Earth Observing System, Longyearbyen, pp 236–251. <https://doi.org/10.5281/zenodo.4294084>
- Schuler TV, Kohler J, Elagina N, Hagen JOM, Hodson AJ, Jania JA, Kääh AM, Luks B, Matecki J, Moholdt G, Pohjola VA, Sobota I, Van Pelt WJJ (2020) Reconciling Svalbard glacier mass balance. *Front Earth Sci* 8:156. <https://doi.org/10.3389/feart.2020.00156>
- Sen PK (1968) Estimates of the regression coefficient based on Kendall's tau. *J Am Stat Assoc* 63:1379–1389. <https://doi.org/10.2307/2285891>.
- Retelle M, Christiansen HH, Hodson A, Nikulina A, Osuch M, Poleshuk K, Romashova K, Roof S, Rouyet L, Strand SM, Vasilevich I, Wawrzyniak T (2020) Environmental Monitoring in the Kapp-Line- Grønfjorden region. In: Van den Heuvel et al (eds) SESS report 2019, Svalbard Integrated Arctic Earth Observing System, Longyearbyen, pp 84–107. https://sios-svalbard.org/SESS_Issue2
- Sobota I, Nowak M, Weckwerth P, 2016. Long-term changes of glaciers in northwestern Spitsbergen. *Glob Planet Change* 144:182–197.
- Sobota I, Arażny A, Barcikowski A, Birkenmajer K, Grześ M, Gugnacka-Fiedor W, Lankauf RK, Plichta W, Przybylak J, Zubeł P (2013) Geographical environment in the vicinity of the Nicolaus Copernicus University Polar Station – Kafføyra. In: Zwoliński Z, Kostrzewski A, Pulina M (eds.). *Dawne i współczesne geoekosystemy Spitsbergenu: polskie badania geomorfologiczne = Ancient and modern geoecosystems of Spitsbergen: Polish geomorphological research*. Bogucki Wydawnictwo Naukowe, Poznań:181–204.
- Stäblein G (1971) Der polare Permafrost und die Auftauschicht in Svalbard. *Polarforschung* 41:112–120.
- Skakun AA, Chikhachev KB, Ekaykin AA, Kozachek AV, Vladimirova DO, Veres AN, Verkulich SR, Sidorova OR, Demidov NE (2020) Stable isotopic composition of atmospheric precipitation and natural waters in the vicinity of Barentsburg (Svalbard). *Ice and Snow* 60(3):379–394. (In Russian). <https://doi.org/10.31857/S2076673420030046>

- Sidorova OR, Tarasov GV, Verkulich SR, Chernov RA (2019) Surface ablation variability of mountain glaciers of West Spitsbergen. *Arct Antarct Res* 65(4):438–448. <https://doi.org/10.30758/0555-2648-2019-65-4-438-448>
- Sund M (2008) Polar hydrology. Norwegian water resources and Energy Directorate's work in Svalbard. NVE Report 2. Oslo, Norwegian Water Resources and Energy Directorate.
- Szafraniec E, Dobinski W (2020) Deglaciation rate of selected nunataks in Spitsbergen, Svalbard – Potential for permafrost expansion above the glacial environment. *Geosciences* 10(5):202. <https://doi.org/10.3390/geosciences10050202>
- Terekhov AV, Tarasov GV, Sidorova OR, Demidov VE Anisimov MA, Verkulich SR (2020) Estimation of mass balance of Aldegondabreen (Spitsbergen) in 2015–2018 based on ArcticDEM, geodetic and glaciological measurements. *Ice and Snow* 60(2):192–200. <https://doi.org/10.31857/S207667342002003>
- Van Pelt W, Pohjola V, Pettersson R, Marchenko S, Kohler J, Luks B, Hagen JO, Schuler T, Dunse T, Noel B, Reijmer C (2019) A long-term dataset of climatic mass balance, snow conditions, and runoff in Svalbard (1957–2018). *The Cryosphere*, 13, 2259–2280. <https://doi.org/10.5194/tc-13-2259-2019>
- Vikhamar-Schuler D, Isaksen K, Haugen JE, Tømmervik H, Luks B, Schuler TV, Bjerke JW (2016) Changes in winter warming events in the Nordic Arctic region. *J Climat* 29:6223–6244. <https://doi.org/10.1175/JCLI-D-15-0763.1>
- Verkulich S, Zazovskaya E, Pushina Z, Savelieva L, Soloveva D, Demidov N, Shishkov V, Dercon G (2018) The postglacial environmental changes in vicinity of the Barentsburg settlement (West Spitsbergen). EGU General Assembly, Vienna, Austria, 8-13 April 2018. EGU 2018-7729.
- Vtyurin B I (1994) The contemporary periglacial environment in the polar regions. *Polar Geogr* 18(1):44-62. <https://doi.org/10.1080/10889379409377530>
- Wawrzyniak T, Osuch M, Nawrot A, Napiórkowski JJ (2017) Run-off modelling in an Arctic unglaciated catchment (Fuglebekken, Spitsbergen). *Ann Glaciol* doi: 10.1017/aog.2017.8.
- Wawrzyniak T, Osuch M (2020) 40 years High Arctic climatological dataset of the Polish Polar Station Hornsund (SW Spitsbergen, Svalbard). *Earth Syst Sci Data* 12:805–815, <https://doi.org/10.5194/essd-12-805-2020>
- Woo M-K (2012) *Permafrost hydrology*. Springer, Berlin, Heidelberg. ISBN: 978-3-642-23461-3. <https://doi.org/10.1007/978-3-642-23462-0>
- Ødegård RS, Hagen JO, Hamran S (1997) Comparison of radio echosounding (30 MHz–1000 MHz) and high-resolution borehole temperature measurements at Finsterwalderbreen, southern Spitsbergen, Svalbard. *Ann Glaciol* 24:262–267.

Appendix 1

Description of sites where hydrological monitoring is taking place on long-term or semi long-term basis. See Figure 1 for locations.

Site	Site description	Hydrological regime	Institute performing monitoring
Hornsund - Fuglebeken	<p>A deglaciated catchment with an area of 1.27 km². Heterogenous land cover and topography. Elevation range 4–522 m a.s.l. Slopes covered with washed rubble sediments, solifluction tongues, rock streams, alluvial cones and bare solid rock of Hecla Hoek geological formation (Harland 1997). Below the slopes, marine terraces covered with sea gravel are covered by diverse tundra vegetation.</p> <p>Close to the eastern boundary of the catchment is the lateral moraine of Hansbreen. The ground has a continuous permafrost layer down to more than 100 m depth (Humlum et al. 2003).</p> <p>Mean annual air temp: -3.7 °C (1979–2019), the warmest month: July (avg. 4.6 °C); the coldest month: March (avg. -10.2 °C). The highest air temperature recorded: 16.5 °C on 25th July 2020. Mean annual precipitation: 463 mm. Snow cover is present approx. 250 days/year. Snow depth 0.3-2.0 m (Wawrzyniak and Osuch 2020).</p>	Restricted to melt season only (usually May–October). Snowmelt rainfall, ground ice melt	Institute of Geophysics, Polish Academy of Science, Poland
Nottinghambukta - Werenskioldbreen	<p>Werenskioldbreen is a land-terminating valley-type polythermal glacier situated in the Wedel-Jarlsberg Land. The glacier has a catchment area of 44.1 km² (glaciated in 61%). Maximum elevation of the firn field is 650 m a.s.l., (Ignatiuk and Migala 2013). Outflows from the Werenskioldbreen take the form of karst springs, geysers and a type Røthlisberberger (R) subglacial outflow channel. The main outflow, located in the northern part of the glacier, originates in an ice gate and creates the Kvislaelva (~80% of the total water yield). In the proglacial zone, tributary rivers originating from the glacier front join and form Breeelva, which drains into the Greenland Sea. The average annual runoff is approx. 80±14x10⁶ m³, which is equivalent to an 1800 mm layer of water from the catchment surface (Majchrowska et al. 2015).</p>	Restricted to melt season only (usually May–October). Snowmelt rainfall, ground ice melt	University of Silesia and University of Wrocław, Poland
Van Keulenfjorden - Finsterwalderbreen	<p>Finsterwalderbreen, is located at 77° 31' N, 15° 19' E on the southern shore of Van Keulenfjorden, southern Spitsbergen. The glacier itself is 12 km long, north facing and flows to the coast from a maximum elevation of 1065 m a.s.l. It is up to 200 m thick, and has a polythermal temperature structure, with a 25–170 m thick cold surface layer, a warm firn accumulation zone and a bed that is mostly temperate, apart from limited areas at the margins (Ødegård et al. 1997). The catchment is mostly devoid of vegetation, except above the most recent glacial trimline and on terminal moraines delimiting the proglacial zone, where a sparse Arctic flora survives. The bedrock geology is diverse, comprising Precambrian basement and Carboniferous through Cretaceous sedimentary units (Hjelle 1993). The mean annual air temperature at 35 m a.s.l. is -3.9 °C, and mean monthly air temperatures are only positive during the summer, although even then they remain <6.0 °C; annual precipitation is in the 180–440 mm w.e. range, with the bulk being delivered as snow during the winter months (Hanssen-Bauer et al. 1990).</p>	Restricted to melt season only (usually May–October). Snowmelt rainfall, ground ice melt	Loughborough University, The United Kingdom

Grønfjorden - Grøndalselva	<p>Glacierised catchment with an area of 98 km², (glacier area–7.4 km²). Elevation range 0–840 m a.s.l. Grøndalen is a trough valley with the main river Grøndalselva, which has 23.5 km. The river has a flat wide valley. Cretaceous deposits protrude on the surface in the delta part of the river. A group of seven large pingos have developed in the central part of the valley (Demidov et al. 2019). Grøndalselva is fed by many tributaries, which collect meltwater discharge from small hanging glaciers. Two larger glaciers, Tavlebreen and Passfjellbreen, as well as their terminal moraines lie in the upper valley part. Glacier runoff made up to 24% of total river discharge in 2017–2018 (Romashova et al. 2019). The permafrost thickness exceeds 100 m (Demidov et al. 2019). Snow cover height (2002–2019) 10–194 cm (mean 58 cm). 50% of total annual runoff falls in June.</p>	Restricted to melt season only (usually May–October). Snowmelt rainfall, ground ice melt, groundwater	The Arctic and Antarctic Research Institute (AARI), St. Petersburg, Russia
Grønfjorden - Aldegondabreen	<p>Glacierised catchment with an area of 9.4 km², (glacier area–5.7 km²). River length–2.6 km. Elevation range 0–720 m. Over the last decades, Aldegondabreen lost more than a half of its ice volume. (Terekhov et al. 2020). Average annual ablation rate on Aldegondabreen was 1.947 m w. e. (or 10.2 million m³) in 2016–2018 (Sidorova et al. 2019), which comprised 47% of the water discharge of the river (Romashova et al. 2019). The drainage system of the Aldegondabreen consists of three tributaries. The streams form a braided system in the moraine area and merge into Aldegondaelva, discharging into Grønfjorden. The river flows through a valley formed by moraine deposits and sandstones with coal seams, shales and some limestones (Elvevold et al. 2007). A small delta with unstable position is formed by the deposited sediments. There are several small lakes (less than 100 m²) in the catchment area formed by the icemelt groundwater (Romashova et al. 2019). Snow depth on the glacier (2002–2019) was 78–238 cm (mean 157 cm). 30% of annual runoff falls in July.</p>	Restricted to melt season only (usually May–October). Snowmelt rainfall, ground ice melt	
Grønfjorden - Kongresselva	<p>Non-glacierised catchment area 10.5 km². River length–3.9 km. Elevation range 0–500m. The river flows out of the karst lake Kongress. The catchment area is composed of ancient metamorphosed and sedimentary rocks of the Precambrian, Upper Paleozoic and Mesozoic ages. Ice-wedged polygons and rock streams are common features of the hill slopes in the valley, while the vegetation is sparse on the slopes of bare rock or rocks covered by algae and lichen crusts and develops mostly in depressions. Several tributaries fed by precipitation and underground water contribute to the river flow (Skakun et al. 2020). Snow depth (2016–2019) 10 cm–196 cm (mean 66 cm). 30% of annual runoff falls in June.</p>	Restricted to melt season only (usually May–October). Snowmelt rainfall, ground ice melt	
Adventfjorden - Adventdalen	<p>Partially glacierised catchment with an area of 500 km². Elevation range 0–1130m a.s.l. Adventdalen is a large U-shaped valley approx. 30 km long and approx. 4 km wide. The main river flowing through it, Adventelva, is extremely braided and flows into Adventfjorden that then connects to Isfjorden. Adventelva collects runoff from several glacierised valleys with different types of thermal regime. Glacially derived freshwater carries a high sediment load. Some of the sediment is also deposited at the valley bottom, creating a fluviially active region. During winter, the river freezes to the bottom, and the valley is covered in a thin layer of snow due to prevailing strong easterly winds.</p> <p>The area is underlain by a continuous permafrost ranging from 100 m to 500 m (Humlum et al. 2003). The valley also contains alluvial fans, extensive aeolian deposits in the central part of the valley, marine terraces, pingos (both open and closed system) and rock glaciers. The geomorphology around the valley is dominated by mountain plateaus covered in extensive blockfields and ice wedge polygons and other periglacial features in the valley bottom. The bedrock geology of the catchment mainly consists of sedimentary rocks, while the unconsolidated sediments are dominated by different slope deposits and glacio-fluvial deposits (personal communication with L Rubensdotter).</p>	Restricted to melt season only (usually May–October). Snowmelt, rainfall, ground ice melt	The University Centre in Svalbard (UNIS), Department of Arctic Geology, Norway
Sassenfjorden - De Geerdalen	<p>Glacierized catchment, area–79.1 km², of which 10% is glacier covered. Includes several glaciers. The monitoring station is located in a narrow gorge in part of a waterfall with a stable rock profile. Meteorological measurements were carried out for a few years in the early 1990's as part of the first water balance studies used to estimate precipitation-elevation gradients (Killingtveit et al. 1994)</p>	Restricted to melt season only (usually May–October). Snowmelt, rainfall, ground ice melt	The Norwegian Water Resources and Energy Directorate (NVE), Norway

Petuniabukta	Small scale catchments with different level of glacier cover from 0 to approx. 60%. Elevation ranges from 0 to 935 m a.s.l. The highest point is the Pyramiden mountain. The region is characterised by rather continental climate with low winter temperatures and high summer temperatures and generally low precipitation (around 400 mm per year). Local climate is also affected by long duration of sea ice (usually November–June). This has resulted in low level of glacier coverage, especially in the western part (Dickson land), where even large catchments do not have glaciers.	Restricted to melt season only (usually May–October). Snowmelt, rainfall, ground ice melt	The Polar Geo-Lab, Masaryk University, Czech Republic and Adam Mickiewicz University, Poland
Kaffiøyra - Waldemarbreen	A glacierised catchment, area approx. 16km ² , 16% of which is occupied by a polythermal valley glacier Waldemarbreen. Elevation range 0–770 m a.s.l. In the north and east, it borders the Prins Heinrichfjella ridge (500–770 m a.s.l.) and in the south Gråfjellet (300–350 m). The hydrological network in the region consists of multiple glacier-fed braided rivers covering up to 40 km ² . The monitoring station on Waldemarelva (approx. 5.5 km long) is in the upper section of the river, close to the moraines, where the water flows onto the outwash plain. Between 1997 and 2019, the average discharge was 0.9 m ³ /s and ranged from 0.5 to 1.4 m ³ /s. Waldemarbreen consists of two distinct parts, separated by a medial moraine. It is approximately 1 km long and 600 m wide with an area of 2.4 km ² . The mean annual mass balance of Waldemarbreen in 1996–2019 was -0.84 m w.e. The only positive year was 1996 (+0.02 m w.e.). From the time of the maximum advance, Waldemarbreen decreased by c. 35% (Sobota et al. 2013)	Restricted to melt season only (usually May–October). Glacier melt, Snowmelt, Rainfall, Ground ice melt	The Nicolaus Copernicus University in Torun, Faculty of Earth Sciences and Spatial Management, Polar Research Center, Poland
Kongsfjorden-Bayelva	A glacierised catchment, area–approx.32 km ² , 50% of which is occupied by cold-based valley glaciers. Elevation range 4–742 m a.s.l. The southern and eastern part of the watershed is underlain by red sandstones, quartzite and phyllite, while the northern and western areas are underlain by sedimentary rocks, such as sandstone, shale, dolomite and limestone (Orvin 1934; Hjelle 1993). The area of the catchment is almost entirely underlain by permafrost with a seasonal active layer measuring from 0.5 to 1.5 m (Killingtveit 2004).	Restricted to melt season only (usually May–October). Glacier melt, Snowmelt, Rainfall, Ground ice melt	The Norwegian Water Resources and Energy Directorate (NVE), Norway
Kongsfjorden-Londonelva	A small de-glacierised catchment, area–0.7 km ² , located on Blomstrandøya (a small island in Kongsfjorden) The elevation ranges from 15 to 149 m a.s.l. It is the only catchment under long-term monitoring that is entirely underlain by carbonate rocks (karst).	Restricted to melt season only (usually May–October). Snowmelt rainfall, ground ice melt	

Appendix 2

Data Sources

Dataset	Parameters	Period	Location or area	Metadata / Data access (URL, doi)	Data provider, reference
1. Meteorological 2. Hydrological	1. Mean daily air temperature, daily sum of precipitation and PET 2. Water discharge	1. 1979–2019 2. 2014–2019 (measured)	Hornsund	SIOS data access portal: https://bit.ly/3mn1WAJ SIOS data access portal: https://bit.ly/2Kw49fV	IG PAS, Tomasz Wawrzyniak tomasz@igf.edu.pl
Hydro-meteorological	Mean daily air temperature, daily sum of precipitation and mean daily flow	1970–1974, 1979, 1980, 1983, 1986, 1988, 1998, 2007–2013, 2017–2020	Nottinghambukta (Werenskioldbreen)	Polish Polar DataBase of the Centre for Polar Studies, University of Silesia, http://ppdb.us.edu.pl/geonetwork/ SIOS data access portal: https://bit.ly/2KA2dTJ	University of Silesia, Centre for Polar Studies, Poland, Elżbieta Łępkowska elzbieta.majchrowska@us.edu.pl
Hydro-meteorological	Winter balance, summer balance, air temperature, relative humidity, wind speed, global and net radiation, precipitation, runoff and flow and hydraulic head in proglacial subsurface	1999–2000	Van Keulenfjorden	SIOS data access portal: https://bit.ly/37c0AUZ	Richard Hodgkins, Loughborough University, United Kingdom r.hodgkins@lboro.ac.uk
Hydrological model	Flow-recession analyses and linear-reservoir simulation of runoff time series	1999–2000	Van Keulenfjorden	SIOS data access portal: https://bit.ly/2KKDgFn	Richard Hodgkins, Loughborough University, United Kingdom r.hodgkins@lboro.ac.uk
Hydrological	Mean snow cover depth, density of the snow cover, snow water equivalent, mean daily discharge, and chemical composition	2002–2019	Grøn fjorden	Submitted to the PANGAEA repository	Arctic and Antarctic Research Institute, Russia Rae-s@aari.ru , hydrology2@aari.ru
Hydrological model and meteorological data	1. Water discharge 2. Air temperature and precipitation 3. Active layer temp. 4. Permafrost temp.	1. 1991–2019 2. 1989–ongoing 3. 2000–ongoing 4. 2008–ongoing	Adventdalen	1. Metadata will be made available in the SIOS data portal in Q1 of 2021 2. Adventdalen: SIOS data access portal: https://bit.ly/37gFLb4 Svalbard Airport https://www.eklima.met.no 3. https://www2.gwu.edu/~calm/data/north.htm 4. http://gtnpdatabase.org/boreholes and https://geo.ngu.no/kart/permafrost_svalbard/	Hydrological data: Aga Nowak, the University Centre in Svalbard aga.nowak@unis.no Active layer: CALM Permafrost: Global Terrestrial Network for Permafrost (GTN-P)

Dataset	Parameters	Period	Location or area	Metadata / Data access (URL, doi)	Data provider, reference
Hydrological	Water discharge	1.1992–ongoing 2.1991–ongoing	1.Londonelva 2.De Geerdalen	Personal communication	The Norwegian Water Resources and Energy Directorate
Hydrological	Daily discharge	1. 2011–2014 2. 2001–2014	Petuniabukta	1. SIOS data access portal: https://bit.ly/2KLZ5V5 2. Personal communication	1. Polar Geo-Lab, Masaryk University, Czech Republic 2. Adam Mickiewicz University, Poznan, Poland
Hydrological and meteorological	1. Meteorological conditions 2. Glacier mass balance (part of WGMS) 3. Water discharge 4. Permafrost and active layer thickness (part of CALM program)	1.1975–ongoing 2.1996–ongoing 3.1970's (sporadic), 1996–ongoing 4.1996–ongoing	Kafføyra	1. Personal communication 2. https://wgms.ch/data_exploration/ 3. Personal communication 4. https://www2.gwu.edu/~calm/data/north.htm	The Polar Research Center, Nicolaus Copernicus University, Ireneusz Sobota irso@umk.pl CALM
Hydrological	1. Glaciological 2. Hydrological 3. Water temp. 4. Conductivity: 5. Sediments	1.1963–ongoing 2.1974–1978, 1989–ongoing 3.1991–ongoing 4.2004–ongoing 5.1989–ongoing	Bayelva	1. https://data.polar.no/dataset/ad6c4c5a-e926-11e2-b06b-005056ad0004 2-5. Personal communication	1. The Norwegian Polar Institute 2-5. The Norwegian Water Resources and Energy Directorate
Meteorological	Mean daily air temperature and precipitation	1967–ongoing	Kongsfjorden Svalbard Airport	https://www.eklima.met.no	The Norwegian Meteorological Institute

Satellite and modelling based snow season time series for Svalbard: Inter-comparisons and assessment of accuracy (SATMODSNOW)

Eirik Malnes¹, Hannah Vickers¹, Stein Rune Karlsen¹, Tuomo Saloranta², Mari Anne Killie³, Ward Van Pelt⁴, Veijo Pohjola⁴, Jie Zhang⁴, Laura Stendardi⁵, and Claudia Notarnicola⁵

1 NORCE Norwegian Research Centre, Bergen, Norway

2 The Norwegian Water Resources and Energy Directorate (NVE), 0368 Oslo, Norway

3 The Norwegian Meteorological Institute, 0371 Oslo, Norway

4 Department of Earth Sciences, Uppsala University, Uppsala, Sweden

5 Eurac Research, Institute for Earth Observation, Bolzano, Italy

Corresponding author: Eirik Malnes, eima@norceresearch.no

ORCID number: 0000-0001-9824-9696

Keywords: Snow, remote sensing, modelling, snow cover, snow water equivalent

DOI: <https://doi.org/10.5281/zenodo.4294072>

1. Introduction

Consistent long-term datasets on snow cover and snow depth/snow water equivalent over Svalbard are scarce and affected by great uncertainties. Remote sensing provides a good platform for large-scale snow monitoring. Due to the scarcity of synoptic stations that measure snow (particularly before 2008) and lack of suitable satellite data, models of snow cover and associated parameters can be an alternative source of data. However, the reliability of snow models is often questionable since the input data used are predominantly based on modelling assumptions and large-scale numerical reanalysis. In this study, currently available models are reviewed and snow model products are compared with remote sensing datasets by evaluating their overall performance for the part of Svalbard where seasonal snow exists.

The following objectives are specifically addressed:

- To identify years/periods where models and Earth Observation (EO) datasets differ significantly
- To identify areas where models and EO datasets differ significantly
- To cross-compare EO datasets at variable scales (AVHRR, MODIS, Sentinel-2) and suggest methods for how newer high-resolution data can be used in combination with moderate or low-resolution data to construct high resolution and long timeseries datasets by making corrections to earlier datasets based on their sensor resolution bias

2. Overview of existing knowledge

This section gives an overview of the datasets used in this study with emphasis on the periglacial landscape in Svalbard (i.e., the non-glaciated land in Svalbard where seasonal snow exists). Table 1 provides an overview of all datasets used in this project. Table 2 contains more information on the details in the different datasets used.

2.1. Satellite data

Remote sensing satellite data have been available since 1978. The earliest satellites generally had coarse resolution except for Landsat.

2.1.1. MODIS

Optical data from the Moderate Resolution Imaging Spectroradiometer (MODIS) onboard Terra and Aqua satellites have been available since 2000. A 20-year snow cover fraction dataset for Svalbard based on the NASA MOD10A1-product (Hall et al., 2002) from the MODIS Terra satellite has been described by Vickers et al. (2020). The MOD10A1-product uses the spectral band 4 (visible light)

and band 6 (short wave infrared) to estimate the normalized differential snow index (NDSI) defined by the relation $NDSI = (band4 - band6) / (band4 + band6)$. The snow cover fraction (SCF) as a percentage is then estimated using the relation $SCF = (0.06 + 1.21NDSI) \times 100$. In addition, cloud cover is detected and masked out. In Svalbard, the polar night period is present from mid-October to mid-February. Since MODIS is an optical sensor, there is no data coverage during the dark period and the MOD10A1 product is only provided from March 1 to November 1. During the polar night, SCF is set to 100 %. The NORCE-derived product provides SCF for the entire periglacial landscape in Svalbard as a temporally interpolated product at daily intervals and 500 m resolution. This is a compromise between the 250 m resolution for the visual channels of MODIS, and the infra-red channel used for cloud discrimination. Since MODIS has moderate spatial resolution and excellent temporal overlap with the other satellite and modelled data products in this study, the MODIS dataset is used throughout this SESS report as a baseline for comparisons.

2.1.2. AVHRR

The Advanced Very High Resolution Radiometer (AVHRR) instrument has flown onboard polar orbiting satellites since the late 1970s. The instrument has approximately 1 km resolution, but only data at a reduced effective resolution of approximately 4 km is permanently archived and available with global coverage. From the AVHRR Global Area Coverage (GAC) data, a fundamental climate data record (FCDR) for radiances and brightness temperatures has been made available by the EUMETSAT Climate Monitoring Satellite Application Facility (CM SAF). The current release 'CLARA-A2' covers 1982–2015 (Karlsson et al., 2017).

Using the probabilistic snow cover algorithm provided by MET Norway, a time series of daily snow cover maps covering the Svalbard archipelago at 4 km grid spacing has been derived from the CLARA-A2 FCDR. The snow cover algorithm uses a set of signatures (instrument channel combinations) and statistical coefficients. The latter are derived from prior knowledge of the typical behaviour of the surface classes across the spectrum. Cloud-free pixels from the AVHRR GAC swath products are averaged and gridded to produce daily maps of average snow probability. A threshold of 50 % is applied to the snow probability maps to derive a binary snow/no snow product. Since the algorithm uses satellite measurements of reflected sunlight, there will be areas of no data due to winter darkness, therefore limiting data coverage between March 1 and September 30 each year. Therefore, the melting season is well covered, but the onset of the snow season is concealed due to the onset of the polar night period. In addition, temporal gap filling has been applied to achieve daily cloud-free mosaics.

2.1.3. Sentinel-2/Landsat-8

The Sentinel-2 (S2) A and B satellites have been delivering data over Svalbard since spring 2016 (Sentinel-2 User guide). The instrument provides data with nominal 10 m pixel spacing and is very well suited for snow cover mapping under cloud-free conditions. Since the launch of the Sentinel-2B

satellite in 2017, daily coverage of Svalbard has been possible. Furthermore, the Landsat-8 satellite has comparable spatial resolution (30 m) and was launched in 2014, thereby extending the period with high-resolution data coverage. Prior to this, only a few datasets for Svalbard were available, provided by Landsat-5 and Landsat-7 satellites.

In this report, we use a time-series of S2 NDSI products interpolated in the temporal dimension between cloud free observations. For the NDSI, we derive the SCF using the same relation as for MODIS (section 2.1.1). We thus obtain daily cloud free SCF-maps with 10 m resolution that can be directly compared with the MODIS dataset. Only the years 2018 and 2019 were available to use in this study.

2.1.4. Other remote sensing datasets

A range of microwave sensors can also be used for remote sensing of snow. Passive microwave sensors such as the Special Sensor Microwave/Imager (SSM/I) have provided decadal-long time series of snow water equivalent (SWE) estimates (e.g. Pulliainen et al., 2020), but the very coarse spatial resolution (~10-20 km) and lack of sensitivity over mountainous areas make these sensors less suitable for Svalbard, which is dominated by mountainous topography.

Microwave scatterometers have somewhat better resolution (~5km) and have also been used to some extent for studies in Svalbard. Rotschky et al. (2011) studied the spatio-temporal variability of snowmelt in Svalbard during 2000–2008 using QuikSCAT. A drawback associated with using active microwave sensors is their poor ability to distinguish between dry snow and bare soil. The main detection method for snowmelt is based on the high contrast between wet snow and dry snow/bare soil, which can also be applied to Synthetic aperture radar (SAR) data to quantify wet snow events (Nagler and Rott, 2000). In the current SIOS project, NORCE is adapting a time series of Envisat ASAR, Radarsat-2 and Sentinel-1 (S1) images over Svalbard to produce wet snow maps for the period 2002–2020. Stendardi (2020, PhD dissertation) has also studied the detailed melting patterns in

Adventdalen using combinations of S1 and S2. Similar studies of the freeze/thaw conditions on Kapp Linne have been published by Eckerstorfer et al. (2020). Multi-sensor approaches which combined optical and SAR data were also studied by Malnes et al. (2010).

ESA CCI Snow will provide global datasets for snow extent and SWE (1979–2018)¹² 'global' snow extent service provides daily data over continental Europe at 500m spatial resolution but excludes Svalbard and is hence not relevant. A high-resolution Fractional Snow Cover product has recently been made available by Copernicus based on Sentinel-2³ This product will, however, only cover areas up to 66°N and is therefore also unfortunately irrelevant for Svalbard (Gascoin et al., 2019).

2.2. Snow models

Snow models can simulate the evolution of relevant snow parameters continuously in space and time and are therefore an important tool to fill spatial and temporal gaps in observational datasets and simulate snow over longer time-periods and larger spatial domains. They require a surface meteorological forcing, which may come from regional climate model output or reanalysis datasets for large-scale modelling. Seasonal snowpack evolution on land areas in Svalbard is dominated by snow accumulation during autumn and winter and subsequent melting during late spring and summer. While cumulative snow accumulation and spring maximum snow depth is mostly determined by cumulative precipitation (snowfall) in autumn and winter, snow melt depends on atmosphere-surface interactions and can be estimated using simple melt-air temperature relationships (positive-degree day model) or more sophisticated models that solve the surface energy balance. Subsurface models may vary in terms of complexity but typically track at least the evolution of subsurface density, temperature and water content. In situ and/or remote sensing snow products (e.g. SWE, snow depth, density, temperature and water content) are

essential for model calibration and validation.

2.2.1. SeNorge

Up-to-date information on snow conditions is a crucial element for forecasting of natural hazards such as avalanches, slush flows and snow melt floods. Operational daily maps of simulated snow conditions have already existed for 15 years for mainland Norway⁴. However, no such detailed and spatiotemporal information with good cover on snow conditions on Svalbard currently exists, despite the obvious relevance and need for such snow information in for example, natural hazard forecasting on Svalbard and planning of outdoor and tourism activities. Consequently, in a research and development project in 2019-2020 NVE endeavours to set up an operational numerical snow model for mapping snow conditions (snow depth, density and water equivalent, fraction of snow-covered area plus others) in Svalbard at 1x1 km resolution. The time series of simulated snow maps start in autumn 2012 and will be continuously updated until the present day, and even 2–3 days ahead from that in the short-term weather forecast period.

This study uses the seNorge snow model (Saloranta, 2016), which requires the 3-hourly or daily mean air temperature [°C] and the sum of precipitation [mm/3h] as its input forcing. The liquid and solid precipitation fractions are defined by a threshold air temperature (solid precipitation occurring if air temperature is ≤ 0.5 °C). The snow and ice melt are calculated using the extended degree-day model including air temperature and solar radiation terms. Subsequently, the two parameters of the melt algorithm have been estimated based on 3356 quality controlled daily melt rates observed by the Norwegian snow pillow network (Saloranta, 2014). The sub-grid snow distribution algorithm in the model (Saloranta, 2012) assumes that snow is distributed uniformly within the grid cells, i.e., all SWE values between a defined minimum and maximum value are equally likely within a grid cell. In addition, an even layer of new snow can form

1 <http://snow-cci.enveo.at/>

2 <https://land.copernicus.eu/>

3 <https://land.copernicus.eu/pan-european/biophysical-parameters/high-resolution-snow-and-ice-monitoring>

4 see www.senorge.no

on top of the uniformly distributed 'old' snowpack (SCA is then set to 1). The main effect of the sub-grid snow distribution is to reduce the grid cell average melting rates towards the late melt season rates when significant areas of bare ground are present in the grid.

The input data are aggregated from the hourly meteorological forcing data obtained and downscaled from the AROME Arctic numerical weather prediction model (NWP). Input precipitation in the current model application is scaled by a factor 0.75, based on initial evaluation of the first model results. The model parameter values are set to the same values as those in the application for mainland Norway, except the spatial snow distribution parameter CF is increased from the default value of 0.5 to 0.85, giving larger variance for sub-grid snow distribution. The model application for Svalbard starts at bare ground initial conditions in September 2012. Afterwards, snow/firn older than 1 year is removed from the model's snow store on 1st September each year. The two first snow seasons may thus be considered as a model 'spin-up' period at higher elevation areas with perennial snow.

The seNorge simulation data used and evaluated in this report are produced from the mid-term project version and updated and improved versions of the dataset may be produced during the ongoing project period until the end of 2020.

2.2.2. Snow modelling at Uppsala University (UU)

Using the snow modelling system SnowModel (Liston et al. 2006), Van Pelt et al. (2016) simulated the seasonal snowpack evolution across Svalbard at 1x1 km spatial resolution and a 3-hourly temporal resolution for 1957–2012. Driven by downscaled meteorological fields of precipitation, air temperature, relative humidity, wind speed and direction, and incoming shortwave and longwave radiation from the High Resolution Limited Area Model (HIRLAM; Reistad et al. 2009), SnowModel solves the surface energy balance and simulates the snow depth, density and temperature evolution. Precipitation was downscaled using an elevation

relation, calibrated against a set of 1,442 SWE measurements collected on glaciers across Svalbard, to account for the effect of local topography on the precipitation distribution. For more details about the methods and dataset, the reader may refer to Van Pelt et al. (2016). The output of SWE is extracted from the model dataset and includes only seasonal snow, implying that multi-year (perennial) snow is excluded in this product.

A second snow model product has been extracted from a recent dataset of combined glacier climatic mass balance, seasonal snow and runoff, presented in Van Pelt et al. (2019). As such, driven by downscaled meteorological input from a regional climate model, a surface energy balance model calculates surface melt and temperature, and provides upper boundary conditions for a subsurface model, simulating the multi-layer evolution of snow density, temperature and water content (Van Pelt et al. 2012). More details on the model physics and calibration/validation can be found in Van Pelt et al. (2019). Here, SWE values are extracted from the model dataset and include both seasonal and multi-year snow. In this study, SWE derived from the 'older' (Van Pelt et al., 2016) SnowModel and the more recent, 'newer' (Van Pelt et al., 2019) SWE dataset described here are used in comparisons with the MODIS SCF products.

2.2.3. Other snow models

As part of the ongoing research and development at NVE, two other snow models are currently being run and evaluated in addition to the seNorge snow model. These are the single- and multi-layer snow schemes D95 and ISBA-ES of the land surface model SURFEX, which is part of the AROME NWP model system operated by the Norwegian Meteorological Institute (MET). The snow simulation results from D95 and ISBA-ES snow models are run with the same forcing data and spatial resolution as the seNorge model but are currently available only for the one-year period 1st September 2018–1st September 2019 due to higher computational requirements. The evaluation of the results from these two models will be described in the forthcoming final report from the project (expected to be published in early 2021).

2.3. Methods for comparison

2.3.1. Comparison of MODIS with AVHRR

The AVHRR 4 km gridded snow cover extent dataset uses the Lambert Azimuthal Equal Area projection. The two main products available are: 1) classed product corresponding to 5 classes (water, no data, snow-free pixels, snow-covered pixels, clouds) 2) gap-free classed product, a snow cover product corrected for cloud cover using information from cloud-free pixels up to 9 days forward or backward in time to correct for cloud-covered pixels in the present image and indicates whether the pixels are covered by snow or not together with the age of the reference image used to make the cloud cover corrections. This product gives in total 4 additional classes, with 3 classes each for both snow-free pixels and snow-covered pixels, and is used for the comparison as it allows a greater number of pixels to be used in the averaging of the AVHRR images.

The MODIS snow cover extent dataset uses a UTMZ33N projection at 500 m resolution. Therefore, the AVHRR dataset is re-projected to the MODIS grid before a comparison can be made. In addition, a vegetation map is used to mask out glaciers in the AVHRR dataset, as done to produce the MODIS SCF data (Vickers et al., 2020). In order to extract the snow cover fraction, the total number of snow-covered pixels in the AVHRR images are divided by the total number of remaining unmasked

pixels in the image i.e., all pixels not classed as water, cloud, glacier or no data. Further, to extract the corresponding snow cover fraction from the MODIS images on the same day of year, the MODIS SCF is averaged over the same unmasked pixels as obtained from the AVHRR image. A 'land-averaged' snow cover extent/fraction product is therefore obtained for each day of year between March 1st and September 30th using the same pixels from both AVHRR and MODIS images.

2.3.2. Comparison of MODIS with Sentinel-2

A systematic comparison between MODIS and S2 for entire Svalbard is beyond the scope of the project, but a few direct comparisons have been done to assess the differences. Since S2 has 20m resolution and MODIS has 500m resolution, there is expected bias in the MODIS data when re-scaled to the same grid size as the S2 data. The same regression formula is used to calculate S2 SCF as was used for MODIS. The MODIS regression has been thoroughly validated, whereas the S2 regression to transform S2 NDSI to SCF is more uncertain. An example of snow cover maps obtained with S2 and MODIS for the Nordenskiöld Land region is presented in Figure 1. The regression between S2 and MODIS for the entire Nordenskiöld Land region has also been examined using the available 2-year dataset, but a longer time-series will be more advantageous.

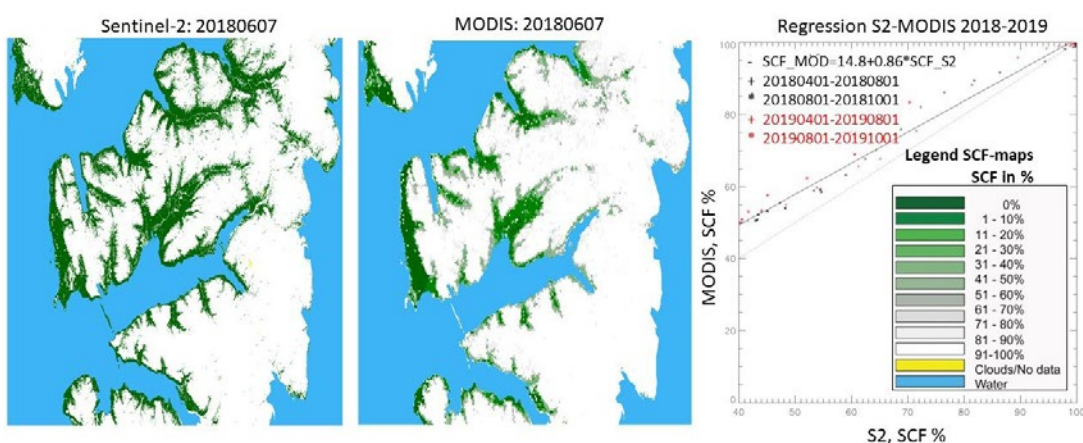


Figure 1: SCF-map for S2 (left) and MODIS (centre) for 20180607. Right: Regression between average SCF over Nordenskiöld Land for S2 and MODIS corresponding days in 2018 and 2019. Colours and symbols show differences between melting season (April–July) and fall (Aug–Nov).

2.3.3. Comparison of MODIS with SWE models (UU, NVE)

For the comparison of the two SWE datasets with the MODIS products, MODIS SCF maps were first georeferenced to the same grid as the SWE datasets. A glacier mask was also applied to the SWE data in the same way that the MODIS products have been masked. In order to obtain a comparable product, a threshold was applied to the SWE data such that pixels with a value below the threshold were classified as 'no snow' and those exceeding the threshold were considered snow covered. This allowed us to produce binary snow cover maps from the SWE data, from which an estimate of the land-averaged snow cover fraction could be derived, for each day of year in the time series. The optimal threshold was determined by trying 10 different thresholds on SWE ranging from 0.01 to 0.1 m and obtaining the land-averaged snow cover fraction time series resulting from the binary maps produced at each threshold. The difference between the SWE-derived SCF time series and the MODIS-derived SCF time series was calculated for each day of the year and the squared difference was summed over the whole year, for each year in the dataset. The threshold producing land-averaged SCF time series that gave the smallest squared-sum was identified as the best threshold for that year. Except for two years (2003 and 2004) where the optimal threshold was determined to be 0.02 m using the older dataset delivered by UU, the optimal threshold for the remainder of the dataset was found to be 0.01 m. Hence, the SWE-derived snow cover fraction time series obtained from the binary snow cover maps corresponding to a threshold of 0.01 m applied to the SWE data, were used to obtain the general relationship between the SWE and MODIS datasets.

Using the land-averaged snow cover fraction time series, the algorithm used to estimate the first snow free day (FSFD) from the MODIS dataset was

applied to the SCF time series derived from the threshold SWE model maps. The same algorithm was also applied to the land averaged SCF time series produced using the re-gridded MODIS data. Note that this may not have necessarily produced the same results as for example, calculating the FSFD per pixel in the MODIS data and subsequently averaging all FSFD estimates over all land pixels.

2.3.4. Comparison of MODIS with seNorge snow-covered area

In addition to the SWE model provided by seNorge, snow-covered area (SCA) estimates were provided at 3-hour intervals on a daily basis for the years 2012–2019. This allowed an opportunity to directly compare SCF time series as well as SCA at a pixel level, after reprojecting the MODIS data to the same grid as the seNorge snow-covered area. SCA maps corresponding to 1200 UTC have been used to compare with the MODIS-derived SCF estimates.

2.3.5. Geographical comparison of snow cover

In the final part of the comparisons between the datasets, the difference in number of days with snow derived from each of the data products, compared with that obtained from MODIS is mapped. In order to make this geographical comparison, a binary snow map was created, in the case of the SWE datasets by thresholding at 0.01 cm and for MODIS SCF, by thresholding at 50%. Since the AVHRR maps already represented a binary snow cover extent, adapting this product was not needed. Hence, for each pixel in the grid, the number of days in a year the pixel was classified as snow covered/not snow covered during each year using the AVHRR, MODIS and SWE datasets was calculated. The difference in number of days with snow cover between AVHRR and MODIS, and the SWE datasets and MODIS was then calculated at each pixel.

3. Results

For the comparison of land-averaged SCF derived from AVHRR snow cover extent maps, the AVHRR SCF estimates were found to be systematically greater than MODIS SCF for all years studied, as shown by the time series plots in Figure 2 and the

scatter plot comparison for the general relationship for these land averaged SCF estimates shown in Figure 3. The relationship was nonlinear, with differences of up to 30 %. For the lowest and highest SCF the two methods tended to converge.

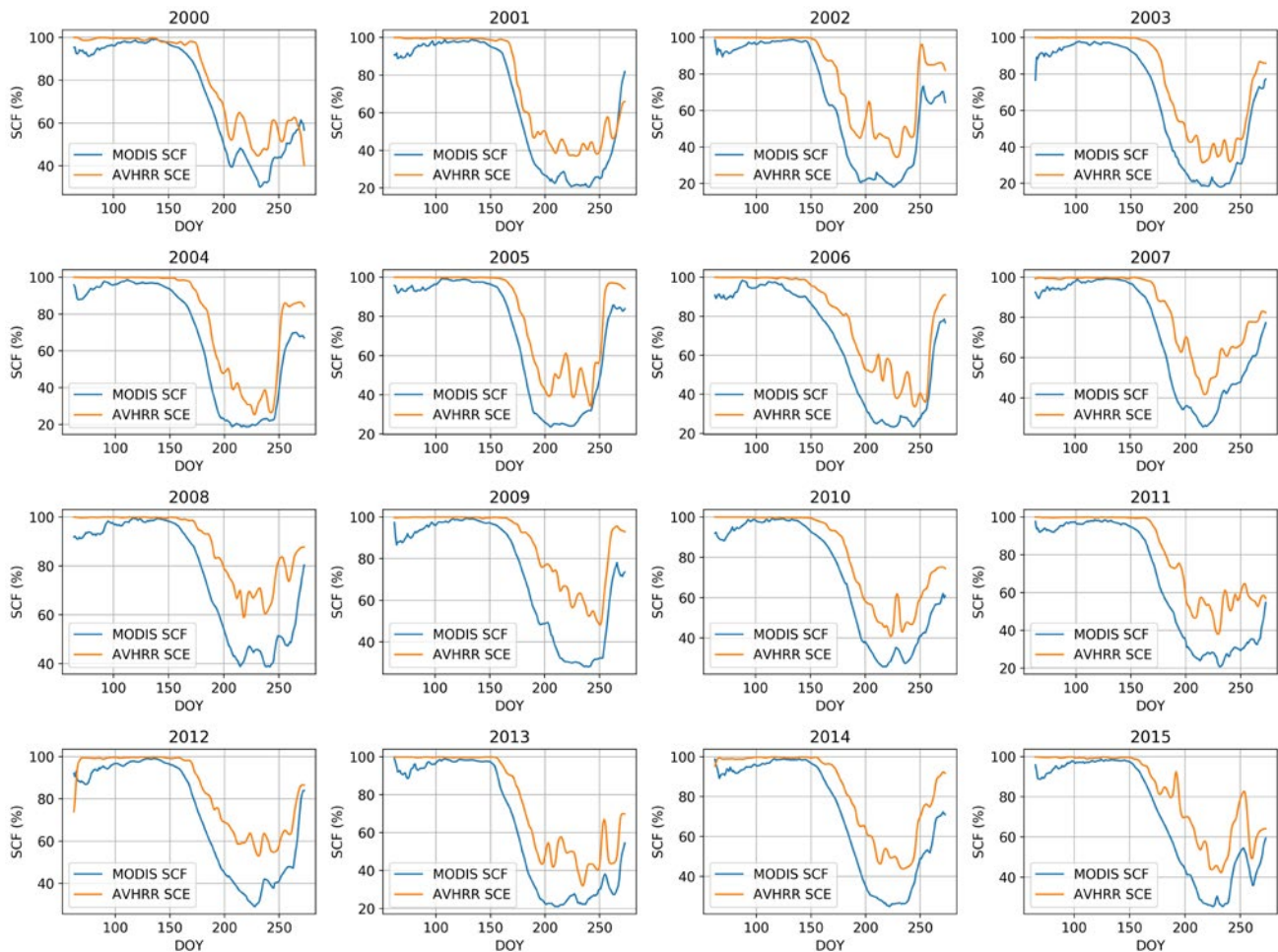


Figure 2: Comparison of SCF time series from AVHRR (orange) and MODIS (blue) for 2000–2015, using the maximum cloud-free gap of 9 days to select AVHRR data.

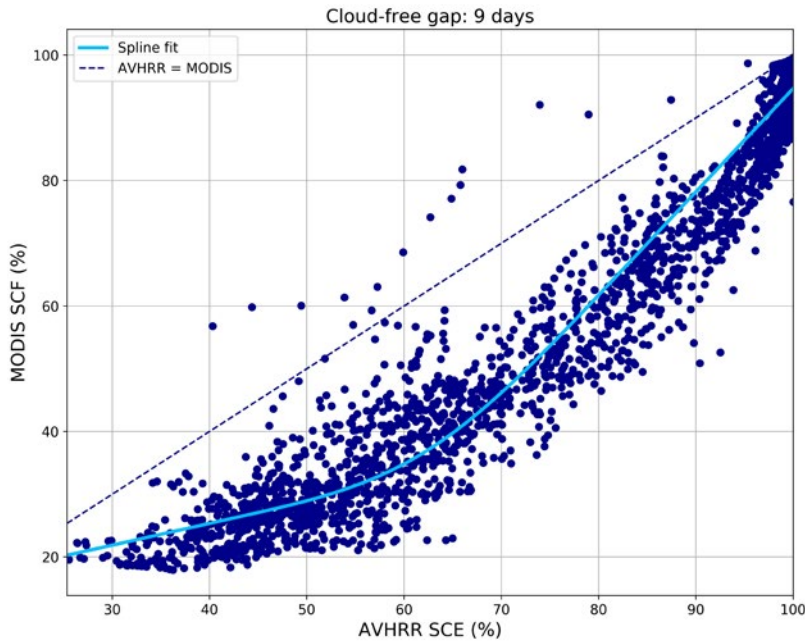


Figure 3: Comparison of SCF from AVHRR and MODIS as a scatter plot, combining the land-averaged estimates from all days of the year and all years (2000–2015), using the maximum cloud-free gap of 9 days. A fitted spline curve is shown in light blue and a dashed line indicates where the land-averaged estimates from both sensors would be equal, implying that in this case, the MODIS SCF is consistently lower than those derived from AVHRR.

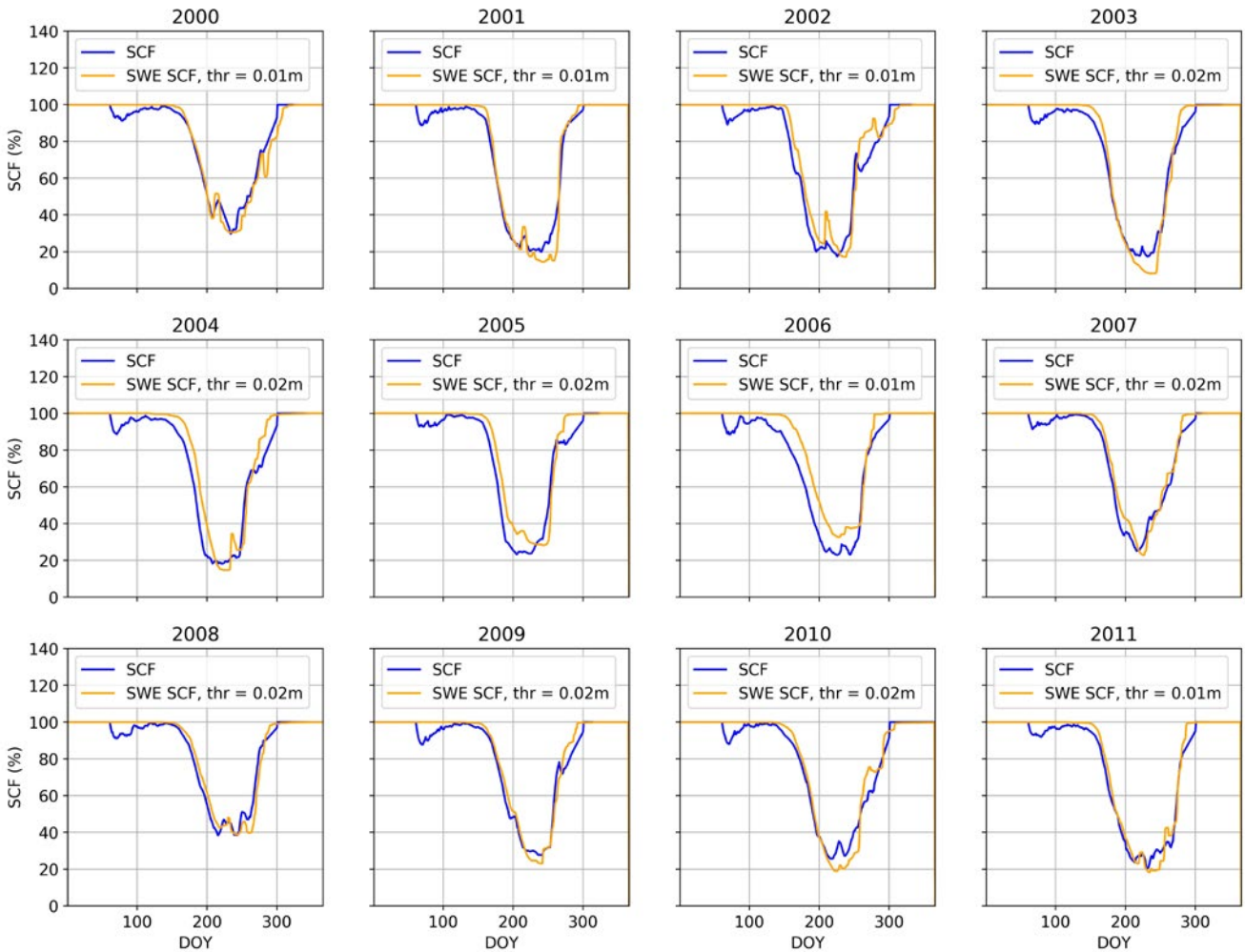


Figure 4: Comparison of SCF time series from thresholding of the older UU snow model SWE data and MODIS for all years with overlapping data (2000–2011 inclusive). The SWE thresholds producing best agreement with the MODIS data are given in the legends. The best agreement was determined by minimizing the squared differences over the yearly time series.

When SWE (UU) datasets underwent thresholding to estimate SCF, a somewhat closer agreement with the MODIS land-averaged SCF was obtained, indicated by the time series comparisons in Figure 4 and the scatter plots (Figure 5) with a positive bias in the SWE-derived SCF of approximately 10 % when MODIS SCF was >40 %. Below these values, the relationship was less linear, and the fitted spline curve suggests that MODIS estimates were on average greater than those derived from SWE. For first snow-free day estimates using

MODIS and SWE SCF (Figure 6) the correlation was rather weak and MODIS estimates were generally earlier than those obtained using the SCF time series derived from SWE datasets. Interestingly in Figure 7, there was very good agreement for the estimates of the last snow free day obtained using both the MODIS and SWE-derived SCF time series. Figure 7 also shows that the strongest correlation was obtained for last snow free day using the SCF time series derived from the older SWE dataset ('SnowModel-1').

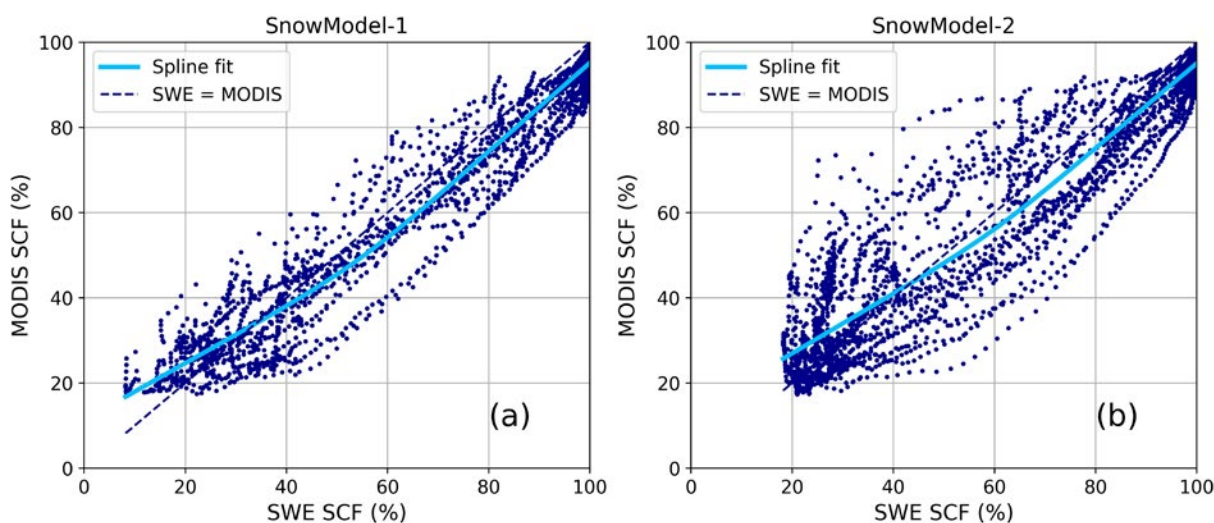


Figure 5: (a) Comparison of SCF from thresholding the older UU snow model SWE maps (SnowModel-1) and MODIS as a scatter plot, combining the land-averaged estimates from all DOY and all years (2000–2011). A fitted spline curve is shown in light blue. (b) same as for Figure 5a but using the newer UU SWE dataset for 2000–2017 inclusive (SnowModel-2).

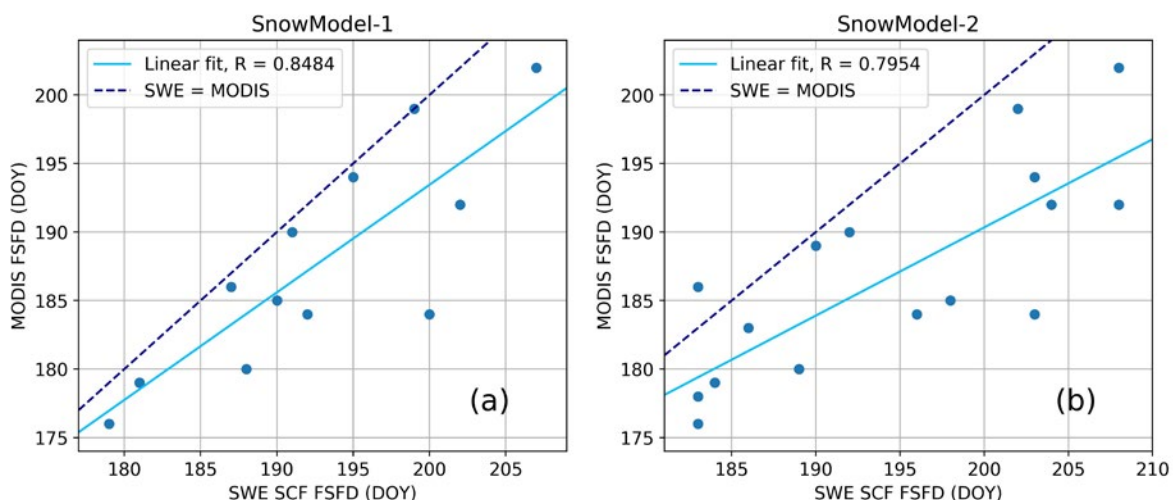


Figure 6: (a): Comparison of the first snow free day (FSFD) derived using the older UU snow model SWE (SnowModel-1) derived land-averaged SCF time series and the MODIS first snow free day derived from the land-averaged SCF time series. (b) same as for Figure 6a but using the newer UU snow model SWE dataset (SnowModel-2). In both figures, a dashed line indicates where FSFD would be the same in both datasets, while a light blue solid line shows the linear fit. Correlation coefficient R is stated in the legend.

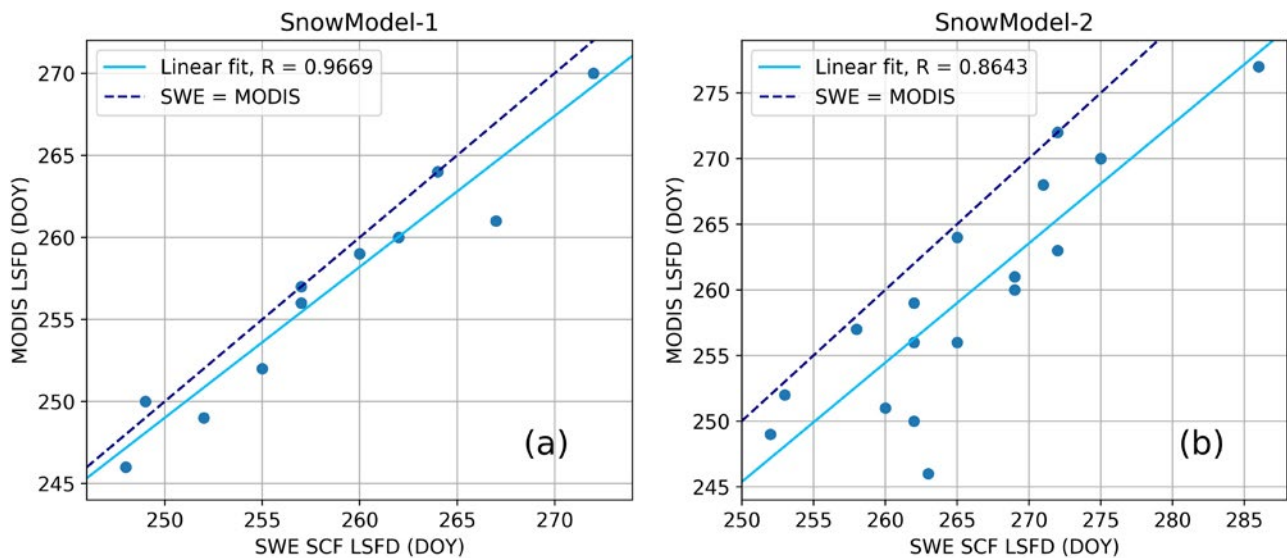


Figure 7: (a): Comparison of the last snow free day (LSFD) using the older UU snow model SWE (SnowModel-1) derived land-averaged SCF time series and the MODIS last snow free day derived from the land-averaged SCF time series. (b) same as for Figure 7a but comparing last snow free day using the newer UU snow model SWE snow model dataset (SnowModel-2). As for Figure 6, a light blue solid line indicates the linear fit to the two datasets and the dashed line shows where the LSFD from both datasets would be equal.

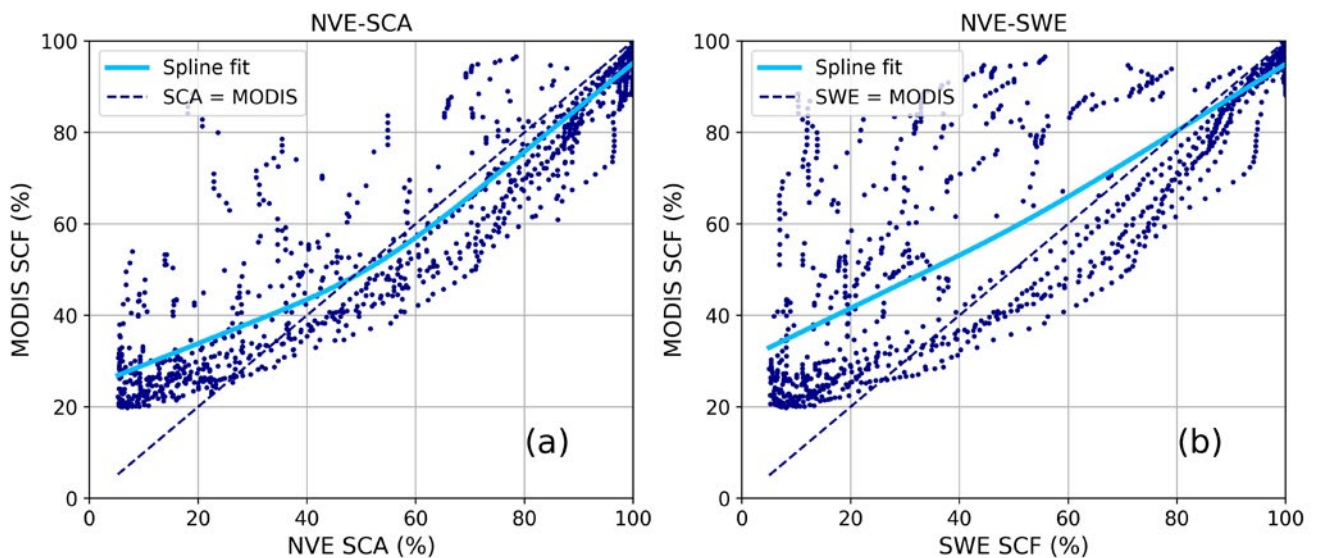


Figure 8: (a) Same as for Figure 5 but showing snow covered area from NVE (2013–2019) and (b) derived from thresholding of the NVE SWE dataset. A spline fit is shown by the light blue curve while a dashed line indicates where the two estimates would be equal.

In the case of the NVE seNorge SCA and SWE datasets, the seNorge SCA was generally lower than that obtained using the MODIS dataset for minimum snow cover during the summer months, but the degree of underestimation with respect to the MODIS dataset was greater when the SWE-derived snow cover fraction was compared. Figures 7a and 7b show the general relationship between seNorge (SWE-derived SCF) and MODIS SCF and between seNorge SCA and MODIS SCF respectively, which illustrate the underestimation

of seNorge with respect to MODIS for lower snow cover fraction. For $SCF > 50\%$, the fitted spline curve in Figure 8b shows that the MODIS SCF is on average slightly lower than that obtained from theseNorge product. Qualitatively, there was better agreement between the seNorge and MODIS time series during the first part of the year when SCF decreases toward minimum; after minimum there is less agreement leading to a lack of correlation between estimates of the last snow free day obtained from MODIS and seNorge (not shown).

For first snow free day (Figure 9), there is a more obvious linear relationship but the correlation is not particularly high and relatively similar when

correlating the first snow free day derived from both SCA and thresholded SWE time series ($R = 0.72$ and 0.79 respectively).

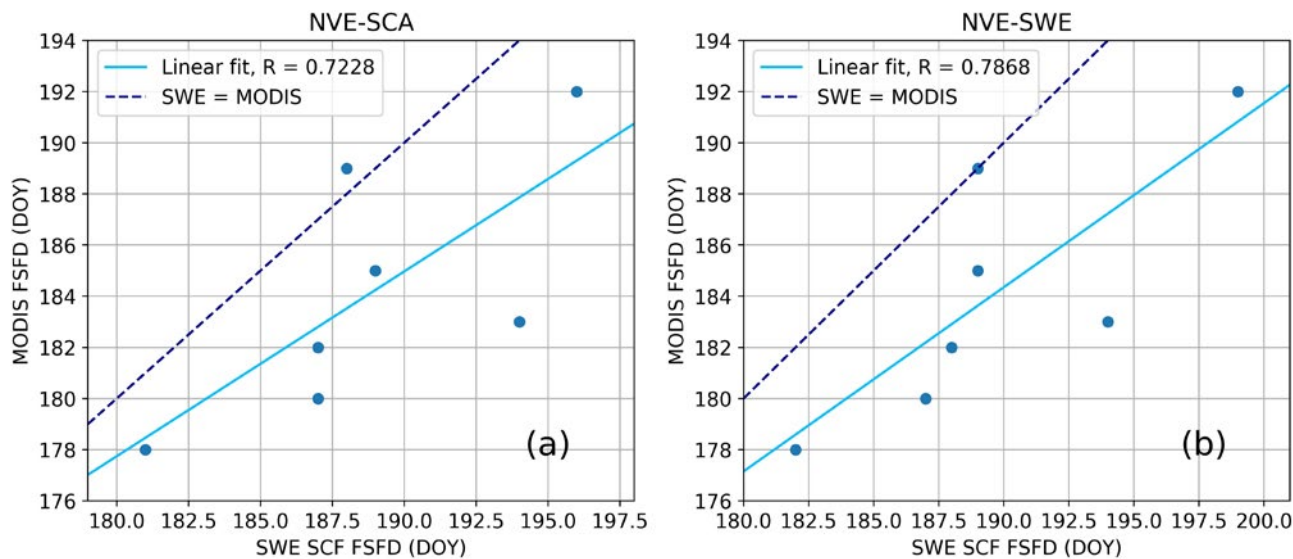


Figure 9: (a) Comparison of the first snow free day from MODIS and those derived using the seNorge land-averaged SCA time series and (b) thresholded SWE (seNorge) land-averaged SCF time series. As for Figures 5 and 6, a light blue solid line indicates the linear fit to the two datasets and the dashed line shows where the LSFd from both datasets would be equal.

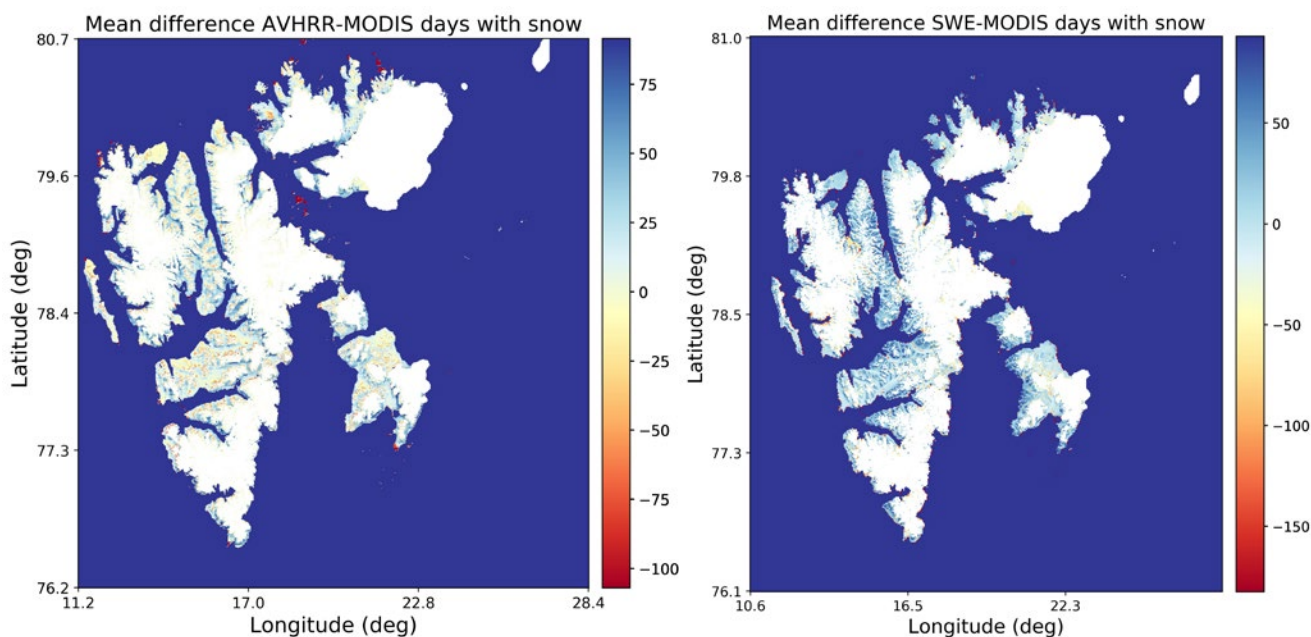


Figure 10: a (left) Average difference in number of days with snow cover over Svalbard for 2000–2015, comparing AVHRR SCE with MODIS SCF. The MODIS SCF has undergone thresholding at 50% to obtain a binary SCE map and b (right) same as for Figure 10a but using SCE derived from the older UU snow model SWE dataset (2000–2011).

For the average differences in number of days with snow cover per year estimated by AVHRR and MODIS, Figure 10a indicates that no clear regional differences are present, but qualitatively, the differences are more altitude dependent. Figure 10a shows that the mean difference between AVHRR and MODIS is primarily positive in the valleys and around the coast while at mid- and higher elevations the difference is increasingly negative, i.e., AVHRR tends to estimate more days with snow per year compared with MODIS in the low-lying areas while at higher elevations, there is an apparent underestimation of snow cover in mountainous areas. Considering the geographical distribution of the mean difference in number of days with snow cover from the UU SWE datasets (Figure 10b), there is a tendency toward positive differences across most of the archipelago i.e., the number of days with snow cover from thresholding the 1 km resolution SWE maps, is mostly greater than the number of days of snow estimated by thresholding the 500 m resolution MODIS SCF maps.

This altitude dependency exhibited in Figure 10a is largely confirmed by Figure 11, which shows the mean difference distributed in bins of 100 m

from 0 to 1600 m. At the lowest altitudes of up to 200 m.a.s.l, the bin averages are around 13 days, while for the highest altitude bin at 1500–1600 m.a.s.l the bin average is of the order of -10 days i.e., AVHRR estimates on average 10 days per year less snow cover compared to MODIS in this height range. There also exist dark red regions and islands around Nordaustlandet, which represent areas not mapped by the AVHRR dataset, resulting from the resolution difference between MODIS and AVHRR. The difference is therefore large and negative since there is no snow cover data here using AVHRR. For the UU SWE dataset, an almost opposite altitudinal pattern to that for the AVHRR data was obtained (not shown); at lower elevations of up to 200 m.a.s.l, there are on average fewer days with snow cover estimated from thresholding the SWE data when compared with the MODIS dataset, while at higher elevations the SWE dataset tends to estimate more days with snow each year compared with the MODIS SCF data. In the elevation band 700–900 m.a.s.l the thresholded SWE dataset estimates on average around 30 more days with snow cover per year when compared with MODIS at these altitudes.

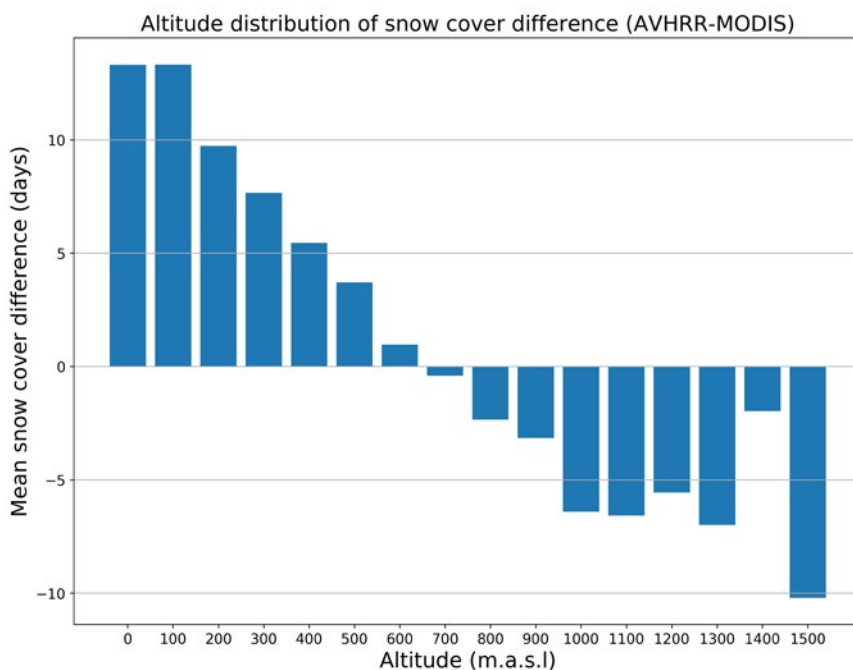


Figure 11: Altitude distribution of the mean difference in number of days with snow cover (cf. Figure 10a) comparing snow cover maps from AVHRR and MODIS for the period of 2000–2015. This figure shows clearly that the differences are positive at low altitudes (< 700 m.a.s.l.) while at higher altitudes (>800 m.a.s.l.) the mean difference in days with snow cover is negative, indicating that AVHRR overestimates the number of days with snow with respect to MODIS at low altitudes, while at high altitudes AVHRR underestimates number of days with snow with respect to MODIS. Best agreement for number of days with snow is found at altitudes between 700–800 m.a.s.l.

For the Sentinel 2–MODIS comparison, Figure 1 shows an example of the snow cover fraction maps for a part of Nordenskiöld Land in central Svalbard for 7th June 2018. Qualitatively, some differences can be observed as the S2 SCF map exhibits smaller variation in the range of SCF than the MODIS map. This may be explained by the large difference in spatial resolution between the two sensors, whereby MODIS tends to smooth out

snow cover with intermediate snow cover fractions to a greater extent than S2. Since S2 only is available for two years during the SATMODSNOW project, a thorough intercomparison between the two datasets has not been performed here. With ongoing acquisition of further data from S2 it is hoped that within a few years, a larger database will allow a more in-depth comparison of SCF estimated by the two sensors, qualitatively and quantitatively.

4. Connections and synergies with other SESS report chapters

4.1. This year

[Killie et al. \(2021\)](#): ‘Svalbard long-term variabilities of terrestrial-snow and sea-ice cover extent’. There are clear synergies between this and the current study. In the case of comparing terrestrial snow and sea-ice cover, a parallel study using the MODIS snow cover dataset was carried out by Vickers et al. (2020), which is a pre-cursor to the current SESS project.

[Salzano R. et al. \(2021\)](#): ‘Terrestrial Photography Applications on Snow cover in Svalbard’. The methods used by Salzano should have synergies when validating satellite data. In particular, it could be interesting to translate the long-term time series of webcam data on the Zeppelin mountain into a georeferenced snow cover dataset, perhaps used as a long-term reference dataset to quantify differences in SCF estimates using different sensors with variable spatial resolution.

4.2. Previous years

Karlsen et al. (2020): ‘Sentinel based mapping of plant productivity in relation to snow duration and

time of green-up’. This report focuses on in-situ and satellite data from the Adventdalen region linked to plant productivity measurements. Current high-resolution Sentinel-1&2 sensors are well suited to accurately map the plant phenology and determine plant productivity. There are obvious synergies between the datasets used in Karlsen et al. (2019) and in this study, and the S2 dataset used is simply a by-product of the S2 NDVI dataset used. Synergies by combining various snow products are shown in the current report and could be extended to plant productivity.

Gallet et al. (2019): ‘Snow research in Svalbard: current status and knowledge gaps. The authors provide an overview of current snow research on Svalbard and identify needs for further research within the three main fields: glacial snow, seasonal snow on land and impacts of contaminants in snow. Based on the recommendations in this report (specifically related to seasonal snow on land), we believe that the SATMODSNOW project has at least partially provided answers to these recommendations by promoting scientific exchanges of data and interdisciplinary work (remote sensing/hydrology).

5. Unanswered questions

While this review has been able to address the first two objectives (outlined in section 1), as summarized in section 4, the third objective has only been answered to a certain extent in terms of suggesting potential methods to improve low resolution datasets (e.g. AVHRR) using higher-resolution datasets (e.g. MODIS or S2). In the results, the relationships between MODIS datasets and the AVHRR and snow model products are described. The remote sensing comparisons suggest that lower resolution sensors tend to overestimate SCF with respect to the higher resolution sensors (e.g. AVHRR-MODIS, MODIS-Sentinel 2 comparisons). This overestimation can be up to several tens of per cents. However, due to the Sentinel-2 dataset in this analysis being comparatively small in terms of temporal (two seasons) and spatial coverage, further analysis is required to fully establish the correction required to improve the lower resolution

MODIS dataset. Acquiring additional Sentinel-2 scenes covering a greater area of Svalbard over the forthcoming years would contribute greatly to the understanding of the differences in SCF obtained at high and moderate spatial resolutions. Once this is ascertained, a corrected MODIS dataset should be used to update the regression obtained with the AVHRR dataset, thereby propagating the corrections down to the lowest sensor resolutions and allowing a long time series of SCF to be reconstructed at high spatial resolution. The potential of fusing models for SWE with satellite observations of snow cover is also high and should be used for improving models in the future. Various approaches could be envisioned for obtaining more realistic snow distributions but finding an acceptable compromise between the satellite observations and the input fields (mainly temperature and precipitation) used in the hydrological models is crucial.

6. Recommendations for the future

- The results in SATMODSNOW and other snow services such as CCI Snow should be utilized to compile a long-term time series of snow cover data for 1978–2020 with as high spatial resolution as possible. Such a consolidated dataset could play an important role in future snow research on Svalbard as well as interdisciplinary research within e.g. ecology, geophysics and climate research.
- Future efforts to integrate multi-source EO data (in situ, airborne and satellite observations) with new techniques (e.g. artificial intelligence and data assimilation) are highly recommended for further improving the characterization of snow cover and SWE in Svalbard.
- Methods to utilize EO data to improve hydrological models should be sought in order to better capture the snow cover distribution simultaneously as SWE estimates are improved.
- The snow measurement infrastructure on Svalbard needs improvements for providing more validation/ground truthing for both models and EO datasets. In addition to traditional ground instruments (met-stations, snow field surveys), datasets providing spatial coverage such as air- or UAV-borne are also needed, among others to reveal more details on the spatial snow distribution. Sensors that can measure additional snow properties such as temperature and liquid water content are also of interest.
- Upcoming datasets from EO (e.g. wet snow from SAR) should be compared and validated using corresponding layers from hydrological modelling (e.g. liquid water content) in the future.

7. Data availability

Table 1: Overview of all the data used in the project, and the availability of the datasets.

Dataset	Parameters	Period	Location or area	Metadata / Data access (URL, DOI)	Data provider, reference
MODIS	Snow cover fraction	2000–2020	Svalbard	Available in the SIOS data access portal in Q1 2021 https://doi.org/10.3390/rs12071123	NORCE
AVHRR	Snow probability	1982–2015	Svalbard	SIOS database; the URL will be added before the SESS report will be published	METNO
Sentinel-2	Snow cover fraction	2017–2020	Nordenskiöld Land	-	NORCE skar@norce-research.no
SeNorge	Snow water equivalent, Snow covered area	2012–2019	Svalbard	www.senorge.no	NVE, tus@nve.no
SnowModel	Snow water equivalent	2000–2011 and 1957–2018	Svalbard	SIOS data access portal: https://bit.ly/3nkfu18	Uppsala University (UU), ward.van.pelt@geo.uu.se

Table 2: Datasets overview showing a comparison of the remote sensing datasets (Sentinel-2, MODIS, AVHRR) and SWE datasets derived from snow models (seNorge, UU) in terms of the time period with data coverage, spatial resolution, snow cover variables and if the polar night period is available.

	Sentinel2	MODIS	AVHRR	SeNorge	UU
<i>Time-period</i>	2016-	2000–2020	1982–2015	2012–2019	2000–2011(old) 1957–2018(new)
<i>Spatial resolution</i>	20 m	500m	4km	1km	1km
<i>Wavelengths used</i>	510–580 nm 860–1040 nm	545–565 nm 1628–1652 nm	580–680 nm 3550–3930 nm	N/A	N/A
<i>Snow extent</i>	Snow cover fraction	Snow cover fraction	Snow probability	Separate SCF layer or derived from SWE using 1 cm threshold	Derived from SWE using 1 cm threshold, (2 cm in 2003/2004)
<i>Snow mass</i>	N/A	N/A	N/A	SWE/snow depth	SWE
<i>Polar night</i>	N/A	N/A	N/A	Yes	Yes

Acknowledgements

This work was supported by the Research Council of Norway, project number 251658, Svalbard Integrated Arctic Earth Observing System – Knowledge Centre (SIOS-KC).

List of abbreviations

AVHRR	Advanced Very High Resolution Radiometer
EO	Earth Observation
FSFD/LSFD	First/Last Snow Free Day
MODIS	Moderate Resolution Imaging Spectroradiometer
NDSI/NDVI	Normalized Differential Snow/Vegetation Index
NVE	The Norwegian Water Resources and Energy Directorate
NWP	Numerical weather prediction model
S2	Sentinel-2
SCE	Snow Cover Extent
SCF/SCA	Snow Cover Fraction/Snow Covered Area
SWE	Snow Water Equivalent
UU	Uppsala University

References

- Eckerstorfer M, Malnes E, Christiansen HH (2017) Freeze/thaw conditions at periglacial landforms in Kapp Linné, Svalbard, investigated using field observations, in situ, and radar satellite monitoring. *Geomorphology* 293:433–447.
- Gallet JC, Björkman MP, Borstad CP, Hodson AJ, Jakobi H-W, Larose C, Luks B, Spolaor A, Schuler TV, Urazgildeeva A, Zdanowicz C (2019) Snow research in Svalbard: current status and knowledge gaps. In: Orr et al. (eds): SESS report 2018. Svalbard Integrated Arctic Earth Observing System, Longyearbyen, pp 83–107. https://sios-svalbard.org/SESS_Issue1
- Gascoin S, Grizonnet M, Bouchet M, Salgues G, Hagolle O (2019) Theia Snow collection: High-resolution operational snow cover maps from Sentinel-2 and Landsat-8 data. *Earth Syst Sci Data* 11(2).
- Hall DK, Riggs GA, Salomonson VV, DiGirolamo NE, Bayr KJ (2002) MODIS snow-cover products. *Remote Sens Environ* 83:181–194.
- Karlsson KG, Anttila K, Trentmann J, Stengel M, Fokke Meirink J, Devasthale A, Hanschmann T, Kothe S, Jääskeläinen E, Sedlar J, Benas N, van Zadelhoff GJ, Schlundt C, Stein D, Finkensieper S, Håkansson N, Hollmann R (2017) CLARA-A2: the second edition of the CM SAF cloud and radiation data record from 34 years of global AVHRR data. *Atmos Chem Phys* 17:5809–5828.
- Karlsen SR, Stendardi L, Nilsen L, Malnes E, Eklundh L, Julitta T, Burkart A, Tømmervik H (2020) Sentinel satellite-based mapping of plant productivity in relation to snow duration and time of green-up (GROWTH). In: Van den Heuvel et al. (eds): SESS report 2019. Svalbard Integrated Arctic Earth Observing System, Longyearbyen, pp 43–57. https://sios-svalbard.org/SESS_Issue2
- Killie MA (2018) Validation of a satellite-based Snow Cover Index for Svalbard, [SIOS Access project 2018_0007](https://sios-svalbard.org/SESS_Issue2)
- Killie MA, Aaboe S, Isaksen K, Van Pelt W, Pedersen ÅØ, Luks B (2021) Svalbard snow and sea-ice cover: comparing satellite data, on-site measurements, and modelling results. In: Ibáñez et al (eds) 2021: SESS report 2020, Svalbard Integrated Arctic Earth Observing System, Longyearbyen, pp 220–235. <https://doi.org/10.5281/zenodo.4293804>
- Malnes E, Karlsen SR, Johansen B, Haarpaintner J, Hogda KA (2010) Monitoring of the snow coverage and its relation to vegetation and growing seasons on Svalbard using ENVISAT ASAR and TERRA MODIS data. *ESASP* 686:265.
- Nagler T, Rott H (2000) Retrieval of wet snow by means of multitemporal SAR data. *IEEE Trans Geosci Remote Sens* 38:754–765.
- Pulliainen J, Luojus K, Derksen C, Mudryk L, Lemmetyinen J, Salminen M, Ikonen J, Takala M, Cohen J, Smolander T, Norberg J, J (2020) Patterns and trends of Northern Hemisphere snow mass from 1980 to 2018. *Nature* 581(7808):294–298.
- Rotschky G, Vikhamar Schuler T, Haarpaintner J, Kohler J, Isaksson E (2011) Spatio-temporal variability of snowmelt across Svalbard during the period 2000–08 derived from QuikSCAT/SeaWinds scatterometry. *Polar Res* 30(1):5963.
- Saloranta TM (2012) Simulating snow maps for Norway: description and statistical evaluation of the seNorge snow model. *The Cryosphere* 6(6):1323.
- Saloranta TM (2014) New version (v.1.1.1) of the seNorge snow model and snow maps for Norway, Rapport 6-2014, Norwegian Water Resources and Energy Directorate, Oslo, Norway, p 30. Available at http://publikasjoner.nve.no/rapport/2014/rapport2014_06.pdf
- Saloranta TM (2016) Operational snow mapping with simplified data assimilation using the seNorge snow model. *J Hydrol* 538:314–325.
- Salzano R, Aalstad K, Boldrini E, Gallet JC, Kępski D, Luks B, Nilsen L, Salvatori R, Westermann S (2021 a) Terrestrial photography applications on snow cover in Svalbard. In: Moreno-Ibáñez et al (eds) SESS report 2020, Svalbard Integrated Arctic Earth Observing System, Longyearbyen, pp 236–251. <https://doi.org/10.5281/zenodo.4294084>
- Sentinel-2 User guide: <https://sentinel.esa.int/web/sentinel/user-guides/sentinel-2-msi>
- Stendardi L (2020) Detection of vegetation phenology in cold regions using a combination of radar and optical satellite data. PhD Thesis, University of Bolzano/Bozen (Italy)
- Van Pelt WJJ, Oerlemans J, Reijmer CH, Pohjola VA, Pettersson R, van Angelen JH (2012) Simulating melt, runoff and refreezing on Nordenskiöldbreen, Svalbard, using a coupled snow and energy balance model. *The Cryosphere* 6:641–659.
- Van Pelt WJ, Kohler J, Liston GE, Hagen JO, Luks B, Reijmer CH, Pohjola VA (2016) Multidecadal climate and seasonal snow conditions in Svalbard. *J Geophys Res: Earth Surface* 121(11):2100–2117.
- Van Pelt WJJ, Pohjola VA, Pettersson R, Marchenko S, Kohler J, Luks B, Hagen JO, Schuler TV, Dunse T, Noël B, Reijmer CH (2019) A long-term dataset of climatic mass balance, snow conditions and runoff in Svalbard (1957–2018). *The Cryosphere* 13:2259–2280.
- Vickers H, Karlsen SR, Malnes E (2020) A 20-Year MODIS-Based Snow Cover Dataset for Svalbard and Its Link to Phenological Timing and Sea Ice Variability. *Remote Sens* 12(7):1123.

Svalbard snow and sea-ice cover: comparing satellite data, on-site measurements, and modelling results (SvalSCESIA)

Mari Anne Killie¹, Signe Aaboe¹, Ketil Isaksen¹, Ward Van Pelt², Åshild Ø. Pedersen³, and Bartłomiej Luks⁴

¹ The Norwegian Meteorological Institute, Postboks 43 Blindern, 0371 Oslo, Norway

² Department of Earth Sciences, Uppsala University, SE-75236 Uppsala, Sweden

³ The Norwegian Polar Institute, FRAM Centre, NO-9296 Tromsø, Norway

⁴ Institute of Geophysics, Polish Academy of Sciences, Księcia Janusza 64, 01-452 Warsaw, Poland

Corresponding author: Mari Anne Killie, mariak@met.no

ORCID number 0000-0001-5594-2124

Keywords: In-situ, modelling, remote sensing, sea-ice area, snow cover extent

DOI: <https://doi.org/10.5281/zenodo.4293804>

1. Introduction

The presence of snow cover has a large impact on Arctic ecosystems, human activities, atmospheric processes and the Earth's surface energy balance. However, the snow cover is challenging to map for larger regions due to its large spatial and temporal variability and its changing properties influenced by temperature, precipitation, wind, vegetation and local topography. Also, the sparse number of weather stations with snow cover measurements contributes to a poor observational database. Svalbard is located on the border between the ice-covered Arctic Ocean and the warmer North Atlantic sector; therefore the sea becomes a controlling factor of the climate. By using satellite remote sensing monitoring, it is possible to get a

better overview of the snow conditions on land.

In this study, we use existing long-term climate data records of the snow cover on Svalbard and the sea-ice area in the adjacent sea, based on satellite data, to investigate how they are related to each other. The long-term climate data record of the snow cover on Svalbard (Killie 2019) is combined with the snow model output for snow water equivalent and in-situ measurements of snow cover and snow-off dates. Temporal as well as spatial trends are investigated. From existing global satellite climate data records of sea-ice concentration, the sea-ice trends in a selected Svalbard region are investigated in relation to the snow cover trends.

2. Overview of existing data

The datasets contributing to this study include long-term satellite data records (section 2.1.1 and 2.1.4), long-term in-situ ground measurements (section 2.1.2), as well as output extracted from a long-term model dataset of climatic mass balance, snow conditions and runoff in Svalbard (section 2.1.3). We also include a shorter data record from in-situ measurements of ground surface temperature [COAT (Pedersen et al. 2020), section 2.1.2]. A common grid and overlapping time span are selected where possible. The satellite-based snow cover data record covers 1982–2015, and thus the sea-ice concentration data, in-situ ground data and snow modelling data are restricted

to cover the same time period. Over land, the snow model data are re-projected to the same 4 km resolution grid as the satellite snow cover data record. The coastal zone is masked, and for quantitative analysis, glaciated land pixels are masked as well. Figure 1 shows land pixels (snow-covered or snow-free) and glaciated pixels. The inset map shows the regions used for comparison with in-situ data.

In section 2.1, the datasets are presented in separate sub-sections, and in the following section 2.2, potential correlations are investigated.

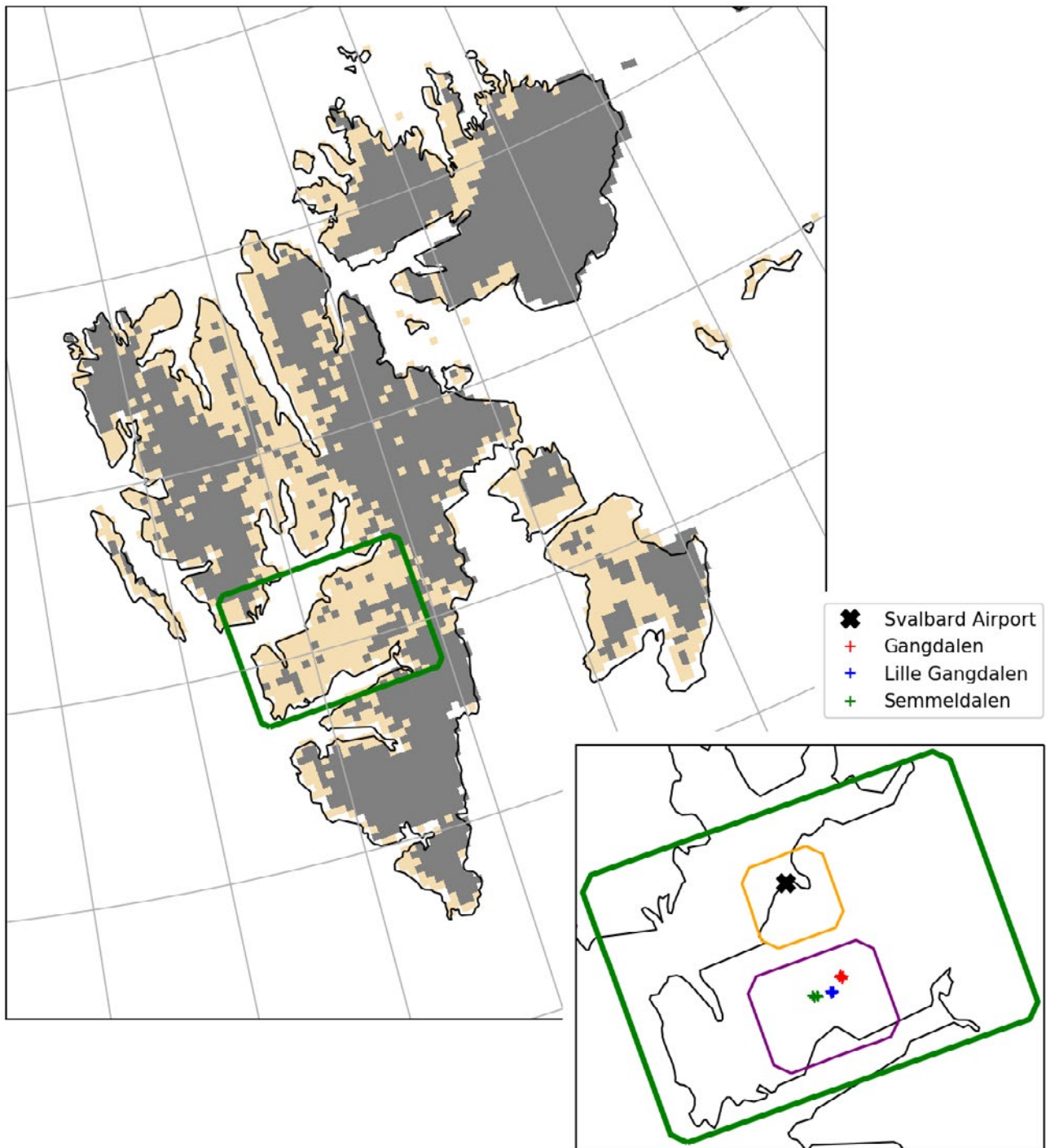


Figure 1: Map of Svalbard showing the study area in Central Spitsbergen. Glaciated pixels are shown in grey. The inserted map shows the regions that are used for comparison between the satellite snow product against in-situ snow cover data (orange square) observed at the manned weather station at Svalbard Airport (marked with a black marker), and against in-situ spatial data on snow-off dates (purple square) in three valleys on Nordenskiöld Land – Gangdalen, Lille Gangdalen and Semmeldalen – marked with red, blue, and green markers, respectively.

2.1 Dataset description

2.1.1 Satellite data for terrestrial snow

The Advanced Very High Resolution Radiometer (AVHRR) instrument is a versatile imaging instrument used for monitoring cloud cover, land and water surfaces. Sea surface temperature, snow cover, ice cover and vegetation characteristics are parameters that can be derived from AVHRR data. The instrument has flown onboard polar-orbiting satellites since the late 1970s. The resolution is approximately 1 km, but only data at a reduced resolution of approximately 4 km is permanently archived and available with Global Area Coverage (GAC). A Fundamental Climate Data Record (FCDR) for radiances and brightness temperatures from the AVHRR GAC data has been made available by the EUMETSAT Climate Monitoring Satellite Application Facility. The current FCDR covers 1982–2015 and is the basis for the satellite-based product for terrestrial snow cover discussed in this chapter. An updated FCDR, with an extended data period including 2020, is planned for release within 2021 and will allow for a larger overlap in time with more modern snow or snow-proxy in-situ observations, such as the in-situ data described in section 2.1.2.

MET Norway's probabilistic snow cover algorithm, normally used in conjunction with AVHRR data for the mainland of Norway (Killie et al. 2011), has been adjusted to be used for the Svalbard archipelago. The algorithm uses a set of signatures (instrument channel combinations) and statistical coefficients derived from training datasets of typical surface classes. Satellite swath products from 24 hours are aggregated into daily products at 4 km grid spacing, and a threshold at 50% probability for snow is set, giving a daily, binary snow/no snow product. This snow cover product has been validated against ground observations of snow depth from weather stations at Ny Ålesund, Svalbard Airport, Hornsund, Barentsburg, Bjørnøya and Sveagruva, and from samplings of snow depths across Nordenskiöld Land. The total hit rate for snow was in the 92–98%

range for the different observation sites, and the total hit rate for snow-free land was in the 52–64% range. Representation error is a challenge when validating a 4 km satellite product against point observations. The location of the weather station does not necessarily represent the surrounding terrain well. This can be particularly challenging for Svalbard, which is characterized by a narrow coastal zone and steep terrain. In some cases, the ground observation is located near glaciers, and the corresponding satellite grid cell is dominated by the radiative properties of the glacier.

In addition to the relatively coarse resolution, AVHRR data are also limited by clouds. Due to frequent cloud cover in the Arctic regions, a 24-hour aggregation period is normally insufficient to give a cloud-free product for Svalbard. Therefore, the dataset contains a gap-filled product as well, where the nearest-in-time cloud-free information searching up to 9 days forward or backward in time is filled in when needed. In the following analysis, the gap-filled product is used.

The algorithm uses reflected sunlight from the surface, and only the pixels for which the solar elevation is 10 degrees or more above the horizon are processed. The Svalbard dataset is therefore constrained to March through September for each year of 1982–2015. This means that the melting season is well covered, but the onset of the snow season later than September is not covered. From this binary product, the following parameters can be derived: The number of snow-free days (SFD) is calculated for each pixel as the number of days with no snow over a time period of interest; the snow-covered fraction (SCF) is the ratio of snow-covered pixels to the total number of land pixels per day; and the land-covered fraction (LCF) is similarly the ratio of snow-free pixels to the total land pixels. The snow cover extent (SCE) shows the accumulated area of snow-covered pixels in square kilometres and is useful for comparing monthly or interannual variations.

In Figure 2, the upper right panel shows the SCF for each day in 1982–2015. A 9-days moving average has been applied to reduce high frequency noise. As seen by the seasonal time series, the melting detected from this dataset typically starts between the second half of May and end of June. The years are coloured depending on their decade and thereby indicate a shift towards an earlier melting start and advanced spring season. The lower right panel shows the trend of the melt onset by plotting for each year the day-of-year when the SCF falls below 95%. The linear trend of the melting onset is found to have a negative rate of 2.6 days per decade (significant to the 0.05 level). This corresponds to well a week earlier melt-start over the 30+ years of satellite data studied here.

Figure 3 shows the spatial distribution of the trend over the 1982–2015 period in the total SFD during May to August, as well as a histogram of all land pixels as a function of height, where the colour represents the trend values. About 77% of the pixels showing a significant trend have an increase in the number of snow-free days (red colour), while 23% show a decrease (blue colour). The areas of largest positive trends are concentrated in regions that are dominated by lowland valleys and coastal plains. Most noticeable are the trends centred near the large valleys on Nordenskiöld Land: Adventdalen, Reindalen and Sassendalen. Here, a positive trend in the range of 1 to 2 days per year is found. The areas with a decrease in SFD (blue regions) are less dependent on elevation.

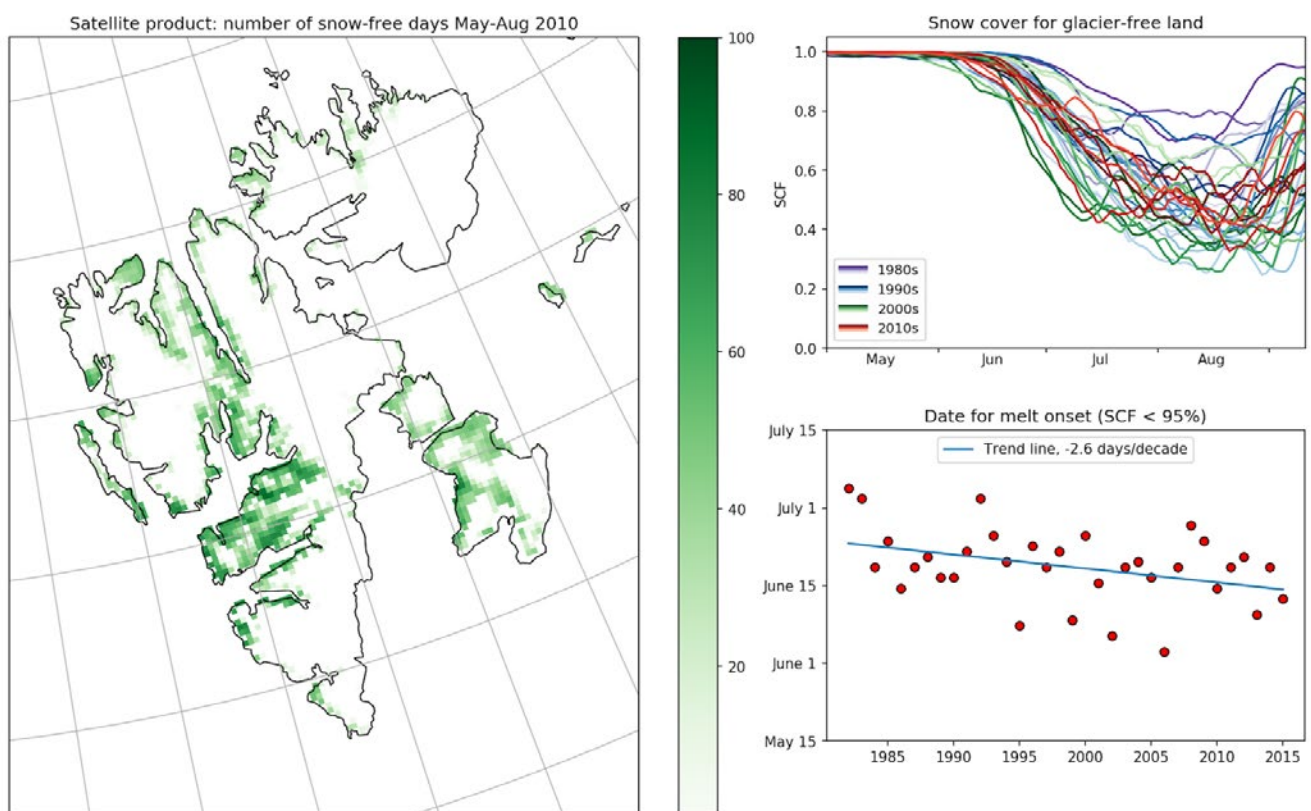


Figure 2: The left panel shows the number of snow-free days for the summer period May–August for 2010. The upper right panel shows the total ratio of snow-covered area (the SCF from which glacier areas are excluded) during May to mid-September. Each year of the 1982–2015 period is indicated by a separate line. A 9-days moving average has been applied. The lower right panel shows a scatter plot for the day-of-year for which the SCF shrinks below 95%, ref: upper right panel.

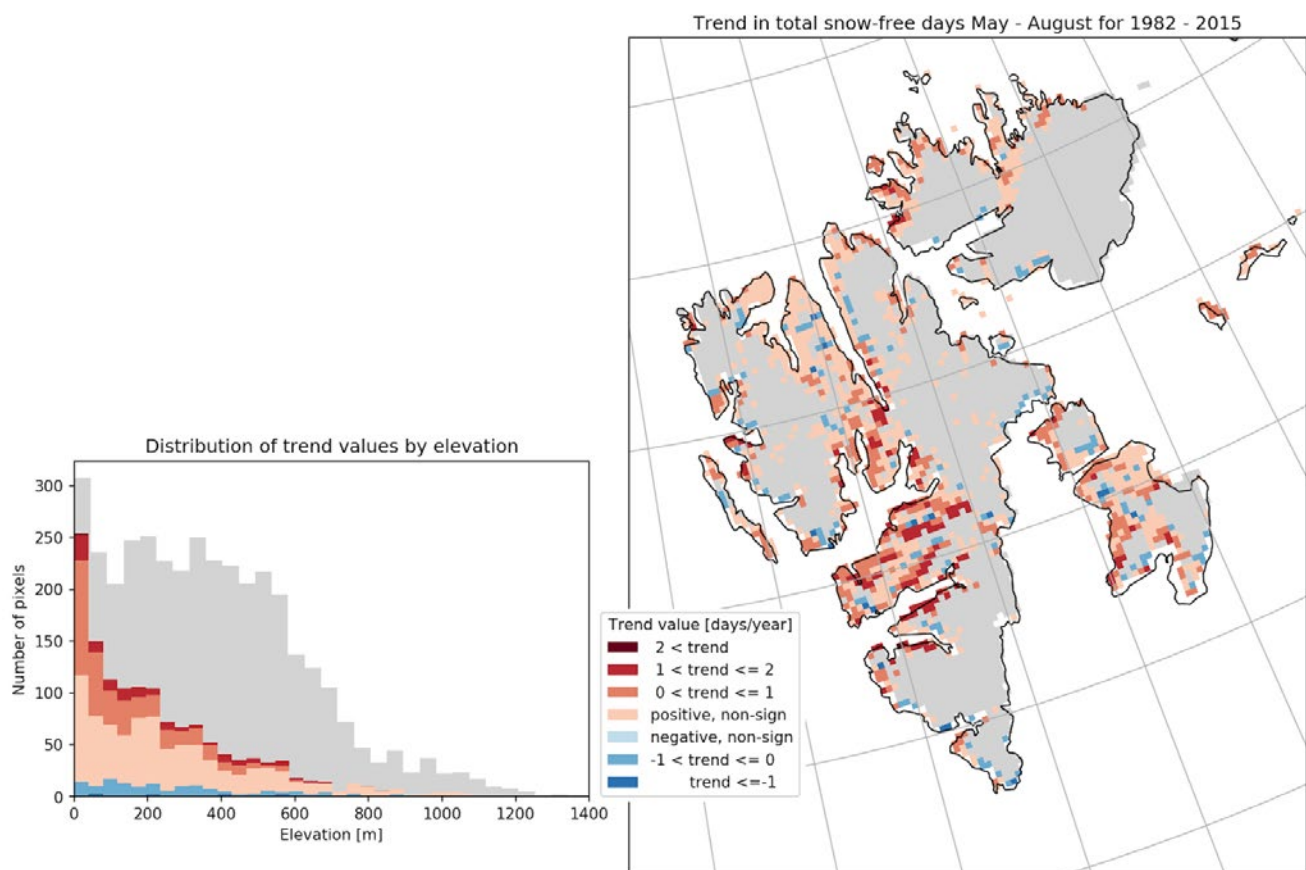


Figure 3: Right panel: Trend map in the total number of SFD from May to August over the 1982–2015 period. Grey areas are glaciated pixels (masked). Positive trends are shown in red, and negative trends are shown in blue. Non-significant trends are shown in light red/light blue. Left panel: The histogram shows the trend values as a function of elevation. The grey background shows how the glaciated pixels are distributed as a function of elevation.

2.1.2 In-situ data for snow

In this study, we use two different types of in-situ snow data: snow-off dates derived from temperature loggers from the COAT observation system and manually observed records for snow cover from a weather station. Both datasets are described briefly in this section and compared with the satellite snow product in section 2.2.1.

The long-term Climate-ecological Observatory for Arctic Tundra (COAT) observation system monitors several state variables, including the timing of snowmelt, locally in a network of temperature loggers on the ground surface (Ims et al. 2013). In 2009, a spatial design was implemented to cover the two most important Svalbard reindeer habitats (Loe et al. 2016). COAT builds on this and its own established network of loggers. “Ground surface temperature” is defined as the surface or near-surface temperature of the ground

(bedrock or surficial deposit), as measured in the uppermost centimetres of the ground. Ground surface temperature data loggers are currently spatially widespread within the COAT regions on Nordenskiöld Land and along the west coast (Brøggerhalvøya and Forlandssundet). With the data from these loggers, it is possible to calculate the snow-off dates (c.f. Staub and Delaloye, 2017). Let’s take an example from three valleys on Nordenskiöld Land (see inset in Figure 1). Here, ground temperature loggers (iButton DS1921G; Maxim Integrated, San Jose, California, USA) have been placed in the soil surface in the ridge (dominated by *Salix polaris*) and sub-ridge vegetation (dominated by *Luzula confusa* and/or *Poa spp.*) at 48 locations, along elevational gradients throughout the study area. Ridge and sub-ridge vegetation types were selected because they constitute the main feeding habitat for reindeer in winter (Hansen et al. 2010). Wind-induced snow transport processes result in a strong heterogeneity of the winter snow cover (e.g. Luce

et al. 1998; Mott et al. 2012). The spatial variability of the snow depth distribution at the time of peak accumulation and the local energy balance result in a gradual development of a patchy snow cover during the ablation period (Mott et al. 2012). The COAT ridge and sub-ridge sites used here are exposed to wind, and snow depths are generally thinner (typically snow depth is 35 cm in March according to Loe et al. 2016) than those in other areas of the landscape where snow accumulates as deep drifts in sheltered spots and where it remains until early summer (snowbed communities). Thus, these sites must be regarded as sites representing early snow-off dates. Each logger recorded the soil surface temperature every fourth hour throughout the year with accuracy of 0.5 degrees C. Data description and protocols are further described in Loe et al. (2016).

In-situ observations of snow cover (SC) are manually performed by the Norwegian Meteorological Institute in a radius of 1 kilometre around the weather station at Svalbard Airport (see Figure 1). The observations are made in line with national and international guidelines for observations of snow cover. SC is an estimated assessment made by an observer and the results may be slightly dependent on the person. SC is reported using codes 0–4: 0 – No snow, 1 – Mostly bare ground, but some snow patches, 2 – Half the ground is snow covered, 3 – Mostly snow-covered ground, but some bare patches and 4 – Full snow cover.

2.1.3 Snow model data

Van Pelt et al. (2019) present a dataset of simulated glacier climatic mass balance, seasonal snow conditions and runoff for the entire land-area of Svalbard. Driven by a meteorological forcing from a regional climate model, the model solves the surface energy balance to estimate surface temperature and melt and simulates the multi-layer evolution of snow temperature, density and water content (Van Pelt et al. 2012; Van Pelt and Kohler 2015). For 1957–2018, Van Pelt et al. (2019) found, for Svalbard, a non-significant trend in snow disappearance date (0.0 ± 0.9 days decade⁻¹) and a significant increase in snow onset date (1.4 ± 0.9 days decade⁻¹). Here, the model output of snow

water equivalent (SWE), including both seasonal snow and multi-year snow (firn), is used. The SWE data are projected from the original 1-km resolution model grid to the 4-km resolution satellite product grid by means of linear interpolation. From the SWE data, the number of SFD is calculated by assuming that snow-free conditions apply when SWE is below 0.01 m water equivalent. The snow model data is compared with the satellite-based snow cover product in section 2.2.2.

2.1.4 Satellite data for sea ice

For more than four decades, sea ice has been monitored in the polar regions by using satellite remote sensing. In this study, we use the global sea-ice concentration climate data record, version 2, from the EUMETSAT Ocean and Sea Ice Satellite Application Facility (OSI SAF). Sea-ice concentration (SIC) is computed from a combination of brightness temperatures from the long-term series of satellite passive microwave instruments SMMR, SSM/I and SSMIS. The product is provided on a 25-km resolution grid but the true spatial resolution is closer to 50 km. The data record contains daily files for the 1979–2015 period, which covers the full-time series of the satellite snow product (section 2.1.1). All daily files and product documentation are available from the OSI SAF web portal (Table 1). More details on the retrieval method and product validation are also found in Lavergne et al. (2019). It must be noted that due to the coarse spatial resolution and potential coastal noise, this product is not meant to monitor the ice cover in the long narrow fjords but mainly represents the conditions in the open adjacent sea.

During winter months, Svalbard is almost encapsulated by sea ice except for the western part with much-reduced sea ice due to the influence of the warm Atlantic water in the West Spitsbergen Current. In the summer months, the ice edge retreats northward and is often completely detached from the coast of Svalbard. Typically, the ice cover is the largest around March, and the sea-ice minimum occurs around September [see Figure 4 (upper two panels)].

In order to investigate how the presence of sea ice might influence the onset and speed of snow melting on land, a time series of daily sea-ice area (SIA) is derived from the SIC data within a region around Svalbard (0–40°E longitude, 72–85°N latitude). SIA is defined as the accumulated area of the ocean surface covered by any amount of ice (with SIC > 0%). Figure 4 (lower left panel) shows the seasonal curves of the Svalbard SIA for 1982–2015 with each year coloured differently. SIA has large seasonal and interannual variabilities; however, an overall trend of decreasing SIA values per decade is visible throughout the year.

Figure 4 (lower right panel) shows the spatial distribution of the concentration trends in June, as computed in each pixel over the 1982–2015

period. June is a typical melting month midway between maximum and minimum ice conditions, and the ice concentrations are seen to be dominated by negative trends (red) in the Svalbard region, especially along the ice edge east of Svalbard into the northern Barents Sea. A dominance of negative trends in the Svalbard region is found for all months in the year with the strongest trends in the mid-winter months of November to February (not shown). The negative trends suggest a more retained ice edge and a less dense ice cover around Svalbard, which, again, may result in more direct interaction between the relatively warm open ocean and the cold winter atmosphere. Section 2.2.3 contains an analysis of the sea ice trends in relation to the trends for the snow cover derived from the satellite dataset.

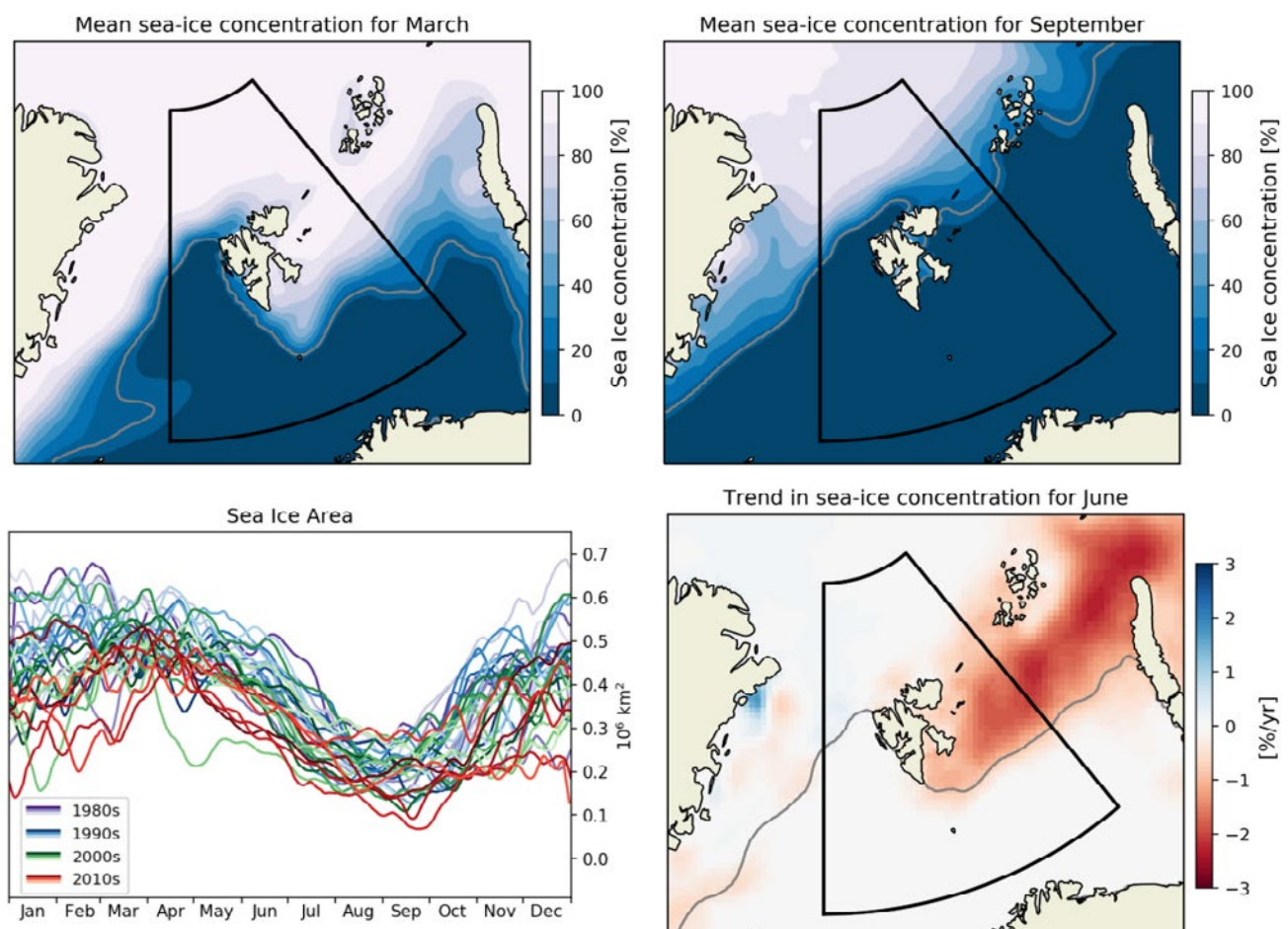


Figure 4: The upper two panels show the mean sea-ice concentration (1982–2015) in March and September, representing the maximum and minimum ice condition around Svalbard. The lower left panel shows the seasonal sea-ice area where each year from 1982 to 2015 is indicated by a separate line. A 9-day moving window average has been applied. The lower right panel shows the trend in the mean sea-ice concentration in June over the 1982–2015 period, with red and blue colours indicating negative and positive trends respectively. For the map plots, the grey contour line along the ice edge represents the 15% line of concentration. The black box on the maps is the Svalbard region over which the sea-ice area is computed. Data source: EUMETSAT OSI SAF global sea-ice concentration climate data record (version 2).

2.2 Data analysis

2.2.1 Comparison of satellite snow with in-situ data

The overlap between the satellite snow cover product (1982–2015) and the in-situ snow-off date data (2010–2015) from COAT is too short for trend analysis, but the comparison and discussion are included here. We focus on three areas on the central Nordenskiöld Land: Gangdalen, Lille Gangdalen and Semmeldalen (see Figure 1). In Figure 5, the upper left panel shows a comparison of the median number of snow-free days from May to July for the in-situ snow-off data for 16 monitoring sites, each within the three areas for each year in 2010–2015 with an average number of SFD from the satellite product collected for a surrounding region (see Figure 1, purple square). Two different elevations are used as maximum, in order to restrict the satellite extract to lower-lying areas. The in-situ monitoring sites are mostly located at or near the base of the valley.

Comparing the ratio of snow-free land according to the satellite product (the LCF) for the same region, as restricted to four different maximum elevations, we find that here the median snow-off date takes place for a low LCF (see Figure 5, upper right panel). The maximum snow-off date corresponds

to LCFs in the range of 0.5 to 0.9, depending on the maximum pixel elevation. Considering that the in-situ sites generally represent early snow-off dates, these results are reasonable.

Comparisons are also drawn between the satellite snow product and the in-situ observations of snow cover around Svalbard Airport, as described in section 2.1.3. Satellite data are collected for a region near the weather station (see Figure 1, orange square), and is limited to only contain pixels between sea surface level and up to an elevation of 200 meters. The SCF for this region is shown in Figure 5 (lower left panel) as a function of the day. The median value together with the 10 and 90 percentiles are shown in the same panel (red lines). Blue lines show the median and the 10 and 90 percentiles for the SC code from the in-situ snow data. The lower right panel shows in-situ snow cover data with dashed lines and satellite data with solid lines. Here, the data are gathered in decades, and median values are shown. Both the in-situ snow cover data and the satellite data show a shift towards earlier melting of snow. Svalbard Airport is located at the outermost part of Adventdalen and near the fjord Isfjorden and is exposed to strong winds, which means that it only has a thin snow cover in winter and, like the COAT data, is early snow-free. The observed differences between the satellite product and station data are reasonable.

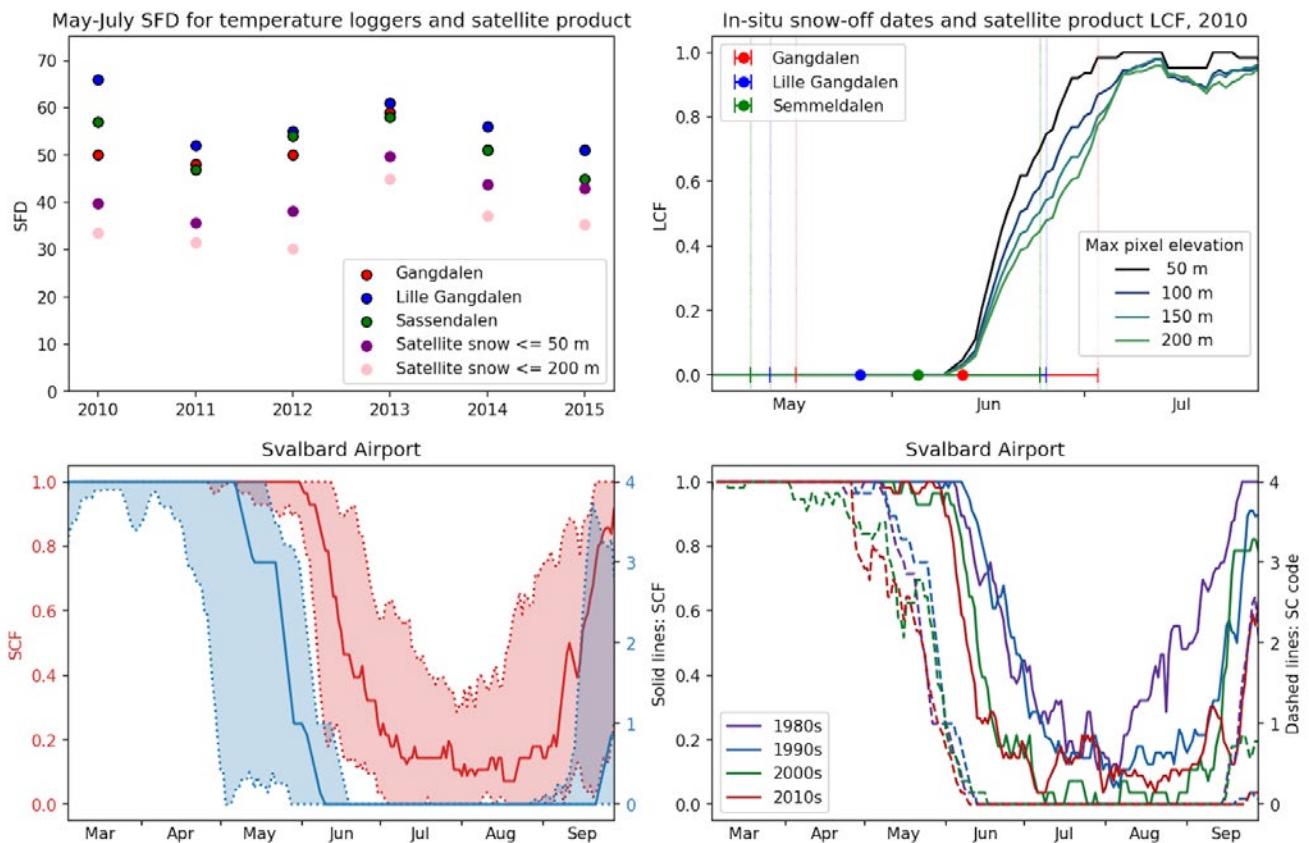


Figure 5: The upper left panel shows the number of SFD during May–July from the in-situ snow-off data from three valleys, using the median values derived from 16 monitoring sites in each of the three valleys. The plot also shows an average number of SFD for the same period from two extracts of the satellite data. One extract (shown in purple) takes unglaciated satellite pixels up to a maximum elevation of 50 meters. The total number of snow-free pixels within the region is summed and divided by the total number of pixels. The process is then repeated with a maximum elevation of 200 meters (shown in pink). The upper right panel shows a comparison of snow-off dates for the iButton loggers with the ratio of snow-free land (the LCF) from the satellite product. The year 2010 is shown here. For the satellite product, 4 maximum elevations are set. The lower panels illustrate comparisons of the satellite snow product with in-situ SC data around Svalbard Airport. The left panel shows the median value for the satellite SCF for the orange square indicated in Figure 1 (averaged over 9 days) together with two percentiles in red, and the median value for the in-situ SC code together with two percentiles in blue. In the lower right panel, the data from the lower left panel are grouped in decades, and median values are shown.

2.2.2 Comparison of snow cover from the satellite with snow model

From the satellite data and the snow model data, the SFD for May–August has been found for each pixel for each year in the 1982–2015 period. Figure 6 compares the averaged total May–August SFD (top) and the trends (bottom). Trends are only shown for the non-glacier domain and for when the trend is significant at a 95% confidence level. Overall, the model and satellite products produce similar spatial patterns of both the average SFD and the associated trends. Both products find the highest SFD (up to 100 days) at low elevations in central Spitsbergen, where the strongest positive trends are also found (up to 2 days per year). The

latter high trends, implying a > 60 days increase in snow-free-season length over 1982–2015, can only be explained by the complete melting of multi-year snow patches during the study period. In other parts of Svalbard, trends are mostly non-significant, in part because of high inter-annual variability. A difference between the two products is that, in contrast to the satellite observations, the model SFD trend distribution does not show an alternating pattern of negative and positive trends in central Svalbard, but shows a more homogeneous positive trend.

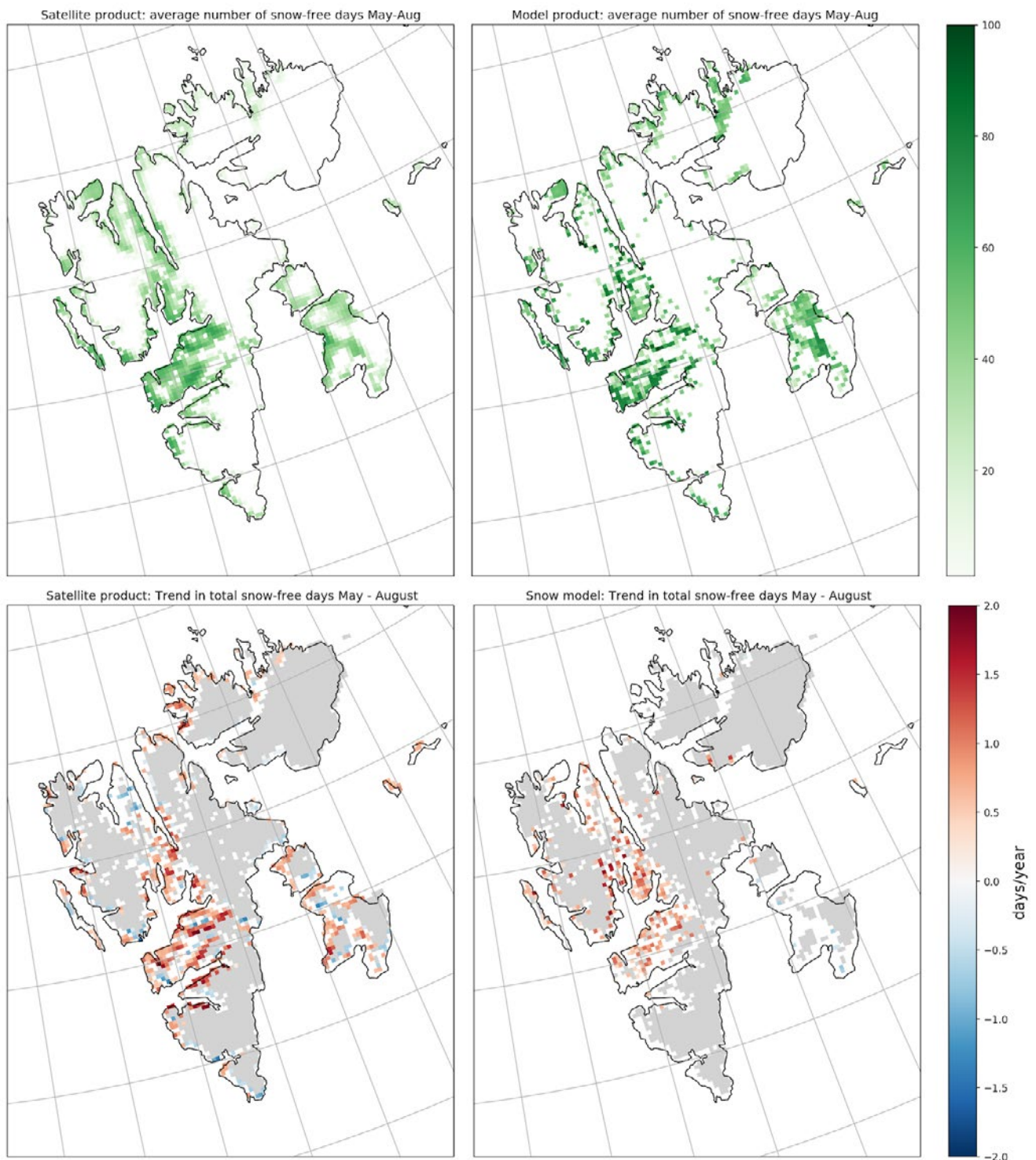


Figure 6: The upper panels show the mean SFD) for May–August over the 1982–2015 period for the satellite product (left) and the snow model interpolated to the satellite grid (right). The lower panels show the trend in total SFD for May–August over the same years, again with the satellite product (left) and snow model (right). Here, glaciated pixels are masked (grey), and only pixels significant to the 5% p-level are coloured.

2.2.3 Correlation between snow on land and sea ice

In the previous sections that presented the long-term satellite datasets of terrestrial snow in Svalbard and sea ice in the adjacent sea, negative trends dominated both datasets over the 34-year period from 1982 to 2015. The onset of snow melting has, on average, advanced more than a week from late June to mid-June, and the sea-ice conditions show dominantly negative trends in the Svalbard region for each month of the year. Despite the long-term negative trends in common, how well does the interannual variability of the snow cover on land and the amount of ice-covered adjacent seas relate to each other? The monthly averaged values of the SIA and SCE are compared with a range of time lag combinations: SCE for May to August against SIA for January to August. Both datasets are linearly detrended in order to avoid high correlation without causation. Instead, we are seeking the correlation of their respective interannual variations.

The first comparison of SIA with SCE, including all land pixels (excluding glaciers), results in positive but non-significant correlations for all time lag combinations. This correlation between sea-ice area and Svalbard total snow cover is also supported by a recent study by Vickers et al. (2020), who compared the Svalbard snow cover based on remote-sensing MODIS data and the regional sea ice in the 2000–2019 period. In the following comparisons, we therefore account for the elevation of the land pixel. The trend in the

duration of the snow cover was found to be strongly dependent on the land elevation (Figure 3), and it is thus reasonable to assume that any atmospheric effect from an ice-covered/ice-free ocean will also have a larger influence on the lowlands rather than on the higher mountains where temperatures are colder and often below 0 degrees.

The combinations giving the highest correlations are presented in Figure 7 (left panel) as a function of the selected maximum pixel elevations between 50 m and 250 m a.s.l. Comparison of the SCE for June and SIA for June results in significant positive correlations for all the lowland elevations (green line). A significant positive correlation with a 2-month time lag is also found between SCE (up to 150 m pixel elevation) for June and SIA for April. Beyond that, overall positive correlations are found between SCE for June and SIA for January to March and May, but they may not be significant to a 5% p-level. That the June values of SCE caused the highest correlations against the SIA does not come as a surprise as June represents the time of onset of snow melting, which is again most probably affected by the ocean-air interactions and transport of warmer or colder winds from an open ocean or ice-covered ocean, respectively, over land. The significant linear relationship in June ($R=0.45$, $P=0.009$) is shown in the scatter plot in Figure 7 of SIA against SCE for land pixels of maximum 50 m elevation. Both monthly datasets are detrended, and each dot represents a year within the 1982–2015 period, coloured with respect to their decadal affiliation.

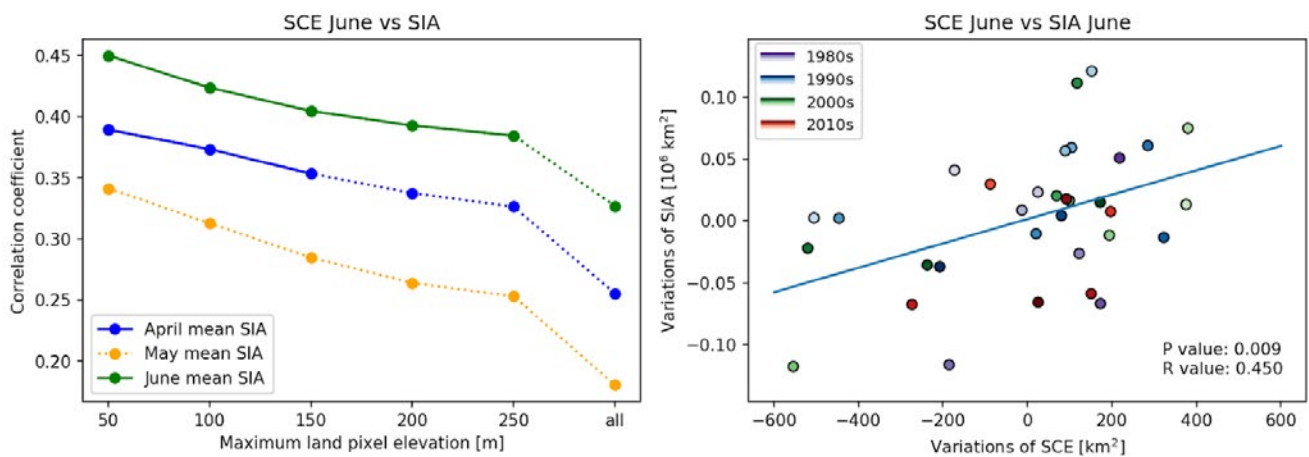


Figure 7: Left panel shows the correlation between the SCE in June and SIA for April, May and June, which gave the highest correlations. Correlations are plotted against the maximum pixel elevation from 50 m to 250 m, and also includes correlation using all land pixels (glacier excluded). The solid line represents when correlation is significant to 5%, whereas the dotted line represents non-significant correlation. Right panel shows the scatterplot of SCE against SIA for June (with no time lag), which had the highest correlation ($R=0.45$, $P=0.009$). Each yearly dot is coloured with respect to its decadal affiliation.

3. Connections and synergies with other SESS report chapters

The data and analysis of snow in Svalbard presented in this chapter are related to other chapters in this issue. The chapter “Satellite and modelling-based snow season time series for Svalbard: Inter-comparisons and assessment of accuracy” (Malnes et al. 2021) compares a MODIS-based time series of fractional snow cover (2000–2020) with other satellite-based snow datasets (including the satellite snow time series discussed herein) and with snow models (including the snow model used in this chapter). They focus on differences between the datasets and investigate whether the datasets can build on each other and thereby provide a long-term time series of snow cover data.

The chapter “Terrestrial Photography Applications on Snow Cover in Svalbard (PASSES)” (Salzano et al. 2021) gives an overview of time-lapse camera systems working in Svalbard, with special focus on snow cover applications. The PASSES initiative has managed to identify a large number of image providers, archived imagery and processed datasets dating back to the year 2000. Despite the differences in spatial resolution, the identified time-lapse imagery and fractional snow cover products might be an important source of data for calibration and validation of both snow (Aalstad et al. 2020) and sea ice satellite products.

4. Unanswered questions

Here we list some questions that still remain to be explored to fill the gaps we have identified.

- What are the changes/dynamics in snow cover extent during the polar night period?
- The alternating pattern of negative and positive trends in central Svalbard seen in the satellite product should be investigated. It is not found in the snow model. Is this an artefact, or does it reflect the increase in precipitation seen over Svalbard (cf. Hanssen-Bauer et al. 2019)?
- In the present study, temporal variation in the snow was compared directly with sea-ice area variability. However, how is this relation affected by other geophysical factors such as temperature, wind, and humidity?
- In the analysis of different time-lag combinations between snow and sea ice, a negative correlation was found between late-summer snow and mid-winter sea-ice conditions. This is out of the scope of this chapter, but an unanswered question is whether a reduced sea-ice cover early in the year might affect a long-lasting snow cover in Svalbard. Could it be a chain reaction where less ice causes more ocean–air interaction, thereby causing more humidity over land, which again results in more snow precipitation?

5. Recommendations for the future

Focus on snowpack properties: The ecosystem impact of changing snowpack properties, snow cover extent and duration in a warming climate is a particularly central theme in COAT and a generally important arena for interdisciplinary research between ecology and geophysics. Besides the need for co-location of research infrastructure, there is a need to develop a data-model fusion system that merges available observational datasets on snow properties with state-of-the-science, high-resolution (1- to 500-meter scale), physically based snow models. The goal of this data-enhancement system is to create accurate, spatially distributed and time evolving datasets that can be used to better understand relationships between drivers (predictors) and biotic responses and ecosystem processes. Several climate impact pathways formalized by COAT conceptual models are driven by changes in snowpack properties, snow cover extent and duration. State-of-the-art monitoring of such pathways is dependent on snow modelling products, and joint efforts will contribute to this. See further details in Pedersen et al. (2020).

Focus on spatially and temporally explicit sea-ice maps: Wildlife use sea ice as hunting and migration corridors, and the lack of high-quality maps at the relevant spatial and temporal scales relevant to wildlife is hampering the possibility of analysing data at ecologically relevant scales to the long-term monitoring of climate change effects of the COAT program. Such products may also be essential in the continuation of understanding the linkages between sea ice and terrestrial primary productivity (Macias-Fauria et al. 2017).

Strengthen the collaboration: The scientific community will benefit from a more coordinated cooperation between snow research groups operating in and outside the SIOS infrastructures and the wider snow remote sensing community. Remote sensing products need high-quality calibration and validation data series. Discovery and assimilation of archival and on-going snow depth, snow water equivalent and snow cover extent datasets (especially archival, dating back to the 80's) would be extremely helpful in calibration and validation of long-term satellite products and models.

6. Data availability

Table 1 contains a list of the datasets used, including the data owner and how to access the data.

Table 1: A list of the datasets used in this study

Dataset	Parameters	Period	Location	Metadata/Data Access	Data provider, reference
1982–2015 daily, binary snow cover maps for Svalbard	Snow cover	1982–2015	Svalbard archipelago	Available in the SIOS data access portal in Q1 2021	MET Norway
COAT data	Snow-off dates derived from temperature loggers (iButton)	2010–2015	Nordenskiöld Land	COAT database (not published yet) ¹ Research/Data/COAT-Data-Portal	NMBU (Leif Egil Loe)
Snow cover data from the Svalbard Airport	Manually observed in-situ data -	1982–2015	The manned station at Svalbard Airport	frost.met.no	MET Norway
A long-term model dataset of climatic mass balance, snow conditions and runoff in Svalbard (1957–2018)	SFD extracted from modelled SWE data	1982–2015	Svalbard archipelago	SIOS data access portal: https://bit.ly/3fG7pAZ	Uppsala University https://doi.org/10.5194/tc-13-2259-2019 , https://doi.org/10.6084/m9 .
Global sea-ice concentration climate data record 1979–2015 (v2.0, 2017), OSI-450	Sea-ice concentration from passive microwave data (SMMR/SSMI/SSMIS). Grid resolution of 25 km.	1982–2015	Northern Hemisphere	EUMETSAT OSI SAFdoi: 10.15770/EUM_SAF_OSI_0008, Data extracted: 1982–2015, 72–85N 0–40E, accessed Sep 2020.	http://osi-saf.eumetsat.int

Acknowledgements

This work was supported by the Research Council of Norway, project number 291644, Svalbard Integrated Arctic Earth Observing System –

Knowledge Centre, operational phase. We thank Leif Egil Loe, NMBU, for use of the temperature logger data for this purpose.

¹ <https://www.coat.no/en/>

References

- Aalstad K, Westermann S, Bertino L (2020) Evaluating satellite retrieved fractional snow-covered area at a High Arctic site using terrestrial photography. *Remote Sens Environ* 239:111618. <https://doi.org/10.1016/j.rse.2019.111618>
- EUMETSAT Ocean and Sea Ice Satellite Application Facility, Global sea ice concentration climate data record 1979-2015 (v2.0, 2017), OSI-450. doi: 10.15770/EUM_SAF_OSI_0008, Data extracted: 1982-2015, 72-85N 0-40E. Accessed 8 September 2020. Hansen BB, Isaksen K, Benestad RE, Kohler J, Pedersen ÅØ, Loe LE, Coulson SJ, Larsen JO, Varpe Ø (2014) Warmer and wetter winters: characteristics and implications of an extreme weather event in the High Arctic. *Environ Res Lett* 9:114021. <https://doi.org/10.1088/1748-9326/9/11/114021>
- Hanssen-Bauer I, Førland EJ, Hisdal H, Mayer S, Sandø AB, Sorteberg A (eds.) (2019) Climate in Svalbard 2100 – a knowledge base for climate adaptation, NCCS Report No. 1/2019. <https://www.miljodirektoratet.no/globalassets/publikasjoner/M1242/M1242.pdf>
- Ims RA, Jepsen JU, Stien A, Yoccoz NG (2013) Science plan for COAT: Climate-ecological Observatory for Arctic Tundra. Fram Centre, Tromsø. <https://www.coat.no/en/Publications/COAT-science-plan>
- Killie MA (2019) Validation of a Satellite based snow cover index for Svalbard. Project report for SIOS ACCESS project 2018_0007. https://sios-svalbard.org/sites/sios-svalbard.org/files/common/SvalSCE_2018_0007_correctedfigure.pdf
- Killie MA, Godøy Ø, Eastwood S, Lavergne T (2011) Algorithm theoretical basis document for the EUMETSAT ocean & sea ice satellite application facility regional ice edge product. Ocean & Sea Ice SAF project report no. OSI-146, Version 1.2.
- Lavergne T, Sørensen AM, Kern S, Tonboe R, Notz D, Aaboe S, Bell L, Dybkjær G, Eastwood S, Gabarro C, Heygster G, Killie MA, Kreiner MB, Lavelle J, Saldo R, Sandven S, Pedersen LT (2019) Version 2 of the EUMETSAT OSI SAF and ESA CCI sea-ice concentration climate data records. *The Cryosphere* 13:49–78. <https://doi.org/10.5194/tc-13-49-2019>
- Loe LE, Hansen BB, Stien A, Albon SD, Bischof R, Carlsson A, Irvine RJ, Meland M, Rivrud IM, Ropstad E, Veiberg V, Mysterud A (2016) Behavioral buffering of extreme weather events in a high-Arctic herbivore. *Ecosphere* 7:1. <https://doi.org/10.1002/ecs2.1374>
- Luce CH, Tarboton DG, Cooley KR (1998) The influence of the spatial distribution of snow on basin-averaged snowmelt. *Hydrol Process* 12:1671–1683. [https://doi.org/10.1002/\(SICI\)1099-1085\(199808/09\)12:10<1671::AID-HYP688>3.0.CO;2-N](https://doi.org/10.1002/(SICI)1099-1085(199808/09)12:10<1671::AID-HYP688>3.0.CO;2-N)
- Macias-Fauria M, Karlsen SR, Forbes BC (2017) Disentangling the coupling between sea ice and tundra productivity in Svalbard. *Sci Rep.* 7 8586 <https://doi.org/10.1038/s41598-017-06218-8>
- Malnes E, Vickers H, Karlsen SR, Saloranta T, Killie MA, Van Pelt W, Pohjola V, Zhang J, Stendardi L, Notarnicola C (2021) Satellite and modelling based snow season time series for Svalbard: Inter-comparisons and assessment of accuracy. In: Moreno-Ibáñez et al (eds) SESS report 2020, Svalbard Integrated Arctic Earth Observing System, Longyearbyen, pp. 202 – 219. https://sios-svalbard.org/SESS_Issue3
- Mott R, Gromke C, Grünewald T, Lehning M (2012) Relative importance of advective heat transport and boundary layer decoupling in the melt dynamics of a patchy snow cover. *Adv Water Resour* 55:88–97. <https://doi.org/10.1016/j.advwatres.2012.03.001>
- Pedersen ÅØ, Stien J, Albin S, Fuglei E, Isaksen K, Liston G, Jepsen JU, Madsen J, Ravolainen VT, Reinking AK, Soininen EM, Stien A, van der Wal R, Yoccoz NG, Ims RA (2020) COAT – Climate-ecological Observatory for Arctic tundra. In: Van den Heuvel et al. (eds): SESS report 2019, Svalbard Integrated Arctic Earth Observing System, Longyearbyen, pp. 58–83. https://sios-svalbard.org/SESS_Issue2
- Salzano R, Aalstad K, Boldrini E, Gallet JC, Kępski D, Luks B, Nilsen L, Salvatori R, Westermann S (2021) Terrestrial photography applications on snow cover in Svalbard. In: Moreno-Ibáñez et al (eds) SESS report 2020, Svalbard Integrated Arctic Earth Observing System, Longyearbyen, pp. 236 – 251. https://sios-svalbard.org/SESS_Issue3
- Staub B, Delaloye R (2017) Using near-surface ground temperature data to derive snow insulation and melt indices for mountain permafrost applications. *Permafrost. Periglac. Process* 28:237–248. <https://doi.org/10.1002/ppp.1890>
- Van Pelt WJJ, Oerlemans J, Reijmer CH, Pohjola VA, Pettersson R, Van Angelen JH (2012) Simulating melt, runoff and refreezing on Nordenskiöldbreen, Svalbard, using a coupled snow and energy balance model. *The Cryosphere* 6:641–659. <https://doi.org/10.5194/tc-6-641-2012>
- Van Pelt W, Kohler J (2015) Modelling the long-term mass balance and firn evolution of glaciers around Kongsfjorden, Svalbard. *J Glaciol* 61:731–744. <https://doi.org/10.3189/2015JoG14J223>
- Van Pelt W, Pohjola V, Pettersson R, Marchenko SA, Kohler J, Luks B, Hagen JOM, Schuler T, Dunse T, Noel B, Reijmer C (2019) A long-term dataset of climatic mass balance, snow conditions, and runoff in Svalbard (1957–2018). *The Cryosphere* 13:2259–2280. <https://doi.org/10.5194/tc-13-2259-2019>
- Vickers H, Karlsen SR, Malnes E (2020) A 20-year MODIS-based snow cover dataset for Svalbard and its link to phenological timing and sea ice variability. *Remote Sens.* 12:1123. <https://doi.org/10.3390/rs12071123>

Terrestrial photography applications on snow cover in Svalbard (PASSES)

Roberto Salzano¹, Kristoffer Aalstad², Enrico Boldrini¹, Jean-Charles Gallet³, Daniel Kępski⁴, Bartłomiej Luks⁴, Lennart Nilsen⁵, Rosamaria Salvatori⁶, and Sebastian Westermann²

1 Institute of Atmospheric Pollution Research, National Research Council of Italy, via Madonna del Piano 10, 50019 Sesto Fiorentino (Firenze), Italy

2 Department of Geosciences, University of Oslo, P.O. Box 1047, Blindern, 0316 Oslo, Norway

3 Norwegian Polar Institute, Hjalmar Johansens gt. 14, NO-9296, Tromsø, Norway

4 Institute of Geophysics, Polish Academy of Sciences, Księcia Janusza 64, 01-452 Warsaw, Poland

5 Department of Arctic and Marine Biology, UiT, The Arctic University of Tromsø, Hansine Hansens veg 18, N-9019 Tromsø, Norway

6 Institute of Polar Sciences, National Research Council of Italy, Via Salaria km 29.300, 00015 Monterotondo (Roma), Italy

Corresponding author: Roberto Salzano, roberto.salzano@cnr.it
ORCID number 0000-0002-0750-0097

Keywords: Cryosphere, snow, fractional snow cover, time lapse photography

DOI: <https://doi.org/10.5281/zenodo.4294084>

1. Introduction

Mapping the evolution of the snow cover in Arctic regions is a critical task that must be addressed in order to estimate how the environment is affected and adapts to climate change. The snow cover characterization and its spatiotemporal evolution represent important factors to be considered in the framework of climate modelling at a global scale. Furthermore, snow cover is an Essential Climate Variable (ECV) of the Global Climate Observing System (GCOS), and high priority is assigned to enhancing and maintaining snow observations (World Meteorological Organization 2016). From this perspective, the continuous monitoring of snow cover is a major contemporary scientific challenge, and the advances in remote sensing explain why optical data are so commonly used for this purpose (Dietz et al. 2012; Petäjä et al. 2020). The description of snow cover comprises different parameters, and two variables – its extent and albedo – can be investigated using optical remote sensing (Gascoin et al. 2020; Vermote et al. 2016; Riggs et al. 2017). However, two different aspects must be considered for the enhancement of the final output: time and spatial resolution. Both components are connected using remotely sensed data (Dietz et al. 201), since the higher the spatial resolution (below hundreds of meters), the lower the revisit frequency will be (more than 1 week). The major advantage of monitoring the snow with remotely sensed data is the possibility of deriving area-wide and spatially comprehensive surface information with a regular and repeatable set of measurements, even in remote areas. In mountain areas, where the surface heterogeneity is greater, additional problems could affect the results. The state-of-the-art snow products concerning the snow extent are derived using remotely sensed data, and they are based mainly on the relation between the radiative behaviour of the surface and the Fractional Snow Cover (FSC), also defined as the Fractional Snow-Covered Area (f_{SCA}). This parameter describes the fraction of surface covered by snow in the picture element (pixel) of a remotely sensed image. The relation between the FSC and the optical behaviour of the surface represents the most common inference required by remote sensing

studies (Gascoin et al. 2020; Riggs et al. 2017; Vermote et al. 2016). There are many options for estimating this relation: combining satellite products with a different spatial resolution (Salomonson and Appel 2006, Yin et al. 2013), using spectral unmixing (Painter et al., 2009), and using ground-truth information (Aalstad et al 2020; Gascoin et al. 2020; Salzano et al. 2019). From this perspective, terrestrial photography provides an opportunity to have accurate ground truth when satellite overpass occurs, this ground truth could represent robust information useful for estimating site-specific relations between retrievals from different satellite platforms and FSC. The available time-lapse and webcam networks are important data sources for calibrating and validating satellite products, but a survey about available image datasets and the homogenization of the different data chains is needed to create a regional infrastructure. The availability of a time series concerning the snow cover is an important gap that can be filled by using terrestrial time-lapse photography. The use of terrestrial photography is not limited only to the estimation of the snow-covered area, but it has also shown potential in assessing other snow parameters. The optical calibration of the camera system can be useful for albedo-oriented applications, where the use of reference targets supports the description of the optical behaviour of snow (Corripio 2004; Garvelmann et al. 2013). Furthermore, modifications of the spectral sensitivity of the camera can be used for the retrieval of relationships between the reflectance in the near-infrared wavelength domain and the snow microphysics (Matzl and Schneebeli 2006). Additional snow features can be extracted from terrestrial images focussed on reference targets that can geometrically evidence the snow height (Bongio et al. 2019; Garvelmann et al. 2013; Parajka et al. 2012). Finally, terrestrial photography applications can also be adapted to other disciplines in order to study glacier dynamics (How et al. 2019; Vallot et al 2019), coastal processes (Nicu et al. 2020), and vegetation phenology at Arctic sites (Anderson et al. 2016; Beamish et al. 2020; Kępski et al. 2017). From this perspective, terrestrial photography provides a large variety of snow cover

applications with different maturity levels. Hardware limitations can nowadays be easily bypassed, since the technological developments and the limited costs support the availability of reliable devices that can operate under severe environmental conditions. Image processing represents the challenging component of this approach, since different algorithms are proposed, but the definition of a standardized procedure could be an important requirement. This summary is aimed

at defining the background where a snow camera network could be implemented in the framework of Svalbard Integrated Arctic Earth Observing System. The proposed contribution will be composed of the following sections: an overview of available webcams in the Svalbard archipelago; a first survey about available camera systems; the definition of a metadata profile useful for characterizing every camera node; and the description of processed datasets.

2. Overview of existing data

There is a large number of network cameras in Svalbard that can potentially be used for assessing the evolution of the snow cover. The knowledge about available datasets, their metadata descriptions, their processing chains, and their product specifications are all important factors for obtaining a complete overview of terrestrial

photography applications in such a remote area. The overview of cameras operating in the Svalbard archipelago has been approached by searching for specific applications on the snow cover and by collecting information about images that can be found on the web – that are not solely focussed on research purposes in the cryospheric domain (Figure

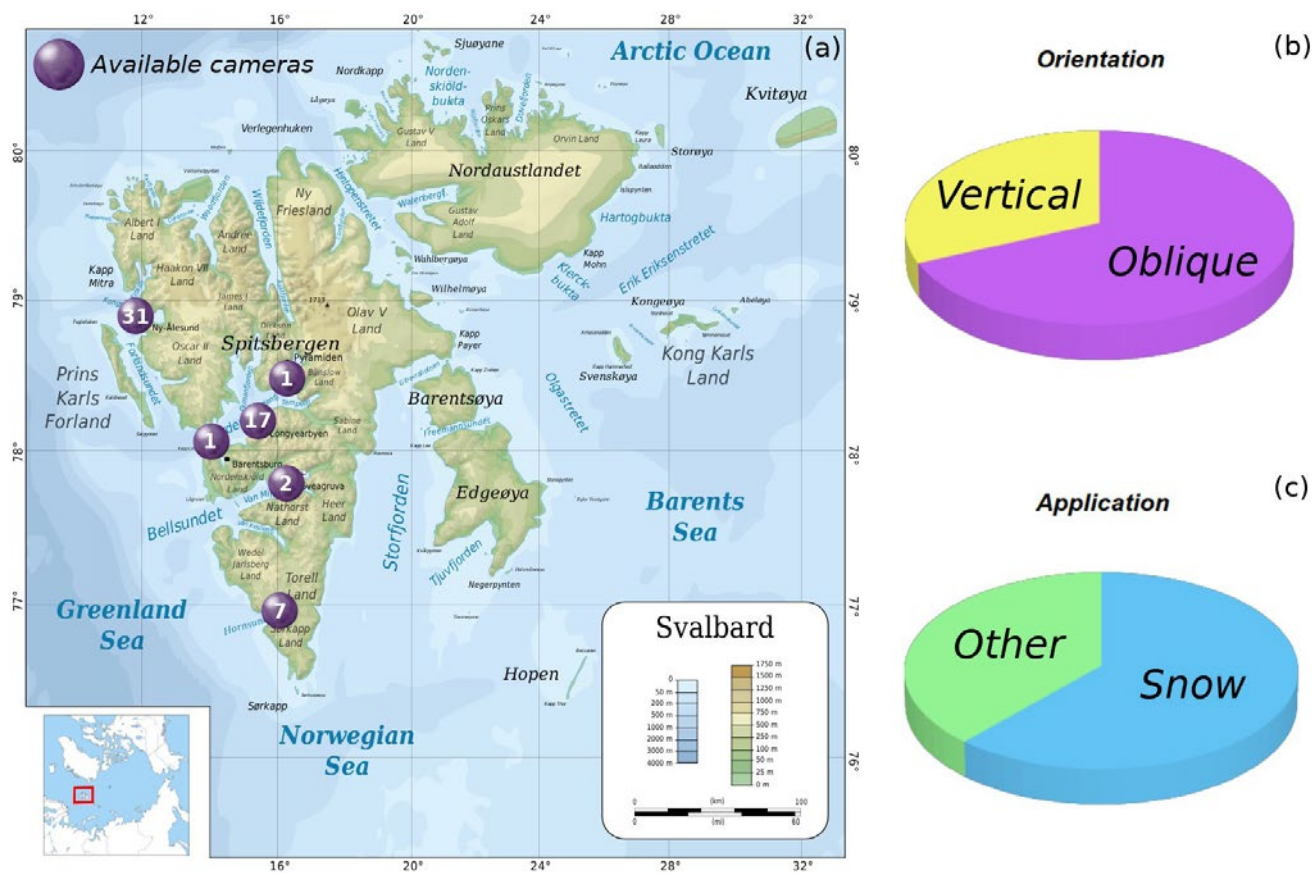


Figure 1: Distribution map of available cameras in Svalbard (a). Fraction of cameras with vertical versus oblique setups (b) and fraction that show snow cover (c).

1). The first step in defining a webcam network aimed at estimating the snow coverage with time-lapse cameras is to designate a metadata profile suitable for creating a registry of available devices.

2.1. Metadata profiling of terrestrial cameras

This primary task can be approached following the guidelines prepared by SIOS (Godøy and Holmen 2017), where the core of a metadata profile is based on mandatory information. This first component must be coupled with an expansion specific to instrumental devices and can possibly be enriched by additional data that are prepared for similar applications or to identify specific FSC estimations. The first component is described in the ISO 19115, where a general-purpose metadata is described. More detailed models for some aspects of resource description, including quality, data structure, or imagery, are defined in other ISO geographic information standards. The metadata

model described herein enables the implementation of domain-specific user extensions based on a common pattern to facilitate the implementation of software using those extensions. Extensions have been prepared considering the experience of other communities on similar camera networks (Peltoniemi et al. 2018; Seyednasrollah et al. 2019; Wingate et al. 2015) for other purposes such as vegetation phenology or ski resort monitoring. The increasing interest in establishing snow-related camera networks in the European Alps (Flöry et al. 2020; Portenier et al. 2020) has supported the identification of specific expansion components (Figure 2) for collecting information on: (i) already tested camera setups; (ii) repositories where imageries are archived; (iii) ortho-rectification approaches; (iv) quality check procedures; and (v) snow classification algorithms. Once a network is established, additional expansions can be defined in order to characterize site-specific conditions and uncertainties about the monoploting procedures and the snow cover retrievals.

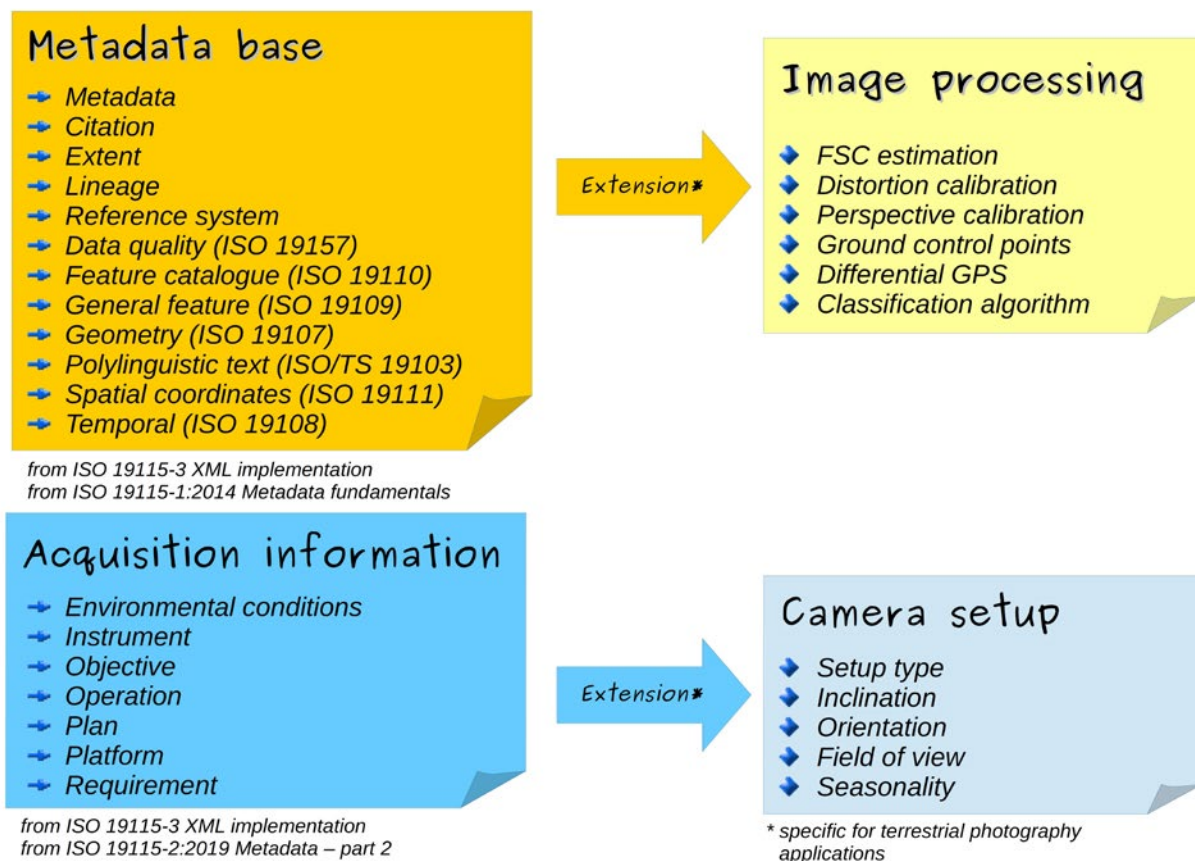


Figure 2: Identified components for describing the metadata profile required by a terrestrial camera network.

The collection of this information will be useful for: (i) an overview of the already tested camera setups; (ii) identification of the repositories where imageries are archived; (iii) survey of approaches focussed on ortho-rectification; (iv) censoring of quality check procedures; and (v) identification of snow classification algorithms.

2.2. Overview of cameras available in Svalbard

The overview of cameras operating in the Svalbard archipelago has been approached by searching for specific applications on the snow cover and by collecting information about images that can be found on the web – that are not solely focussed on research purposes in the cryospheric domain (Figure 1). The survey identified at least 60 cameras operating in the region that are managed by research institutions (87%) and local private companies (13%). The collected information includes facilities operated by 4 nationalities (Norway, Poland, Italy and France), by 8 SIOS members and by 8 non-SIOS member institutions. Further censoring activities are still necessary in order to involve parties in providing more detailed information, but this incomplete picture points us to the important constraints about the framework on terrestrial photography applications. Around 61% of the registered devices are involved in activities focussed on assessing the snow cover condition of the surface. About 70% of these cameras are actually operating, and about 30% are discontinued or under maintenance. Furthermore, while 32% of the imaging sensors are provided by systems with a vertical setup and a limited field of view, the rest are acquired by oblique-oriented systems, with a larger field of view. The number of motorized systems is increasing and pan/tilt/zoom cameras are available with large panoramic views. From this perspective, the identified systems can be categorized into four different classes defined by combining the orientation, site location and the resulting perspective (Table 1).

The installation of the registered cameras is affected by logistic issues (power supply, network connection, maintenance and other environmental problems), and the available

locations are consequently limited to a few areas where settlements are present: Longyearbyen, Ny-Ålesund and Hornsund. Mature snow-cover estimations from camera systems are limited to a few locations that will be described in the next sections. The rest of the cameras are not processed in terms of snow cover, and they are usually not archived in order to be compliant with the national regulations on privacy. This summary is focussed on the description of the datasets that have been designed for snow-related studies, are maintained at the moment and accessible to the scientific community.

Table 1: Classification of different camera setups

Orientation	Camera setup	Camera type	Coverage
Vertical	Close range	Standard	1–10 m ²
Oblique	Close range	Standard	< 1 km ²
	Long range	Standard	1–5 km ²
	Multiple views	Motorized	> 5 km ²

2.3. Ny-Ålesund

2.3.1. The Zeppelin Observatory

The Zeppelin Observatory is a research infrastructure managed by the Norwegian Polar Institute where a combination of different time-lapse cameras have been operating since 2000. The facility is located close to the top of the Zeppelin mountain (at 475 m a.s.l.) facing the Kongsfjorden in front of the Ny-Ålesund village. This dataset represents the longest camera time series available in Svalbard (Pedersen 2013), and different devices have been involved in acquiring images. The longest component of this dataset is the view looking at Ny-Ålesund village, where different cameras have been used during the acquisition history. This imagery has been provided by a fixed and oblique setup with a projected covered area ranging from 3 to 5 km². The camera system, upgraded from a low resolution sensor to the latest AXIS P5635-E-MKII device, has increased the image size from a

480sd to a 1080p format. Furthermore, the final acquisition timing has been fixed at an hourly scale, and all of the images have been archived, streamed online and made publicly available. The second component of this dataset is constituted by the imagery acquired by a pan/tilt/zoom device that now provides 4 different views of the Kongsfjorden once per day. The perspective is assessed by having at least ten ground control points (buildings, infrastructures, etc.) but all of the images are controlled in terms of alignment using customized procedures based on recognized patterns or objects

in each image (mainly identified from coastline and topography). Finally, projected pixels are grouped in satellite-derived grids (Sentinel, Landsat and MODIS are considered at the moment), and only grid elements with a consistent number of pixels included (100 pixels) are selected for the FSC retrieval. The analysis of this long time series provided a description of snow cover evolution over a decadal temporal range (Figure 3) and the obtained dataset was combined with different satellite platforms (Petäjä et al. 2020).

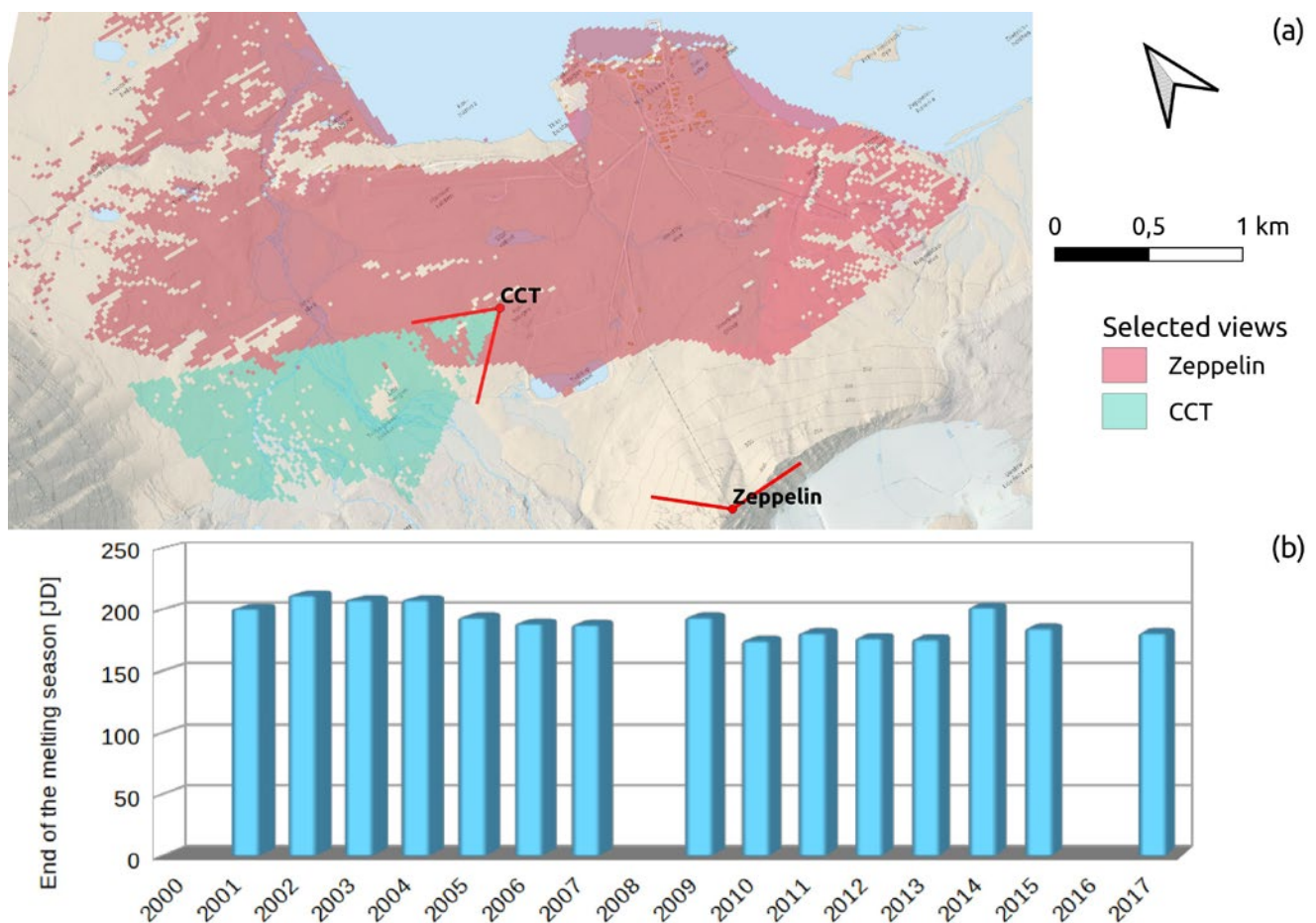


Figure 3: Representation of the projected areas covered by the different available cameras (a) on Zeppelinfjellet and close to the Amundsen-Nobile Climate-Change Tower (CCT). Estimation of the first snow-free day in the Brøggerdalen area (b).

2.3.2. The Climate Change Tower

Two cameras are located close to the Amundsen-Nobile Climate Change Tower at the Kolhaugen site: one with a vertical setup and one with an oblique orientation and a limited field of view. While the first device is positioned at 3 m above the ground, the second one is installed 15 m above the surface. Both are customized systems where the sensor is a Sony IMX219 with an 8 megapixel resolution. The projected area covered by each perspective view is controlled by each setup, and it can be estimated to be 5 m² and 1.2 km² respectively. Furthermore, both cameras acquire images hourly, and they have been operating since 2015 (vertical) and 2018 (oblique). Data are routinely downloaded to the CNR servers and are processed in terms of fractional snow cover using algorithms based on the blue-channel thresholding (Salvatori et al. 2011) and the

spectral similarity approach (Salzano et al. 2019). The perspective, especially for the oblique setup, is assessed by having at least ten ground control points but all of the images are controlled in terms of alignment using customized procedures based on recognized patterns or objects in each image. Finally, projected pixels are grouped in satellite-derived grids (Sentinel, Landsat and MODIS are considered at the moment), and only grid elements with a consistent number of pixels included (100 pixels) are selected for the FSC retrieval (Figure 4). The aims of these devices are: (i) to approach the multi-scale issue through different perspectives with different spatial resolutions (Petäjä et al. 2020); and (ii) to integrate the FSC assessment with the retrieval of spectral reflectance obtained by other instruments (Salzano et al. 2016).

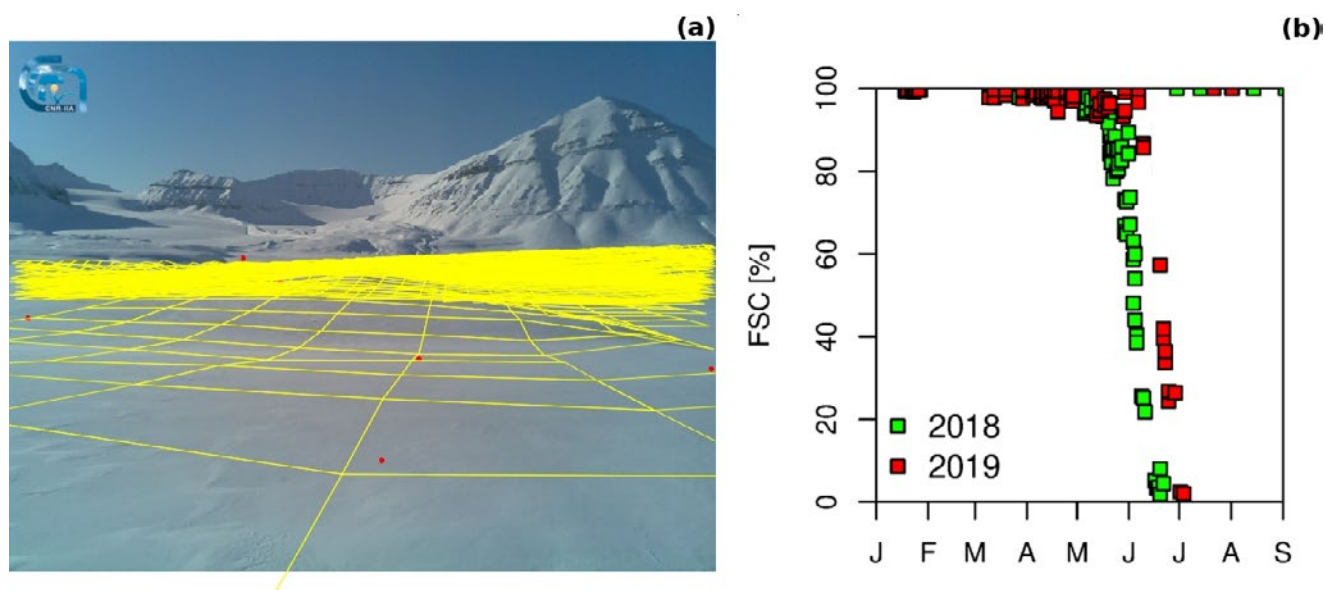
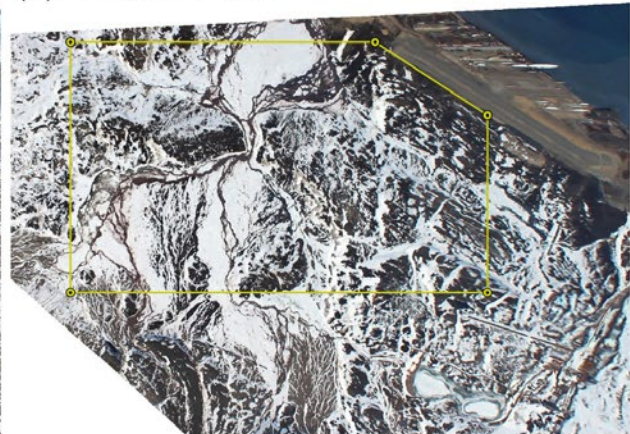


Figure 4: Example of a 20x20 m resampling grid projected on the image (a). Evolution of the melting season close to the Climate Change Tower (b).

(a) Time-lapse photograph



(b) Orthorectified



(c) Cropped



(d) Classified

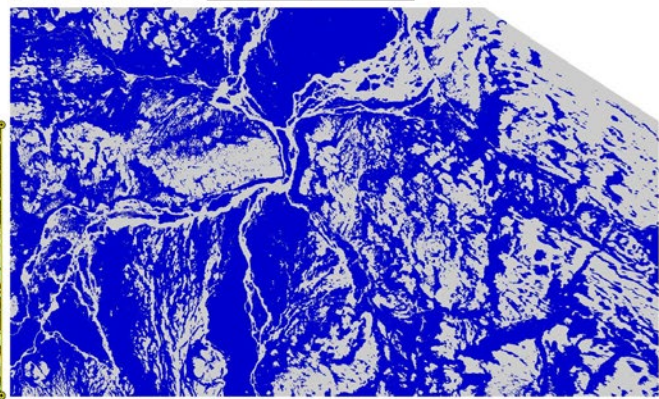


Figure 5: An example of the processing chain for the Scheteligfjellet camera: (a) a raw time-lapse photograph (10:31Z 03.06.2016); (b) the orthorectified version of this photo (the area of interest [AOI] is in the yellow polygon); (c) the same orthoimage cropped to the AOI; and (d) the final classified orthoimage with bare ground pixels in grey and snow-covered pixels in blue. Adapted from Aalstad et al. (2020).

2.3.3. The Scheteligfjellet site

An automatic camera system was deployed at 562 m a.s.l. near the summit of Scheteligfjellet (719 m a.s.l.) to monitor snowmelt patterns in the Bayelva catchment. The system consisted of a Canon EOS 1100D digital single-lens reflex camera triggered by a Harbortronics time-lapse package. It was maintained and installed for each ablation season (May–August) in the years 2012–2017 by scientists from the Department of Geosciences at the University of Oslo. The camera delivered hundreds of high-quality oblique daily images except in rare periods with low cloud cover, artifacts, or system malfunction that were later filtered out. These images were orthorectified with a camera calibration toolbox using a high-quality reference DEM and orthophoto. An independent validation indicated an average georeferencing error of under 2 m with no systematic shifts. These 0.5 m resolution orthoimages were then cropped

to a 1.77 km² AOI to avoid edge distortions and significant anthropogenic disturbances. Subsequently, each of these images was individually and manually classified into binary snow-covered and snow-free pixels using an image-specific threshold on the blue band histogram. These high-resolution orthorectified binary snow cover images can be spatially aggregated and applied to validate satellite retrievals of FSC (Figure 5).

A more detailed description of the processing chain for this camera system is provided in Aalstad et al. (2020). Therein, this imagery is used to validate FSC retrieved from several optical satellite sensors – namely Terra/Aqua MODIS, Landsat 8 OLI and Sentinel-2A/2B MSI – using algorithms varying in complexity from thresholding to spectral unmixing. A subset of the imagery was used in an earlier snow data assimilation experiment (Aalstad et al., 2018) for validation and to provide observation error variance estimates for the assimilated satellite

retrievals. These error estimates were also used in a subsequent high resolution snow data assimilation framework that was implemented over the Swiss Alps (Fiddes et al., 2019).

2.4. The Adventdalen area

With support from the SIOS InfraNor project since 2018, the University of Tromsø established an automatic system for monitoring vegetation and environmental seasonal changes in Svalbard. Ten racks were distributed within the lower part of Adventdalen, south of Longyearbyen. All racks had basic equipment comprising one RGB camera, one

non-imaging NDVI sensor and a sensor measuring both soil moisture and temperature. In addition, five racks were equipped with a thermal infrared sensor measuring surface temperature, and two racks had sensors recording the photochemical reflectance index (PRI). For calibration purposes, hemispheric NDVI and PRI sensors were mounted on three racks measuring incoming radiation. The cameras used were WingScapes TimeLapseCam cameras (WCT-00122; Ebsco Industries, China), with a resolution of 8 MP and were taking RGB images from a vertical position at a height of 2 m. The project has been operational with ten cameras since 2016.

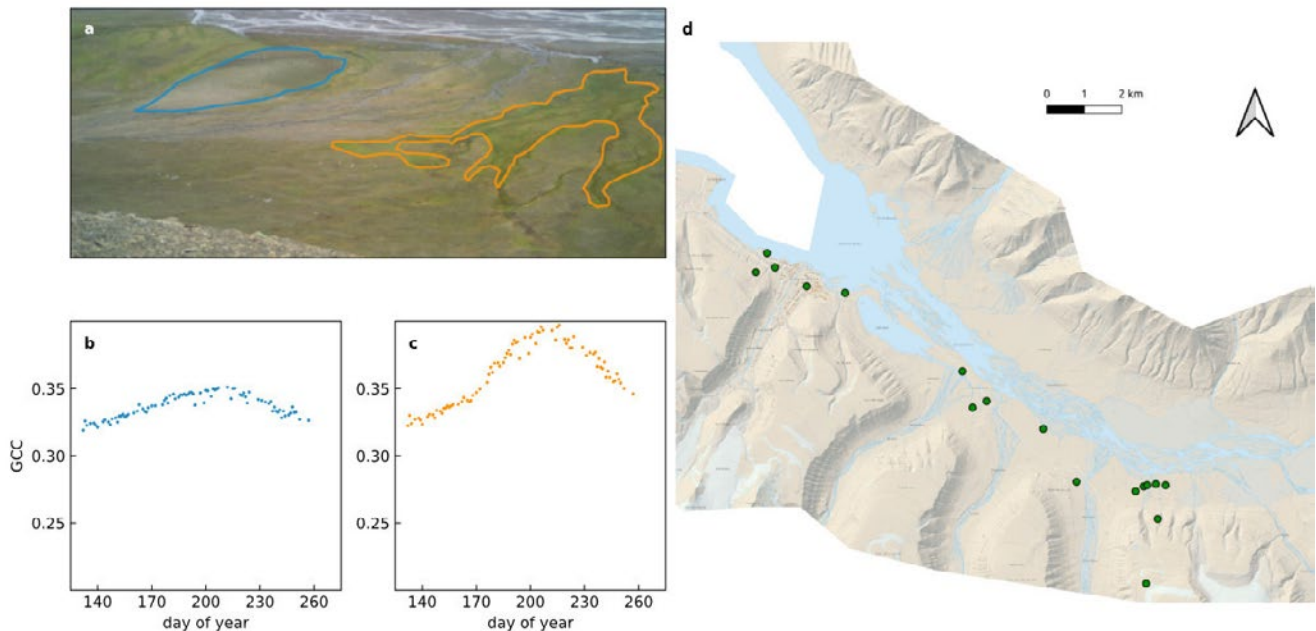


Figure 6: Examples of RGB indices derived from different regions of interest (ROI) during the growing season. The blue encircled area (a) has a low vegetation cover, which leads to lower values of the Green Chromatic Coordinate (GCC) index (b). The orange outline encircles dense vegetation which leads to a higher value of GCC (c). Distribution map of the available camera racks (d).

A landscape camera (CuddeBack H-1453, CuddeBack Digital, RGB, 20 Megapixel) is mounted up in the hillside of the Breinosa mountain, facing the Adventdalen river and surveilling 4 of the racks and their surroundings. The CuddeBack camera has been operative since 2018. Both the rack cameras and the landscape camera are set up in late April / early May and taken down again by the

end of September. The main purposes of the rack cameras are to document, on a daily basis, the plant phenology at the plot and species level, as well as to generate vegetation indices (greenness indices). The landscape camera will monitor and document, on a daily basis, the appearance, growth and withering of plant communities surrounding the racks (Figure 6).

2.5. The Hornsund area

Seven time-lapse cameras are located in the neighbourhood of Polish Polar Station, Hornsund, which is managed by the Institute of Geophysics, the Polish Academy of Sciences. Two of them were installed in 2014, primarily for snow cover applications: one near the Fugleberget summit (550 m a.s.l.) overlooking the small Fuglebekken catchment and the second on a small container in the catchment (5 m a.s.l.) facing towards the slopes of the Fugleberget mountain. The devices used in those setups were Harbortronics Digisnap 2000 time-lapse camera systems, which originally provided 12.2 megapixel resolution. The one at the summit was replaced later by its modernized continuation rebranded as Cyclapse Pro. The one overlooking the slopes of Fugleberget was

uninstalled in 2015. Both sets take photos every hour starting in the spring before the ablation season begins. The camera mounted near the summit was used for providing fractional snow cover estimates during the melting period for an area of about 0.7 km² (Figure 7). Snow classification was performed using blue-channel thresholding applied to the orthorectified imagery, originally to study the timing of snow disappearance from various tundra vegetation communities (Kępski et al. 2017). Other cameras installed in the Hornsund area are in-house developed systems based on DSLR cameras. They were designed for tracking the position of the glacier front, changes of the coastline and sea-ice dynamics. These cameras operate within the framework of oceanographic monitoring of the Polish Polar Station at Hornsund.

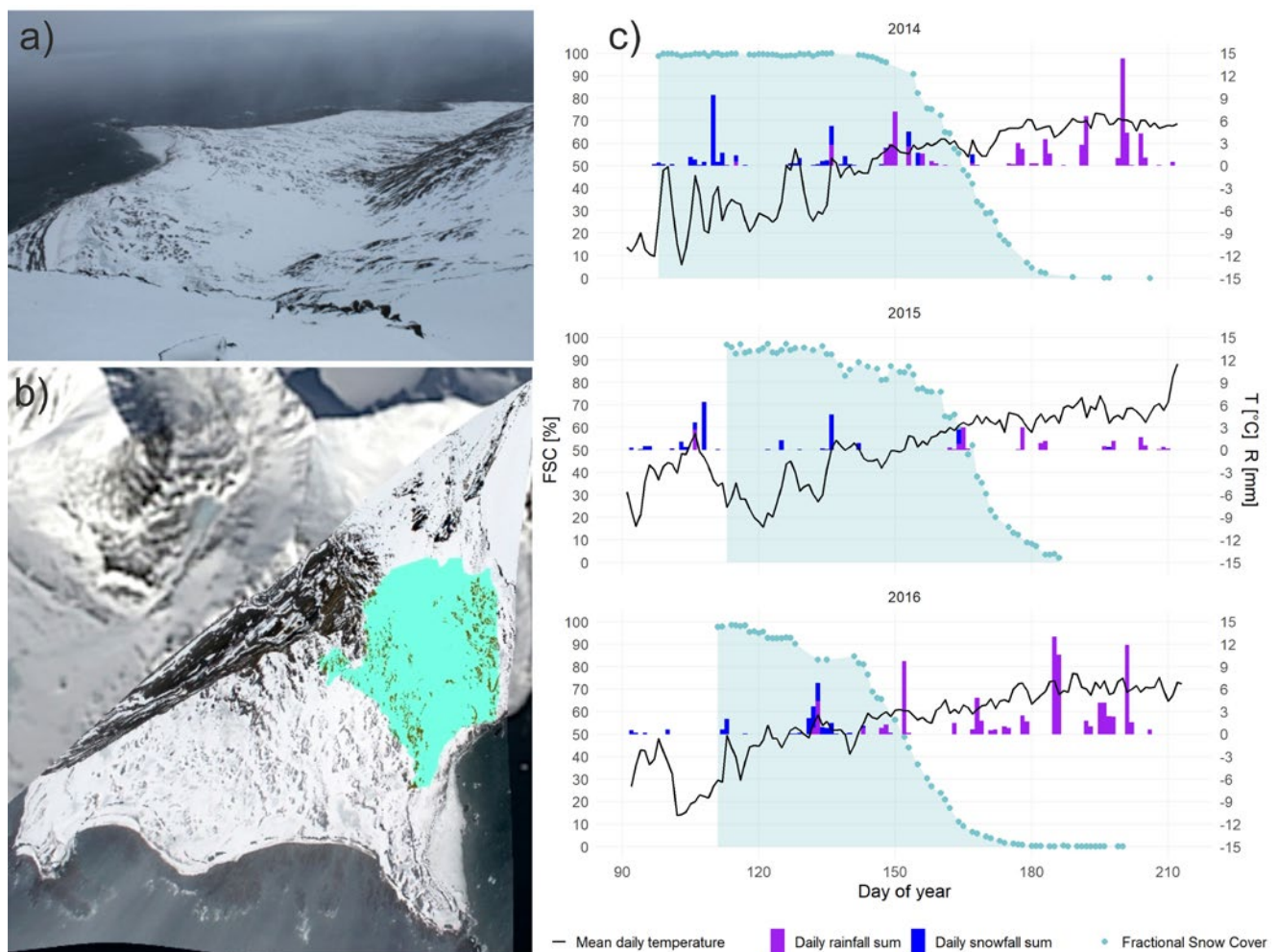


Figure 7: Time-lapse camera mounted near the Fugleberget summit in Hornsund: a) raw image; b) orthorectified image with binary classified snow surface clipped to mask with the smallest distortions of terrain (marked in cyan); and c) fractional snow cover in melting seasons 2014–2016.

3. Connections and synergies with other SESS report chapters

This data summary has different connections with previous SESS reports where the imagery provided by time-lapse cameras were mentioned as tools useful for studying snow-covered areas (Gallet et al. 2019) and as a ground-truth technique for vegetation-related studies based on remote sensing (Karlsen et al. 2020). Terrestrial photography is in fact an ideal approach for observing the evolution of the snow cover through a broader perspective than standard point measurements. Furthermore, the snow cover evolution affects the vegetation phenology, and, especially when the melting season is over, additional information about vegetation growth can be extracted from oblique or vertical time-lapse images. The contribution of terrestrial photography presented in this

chapter also offers important synergies with other disciplines concerned with other chapters available in this report: (i) Svalbard long-term variabilities of terrestrial-snow and sea-ice cover extent (Killie et al. 2021); and (ii) satellite and modelling-based snow season time series for Svalbard: inter-comparisons and assessment of accuracy (Malnes et al. 2021). In both cases, terrestrial photography can offer an important source of ground truth, which is useful for combining different satellite observations obtained with different temporal and spatial resolutions. The seasonal description of the snow cover obtained by time-lapse cameras is certainly limited in terms of spatial coverage but it is almost continuously independent from the cloud cover.

4. Unanswered questions

The collected information showed a considerable availability of cameras located in the Svalbard archipelago that could be important data sources to be integrated between different disciplines. We defined a key background of the camera nodes useful for preparing the groundwork for establishing a snow-related camera network in Svalbard. The defined framework highlighted the need for key information from all of the identified systems. The survey is still ongoing since only 40% of the contacted camera operators have responded positively and are ready to provide details in line with the metadata profile, which would be useful for characterizing the data processing components.

We defined a specific questionnaire that could represent a key tool for continuing the censusing activity developed in the PASSES website¹. The dataset on available cameras is complete with respect to the most mature nodes (6) included in this contribution, and which were identified between the involved partners, but it still needs more effort for completing the harvesting of information from other research groups.

Networking is a critical task and the aim of such an effort is to increase the number of locations investigated for snow cover purposes. Camera systems are, at the moment, available in a few selected sites where the logistical support can be easily provided: Longyearbyen, Ny-Ålesund and Hornsund. A few additional sites are present, but data chains from those have a lower maturity level, with images not being processed in terms of snow cover and/or not being archived due to privacy issues. More high-level nodes are necessary in order to obtain a good spatial distribution representing the different environmental conditions available in the archipelago.

Looking at the data processing, we identified the most important high-maturity datasets and analysed them in order to identify the key components that must be harmonized for having a standardized snow cover product. There are different setups that range from heterogeneous camera devices (different sensor resolutions, fore optics, sensor types), to installation features (site elevation, perspective coverage, acquisition seasoning), image data

¹ <https://niveos.cnr.it/passes/>

processing (ortho-rectification and classification), and finally to the uncertainty estimation. There is a need for a shared strategy for the different components of these data processing chains, and the final solution will be a compromise between maintenance issues, logistic requirements, resource allocation and data/privacy constraints.

Once the strategy has been defined, such an infrastructure will be important for different disciplines (glaciology, hydrology, plant and animal ecology, coastal processes, sea-ice tracking, satellite cal/val) and it will be ready to be integrated with other SIOS and COPERNICUS infrastructures.

This data summary could contribute to laying the groundwork for a regional service aimed at describing the FSC using terrestrial photography. Furthermore, the availability of different datasets can represent a training infrastructure for novel algorithms and innovative approaches focussed on integrating and assimilating different data sources. By defining the regional framework of available datasets – some of which are already connected to the SIOS data infrastructures – the Earth System Science community could increase the opportunity to fill the multi-scale gap present between different disciplines such as remote sensing and snow micro-physics.

5. Recommendations for the future

1. The aforementioned problems and knowledge gaps hinder the full use of the opportunities presented by terrestrial photography. To enhance its usefulness for snow cover and other related studies, we propose the following actions that can be taken by the SIOS community to support research in this field:
2. Promote actions and projects that assume usage of time-lapse cameras, especially in more remote areas of Svalbard. Most terrestrial photography setups focus on the Spitsbergen shores, close to human settlements. There are no cameras that cover the field of view of higher-elevation terrain.
3. Stimulate the creation of a Svalbard camera system network. Although all cameras provide valuable scientific data, it is currently difficult to use them collectively for one scientific purpose. There is a need to create a common and easy-to-apply algorithm for processing large quantities of images from different devices for snow cover applications.
4. Create a space on the SIOS website that gathers information about actively maintained camera systems on Svalbard. As a preliminary version, we propose the website created during the preparation of this report².
5. Promote the estimation of the fractional snow-covered area from images obtained by time-lapse cameras not specifically devoted to snow studies. This action will facilitate the involvement of local communities in the framework of citizen science, even if some privacy issues must be resolved first.
6. Stimulate the use of time-lapse cameras by different disciplines where high time-resolved information can be retrieved for different purposes (glaciology, hydrology, plant and animal ecology, coastal processes, sea-ice tracking, satellite cal/val).

² <https://niveos.cnr.it/passes/>

6. Data availability

Dataset	Parameters	Period	Location	Metadata/Data Access	Data provider, reference
Svalbard cameras	Camera locations and ancillary information	2000–2020	Svalbard archipelago	http://iadc.cnr.it/cnr/metadata_view.php?id=113 SIOS data access portal: https://bit.ly/3fJugLZ	https://doi.org/10.5281/zenodo.4036510
Brøggerdalen	Raw imagery	2018–2020	Brøggerdalen	http://iadc.cnr.it/cnr/metadata_view.php?id=112	Data request (Roberto Salzano: roberto.salzano@cnr.it)
Brøggerdalen	Fractional snow cover	2018–2019	Brøggerdalen	http://iadc.cnr.it/cnr/metadata_view.php?id=80	Data request (Roberto Salzano: roberto.salzano@cnr.it)
CCTower	Raw imagery	2015–2020	Kolhaugen	http://iadc.cnr.it/cnr/metadata_view.php?id=110	Data request (Roberto Salzano: roberto.salzano@cnr.it)
Fuglebergsletta	Raw imagery	2016–2020	Hornsund	SIOS data access portal: https://bit.ly/37hfc5M	Data request (Mateusz Moskalik: mmosk@igf.edu.pl)
Fuglebekken catchment	Raw imagery	2014–2019	Hornsund	SIOS data access portal: https://bit.ly/2JcyqjK	Data request (Barttomiej Luks: luks@igf.edu.pl)
Fuglebekken catchment	Fractional snow cover	2014–2016	Hornsund	https://doi.pangaea.de/10.1594/PANGAEA.874387 SIOS data access portal: https://bit.ly/39rYEt4	Kępski et al. (2017)
Zeppelin observatory	Raw imagery	2000–2020	Ny-Ålesund	https://doi.org/10.21334/npolar.2013.9fd6dae0 SIOS data access portal: https://bit.ly/39iFlgm	Pedersen (2013)
Zeppelin observatory	Fractional snow cover	2014–2019	Ny-Ålesund	http://iadc.cnr.it/cnr/metadata_view.php?id=111	Data request (Roberto Salzano: roberto.salzano@cnr.it)
Scheteligfjellet	Raw imagery	2012–2017	Ny-Ålesund	https://doi.pangaea.de/10.1594/PANGAEA.846617 SIOS data access portal: https://bit.ly/2J58lXL	Aalstad et al. (2020)
Scheteligfjellet	Fractional snow cover	2012–2017	Ny-Ålesund	SIOS data access portal: https://bit.ly/2K2vir8	Aalstad et al. (2020)
Adventdalen landscape	Raw imagery, vegetation index	2016–2020	Adventdalen	Available in the SIOS data access portal in Q1 2021	Data request (Lennart Nilsen: lennart.nilsen@uit.no)
Adventdalen racks	Raw imagery, NDVI, soil moisture, temperature (soil and surface)	2016–2020	Adventdalen	Available in the SIOS data access portal in Q1 2021	Data request (Lennart Nilsen: lennart.nilsen@uit.no)

Acknowledgements

The information acquired during the preparation of this contribution has been included in a website prepared by Maria Annunziata Liberti, who also implemented the data sharing and privacy policies in the specific documents. Massimiliano Olivieri supported the preparation of the image repository provided by CNR-IIA. Simone Berti for the project financial management. These activities were carried out using funds from the European Union's Horizon 2020 research and innovation programme under grant agreement No 689443 via project iCUPE (Integrative and Comprehensive Understanding on Polar Environments). The logistic support was provided by Mauro Mazzola, the Italian Arctic Station at the Climate Change Tower and the Italian Arctic Data Center. Sebastian Westermann and Kristoffer Aalstad gratefully acknowledge funding from the SatPerm project (#239918; Research Council of Norway) and the European Space Agency Permafrost CCI project³. The acquisition of time-lapse imagery from Hornsund

was funded by the SMACS project (No. 236768/E10; Research Council of Norway) and the Polish Polar Station, Hornsund. The processing and data curation from Hornsund was funded within statutory activities No. 3841/E-41/S/2020 of the Ministry of Science and Higher Education of Poland. Lennart Nilsen acknowledges Hans Tømmervik from the Norwegian Institute for Nature Research (NINA) for assisting in the practical fieldwork in Adventdalen, as well as for extending financial support. Likewise, he acknowledges Dr. Frans-Jan Parmentier at the University of Oslo, Section for Meteorology and Oceanography for his contribution to data preparation and quality check through his participation in the SnoEco project led by Dr. Elisabeth Cooper (University of Tromsø). This work was supported by the Research Council of Norway, project number 291644, the Svalbard Integrated Arctic Earth Observing System – Knowledge Centre, operational phase.

References

- Aalstad K, Westermann S, Bertino L (2020) Evaluating satellite retrieved fractional snow-covered area at a high-Arctic site using terrestrial photography. *Remote Sens Environ* 239:111618. <https://doi.org/10.1016/j.rse.2019.111618>
- Aalstad K, Westermann S, Schuler TV, Boike J, Bertino L (2018) Ensemble-based assimilation of fractional snow-covered area satellite retrievals to estimate the snow distribution at Arctic sites. *Cryosphere*, 12:247–270. <https://doi.org/10.5194/tc-12-247-2018>
- Anderson HB, Nilsen L, Tømmervik H, Karlsen SR, Nagai S, Cooper EJ (2016) Using ordinary digital cameras in place of near-infrared sensors to derive vegetation indices for phenology studies of High Arctic vegetation. *Remote Sens* 8(10):847. <https://doi.org/10.3390/rs8100847>
- Beamish A, Reynolds MK, Epstein H, Frost GV, Macander MJ, Bergstedt H, Bartsch A, Kruse S, Miles V, Tanis CM, Heim B, Fuchs M, Chabrilat S, Shevtsova I, Verdonen M, Wagner J (2020) Recent trends and remaining challenges for optical remote sensing of Arctic tundra vegetation: A review and outlook. *Remote Sens Environ* 246:111872. <https://doi.org/10.1016/j.rse.2020.111872>
- Bongio M, Arslan AN, Tanis CM, De Michele C (2019) Snow depth estimation by time-lapse photography: Finnish and Italian case studies. *Cryosphere Discuss.* <https://doi.org/10.5194/tc-2019-193>
- Corripio, JG (2004) Snow surface albedo estimation using terrestrial photography. *Int J Remote Sens* 25(34):5705–5729. <https://doi.org/10.1080/01431160410001709002>
- Dietz AJ, Kuenzer, C, Gessner, U, Dech, S (2012). Remote sensing of snow—A review of available methods. *Int J Remote Sens* 33(12):4094–4134. <https://doi.org/10.1080/01431161.2011.640964>
- Fiddes J, Aalstad K, Westermann S (2019) Hyper-resolution ensemble-based snow reanalysis in mountain regions using clustering. *Hydrol Earth Syst Sci* 23:4717–4736. <https://doi.org/10.5194/hess-23-4717-2019>
- Flöry S, Ressler C, Hollaus M, Pürcher G, Piermattei L, Pfeifer N (2020) WEBSNOW: Estimation of snow cover from freely accessible webcam images in the Alps. *ISPRS Ann Photogramm Remote Sens Spatial Inf Sci V-2-2020:695–701.* <https://doi.org/10.5194/isprs-annals-V-2-2020-695-2020>

³ <http://cci.esa.int/Permafrost>

- Gallet JC, Björkman MP, Borstad CP, Hodson AJ, Jakobi H-W, Larose C, Luks B, Spolaor A, Schuler TV, Urazgildeeva A, Zdanowicz C (2019) Snow research in Svalbard: current status and knowledge gaps. In: Orr et al. (eds): SESS report 2018. Svalbard Integrated Arctic Earth Observing System, Longyearbyen, pp. 83–107. https://sios-svalbard.org/SESS_Issue1
- Gascoin S, Dumont Z B, Deschamps-Berger C, Marti F, Salgues G, Lopez-Moreno JI, Revuelto J, Michon T, Schattan P, Hagolle O (2020) Estimating fractional snow cover in open terrain from Sentinel-2 using the normalized difference snow index. *Remote Sens* 12:2904. <https://doi.org/10.3390/rs12182904>
- Garvelmann J, Pohl S, Weiler M (2013) From observation to the quantification of snow processes with a time-lapse camera network. *Hydrol Earth Syst Sc* 17(4):1415–1429. <https://doi.org/10.5194/hess-17-1415-2013>
- Godøy Ø, Holmen K (2017) SIOS Data Management Plan (ver 0.3). https://sios-svalbard.org/sites/sios.metsis.met.no/files/common/SIOS_Data_Management_Plan_20170428_ToBeApproved.pdf. Accessed 1 September 2020
- How P, Schild KM, Benn DI, Noormets R (2019) Calving controlled by melt-under-cutting: detailed calving styles revealed through time-lapse observations. *Ann Glaciol* 60(78):20–31. <https://doi.org/10.1017/aog.2018.28>
- Karlsen SR, Stendardi L, Nilsen L, Malnes E, Eklundh L, Julitta T, Burkart A, Tømmervik H (2020) Sentinel satellite-based mapping of plant productivity in relation to snow duration and time of green-up (GROWTH). In: Van den Heuvel et al. (eds): SESS report 2019. Svalbard Integrated Arctic Earth Observing System, Longyearbyen, pp. 43–57. https://sios-svalbard.org/SESS_Issue2
- Kępski D, Luks B, Migala K, Wawrzyniak T, Westermann S, Wojtuń B (2017) Terrestrial remote sensing of snowmelt in a diverse high-arctic tundra environment using time-lapse imagery. *Remote Sens* 9:733. <https://doi.org/10.3390/rs9070733>
- Killie MA, Aaboe S, Isaksen K, Van Pelt W, Pedersen ÅØ, Luks B (2021) Svalbard snow and sea-ice cover: comparing satellite data, on-site measurements, and modelling results. In: Ibáñez et al (eds) 2021: SESS report 2020, Svalbard Integrated Arctic Earth Observing System, Longyearbyen, pp. 220–235. <https://doi.org/10.5281/zenodo.4293804>
- Malnes E, Vickers H, Karlsen SR, Saloranta T, Killie MA, Van Pelt W, Pohjola V, Zhang J, Stendardi L, Notarnicola C (2021) Satellite and modelling based snow season time series for Svalbard: Inter-comparisons and assessment of accuracy. In: Ibáñez et al (eds) 2021: SESS report 2020, Svalbard Integrated Arctic Earth Observing System, Longyearbyen, pp. 202–219. <https://doi.org/10.5281/zenodo.4294072>
- Mariash H, McLennan D, Rosqvist GN, Sato A, Savela H, Schneebeli M, Sokolov A, Sokratov SA, Terzago S, Vikhamar-Schuler D, Williamson S, Qiu YB, Callaghan TV (2016) Changing Arctic snow cover: A review of recent developments and assessment of future needs for observations, modelling, and impacts. *Ambio* 45:516–537. <https://doi.org/10.1007/s13280-016-0770-0>
- Matzl M, Schneebeli M (2006) Measuring specific surface area of snow by near-infrared photography. *J Glaciol* 52(179):558–564. <https://doi.org/10.3189/172756506781828412>
- Nicu JC, Stalsberg K, Rubensdotter L, Martens VV, Flyen AC (2020) Coastal erosion affecting cultural heritage in Svalbard. A case study in Hiorthhamn (Adventfjorden) – an abandoned mining settlement. *Sustainability* 12:2306. <https://doi.org/10.3390/su12062306>
- Painter T, Rittger K, McKenzie C, Slaughter, P, Davis RE, Dozier J (2009) Retrieval of subpixel snow-covered area, grain size, and albedo from MODIS. *Remote Sens Environ* 113:868–879. <https://doi.org/10.1016/j.rse.2009.01.001>
- Parajka J, Haas P, Kirnbauer R, Jansa J, Blöschl G (2012) Potential of time-lapse photography of snow for hydrological purposes at the small catchment scale. *Hydrol Process* 26(22):3327–3337. <https://doi.org/10.1002/hyp.8389>
- Pedersen C (2013) Zeppelin web camera time-series [Dataset] Norwegian Polar Institute, <https://doi.org/10.21334/npolar.2013.9fd6dae0>
- Peltoniemi M, Aurela M, Böttcher K, Kolari P, Loehr J, Karhu J, Linkosalmi M, Tanis CM, Tuovinen JP, Arslan AN (2018) Webcam network and image database for studies of phenological changes of vegetation and snow cover in Finland, image time series from 2014 to 2016. *Earth Syst Sci Data* 10:173–184. <https://doi.org/10.5194/essd-10-173-2018>
- Petäjä T, Duplissy EM, Tabakova K, Schmale J, Altstädter B, Ancellet G, Arshinov M, Balin Y, Baltensperger U, Bange J, Beamish A, Belan B, Berchet A, Bossi R, Cairns WRL, Ebinghaus R, El Haddad I, Ferreira-Araujo B, Franck A, Huang L, Hyvärinen A, Humbert A, Kalogridis AC, Konstantinov P, Lampert A, MacLeod M, Magand O, Mahura A, Marelle L, Masloboev V, Moiseev D, Moschos V, Neckel N, Onishi T, Osterwalder S, Ovaska A, Paasonen P, Panchenko M, Pankratov F, Pernov JB, Platis A, Popovicheva O, Raut JC, Riandet A, Sachs T, Salvatori R, Salzano R, Schröder L, Schön M, Shevchenko V, Skov H, Sonke JE, Spolaor A, Stathopoulos VK, Strahlendorff M, Thomas JL, Vitale V, Vratolis S, Barbante C, Chabrillat S, Dommergue A, Eleftheriadis K, Heilimo J, Law KS, Massling A, Noe SM, Paris JD, Prévôt ASH, Riipinen I, Wehner B, Xie Z, Lappalainen HK (2020) Overview: Integrative and Comprehensive Understanding on Polar Environments (iCUPE) – concept and initial results. *Atmos Chem Phys* 20:8551–8592. <https://doi.org/10.5194/acp-20-8551-2020>
- Portenier C, Hüsler F, Härer S, Wunderle S (2020) Towards a webcam-based snow cover monitoring network: Methodology and evaluation. *Cryosphere* 14:1409–1423. <https://doi.org/10.5194/tc-14-1409-2020>
- Riggs GA, Hall DK, Román MO (2017) Overview of NASA's MODIS and Visible Infrared Imaging Radiometer Suite (VIIRS) snow-cover Earth System Data Records. *Earth Syst Sci Data* 9:765–777. <https://doi.org/10.5194/essd-9-765-2017>

- Salomonson VV, Appel I (2006) Development of the Aqua MODIS NDSI fractional snow cover algorithm and validation results. *IEEE T Geosci Remote* 44:1747–1756. <https://doi.org/10.1109/Tgrs.2006.876029>
- Salvatori R, Plini P, Giusto M, Valt M, Salzano R, Montagnoli M, Cagnati A, Crepaz G, Sigismondi D (2011) Snow cover monitoring with images from digital camera systems. *Ital J Remote Sens* 43:137–145. <https://doi.org/10.5721/ITJRS201143211>
- Salzano R, Salvatori R, Valt M, Giuliani G, Chatenoux B, Ioppi L (2019) Automated classification of terrestrial images: The contribution to the remote sensing of snow cover. *Geosciences* 9:97. <https://doi.org/10.3390/geosciences9020097>
- Salzano R, Lanconelli C, Salvatori R, Esposito G, Vitale V (2016) Continuous monitoring of spectral albedo of snowed surfaces in Ny-Ålesund. *Rend Lincei Sci Fis* 27:137–146. <https://doi.org/10.1007/s12210-016-0513-y>
- Seyednasrollah B, Young AM, Hufkens K, Milliman T, Friedl MA, Frohling S, Richardson AD (2019) Tracking vegetation phenology across diverse biomes using Version 2.0 of the PhenoCam Dataset. *Sci Data* 6:222. <https://doi.org/10.1038/s41597-019-0229-9>
- Vallot D, Adinugroho S, Strand R, How P, Pettersson R, Benn DI, Hulton NRJ (2019) Automatic detection of calving events from time-lapse imagery at Tunabreen, Svalbard. *Geosci Instrum Method Data Syst* 8:113–127. <https://doi.org/10.5194/gi-8-113-2019>
- Vermote E, Justice C, Claverie M, Franch B (2016) Preliminary analysis of the performance of the Landsat 8/OLI land surface reflectance product. *Remote Sens Environ* 185:46–56. <https://doi.org/10.1016/j.rse.2016.04.008>
- Wingate L, Ogée J, Cremonese E, Filippa G, Mizunuma T, Migliavacca M, Moisy C, Wilkinson M, Moureaux C, Wohlfahrt G, Hammerle A, Hörtnagl L, Gimeno C, Porcar-Castell A, Galvagno M, Nakaji T, Morison J, Kolle O, Knohl A, Kutsch W, Kolari P, Nikinmaa E, Ibrom A, Gielen B, Eugster W, Balzarolo M, Papale D, Klumpp K, Köstner B, Grünwald T, Joffre R, Ourcival JM, Hellstrom M, Lindroth A, George C, Longdoz B, Genty B, Levula J, Heinesch B, Sprintsin M, Yakir D, Manise T, Guyon D, Ahrends H, Plaza-Aguilar A, Guan JH, Grace J (2015) Interpreting canopy development and physiology using a European phenology camera network at flux sites. *Biogeosciences* 12:5995–6015. <http://doi.org/10.5194/bg-12-5995-2015>
- World Meteorological Organization (2016) The Global Observing System for climate: Implementation needs. GCOS report 200, Geneva, Switzerland. https://unfccc.int/sites/default/files/gcos_ip_10oct2016.pdf
- Yin DM, Cao X, Chen XH, Shao YJ, Chen J (2013) Comparison of automatic thresholding methods for snow-cover mapping using Landsat TM imagery. *Int J Remote Sens* 34:6529–6538. <https://doi.org/10.1080/01431161.2013.803631>

A multi-scale approach to snow cover observations and models (SnowCover)

Roberto Salzano¹, Mari Anne Killie², Bartłomiej Luks³, Eirik Malnes⁴

1 Institute of Atmospheric Pollution Research, National Research Council of Italy, Sesto Fiorentino (Firenze), Italy

2 The Norwegian Meteorological Institute, Oslo, Norway

3 Institute of Geophysics, Polish Academy of Sciences, Warsaw, Poland

4 NORCE Norwegian Research Centre, Bergen, Norway

Corresponding author: Roberto Salzano, roberto.salzano@cnr.it

ORCID number 0000-0002-0750-0097

DOI: <https://doi.org/10.5281/zenodo.4294092>

1. Highlights

- The description of the snow cover in the Arctic can be approached with different spatial and time scales. This large variability is not a weakness; rather, it represents a relevant opportunity to fill the multi-scale gap that affects snow cover monitoring.
- The availability of long time series is the key to observing long-term climate changes. A combination of different methodologies based on several data sources (terrestrial and satellite observations) is the most reliable solution.
- Terrestrial photography contributes by offering high-resolution and high temporally resolved ground truth for satellite imagery, but it is limited in terms of spatial extension. This approach is unaffected by cloud cover but requires a large number of observing sites distributed across the region.
- The long-term climate data record for the terrestrial snow cover in Svalbard with snow model output for snow water equivalent and in situ measurements of snow cover and snow-off dates are important for many scientific disciplines.
- Time series offer the opportunity to study the relationships between satellite observations and snow-related models.

2. Background

The snow cover can be studied by combining different data sources and integrating several data types. Snow cover data is relevant not only for the study of snow *per se*, but it is also used as input for different models (e.g. snow models) and to verify simulation output. Earth observation (EO) of snow involves the gathering of information on the physical properties of snow via remote sensing technologies as well as in situ measurements. Snow is characterised by many properties, including snow cover, snow depth, temperature, density, grain size, shape, etc. Different sensors have variable capabilities of measuring snow. In situ sensors or sensors close to the site measure the properties more efficiently, in terms of time resolution, than remote sensing at the cost of being only valid as a point measurement. Remote sensors cover a wider area but are usually less timely resolved. Spatial and temporal scales are the most critical features that must be taken into account in order to fill the existing gap between the different observation methods.

On the one hand, in situ point measurements can be extremely detailed over time but limited in terms

of spatial extension. On the other hand, satellite acquisitions can provide complete spatial coverage across Svalbard but have limitations associated with revisiting time and the cloud cover. In the past five years, since the deployment of the first Sentinel-2 platform, the gap between satellite and in situ observations has reduced thanks to technological improvements, with the availability of automated measurement stations on one side and, on the other, the introduction of new satellite platforms that are becoming more efficient in terms of numbers (constellations of platforms) and sensor capabilities. There have also been significant improvements in the range between satellite and in situ observations with the development of intermediate methodologies: airborne platforms, unmanned aerial vehicles, terrestrial photography, etc. All these approaches can contribute to the integration of new, recent and past observations.

This report includes three data summaries that contribute to this important task, focusing on integrating different data sources for the assessment of the state of the snow cover. The first (PASSES) provides a picture of terrestrial

photography applications focused on the snow cover with information about the facilities operated by different nationalities and the maturity level of datasets in terms of fractional snow cover retrieval. The second (SvalSCESIA) compares the existing satellite-based long-term climate data record for terrestrial snow cover in Svalbard with snow model output for snow water equivalent and in situ measurements of the snow cover and snow-off dates. Spatial and temporal trends are investigated and viewed in relation to trends in sea-ice area for the adjacent sea, derived from a long-term climate data record for sea-ice concentration. The third (SATMODSNOW) compares satellite observations

with outputs from hydrological snow models and quantifies the differences. All three present a full picture for every single approach and suggest the need for more efforts in the comparison between tools providing estimations of the same variable obtained with different spatial and time resolutions. Comparisons and the understanding of the uncertainties may also provide insight and help reduce observational and modelling uncertainty in the future. Furthermore, these approaches show the potential impact of a holistic approach on the final description of processes occurring in the Arctic ecosystem.

3. Summary

The description of the snow cover represents important knowledge useful for the calibration and validation of the snow process and hydrological models. From this perspective, the availability of long time series is a critical task that can be approached using ground-based as well as remotely sensed data. The current SESS report includes three different chapters about data sources that can provide important datasets with different time and spatial resolutions. These differences are not a limitation but represent an opportunity to develop a multi-scale analysis and obtain reliable input for climate and ecological models. The chapter 'PASSES' ([Salzano et al. 2021](#)), focuses on terrestrial photography applications, provides an overview of the cameras operating in Svalbard looking at specific applications on the snow cover and collecting information about the images discoverable and/or accessible on the web. These data sources can provide information about the state of the snow cover that is limited in terms of spatial extension (10 m² up to 10 km²) but almost independent from the meteorological conditions and characterised by high time resolution.

The availability of a network of cameras, potentially operating for a long time (the longest time series covers about 20 years), offers the opportunity to have continuous ground truth for validating remotely sensed data. Looking for an upscaling

strategy from in situ observations to satellite data, terrestrial photography can be easily linked to the satellite sensors characterised by higher spatial resolution (Sentinel-2, Landsat 8, etc.). This is the case with the results presented in the third chapter 'SATMODSNOW' ([Malnes et al. 2021](#)), where sensors characterised by higher spatial resolution are considered. Data provided by AVHRR, MODIS and Sentinel-2 Multi-Spectral Instrument (MSI) cover the 2000–2020 time interval, providing a snow cover description with a spatial resolution ranging from 4 km to 10 m and time resolution spanning from 5 days to half a day. In SATMODSNOW, several hydrological snow models were compared with snow cover fractions from satellites. The comparisons show that there are significant differences between the datasets, both with respect to the geographical snow distribution and the timing of the snow cover. The main reason for the differences is possibly inaccurate precipitation/temperature inputs to the snow models. Improvements are foreseen in the future when snow models can assimilate satellite data as well.

Furthermore, the description of the snow cover seasonality at different spatial scales contributes to the assessment of climate changes. Potentialities have been highlighted in this direction by the chapter 'SvalSCESIA' based on the AVHRR platform

(Killie et al. 2021). This dataset covers the 1982–2015 time interval and provides a snow cover description with a 4 km spatial resolution and a daily time resolution. Satellite monitoring showed an earlier onset of snow melting in Svalbard, with the most pronounced decrease in the valleys by 1–2 days/year. The variability of the snow cover in the lowlands correlates with the variability of sea ice in the adjacent sea, especially in the month of June. This chapter confirmed the need to develop a data model fusion system that would merge the available observational datasets on snow properties

with state-of-the-art, high-resolution (1 to 500 m scale) and physically based snow models. The goal of this data-enhancement system is the creation of accurate, spatially distributed and time-evolving datasets for better understanding the relationships between ecosystem processes. Additionally, integration with other snow parameters such as snow depth, snow water equivalent and snow-cover extent datasets (especially archival dating back to the 80s) would be extremely helpful in the calibration and validation of long-term satellite products and models.

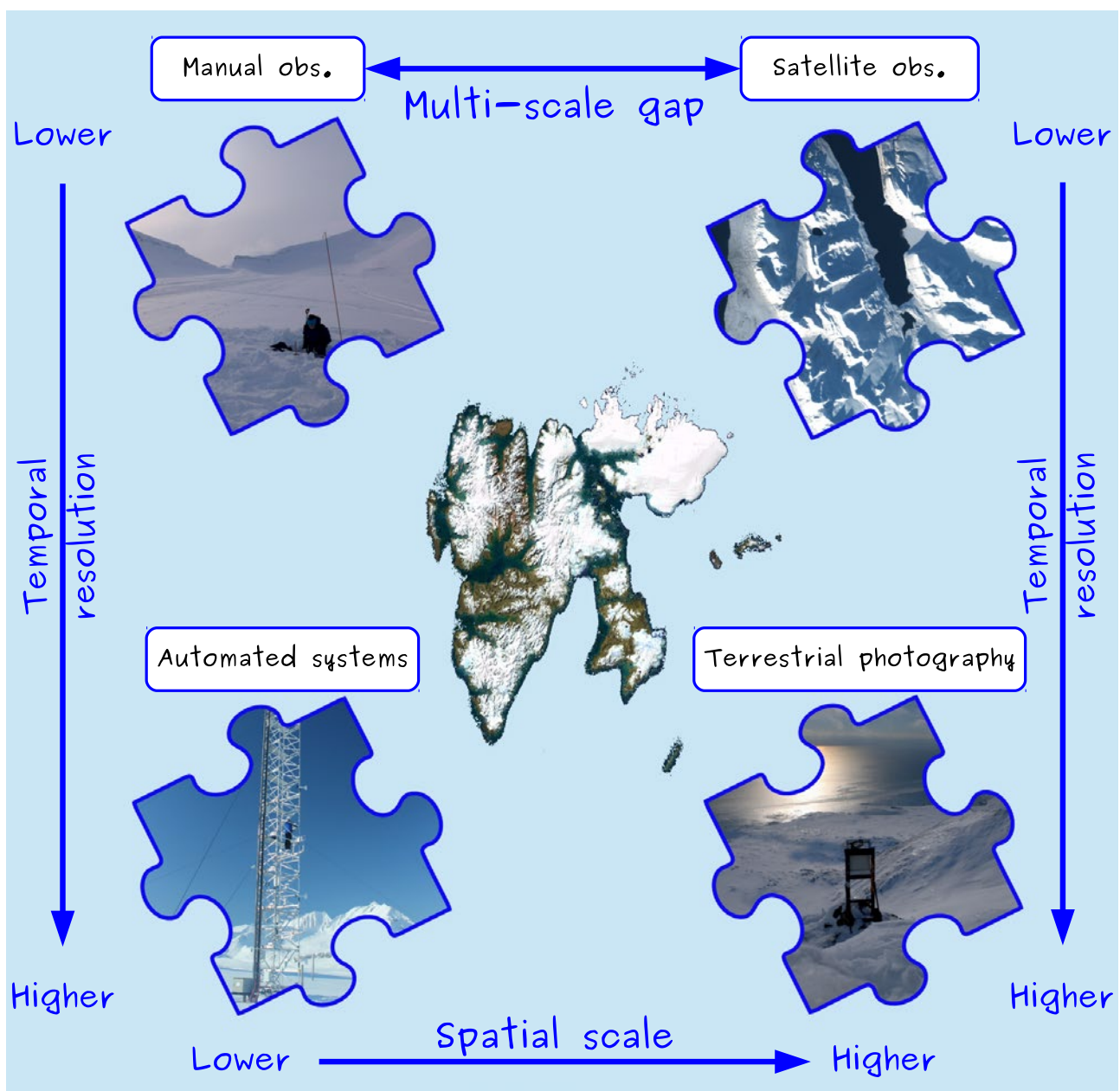


Figure: The representation of a multi-scale strategy aimed at solving the gap existing between in situ measurements and satellite observations: the snow cover observed from different perspectives. The gaps between different spatial and temporal scales need to be bridged using sensors in the intermediate scale range (e.g., airborne sensors) to understand and remove uncertainties in long-term snow time series based on coarse-scaled satellite data and modelling.

4. Joint recommendations

- Intercomparisons (and intercalibrations) of snow products from coarse scale (4km, AVHRR), via medium scale (500m, MODIS) and detailed (10–20m, S2-MSI) to sub-meter scale (time-lapse cameras) could be investigated; this will help in better understanding detailed melting patterns.
- A SIOS/Svalbard supersite for remote sensing of snow should be established to provide sustained in situ reference snow measurements that can be used for cal/val activities.
- Attempts should be made to map, harvest and maintain (if possible) all kinds of EO products of snow over the archipelago and validate/quantify errors in each of the datasets.
- The assimilation of EO data in snow hydrology and snow process models needs to be further investigated.

References

Killie MA, Aaboe S, Isaksen K, Van Pelt W, Pedersen ÅØ, Luks B (2021) Svalbard snow and sea-ice cover: comparing satellite data, on-site measurements, and modelling results. In: Moreno-Ibáñez et al (eds) SESS report 2020, Svalbard Integrated Arctic Earth Observing System, Longyearbyen, pp 220-235. <https://doi.org/10.5281/zenodo.4293804>

Malnes E, Vickers H, Karlsen SR, Saloranta T, Killie MA, Van Pelt W, Pohjola V, Zhang J, Stendardi L, Notarnicola C (2021) Satellite and modelling based snow season time series for Svalbard: Inter-comparisons and assessment of accuracy. In: Moreno-Ibáñez et al (eds) SESS report 2020, Svalbard Integrated Arctic Earth Observing System, Longyearbyen, pp 202-219. <https://doi.org/10.5281/zenodo.4294072>

Salzano R, Aalstad K, Boldrini E, Gallet JC, Kępski D, Luks B, Nilsen L, Salvatori R, Westermann S (2021) Terrestrial photography applications on snow cover in Svalbard. In: Moreno-Ibáñez et al (eds) SESS report 2020, Svalbard Integrated Arctic Earth Observing System, Longyearbyen, pp 236-251. <https://doi.org/10.5281/zenodo.4294084>

Ground ice content, drilling methods and equipment and permafrost dynamics in Svalbard 2016–2019 (PermaSval)

Hanne H. Christiansen¹, Graham L Gilbert^{1,2}, Ullrich Neumann³, Nikita Demidov⁴, Mauro Guglielmin⁵, Ketil Isaksen⁶, Marzena Osuch⁷, and Julia Boike⁸

¹ University Centre in Svalbard, UNIS, Arctic Geology Department, Longyearbyen, Norway.

² Norwegian Geotechnical Institute, Natural Hazards Division, Oslo, Norway.

³ Kolibri Geo Services, Risor, Norway

⁴ Arctic and Antarctic Research Institute, AARI, Ministry of Natural Resources and Environment, Russia.

⁵ Insubria University, Department of Theoretical and Applied Science, Varese Italy.

⁶ Norwegian Meteorological Institute, Research and Development Department, Oslo, Norway.

⁷ Institute of Geophysics, Polish Academy of Sciences, Poland.

⁸ Alfred Wegener Institute for Polar and Marine Sciences, Potsdam, & Geography Department, Humboldt-Universität Berlin, Germany

Corresponding author: Hanne H. Christiansen, hanne.christiansen@unis.no

ORCID number 0000-0002-6218-3493

Keywords: Permafrost, ground temperature, active layer, ground ice content, drilling methods, Svalbard

DOI: <https://doi.org/10.5281/zenodo.4294095>

1. Introduction and objectives

Permafrost plays an important role in the Earth system, underlying 25% of the terrestrial parts of Planet Earth. In Svalbard, permafrost underlies almost all land areas not covered by glaciers. Permafrost is often near its freezing point and thus is sensitive to climatic changes. The thermal state of permafrost and active layer thickness are the two essential climate variables (ECVs) monitored to quantify the effects of climate change on permafrost conditions. We presented the observations of these ECVs in Svalbard in the first SESS report (Christiansen et al. 2019), focusing on their meteorological controls and provided an update in our SESS report card (Christiansen et al. 2020). The response of permafrost landscapes to thawing can be largely affected by the amount of ground ice in the stratigraphy, as was identified as a recommendation for future permafrost studies in both earlier SESS reports. When ice-rich permafrost thaws, melting ground ice often results in ground subsidence and instability. Therefore, the amount of ground ice provides a good indication of the sensitivity of permafrost landscapes to climate-induced changes. Additionally, thawing permafrost impacts infrastructure, nutrient and sediment transport into rivers and fjords, and landslide regimes, resulting in important links to large parts of the SIOS observation system.

A variety of drilling methods and monitoring equipment have been used to establish boreholes for permafrost thermal observation in different landforms and types of sediment, soil,

and bedrock in Svalbard. In some cases, core samples were extracted during drilling these boreholes, allowing for ground ice determination and classification of stratigraphy. Permafrost drilling is typically conducted during winter, as rig transport must be done on frozen and snow-covered ground. Weather conditions during drilling operations are often demanding for both personnel and machines. Additionally, drilling and sampling in Arctic permafrost are logistically and technically challenging, requiring specialized techniques, custom drilling equipment, knowledge and experience from the drillers and project coordinators.

In this SESS report, we, therefore, focus on how to obtain samples and determine the ground ice content by presenting the research and drilling infrastructure currently available in Svalbard. We also present and discuss the ground ice content from the observation sites as a key factor for assessing the response of the Svalbard permafrost landscape to changes in climate. The objectives of this chapter are: (1) to provide a technical overview of the methods and drilling equipment used in permafrost in Svalbard and an overview of the available equipment for permafrost coring, (2) to summarise the currently available data on ground ice content and stratigraphy from the permafrost ECV observation sites, and (3) to summarise the observational time series of the Svalbard permafrost ECVs from the hydrological years starting in summer 2016 to summer 2019.

2. Connections and synergies with other SESS report chapters

In the introduction, we have made reference to our earlier SESS chapters and explained how this chapter advances our two earlier permafrost SESS contributions. As this contribution shows, assessing the permafrost changes needs access to meteorological observations as an important controlling factor. These have unfortunately not yet been analysed in large separate detail in SESS reports;

but many chapters use different meteorological data available and, in this report, there is a chapter on meteorological modelling (Gjermundsen et al. 2021). Permafrost changes are relevant for the hydrological observations presented in a review in this report (Nowak et al. 2021). Permafrost observations are influenced by snow dynamics as is described by Killie et al. (2021). Clearly, surface hydrology,

groundwater, and snow cover dynamics are related to permafrost; e.g. insulation effects of snow cover,

convective and advective heat transfers of water in the active layer and frozen soils.

3. Overview of drilling equipment

A drill rig is typically needed to establish boreholes down to DZAA in permafrost (Gilbert et al. 2015). To also record the amount of ground ice in the permafrost, the drill rig needs to be able to collect cores during drilling. Here, we provide a first overview of the drilling methods and equipment used for permafrost drilling in Svalbard.

3.1. Drilling methods

Rotary drilling is used for all sites. The drill engine is mounted on a mast or tower that allows for vertical movement. It inserts rotation, thrust, torque and flushes fluid (water or air) through the drill rods to the drill bit. However, drill bit design differs for the five systems used in Svalbard and can be categorised into rotary percussion drilling and rotary core drilling. While rotary percussion drilling is developed for advancing into the ground efficiently, the latter is intended for retrieving core samples of the best possible quality.

3.1.1. Rotary percussion drilling

Down-the-hole hammer drilling (DTH) is most commonly used for boreholes in Svalbard. The percussion introducing unit is located right behind the drill bit in the borehole. It is powered by compressed air that flows through the drill rods. Combined with the rotation drill engine, small fragments are broken loose by carbide tungsten inserts in the drill bit front (Figure 1D). Cuttings are flushed up and out above the ground surface by the excess air of the hammer, allowing for the collection of bulk, bag samples. Besides the drill rig, the air compressor is the vital machinery providing enough energy to drive the hammer and remove the cuttings/the loose material being blown out of the borehole. This method was used for the following boreholes: Old Aurora Station, Endalen, Janssonhaugen, UNIS east, DBNyÅlesund, Kapp Linné 1, Kapp Linné 2, and Hornsund (Table 1). At Bayelva, a top hammer was used. In this set-up, the percussion introducing unit is situated above the borehole, in or near the drill motor. During rotation, percussion is applied to the drill bit through the drill rods.

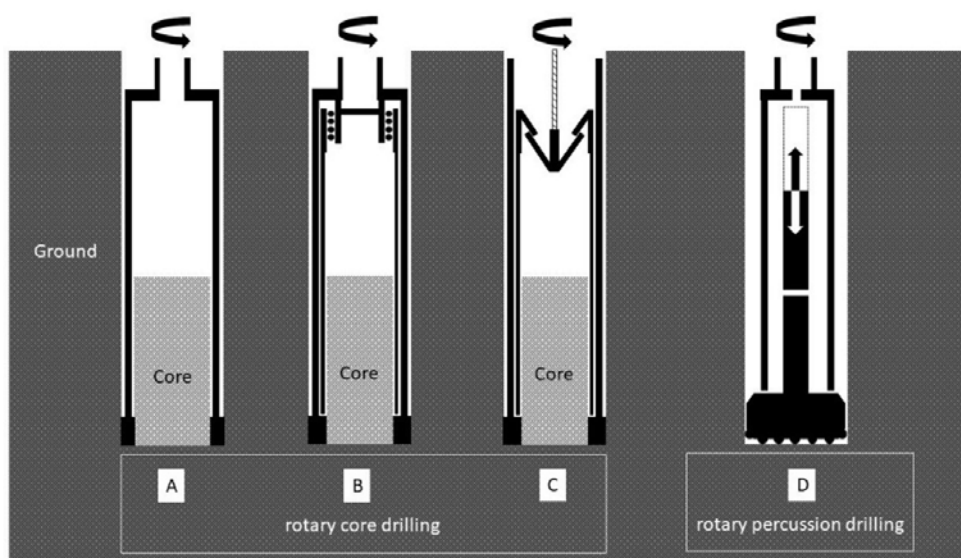


Figure 1: Schematic view of the drill bit and core assembly for rotary drilling: A – single core barrel. B – double core barrel. C – wire-line. D – Down-the-hole (DTH) hammer.

Table 1: Drill equipment information for permafrost boreholes presented in this report.

Drill equipment			Borehole									
Rig category	type	Operator	weight (ton)	Available drill methods	Location	rental	Location	Location	Borehole name/ID	Borehole depth (m)	Drill method used	
Construction	Atlas-Roc 701	Store Norske Spitsbergen Kulkompani AS	10	DTH	Drill rig no longer available	No	Adventdalen	Adventdalen	Jansonhaugen P10	102	DTH	
	Nemek 510	Anleggsdrift AS	10	DTH	Longyearbyen	Yes	Adventdalen	Adventdalen	Jansonhaugen P11	15	DTH	
	Nemtek 300 TS	Kings Bay AS	10	DTH	Ny-Ålesund	Yes	Ny-Ålesund	Adventdalen	NGTS Adventdalen	30	DTH	
Geotechnical	Geotech 504	SINTEF	2.5	Core drilling, auger, sounding, DTH	Longyearbyen	Yes	Adventdalen	Adventdalen	Old Aurora Station2	9,85	DTH	
	GM 50 GT Combi	Polish Polar Station, Hornsund	2.0	Core drilling, auger, sounding, DTH	Hornsund	Yes	Hornsund	Kapp Linné	Endalen	19	DTH	
									Kapp Linné 1	29	DTH	
									Kapp Linné 2	38	DTH	
									Meteo	12	DTH	
Purpose build	UKB 12/25	Arctic and Antarctic Research Institute (St. Petersburg)	0.1	Core drilling	Barentsburg	Collaboration only	Barentsburg	Barentsburg	Brzuchorzęska	5	DTH	
									Lisek	10	DTH	
									Brzydal	10	DTH	
									Lola	20	DTH	
									Renifer	20	DTH	
Exploration	UNIS permafrost rig LB 1200 (modified)	University Centre in Svalbard, Kolibri Geo Services	0.6	Core drilling, DTH	Longyearbyen	Yes	Ny-Ålesund	Ny-Ålesund	DBNyÅlesund	48,5	DTH /double core barrel	
	Onram 1500	Store Norske Spitsbergen Kulkompani AS	3	Core drilling (Wireline)	unknown	yes	Adventdalen	Adventdalen	Verlegenhukken	31	DTH / double core barrel	
									Breirosa	335	Wireline	

3.1.2. Rotary core drilling

A steel cylinder that accommodates the core is equipped with a barrel head to connect to drill rods and a drill bit that drills directly into the ground. The simplest coring equipment used is the single core barrel. It can consist of one piece or be made of several interchangeable elements (Figures 1A and 2A). The single core barrel is used “dry”, where no flushing medium (water, air, mud, foam) is used. The borehole in Barentsburg was drilled this way. There the core barrel was fitted with tungsten carbide bit inserts.

To retrieve samples from the borehole at DBNyÅlesund, a double core barrel was used with

impregnated diamond drill bits. The inner core barrel, held by ball bearings, does not allow contact of the core with the rotating outer core barrel (Figure 1B). An air compressor was used to cool the drill bit and flush cuttings to the surfaces. This method was used only to drill the upper part of the borehole.

Drilled as an exploration borehole, Breinosa was drilled using a wire line system (Figure 1C). As a “lazy” modification of the double core barrel, here the inner core barrel can be retracted by means of a steel wire. The outer rotating casing including the core barrel supports the borehole walls during operation. Cooling of the drill bit and removal of cuttings are carried out by water with salt as an additive to hinder freezing.



Figure 2: Location of relevant permafrost observation sites in Svalbard.



Figure 3: A) Single core barrel. Squared tungsten carbide inserts form the crown of the drill bit. (Photo: Ullrich Neumann), B) Borehole being drilled in Janssonhaugen. Drill rig, air compressor and accessories are placed onto one large sledge (Photo: Johan Ludvig Sollid). C) Rotary percussion drilling at Endalen borehole with the Geotech 504 geotechnical drill rig. (Photo: Håvard Juliussen). D) The Hornsund GM 50 GT Combi drill rig. (Photo: Tomasz Wawrzyniak). E) Russian drill rig in operation near Barentsburg. (Photo: Ullrich Neumann) F) UNIS permafrost drill rig drilling the DBNyÅlesund borehole. Kings Bay AS supplied the air compressor (Photo: Ullrich Neumann).

3.2. Equipment categories

3.2.1. Construction drill rigs

Designed for construction and mining purposes, construction drill rigs are very efficient drilling tools. Both machinery and methods are well established utilizing rotary percussion drilling methods. However, the rather high mass of around 10 tons makes them ineffective for boreholes far away from general infrastructure. Including the compulsory air compressor, the total weight is often over 20 tons. Generally, the rig can reach a depth of 300 m with a diameter of up to 300 mm. While the UNIS East borehole could be accessed by road, Janssonhaugen (Figure 2) was reached by a caterpillar towing the rig and accessories on a sledge in winter. Examples of such rigs and the boreholes they have drilled are as follows: Atlas-Roc 701 (Janssonhaugen; Figure 3B), Nemek 501 (UNIS east) and Nemek 300 TS (Bayelva).

3.2.2. Exploration drill rig

The Breinosa 335 m deep borehole was established using an exploration drill rig, prospecting for coal. The rig has a capability of 1000 m and more with a wireline system. A large logistical effort is necessary to supply supercooled water as a drill fluid on-site, and all necessary equipment must be airlifted in place. Today, this rig is no longer located in Svalbard.

3.2.3. Geotechnical drill rigs

Geotechnical drill rigs offer a broad spectrum of drilling and sampling methods for ground investigations. These rigs are self-propelled by tracks, have a weight of around 2 tons, and are operated by a crew of two. Geotechnical rigs offer rotary core drilling, auger, sounding, and DTH. Borehole diameters of up to 160 mm are possible. Both rigs, the Geotech 504 stationed at UNIS (Figure 3C) in Longyearbyen and the GM 50 GT Combi in Hornsund (Figure 3D) used DTH drilling methods to establish boreholes.

3.2.4. Purpose built permafrost drill rigs

The DBNyÅlesund and the new SIOS InfraNOR boreholes around Longyearbyen and Adventdalen were drilled by the UNIS permafrost drill rig, jointly developed by Lutz Kurth Drill systems, Kolibri Geo Services, and UNIS scientific staff, for drilling in remote locations in Svalbard and Greenland, mainly during winter (Figure 3F). The hydraulic rig, powered by a gasoline engine, has a weight of 600 kg and uses coring and percussion drilling methods. A total depth of 50 m can be reached with borehole diameters of up to 116 mm. Without propulsion, the rig is towed on a sledge by a snowmobile, pushed on wheels, or airlifted in place. It has been sent by the medium-sized Dornier airplane from Svalbard to N and NE Greenland for drilling permafrost monitoring boreholes there as well. This drill rig is presently being further developed to improve drilling into as many types of sediments in permafrost landscapes as possible, as part of the SIOS InfraNOR project.

Originally developed for ground investigations in remote areas of Siberia, the Russian drill rig has a total weight of approximately 100 kg (Figure 3E). Both thrust and lifting are done by a manually operated winch, while a one-cylinder, two-stroke engine rotates the drill. The drill operation in Barentsburg used dry coring with a single core barrel with a 50–120 mm diameter range. A maximum depth of 50 m has been reached in peat deposits in northern Russia.

For climate change-related investigations, often a hand drill can provide important information about the ground ice content in the upper meters of the permafrost depending on the sediment type. At UNIS, a STIHL™ BT 121 Earth Auger with drilling extensions and an unflighted (smooth-walled) core barrel with diamond cutting teeth is used for hand drilling to obtain shallow cores (Gilbert et al. 2015).

4. Ground ice and stratigraphy

A great deal of information about stratigraphy and ground ice content was collected during the drilling and installation of the boreholes included in this and earlier SESS reports on permafrost. Even for sites where cores and samples were not recovered, driller observations can provide valuable insight into the stratigraphy and ground ice content. Here, we provide the first overview of the stratigraphy and ground ice conditions at all the observation permafrost boreholes included in this report.

Drill records from the DBNyÅlesund site (Figure 2 and Table 1) indicate approx. 3.5 m of overburden sediment, likely moraine material, overlying bedrock. Observations indicate that the transition to bedrock is likely gradational and extends over a few vertical meters. During drilling, cores were retrieved in the upper 3 m of the borehole.

Disturbed cutting samples were collected in the bedrock interval. The gravimetric ground ice content varies significantly, from between 5% and up to 40% in the upper 3 m (Figure 4A). No excess or visible ground ice was documented. A few samples from the bedrock interval were also analysed, but should be interpreted with caution, as they are disturbed samples. They show rather low ground ice contents of around 10%. Unfortunately, no drilling log is available from the Bayelva site in Ny-Ålesund.

The Old Aurora Station 2 in central Adventdalen has a sediment cover that is approx. 60 m thick and is comprised of a complex stratigraphy recording both marine (deltaic and fluvial) and terrestrial (aeolian loess) sedimentary infilling and development of a fjord-valley system following deglaciation (Gilbert

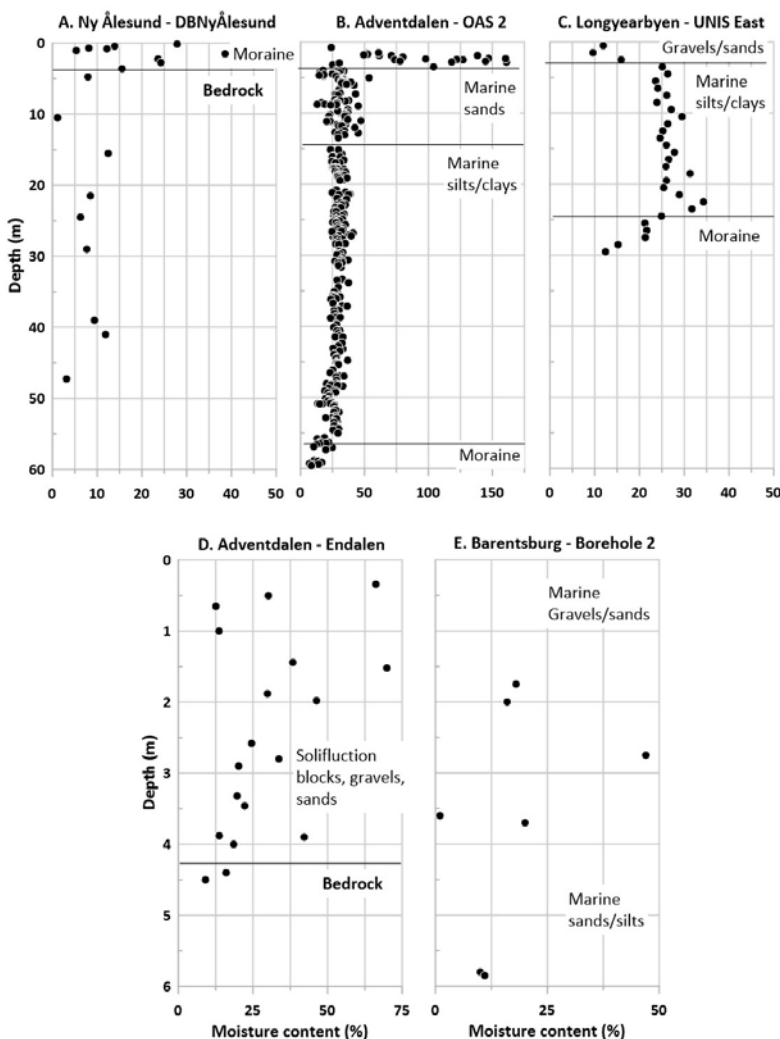


Figure 4: Permafrost gravimetric ice content in percent from the permafrost observations sites. Note that vertical scale is very different for A to C compared with D and E, as these boreholes are comparably shallow. The horizontal ice content scale is also adapted to each plot to illustrate the observed range in values in most detail. The depth where bedrock was encountered is indicated by a black horizontal line.

et al. 2018). The ground ice content has been quantified in 350 samples from a borehole located within approx. 100 m radius of the Old Aurora Station 2 site (Gilbert et al. 2018, 2019). These show rather large variability in the top 1.5–3.5 m of terrestrial sediments, from 50% to 160% ground ice content (Figures 4B and 5). The upper 3 m consists of sands and silts deposited as loess and enriched with ice. Below 3 m in fluvial and marine sand, silt, and clay sediments, the ground ice content varies much less and is generally only around 20–40% (Gilbert et al. 2018).

The UNIS East site consists of 4 m of sands and gravels overlying 21 m of marine clays overlying 5 m of moraine material. The amount of ground ice is rather low for this fine-grained site with a maximum of around 30% at 20 m depth, whereas the top permafrost has only around 10% ground ice (Figures 4C). Bedrock was not encountered during drilling of the borehole included in this report but is known to lay between 25 m and 35 m below the terrain surface in this area.

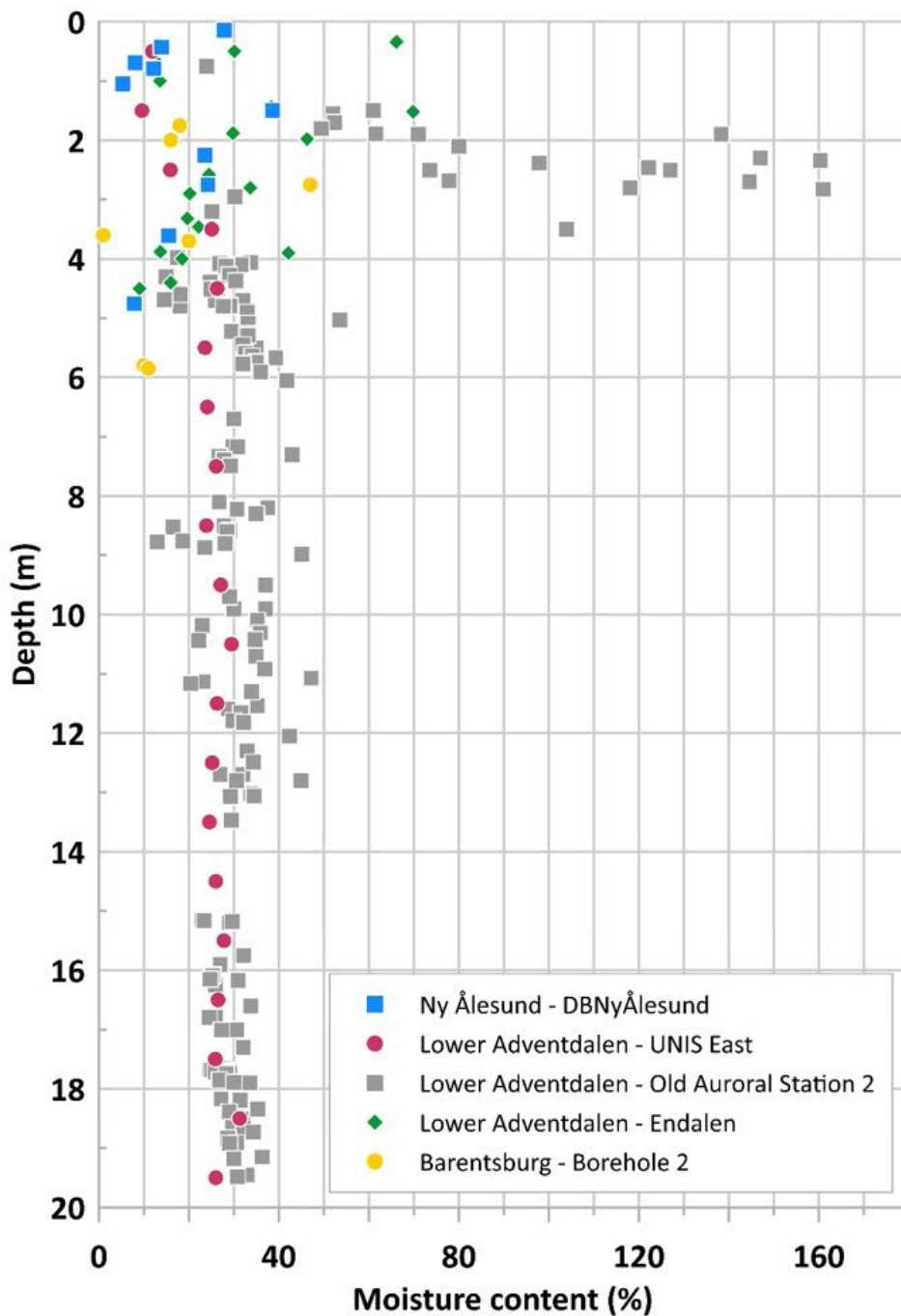


Figure 5: Permafrost gravimetric ice content in percent for all permafrost observation sites in Svalbard, allowing for direct comparison for the top 20 m.

The Endalen solifluction site is characterized by approx. 4–5 m of diamict material overlying bedrock. The transition to bedrock is gradational and extends over approx. 4 m. Core sample

analyses of the top 4.5 m indicate that the ice content within the sediment varies quite a lot but ranges up to 70% (Figure 4D). Segregated ground ice is observed at this site (Figure 6E).

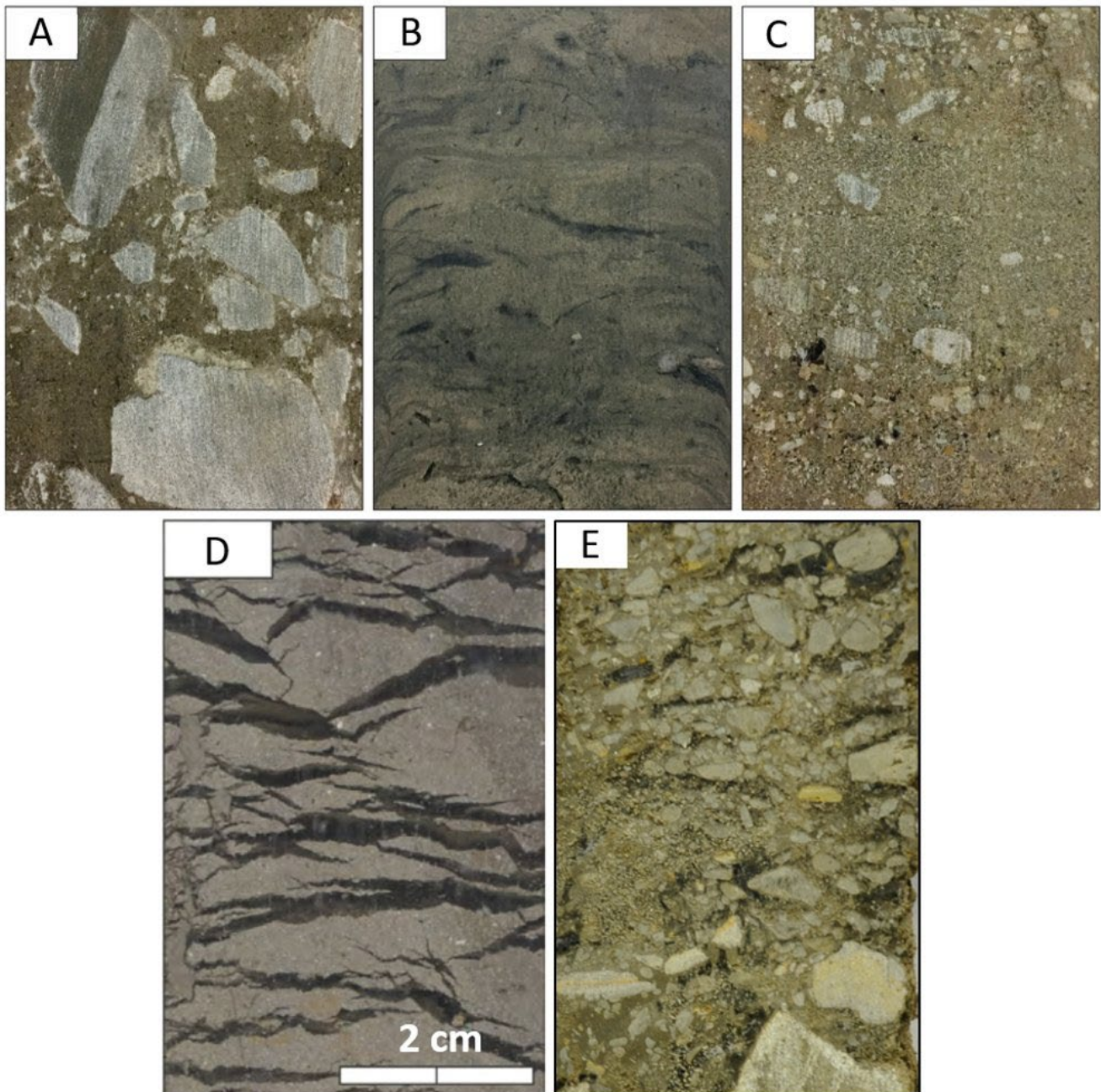


Figure 6: Example images of core samples. A) moraine sediment (UNIS East). B) marine clays (UNIS East). C) ice-poor sands and gravels (UNIS East). D) segregated ice lenses (Old Aurora Station2). E) Segregated ice (black) and gravels (Endalen). A–C reproduced from Gilbert et al. (2019). D reproduced from Gilbert et al. (2018). E Ullrich Neumann.

Stratigraphy at the Breinosa blockfield borehole consists of several meters of weathered bedrock overlying bedrock (Christiansen et al. 2010). Since the borehole was drilled as part of coal prospecting using exploration drilling, no permafrost samples were collected. However, direct field observations in the Breinosa area show high ice contents between individual blocks in the lower active layer in late summer.

The site at Janssonhaugen is drilled using the DTH technique into bedrock. Ground ice content data does not exist. However, XRD analyses of well cuttings from the drilling collected at 3–7 m intervals, show high quartz content interpreted as sandstone (Isaksen et al. 2000). Ice lenses were identified down to 6–7 m depth, just as clean ice chips were blown up during drilling from the most fractured parts (Isaksen et al. 2000).

The Meteo borehole in Hornsund is drilled in crystalline quartz bedrock. Unfortunately, ground ice data are also not available from this site, which was also drilled using the DTH technique. Kapp Linné 1 was drilled into an outcrop of silicified carbonate and clastic sedimentary bedrock, and Kapp Linné 2 was drilled through 6.2 m of beach ridge gravels overlying the same type of bedrock (Christiansen et al. 2010). Ground ice data are not available from these two sites either as drilling was

done using DTH (Figure 4C) before the UNIS drill rig was developed.

The stratigraphy at borehole 2 in Barentsburg is 1.3 m of sands and gravels overlain by an intermediate soil loam containing different ground ice structures. A gradual transition to bedrock is encountered at approx. 7 m depth. Some ground ice content measurements exist from the top 6 m. These show a large variation even over a short depth from only a few percent to close to fifty percent (Figure 4E). Borehole 12 in Barentsburg was drilled during coal exploration in the early 1930s, and unfortunately, no detailed description of the stratigraphy for this borehole drilled into sediments is available.

The ground ice content in the Svalbard permafrost observation boreholes is generally largest in the permafrost in valley bottom sediments up to 160%. This is clearly much more ice than in the bedrock sites, which typically have below 15% (Figure 6). In Adventdalen, the permafrost has a much higher content of ground ice, reaching 150% in the top 1–3 m, where terrestrial sediments such as loess and solifluction sediment dominate. Ground ice content is typically lower (approx. 25–35%) in the underlying fluvial sands and gravels and marine sediments (silts and clays) (Figure 6).

5. Meteorology 2016–2019

Air temperatures in Svalbard have increased by 1°C per decade since 1971, while total liquid and solid precipitation has increased by 4% per year (Figure 7 upper), with the most increase occurring in the autumn (NCCS 2019). Mean annual air temperatures at both Hornsund and Ny-Ålesund

were reduced by around 2.5°C from 2016 to 2019 (Figure 7 upper). The total amount of precipitation recorded was from around 100 mm (Longyearbyen area) to around 500 mm (Hornsund) less during the 2018–2019 period (compared with 2016–2017 (Figure 7).

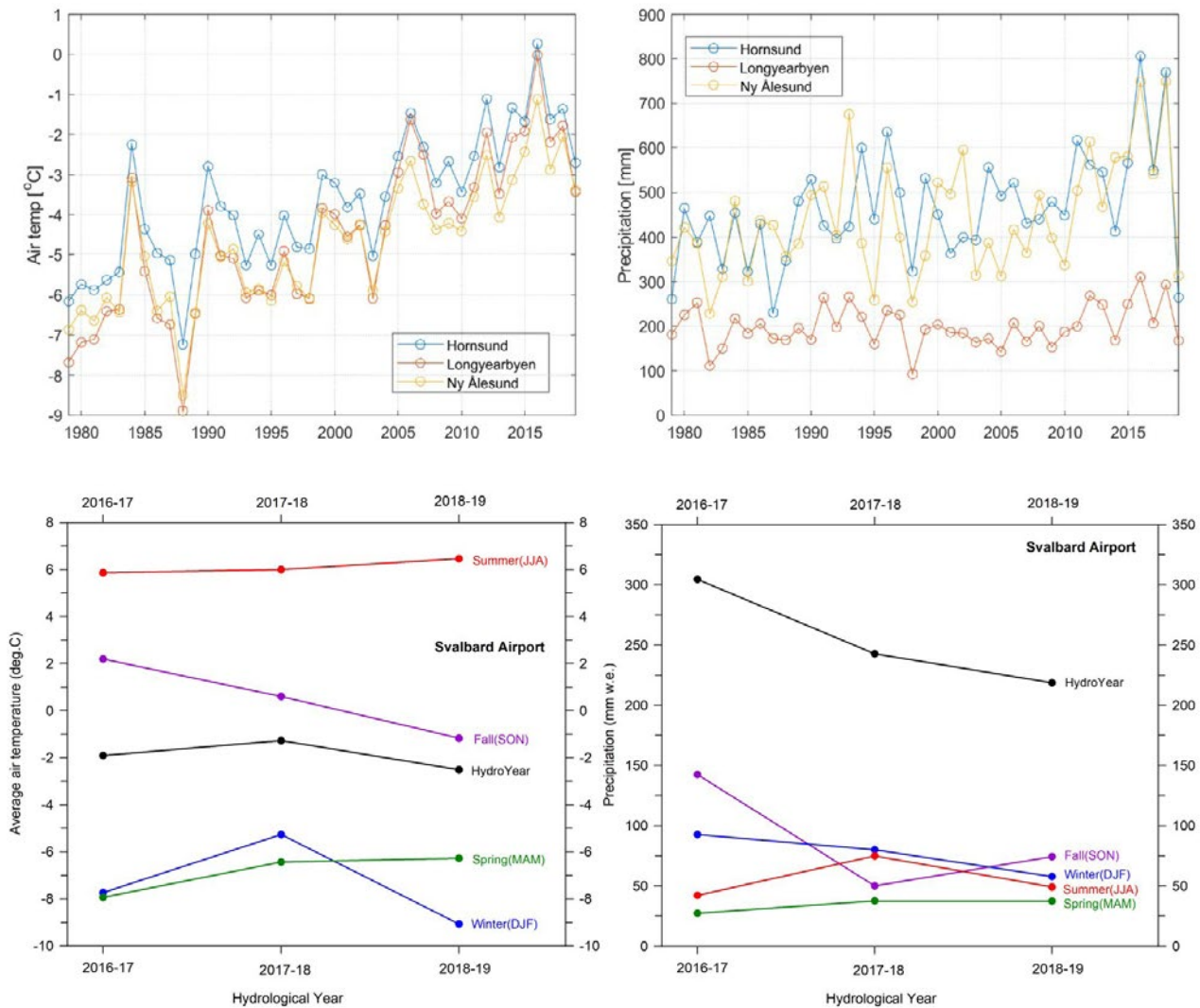


Figure 7: Upper: Meteorological records of mean annual (calendar year) air temperature and precipitation from 1979 to 2019 of 3 stations in Hornsund, Longyearbyen, and Ny-Ålesund, covering the variation in our permafrost observation areas in Svalbard. Lower: Mean annual and seasonal air temperature and precipitation for the hydrological years from 2016–2017 to 2018–2019 at the Svalbard Airport in the Longyearbyen area. Hydrological years run from 1 September to 31 August the year after.

Air temperatures in the calendar year 2016 reached a record high mean annual value of -0.1°C recorded at Svalbard Airport (Figure 7 upper), characterised by a particularly warm and wet autumn (Christiansen et al. 2019) (Figure 7 lower). During the 2016–2017 hydrological year (from 1 September to 31 August), mean annual air temperature was -1.9°C , and 305 mm of precipitation was recorded, an above-average amount. During the observation period we report on in this PermaSval contribution mean hydrological annual air temperatures have varied from -1.3°C in 2017–2018 to -2.5°C in 2018–2019 at the Svalbard Airport. Seasonally, at Svalbard Airport, the largest changes are a 1°C cooling in the autumns, but only to a value of -1.2°C

in the 2018 autumn. Summers and springs have remained relatively stable with only small increases in the summer of 2019, and from spring 2017 to spring 2018. The largest seasonal variability was observed in the winter air temperatures, which ranged from -5.3°C in 2017–2018 to -9.1°C in 2018–2019. Precipitation has generally been low in all seasons, reflecting the overall dry climate, particularly in central Svalbard. The reduction in precipitation of approx. 100 mm is attributed to drier autumns after the record wet autumn 2016 value of 142 mm (September–November 2016). Autumn 2016 had 47% of the annual precipitation of that hydrological year, with a value clearly much higher than any other season that hydrological year.

6. Permafrost thermal state and active-layer thickness 2016–2019

The permafrost thermal state is presented for the five main permafrost observation sites in Svalbard: Ny-Ålesund, Adventdalen, Kapp Linné, Barentsburg, and Hornsund (Figure 2). Borehole locations and instrumentation at each site were previously described in detail in Christiansen et al. (2019), Gilbert et al. (2019), Boike et al. (2018), Demidov et al. (2016), and Isaksen et al. (2001). We present hydrological year data, calculated from 1 September to 31 August the year after.

Permafrost temperature at the depth of zero annual amplitude (DZAA) is typically found between 10 to 20 m and reflects climate and ground conditions over a longer duration. Temperature at the DZAA is commonly used to interpret the response of permafrost to climate changes. The top permafrost temperatures respond to annual and even seasonal variations and are thus more directly sensitive to short-term meteorological fluctuations.

Interpolation is used at the end of the thawing season to calculate active-layer thickness from the borehole temperature data. For the three CALM grids in Svalbard, located in Adventdalen (UNISCALM), near Barentsburg, and in Ny-Ålesund (Christiansen & Humlum 2008; Shiklomanov et al. 2012; Christiansen et al. 2019), the active layer

thickness is determined by manual probing at 121 points, spaced evenly in a 100 m x 100 m grid, reporting the mean for the entire grid.

6.1. Permafrost thermal state

The permafrost surface temperatures, determined from the upper-most temperature sensor within the permafrost, typically varied less between the observation sites in Svalbard than the deeper permafrost temperatures during this observation period, with a range only from around -1°C to -4.5°C (Figure 8a). There is a general decline observed in all sites ranging from 0.3°C to 1.2°C , in response to decreasing mean annual air temperatures and precipitation during the three-year period.

The lowest permafrost temperatures at DZAA are observed in boreholes at inland mountain sites at higher elevations, such as Breinosa (677 m a.s.l.) and Janssonhaugen (254 m a.s.l.), and in sites with thin winter snow cover and winter cold air drainage such as in Adventdalen Old Aurora Station 2 (Figure 8). In these sites, observed permafrost temperatures are around -5°C , with a slightly positive trend over the observation period only for Janssonhaugen. Sites where winter snow cover (e.g. UNIS East) is thicker and/or with a thick, moisture-rich active layer (e.g.

Endalen), have characteristically higher permafrost temperature from -4° to -2.5°C , also with a slightly positive trend. Permafrost temperatures at DZAA are higher in the more coastal lowland sites in Ny-Ålesund (25 m and 55 m a.s.l.), Barentsburg (95 m a.s.l.), and Kapp Linné (20 m a.s.l.), ranging from -2.2°C to -3.1°C . These coastal sites also had a smaller increase in permafrost temperatures. The

highest permafrost temperature observations at DZAA are from Hornsund, where temperatures are only -1.2°C at 12 m depth. This value has been rather stable over the two-year observation period (Figure 8B). Clearly, most of the deeper permafrost temperatures still increase slightly, responding to the overall decadal warming that has been going on in Svalbard.

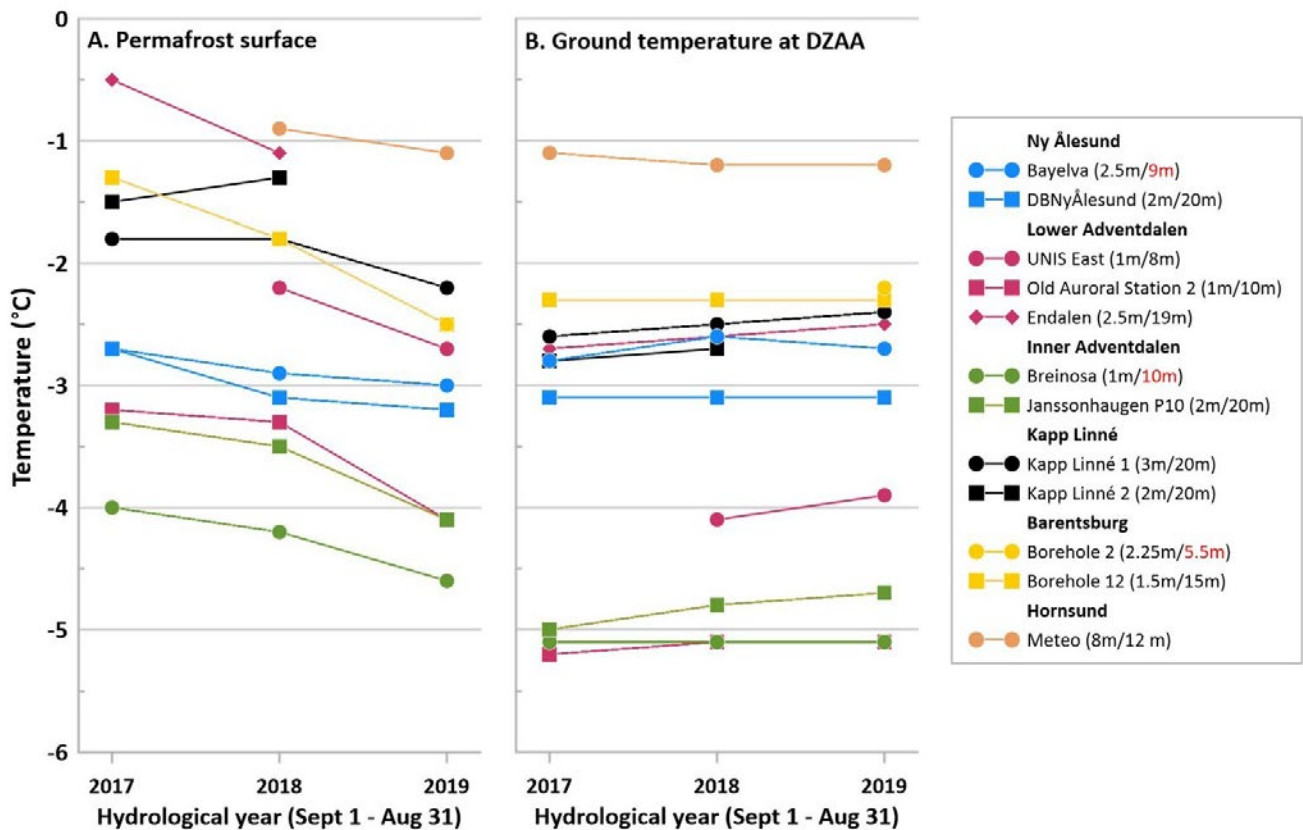


Figure 8: Mean annual ground temperature development as recorded at (A) the permafrost surface (represented by the upper-most temperature sensor in the permafrost) and (B) the depth of zero annual amplitude (DZAA) or deepest sensor for the hydrological years 2016–2017 to 2018–2019. DZAA (black text) or location of the deepest sensor (red text) is given in brackets beside each borehole in the legend. Borehole location areas are shown in Figure 5.

6.2. Active layer thickness

Most of the active layer thickness observations fall in a range from 100 to 200 cm (Figure 9). However, in the highest located borehole at Breinosa, the active layer has been as shallow as 49 cm, and we observe much thicker active layers in the bedrock coastal site at Kapp Linné around 3 m and at Hornsund around 5 m. The active layer is generally thinnest at sites with well-drained sediments in the Adventdalen area such as Breinosa, UNIS East, and the Old Aurora Station 2, ranging from 50 to 100 cm. Observations from boreholes in sediment and

moraine, e.g. Ny-Ålesund and Barentsburg, suggest an active-layer thickness of approx. 150 cm. Thicker active layers in slopes e.g. Endalen and in bedrock boreholes e.g. Kapp Linné and Janssonhaugen, are observed all around 175 to 200 cm. The deepest thaw depth is recorded at the Meteo borehole in Hornsund – approx. 500 cm. The observations at Hornsund are quite exceptional and might reflect a more complicated situation at the site than simple heat conduction. The very thick active layer may be influenced by groundwater flow during summer, but it is also possible that the quartzite bedrock with its high thermal conductivity causes this.

The active-layer thickness has doubled at the blockfield bedrock site at Breinosa to 98 cm and has increased by 75 cm at the Meteo raised beach bedrock site in Hornsund over only 1 year (Figure 9). At the Barentsburg Borehole 12, the active layer thickness decreased by 37 cm over the observation

period. At the Janssonhaugen and the Kapp Linne bedrock borehole sites active-layer thickness increased slightly over the three-year observation period, while a slight decrease was observed at all other sites.

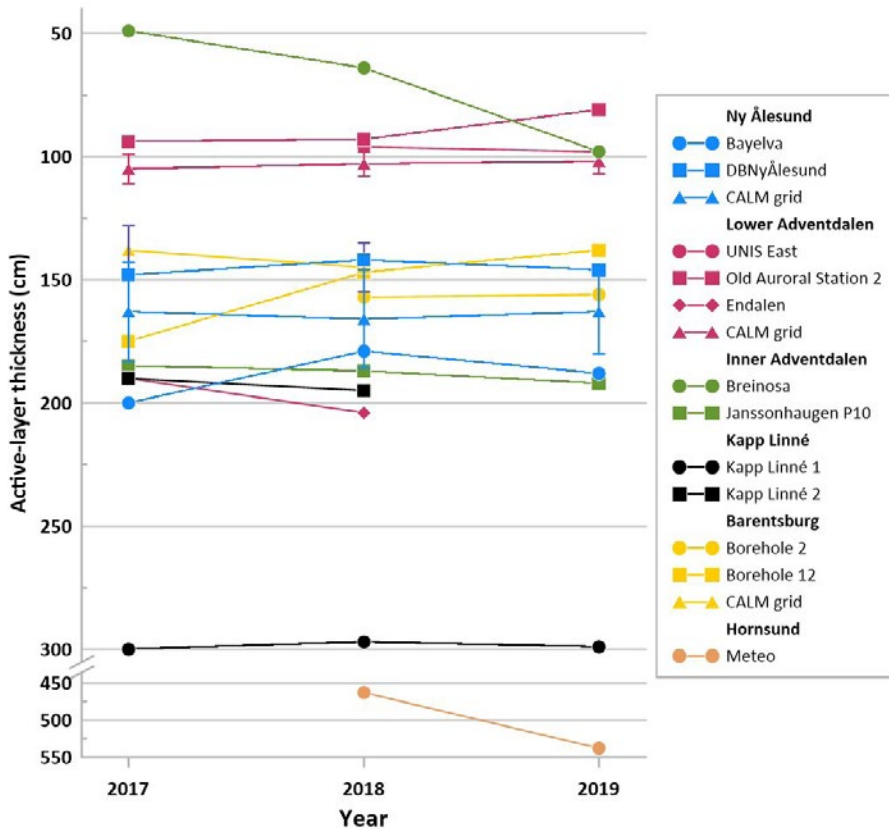


Figure 9: Active-layer thickness through the 2017–2019 period. Values are reported in autumn of each year. The active-layer thickness is determined by interpolating the temperature profiles at the end of the thawing season. CALM grid means also show one standard deviation. Note the break and change in the vertical axis and spacing to accommodate observations from Hornsund.

7. Conclusion

Being able to combine the information on the ground ice content with the permafrost ECVs allows for an improved understanding of the permafrost ECV dynamics during the observation period 2016–2019 in Svalbard. The presented permafrost ECV data range from either no warming (Breinos at 10 m depth; DBNyÅlesund at 20 m depth; Borehole 12 Barentsburg at 15 m depth) up to 0.15°C/y warming (Janssonhaugen at 20m depth) at 10–20 m depths. This shows that there is still a response to the general warming that Svalbard has seen over the last decades. On the rather short time scale of

our three-year observation period in which mean annual air temperature declined and there was reduction in the annual amount of precipitation, the temperature in the top permafrost decreased in all observation sites ranging from 0.2°C/y (Kapp Linne 1) to 0.6°C/y (Borehole 12 Barentsburg) as a response to this small-scale variability.

The active layer has generally decreased slightly in thickness, ranging from 1 cm/y (DBNy-Ålesund) to 6.5cm/y (Old Aurora Station Adventdalen), but two sites had small increases from 1 cm/y (Kapp

Linne 1) to 3.5 cm/y (Janssonhaugen). However, two other sites experienced larger changes. In the blockfield at Breinosa, the active layer increased by 24.5 cm/y, while in the raised marine sediments at Borehole 12 in Barentsburg, the active layer thinned by 18.5 cm/y in the two-year observation period from summer 2017 to summer 2019.

Less than half of the observation boreholes have detailed ground ice information, but the ones that have this information represent both bedrock and sediments and thus allow us to extrapolate this information and use it at a general level to interpret the results from all the permafrost observation sites. Most of the permafrost observation sites have warmed only slightly at 10–20 m depth but at the same time show consistent cooling in the top permafrost and small-scale thinning of the active layer in response to the cooling over the observation period 2016–2019. However, two sites have not seen warming at 10–20 m depth and had cooling of the top permafrost and decreasing active layer thicknesses (DBNyÅlesund and Borehole12 Barentsburg). Both had relatively high ground ice contents in the top permafrost, which is sedimentary. Bedrock underlies the Ny-Ålesund site, while the entire borehole is in sediment in Borehole 12 in Barentsburg. This shows how high ground ice contents protect and preserve the permafrost.

The blockfield observation site at Breinosa had no warming at 10 m, exhibited permafrost top cooling, and at the same time experienced an active layer doubling. Clearly, more air circulation must be the main reason why the active layer doubled in this landform, with no other landforms having this response. This, clearly, was not directly air temperature driven, but was probably also caused by less precipitation. The only other site which had a small-scale active layer increase (3.5 cm/y) was the hilltop Janssonhaugen borehole site, which had permafrost warming at 20 m, while the permafrost top cooled. This presumably reflects the influence of the slight summer warming in combination with the exposed nature of the hilltop, which prevents snow accumulation at this site and allows quick heat conduction into the bedrock which probably has low ground ice content.

Additionally, the overview of the drilling equipment clearly demonstrates how well-equipped Svalbard now is for drilling boreholes with both methods and a range of equipment, allowing for both deep and shallow boreholes. The review of the drilling methods used for the present observation boreholes also shows that most drilling operations, even though made for permafrost observation, did not collect cores, and some did not even have any stratigraphical record.

8. Unanswered questions and recommendations for the future

- *Always collect ground ice and stratigraphy information from long-term permafrost observation sites* – This reporting shows how important data on stratigraphy and ground ice content are to best understand the detailed responses of permafrost to climatic changes. Therefore, it is a clear recommendation to invest in obtaining and analysing the ground ice content of cores collected through drilling of all new boreholes being established for permafrost ECV observation. This is more costly but clearly provides important data for interpreting the observed permafrost ECV data in larger detail and thus allows us to better predict future responses to climatic changes. Also, the present drilling equipment in Svalbard will be/is now offering a very good variety of methods which suit most needs from shallow to deep boreholes.
- *Consider expanding the permafrost observation network* – Expand the network to make sure it contains not only all the different parts of Svalbard but also covers the landform variability. The presented results clearly show how different landforms can respond very differently to the same climatic forcing. Other types of site-specific forcing are also very important, such as grain size, lithology, ground ice content, aspect, and vegetation cover.

- *Perform ground ice studies from slopes* – Current knowledge about ground ice in Svalbard is focused on coastal lowlands, valley bottoms, and periglacial landforms such as pingos and solifluction sheets. Climate change is expected to impact landslide frequency in sloping terrain. However, knowledge about the amount and distribution of ground ice in slope deposits is sparse but could improve estimates of the future stability of slopes in Svalbard. New boreholes should be drilled in slopes with cores retrieved and laboratory studies carried out to quantify the ground-ice content and stratigraphy.

Temperature and pore water pressure sensors should be installed in such boreholes to improve our understanding of their sensitivity to climate change and for preparedness situations in populated areas.

- *Get more permafrost ECV and SIOS SCD operational and online* – New boreholes, or old boreholes getting new instrumentation, should be using modern technology that provides online access to the permafrost data for improved direct scientific and societal use.

9. Data availability

The permafrost ECV data included is generally available through the Global Terrestrial Network for Permafrost (GTN-P) database. These two types of permafrost ECV data are both SIOS core data, and therefore, also available through the SIOS data access portal. An overview of the permafrost

temperature data are included in Table 2. Ground ice content data are available through the references included in this report or by contacting the authors. The information about the drilling equipment is all included in the text, figures, and Table 1.

Table 2. Permafrost temperature data in GTN-P and as appearing in the SIOS data access portal.

Dataset	Period	Location	Metadata/Data Access
GTN-P Barentsburg Borehole 12	2016–2017	Barentsburg	SIOS data access portal: https://bit.ly/346AVLN
GTN-P DBNyÅlesund	2016–2017	Ny-Ålesund	SIOS data access portal: https://bit.ly/2Wr2co5
GTN-P Breinosa (E-2009)	2009–2020	Breinosa	SIOS data access portal: https://bit.ly/2Kp3ygh
GTN-P Kapp Linne 1	2008–2020	Kapp Linne	SIOS data access portal: https://bit.ly/3oRhH4F
GTN-P Kapp Linne 2	2008–2018, 2019–2020	Kapp Linne	SIOS data access portal: https://bit.ly/3mizyzZ
GTN-P Endalen PYRN	2008–2020 (with some gaps)	Endalen	SIOS data access portal: https://bit.ly/3qYJan4
GTN-P Old Auroral Station PYRN	2008–2019	Adventdalen	SIOS data access portal: https://bit.ly/3oRHbyY

Acknowledgements

We are grateful to SIOS for supporting the development of this report. The permafrost data that this report is based on has been funded by our national research councils and the participating institutions where the authors are based. Financial support at Hornsund was provided by the Polish National Science Centre through grant No.

2016/21/B/ST10/02509. This work was supported by the Research Council of Norway, project number 291644, Svalbard Integrated Arctic Earth Observing System - Knowledge Centre, operational phase. Thanks to Sarah Strand for checking the language and for uploading data into GTN-P.

References

- Boike J, Juszak I, Lange S, Chadburn S, Burke E, Overduin PP, Roth K, Ippisch O, Bornemann N, Stern L (2018) A 20-year record (1998–2017) of permafrost, active layer and meteorological conditions at a high Arctic permafrost research site (Bayelva, Spitsbergen). *ESSD* 10:355
- Christiansen HH, Etzelmüller B, Isaksen K, Juliussen H, Farbrod H, Humlum O, Johansson M, Ingeman-Nielsen T, Kristensen L, Hjort J, Holmlund P, Sannel ABK, Sigsgaard C, Åkerman HJ, Foged N, Blikra LH, Pernosky MA, Ødegård RS (2010) The thermal state of permafrost in the Nordic area during the international polar year 2007–2009. *Permafrost Periglacial Process* 21:156–181
- Christiansen HH, Humlum O (2008) Interannual variations in active layer thickness in Svalbard. In: Kane, DL & Hinkel, KM (eds) 9th Int. Conf. on Permafrost Proceedings, Institute of Northern Engineering, University of Alaska, Fairbanks, USA, pp 257-262
- Christiansen HH, Gilbert GL, Demidov N, Guglielmin M, Isaksen K, Osuch M, Boike J (2019) Permafrost thermal snapshot and active-layer thickness in Svalbard 2016-2017. In Orr et al (eds): SESS report 2018, Svalbard Integrated Arctic Earth Observing System, Longyearbyen, [pp 26-47 https://sios-svalbard.org/SESS_Issue1](https://sios-svalbard.org/SESS_Issue1)
- Christiansen HH, Gilbert GL, Demidov N, Guglielmin M, Isaksen K, Osuch M, Boike J (2020) Permafrost temperatures and active layer thickness in Svalbard during 2017/2018. In: Van den Heuvel et al (eds): SESS report 2019, Svalbard Integrated Arctic Earth Observing System, Longyearbyen, [pp 236-249 https://sios-svalbard.org/SESS_Issue2](https://sios-svalbard.org/SESS_Issue2)
- Demidov NE, Verkulich SR, Karaevskaya ES, Nikulina AL, Savatyugin LM (2016) First results of permafrost monitoring on the cryospheric site of Russian Scientific Center on Spitsbergen (RSCS). *Problems of Arctic and Antarctic* 110: 67-79
- Gilbert GL, Christiansen HH, Neumann U (2015) Coring of unconsolidated permafrost deposits: Methodological successes and challenges. *GeoQuebec 2015*, 68th Canadian Geotechnical Conference and 7th Canadian Permafrost Conference. In: Gilbert, GL (2018) *Cryostratigraphy and sedimentology of high-Arctic fjord-valleys*. Ph.D. thesis, University of Bergen & UNIS, paper II
- Gilbert GL, O'Neill HB, Nemeč W, Thiel C, Christiansen HH, Buylaert JP (2018) Late Quaternary sedimentation and permafrost development in a Svalbard fjord-valley, Norwegian high Arctic. *Sedimentology* 65: 2531-2558
- Gilbert GL, Instanes A, Sinitsyn A, Aalberg A (2019) Characterization of two sites for geotechnical testing in permafrost: Longyearbyen, Svalbard. *AIMS Geosciences*. 5: 868–885
- Gjermundsen A, Graff LS, Bentsen M, Breivik LA, Debernard JB, Makkonen R, Olivie DJL, Seland Ø, Zieger P, Schulz M (2021) How representative is Svalbard for future Arctic climate evolution? An Earth system modelling perspective. In: Moreno-Ibáñez et al (eds) SESS report 2020, Svalbard Integrated Arctic Earth Observing System, Longyearbyen, [pp. 38-59 https://doi.org/10.5281/zenodo.4034104](https://doi.org/10.5281/zenodo.4034104)
- Hanssen-Bauer I, Førland E, Hisdal H, Mayer S, Sandø A, Sorteberg A (red.) 2019. *Climate in Svalbard 2100 – a knowledge base for climate adaptation*. Norwegian Centre for Climate Services (NCCS)
- Isaksen K, Mühl D, Gubler, H, Kohl T, Sollid, JL (2000). Ground surface temperature reconstruction based on data from a deep borehole in permafrost at Janssonhaugen, Svalbard. *Ann Glaciol* 31: 287-294
- Isaksen K, Holmlund P, Sollid JL, Harris C (2001) Three deep Alpine-permafrost boreholes in Svalbard and Scandinavia. *Permafrost Periglacial Process* 12, 13-25
- Killie MA, Aaboe S, Isaksen K, Van Pelt W, Pedersen ÅØ, Luks B (2021) Svalbard snow and sea-ice cover: comparing satellite data, on-site measurements, and modelling results. In: Moreno-Ibáñez et al (eds) SESS report 2020, Svalbard Integrated Arctic Earth Observing System, Longyearbyen, [pp. 220-235 https://doi.org/10.5281/zenodo.4293804](https://doi.org/10.5281/zenodo.4293804)
- Nowak A, Hodgkins R, Nikulina A, Osuch M, Wawrzyniak T, Kavan J, Łepkowska E, Majerska M, Romashova K, Vasilevich I, Sobota I, Rachlewicz, G (2021) From land to fjords: The review of Svalbard hydrology from 1970 to 2019. In: Moreno-Ibáñez et al (eds) SESS report 2020, Svalbard Integrated Arctic Earth Observing System, Longyearbyen, [pp. 176-201 https://doi.org/10.5281/zenodo.4294063](https://doi.org/10.5281/zenodo.4294063)
- Shiklomanov NI, Streletskiy DA, Nelson FE (2012) Northern hemisphere component of the global circumpolar active layer monitoring (CALM) program. In: Proc. 10th Int. Conf. on Permafrost, 1, pp 377-382

Frequently Asked Questions

How representative is Svalbard for future Arctic climate evolution? An Earth system modelling perspective (SvalCLIM)

What is Arctic Amplification?

The world warms in response to anthropogenic greenhouse gas (GHG) emissions, but there are substantial regional differences in the rate of the warming. In particular, the Arctic warms at a much greater rate than the rest of the world. This accelerated warming is often called Arctic Amplification.

What causes Arctic Amplification?

Several mechanisms cause Arctic amplification. As early as 1869, Swedish scientist Svante Arrhenius realised that changes in atmospheric CO₂ concentration could alter the surface temperature and that the change would be especially large in polar regions due to reduced albedo as the snow and ice retreated. Additional causes of enhanced warming in the Arctic are changes in clouds, a flattening of the atmospheric vertical temperature gradient, increased water vapour content and surface fluxes as well as changes in atmospheric and oceanic energy transports.

What is CMIP6?

CMIP6 stands for Coupled Model Intercomparison Project Phase 6. This project coordinates climate model experiments involving 33 international modelling teams. Using many different models and scenarios, they try to: 1) find out how the earth system responds to various climate forcings; 2) identify causes of systematic bias in the models; and 3) figure out how best to predict climate change, given climate variability and uncertainties in the scenarios.

Why are so many models and scenarios used to project climate change?

Climate change involves many factors: emission of greenhouse gases (such as carbon dioxide, methane, nitrous oxide), airborne particles (aerosols, dust, smoke, and soot), physical and chemical processes. How the climate evolves will also depend on how society acts to adapt and mitigate to future changes and thus several future scenarios are used for future projections. By using an ensemble of models and scenarios, researchers can obtain a range of possible future states and better understand the uncertainties.

What are climate feedbacks?

Climate feedbacks are processes that can either amplify or diminish the effect of the drivers of the climate, the so-called climate forcings.

Positive climate feedbacks accelerate the effects of climate forcers, while negative feedbacks slow them down. One example is the ice and snow albedo feedback. Surfaces covered with ice and snow efficiently reflect solar radiation back to space. As temperatures rise, ice and snow melt and the bright surface is replaced by darker land and ocean which absorb solar radiation, hence accelerating warming.

Space Physics in Svalbard: A study of the energy input into the polar ionosphere using SuperDARN

What causes the aurora and how high is it?

The aurora occurs when high energy particles from the Sun collide with oxygen and nitrogen gas particles in the Earth's upper atmosphere at high latitudes. These collisions occur from approximately 100 to 250 km altitude, depending on the energy of the incoming particles. Collisions with different types of gas particles produce different colours. The green auroral emission occurs at about 100 km altitude, and the red emission up to about 250 km.

Why is Svalbard an important location for studying the aurora?

Svalbard is ideally located for studying a funnel-shaped region of the Earth's magnetic field called the "cusp". This region provides a pathway for particles from the Sun to enter the Earth's atmosphere and produce a unique type of aurora. During the polar night, it is possible to see this aurora when Svalbard rotates under the cusp between about 08:00-12:00 local time. Due to its location and supporting infrastructure, Svalbard is the only place on Earth where it is both possible and practical to study the cusp aurora from the ground.

What is "Space weather" and why is it important?

Space weather occurs when the Earth's space environment is disturbed by solar activity such as large explosions and X-ray flares. These disturbances can have a significant impact on technology including satellite navigation systems and long-distance radio communication, especially at high latitudes. Space weather events may also damage satellites and electric power grids, and pose a radiation risk to astronauts. It is important to understand Earth's space environment so that space weather events can be predicted.

How can radars be used to study the upper atmosphere (and magnetosphere)?

At latitudes above 65°, the Earth's upper atmosphere is constantly in motion due to the interaction between the Sun's and Earth's magnetic fields. Typical speeds are 500-1000 m/s, but can sometimes exceed 3000 m/s! Radars can be used to observe this motion by transmitting signals up into the atmosphere and then measuring the Doppler shift caused by the motion. Some radars can also measure the temperature and density of the atmospheric particles, which depends on collisions between particles and the motion of the atmosphere as a whole.

Scientific Applications of Unmanned Vehicles in Svalbard (UAV Svalbard)

What are the biggest challenges to flying drones in the Arctic?

The main challenge is low air temperatures, which make piloting drones difficult and reduces their battery capacity.

Svalbard's high latitude can mean interference in the magnetic field and low GPS coverage, perturbing the drone's positioning system.

Wildlife can pose problems. Seabirds can attack drones and pilots operating near breeding or feeding grounds. Mammalian wildlife may be frightened by the rotor noises. Stressing Svalbard's fauna is prohibited.

High winds, visibility, and icing can cause problems, restricting operations to fair weather.

What do I have to do to fly a drone on Svalbard?

Norwegian regulations for drone operations currently apply to Svalbard. For simple missions this means:

- Disturbing Svalbard's wildlife is prohibited
- Fly no higher than 120 meters above ground
- Keep 150 meters away from people, buildings, boats, etc
- You must always be able to see your drone
- Familiarize yourself with rules about filming and photographing other people
- Flying drones in the dark is prohibited
- Stay at least 5 km away from airports in Longyearbyen and Svea. Obey the 20 km no-fly zone around Ny-Ålesund

Starting 1 January 2021, the new EU drone laws will apply.

How are drones used for science in Svalbard?

Drones are used scientifically in many ways in Svalbard. Most scientists use simple drones to take pictures from above. This method can generate maps and 3D landscape models that are useful for many scientific disciplines in Svalbard. Examples include assessing vegetation covers, counting reindeer, mapping glacier crevasses, identifying geohazards, digitizing geological outcrops, etc. Some scientists use more sophisticated drones, such as fixed-wing drones, for more advanced purposes, like atmospheric measurements or mapping of large areas.

I want to use drones in Svalbard. How can I get access to drone infrastructures?

Several facilities can be used to obtain access to drones on Svalbard. The University Centre in Svalbard (UNIS) and the Svalbard Integrated Arctic Earth Observing System (SIOS), both offer drone and pilot rental services.

I am using drones for science in Svalbard. Why should I share and long-term store my results?

Data collected with drones can potentially be useful for others in ways that the original drone operators cannot easily predict. For example, a drone campaign mapping glacier surfaces to study crevasses could be used in the future to monitor long-term changes in the glacier's volume and extent. Researchers must share their results with the scientific community and ensure long-term storage of their data. Most university libraries can help with long-term storage of research data and open-access and can advise on general data management strategies.

Arctic haze in a climate changing world: the 2010-2020 trend (HAZECLIC)

What is the Arctic haze?

Arctic haze is a "mist" made of fine (submicrometric) particles, mainly anthropogenic in origin, due to emissions from mid-latitude areas (especially Europe and the former Soviet Union). The particles

are transported to and trapped in the Arctic air mass during winter and early spring.

How does Arctic haze affect daily life in Svalbard?

The fine particles composing the haze are very efficient at scattering visible solar radiation, leading to a cooling of the atmosphere. Haze also weakly absorbs light due to the presence of black carbon. The net result is a noticeable reduction of visibility to a few kilometres and the "weak" absorption may strongly affect climate when carbon settles on the highly reflecting Arctic snow and ice pack.

Moreover, haze contains toxic species (e.g. heavy metals) potentially harmful to man and environment on both short and long-term scales.

How can the Arctic haze be traced and monitored?

By measuring the concentration of selected chemical species in atmospheric aerosols collected at strategic sites, it is possible to detect and track changes in the extent and features of Arctic haze. Particularly relevant markers are sulphate, ammonium, nitrate, and elemental and organic carbon.

Is there a long-term trend in the Arctic haze?

Sulphate concentrations show a significant decrease over the last few decades, consistent with the decrease in SO₂ emissions since the early 1990s. This decline is still ongoing and sulphate needs to be monitored further to reliably assess the climatic and environmental impact of the Arctic haze.

Microplastics in the realm of Svalbard: current knowledge and future perspective (MIREs)

What are microplastics?

Microplastics are small bits of plastic (<5 mm) which are not different from any other plastic except the size. On the basis of their origin, microplastics can be divided into two categories: primary and secondary. Primary microplastics are manufactured with a function in that size category

and are commonly used as exfoliants/scrubbers in cosmetics and industrial abrasives. In contrast, secondary microplastics originate from the fragmentation of larger plastics under the influence of light, mechanical abrasion, and temperature fluctuations.

How do microplastics travel to Svalbard and where do they come from?

Microplastics can travel to Svalbard with atmospheric currents, ocean currents and migratory birds, from local and distant sources. Local sources include commercial activities like fishing, shipping, and tourism, household activities such as washing of synthetic textile clothing, personal care products (e.g. toothpaste, exfoliants, etc.), as well as dumpsites and landfills, sewage, car/truck tyres and snowmobile belt wear dust, etc. Long-distance sources are mostly from similar to the local sources but on a larger scale.

How far can microplastics travel?

Microplastics may be transported over vast distances, from densely populated areas to the most remote places on Earth, including Antarctica and the Arctic. Researchers estimate that each year the atmosphere transports 140 metric kilotonnes (kt) of traffic-produced particles into the world's oceans – equivalent to the amount delivered by rivers – and 86.1 kt to the world's ice and snow.

Environmental status of Svalbard coastal waters: coastscapes and focal ecosystem components (SvalCoast)

Will we lose the fjord ice in western Svalbard in the near future?

In no recent year has ice been completely absent from western Svalbard fjords. Between 1973 and 2000 there was around 12 000 km² of sea ice that lasted two months or more, while in 2014-2019 the sea-ice extent fell to half (6000 km²). A further 2°C increase in mean winter air temperatures will most likely result in only 2000 km² of fast ice with very little ice in the innermost fjord arms of western Svalbard.

Has there been a huge increase in cruise tourism in Svalbard the last decade (before COVID-19)?

Although fewer oceangoing cruise ships come to Svalbard after the use of crude oil fuel was banned in 2015, these ships have become larger so the number of passengers has increased by ~30% to around 40 000 in 2019. Smaller expedition ships have increased from <20 ships in 2008 to 73 in 2019. The number of day-tourists in the Isfjorden–Ny-Ålesund area has also increased, from <10 000 in 2009 to ~30 000 in 2019. The boat season now starts earlier and ends later due to the reduction in sea ice.

Will warmer sea temperatures lead to new opportunities for fisheries in Svalbard?

Schools of Atlantic cod in Svalbard fjords are nothing new. In 1874-1882 there was a rich cod fishery in Svalbard. Cod was also plentiful around 1939 and from 1960 to the end of the 1970s. The past decade's abundance of cod is explained by unusually strong year classes and incursion of Atlantic water into the fjords. Today, the main commercial fishing in Svalbard fjords is for shrimp. In the future it may be possible to catch snow crab here, but so far only one two snow crabs have been detected in Svalbard fjords, in Raudfjorden in 2017 (by UNIS).

Which seabird species are most threatened by climate change?

Seabird populations are declining worldwide and climate change is considered to be one of their main threats. In Svalbard, we observe that "Arctic species" like Brünnich's guillemots, glaucous gulls and ivory gulls grow less numerous year after year. However, some species might cope better with global warming; some may even benefit from it. For example, species like the great skua, northern gannet and common guillemot, which normally breed in temperate environments, are doing well and their populations have been rapidly increasing in Svalbard.

From land to fjords: The review of Svalbard hydrology from 1970 to 2019 (SvalHydro)

The Arctic, including Svalbard, is warming twice as fast as the global average: why is that?

The Arctic atmosphere is relatively thin, so any additional energy will affect proportionally more of it. The snow and ice cover of the land and ocean act as an energy sink: large amounts of atmospheric energy are consumed simply in melting it. As snow and ice extent decreases, less energy is used in this way, so more is available to warm the surface. Third, and most importantly, the loss of snow and ice, particularly over the ocean, greatly reduces surface reflectivity, and allows more atmospheric energy to be absorbed: this melts snow and ice faster and further reduces reflectivity, in a highly effective feedback loop. [RH]

How is climate change affecting local environment in the Arctic (hydrology in particular)?

The most visible effect is rapid retreat of glaciers and thinning of ice caps. Climate warming means that summer is longer, warmer and wetter as we see more rainfall (even in winter). It is no longer a polar desert. All this affects plants and animals, rivers, lakes, fjords, seas and oceans. In general, we see an initial increase of freshwater as glaciers melt, releasing water that used to be frozen, but we do not know how long this overall increase will last. In places where glaciers are small, and their retreat is significant, we already observe a decrease in freshwater production. There are many uncertainties in Arctic hydrology and the entire story of change remains to be told. [JK, AN]

Why is it necessary to study water bodies in the Arctic if they are frozen for most of the year?

Arctic water bodies are sensitive to the rapid climate changes occurring today. We don't know how these changes will affect the whole region in the future, especially its ecosystems. Ultimately, we aim to predict changes under different future climate scenarios. To do that we need to collect data on site and maintain long-term monitoring, which unfortunately can be labour-intensive and costly. [AARI]

What would happen to the river flowing from a glacier if/when that glacier melts away completely?

It is hard to estimate exactly, but we expect that annual river runoff will decrease by the amount that comes from annual glacier melt. In low-water periods without rainfall the river will be more likely to dry up. However, the Arctic is getting wetter. So, the absence of glacier meltwater could potentially be balanced by input from rainfall, snowmelt, water exchange with permafrost active layer and other underground sources. We simply don't know. That is why these elements of water balance should be studied more extensively. [AARI]

What are the changes in precipitation patterns and how do they influence hydrology in Svalbard?

An immediate consequence of the continuous increase in air temperature is an increase in the amount of liquid precipitation and a prolongation of the melt season across Svalbard. Melting is starting earlier, while the winter freeze-up is starting later. This results in a reduction of the snowpack and a shift of the hydrological regime. High flows occur more commonly in autumn and early winter rather than spring. Catchments dominated by snow are transitioning to mixed rain and snow dominance, and in future will shift towards rain-dominated. [IG]

Satellite and modelling based snow season time series for Svalbard: Inter-comparisons and assessment of accuracy (SATMODSNOW)

How is snow measured in Svalbard?

Snow depth is measured at a few meteorological stations, and snow campaigns provide more detailed measurements over wider areas. Optical satellites can measure *snow cover fraction* during daylight on clear days, and radar satellites can detect wet snow despite clouds and (polar) night. New satellites give higher resolution data than the old ones. Measuring *snow mass* requires new and more sensitive radar sensors. Satellite sensors are not yet sensitive enough to measure snow depths, but ground-penetrating radars on snowmobiles or drones can survey limited areas.

How does snow modelling work?

Hydrological snow models mainly use temperature and precipitation data from the meteorological service. The model aggregates precipitation as snow during cold periods and melts snow when temperatures are above 0°C. The uncertainty of the meteorological data on Svalbard is high since there are few meteorological stations that can provide input to the model. This uncertainty is propagated as increased uncertainty in the hydrological snow models.

Can the snow models be improved to more accurately predict snow depths on Svalbard?

Yes. Snow model performance is currently limited by the sparseness of input data. Addition of new meteorological stations has already expanded access to local data. Ongoing development of radar satellite sensors that can measure snow all over Svalbard will further improve the models. Comparison of the first and last snow-free days predicted by models versus historical satellite time series may allow us to refine the input data (precipitation and/or temperature) used in historical models and thus improve model performance.

Svalbard snow and sea-ice cover: comparing satellite data, on-site measurements, and modelling results (SvalSCESIA)

What is the difference between sea-ice area and sea-ice extent?

Both sea-ice extent and sea-ice area are measures of the ice-covered area in a region, and sea-ice extent is always larger than sea-ice area. Sea-ice area is the total area of the sea ice itself, whereas sea-ice extent describes the total sea surface that is ice-covered according to some ice concentration threshold (15% ice concentration is a commonly used threshold). This means that the sea-ice extent also includes many square kilometres of ice-free water between ice floes, which is the reason why sea-ice area should be preferred for some applications.

Terrestrial photography applications on snow cover in Svalbard (PASSES)

What are the advantages of participating in the PASSES survey?

By sharing your information, you could be involved in future opportunities where your facilities could be used for snow cover studies.

Who can participate in the Survey?

Whether organisation or private citizen, anyone who is interested in extracting information from their time-lapse images and helping monitor climate change is welcome to participate.

How do I sign up for the Survey?

It's easy! All you need to do is go to <https://niveos.cnr.it/passes/>, click on the "REGISTER NOW!" link and fill in your information.

What kind of information does PASSES require?

The first contact requires only basic information about your setup (location, coordinates, purpose) and acceptance of terms (use and privacy).

How can I protect my data? Will I still own them?

We are collecting only information (metadata) and your data are not requested. We wish in the future to establish a camera network that gives users an overview of where the cameras are and what is required for processing the data.

Is there a need for professional/paid software to process the data?

No, in the future we hope to have resources to prepare a standardised methodology for processing your data without efforts from your side.

Ground ice content, drilling methods and equipment and permafrost dynamics in Svalbard 2016-2019 (PermaSval)

What is the temperature of the permafrost in Svalbard?

That varies depending on where in the permafrost it is measured. At 10-20 m depth where the annual air temperature fluctuations do not have any influence, mean annual temperatures range from -5°C to -1.2°C . In the top permafrost we recently have less variation as mean annual temperatures there range from -1°C to -4.5°C .

What is ground ice and why is it important?

This is ice formed due to freezing conditions in the permafrost. The ground ice content can be either high or low. If the ground ice content is high, this means that thawing of permafrost in a climate that is warming will take longer time, as all the ice needs to melt before the permafrost can thaw.

Why is it called permafrost thaw and not melt?

Permafrost can contain ground ice, sediment, rock or organic material. Of these, only ice melts, when changing from solid to liquid form, when the temperature increases above 0°C . Neither sediment nor rock nor organic material will physically change state or melt at that temperature. You can remember this if you think of permafrost as a chicken. If you want to eat a frozen chicken for dinner, you must defrost it before you can eat it. Your frozen chicken can only thaw, it doesn't melt!

You can find this and previous SESS reports on our webpage:

<https://sios-svalbard.org/SESSreport>



Visit the SIOS data access portal to find metadata and datasets described in this report: https://sios-svalbard.org/metadata_search

